SHAFT RESISTANCE OF AXIALLY LOADED PILES IN CLAY

A thesis submitted to the University of London
(Imperial College of Science and Technology)

in partial fulfilment of the requirements
for the Degree of Doctor of Philosophy in
the Faculty of Engineering

by

JOHN PAUL MARTINS, M.A., M.Sc., D.I.C.

January 1983

To my wife and to my parents

ABSTRACT

This thesis describes an investigation into the behaviour of axially loaded piles in clay. The philosophy adopted has been to simplify the problem as far as possible in order that details of the load-transfer mechanism might be examined; the study was made more relevant to field conditions as understanding was gained.

The load transfer mechanism is dominated by the severe kinematic restraints imposed by the presence of the pile, and it was decided to employ three independent, although complementary, approaches:-

(i) laboratory scale model pile tests;

(ii) investigations of micro-fabric changes induced in the clay as a result of both pile installation and pile loading;

(iii) theoretical (finite element) analyses employing an elasto-plastic constitutive law (Modified Cam Clay).

The first series of model pile tests was conducted on rigid piles installed with a minimum of disturbance into samples of Speswhite Kaolin which were consolidated to a range of initial stress ratios, K. The pile loadings were conducted under drained conditions, and in such a manner that only shaft resistance was generated. The results of tests conducted on nine normally-consolidated samples and one over-consolidated sample suggest that the peak angle of shaft friction is independent of the initial stress ratio in the clay ($0.7 < K < 1.5$), and is slightly less than $\phi'_{triaxial}$. When loaded axially, the lateral effective stresses on the pile shaft decrease with increasing pile load for piles in normally-consolidated clay, but may increase for those in over-consolidated clay. The adhesion factors, α, back calculated from the tests on piles in normally-consolidated clay, are in excess of unity. Micro-fabric studies confirmed that the pile installation procedure employed caused minimal fabric disturbance to the clay adjacent to the pile. The progressive development of micro-fabric features in the clay with pile displacement is demonstrated; once residual load conditions are reached, there exists a thin, continuous, displacement discontinuity parallel to the pile.

Finite element modelling of the above laboratory tests has given very encouraging agreement with the experimental observations, and has led to a better understanding of the influence of the kinematic restraints on the effective stress changes occurring in the clay beside loaded piles.

A second, shorter, series of model tests was performed to examine the behaviour of jacked and driven piles. On the basis of micro-fabric studies, and an examination of the pile load-displacement behaviour, it is concluded that fabric disturbance caused by pile installation may significantly affect the future behaviour of the pile. A method is proposed whereby a conservative estimate of the ultimate capacity of long compressible driven piles may be calculated, without the need to resort to empirical coefficients. Predictions based on this new method are shown to be in good agreement with field measurements.

ACKNOWLEDGEMENTS

The work described in this thesis was conducted in the Soil Mechanics Section of the Department of Civil Engineering, headed by Professor J.B. Burland. I am grateful to Professor Burland for the interest that he has taken in my work. The author was supported in the first year by a grant from the Science Research Council, before being appointed, for the remaining two years, to the post of Research Assistant. This was financed by an award from the Science and Engineering Research Council Marine Technology Directorate, and I greatly appreciate their support.

I wish to express my gratitude to Dr. R.J. Chander for his interest, guidance and encouragement during my research. I also appreciate his attempts to broaden my knowledge of other aspects of soil mechanics.

I am indebted to Dr. A. Skinner and to Dr. P.R. Vaughan for the numerous discussions which we have had, and for their generosity with ideas.

Special thanks are due to Dr. D.M. Potts from whom I have learned a great deal. I am most grateful for his collaboration and encouragement, and I have much enjoyed his friendship. Similar thanks are extended to Dr. Gens whose company I have also found most stimulating.

I should also like to thank other members of the academic staff at Imperial College, Professor A.W. Skempton, Professor J.N. Hutchinson, Professor N.N. Ambraseys, Dr. S. Cavounidis, and particularly, Mr. D.W. Hight for their interest and assistance.

Particular thanks are also due to my friends and colleagues Tacio de Campos, Andy Fourie, Luis Lemos, Franco Lupini, Richard Jardine, and of course Matthew Symes, for their comradeship and innumerable discussions.

I am most grateful to the technical staff of the Soil Mechanics Laboratory, supervised by the late Mr. D. Evans, for the assistance that they have given me in the course of my experimental work. Graham Keefe was responsible for building most of the equipment, and Steve Ackerley was always ready to help with any electronics problem (generally the more difficult the better!). I also acknowledge the assistance from Messrs. Fred Evans, Lou Spall and Alan Bolsher, and from Mrs. Eileen Gibbs.

Miss Joyce Gurr provided invaluable assistance with all of the photography which I undertook. I should like to thank her for her time and enthusiasm,

and for trying to teach me a little of the art of technical photography.

Mr. Kevin Schrapel from the Department of Geology, Queen Mary College, London was responsible for the preparation of all of the thin sections discussed in this thesis. Kevin's skill and constructive approach are much appreciated.

I am also glad to acknowledge my many colleagues in the Soil Mechanics Section for their discussions and help in many ways, M. Chandler, M. Hamza, F. Lopes, M. Martins, J. Maswoswe, S. Shibuya, M. Takahashi, D. Toll and J.C. Ziolkowski.

Many thanks are due to Mrs. Marjorie Carter and Mrs. Kay Crooks for their assistance in the most efficiently run library.

Miss Cynthia Collins undertook the onerous task of typing this thesis. The typing was always performed promptly and accurately, and I am most grateful.

My profound gratitude is expressed to my parents and brother who have always been of the greatest encouragement to me, throughout my education.

I am glad of the opportunity to record my appreciation of the interest which my wife's parents have shown in my work, and finally I find it hard to express my thanks and commiserations to my wife, Charlotte, for the continuous encouragement and comradeship which she has given me in the course of this thesis.

Among the innumerable mortifications which waylay human arrogance on every side may well be reckoned our ignorance of the most common objects and effects, a defect of which we become more sensible by every attempt to supply it. Vulgar and inactive minds confound familiarity with knowledge and conceive themselves informed of the whole nature of things when they are shown their form or told their use; but the speculatist, who is not content with superficial views, harasses himself with fruitless curiosity, and still, as he inquires more, perceives only that he knows less.

Samuel Johnson,
The Idler
(Saturday, 25th November, 1758)

NOTATION

A	surface area
b	Bishop's parameter, $(\sigma_2' - \sigma_3')/(\sigma_1' - \sigma_3')$
C'	effective cohesion intercept
C_a'	effective adhesion intercept
$C_{u,o}$	undrained shear strength in triaxial compression before pile installation
$C_{u,i}$	undrained shear strnegth, at a Lode angle of zero, after pile installation and consolidation
c_v	coefficient of consolidation
e	void ratio
E	Young's modulus
F	yield function; axial load on pile
g	function defining shape of yield surface in the deviatoric plane
G	elastic shear modulus
J	second invariant of the stress tensor $\{1/6((\sigma_1' - \sigma_2')^2 + (\sigma_2' - \sigma_3')^2 + (\sigma_3' - \sigma_1')^2)\}^{\frac{1}{2}}$
k	permeability
K	stress ratio, σ_r'/σ_z'
K_{OnC}	in situ stress ratio for one-dimensional normally-consolidated clay
K_B	elastic bulk modulus
M	slope of critical state line
P'	mean effective stress $(\sigma_1' + \sigma_2' + \sigma_3')/3$
P_o'	value of P' at intersection of current swelling line and virgin consolidation line
P_f'	value of P' at failure
L	pile length.

q	deviatoric stress $\sigma_1' - \sigma_3'$ in triaxial stress space
Q	plastic potential function
r	coordinate direction radius
r_o	initial radius, or pile radius
R	radius
$\underset{\sim}{s}$	deviatoric stress tensor
S	stress measure
$S_1 \ldots . S_n$	family of shear structures
T	time factor (dimensionless coefficient)
u	displacement, excess pore pressure
v	specific volume; angle of dilation
v_1	specific volume at unit pressure on the virgin consolidation line
v_s	specific volume at unit pressure on current swelling line
x	coordinate direction
X	variable employed in describing the plastic potential function
y	coordinate direction
Y	variable employed in describing the plastic potential function
z	coordinate direction
Z	variable employed in describing the plastic potential function
α	adhesion factor (the ratio of the peak unit shaft resistance to initial undrained shear strength in triaxial compression); angle of inclination
β	effective stress coefficient introduced by Burland; angle of inclination
γ'	effective unit weight
γ	shear strain

γ_{rz}	shear strain in r-z plane
δ'	mobilised angle of friction along the pile shaft
δ	displacement
ε	direct strain
θ	Lode angle; cylindrical coordinate direction
κ	slope of swelling line in v-$\ell n(P')$ space
λ	slope of consolidation line in v-$\ell n(P')$ space
μ	coefficient introduced in new method for pile design
$\sigma'_r, \sigma_\theta, \sigma'_z$	effective normal stresses in cylindrical coordinate directions
$\sigma'_1, \sigma'_2, \sigma'_3$	principal effective stresses
τ	shear stress
τ_{max}	maximum shear stress on pile shaft
τ_{rx}	shear stress mobilised on r-z plane
$\bar{\tau}$	average shear stress on pile shaft
ϕ'	effective angle of shearing resistance
ψ	inclination of major principal stress with respect to the vertical direction
ω	water content

Subscripts

f	failure value
i	initial value; or value after pile installation and consolidation
N.C.	normally-consolidated value
o	value before pile installation; in situ
P	peak value
r	residual value
r	radial direction
θ	hoop direction
z	axial direction
1,2,3	major, intermediate, minor

Superscripts

E	elastic component
P	plastic component
T	total value
·	incremental value
-	average value

Sign Convention

Compressive direct stresses and strains are reckoned positive, as are shear stresses inducing anti-clockwise moments.

Units

Except where stated to the contrary, all quantities are measured in S.I. units.

Table of Contents

			Page
Abstract			i
Acknowledgements			iii
Notation			vi
Table of Contents			x
CHAPTER 1:		INTRODUCTION	1
	1.1	INTRODUCTION	1
	1.2	GENERAL THEORY OF PILE BEHAVIOUR	2
	1.3	METHODS OF RESEARCH INTO PILE BEHAVIOUR	3
	1.4	OUTLINE OF THE PRESENT INVESTIGATION	4
		1.4.1 Object of the Research	4
		1.4.2 Approaches Employed	4
		1.4.3 Model Pile Tests	5
		1.4.4 Microfabric Studies	6
		1.4.5 Theoretical Analyses	6
CHAPTER 2:		LITERATURE REVIEW	7
	2.1	INTRODUCTION	7
	2.2	FIELD PILE TESTS	8
		2.2.1 The Effects of Installing Displacement Piles	8
		2.2.1.1 Introduction	8
		2.2.1.2 Ground movements during pile installation	8
		2.2.1.3 Excess pore-pressures generated during the installation of displacement piles	10
		2.2.1.4 Total stress changes induced by pile installation	11
		2.2.2 Consolidation Following Pile Installation	12
		2.2.2.1 Introduction	12
		2.2.2.2 Field observations	12

Page

		2.2.3 Fabric Disturbance caused by the Installation of Driven Piles	14
		2.2.4 Pile Loading Tests	15
		2.2.4.2 Stress measurements during pile loading	16
		2.2.4.3 Post-peak behaviour of loaded piles	17
	2.3	LABORATORY SCALE MODEL PILE TESTS	18
		2.3.1 Introduction	19
		2.3.2 Model Pile Tests	18
		2.3.3 Interface Behaviour	24
	2.4	DEVELOPMENT OF EFFECTIVE STRESS METHODS OF PILE DESIGN	25
		2.4.1 Introduction	25
		2.4.2 Initial Development of an Effective Stress Theory of Pile Design	26
		2.4.3 Development of a Generalised Effective Theory of Pile Design	28
	2.5	MICROFABRIC STUDIES	34
		2.5.1 Introduction	34
		2.5.2 Preparation of Thin Sections	34
		2.5.3 Effects of Impregnating Clay Samples	34
		2.5.4 Observation of Thin Sections under Polarised Light	35
		2.5.5 Shear-induced Particle Orientation	35
TABLE			37
CHAPTER 3:		DESIGN OF EXPERIMENTAL APPARATUS	38
	3.1	INTRODUCTION	38
	3.2	BOUNDARY CONDITIONS	39
		3.2.1 Outer Circumferential Boundary	39
		3.2.2 Top and Bottom Boundaries	40
	3.3	PRINCIPLES BEHIND THE PILE INSTALLATION PROCEDURES (TO CAUSE MINIMAL DISTURBANCE)	41

			Page
3.4	APPARATUS		42
	3.4.1	General Layout	42
		3.4.2.1 Introduction	42
		3.4.2.2 Drainage	42
		3.4.2.3 Provision for pile entry and exit	43
	3.4.3	Sample Loading	43
	3.4.4	Piles	44
		3.4.4.1 Introduction	44
		3.4.4.2 Non-instrumented piles	44
		3.4.4.3 Instrumented piles	45
		3.4.4.4 Displacement piles	47
	3.4.5	Pile loading system	47
3.5	CALIBRATIONS		48
	3.5.1	Introduction	48
	3.5.2	Pressure Transducers	48
	3.5.3	Load Cells	49
	3.5.4	Displacement transducers	49
	3.5.5	Axial Stresses on the Samples in Hydraulic Triaxial Cell	49
TABLE 3.1		Comparison Between Different Methods of Installation	51
FIGURES			52
APPENDIX 3.1		Preparation of Membranes	60
CHAPTER 4:		SAMPLE PREPARATION AND TESTING PROCEDURES	61
4.1		INTRODUCTION	61
4.2		CLAY SELECTED FOR EXPERIMENTAL PROGRAMME	61
	4.2.1	Reasons for Selection	61
	4.2.2	Properties of Speswhite Kaolin	62
4.3		SAMPLE PREPARATION	63
	4.3.1	Introduction	63
	4.3.2	Preparation of Slurry	63
	4.3.3	One-dimensional Consolidation	63
	4.3.4	Consolidation in the Hydraulic Triaxial Cell	64

Page

4.4 TESTS EMPLOYING NON-INSTRUMENTED, ZERO-DISPLACEMENT PILES 66
4.4.1 Introduction 66
4.4.2 Unloading the Sample 66
4.4.3 Forming the Hole through the Sample 67
4.4.4 Introduction of a Non-instrumented Model Pile 67
4.4.5 Grouting the Pile in Place 68
4.4.6 Re-application of Total Radial Stress to the Sample 68
4.4.7 Pile Loading Procedure 68
4.5 PILES INCORPORATING A DEVICE FOR MEASURING RADIAL STRESSES 69
4.5.1 Introduction 69
4.5.2 Assembly of the Pile Core 69
4.5.3 De-airing of the Hydraulic System 70
4.5.4 Fitting a Membrane to the Central Section of the Pile 70
4.5.5 Calibration of the Membrane 71
4.5.6 Attachment of Shear Reinforcement 71
4.5.7 Pile Installation 71
4.5.8 Re-application of Total Radial Stress to the Sample 72
4.5.9 Pile Loading 72
4.6 TESTS EMPLOYING FULL-DISPLACEMENT PILES 72
4.6.1 Introduction 72
4.6.2 Driven Piles - Introduction 73
4.6.3 Pile Driving 73
4.6.4 Jacked Pile - Introduction 74
4.6.5 Pile Jacking 74
4.7 THIN SECTION PREPARATION 75
4.7.1 Introduction 75
4.7.2 Impregnation Procedure 75
4.7.3 Preparation of Thin Sections 76
4.7.4 Observation of Thin Sections 76
TABLES 4.1 Speswhite Kaolin - Properties 77
4.2 Strength and Consolidation Properties of Speswhite Kaolin 78
FIGURES 79
APPENDIX 4.1 Residual Shear Strength of Kaolin 87

			Page
CHAPTER 5:		EXPERIMENTAL RESULTS - EXCLUDING MICRO-FABRIC STUDIES	95
	5.1	INTRODUCTION	95
	5.2	TESTING PROGRAMME	95
		5.2.1 Introduction	95
		5.2.2 Piles Installed with Minimal Disturbance	95
		5.2.3 Full-displacement Piles	97
	5.3	RESULTS OBTAINED DURING SAMPLE PREPARATION	97
		5.3.1 Introduction	97
		5.3.2 One-dimensional Consolidation	97
		5.3.3 Anisotropic Consolidation within the Hydraulic Triaxial Cell	98
		5.3.3.1 Normally-consolidated samples	98
		5.3.3.2 Over-consolidated sample	98
	5.4	INSTALLATION OF PILES WITH MINIMAL DISTURBANCE	99
		5.4.1 Introduction	99
		5.4.2 Results: Excluding measurements of the Radial Stresses Acting on Piles	99
		5.4.2.1 Introduction	99
		5.4.2.2 Measurements of total stress changes	99
		5.4.3 Water-content Profiles	101
		5.4.4 Instrumented Model Piles	102
		5.4.4.1 Introduction	102
		5.4.4.2 Membrane inflation pressures	102
		5.4.4.3 Installation of the instrumented pile in Test 15	102
		5.4.4.4 Installation of the instrumented pile in Test 17	103
	5.5	LOADING BEHAVIOUR OF PILES INSTALLED WITH MINIMAL DISTURBANCE	104
		5.5.1 Introduction	104
		5.5.2 Load-displacement Behaviour	104
		5.5.2.1 Tests conducted to investigate the development of micro-fabric changes with pile loading (Nos. 9,10,12,13)	104

Page

5.5.2.2 Effects of initial stress ratio on the pile load-displacement behaviour 105

5.5.2.3 Pile installed in over-consolidated Kaolin (OCR 5) 106

5.5.3 Measurements of Radial Stresses Acting on Pile Shafts During Pile Loading 107

5.5.3.1 Introduction 107

5.5.3.2 Test 15 107

5.5.3.3 Test 17 108

5.6 A DISCUSSION OF THE RESULTS FROM THE TESTS CONDUCTED ON PILES INSTALLED WITH MINIMAL DISTURBANCE 108

5.6.1 Variations of the Angles of Shaft Friction and the Radial Effective Stress During Pile Loading 108

5.6.1.1 Variation of the radial effective stress on loading to residual conditions 108

5.6.1.2 Determination of the peak angles of shaft resistance 109

5.6.1.3 Discussion of the post-peak behaviour 110

5.6.2 Comparison between the Test Results and Predictions Based on Effective Stress Methods of Pile Design 111

5.6.3 Comparison between the Test Results and Predictions based on Total Stress Design Methods 113

5.7 TESTS ON FULL-DISPLACEMENT PILES 113

5.7.1 Introduction 113

5.7.2 Driven Piles 114

5.7.2.1 Sample preparation 114

5.7.2.2 Pile driving 114

5.7.2.3 Pile loading 115

5.7.2.4 Sample removal 116

5.7.2.5 Comments 116

Page

5.7.3 Jacked Piles 117
5.7.3.1 Sample preparation 117
5.7.3.2 Pile jacking 117
5.7.3.3 Pile loading 117
5.7.3.4 Sample removal 118
5.7.3.5 Comments 118

TABLE 5.1 Summary of Model Pile Tests 119

TABLE 5.2 Summary of the Results of the Model Pile Tests 120

TABLE 5.3 Water Contents Measured during Pile Installation (supplementary) 121

FIGURES 122

APPENDIX 5.1 The use of Strain Increment Vectors to Monitor Consolidation 149

APPENDIX 5.2 Total Stress Changes Measured during Pile Installation 151

APPENDIX 5.3 The Results of Fast Ring-shear Tests 158

CHAPTER 6: MICRO-FABRIC INVESTIGATIONS 169
6.1 INTRODUCTION 169
6.2 DEVELOPMENT, WITH PILE DISPLACEMENT, OF MICRO-FABRIC CHANGE WITHIN THE CLAY ADJACENT TO LOADED MODEL PILES INSTALLED WITH MINIMAL DISTURBANCE 170
6.2.1 Introduction 170
6.2.2 Fabric Disturbance Caused by the Drilling Operation 171
6.2.3 Test Stopped at 70% of Peak Load 171
6.2.4 Test Stopped at 95% of Peak Load 172
6.2.5 Test Stopped Immediately Post-peak 173
6.2.6 Test Pile Displaced to Residual Conditions 175
6.2.7 Comments 177
6.3 THE EFFECT OF THE INITIAL STRESS RATIO ON THE MICRO-FABRIC CHANGES INDUCED IN THE CLAY SURROUNDING LOADED PILES 177
6.3.1 Introduction 177
6.3.2 Test Conducted at an Initial Stress Ratio of 1.5 178

Page

6.3.3 Test Conducted at an Initial Stress Ratio of 1.11 178

6.3.4 Test Conducted at an Initial Stress Ratio of 0.74 179

6.3.5 Comparison between the Observed Modes of Deformation 180

6.4 TEST CONDUCTED ON A PILE INSTALLED IN OVER-CONSOLIDATED KAOLIN 181

6.4.1 Introduction 181

6.4.2 Observed Micro-fabric Changes 181

6.4.3 Comments 182

6.5 SUMMARY OF MICRO-FABRIC FEATURES OBSERVED AS A RESULT OF LOADING PILES INSTALLED WITH MINIMAL DISTURBANCE 183

6.6 TESTS TO EXAMINE FABRIC DISTURBANCE CAUSED BY INSTALLING AND LOADING DISPLACEMENT PILES 183

6.6.1 Introduction 183

6.6.2 Pile Driven into Clay Sample, but not Loaded 183

6.6.2.1 Introduction 183

6.6.2.2 General description of deformations around the pile 184

6.6.2.3 Deformations around the pile shaft 185

6.6.2.4 Soil deformations beneath the advancing pile tip 185

6.6.2.5 Comments 186

6.6.3 Pile Driven and Slowly Loaded to Residual Conditions 187

6.6.3.1 Introduction 187

6.6.3.2 Fabric changes adjacent to the pile shaft 187

6.6.3.3 Comments 188

6.6.4 Pile Jacked and then Slowly Loaded to Residual Conditions 188

6.6.4.1 Introduction 188

6.6.4.2 Micro-fabric changes beside the pile 189

6.6.4.3 Comments 190

Page

6.7 DISCUSSION OF THE BEHAVIOUR OF DISPLACEMENT PILES 190
6.7.1 Summary of the Results from the Model Tests on Displacement Piles 190
6.7.2 Field Tests on Jacked and Driven Piles in London Clay 191
6.7.2.1 Introduction 191
6.7.2.2 Comparison between the behaviour of jacked and driven piles 191
6.7.2.3 Stresses acting on a continuously jacked pile in London Clay
6.7.3 Conclusions 194

FIGURES 195

APPENDIX 6.1 End Effects in Model Pile Tests 237
6.2 Micro-fabric Changes around the Radial-stress Measuring Devices 242

CHAPTER 7: FINITE ELEMENT ANALYSES 250
7.1 INTRODUCTION 250
7.2 FINITE ELEMENT PROGRAM 252
7.3 MESH GEOMETRIES EMPLOYED 252
7.3.1 Introduction 252
7.3.2 Mesh to Analyse the Ideal Behaviour 253
7.3.3 Mesh to Analyse the Experimental Conditions 254
7.4 SOIL CONSTITUTIVE MODELS 254
7.4.1 Introduction 254
7.4.2 Constitutive Model in Triaxial Stress Space 255
7.4.2.1 Introduction 255
7.4.2.2 Consolidation behaviour 255
7.4.2.3 Yield function and plastic potential 255

Page

7.4.3 Constitutive Models in Generalised Stress Space 256
7.4.3.1 Introduction 256
7.4.3.2 General expressions for the yield function and the plastic potential 258
7.4.3.3 Elastic behaviour 260
7.4.1 Discussion of some Implications of the chosen Soil Models 261
7.4.5 Parameters selected for the Soil Models Employed 262

FIGURES 263

APPENDIX 7.1 Determination of Appropriate Mesh Geometry 272
7.2 Selection of Increment Sizes 274
7.3 Relationship between the Lode Angle and Bishop's Parameter b 276
7.4 The Relationship between q, J and θ 278
7.5 Relationship between $g(\theta)$, θ and ϕ' 279

TABLE A.7.5.1 The Variations in ϕ' implied by selecting Constant Values of $g(\theta)$ 280

CHAPTER 8: THEORETICAL ANALYSES OF MODEL PILE TESTS 281
8.1 INTRODUCTION 281
8.2 STRESS CONDITIONS WITHIN THE EXPERIMENTAL APPARATUS 281
8.2.1 Introduction 281
8.2.2 Stress Distribution around the Model Piles 282
8.2.3 A Comparison between the Stresses predicted in the Clay Adjacent to an Experimental Model Pile and those adjacent to an Element of a Long Pile in Kaolin of Vast Extent 282
8.2.4 Discussion 283

Page

8.3 EFFECTS OF INITIAL STRESS CONDITIONS ON THE LOADING BEHAVIOUR OF PILES 283

8.3.1 Introduction 283

8.3.2 Stress Changes Occurring on Drained Loading 283

8.4 COMPARISON BETWEEN THEORETICAL PREDICTIONS OF STRESS CHANGES AND EXPERIMENTAL RESULTS 285

8.4.1 Introduction 285

8.4.2 Comparison between Predicted and Observed Pile Loading Behaviour 286

8.4.3 Conditions obtaining at Peak Load 286

8.4.3.1 Angle of shaft resistance 286

8.4.3.2 Changes in the radial effective stress 286

8.4.4 A Comparison between the Observed Pile Capacities and Predictions based on Conventional Pile Design Methods 287

8.4.5 Comments 288

8.5 DEFORMATION BEHAVIOUR OF THE SOIL SURROUNDING LOADED PILES 289

8.5.1 Kinematic Restraints 289

8.5.2 Strains within the Clay adjacent to a Loaded Pile 289

8.5.3 Radial distribution of Shear Strains and Axial Displacements 291

8.5.4 Zero Extension Lines 292

8.6 COMPARISON BETWEEN THE PREDICTED SOIL DEFORMATION BEHAVIOUR ADJACENT TO LOADED PILES AND OBSERVATIONS OBTAINED BY MEANS OF MICRO-FABRIC STUDIES 293

8.6.1 Introduction 293

8.6.2 Shear Strains in the Clay adjacent to Loaded Piles 294

8.6.3 Radial distribution of Axial Displacements 294

8.6.4 Riedel Structures 295

Page

8.7 DISCUSSION OF THE WORK RELATED TO NON-DISPLACEMENT PILES 297
8.7.1 Introduction 297
8.7.2 Model Pile Tests and Micro-fabric Results 297
8.7.3 Model Pile Tests and Theoretical Predictions 298
8.7.4 Micro-fabric Studies and Theoretical Predictions 298
8.7.5 Conclusions 299
8.8 UNDRAINED LOADING OF PILES 299
8.8.1 Introduction 299
8.8.2 Undrained Loading 299

FIGURES

CHAPTER 9: DISPLACEMENT PILES 337
9.1 INTRODUCTION 337
9.2 THE LOADING BEHAVIOUR OF FULL-DISPLACEMENT PILES 337
9.2.1 Introduction 339
9.2.2 Piles in Normally-consolidated Boston Blue Clay 339
9.2.3 Dissipation of Excess Pore Pressures around Loaded Piles 340
9.2.4 Pile installed in Over-consolidated London Clay 342
9.2.5 Simplified Analyses and Pile Loading 343
9.2.6 Undrained Pile Loading 344
9.3 PARAMETRIC STUDIES 346
9.3.1 Introduction 347
9.3.2 Shape of the Yield Surface in the Deviatoric Plane 347

Page

9.3.3 The Effects of Deviations of the Stress Conditions (around displacement piles) from the Values Predicted on the Basis of Cavity Expansion Analyses 349

9.3.3.1 Introduction 349

9.3.3.2 Departures from normally-consolidated conditions adjacent to displacement piles 350

9.3.3.3 Influence of the initial stress ratio 350

9.3.4 Effect of Changes in the Parameters describing the Soil Model on the behaviour of Full-displacement Piles 351

9.3.4.1 Introduction 351

9.3.4.2 Angle of shearing resistance ϕ' 351

9.3.4.3 $G/C_{u,i}$ 352

9.3.4.4 λ and κ 352

9.3.5 Comments 353

9.4 LOW DISPLACEMENT PILES 354

9.4.1 Introduction 354

9.4.2 Drained and Undrained Pile Loadings 354

9.5 DISCUSSION OF RESULTS 355

9.5.1 Introduction 355

9.5.2 Pore Pressure Generation 355

9.5.3 Changes in Radial Stresses acting on Loaded Piles 356

9.5.4 Pile Capacities 357

9.5.4.1 Introduction 357

9.5.4.2 Full-displacement piles 357

9.5.4.3 Low-displacement piles 359

9.5.4.4 Comparison with field and laboratory measurements 359

Page

9.5.5 The Possible Influence of Fabric Disturbance caused during Pile Installation 360
9.5.5.1 Introduction
9.5.5.2 Theoretical analyses of pile loading incorporating allowances for the presence of pre-existing shear surfaces 362

9.6 THE POSSIBLE USE OF THE SIMPLE SHEAR TEST IN PILE DESIGN 363
9.6.1 Introduction 363
9.6.2 Undrained Pile Loading 363
9.6.3 Drained Loading of Piles 364

9.7 A SIMPLE METHOD FOR DETERMINING LOWER BOUNDS TO THE CAPACITIES OF LONG DRIVEN PILES 365
9.7.1 Introduction 365
9.7.2 Ultimate Angle of Shaft Friction 366
9.7.3 Ultimate Value of the Radial Effective Stress 366
9.7.4 Evaluation of the Shaft Resistance 367
9.7.5 Comparison between Predictions and Field Measurements 368
9.7.5.1 Introduction 368
9.7.5.2 Derivation of equivalent α values 369
9.7.5.3 Derivation of equivalent β values 370
9.7.5.4 Derivation of equivalent λ values 370
9.7.5.5 Comparisons between predicted values of α, β and λ with field results 370

TABLE 9.1 Predicted Values of α and β assuming the Clay to be intact $\phi' = 25°$ 372
9.2 Properties of a Selection of Clays 373
9.3 Predicted Lower Bounds for the Coefficients α, μ or β_{min} and λ 374

FIGURES 375

APPENDIX 9.1 Consolidation around Piles 400
9.2 Derivation of a Variety of Equations Employed in the text 406

			Page
CHAPTER 10		CONCLUDING REMARKS	410
	10.1	CONCLUSIONS	410
	10.2	IMPLICATIONS FOR THE DESIGN	413
		10.2.1 Prediction of the Capacities of Compressible Piles	413
		10.2.2 The Design of More Efficient Piles	413
	10.3	SUGGESTIONS FOR FUTURE RESEARCH	415
		10.3.1 Field Measurements of Stresses	415
		10.3.2 Interface Behaviour	415
		10.3.3 Industrially Important Problems	415
REFERENCES			417

CHAPTER 1

INTRODUCTION

1.1 INTRODUCTION

Traditionally the design of piles in clay has been performed with the aid of total stress methods in which the average shaft adhesion is related to the mean undrained shear strength of the clay prior to pile installation by an empirically determined parameter, α. The magnitude of α depends on many factors which include the type of pile, its method of installation and the nature and stress history of the clay into which it is installed. The method has worked satisfactorily on land (where it was developed) because appropriate α values may be selected on the basis of past experience, coupled with additional pile tests if necessary.

However, the design of offshore piled foundations to support heavy structures in increasingly deep waters is a much more demanding task, because of both the nature and the magnitudes of the loads transmitted to individual piles. As a result of the cyclic nature of the loadings, the load-deformation behaviour of individual piles influences the dynamic response of the supported structure, and hence the stresses in its members. These in turn affect the fatigue life of the structure, and so it is important to be able to predict the pile behaviour at working loads. Unfortunately, the dimensions of the piles and the geological site conditions are now well outside the data-base established by means of land based tests, and tests on relatively short piles offshore. Because tests on large piles in deep waters are very costly and time consuming operations, very few have been performed and so it has been necessary to extrapolate the largely empirical design procedures (such as the α, β and λ methods; see Skempton (1959), Burland (1973) and Vijayvergiya and Focht (1972) respectively) beyond their data base, which is always an undesirable practice. The reader is referred to St. John (1980) for a review of current practice in the design and installation of piles for offshore structures.

As the exploration for, and the production of, oil is extended to still deeper waters, the shortcomings of existing procedures will be accentuated. This will be especially true in the case of the proposed Tension Leg Platforms in which the anchoring piles will be subject to

continuous cyclic tension loadings.

Clearly, there is a need for a general theory for the prediction of pile behaviour both in terms of capacity and of load-deflection response. Such a theory should eventually be able to account for the effects of tension loading, cyclic loading and the rate of loading.

1.2 GENERAL THEORY OF PILE BEHAVIOUR

It has been long established that the behaviour of soil is largely determined by the effective stresses acting within it, and for this reason many investigators have sought to describe the behaviour of piles in terms of the effective stresses acting in the adjacent soil. Because the behaviour of soil depends on its stress history, any general theory must be capable of modelling all the major stages involved in the history of the soil around the pile under consideration. In order to do this a good understanding of the mechanisms involved is required, in addition to a general constitutive law to describe the soil response. In principle, it should be possible to incorporate the effects of rate of loading or cyclic loading through the constitutive law.

The development of the effective stress approach is briefly charted in Chapter 2, and so only the current position is described here. The history of the soil around a pile may conveniently be considered in four phases:

(i) soil deposition/erosion: in principle it is possible to establish the main features of the stress history by means of laboratory tests conducted on samples obtained during the site investigation;

(ii) pile installation: for displacement piles this has been modelled mathematically as the undrained expansion of a cylindrical cavity under plane strain conditions (e.g. Butterfield and Bannerjee (1970), Kirby and Wroth (1977) and Randolph, Carter and Wroth (1979));

(iii) consolidation following installation: this has been treated as a radial consolidation problem (e.g. Randolph et al (1979)).;

(iv) pile loading.

Considerable effort has been devoted to establishing the stresses acting in the soil around a pile after driving. Originally the soil was modelled as an elastic plastic material (Butterfield and Bannerjee, 1970), whereas more recently the work-hardening elasto-plastic Modified Cam Clay constitutive law (Roscoe and Burland, 1968) has been incorporated (Randolph et al, 1979). Significant advances have been made, and some of the predictions (for instance pore pressures generated on driving) have been broadly confirmed by field measurements, whereas others (including the important radial effective stress acting on the shaft after complete consolidation) are yet to be confirmed for lack of suitable field measurements.

However, to date the nature of the soil behaviour during pile loading has received relatively little attention, and it is this that forms the subject of this thesis.

1.3 METHODS OF RESEARCH INTO PILE BEHAVIOUR

There are essentially four methods of research available, varying considerably in cost and generality. They are: field loading tests on full sized piles; field tests on small scale model piles; laboratory testing, and theoretical analysis.

Tests on full sized piles offshore are extremely costly and as a result only a few have been performed, for example only one reliable test has been performed in the North Sea, at West Sole. The results from such tests can only record the behaviour of a particular pile at a specific location, and in the absence of a well developed theoretical framework cannot provide much insight into the mechanisms involved.

Land-based tests on smaller, well instrumented piles are potentially extremely valuable, particularly if the soil conditions are similar to those around the prototype piles. Unfortunately, the instrumentation of model piles (particularly in respect of measurements of radial stresses) has proved very difficult and field tests have yielded relatively little information about the stresses acting in the soil during installation and loading. Once again, the results from such tests are potentially far more valuable if they can be incorporated into a general theoretical framework.

Laboratory scale model tests, on the other hand, are potentially very flexible, and provide the means whereby a wide range of conditions

may be investigated at a comparatively low cost. Model tests are generally performed for one of two purposes; either to simulate as exactly as possible (within limits established by the scaling laws) the behaviour of a prototype structure, or to investigate individual mechanisms of behaviour in simplified problems so that a reliable theoretical framework can be established. Tests to model prototype behaviour are often complex and fairly expensive (e.g. centrifuge testing) whereas the second category of tests are often simpler and cheaper.

The fourth approach involves the development of theoretical (commonly numerical) models of the behaviour. Often the theoretical models are developed in conjunction with laboratory tests performed to investigate mechanisms of behaviour. Once the theoretical procedure has been verified, it may then be used in a predictive capacity.

The four approaches to piling research are each of comparatively limited value if employed in isolation, whereas they are very powerful if used in conjunction with each other.

1.4 OUTLINE OF THE PRESENT INVESTIGATION

1.4.1 Object of the Research

The work presented is intended as a contribution towards the development of a general theory of pile behaviour, and considers the development of shaft resistance beside a rigid pile, in response to monotonic pile loading.

The aim has been to examine the mechanisms of load transfer between a loaded pile and the surrounding clay, starting from the simplest conditions that can be modelled and extending to more realistic conditions as understanding is gained. It was intended to isolate, as far as possible, the effects of pile loading from those of the disturbance usually caused by pile installation. The results from the experimental investigations were then used to aid the development of a theoretical (numerical) model of pile behaviour.

1.4.2 Approaches Employed

The behaviour of the soil adjacent to a loaded pile is dominated by the local kinematic constraints, and it was decided to adopt three separate, although complementary approaches to the problem of load transfer.

(i) carefully controlled model pile tests;

(ii) a study of microfabric changes induced in the clay as a result of both pile installation and pile loading;

(iii) theoretical (numerical) modelling, employing an appropriate elasto-plastic constitutive law to represent the clay, and drawing on the results of the model tests and the microfabric studies for verification.

A brief description of these three approaches is now presented.

1.4.3 Model Pile Tests

The purpose of the tests was to represent the behaviour on drained axial loading,of a short element of a long rigid pile installed in clay. In the first series of tests, the piles were installed with a minimum of disturbance to either the stress field within, or the microfabric of, the clay surrounding the piles. The intention was not to model any particular type of pile or installation procedure employed in the field, but rather to reduce the problem of pile loading to its simplest terms. In the second, shorter, series of tests the behaviour of piles installed by jacking or by driving were considered.

With the exception of one test, the experimental work considered normally-consolidated clay. The two main reasons for the restriction were a concern for the possibility of progressive failure along the pile if over-consolidated clay were employed in the proposed apparatus, and also for ease of interpretation of the results. It was considered that by conducting a series of the idealised model tests on piles installed in clay normally consolidated to a range of initial stress ratios ($K = \sigma'_r/\sigma'_z$), some important information about the mechanism of load transfer between the pile and the clay might be obtained. It was also anticipated that the results from such a series of tests would be of value when assessing the validity of various theoretical procedures for analysing pile loading behaviour.

1.4.4 Microfabric Studies

After each of the above model tests, thin sections were prepared from the material at the pile-clay interface. The sequence of development, with pile loading, of microfabric changes within the clay was established, and the influence of the initial stress conditions was also considered.

Thin sections prepared from the clay around the jacked and driven piles were used to investigate the nature of the fabric disturbance caused by the installation of full-displacement piles.

1.4.5 Theoretical Analyses

The results from the first series of model tests clearly indicated that the behaviour of the soil surrounding piles cannot be considered elastic. Finite element analyses (employing an appropriate elasto-plastic constitutive law) of the model test conditions were performed and the predictions were compared with the experimental results. Encouraging agreement was obtained and the theoretical analyses were extended to consider the behaviour of displacement piles. The resulting predictions were compared with the available field data.

CHAPTER 2

LITERATURE REVIEW

2.1 INTRODUCTION

This chapter considers the literature relevant to the development of a generalised effective stress theory of pile design. Attention is largely restricted to the behaviour of displacement piles installed in normally, or lightly over-consolidated clays; conventional cast-in-situ bored piles in over-consolidated clays are not discussed. The review is organised into four main sections:

(i) results from carefully conducted field pile tests (the effects of pile installation, the subsequent consolidation, and pile loading are considered separately where possible);

(ii) results from carefully controlled model tests (usually at the laboratory scale);

(iii) the development of a generalised effective stress theory of pile design;

(iv) a brief summary of the literature relevant to micro-fabric investiations.

For details of currently adopted methods of pile design and of pile installation procedures, the reader is referred to a recent, comprehensive, review by St. John (1980).

Simultaneous measurements of the radial total stresses, shear stresses and pore-pressures acting on the face of a pile during installation, consolidation following installation, and during pile loading are of considerable importance to the development of a generalised theory of pile design. Unfortunately, however, records of such measurements are scarce, and it is evident from the literature that it has proved to be particularly difficult to measure the radial total stresses acting on a pile shaft.

The development of a generalised effective stress theory of pile design is traced from the very simple methods which were first proposed

(considering the effects of pile installation, consolidation and loading altogether),to the more recent approaches which aim to follow the stress history of the clay surrounding a pile. The latter employ relatively sophisticated work-hardening, elasto-plastic, constitutive laws to describe the clay behaviour; unfortunately the dearth of suitable field measurements has hampered the verification of the more recent developments.

2.2 FIELD PILE TESTS

2.2.1 The Effects of Installing Displacement Piles

2.2.1.1 Introduction

When displacement piles are installed, they must displace an equivalent volume of soil. At small pile penetrations a large proportion of the displaced material appears as surface heave (e.g. Cooke and Price, 1973), whereas at greater depths the soil appears to be displaced in a predominantly radial direction. The effect of the radial displacements in the soil is to increase the total stress level in the soil close to the pile, and to cause the generation of excess pore-water pressures; the latter result from both the increased total stress levels and the severe shear straining to which the soil is subjected. With time, the excess pore-pressures dissipate and both the local undrained shear strength of the clay and the effective stress levels increase. As a result of this consolidation, the available pile capacity increases with time; this phenomenon is also responsible for the 'set-up' observed during pile driving operations. Published measurements of the stresses and pore-pressures acting in the clay around displacement piles are considered below, although the reader is also referred to two recent literature reviews on this subject presented by Swann (1979) and by Chodorowski (1982).

Another very important effect of the installation of displacement piles is the fabric disturbance induced in the clay as a result of the large relative displacements between the pile and the clay. Although this phenomenon may have a considerable influence on pile capacities, it has received surprisingly little attention to date. The available field evidence is considered below.

2.2.1.2 Ground Movements during Pile Installation

The displacements of clay around isolated displacement piles have been investigated by several workers, e.g. Cummings et al (1950),

Zeevaert (1950), Fellenius (1972), Cooke and Price (1973), Massarsch (1976) and Cooke, Price and Tarr (1979).

The results presented by Cooke, Price and Tarr (1979) are the most comprehensive, and were obtained from tests employing piles (5 metres long, and 0.17 metres diameter) which were jacked into London Clay. The radial variations of the vertical components of deformation were established at different levels within the clay, as the piles were jacked and later loaded.

It was found that at small pile displacements the volume of clay displaced by the piles was almost entirely accommodated by vertical heave which was detected at distances of more than forty pile radii from the piles. At greater pile penetrations (> 20 pile diameters) the displacements around the piles became predominantly radial, although the incremental ratio of heave volume to embedded pile volume was still as much as 25% to 40%. Cooke et al. also noted that significant downward movements were initiated in the clay when the pile tip was about two pile diameter above the observation level, and that the clay within about one diameter from the shaft was considerably disturbed during the installation.

Several other workers have quoted heave measurements obtained during the installation of pile groups, e.g. Klohn (1961), Orrjie and Broms (1967), Hagerty and Peck (1971), Torstensson (1973), Fellenius and Samson (1976), and Blanchet, Tavernas and Garneau (1980).

Orrjie and Broms (1967), working with precast concrete piles in soft, sensitive, silty clay report volumes of vertically displaced soil equal to 40% of the total volume of the piles in a group. Hagerty and Peck (1971) measured the heave caused by driving a group of piles in a non-sensitive clay and report that 50% of the pile volume was obtained as heave of the ground surface within the pile group. Similar results are presented by Torstensson (1973) and by Fellenius and Samson (1976). Blanchet, Tavernas and Garneau (1980) report somewhat smaller heave (35%) in soft, sensitive clays.

From the work of Cooke et al (1979), it would appear that in order to obtain reliable measurements of the volumes of surface heave, it is necessary to record ground movements to distances in excess of forty pile diameter from the shaft. Unfortunately, the measurements quoted by most other workers seldom extend to such large distances from the piles in question.

The deformations within the clay immediately adjacent to piles are considered in section 2.2.3.

2.2.1.3 Excess Pore-Pressures Generated during the Installation of Displacement Piles

The pore-pressure acting on the face of a pile is the easiest component of stress to measure, and results of such measurements have been reported by many workers, e.g. Bjerrum and Johannessen (1961), Milligan et al. (1962), Lo and Stermac (1965), Orrjie and Broms (1967), Koizumi and Ito (1967), Airhart et al (1969), Roy (1979), Rigden et al (1979), Appendino et al (1979), Blanchet et al (1980), Grosch and Reese (1980), Roy et al (1981), and Roy et al (1982).

The measurements typically show that high excess pore pressures are generated very close to the pile, and that these pressures decrease almost logarithmically with radial distance from the pile; at a distance of about 15 diameters from the pile the excess pressures are usually negligible. Typical distributions are presented by Bjerrum and Johannessen (1961), Lo and Stermac (1965) and Koizumi and Ito (1967).

The excess pressures measured at the pile face generally lie in the range $5 < \Delta u/Cu < 6$ for full displacement piles, the higher values often being recorded adjacent to piles installed in sensitive clays. Pore pressures corresponding to $\frac{\Delta u}{Cu} = 4$ are typically encountered around low displacement piles. The excess pore pressures around full displacement piles may exceed the local total overburden stresses and it has been suggested by Massarsch and Broms (1977) that this results in local hydraulic fracturing of the soil close to the pile. However, this view does not seem to have gained general acceptance.

The pore-pressures generated at the tip of an advancing pile have frequently been observed to be significantly greater than those acting on the pile shaft some distance from the tip. The reason for the greater pore-pressures at the tip is probably that the total stresses are greater. Such measurements have been presented by Rigden et al (1979), Blanchet et al (1980), Roy (1980), and by Roy et al (1981).

Rigden et al considered piles driven into a glacial till, and showed that the maximum pore-pressure changes at the tips were about 6 Cu, whereas those generated along the shafts were only about 4 Cu. Roy et al

(1981) present the results of pore-pressure measurements obtained around piles driven into a soft, sensitive, clay. The excess pore-pressures at the pile tips were around 7 Cu, whereas the pressures decayed to a steady value of about 3.5 Cu at a distance along the piles of between five and ten pile diameters from the tip.

2.2.1.4 Total Stress Changes Induced by Pile Installation

It is unfortunate that there have been very few reliable simultaneous measurements of both the radial total stresses and the pore pressures at the faces of driven piles.

Koizumi and Ito (1967) measured both the pore-pressure and the radial total stress during the installation of a jacked pile into a sensitive clay. The results indicated that the radial effective stresses acting on the pile shaft during jacking were very close to zero.

Rigden, Pettit, St. John and Poskitt (1979) present measurements of both the total radial stresses and the pore-pressures acting on two steel piles driven into a glacial till. These results also showed that the radial effective stresses acting on the pile shafts during and immediately after installation were small in relation to excess pore-pressures.

Butterfield and Johnston (1973) present measurements of the local radial total stresses and shear stresses acting on the face of a continuously jacked pile in London Clay; pore pressures were unfortunately not measured. The jacking of the 100 mm diameter pile was slow (0.35 mm/sec), and it is argued by the authors that the excess pore-pressures along the shaft were probably small as a result. The radial total stress was seen to vary directly with the local undrained shear strength; the ratio of the radial total stress to the local initial undrained shear strength ranged between 8 at the pile tip, and about 5 along the shaft away from the tip. If, in fact, the excess pore-pressure along the shaft had largely dissipated during the jacking, then the equivalent angles of shaft friction are shown to have ranged between 10° ± 3°; (it may be noted that the residual angle of shearing resistance of London Clay is typically about 10°). During the jacking the equivalent α value ($\bar{\tau}/\bar{C}u$) in the lower half of the pile was between 0.7 and 0.9, whereas on extraction the value was only 0.6. There is some evidence that during the jacking the shear stresses acting on the pile close to the tip were up to four times greater than the average value acting on the pile shaft.

2.2.2 Consolidation Following Pile Installation

2.2.2.1 Introduction

The excess pore-pressures generated during pile installation dissipate with time, leaving the clay adjacent to the pile at a higher effective stress level and a lower water content. Further away from the pile, the migration of water causes a small increase in the water-content of the clay. Depending on the sensitivity of the clay, the final undrained shear strength of the clay adjacent to the pile may be higher than the initial in-situ value.

As the effective stresses acting on the pile face increase with time, so too does the shaft resistance of the pile; the variation of shaft capacity with time has been measured by several investigators who performed successive pile tests at various intervals after pile installation.

2.2.2.2 Field Observations

The decay with time of excess pore-pressures acting on displacement piles has been studied by many investigators, e.g. Seed and Reese (1955), Yang (1956), Lo and Stermac (1965), Orrjie and Broms (1967), Koizumi and Ito (1967), Fellenius and Samson (1976), Rigden et al (1979), Blanchet et al (1980) and Roy et al (1981).

Koizumi and Ito (1967) and Rigden et al (1979) also measured the corresponding variation of the radial total stresses on the pile. The results from both sets of workers suggest that after full consolidation the radial effective stresses acting on the piles were approximately equal to the effective overburden stresses.

Several workers have conducted pile loading tests at various intervals after installation. They include Seed and Reese (1955), Eide, Hutchinson and Landva (1961), Stermac, Selby and Devata (1969), McCammon and Golder (1970),Flaate (1971), Thorburn and Rigden (1980), and Bergdahl and Hult (1981). The results presented by Seed and Reese (1955) are discussed below.

Measurements of changes in the water-contents and undrained shear strengths of the clay beside displacement piles, as a function of time since installation, have been reported by fewer investigators, e.g. Seed and Reese (1955), Eide et al (1961), Orrjie and Broms (1967), Fellenius and Samson (1976) and Roy et al (1981). The water contents of the clay beside the piles were observed to decrease with time after

installation. The local undrained shear strengths of the clays close to the piles often decreased initially (particularly in sensitive soils) but increased with consolidation, and often the final value was in excess of the initial in-situ value. Seed and Reese (1955) present the most comprehensive set of measurements of the consolidation process, and the results are now briefly considered.

Seed and Reese (1955) performed a study in which closed-end steel piles (150 mm diameter) were driven into 'Bay Mud', an organic silty clay. One of the piles was instrumented such that the distribution of axial loads and pore-pressures could be measured during and after installation. The variation, with time, of the properties of the clay beside the non-instrumented piles was established by taking samples at different times after installation, as well as by performing a series of field vane tests. Pile loading tests were conducted at various intervals after driving.

The authors compared the gains in pile capacities with the decreasing excess pore pressures beside the piles, and with the gains in the local undrained shear strengths of the clay. Excellent agreement was found between the rate of dissipation of excess pore-pressures and the gain in undrained shear strength close to the piles, whereas the pile capacities increased at a somewhat slower rate. It is unfortunate that no measurements of the radial stresses acting on the pile were made, because an interpretation in terms of effective stresses might have been more illuminating.

The pile capacities were observed to increase by more than 5.4 times during the dissipation of the excess pore-pressures. The local undrained shear strengths of the clay beside the piles finished at values roughly 1.5 times the initial 'undisturbed' value, and about three times the initial remoulded strength. Loading tests performed during the consolidation showed the average shaft resistance per unit area was always less than the current local undrained shear strength. For instance, 33 days after installation, the average shaft resistance per unit area was about 12 KN/m^2 which compares with the current mean undrained shear strength of 18 KN/m^2. However, as the initial undrained shear strength of the clay was about 12 KN/m^2, the final α value was unity.

It has been observed by several investigators that the nature of the pile material may significantly affect both the rate of consolidation and the final strengths obtained, e.g. Lo and Stermac (1964), Orrjie and

and Broms (1967), and Stermac, Selby and Devata (1969). The general conclusion is that the clay around timber piles consolidates the fastest, and that around steel piles the slowest. Data compiled by Kraft, Focht and Amerasinghe (1981) show clearly that timber piles generally develop higher shaft adhesions than either precast concrete or steel piles. The differences in behaviour between the pile types is thought to be attributable to the porosities and permeabilities of the pile materials.

2.2.3 Fabric Disturbance Caused by the Installation of Driven Piles

As a pile tip is advanced in soil, the soil ahead of the tip is displaced both radially and vertically. Close to the line of the pile the soil is forced downwards, whereas at a short distance from the pile heave occurs (see Cooke, Price and Tarr (1979) for field measurements). This has also been demonstrated experimentally by Robinsky and Morrison (1964) in sands, and by Randolph, Steenfelt and Wroth (1979) in clays. As the pile is further advanced the soil beside the pile is severely distorted and eventually a principal displacement shear surface is formed parallel to the pile.

Cummings, Kerkhoff and Peck (1950), Krynine (1950), Zeevaert (1950) and Tomlinson (1970(a) and (b)) present the results of observations obtained by excavating around displacement piles to examine fabric disturbance. The authors have shown that close to the pile, originally horizontal layers have been forced to lie parallel to the pile shaft, whereas at a distance of about one pile radius from the shaft, the horizontal bedding is apparently undisturbed. Photographs of this phenomenon are presented by Cummings et al (1950) and by Tomlinson (1970(a) and (b)).

Several investigators have reported that failure around displacement piles in clays occurs on a well defined slip surface within the clay, at a small distance from the shaft. Thus failure appears to occur as a soil-soil rather than a soil-pile phenomenon. Koizumi and Ito (1967) discovered a failure surface at a distance of roughly 30 mm away from the face of a 300 mm diameter pile, and Grosch and Reese (1980) encountered a slip surface at a distance of 2.5 mm from a 25 mm diameter model pile. Tomlinson (1970(a) and (b))) has conducted the most thorough investigation of this phenomenon, and his work is briefly reviewed below. All of the above investigators reported that the clay adjacent to the piles (steel) was found to adhere strongly to the piles, even on extraction of

the piles.

Tomlinson examined the behaviour of displacement piles which were either driven or jacked into London Clay. Following the pile tests, the clay around the piles was excavated. It was found that for the piles in uniform London Clay a thin, almost continuous, layer of clay between one and six millimeters thick adhered to the pile shaft; this skin was seen to be comprised of numerous vertical laminations. Furthermore, it was evident in each case that the failure of the pile under load was associated with slip on slickenslided surfaces between the outer periphery of the adhering skin and the surrounding clay, and not at the pile-clay interface. Photographs of both the distorted clay away from the piles and the slickenslided surfaces of the adhering clay are presented. Electron-micrographs of the adherent clay were also obtained from around a jacked and a driven pile. These showed that the slickenslided shear surface around a jacked pile was somewhat smoother than that observed around a driven pile; very similar results have been obtained in the experimental study presented in this dissertation.

It should be remembered that these observations reported by Tomlinson were obtained from a plastic clay, and it is anticipated that the micro-fabric changes occurring around piles driven into low plasticity clays (such as glacial tills) might be rather different; this requires investigation.

2.2.4 Pile Loading Tests

2.2.4.1 Introduction

Large numbers of pile tests have been performed in order to establish the ultimate capacities of piles, and the results have usually been interpreted in terms of total stress analyses. The major factors influencing pile capacities have been reviewed by Meyerhof (1976), St. John (1980) and Kraft, Focht and Amerasinghe (1981). The purpose of the present review is primarily to consider those measurements obtained during pile tests which can be used to evaluate quantities relevant to effective stress methods of pile design.

In order to calculate the peak shaft resistance of a pile by means of an effective stress approach, it is necessary to be able to predict both the radial effective stresses and the angles of shaft friction acting at peak conditions. As described earlier, the radial

effective stresses in the soil may be significantly altered by the installation of a pile; the stresses may be expected to change further during the loading of the pile. If the pile installation process were to cause no disturbance to the soil micro-fabric then the peak angle of shaft friction might be expected to approach the intact angle of shearing resistance for a material (this has in fact been observed in some of the model tests described in this dissertation). However, as has been seen in Section 2.2.3, the installation of displacement piles may cause considerable fabric disturbance, possibly involving the formation of slickenslided shear surfaces which would have the effect of reducing the peak angle of shaft friction. In order to establish the radial effective stress and the angle of shaft friction mobilised during a pile test, it is necessary to measure the radial total stresses, the pore water pressures and the shear stresses acting on the pile. The results of published field measurements are considered below; it is unfortunate that in only one paper are simultaneous measurements of the three stresses presented.

2.2.4.2 Stress Measurements during Pile Loading

Puech and Jezequel (1980) present measurements of changes in the radial total stress and pore-pressure acting on the shaft of a driven steel pile. The quoted measurements were obtained during tension loading of the pile, from transducers installed at a height of roughly seven pile diameters above the tip. The results show that both the radial total stress and the pore pressure increased during loading in such a manner that the radial effective stress decreased by about 23% of the effective overburden stress (unfortunately the value of the radial effective stress acting on the pile prior to loading is not quoted).

Roy, Blanchet, Tavernas and La Rochelle (1981) present measurements of pore-pressure changes determined during the loading of a steel pile driven into soft, sensitive, Champlain Clay. The pore-pressures were recorded at the face of the pile and at a variety of distances from the shaft during a loading test. The peak excess pore-pressures measured at the pile face were up to 1.5 times the initial undrained shear strength, whereas at a distance of two pile radii from the shaft no effect was recorded. This suggests that the generation of excess pore-pressures on loading the pile is much more localised than that caused by pile driving, when pressure increases were measured at distances of up to 20 radii from the shaft.

Clark and Meyerhof (1972,a) measured the total stress and pore-pressure changes during the loading of a 75 mm diameter pipe pile driven into a drum of clay. The stresses were measured at a distance of about one pile radius from the shaft; excess pore pressures of between 0.2 Cu and 0.6 Cu were generated, and the radial effective stress decreased by between 0.1 Cu and 0.3 Cu.

Measurements of pore-pressure changes during the loading of displacement piles have also been reported by Massarsch, Broms and Sundquist(1975), by Airhart, Coyle, Hirsch and Buchanan (1969) and by Lo and Stermac (1964). Table 2.1 summarises the available measurements of pore-pressure changes.

Butterfield and Johnston (1973 and 1980) present measurements of the radial total stresses and the shear stresses acting on a continuously penetrating pile shaft in London Clay. If, as the authors argue, the excess pore-pressures along the shaft had largely dissipated during the jacking process then the angle of shaft friction was $10° \pm 3°$, which is of the same order as typical Ring shear measurements of the residual angle of friction in London Clay. It may be recalled that Tomlinson (1970,b) observed slickensided shear surfaces adjacent to displacement piles installed in London Clay.

2.2.4.3 Post-peak Behaviour of Loaded Piles

On first time loading, the load-displacement behaviour of most piles exhibits a brittle post-peak response, as measured by constant rate of penetration tests. For examples of the behaviour of driven piles reference may be made to the following papers; Meyerhof and Murdock (1953), Coyle and Reese (1966), Tomlinson (1970,b), McCammon and Golder (1970), Heerema (1979), Thorburn and Rigden (1980), and Kraft, Ray and Kagawa (1981). For jacked piles see Tomlinson (1970,b), and for bored piles in over-consolidated clays see Burland, Butler and Dunican (1966), Reese, Hudson and Vijayergiya (1969), O'Neill and Reese (1972) and O'Riordan (1982). After post-peak displacements of the order of a few millimeters the shaft resistance reaches a residual value which is not affected by unloading and re-loading the pile (see Tomlinson (1970,b) and O'Riordan (1982)).

The post-peak brittleness may be affected by stress-path softening, but is considered to be largely the result of the development of shear surfaces in the clay beside the piles along which the clay particles exhibit a high degree of preferred orientation. A very

interesting comparison between the behaviours of driven and jacked piles in London Clay is presented by Tomlinson (1970,b); the results are discussed at some length in Chapter 6 of this dissertation.

An important consequence of the brittle behaviour of piles is that long, and therefore relatively compressible, piles are subject to progressive failure which has the effect of reducing the available pile capacities. The effect of compressibility of piles on their shaft capacities is clearly illustrated by Kraft, Focht and Amerasinghe (1981).

2.3 LABORATORY SCALE MODEL PILE TESTS

2.3.1 Introduction

The majority of the reported pile tests have been performed to duplicate, on a small scale, the behaviour of driven and jacked piles in the field. In general the results were interpreted in terms of total stress methods, rather than effective stress methods.

Until the late 1970's little attempt was made to measure the pore-pressures, radial and shear stresses acting on the faces of the model piles. More recently, some success has been obtained with pore-pressure measurements, but the radial stresses have proved to be very difficult to measure reliably.

Investigations into soil deformations during pile installation have been performed but, to date, the nature of the micro-fabric changes caused by pile installation and loading does not appear to have been studied experimentally. The results of studies performed to examine the behaviour of soils when sheared against rigid interfaces are considered below.

2.3.2 Model Pile Tests

Coyle and Reese (1966) performed laboratory tests on model piles in a plastic clay (PI = 47%). Each steel pile (of diameter 12.5 mm or 9.5 mm) was placed in a triaxial cell, and the clay was consolidated around the pile under conditions of zero axial strain. After consolidation the clay sample with the included pile was transferred to another triaxial cell, in which isotropic stresses were applied to the clay. The consolidation probably resulted in rigid inclusion effects around the model piles, and the application of isotropic stresses to the sample probably resulted in the development of shear stresses at the pile-soil interface. The pile was then loaded at a constant rate of displacement resulting in 'failure'

in less than two minutes. The pile loadings were probably intermediate in character between being drained and undrained.

The post-peak behaviour was found to be brittle, and residual conditions were achieved after displacements of about 4 mm. The displacements to peak were found to be somewhat less for smooth than for rough piles, and the smooth piles exhibited the most rapid decrease in strength with the initial post-peak displacements. At the higher stress levels employed ($\sigma_n \sim 300$ kN/m^2) the peak capacities of both rough and smooth piles were similar, and α values close to unity were obtained. No measurements were made of the stresses acting on the piles and an interpretation of the tests in terms of effective stresses is therefore not possible.

Clark and Meyerhof (1972, 1973) describe the results of laboratory and field tests to examine the behaviour of driven piles. The laboratory tests consisted of a series of model pile tests, and an investigation of interface shearing behaviour.

The interface tests involved shearing soil samples against flat steel surfaces of different roughnesses, in a modified direct shear box. A facility for measuring pore pressures at the interfaces was provided. The tests showed that both the peak and the residual angles of interface friction depend on the roughness of the interface, and that for the rougher interfaces the peak angle of friction approaches the intact value such as might be established in a conventional shear-box test. Residual conditions were typically achieved after displacements of some 8 mm.

The model pile tests involved driving piles (76 mm diameter x 762 mm long) into a large bed of compacted insensitive clay (559 mm diameter x 762 mm deep). Total stress cells and pore-pressure transducers were installed in the clay bed, about one pile diameter away from the proposed pile centre-line. Linear displacement transducers were also installed to measure the radial soil displacements caused by pile installation; these measurements were later compared with predictions based on elasto-plastic cavity expansion theory, and encouraging agreement was obtained. Changes in pore-pressures and radial total stresses close to the pile were recorded during the installation and the subsequent consolidation, and the variation of the local undrained shear strength was determined by means of vane tests. The undrained shear strength of the clay adjacent to the pile increased by 50% as a result of the consolidation following pile driving; this figure accords well with

predictions based on cavity expansion theory (see Randolph, Carter and Wroth, 1979). After consolidation, the radial effective stress acting at a distance of one pile radius from the pile shaft was found to average 1.6 times the current local undrained shear strength (or 2.5 times the initial undrained shear strength).

In the course of a pile loading test conducted after allowing full dissipation of the driving-induced pore-pressures, the radial effective stress at a distance of one pile radius from the shaft was observed to decrease by about 13%, and excess pore-pressures of about 50% of the initial undrained shear strength were recorded. A significant conclusion drawn by Clark and Meyerhof from this work was that when designing piles by effective stress methods, the peak angle of shaft friction should be taken to be the residual value established by interface tests.

Bea and Doyle (1975) conducted laboratory tests to investigate the influences of normal stress, interface roughness, soil type and rate of loading on the strengths of pile-soil interfaces. Three types of tests were performed; model pile tests, direct shear tests against steel interfaces, and conventional direct shear tests involving soil-soil failure.

The model pile tests were performed using reconsistituted clay which was one-dimensionally consolidated to an axial stress of about 200 kN/m^2. The total stresses were removed and the model pile was introduced into the clay sample by coring a hole through the sample with a sharp, thin-walled cutter and then pushing the pile into the hole. The sample with the included pile was then placed in a triaxial cell and further consolidated under isotropic stresses. It seems probable that the relative movement between the cutter, and later the model pile, against the clay will have caused some local fabric disturbance. The radial stresses acting on the pile after the application of the isotropic stresses and the sample were probably not equal to the cell pressure, because of rigid inclusion effects; the radial stresses acting on the pile were not measured.

The most significant conclusions from this work were that:

(i) the apparent angle of peak shaft friction is significantly less than the peak angle of shearing resistance measured in a soil-soil direct shear test;

(ii) the apparent angle of peak shaft friction decreases with increasing soil plasticity;

(iii) the apparent angle of peak shaft friction depends on the pile roughness, being smaller the smoother the pile;

(iv) the pile capacity is not significantly affected by the rate of loading;

(v) scale effects are insignificant.

These tests investigated a wide range of possible influences on pile capacity. It is unfortunate that the radial stresses acting on the pile were not measured, and that more information about the drained residual strength of steel-clay interfaces was not presented, as this might have aided interpretation of the pile test results.

Holmquist and Matlock (1976) conducted a series of tests on 25 mm diameter model piles which where installed, generally by driving, into a drum of clay (770 mm diameter by 770 mm high). Radial stress was applied to the sample by means of water-filled bags around the circumference. No mention is made of provisions for drainage during the consolidation of the samples. However, with the quoted values of the coefficient of consolidation, even if both top and bottom drainage had been provided, 95% consolidation would have taken about one year which is considerably longer than the periods quoted for 'resting'. The undrained shear strengths measured by vane testing are apparently consistent with an effective confining stress of 68 kN/m^2, rather than the 204 kN/m^2 total stress applied to the sample, confirming that the samples were under-consolidated at the start of pile testing. No measurements of pore-pressures are recorded.

The load-displacement curves obtained on loading the driven piles indicated α values of around unity and exhibited brittle post-peak behaviour. Cyclic loading tests indicated a progressive reduction in strength towards a residual value. In the absence of measurements of either pore-pressures or radial stresses in the clay near the piles it is not possible to interpret the test results in terms of effective stresses.

Bannerjee (1979) discusses the experimental work performed by Fathallah and himself, concerning the stress changes occurring in the

clay around a jacked pile. An instrumented pile (63.5 mm diameter) was jacked into a tank of kaolin, and the changes in the radial total stresses and pore-pressures at the pile surface were measured. Excess pore-pressures of about 4 Cu were recorded at the pile face; as observed by Steenfelt et al (1981) these pore-pressures dissipated more rapidly than predicted. After the tests, the undrained shear strength of the clay close to the piles had increased by about 50%.

Aurora, Peterson and O'Neill (1980, 1981) present the results of laboratory tests in which very slender piles were driven into compacted clays, and then loaded. The piles (25.4 mm diameter by 2667 mm long) were instrumented to measured axial stress distributions along the piles. The pile loading tests were load-controlled so that the post-peak behaviour could not reliably be observed. No axial total confining stresses were applied to the clay samples, and neither pore pressures nor radial stresses were measured. Yet again, it is not possible to interpret the quoted results in terms of effective stresses as too few parameters were measured. The most significant conclusions presented by the authors were that

(i) pile 'failure' occurred by clay-clay slip, rather than clay-pile slip;

(ii) the observed average α values were less than unity;

(iii) the α values corresponding to the upper one-third of the pile decreased with increasing penetration, whereas they remained essentially constant in the lower two-thirds. The explanation presented for this observation is that of pile-whip in the upper third;

(iv) the pile capacities in tension were equal to those in compression;

(v) the α values tended to increase with decreasing clay P.I.

Randolph, Steenfelt and Wroth (1979) present the results of simple model tests designed to observe the soil deformation patterns around open- and closed-ended piles during jacking. The main aim of the tests was to examine the validity of the assumptions employed when modelling the installation of a displacement pile as the expansion of a cylindrical cavity. The studies were performed using a cylindrical

sample of clay which was cut down its longitudinal axis to provide semi-circular specimens. The flat vertical face of each specimen was marked with grid lines and placed against a lubricated perspex sheet. A semi-circular pile was rapidly jacked into the clay, flush with the perspex plate. Photographic records of the process enabled particle trajectories to be determined.

The results show that as the pile tip approaches the level of an arbitrary horizontal plane, the clay particles in the plane appear to move along straight lines radiating from the centre of the pile (similar to spherical cavity expansion). As the pile tip passes the level of the plane, significant additional horizontal movement occurs. This latter phase is analogous to the expansion of a cylindrical cavity. Overall, the results provide a broad corroboration of the principle of modelling pile installation as the expansion of a cylindrical cavity. However, the technique of testing employed did not enable the behaviour of the clay very close to the pile to be observed.

Steenfelt, Randolph and Wroth (1981) present the results of model pile tests performed to examine the behaviour of the clay around displacement piles during installation, consolidation and pile loading. The results are compared with predictions based on cavity expansion theory, using Modified Cam Clay as the constitutive law.

Instrumented model piles (19 mm diameter) were jacked into large cylindrical samples of Speswhite kaolin (250 mm diameter by 600 mm long). The vertical and radial stresses could be varied independently. During the pile installation and loading pore-pressures acting on the face of the pile and within the clay mass were measured, together with the radial stresses acting on the pile. Unfortunately the latter results were unreliable.

During pile installation (by jacking) X-ray photographs of lead-shot embedded within the samples were taken. The results again broadly confirmed that in the bulk of the clay the pile installation may be modelled as the expansion of a cylindrical cavity. However, as in the case ofthe tests performed against the perspex sheet, no information was provided about the clay deformations very close to the pile, especially near the pile tip.

Pore-pressures measured in the bulk of the clay were in reasonable agreement with theoretical predictions based on cavity expansion theory.

However, at the pile interface the pore-pressures were lower than those at a small distance from the shaft which suggests that close to the pile the clay behaviour is more complex than that assumed when modelling the installation as the expansion of a cylindrical cavity. This may have important implications when considering pile capacities because the stresses close to the pile are the most important ones to predict correctly. Consolidation times were in broad agreement with theoretical predictions.

On loading the piles, following full consolidation, α values of between 0.9 and unity were obtained, despite the local increases in the undrained shear strength that may be presumed to have resulted from the consolidation. If, in accordance with predictions based on cavity expansion theory and measurements presented by Clark and Meyerhof (1972) and by Bannerjee (1979), the consolidation increased the local undrained shear strength by about 50%, then this implies that only 60% of the 'available' undrained shear strength of the clay was mobilised parallel to the shaft. It is considered that an explanation for this result may lie in the influence of shear surfaces formed parallel to the piles during installation; this is discussed in Chapters 6 and 9.

2.3.3 Interface Behaviour

Meyerhof and Murdock (1953) sheared London Clay against wet and dry stones in a modified direct shear box. They found that the adhesion at the interface was dependent upon the normal stress and at high stresses (probably approaching the pre-consolidation stress) the adhesion was similar to the initial undrained shear strength of the clay. It was found that the post-peak behaviour was brittle, with the residual strengths being roughly half the peak values.

Potyondy (1961) presents the results of a series of interface tests conducted between a variety of soils and construction materials. Unfortunately, however, the testing procedures are not fully documented, and the results suggest that a mixture of drained and undrained behaviour was observed.

Clark and Meyerhof (1972) conducted a number of interface tests between clays and flat steel plates. Different steel roughnesses were investigated, and the effects of rate of loading were studied too. Pore-pressures were measured at the interfaces during undrained loadings. The most important results were that the peak and residual angles of effective

interface friction were affected by the surface roughness, and that residual conditions were typically achieved following displacements of about 8 mm.

Littleton (1976) also describes interface tests conducted in a modified direct shear box. Two clays, Kaolin and Illitic clay, were employed and they were each consolidated from slurry against a steel interface. Drained and nominally undrained tests were performed, and the results showed that the peak mobilised angles of effective interface friction were slightly less than the angles of shearing resistance measured in triaxial compression tests. Residual angles of friction of roughly half the peak values were reached following displacements of less than 8mm.

Kulhawy and Petersen (1979) report the results of an extensive testing programme to examine the strength and deformation behaviour of sand-concrete interfaces. Several interface roughnesses and sand size mixtures were examined. The results showed that in any given conditions the apparent roughness of the interface depends on the particle size distribution of the sand and that the latter may be used to provide a convenient way of quantifying the roughness of any given interface. For rough interfaces the angle of interface friction (δ') may be greater than the bulk angle of shearing resistance ϕ', whereas for smooth interfaces δ' may be less than ϕ'. Little post-peak brittleness was observed and the residual strength was generally greater than 85% of the peak value.

The behaviour of soil when sheared against a rigid interface is of considerable relevance to the behaviour of piles, but has received surprisingly little attention. In particular, the effect of the rate of shearing on the angle of shearing resistance that can be mobilised does not appear to have been considered in any detail.

2.4 DEVELOPMENT OF EFFECTIVE STRESS METHODS OF PILE DESIGN

2.4.1 Introduction

It has been appreciated for many years that the behaviour of soils is dependent on the effective stress state imposed on them. With this in view, many workers have attempted to relate pile behaviour to the effective stresses existing in the soil beside the pile, rather than to rely on the more empirical total stress methods.

The development of a generalised effective stress theory of pile behaviour has recently received considerable stimulus from the oil industry. Many of the large, heavy, offshore structures which are subject to severe loading conditions are supported by driven piles. The load-deformation response of the piles affects the dynamic response of the structure as a whole, and hence the stresses induced in the structural members. Thus, the fatigue life of the structure is a function of the pile behaviour. The design of such piles currently requires considerable extrapolation of existing total stress design methods from land-based experience and there is felt to be a need to develop a generalised theory of pile behaviour, starting from first principles.

Initially effective stress design methods related pile capacities directly to the initial in-situ stress state in the soil. No explicit account was taken of the stress changes occurring in the soil during the installation and loading history of the pile, although this was appreciated to involve a major simplification. More recently, attempts have been made to model the various stages involved in the history of piles, the stress state predicted at the end of one stage being employed as the initial conditions for the next stage.

2.4.2 Initial Development of an Effective Stress Theory of Pile Design

Effective stress methods were initially proposed by Zeevaert (1960) (in relation to negative skin friction), and by Eide, Hutchinson and Landva (1961) for evaluating the long-term shaft resistance in clays. Eide et al did not use the method, however, because they did not feel confident about assigning specific values to either the angle of shaft friction or to the coefficient of earth pressure around driven piles. Johannessen and Bjerrum (1965) used the method in relation to negative skin friction.

Chandler (1968) analysed the results of a large number of tests on bored piles in over-consolidated London Clay, and concluded that a simple effective stress approach could give good agreement with the field measurements. Chandler assumed that the angle of shaft friction was equal to the effective angle of shearing resistance determined by means of triaxial compression testing, and that the normal effective stress acting on the pile at peak load was equal to the initial in-situ horizontal effective stress.

Burland (1973) argued that there was little fundamental justification for relating shaft adhesion to undrained shear strength because of the severe local disturbance accompanying pile installation, and because local drainage of the soil adjacent to a loaded pile was expected to be very rapid. Burland examined the records of a large number of tests on piles driven into soft clays and showed that a simple effective stress method (characterised by the equation $\tau = \beta.\sigma'_{v,o}$) provides a reasonable lower bound to the available shaft capacities. The results exhibited less scatter than those obtained by total stress methods, particularly where sensitive clays were considered. Burland applied this approach to bored piles in stiff, over-consolidated clay, and like Chandler, found that the assumption of Ko conditions led to a slight over-estimation of pile capacities. This approach was also applied to driven piles in stiff, over-consolidated clays and it was found that an assumption of $\beta = 0.8$ provided a reasonable lower-bound to the observed pile capacities.

This simple model was not intended to replace the traditional empirical methods of estimating shaft capacities, but was thought to be useful for preliminary design purposes and to form the starting point for a more rigorous approach. Meyerhof (1976) extended the simple approach by introducing an expression for the coefficient of earth pressure which took explicit account of the initial over-consolidation ratio of the soil.

Parry and Swain (1977, a and b) and Parry (1980) attempted to consider in more detail the stress conditions existing around piles in normally- and over-consolidated clays. They showed that first failure of the clay may occur on planes inclined to the pile axis, and that the peak mobilised angle of friction will, in general, be less than the angle of shearing resistance, ϕ', for the clay. Their analyses also indicated that if at peak pile load the ratio of the horizontal to the vertical stresses acting in the soil adjacent to the pile tend towards the passive value, then the peak mobilised angle of shaft friction will tend towards zero. Unfortunately, no experimental evidence was produced to substantiate the various assumptions made about the variation of the stress ratio (σ'_r/σ'_z) during pile loading, and so the suggestion that the peak angle of shaft friction will be strongly dependent on the initial stress ratio is not proven. Burland (1979), in written discussion of the first two papers, noted that failure conditions around a pile are likely to be confined to a very narrow zone close to the pile, and that within this zone little constraint will be imposed on the possible variations of σ'_z.

In addition to the aforementioned relatively simple effective stress methods of pile design, simple hybrid methods (combinations of total and effective stress approaches) have also been proposed. Vijayvergiya and Focht (1972) proposed an essentially empirical, but widely used, method for evaluating the capacities of long,and therefore relatively compressible, piles.

2.4.3 Development of a Generalised Effective Stress Theory of Pile Design

In order to develop a generalised effective stress theory of pile design it is necessary to attempt to model the stress history of the soil surrounding the pile. This may conveniently be considered in four main stages:

(i) soil deposition and geological history before pile installation;

(ii) pile installation - a short-term, undrained analysis;

(iii) re-consolidation as the excess pore pressures generated by pile installation dissipate;

(iv) pile loading.

Butterfield and Bannerjee (1970) were the first to model the installation of driven piles as the undrained plane-strain expansion of a cylindrical cavity in the soil, from zero radius to a finite radius. Plane-strain conditions (i.e. no axial total strain) were selected to represent the behaviour of the soil at the centre of a long pile, away from the influences of both the tip and the head of the pile. The soil was modelled as an elastic-plastic material, obeying a Von-Mises' yield criterion, and an analytical solution for the total stresses acting in the soil was obtained. Excess pore-pressures were evaluated by adopting Henkel's (1960) generalisation of the Skempton (1954) pore pressure equation. The analyses predicted that excess pore pressures of between 4.0 and 6.5 times the initial undrained shear strength could be generated at the pile-soil interface, and that these pressures decrease with the logarithm of radius from the interface. Such results are in sensible agreement with the field observations presented by Lo and Stermac (1965) and Koizumi and Ito (1967). At the pile face no immediate change in the radial effective stress was predicted. The dissipation of the excess pore pressures was again modelled as a plane strain problem, but no attempt was made to analyse the loading of the pile.

Kirby and Wroth (1977) and Esrig, Kirby and Bea (1977) published comparison papers in which the installation of a displacement pile was analysed. The concepts of critical state soil mechanics (see Schofield and Wroth, 1968) were employed, and it was assumed that the soil adjacent to the pile would be brought to the critical state by the pile installation. The mean effective stress in soil close to the pile was estimated from a knowledge of the initial conditions within the soil by using the ratio ($P'_{N.C}/P'_{C.S}$) determined from triaxial compression tests. The pore pressures predicted were similar to those derived by Butterfield and Bannerjee (1970). No attempt was made to model in detail the consolidation following the expansion of the cylindrical cavity. Kirby and Wroth (1977) assumed that on consolidation, the effective stress path of the soil adjacent and the pile would follow the critical state line. As a direct consequence of this assumption it was predicted that almost no pore-pressure generation would occur during pile loading (as the soil was taken to be at the critical state no pore pressures were expected to be generated by the imposed shear stresses). The final expression derived for the peak shaft resistance was therefore

$$\tau = \frac{MP'_f}{2} \cos \phi'_{s.s.}$$

where

- M is the slope of the critical state line in q-p' space
- P_f is the value of the mean effective stress, at the current water content, on the critical state line
- $\phi'_{s.s}$ is the angle of shearing resistance at the pile-soil interface

This effective stress model of pile behaviour attempted to consider the main events in the history of the soil immediately adjacent to a displacement pile. Comparison between predicted and actual pile capacities showed, however, that the new model tended to yield unconservative predictions, and with generally more scatter than existing empirical methods. Nevertheless the results were encouraging because it was evident that the model was amenable to several refinements.

Desai (1977) considered the consolidation of the soil around a displacement pile by means of a finite element analysis. The pore pressure distribution around the pile immediately after installation was taken from a cavity expansion analysis similar to that presented by

Butterfield and Bannerjee (1970). The consolidation analysis was a coupled solution, assuming linear elastic soil behaviour. As no plastic behaviour was accounted for during the consolidation, the predicted stresses must be regarded as being very approximate. On the other hand the predicted rates of consolidation may be more realistic.

Miller, Murff and Kraft (1978) discussed the results of a numerical study which was performed to investigate the radial, plane-strain consolidation of soil around a pile. Modified Cam Clay (Roscoe and Burland, 1968) was selected as the soil constitutive law. The aim of the study was to examine the stress path followed by the soil immediately adjacent to the pile during the consolidation, and in particular to determine whether or not the stress path follows the critical state line. In one consolidation analysis the initial stress and pore pressure distributions were taken from the results of a cavity expansion analysis using Modified Cam Clay (details of the expansion analysis were not provided), whereas in other analyses hypothetical distributions were assumed. The results showed that the stress paths do not follow the critical state line; indeed if the initial excess pore pressures are large enough then the soil adjacent to the pile was shown to consolidate under radial K_o conditions such that

$$\sigma'_r > (\sigma'_\theta = \sigma'_z = K_o \sigma'_r)$$

Randolph and Wroth (1979) present an analytical solution for the consolidation around a long displacement pile. The initial stress and pore water pressure distributions were taken from a cavity expansion analysis assuming the soil to behave in an elastic-perfectly plastic manner. During consolidation the soil was assumed everywhere to be unloading in shear and to behave in a linear-elastic manner; the flow of water was assumed to be radial. The analysis predicted that the radial total stress acting on the soil close to the pile remains constant during consolidation and therefore that the full limiting pressure required to expand the cylindrical cavity will finally act as an effective stress against the pile. However, examination of behaviour of the soil immediately adjacent to the pile suggests that in practice the soil may locally undergo plastic loading rather than elastic unloading (also see Miller et al (1978)) and so the stress changes predicted on the basis of an elastic analysis are likely to be significantly in error. On the other hand the rate of consolidation (particularly at longer times) is dominated by the behaviour

of the soil at some distance from the pile and as this will probably behave almost elastically, the predicted rates are expected to be fairly reliable. This has since been experimentally verified by Steenfelt, Randolph and Wroth (1981), and sensible agreement with field observations of the gain of pile capacity with time after installation have been obtained on the basis of elastic consolidation analyses.

Carter, Randolph and Wroth (1979) modelled the installation of full-displacement piles in both elastic-plastic and a work-hardening elasto-plastic soil. A finite deformation formulation of the equilibrium equation was employed, and the analyses were performed numerically using a finite element computer code. The validity of the program was established by comparing the results obtained using the elastic-plastic material with analytical results presented by Hill (1950) and by Gibson and Anderson (1961) for the cavity expansion phase.

The numerical routines used were incapable of considering the expansion of a cavity from zero radius because infinite strains would be implied. However, it was found that the ultimate limit pressure is rapidly approached if a cavity with a finite initial radius (say a_o) is expanded to double the radius ($2a_o$). The installation of a pile of radius r_o was modelled by equating the volumes of the soil displaced (i.e. $r_o^2 = (2a_o)^2 - a_o^2$, or $r_o = a_o\sqrt{3}$). The solution only exists for radii in excess of $2a_o$, and so the stresses in the soil close to the pile (i.e. between $a_o\sqrt{3}$ and $2a_o$) may only be obtained by extrapolation. This is quite an important point because the stresses acting at the pile face are generally the primary quantities required. The elasto-plastic analyses showed that the stress conditions close to the pile are significantly different from those predicted by elastic analyses. In particular, the radial total stress was found to decrease rather than to stay constant.

Randolph, Carter and Wroth (1979) present the results of a parametric study to consider the effects of past consolidation history and soil-sensitivity on the stress changes caused by the installation of full displacement piles. Several significant conclusions were reached:

(i) the stresses adjacent to the pile, when normalised by the initial value of the undrained shear strength, are almost independent of the initial OCR;

(ii) the final undrained shear strength close to the pile, expressed as a proportion of the initial value,

varies between 1.3 and 2.0 depending primarily on ϕ', but is largely independent of the initial OCR;

(iii) the final consolidation stress state close to the pile is one in which the radial stress is the major principal stress, and the minor and intermediate principal stresses are equal (and given by $\sigma'_\theta = \sigma'_z = K_o \sigma'_r$). This result is similar to that obtained by Miller et al (1978).

It is interesting to note that these cavity expansion/ consolidation analyses all predict that on loading the pile, the soil is most likely to fail at the pile-soil interface. In practice shear surfaces are often observed at a small distance from the faces of impermeable piles (e.g. Tomlinson (1970,b)).

Wroth, Carter and Randolph (1980) present a similar parametric study, and suggest some practical guidelines for the design of piles in sensitive clays. They note that on loading a displacement pile the radial effective stress adjacent to the pile will probably decrease, which implies that the value predicted as a result of the consolidation analysis should not be used directly when estimating pile capacities.

Randolph and Carter (1979) considered the effect of pile permeability on the consolidation process following driving and concluded that the rate of consolidation, and hence the rate of gain of pile capacity, would be greater around permeable piles than impermeable piles, and that the final capacities of permeable piles are likely to be greater too. These predictions are supported by field data (e.g. Stermac et al, 1969).

Carter and Randolph (1980) examined, numerically, the performance of closed-ended and open-ended piles on driving. They concluded that low displacement piles (which were assumed not to plug during driving) cause far less widespread disturbance to the stresses in the soil, and as a result the final radial effective stresses and the undrained shear strengths of the soil adjacent to low displacement piles are lower than those around similarly installed full displacement piles. Thus partial displacement piles may be expected to lead to somewhat lower long-term capacities than full displacement piles, but the final capacity

is achieved roughly an order of magnitude faster by the partial displacement piles. This would seem to represent a significant potential advantage of open-ended piles, especially where the piles are driven in groups.

Kirby and Esrig(1980) present some results from True Triaxial tests conducted by D.M. Wood on normally-consolidated Boston Blue Clay. The tests were intended to model the same strain path as is followed by soil during cavity expansion. The resulting stress paths were similar to those obtained during undrained triaxial compression testing following isotropic consolidation. Undrained triaxial tests performed after anisotropic consolidation resulted in very different, brittle, stress paths (also see Ladd (1965), and Gens (1982)). Wood (1981), in a discussion of the paper by Randolph, Carter and Wroth (1979), suggested that the constitutive laws to employ in numerical modelling of the installation of displacement piles would best be selected on the basis of results from strain path testing.

Bannerjee and Fathallah (1979) considered the incremental penetration of a pile into an elasto-plastic half space. They predicted stress changes occurring in the soil close to the pile shaft are very similar to those obtained by means of cavity expansion analyses.

The stress changes occurring in the soil around loaded piles have been considered theoretically by several investigators, using finite element methods, e.g. Lopes (1979), Kirby and Esrig (1980) and Baguelin and Frank (1980). Unfortunately, however, they generally considered the soil to be isotropic-elastic and so in the absence of coupling between the shear and volumetric strains, the analyses predicted no significant changes in either the mean effective stress or the radial effective stress during pile loading. In this dissertation analyses of pile loading, assuming the soil to be a work-hardening elasto-plastic material,are presented.

Randolph and Wroth (1981) discussed the application of constant volume simple shear test results to the prediction of pile capacities. In contrast to the elastic analyses above, the application of simple shear test results seems to imply very considerable changes in the radial effective stresses acting on piles during loading. A discussion of applicability of simple shear test data to pile design is considered at some length in Chapter 9.

2.5 MICROFABRIC STUDIES

2.5.1 Introduction

Investigations into the structure of clays may be performed at a wide range of magnifications, varying from the macroscopic scale at which major joints and fissures might be studied, to the sub-microscopic scale at which individual clay particles may be resolved (employing an electron microscope). The work discussed in this dissertation relates to the intermediate, microscopic, scale which can be studied with the aid of an optical microscope with magnifications of between x 10 and x 300. Mitchell (1956) was one of the first people to develop a simple technique for the preparation of thin-sections of clay (similar to petrological thin sections) without causing significant fabric disturbance; samples of clay could be examined under transmitted plane-polarized light. This technique was later employed by Skempton (1964) to examine shear surfaces in natural clays, and by Tchalenko (1967) to examine microfabric changes occurring during direct shear box tests.

2.5.2 Preparation of Thin Sections

The essential requirement of the technique is that it does not significantly alter the original fabric of the clay, or distort the optical properties of the clay. The samples are typically prepared by impregnating them with either a wax or a resin so that eventually the specimen can be cut and polished by techniques similar to those employed in petrology. Tchalenko (1967) reviewed the advantages of Polyethylene glycol (commonly known as Carbowax 6000) over other possible impregnating materials, and also considered alternative techniques such as freeze drying. He concluded that Carbowax was the only available impregnating agent which was suitable for quantitative studies using polarized light, and also convenient for grinding. The technique which Tchalenko adopted in his research is described in some detail in Tchalenko (1967). The theory behind quantitative studies of microfabric is described in Morgenstern and Tchalenko (1967 (a) and (b)).

2.5.3 Effects of Impregnating Clay Samples

It has been observed by Quigley and Thompson (1966) and by Tchalenko (1967) that the impregnation of clay samples by Carbowax typically results in a linear shrinkage of around 8%. Tchalenko also found that

samples which exhibit a high degree of bulk preferred orientation may also be subject to an additional internal shrinkage of between 0.5% and 1%, which manifests itself in cracks which form parallel to the planes of greatest preferred particle orientation. The fact that these cracks are not observed near, or at the outer faces of the samples, and that Carbowax is generally not present in the cracks,suggests that the cracks form during the cooling phase. Structural features (such as strain and displacement discontinuities) within impregnated samples do not appear to be damaged by these shrinkage cracks. Similar observations about the internal cracking have been made in the current investigation, and, in fact, the cracks have served as useful markers when interpreting micrographs of the thin sections. Mitchell (1956) and Martin (1962, 1966) also confirm that the impregnation does not damage the microfabric.

2.5.4 Observation of Thin Sections under Polarized Light

A single clay particle is birefrigent. If it is illuminated with plane polarized light and viewed through a crossed polarizing filter ('crossed-nicols'), then as the particle is rotated relative to the plane of polarization of the illuminating light, it may be seen to transmit a minimum light intensity when one of the optical axes is parallel to this direction, and a maximum light intensity when an optical axis is at 45° to it.

Tchalenko (1967) and Morgenstern and Tchalenko (1967 (a) and (b)) have shown that the birefrigence of an aggregate of clay particles depends solely on the intrinsic birefrigence of the constituent particles and their spatial configuration. When a random structure is viewed in thin section under crossed-nicols, no variation in transmitted light intensity is observed as the sample is rotated. On the other hand, if the aggregate has a preferred orientation, then the minimum and maximum light intensities will depend on the degree of orientation. The ratio of these intensities may be employed, as described by Morgenstern and Tchalenko (1967 (a) and (b)) to provide a measure of the degree of preferred orientation.

2.5.5 Shear-induced Particle Orientation

Shear straining within clays is known to induce preferred particle orientation. Skempton (1964) noted that the shearing resistance of some clays decreases as a result of post-peak displacements, and

attributed the phenomenon of residual-strength to the formation of a thin band of clay particles which exhibit a high degree of preferred orientation sub-parallel to the direction of relative displacement. The progressive development of shear induced structures within a direct shear box has been studied by Tchalenko (1967). The major conclusions of his work were that fabric discontinuities are associated with local instability phenomena, and that the development of shear induced structures within the clay is dominated by the imposed kinematic constraints. Kinking appears to be the dominant mode of deformation in the generation of major microfabric structures. The development of kink bands in kaolin has been studied by De (1973), and in a geological context has been considered by many authors, e.g. Paterson and Weiss (1966), Ramsay (1967), Tchalenko (1968), Freund (1974), Gay and Weiss (1974) and Weiss (1980). Despite the research effort, the modes of nucleation and propagation of kink bands still do not appear to be well understood.

Microfabric changes induced in clay samples by the installation and loading of model piles are considered in Chapter 6 of this dissertation.

TABLE 2.1: Measurements of Pore Pressures Generated along the Shafts of Displacement Piles during Loading

Reference	Pile diameter/type	Soil type	Pore-pressures /Cu	Comments
Lo and Stermac (1964)	368 mm/timber) 610 mm/Franki)	O.C. Silty-Clay	0.2-0.25	Piezometers located about one pile radius from pile face
Airhart et al. (1969)	406 mm/steel pipe pile	O.C. Beaumont Clay	0-0.13	Measurements at pile face
Clark and Meyerhof (1972(a))	75 mm/steel pipe pile	Medium plasticity clay (PI = 20.4)	0.2-0.6	Measurements at a distance of one pile radius from pile face
Massarsch,Broms and Sundquist (1975)	75-125 mm/steel	Norwegian Quick Clay	0.15-1.25	Measurements along the shaft
Puech and Jezequel (1980)	273 mm/closed-ended steel pile	Silty clay (PI = 28)	0.75-1.3 (very roughly)	Measurements at pile face, Cu not quoted
Roy, Blanchet and Tavernas (1981)	219 mm/steel	Soft, sensitive, Champlain Clay 10% < PI < 27%	0.6-1.5 0	At pile face At a distance of two pile radii from the shaft

CHAPTER 3

DESIGN OF THE EXPERIMENTAL APPARATUS

3.1 INTRODUCTION

As outlined in Chapter 1, the purpose of the first series of tests was to investigate the behaviour on drained axial loading of piles installed into normally-consolidated clay (Kaolin) with a minimum of disturbance. The initial stress ratio K ($= \sigma'_r/\sigma'_z$) was the principal variable in these tests. In nature, initial stresses before pile installation are confined to the K_o condition, but during the installation the stress conditions, and in particular the stress ratio K, are altered. In the laboratory it is possible to vary K and hence study its influence on failure conditions. In order to isolate the influence of K it is necessary to eliminate other more complex effects of field installation procedures, and so the model piles were installed by a special technique which is demonstrated (Chapter 6) to cause a minimum of disturbance to the soil fabric and the stress field in the clay around the pile. Once the behaviour of a pile installed in such an idealised manner was better understood, the experimental programme was extended to consider the behaviour of displacement piles.

In order to be able to control the consolidation stress ratio it was decided to conduct the tests by installing piles in cylindrical samples of Kaolin confined in a large, modified, hydraulic triaxial (stress path) cell in which the axial stresses and cell pressure could be independently varied (Bishop and Wesley, 1975). As the samples were prepared from a high water-content slurry, some consolidation outside the cell was required before the sample was transferred to the stress path and consolidated further to the desired stress level.

The purpose of the apparatus was to be able to conduct element tests representing the behaviour of a short section of a long-rigid, pile installed into a homogeneous, semi-infinite, mass of clay. Below, boundary conditions imposed on the laboratory samples of clay are considered in relation to this ideal.

3.2 BOUNDARY CONDITIONS

3.2.1 Outer Circumferential Boundary

Consider a short element of a very long pile, and a corresponding horizontal 'slice' of soil. On loading the pile all stress components within the soil may change. However, because the element is considered to be part of a very long pile, symmetry dictates that the pile load must be transmitted through the sample by increased shear stresses in the vertical plane, and not by a vertical gradient of axial stresses. Thus, at an arbitrary radius, r, from the centre-line, the pile load, P,is balanced by a shear stress $\tau(r)$, where

$$\underset{rz}{\tau(r)} = P/2\pi rL \qquad (3.1)$$

In practice, of course, no apparatus can have an infinite lateral extent, and so ideally shear reinforcement should be provided on the outer boundary of the sample in order to balance the load of the pile. The provision of shear reinforcement introduces practical complications because the sample must now be able to move relative to the reinforcement in order to ensure that the whole of the pile load is, in fact, transmitted in shear. Further, the reinforcement must not be allowed to interfere with the main consolidation of the sample prior to pile installation. A design capable of overcoming these difficulties would be expensive and time consuming to construct, but might incorporate matching hydraulic pistons above and below the sample to apply a constant axial force. The interference between the external reinforcement and the sample during consolidation might be eliminated by employing two membranes around the sample, the inner membrane being rough but unreinforced, and the outer one being both rough and reinforced. During consolidation, the two membranes could be separated by applying a small excess pressure between them, whereas the space between them could be vented (or evacuated) during the pile loading.

It was decided to perform a series of 'pilot' tests in a simpler piece of apparatus having no provision for shear reinforcement, before attempting to develop a more sophisticated piece of equipment. However, finite element modelling of the pile tests performed in the simpler apparatus showed that for tests employing normally-consolidated clay, the effect on the pile behaviour of omitting the shear-reinforcement in the boundary membrane was negligible for the equipment geometry selected, and so the test programme was completed in the simpler apparatus.

The outer circumferential boundary of the sample must be stress-controlled during consolidation to achieve a range of values of K, and was chosen to be so during pile loading. The influence on the pile behaviour of varying the distance to the stress controlled outer boundary was examined by means of finite element analyses employing Modified Cam Clay as the constitutive law (see Chapter 8), and it was found that for tests employing normally-consolidated clay, the proposed geometry was satisfactory (i.e. increasing the ratio of the sample to pile diameters had no significant effect).

The influence of the imposed boundary conditions on the pile behaviour depends on the geometry of the apparatus and on the behaviour of the soil being tested. So, although finite element modelling has shown the proposed apparatus to be satisfactory when employing normally-consolidated clay, the same design of apparatus would not necessarily be suitable for testing strongly dilatant soils.

3.2.2 Top and Bottom Boundaries

On loading a long pile, the stresses in the soil around the pile (including the axial stresses) will tend to change, and so the imposition of a constant axial stress boundary condition at the top and bottom of the sample is not strictly correct. A constant total axial load condition might be more appropriate, especially if shear reinforcement were provided on the outer circumferential boundary.

In the apparatus employed for the model tests, no shear reinforcement was provided. During the pile loading, the sample height was held constant, and so the pile load was transmitted to the apparatus in the form of a slightly reduced average axial stress on the top of the sample, and a slightly increased mean axial stress on the bottom, with the mean stress at mid-height being almost unaffected. Measurements of the force acting on the lower boundary during pile loading have confirmed that the pile load was shared fairly evenly between the top and bottom loading platens (see Fig. 3.1).

During consolidation of the sample, the top and bottom platens should ideally be lubricated. However, on loading the pile, the platens need to be rough in order to transmit complementary shear stresses, and so it was decided not to attempt to lubricate the ends.

3.3 PRINCIPLES BEHIND THE PILE INSTALLATION PROCEDURES (TO CAUSE MINIMAL DISTURBANCE)

In the first series of tests, the aim was to introduce a rigid pile into the centre of a cylindrical sample of clay with a minimum of disturbance to either the stress field or the soil fabric. There are, of course, several possible ways of introducing a pile, but they all cause some disturbance. The principal advantages and disadvantages of a selection of possibilities are summarised in Table 3.1. The method adopted was the last one (vi) in Table 3.1, which minimises the disturbance caused by the pile installation. The major disadvantage was that measurement of the radial stresses acting on the pile was very difficult, but this was eventually accomplished.

Experimental details of the installation procedure are described in Chapter 4, and the object here is simply to outline the principles on which the procedure relies. The sample was consolidated within the hydraulic triaxial cell to the desired stress state. Free water was expelled from the drainage system, and the height of the sample was maintained constant throughout the remainder of the test. The cell pressure, and hence the radial total stress applied to the sample, was reduced to zero, whilst undrained conditions were maintained. Ideally, because both the volume and the height of the sample were unchanged there should have been neither radial nor axial strains and hence no changes in the effective stresses.

A hole was then drilled through the sample, an undersized brass core of a pile introduced, and the annular space between the core and the walls of the hole grouted with a very low shrinkage epoxy resin. Epoxy resin was selected to avoid base-exchange problems that would have resulted from the use of a micro-concrete. It should be noted that during drilling, the radial total stresses on the sample were reduced to zero, and hence there was no tendency for the hole to collapse onto the drill. Once the resin had set, the cell pressure was returned to the original value, whilst undrained conditions with a constant sample height were maintained.

Ideally the reloading should correspond to plane strain conditions with a Poisson's ratio of one-half, and so no rigid inclusion effects should result (see Jaeger and Cook, 1977), and the radial stress acting on the pile should equal the cell pressure. In practice there were small departures from the ideal conditions, and these would be expected to cause the radial stresses acting on the pile to be slightly greater than the cell pressure (because of rigid inclusion effects). Measurements of the radial stresses acting on

pile shafts in two tests during the re-application of cell pressures indicated that the increases were less than 7%; observations of thin sections prepared from the clay around a hole drilled under the above conditions (see Fig. 6.2) have also confirmed the efficacy of the procedures. The subject of the installation procedures will be considered further in Chapters 4 and 5.

3.4 APPARATUS

3.4.1 General Layout

A schematic diagram of the model pile testing equipment is presented in Figs. 3.2 and 3.3. The primary components of the apparatus are the hydraulic triaxial cell, the sample loading system, the piles and the pile loading system. The majority of the data logging was performed by an a.c. Peekel data logger, although later installation of driven piles was monitored using a storing Oscilloscope.

3.4.2 Hydraulic Triaxial Cell

3.4.2.1 Introduction

The tests were performed in a large hydraulic triaxial cell, which was modified from its original role as a plane strain apparatus (Atkinson, 1973). A description of the operation of hydraulic triaxial cells has been presented by Bishop and Wesley (1975). The radial stress on the sample is controlled by the cell pressure applied to the external circumferential boundary of the sample, and the axial stress is controlled by the pressure applied to the lower chamber of the hydraulic ram. The axial stress on the sample is affected by the cell pressure, and this must be taken into account. The controlling pressures were supplied by means of a system of self-compensating mercury pots (Bishop and Henkel, 1962).

3.4.2.2 Drainage

The final consolidation of the samples (nominally 102 mm diameter x 150 mm long) was effected within the triaxial cell. Both top and bottom drainage was permitted, and this was assisted by spiral wound strip filter paper side drains, although,because of the high permeability of the Kaolin tested, the contribution of the side drains was probably minimal. The end drainage provision comprised a filter paper and metal gauge sandwich, as illustrated in Fig. 3.3. Two drainage connections were provided at each end so that the drainage system could be gently flushed with air to remove as much free

water as possible in advance of the pile installation procedure (this is why the filter paper sandwiches were employed in preference to porous stones). The tests were all performed without the use of back-pressures, and volumes of water expelled from the samples during consolidation were measured by means of a water-paraffin volume gauge. The hydraulic systems involved in the equipment are shown schematically in Fig. 3.4.

3.4.2.3 Provisions for pile entry and exit

As the aim of the tests was to examine the shaft resistance of piles, it was decided that rather than attempt to measure the end bearing resistance of the model piles the apparatus should be designed to eliminate it.

The pile tip was arranged to protrude through the base of the Kaolin sample and into a cavity in the bottom platen (Fig. 3.3). During pile loading the cavity was vented to atmospheric pressure. However, during consolidation before pile installation, the existence of holes in the top and bottom platens would lead to extrusion, and so the cavity in the bottom platen was sealed by a small piston which was held flush with the surface of the platen during consolidation. This was effected by filling the chamber beneath the piston with de-aired water and sealing it hydraulically. A simpler screw-in plug arrangement was used in the top platen. During pile installation both plugs were retracted.

3.4.3 Sample Loading

The cell pressure was supplied by means of self-compensating mercury pots which were manually controlled. Pressures were monitored by means of a 150 p.s.i. Bell and Howell transducer connected to the cell. Occasionally problems with the data logging unit caused the 'zero' readings of the various transducers to shift, and for this reason the hydraulic connections to each pressure transducer were arranged so that the transducers could be connected to a reference pressure at any time, without affecting the pressure that the transducer was originally intended to measure. Another advantage of this arrangement was that the pressure to be applied to the equipment could be accurately pre-set before application.

The axial stress was supplied by means of a hydraulically controlled piston, as described by Atkinson (1973). The piston employed double-acting Bellofram seals and was guided by Rotolin bearings. The axial stress was controlled by altering the pressure in the lower chamber; during calibration

of the system (described later) it was found that there was very little friction in the system, and this result permitted the omission of a force transducer, greatly simplifying arrangements within the triaxial cell. It should be noted that measurements of the axial stress were required primarily to control consolidation and hence the small errors that might have been incurred by the omission of a load cell were considered acceptable.

The axial travel of the hydraulic piston was only 17.5 millimeters, and so after allowing for clearances during sample assembly the available travel was reduced to about 15 mm. This imposed important constraints on the stress levels, and stress ratio that could be employed during consolidation of the Kaolin samples. In order to reduce this problem, the heights of the samples were selected to be 150 mm (rather than the 200 mm which would commonly be used for 102 mm diameter samples failed in triaxial compression).

During consolidation the axial movement deformation of the sample was monitored by means of a submersible linear variable differential transformer (LVDT) connected between the top and bottom platens. Once the consolidation was completed, the height of the sample was kept constant for the rest of the test. This condition was maintained, despite the variations of cell pressure involved in the pile installation procedures, by means of a manually operated hydraulic ram connected to the lower chamber of the axial stress piston, as shown schematically in Fig. 3.4.

3.4.4 Piles

3.4.4.1 Introduction

The main requirements of the piles installed with minimal disturbance were that they were of exactly the same diameter as the hole drilled through the sample, and that they were rigid both axially and radially. The majority of tests employed non-instrumented piles, although eventually a system was developed whereby the radial stresses acting on the pile shaft could be measured. The full-displacement piles employed in the second series of tests were of similar construction although the diameters were no longer critical.

3.4.4.2 Non-instrumented Piles

The piles were constructed by drilling a 15 mm diameter hole through the sample. A rigid brass core of 11 mm diameter was then introduced and the annular gap between the pile core and the hole was grouted in-situ with a strong, low shrinkage, epoxy resin (Araldite CY 219, HY 219 and AY 219 10%;

the manufacturers,Ciba Geigy, quote shrinkage figures of less than 0.1% for resin including 1% of the accelerator). The purposes of the core were to ensure axial rigidity, and to minimise any possible shrinkage of the resin which was thereby limited to a two millimeter thick annulus around the rigid core. The latter was provided with shear keys to prevent relative movement between the resin and the core on loading the pile.

Down the centre of the brass core a three millimeter diameter hole was provided, through which water could be passed in order to inflate a small latex rubber 'packer' membrane at the base of the pile. The purpose of this was to prevent injected resin from escaping into the cavity in the bottom platen. The base of one such pile is illustrated in Fig. 3.3.

3.4.4.3 Instrumented Piles

The piles intended to measure the radial stresses acting on the shaft were constructed in a similar manner to the non-instrumented piles, the main difference being the addition of a pressure-sensing element close to the centre of the pile.

Because the piles were required to be cast in-situ, for the reasons discussed earlier, all instrumentation was difficult at the scale employed. No attempt was made to measure the distribution of shear stress along the pile, particularly as the finite element predictions (Chapter 8) suggested that these stresses were likely to be very uniform, at least when testing normally-consolidated clays.

The major difficulty in developing a device for measuring the radial stresses arose from the need to avoid disturbance to the walls of the pre-drilled hole in the sample whilst installing the device. Therefore, the device could not be fully assembled outside, but had to be expanded, in-situ, to fit the hole exactly. For this reason, the device was constructed on a principle similar to that of a pressuremeter (see Fig. 3.5).

Piles incorporating this radial stress sensing element were installed following similar procedures to those used for the other piles, with the exception that while the injected epoxy resin was still fluid, a 25 mm long cylindrical latex rubber membrane (the preparation of these membranes is discussed in Appendix 3.1) at the centre of the pile was inflated with de-aired water to fit the hole diameter exactly. Once the resin had set, the enclosed volume of water was restrained axially by the resin, and was also restrained by the central brass core of the pile. The annulus of water was connected

via stainless steel hypodermic tubing to a 150 p.s.i. Bell and Howell pressure transducer. Thus, any increase in radial stress applied to the outer surface of the membrane was reflected in a similar increase in the fluid pressure measured by the pressure transducer. The hydraulic system was made as stiff as possible so as to minimise the required deflections of the sensing element. To enable the device to resist shear stresses as the pile was loaded, shear reinforcement was provided in the form of some forty strips of flattened, annealed, copper wire which ran down the outside of the membrane. These strips were embedded at both ends in the resin so that the loads could be transmitted to the brass core. Following Tests 7 and 15, thin sections were prepared through the radial stress measuring devices in order to establish whether the Kaolin around the devices had behaved in a similar manner to that elsewhere along the piles. It may be seen in Appendix 6.2 that the shear reinforcement had worked well.

As a check on the compliance of the hydraulic system, a sensing element, similar to that described above, was cast into a hole drilled in a large cylinder of steel, and the compressibility was measured as a function of the internal pressure, using the equipment shown schematically in Fig. 3.6. Typical results are presented in Fig. 3.7, and these illustrate that, as would be expected, the compliance is greatest at low pressures, but is negligible at higher pressures. The measured compressibility of the system is equivalent to a ratio of peak membrane deflection to length of sensing element of less than 1 in 2,000, which would generally be considered acceptable for devices used in the field. However, this particular application is more restrictive because the re-application of cell pressure should ideally cause no radial strains within the sample which is being reloaded under conditions of constant height and constant volume. Thus, the soil adjacent to the sensing element will be very stiff, and even a small compliance of the device will affect the measurements. It was considered impractical to attempt to construct even stiffer devices and so an alternative technique of operation of the device was developed; this is believed to have enabled reliable measurements to be obtained.

Once the device had been cast into a pile (as described in Chapter 4) the measuring system was isolated. On application of an increment of cell pressure, an equal change in the fluid pressure within the device would ideally occur. Because of the system compliance, however, the incremental response of the device was initially only half of this value, but continued to rise very slowly. In order to overcome this, a small pressure increment was applied

to the device which was again isolated, and the response observed. If the pressure tended to fall, then a small decrement of pressure was applied, and vice-versa; the process was repeated until the 'true' radial stress had been bracketed with sufficient accuracy. A further increment of cell pressure was then applied. The incremental response of the device rapidly improved with increasing pressure, and as the final stress levels were approached corrections proved unnecessary. More information about the operation of the radial stress measuring devices is included in Chapter 4, and within the descriptions of Tests 15 and 17.

The present design of device proved to be both difficult to construct and to operate largely as a result of the small scale involved, and, of course, each device could only be used for a single test. For these reasons the use of such devices was only attempted in three tests (7,15,17). However, it is believed that many of the problems of construction would be greatly alleviated by the use of model piles with diameters in excess of 25 millimeters.

3.4.4.4 Displacement Piles

Displacement piles were used in three tests (16,18 and 19), and none of them was instrumented. In a similar fashion to the cast-in-situ piles described above, these piles incorporated a rigid brass core provided with shear keys, surrounded by an annulus of epoxy resin. The pile employed in test 16 was prepared by casting a brass core within a hole drilled in a spare sample of Kaolin, whereas the piles for Tests 18 and 19 were cast oversized and then trimmed to the required dimensions on a lathe. The brass cores used in these two tests each had a three millimeter diameter hole drilled along the length of the pile so that a brass rod could be inserted; this was used to facilitate the retraction of the piston in the lower platen of the triaxial cell, prior to pile loading (see Chapter 4).

The equipment used for installing the displacement piles is described in Chapter 4, section 6.

3.4.5 Pile Loading System

The requirement was to be able to load the piles in compression at a constant rate of displacement, with the measurement of both pile load and axial displacement. A general view of the equipment is provided in Fig. 3.2. The pile was loaded by means of an electric motor driven through a reduction gearbox and a restrained worm gear, at a displacement rate of about 0.2 millimeters per hour.

In transmitting the load from the gearbox to the pile, it was necessary to fulfil two conditions:

(i) that the axial load be applied without introducing bending moments or significant lateral forces;

(ii) that the pile displacements could be measured to an accuracy of better than one-hundredth of a millimeter.

The arrangement illustrated in Fig. 3.2 satisfied both conditions. The pile was fitted with a stainless-steel knife-edged cap. Onto this was lowered a stainless-steel bar of rectangular cross-section, which pivoted about a knife-edged support which was adjustable in height; this was used to level the bar. The load was applied to the upper face of the bar (as shown in Fig. 3.2) immediately above the pile cap, through a ball-ended extension to a 450 kg Imperial College load cell (El-Ruwayih, 1975). An amplified value (c x 2) of the pile displacement was obtained by measuring the vertical displacement of the far end of the steel bar, employing a particularly sensitive LVDT. Pile displacements smaller than 5×10^{-4} millimeters could be resolved by this means, and the whole system worked well.

3.5 CALIBRATIONS

3.5.1 Introduction

The transducers used in the experiments were generally monitored using an a/c Peekel data logger. Despite its age, the system worked satisfactorily, and proved particularly useful when logging LVDTs as no additional a/c to d/c converter was required. Calibrations of the various transducers employed were repeated at intervals during the testing programme, and no significant differences were found.

3.5.2 Pressure Transducers

The three Bell and Howell 150 p.s.i. pressure transducers were each calibrated using a Budenberg Dead Weight tester. The responses were all essentially linear (see Figs. 3.8(a) and (b)), and a resolution of about 0.13 kN/m^2 was obtained.

The major source of error probably arose from the generally poor temperature control of the laboratory (typically ± 2°C but much worse on occasions). Nevertheless, an overall accuracy of better than ± 0.5 kN/m^2 was obtained, and this was considered satisfactory.

3.5.3 Load Cells

Altogether three 'Imperial College' load cells were employed, and they were all calibrated using the Budenberg Dead Weight tester. One 450 kgf load cell was used to monitor the consolidation of samples prepared outside the hydraulic triaxial cell, and another was used to monitor the pile loads. A 2700 kgf load cell was used during the calibration of the hydraulic ram of the stress path cell.

A typical calibration curve obtained from the load cell employed to monitor the pile load is shown in Figs. 3.9(a) and (b). It may be seen in (a) that the incremental response was not constant. However, it may also be seen in (b) that, over the range of loads used in practice, the representation of the accumulated response by a straight line implies an error of less than 1%. Similar results were obtained from the other load cells, and the linear approximation was considered sufficiently accurate.

3.5.4 Displacement Transducers

Three LVDT's were used in the course of the pile testing; a submersible transducer was used to monitor the consolidation of samples within the hydraulic triaxial cell, a long throw (> 75 mm) transducer was used to monitor the installation of the displacement piles, and a very sensitive device was used to measure the pile displacements on loading. The long throw device was monitored on a recording oscilloscope or a Solartron logger, whereas the other two were monitored on the Peekel logger.

The transducers were calibrated by means of a horizontally mounted vernier system, and the responses were linear and exhibited very little scatter. The resolution of the transducer used to record the pile displacements on loading was about 3×10^{-4} mm; when used in conjunction with the magnifying lever system shown in Fig. 3.2, an accuracy of better than 10^{-3} mm was obtained. The transducer used to monitor the sample consolidation had a resolution of 1×10^{-3} mm, and so an accuracy of better than 5×10^{-3} mm may reasonably be assumed.

3.5.5 Axial Stresses on the Samples in the Hydraulic Triaxial Cell

Preliminary investigations indicated that the friction in the hydraulic ram of the triaxial cell was extremely low. This suggested the possibility that the axial stresses acting on a sample within the cell could be established by measuring the pressure in the lower chamber without the need

for a load cell.

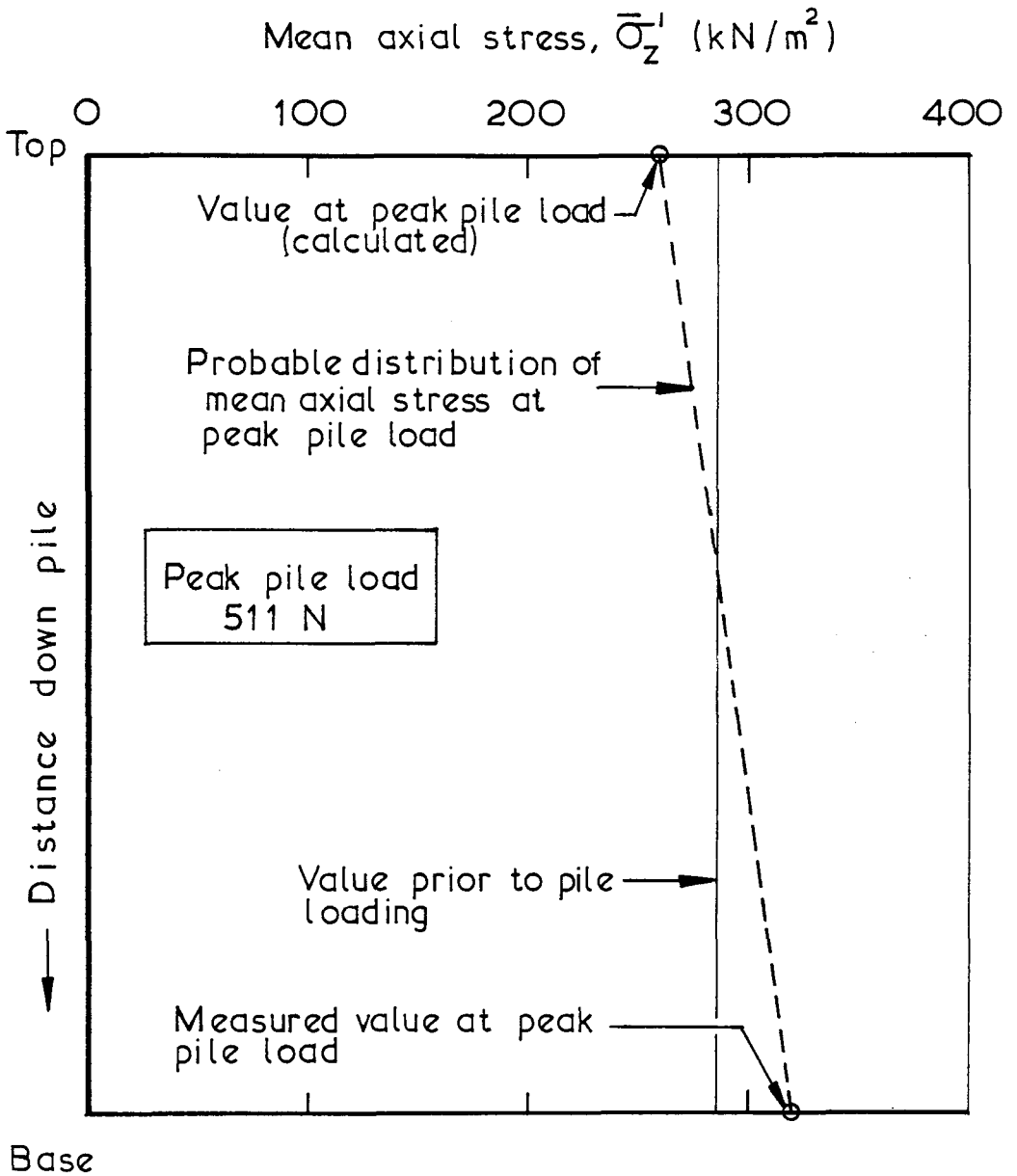
In order to measure the friction involved, and to determine the effective area of the lower piston, the axial system was first calibrated with no pressure applied to the cell. A previously calibrated 2700 kgf load cell was attached to the top-cap of the cell, and the load cell was connected to the hydraulic piston by means of a rigid brass cylinder and a combination of compressible elements. The pressure in the lower chamber was then slowly cycled, and the axial displacement and the load cell response were recorded. This process was repeated with different compressible elements so that the piston travel to achieve full load could be varied. The results showed that the friction in the system was indeed very small and that an error of less than 0.2% was incurred by neglecting it. The effective cross-sectional area of the lower piston was determined to be 7.529×10^{-3} m^2.

Having established that it was reasonable to omit a load cell and to rely on the measurements of pressure in the lower chamber, it was necessary to determine the influence of the cell pressure on the axial stresses. In order to determine the equivalent cross-sectional area of the top piston, the piston was raised to mid-travel and then the lower chamber was hydraulically sealed. The pressure in the lower chamber was then observed as the cell pressure was cycled, and the equivalent cross-sectional area was calculated to be 7.487×10^{-3} m^2.

During a test, the cross-sectional area of a sample varies, and is in general not equal to the equivalent cross-sectional area of the top piston. Thus, in order to calculate the axial stress acting on a sample it is necessary to take into account the diameter of the sample, the pressure in the lower hydraulic chamber, and the cell pressure. A programme was written for a hand-held calculator (HP 41-CV) in order to determine the stresses acting on a sample, taking into account changes in geometry during consolidation.

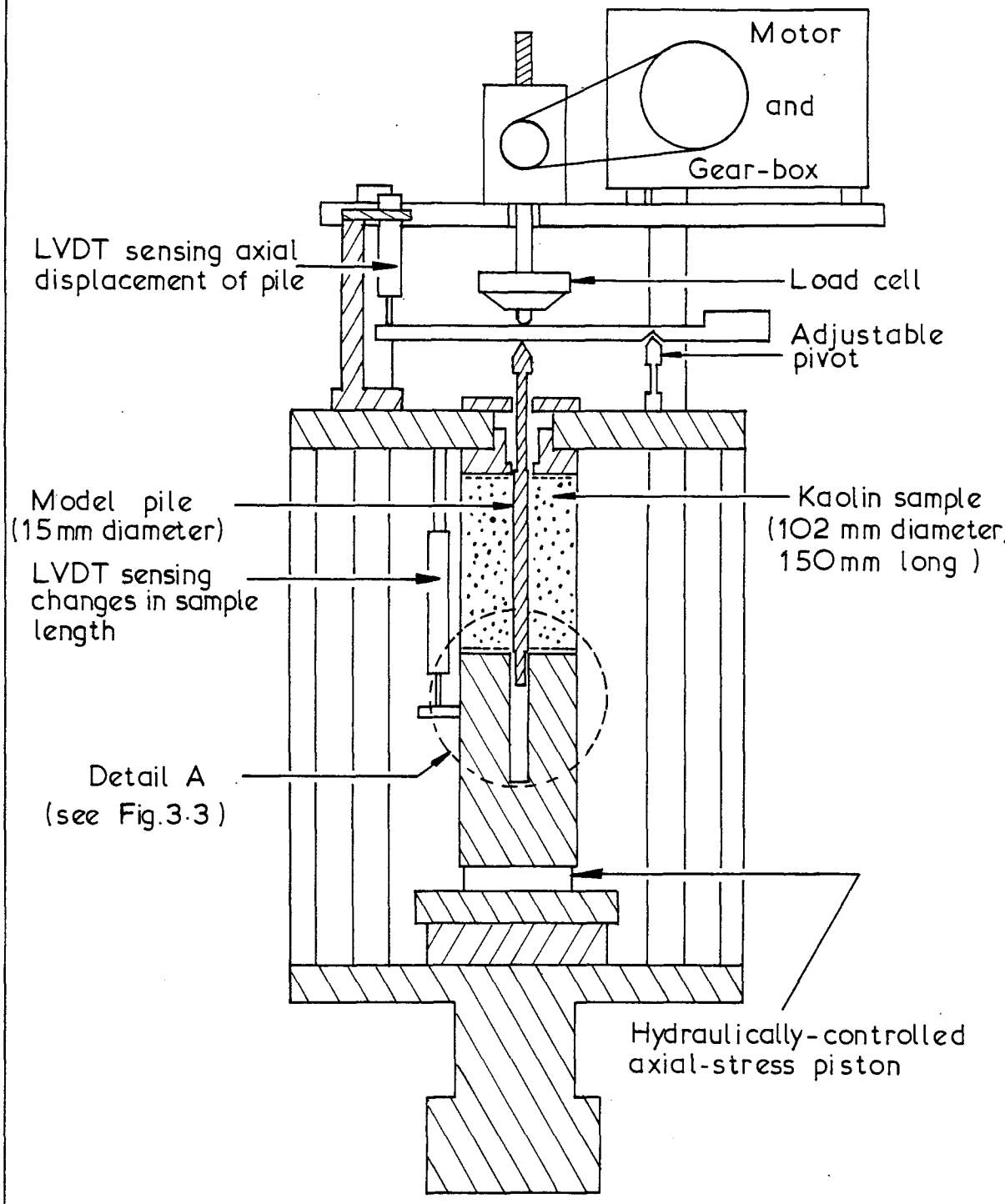
Table 3.1: Comparison between different methods of the installation

Method	Advantages	Disadvantages
(i) Consolidating from slurry around a pile		Severe fabric disturbance if soil can drag against pile during consolidation. Rigid inclusion effects
(ii) Jacking or driving a pile		Disturbance to stress field and soil fabric
(iii) Jacking a thin-walled sample tube with inward directed cutting shoe	Minimal disturbance to stress field	Serious local disturbance to soil fabric; axial and buckling rigidity of tube in question
(iv) Boring a cavity with the sample under stress, and then grouting the cavity	Only suitable for heavily over-consolidated materials	Disturbance to stress field and soil fabric
(v) Boring a cavity with lateral stresses reduced to zero, then introducing a tightly fitting rigid pile; lateral stresses then re-applied	Minimal fabric disturbance if pile undersize	Disturbance to soil fabric if the pile is oversize; disturbance to the stress field if the pile slightly oversize; large disturbance to the stress field if the pile is undersized
(vi) Boring a cavity whilst the radial total stresses are reduced to zero under undrained conditions; cavity then grouted to form a rigid inclusion, of same diameter as cavity; lateral stresses are then re-applied	Minimal to small disturbance to the stress field; minimal fabric disturbance	Any radial stress measuring device must be expanded while it is in place to fit exactly against the side of the hole



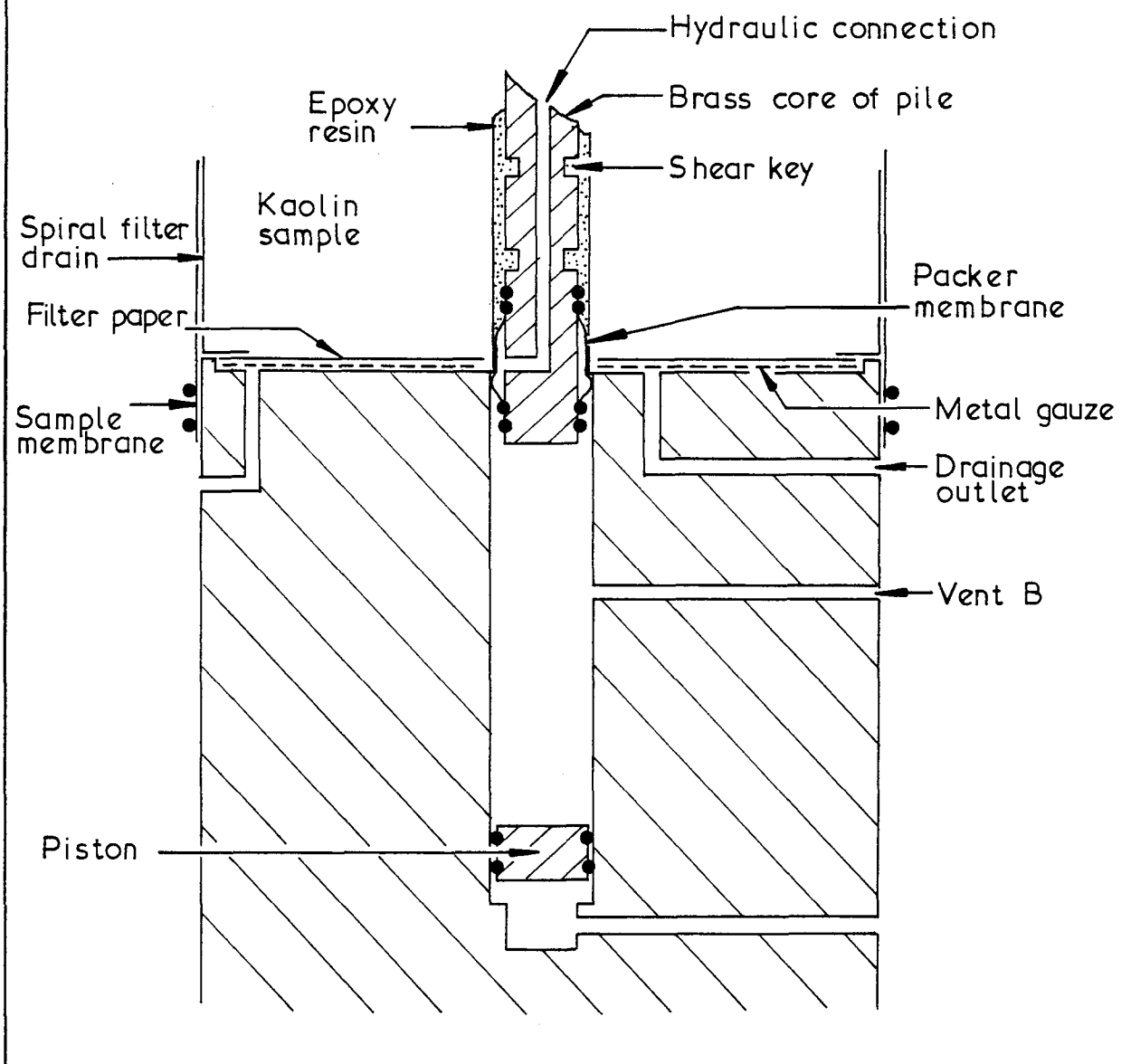
Variation of the mean axial stress acting within the kaolin sample from Test 11, before loading and at peak load.

Fig.3.1



Schematic view of apparatus

Fig.3.2



Detail A in Fig. 3.2 at base of clay sample; the piston is retracted into the position shown during pile installation, when vent B is connected to atmospheric pressure.

Fig. 3.3

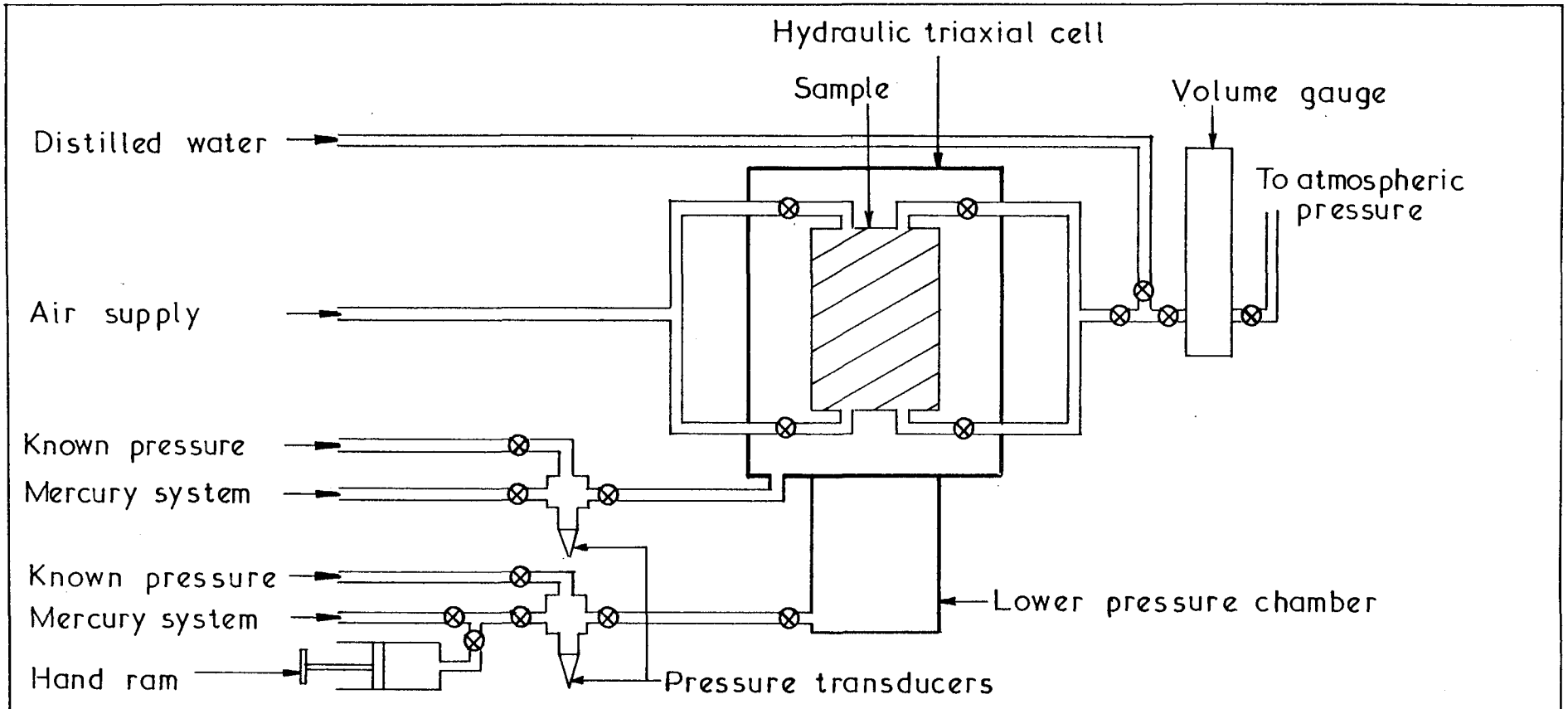


Fig. 3.4

SCHEMATIC VIEW OF HYDRAULIC SYSTEMS

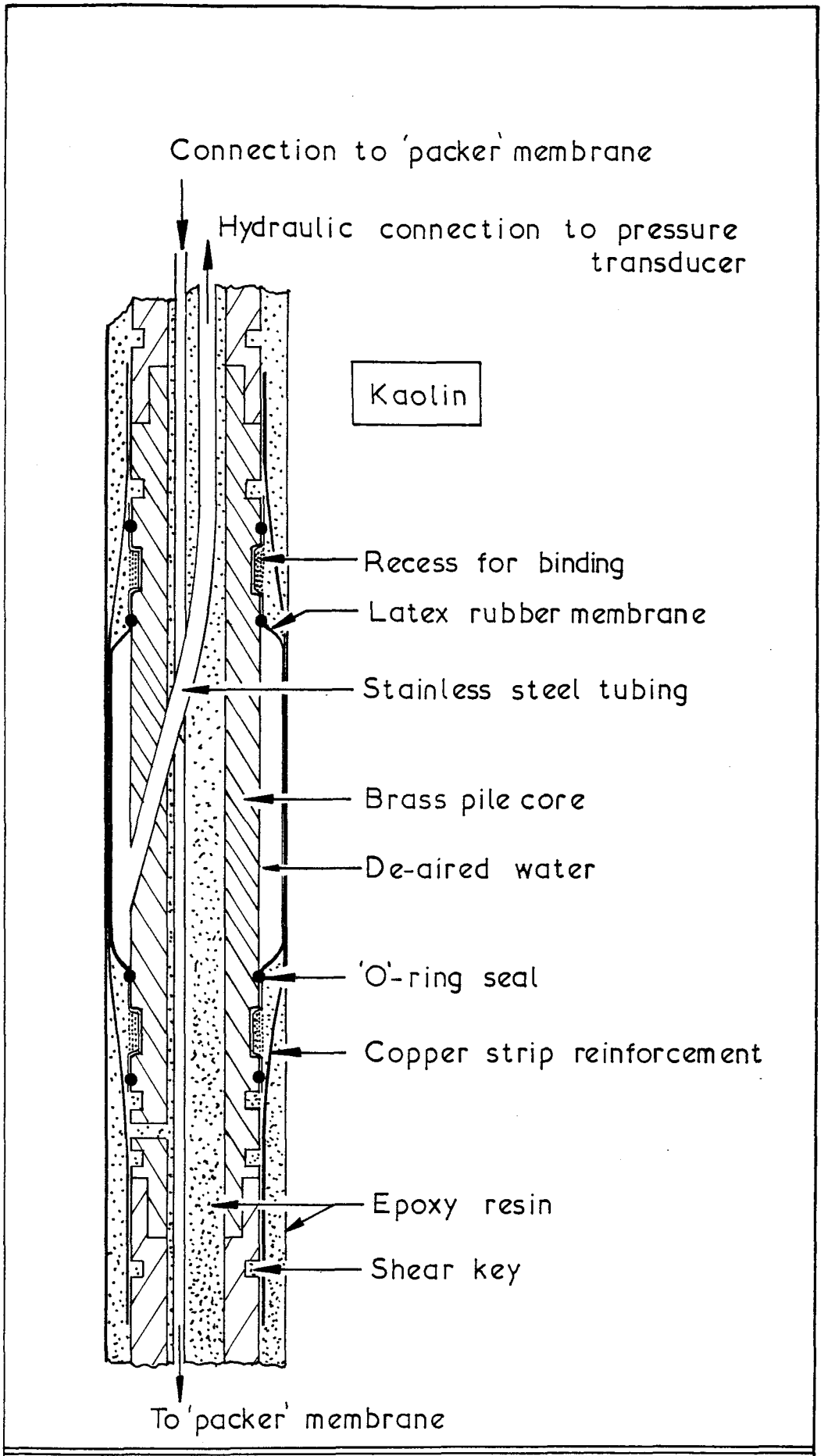
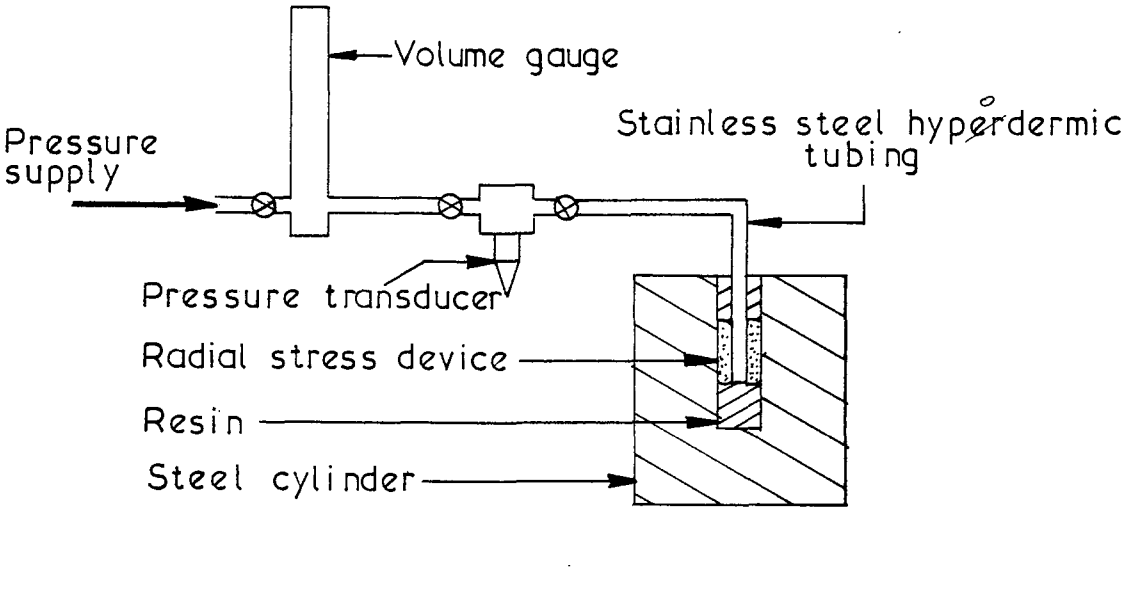
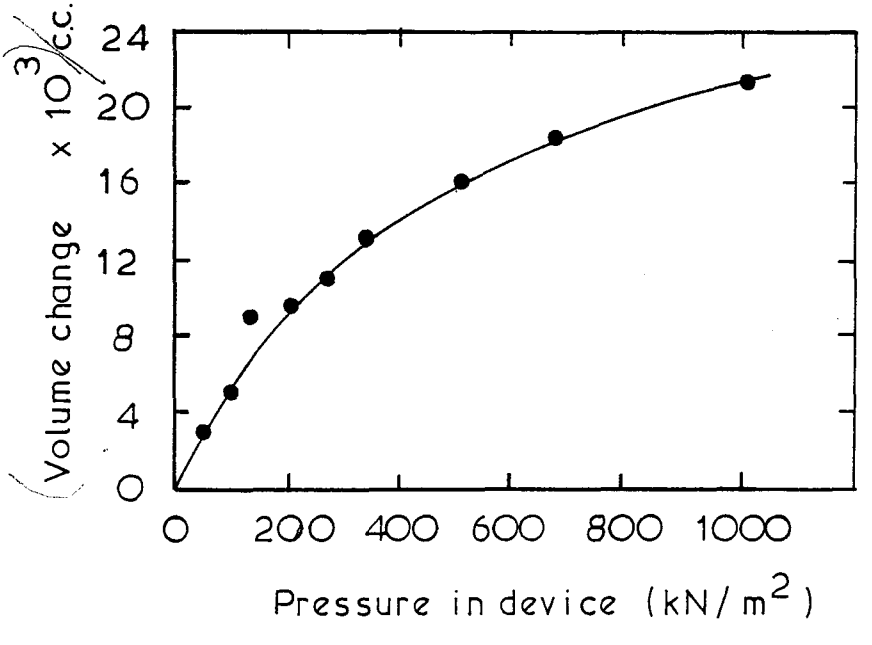

Connection to 'packer' membrane
Hydraulic connection to pressure transducer
Kaolin
Recess for binding
Latex rubber membrane
Stainless steel tubing
Brass pile core
De-aired water
'O'-ring seal
Copper strip reinforcement
Epoxy resin
Shear key
To 'packer' membrane
Radial stress device

Fig. 3.5



Schematic view of apparatus for measuring the compliance of the radial stress device.

Fig. 3.6



Volume change of radial stress -measuring device with pressure.

Fig. 3.7

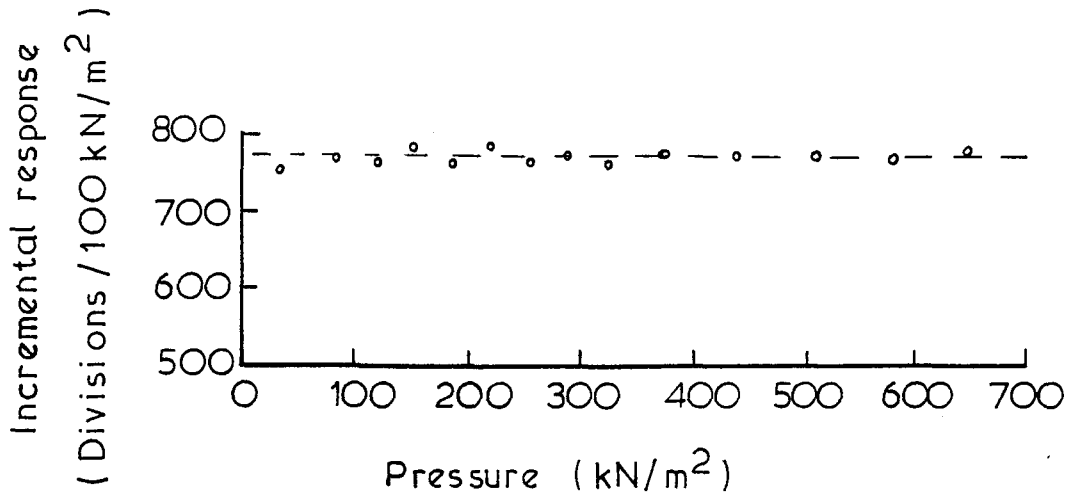


Fig. 3.8 (a)

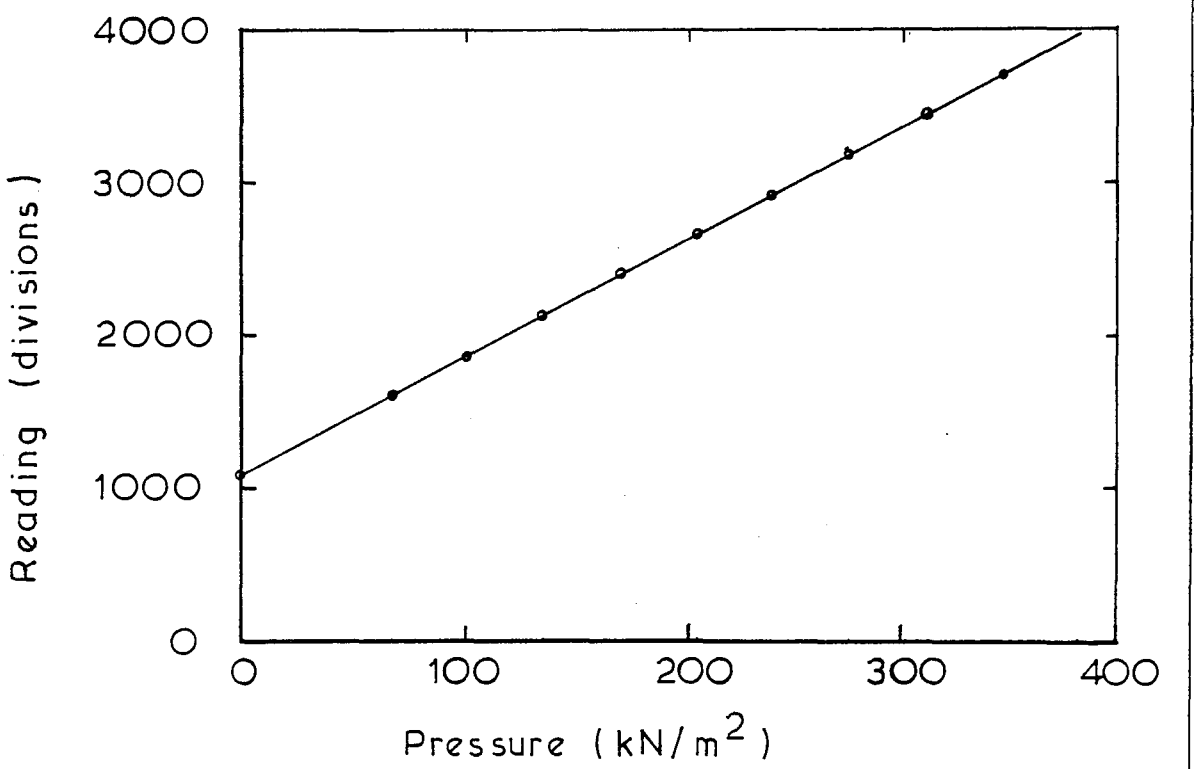


Fig. 3.8(b)

Calibration curves for pressure transducer used to measure radial stresses on piles.

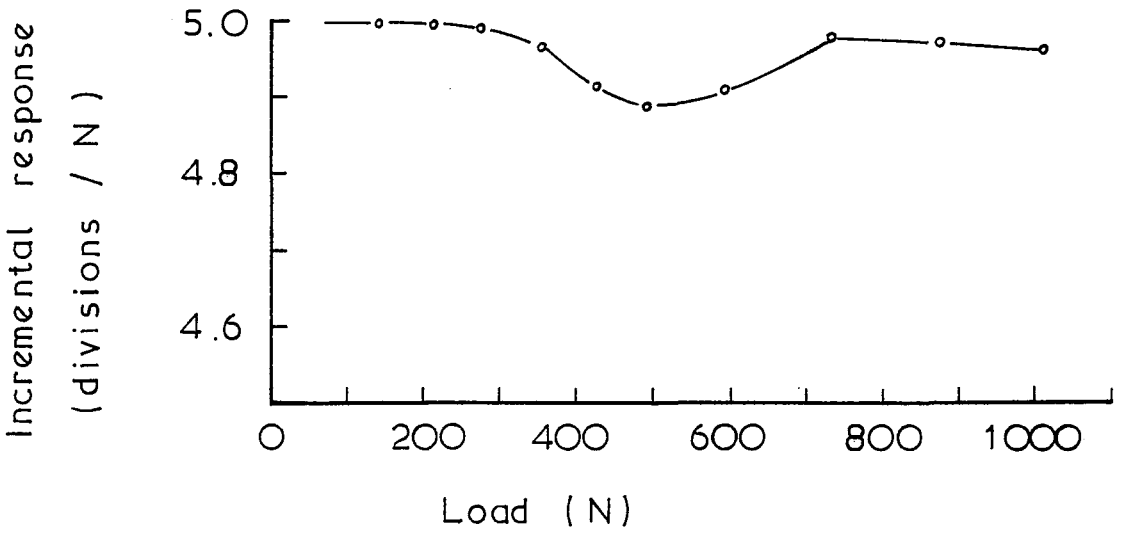


Fig. 3.9(a)

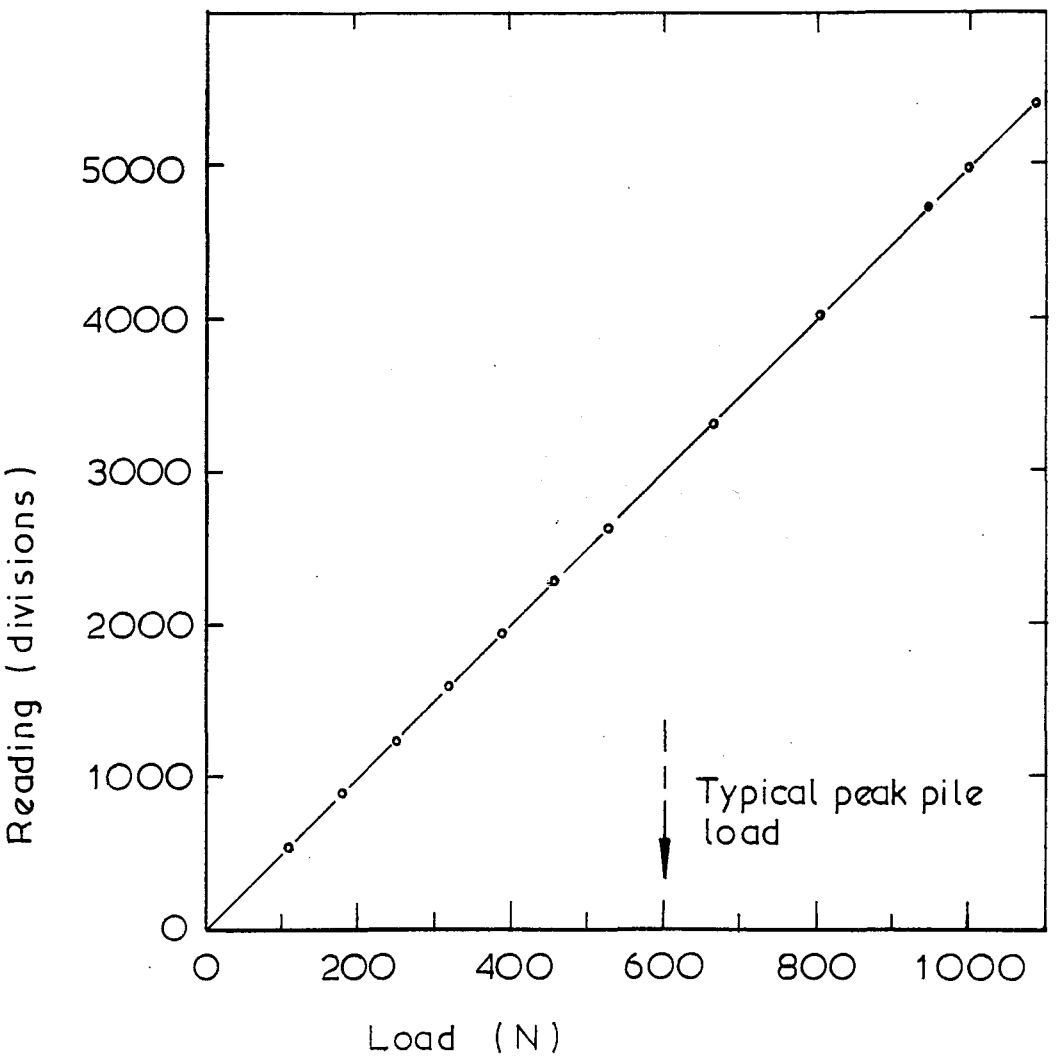


Fig. 3.9(b)

Calibration curves for load cell measuring pile load.

APPENDIX 3.1

PREPARATION OF MEMBRANES

Small diameter (c 12 mm) cylindrical rubber membranes were required to act as 'packers' on the bases of model piles, and others were needed for the radial stress-measuring devices. Both types of membrane were made in the laboratory.

The first technique of fabrication tried,was suggested by Dr. R. Arthur of University College, London. A degreased former was dipped into a coagulant solution (calcium nitrate (60% by weight) and methanol) and then put in an oven to dry. The former was then dipped with pre-vulcanised Latex rubber solution (Revultex) and put in an oven (60°C) to cure. This method was found to produce membranes that were too thick for the present purposes, although it is possible that a change in the consistency of the coagulant would have led to a greater control. However, the use of the coagulant was soon abandoned in favour of a simpler method.

In the alternative method, a degreased brass former (roughly 12 mm dia. x 150 mm long) was dipped into Revultex solution and then suspended until air dried. It was then up-ended, dipped, and allowed to dry. This procedure was repeated until either three or five thicknesses (depending on the intended function of the membrane) had been built up. The membrane was then coated in French chalk, removed from the former and placed into a bath of tap-water in which it was allowed to soak for at least 24 hours in order to leach the membrane. This allowed the membrane to absorb various ions from the water with the result that the membrane was subsequently less susceptible to osmosis. The membrane was then dried, dusted with French chalk and stored in the dark.

CHAPTER 4

SAMPLE PREPARATION AND TESTING PROCEDURES

4.1 INTRODUCTION

An important requirement of the experimental procedures was to prepare homogeneous samples of clay behaving, with the exception of one sample, in a normally-consolidated fashion at the desired stress ratio. In the first series of tests, model piles were introduced into the clay samples with a minimum of disturbance to either the stress field or the clay fabric, and in the second series full displacement piles were either driven or jacked into the clay.

4.2 CLAY SELECTED FOR EXPERIMENTAL PROGRAMME

4.2.1 Reasons for Selection

As homogeneity and repeatability were important, it was necessary to be able to control the whole stress history of the samples. The samples were therefore artificially prepared, starting from a high water content slurry.

Speswhite Kaolin (obtained from the English China Clay Company) was selected as the clay to be investigated for three main reasons:

(i) for a clay, it consolidates very rapidly and hence the relatively large samples required for the test programme could be consolidated in less than one month;

(ii) although Kaolin is still a clay, the particles are relatively large (Mitchell, 1976) and consequently Kaolin exhibits excellent properties for micro-fabric investigations (Morgenstern and Tchalenko, 1967(a) and (b));

(iii) the geotechnical properties of Speswhite Kaolin are similar to those of the now unavailable Spestone Kaolin (see Steenfelt, Randolph and Wroth, 1981). Spestone Kaolin was the subject of twenty years investigation at Cambridge, and it is known that the Modified Cam Clay constitutive law (Roscoe and Burland, 1968) provides a useful generalised mathematical model of the behaviour

of the clay. This constitutive model should, therefore, be of assistance in controlling the consolidation of samples, and in interpreting the results of the tests.

4.2.2 Properties of Speswhite Kaolin

Speswhite Kaolin is an inorganic china clay with a high plasticity, and, as remarked earlier, its behaviour has been found to be similar (Steenfelt, Randolph and Wroth (1981)) to that of the Spestone Kaolin which was used in the development of the 'Cam Clay' and 'Modified Cam Clay' constitutive laws at Cambridge.

The Modified Cam Clay constitutive law provides a very useful framework for the description of the continuum stress-strain behaviour of Kaolin, and requires the establishment, by standard laboratory testing, of the four Cam Clay parameters characteristic of the particular clay;

(i) λ , the slope of the virgin consolidation line in e-ℓn P' space

(ii) κ , the slope of a swelling line in e-ℓn P' space

(iii) $(e_\lambda)_1$, the void ratio at unit confining pressure

(iv) M , the slope of the Critical State Line

For further information about these constitutive laws, the reader is referred to Schofield and Wroth (1968), and Roscoe and Burland (1968).

A general description of the clay is presented in Table 4.1(a), the chemical composition is quoted in Table 4.1(b), and the Index properties are summarized in Table 4.1(c). The strength and consolidation properties were established by laboratory experiments, the results of which are presented in Table 4.2, together with corresponding values reported by other workers (where available).

It was found that the slope of the virgin consolidation line was not absolutely straight in e - ℓn(P') space, the value decreasing slowly with increasing mean effective stress (see Butterfield, 1979), whereas the κ value was constant (within the stress range considered). This may be seen in Fig. 4.1 and will be considered in Chapter 5 in relation to the results obtained during the preparation of samples at a variety of stress ratios.

If a clay is subject to displacements along a shear surface (either within the clay or at a rigid interface) the clay particles adjacent to the

discontinuity become preferentially oriented sub-parallel to the direction of motion (see Morgenstern and Tchalenko (1967, d) and Lupini (1980)). The particle orientation phenomenon typically occurs within a narrow zone (< 100 μ), and as the degree of preferred orientation increases the angle of shearing resistance that can be mobilised on the shear surface decreases until eventually a residual value (ϕ'_r) is reached. The magnitude of ϕ'_r will depend on the normal effective stress and the rate of shearing. The residual strength of Speswhite Kaolin was examined by means of ring shear tests and by direct shear interface tests. A value of ϕ'_r appropriate to the conditions of the model pile tests is presented in Table 4.2, but for further information, the reader is referred to Appendix 4.1.

4.3 SAMPLE PREPARATION

4.3.1 Introduction

As the Kaolin samples were prepared from a high water-content slurry (at roughly twice the liquid limit), consolidation to the desired water contents of around 45% involved a halving in volume. This reduction was greater than could be effected within the hydraulic triaxial cell, and so the consolidation was performed in two stages. The slurry was first consolidated one-dimensionally to a water content of approximately 52%, after which the soft sample was transferred to the triaxial cell. In this second stage of consolidation, the effective stress level within the sample was approximately doubled.

4.3.2 Preparation of Slurry

Dry Speswhite Kaolin powder was mixed with distilled water in a large paddle mixer to form a slurry with a water-content of between 140% and 150% (just over twice the liquid limit). The slurry was allowed to stand for several weeks to ensure full hydration, after which it was stirred under vacuum for at least one week to ensure complete saturation.

4.3.3 One-dimensional Consolidation

This first stage of consolidation was performed in a length (c 330 mm) of 108 mm diameter sample tube. The polished inner wall of the tube was lightly smeared with silicone grease in order to reduce side friction during consolidation. Top and bottom drainage was provided in the form of a sandwich of filter paper and metal gauze at either end (see Fig. 4.2).

Before introducing the slurry, the bottom drainage system was filled with distilled water and sealed. A little more water was then added, the tube tilted, and the slurry gently poured down the sides of the tube which was gradually rotated to ensure uniform distribution of the slurry. Great care was taken to avoid trapping any air bubbles. The slurry was added in layers about 50 mm deep. After each layer,a sample was taken for a water-content determination, and the tube rocked in order to level the surface. The object of the rocking described above was to try to eliminate transverse bedding structures from the final sample. Even when prepared from such a high water content slurry, thin sections prepared later showed that the final samples still retained some of the early structural features (also see Tchalenko, 1967). Although there is no evidence to suggest that they affect the behaviour of the sample, they may slightly confuse interpretation of thin sections prepared after the pile tests.

The tube full of slurry was then placed in a displacement-controlled press and consolidation was effected by compressing the sample at a variety of constant rates of displacement. These were selected, on the basis of a trial consolidation, to minimise excess pore pressures at the centre of the sample. The trial was conducted on a sample of half the normal height. Top drainage was provided, and pore pressures at the base were measured; the rates of compression were varied in order to control the excess pore pressures. The results of the trial are shown in Fig. 4.3.

The one-dimensional consolidation of samples was completed in about ten days. Free water was removed from the drainage systems and the tube taken from the press. The bottom cap was prized off and the sample gently slid out under its own weight. If the sample was not to be used immediately, it was wrapped in Cling-film and sealed with wax before being stored. The difference in water content between the top and bottom of the sample was generally less than 0.5%, which is equivalent to a reduction of axial stress down the sample due to friction of less than 5%; this was considered acceptable.

4.3.4 Consolidation in the Hydraulic Triaxial Cell

The one-dimensionally consolidated sample was trimmed to 102 mm diameter and to a length (around 150 mm) appropriate to the stress ratio to be employed in the subsequent consolidation (it will be recalled that the hydraulic piston had an available travel of only 15 mm). The sample was

then equipped with top, bottom and side drainage and transferred to the triaxial cell.

The stress paths followed by the samples during one-dimensional consolidation and subsequent removal from the sample tube are shown in Fig. 4.4, together with the limiting stress states imposed by the apparatus, the Kaolin and the test procedures followed. The one-dimensional consolidation is represented by the path OA, and the sample removal by AB. Path AB is assumed, as pore pressures within the sample were not measured. Thereafter further consolidation was imposed in the hydraulic triaxial cell, the aim being to produce a sample which behaved in a normally-consolidated fashion at the desired stress ratio.

After transferring a one-dimensionally consolidated sample to the hydraulic triaxial cell, small stress increments (approximately 10 kN/m^2) were applied until positive pore pressures were generated within the sample (this is illustrated by point Q in Fig. 4.4). The drainage system was then flushed with distilled water to remove as much air as possible. The stresses applied to the sample were then increased in steps of about 15 kN/m^2 every twelve hours until the final stress level, corresponding to a water-content of about 45% was reached (see path QJ in Fig. 4.4).

During consolidation the volume of pore-fluid expelled from the sample was measured by a 25 cc water-paraffin volume gauge which was vented to atmospheric pressure at the elevation of the centre of the sample. Changes in length of the sample were measured with the aid of a submersible LVDT. By using these two measurements, the ratio of total strain increments $(\dot{\varepsilon}_s|\dot{\varepsilon}_v)^T$ was monitored during consolidation and the approach of the sample to normally-consolidated behaviour at the imposed stress ratio observed. At first, as stresses were applied in the cell, the sample was strongly influenced by its earlier one-dimensional consolidation, and the approach to true normally-consolidated behaviour was asymptotic with increasing stress level. The effective stress levels were generally doubled during consolidation in the triaxial cell, at which stage the samples were regarded as being truly normally-consolidated at the relevant stress ratio. For further details of the use of stress-increment vectors to monitor consolidation, see Appendix 5.1.

Consolidation along stress paths close to active or to passive conditions result in large axial deformations of the sample, and the limited axial travel of the hydraulic piston meant that the stress ratios which could be employed in the test programme lay between the values of 0.6 and 1.6, at the water contents considered. The lines CD and EF in Fig. 4.4 represent the

limitations imposed by the restricted axial deformations. Further constraints on the available stress states were imposed by the clay behaviour during pile installation, and are considered later.

4.4 TESTS EMPLOYING NON-INSTRUMENTED, 'ZERO'-DISPLACEMENT PILES

4.4.1 Introduction

The aim of the first series of tests was to observe the behaviour, on loading, of model piles installed with a minimum of disturbance to either the fabric of, or the stress field within, the clay surrounding the pile. The principles behind the adopted pile installation procedure are discussed in Chapter 3, section 3, and the experimental details are considered below (the remainder of section 4.4 is applicable to the eight non-instrumented piles, and section 4.5 to the three piles instrumented to measure radial stresses).

4.4.2 Unloading the Sample

Once the sample had been fully consolidated within the hydraulic triaxial cell to the desired stress level, the volume gauge was isolated and the drainage system gently flushed through with air in order to remove as much free water as possible. The cell pressure was then reduced to zero in steps of 10-15 kN/m^2 whilst the height of the sample was kept constant, and undrained conditions maintained. The hydraulic piston was controlled (using a manually operated ram) such that the reading of the submersible LVDT connected between the top and the bottom of the sample, remained constant. The pressure of the fluid in the lower chamber of the hydraulic piston was monitored, so that the variation of the total axial stress with cell pressure could be determined. A typical unloading curve is presented in Fig. 5.4 where it may be seen that initially the slope of the curve is less than the theoretical 45°, but approaches 45° as the cell pressure is reduced further. Samples consolidated to stress ratios exceeding unity theoretically require a negative total stress to be applied on unloading. To provide for this, a vacuum system was available for connection to the drainage system. For this technique to be feasible, the theoretical negative stresses must be less than one atmosphere, and this requirement placed a further restriction on the absolute value of the deviatoric stress during consolidation. This is represented by line HJ in Fig. 4.4. In practice only small negative stresses were encountered. In order to minimise the possibility of cavitation during unloading, cell pressures were limited to about 260 kN/m^2, and this restriction is represented by line FG in Fig. 4.4.

4.4.3 Forming a Hole through the Sample

When the cell pressure had been reduced to zero, the plug was removed from the centre of the top-cap, thereby giving access to the sample. As the total radial stress acting on the sample had been removed, there was no tendency for the clay to extrude through the hole.

A drilling guide was mounted over the sample, and a 13 mm diameter hole was drilled down the centre-line of the sample, using a hand-turned twist-drill which was carefully advanced and then cleared in increments of about 15 mm. The waste clay was used to determine a water-content profile, from which the local undrained shear strengths may be determined. Typically, the water contents were uniform down the pile (± 0.5%) but there was evidence of slight swelling at the ends of the sample. Evidently not all the free water had been removed by flushing the drainage system with air.

Having formed the 13 mm diameter hole, the hydraulic system retaining the small piston in the lower platen was vented to atmospheric pressure, and the piston was pushed to the bottom of its chamber by means of a small diameter rod which was introduced via the top of the sample; care was taken to avoid out the rod touching the sides of the bore hole. The hole was then reamed to 15 mm diameter using a very sharp reaming tool. Throughout the drilling and reaming process the radial total stress acting on the sample was kept at zero so there was no tendency for the hole to collapse. The final hole was always very clearly cut, and it is shown in Chapter 6 that very little disturbance to the local soil fabric resulted from the drilling operations.

4.4.4 Introduction of a Non-instrumented Model Pile

The procedures described here are applicable only to the non-instrumented piles; the installation of instrumented piles was more complex and is considered in section 4.5.

Once a 15 mm diameter hole had been drilled through the sample, an 11.1 mm diameter brass core to a pile (which had been roughened) and de-greased was introduced, taking care to prevent the core from touching the sides of the hole. The core was then clamped at its top such that the centre of the 'packer' membrane was level with the base of the sample, as illustrated in Fig. 3.3. This bore-hole sealing membrane was then inflated with water, via the hole through the pile, to a pressure of about 35 kN/m^2 (the packer system was always tested before use, and the pressure required to seal a cavity 15 mm in diameter was determined experimentally).

4.4.5 Grouting the Pile in Place

To ensure that the final diameter of the pile was equal to that of the hole drilled through the sample, the brass pile-core was grouted into the hole using a very low shrinkage epoxy resin (Araldite CY 219, HY 219 and AY 219, 10% by weight). The grouting was effected using a syringe with a short length of small bore plastic tubing. The low viscosity resin was injected slowly down one side of the pile, with care being taken to avoid trapping any air bubbles. The hole was grouted to the top, the pile-core was vertically aligned and the resin left overnight to set.

4.4.6 Re-application of Total Radial Stresses to the Sample

Once the resin had set hard the cell pressure was increased, again in steps of 10-15 kN/m^2, to the original value. The height of the sample was still kept constant using the hand-ram, and the variation of axial total stress with cell pressure was recorded. Under these conditions, the axial stress acting in a sample having a Poisson's ratio of 0.5 would return to its initial value, and no rigid inclusion effects would result around the pile (if the latter were to occur, they would tend to increase the radial stress acting on the pile; see Jaeger and Cooke, 1977). In practice, however, the axial stress seldom returned exactly to the initial value. Nevertheless, these stresses were not 'corrected', for to have done so would have implied some axial displacement of the sample, and therefore relative movement between the clay and the now rigid pile.

A device was developed to enable the radial stresses acting on the side of a pile during installation and during loading to be measured. The radial stresses on two piles (Tests 15 and 17) were measured during the installation process, and the results showed that the final radial stresses were within about 4% of the cell pressure. This confirms that the pile installation procedure did not cause a significant change in the local stress field. Such disturbance as there was seems to have been repeatable, as illustrated by the pile load-displacement curves from four similarly prepared samples (see Fig. 5.14).

4.4.7 Pile Loading Procedure

After allowing the sample, with its included pile, to settle for about 24 hours following the re-application of the cell pressure, the pile was loaded axially at a constant rate of displacement using the equipment

described in Chapter 3, section 3.4.5.

The selected rate of pile displacement was c 0.25 mm/hour, with the result that peak conditions were achieved after about 9 hours. As is shown in Appendix 4.2 this rate of loading was sufficiently slow to ensure that the pile loading was fully drained. It may be of interest to note that for the pile to be loaded under undrained conditions (i.e. less than 5% dissipation of excess pore pressures at the pile face), peak conditions would need to be achieved within about one second!

During the drained pile loading, the load-displacement behaviour was accurately monitored, and most of the tests were continued to a displacement of about 12 mm by which stage residual conditions were attained. Some tests were stopped at earlier stages in the loading so that thin sections could be prepared.

At the end of each test, the sample was unloaded under the same conditions as those used when installing the pile. The cell was disassembled and the dimensions of the sample, and water contents within it were determined. The sample was then trimmed and placed in a bath of Carbowax so that thin sections could be prepared from the material adjacent to the pile-clay interface. Because of the need to avoid disturbing the clay in the vicinity of the pile, it proved difficult to obtain accurate measurements of water contents adjacent to the pile face.

4.5 PILES INCORPORATING A DEVICE FOR MEASURING RADIAL STRESSES

4.5.1 Introduction

As described in Chapter 3 (section 3.4.4.3) a device was developed to enable the radial stresses acting on the side of a model pile to be measured during pile installation and loading. Because of the importance of avciding disturbance to the soil during pile installation, the device was constructed on similar lines to a pressuremeter. The main requirements of the device were that it should be hydraulically as stiff as possible (and therefore thoroughly de-aired), be securely sealed against leakage, and be capable of resisting longitudinal shear stresses.

4.5.2 Assembly of the Pile Core

For the ease of construction and assembly, the pile-core was made in three sections, which are illustrated in Fig. 4.5(a);

(i) the bottom section accommodated the 'packer'-membrane which sealed the cavity in the lower platen of the triaxial cell to prevent the ingress of epoxy resin. The hydraulic connection for inflating the membrane was made from hypodermic steel tubing because of the limited space within the pile core;

(ii) the central section was designed to incorporate the radial stress sensing element. Stainless-steel hypodermic tubing was used for the hydraulic connection between the sensing element and the pressure transducer both for reasons of space and more particularly to ensure the greatest possible hydraulic stiffness.

(iii) The top section was required to accept the pile loading cap and to permit the two stainless-steel tubes to leave the pile.

The three units were made separately, and then connected with Loctite (Retainer); see Figs. 4.5(a) and (b).

4.5.3 De-airing of the Hydraulic System

The two hyperdermic tubes were connected to their respective hydraulic systems. In Tests 7 and 15, the pressure transducer assembly was de-aired by flushing continuously with de-aired water at a pressure of 1000 kN/m^2 for a period of weeks, whereas the hypodermic tubing was de-aired by flushing at atmospheric pressure. In Test 17, the pile core was sealed into a brass tube which was filled with de-aired water and was provided with a separate hydraulic fitting. The whole system, including the hypodermic tubing and the pressure transducer block was pressurised to 1000 kN/m^2 and continuously flushed with de-aired water under a small differential head for several days.

4.5.4 Fitting a Membrane to the Central Section of the Pile

In order to prevent air from entering the measuring system, the following operations were all effected under de-aired water, and de-aired water was continuously flushed through the hypodermic tubing connected to the central section. The brass pile-core was removed from the brass tube. The 'O' ring grooves and binding sections on the middle section of the pile

were lightly smeared with silicone grease, and a length of membrane (prepared as described in Appendix 3.1) was slipped along the pile and into place. The 'O' rings were then fitted, and the membrane was further sealed with the aid of whipping cotton (this may be seen in Fig. 4.5(c)).

4.5.5 Calibration of the Membrane

The membrane was inflated (unconfined) several times to ensure that there were no obvious leaks. The pile was inserted into a glass tube of 15 mm diameter (the same as that of the final pile) and the membrane was inflated to a variety of pressures and the length of the membrane in contact with the tube was noted. This procedure was repeated several times, and a pressure sufficient to induce a profile such as that shown in Fig. 4.5(c) (with about 20 mm in contact with the wall of the tube) was selected for later use. The results and interpretations of the calibrations are provided in Chapter 5.

4.5.6 Attachment of shear reinforcement

The brass core of the pile was roughened with the aid of a file, and carefully degreased. About 40 lengths of flattened, annealed, copper wire were then attached to the central section of the pile in the form of the 'Chinese-Lantern' shown in Fig. 4.5(d). The pile was now ready to be installed into the sample.

4.5.7 Pile Installation

The sample preparation up to this stage was exactly the same as for the tests incorporating non-instrumented piles. The instrumented pile core was inserted into the 15 mm diameter hole drilled through the sample, and the lower membrane inflated. Epoxy resin was then injected until the measuring system had been covered. After a short delay to allow time for any possible air bubbles to rise to the surface, the central membrane was slowly inflated to the pressure determined during the calibration. A small bleed hole through the brass core between the two membranes ensured that resin was not trapped under pressure. The annular gap between the hole and the pile core was then grouted to the top of the sample, and the system was left overnight for the resin to set.

4.5.8 Re-application of Total Radial Stress to the Sample

The radial stress measuring system was isolated from the pressure supply, and an increment of cell pressure applied to the sample. As described in Chapter 3, section 3.4.4.3, the response of the measuring system was observed, and small changes to the pressure within the device were imposed according to the behaviour of the device. The device was again isolated and a further increment of cell pressure applied. The process was repeated until the original cell pressure was reached. For details of the responses of the radial stress measuring devices, and the corresponding corrections, reference should be made to the descriptions of Tests 15 and 17 in Chapter 5.

4.5.9 Pile Loading

After the re-application of the cell pressure to the sample, it was left for about one day to settle.

The pile was then loaded as described in section 4.4.7, except that the radial stress acting on the pile was also measured. Reference should again be made to the descriptions of Tests 15 and 17, in Chapter 5.

4.6 TESTS EMPLOYING FULL-DISPLACEMENT PILES

4.6.1 Introduction

A set of three tests (Nos. 16,18,19) was performed to examine the nature of micro-fabric changes around,and the load-displacement behaviours of, driven and jacked piles. The results were compared with those obtained from tests on piles installed with minimal disturbance, and with field observations.

The Kaolin samples were prepared by the methods described in section 4.3, and were normally-consolidated to a stress ratio, K, of 0.7. The sample dimensions were the same as those used in the earlier tests, and so the ratio of sample diameter (102 mm) to pile diameter (15 mm) (see Chapter 3, section 3.4.4(c)) was just less than seven. This value is somewhat low for accurate modelling of the effects of installing full displacement piles (according to cavity expansion theory; see Randolph, Carter and Wroth, 1979), and this must be recalled when interpreting the results of the loading tests. However, the micro-fabric close to the pile is unlikely to have been influenced by this limited ratio of diameters.

4.6.2 Driven Piles - Introduction

The intention behind the installation procedures was to ensure that the peak rates of pile penetration during driving were of the same order as those which may occur amongst full-sized piles (for instance, the results presented by Dolwin, Leonard and Poskitt (1979) indicate velocities of the order of two metres per second). No attempt was made to ensure that the overall pile installation process was undrained, for to have done so would have required the pile to be driven in a matter of seconds.

In Test 16, the pile was driven to the mid-height of the sample, so that soil deformation patterns around the toe could be observed (by means of thin-sections). The pile in Test 18 was driven through the sample into the cavity in the bottom platen of the hydraulic triaxial cell. After allowing full consolidation of the Kaolin sample, the pile was slowly loaded to residual conditions, after which thin sections were prepared.

4.6.3 Pile Driving

The equipment used for pile driving is illustrated schematically in Fig. 4.6. It consisted of a steel rod (about 1 m long) which was attached to the pile and held in guides to prevent wobble during driving. Hollow cylindrical weights (c 0.5 kg each) were allowed to slide down the rod and to hit a collar incorporating a micro-switch which triggered a two-trace storage-oscilloscope. The load on the pile was measured using a standard Imperial College load cell (450 kg) and the displacements were monitored with the aid of a long throw LVDT. The results of each blow were recorded on the oscilloscope screen which was then photographed (typical results are shown in Chapter 5). No attempt was made to make the monitoring equipment more sophisticated because the main objective was only to obtain an estimate of the peak rates of pile penetration.

The piles were driven whilst the Kaolin sample was subject to its full consolidation stresses. In order to avoid extrusion when the plug in the top-cap was removed in order to introduce the pile, the sample was unloaded in exactly the same manner as described for the 'zero-displacement' piles. The plug was removed and replaced by the tip of the pile to be driven. The pile was prevented from moving upwards and the stresses were re-applied to the specimen. After allowing the sample to settle for a day the pile was driven. It is suggested for future research that the plug be replaced by the pile from the start of consolidation in the triaxial cell.

During driving, the piles were advanced about two millimeters per blow, the energy of each blow being varied in order to maintain this penetration. Some seventy blows were therefore required to drive the pile in Test 18. This process took about thirty minutes and so the driving cannot be considered to have been undrained. The operation would have been speeded-up considerably had the ultra-violet recording oscilloscope (used for fast ring-shear tests) been available.

After driving the pile in Test 18 to the base of the sample, the pile was restrained whilst a brass rod was pushed through the pile in order to aid the retraction of the piston in the bottom platen. The cavity created was vented to atmospheric pressure so that the pile end-bearing resistance could again be eliminated.

The sample was left overnight to consolidate fully before the pile was loaded (see Steenfelt, Randolph and Wroth (1981) for measurements of the rates of dissipation of excess pore-pressures around displacement piles in Kaolin). Pile loading was conducted in the manner described in section 4.4.7. After the tests, the samples were unloaded and thin sections prepared. Water-content determinations within the Kaolin were made but, as mentioned earlier, the measurement of water contents very close to the pile was hampered by the need to avoid fabric disturbance that would influence the thin sections.

4.6.4 Jacked Pile - Introduction

The rate of installation was selected to be intermediate between the rate of loading employed in the tests on 'zero displacement' piles (4×10^{-3} mm/min) and the peak rate of penetration during pile driving (10^{5} mm/min). The pile in Test 19 was jacked at a mean rate of 4 mm/min, giving a total time for installation similar to that of the driven piles. After allowing full consolidation, the pile was slowly loaded to residual conditions. The main objects of the test were to observe the micro-fabric changes induced around the pile, and also the shape of the load-displacement curve.

4.6.5 Pile Jacking

The pile was jacked using an extended restrained worm-gear, driven through a reduction gear-box by an electric motor. The pile was restrained by vertical guides to prevent wobble during jacking and to ensure that the pile tip accurately located the piston in the lower platen. The pile construction (described in Chapter 3, section 3.4.4.4) was similar to the piles driven in Tests 16 and 18, and included a 3 mm diameter hole through the

centre to facilitate the retraction of the piston in the bottom platen; the hole through the pile was closed during pile installation.

The jacking force was measured during the installation but, unfortunately, the brass extension to the pile (which was used to assist guidance) snagged with the main guide which was below the load cell, and so the load readings were not reliable.

Once jacking was complete, the piston in the lower platen was retracted, the cavity vented to atmospheric pressure, and the sample left overnight to consolidate.

The pile was load-tested in exactly the same manner as the tests described previously, and thin sections were prepared.

4.7 THIN-SECTION PREPARATION

4.7.1 Introduction

The technique for the preparation of thin sections will not be described in detail as it was similar to that employed by Tchalenko (1967). In principle, the 'wet' sample of Kaolin was immersed for three weeks in a bath of warm (60°C) Carbowax 6000 (Polyethylene glycol, molecular weight ~6000), which is completely miscible with water. Water was able to diffuse out of, and Carbowax into, the sample until eventually the pores in the sample were filled with wax-rich pore fluid. On removal of the sample from the warm bath, the wax inside the sample solidified, and the sample could thereafter be treated as a rock specimen. Thin sections were prepared using paraffin as the coolant/lubricant (not water!).

4.7.2 Impregnation Procedure

At the end of a pile test, a parallel sided diametral slice about 25 mm thick was cut from the centre of the sample so as to include the pile (see Fig. 4.7). The specimen was placed in a tightly fitting box made from three sections of coarse steel gauze and the box was then wired together. The sample was then immersed in a large bath of Carbowax (the volume of fresh wax employed was about 20 times that of the sample to be impregnated). The sample was turned over regularly, and the wax stirred frequently, particularly in the first few days. After about three weeks, when the sample was fully impregnated, it was removed from the wax bath and allowed to cool slowly for at least one day before thin sections were prepared.

4.7.3 Preparation of Thin-Sections

The hard sample could now be cut with a diamond saw, and ground and polished in the same manner as a rock specimen. However, as the impregnating wax is miscible with water, great care was taken to prevent water from reaching areas of the sample from which the final thin sections were required. Although the primary cutting could have been performed using oil or paraffin rather than water as a coolant, the latter was selected for reasons of health. However, the final grinding was always performed using paraffin.

A typical cutting and grinding sequence for a specimen is illustrated in Fig. 4.8. Having selected a piece for thin sectioning, the brass core of the pile was removed, leaving the epoxy resin still in contact with the clay (if possible). The removal of the brass core is an important aspect of the procedure, because the resin and the impregnated specimen when ground/polished both wear at a similar rate, whereas the brass core would wear more slowly. Preliminary trials showed that the retention of the brass (or the use of a brass pile) resulted in tapering thin sections which did not appear uniform under polarised light, and were, therefore, difficult to photograph and interpret.

Thin sections were prepared from the cut sections in a manner similar to that described by Tchalenko (1967). The author is very grateful for the services of Mr. Kevin Schrapel of the Geology Department at Queen Mary College, London who prepared the numerous thin sections with such skill.

4.7.4 Observation of Thin Sections

The microscope employed during this investigation is described by Tchalenko (1967) and is a standard 'geological' microscope, incorporating a light-sensitive cell to aid photography. A 35 mm camera was connected to the microscope. Photographs were generally taken at the lowest magnification (x 3 objective), using 125 ASA black and white film (FP4). Frequently, however, it was found that the overall magnification was excessive for the present purposes, and a system suitable for macro-photography was employed. Towards the end of this research, the macro-photography system was made so versatile that the use of the microscope was largely superseded.

Table 4.1: Speswhite Kaolin

(a) General Description

Type	Speswhite fine china clay
Visual appearance	White and floury when dry
Unified classification	'CH' - inorganic clay of high plasticity

(b) Chemical Analysis (from manufacturers)

Constituent	%
SiO_2	46.2
A_2O_3	38.7
Fe_2O_3	0.56
TiO_2	0.09
CaO	0.2
MgO	0.2
K_2O	1.01
Na_2O	0.07
Loss on ignition	13.14

(c) Physical Properties

Property	Symbol	Value	
		This Study	Other Workers
Plasticity index	PI	30	31[1]
Plastic Limit	PL	32	38[1]
Liquid Limit	LL	62	69[1]
Specific Gravity of Solids	G	-	2.61[1] 2.60[2]
Clay fraction	% < 2μ	-	82[2]

Note: Superscript 1 refers to Steenfelt, Randolph and Wroth (1981)
" 2 " " Yong (1979)

Table 4.2: Strength and Consolidation Properties of Speswhite Kaolin

Property	Definition	Value		
		This Study	Comments	Other Workers
Slope of Critical State Line (C.S.L.) (Triaxial compression)	M	0.9	-	0.9[1]
Angle of shearing resistance in triaxial compression	ϕ'_{TC}	~23°	-	~23°[1]
Residual angle of shearing resistance	$\phi'_r = \tan^{-1}(\tau/\sigma'_n)_r$	11.5° - 12°	See Appendix 4.1	
Slope of consolidation lines	$\lambda = -\frac{de}{d(\ell nP')}$	$0.25 \geq \lambda \geq 0.23$	$5 \leq P' \leq 50$ kN/m^2	0.25[1]
		$0.23 \geq \lambda \geq 0.21$	$50 \leq P' \leq 200$ "	0.24[2*]
		$0.21 \geq \lambda \geq 0.18$	$200 \leq P' \leq 350$ "	
Slope of swelling lines	$K = -\frac{de}{d(\ell nP')}$	0.04	$10 \leq P' \leq 350$ "	0.04[2*]
Void ratio at effective pressure P' = 1 kN/m^2	(e_λ) (1-D consolidation)	2.52	$50 \leq P' \leq 100$ kN/m^2 (1-D Consolidation Tube)	2.58[1]
Coefficient of consolidation	C_v ($= k/\gamma m_v$)	5 - 10 m^2/year	1-D Consolidation	16 m^2/yr[1]
		5 - 10 m^2/year	Triaxial Consolidation $50 \leq P' \leq 300$ kN/m^2	8-13.5 m^2/yr[2] ($54 \leq P' \leq 430$)
Coefficient of swelling	C_s	22 m^2/year	P' = 250 kN/m^2	31[1] m^2/yr
Coefficient of 'at-rest' earth pressure	K_o	0.65 ± 0.01	Determined by observing strain increment vectors (Appendix 5.1)	0.64 ± 0.01[2]

Notes: Superscript 1 refers to Steenfelt, Randolph and Wroth (1981)

" 2 " " Yong (1979)

" 2* means result derived from data presented by Yong (1979)

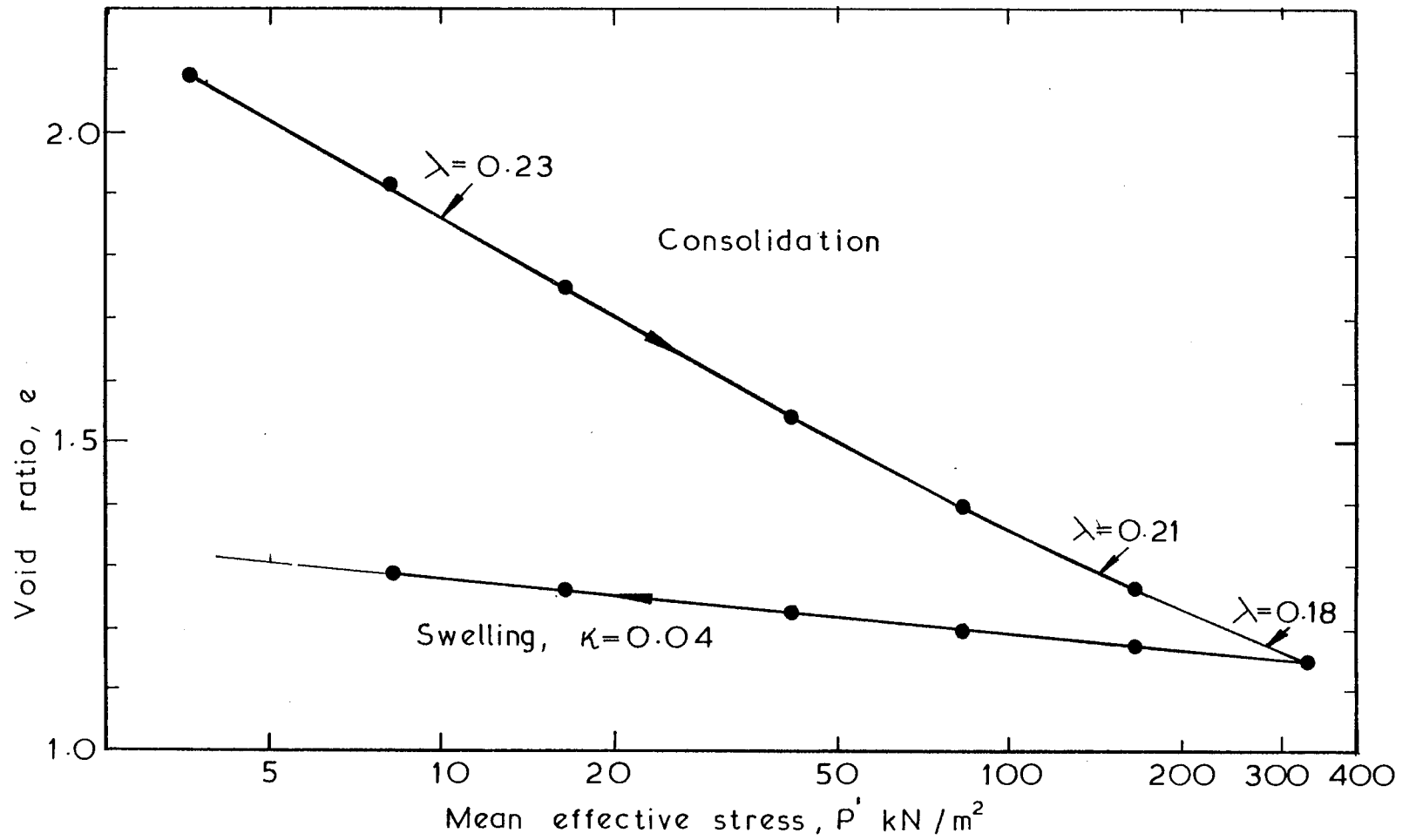
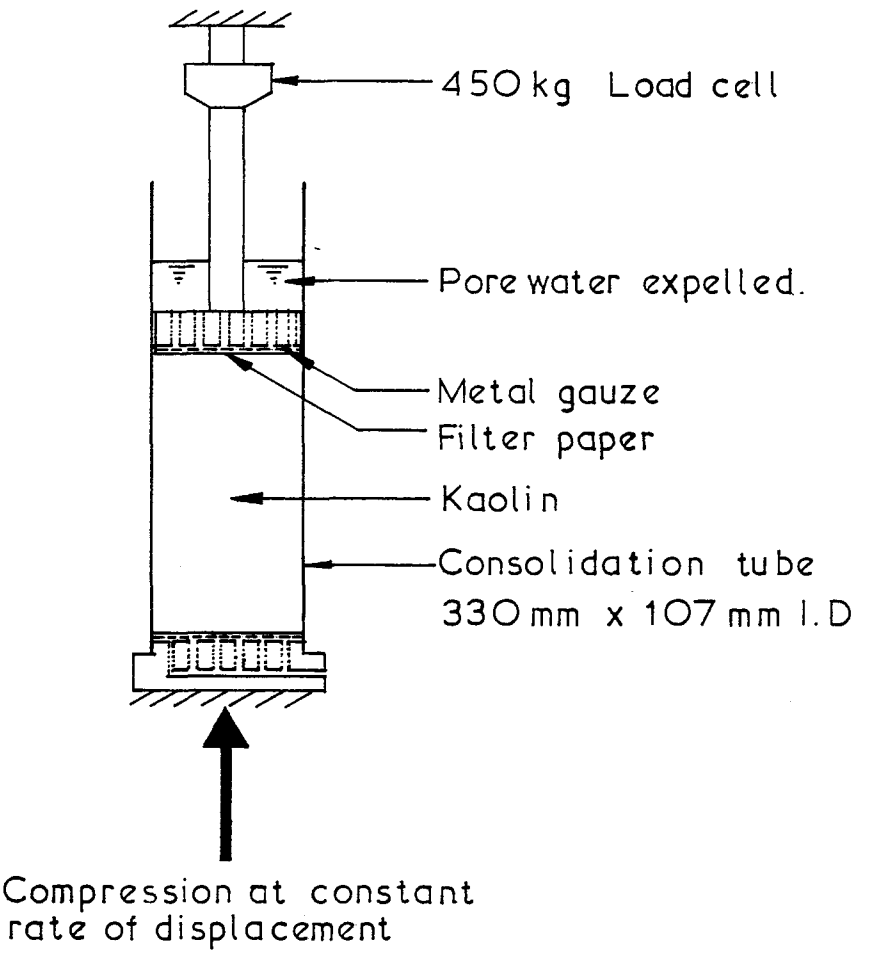


Fig. 4.1

Relation between void ratio and mean effective stress. One-dimensional consolidation



Schematic view of the apparatus for one-dimensional consolidation of samples.

Fig. 4.2

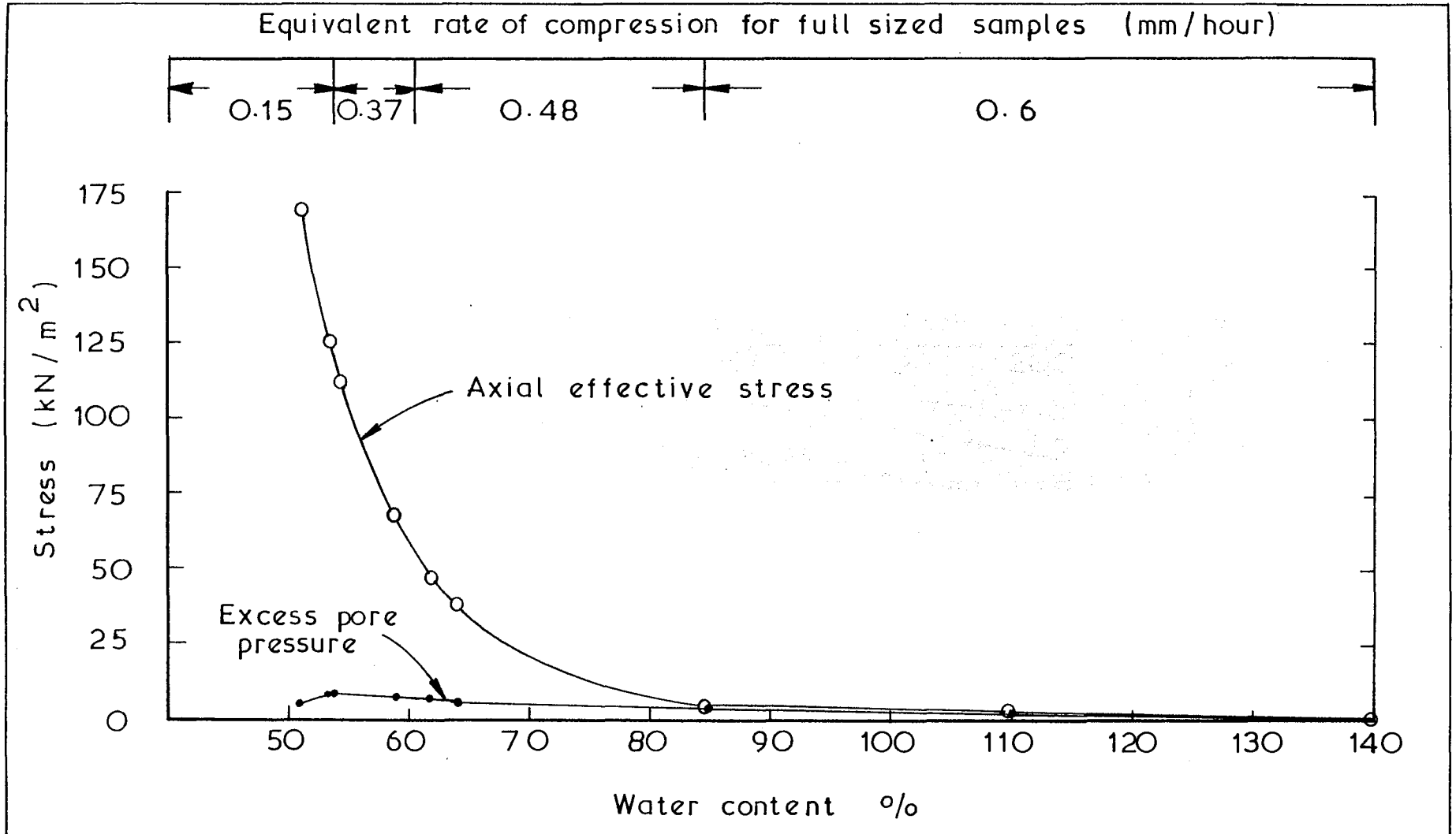
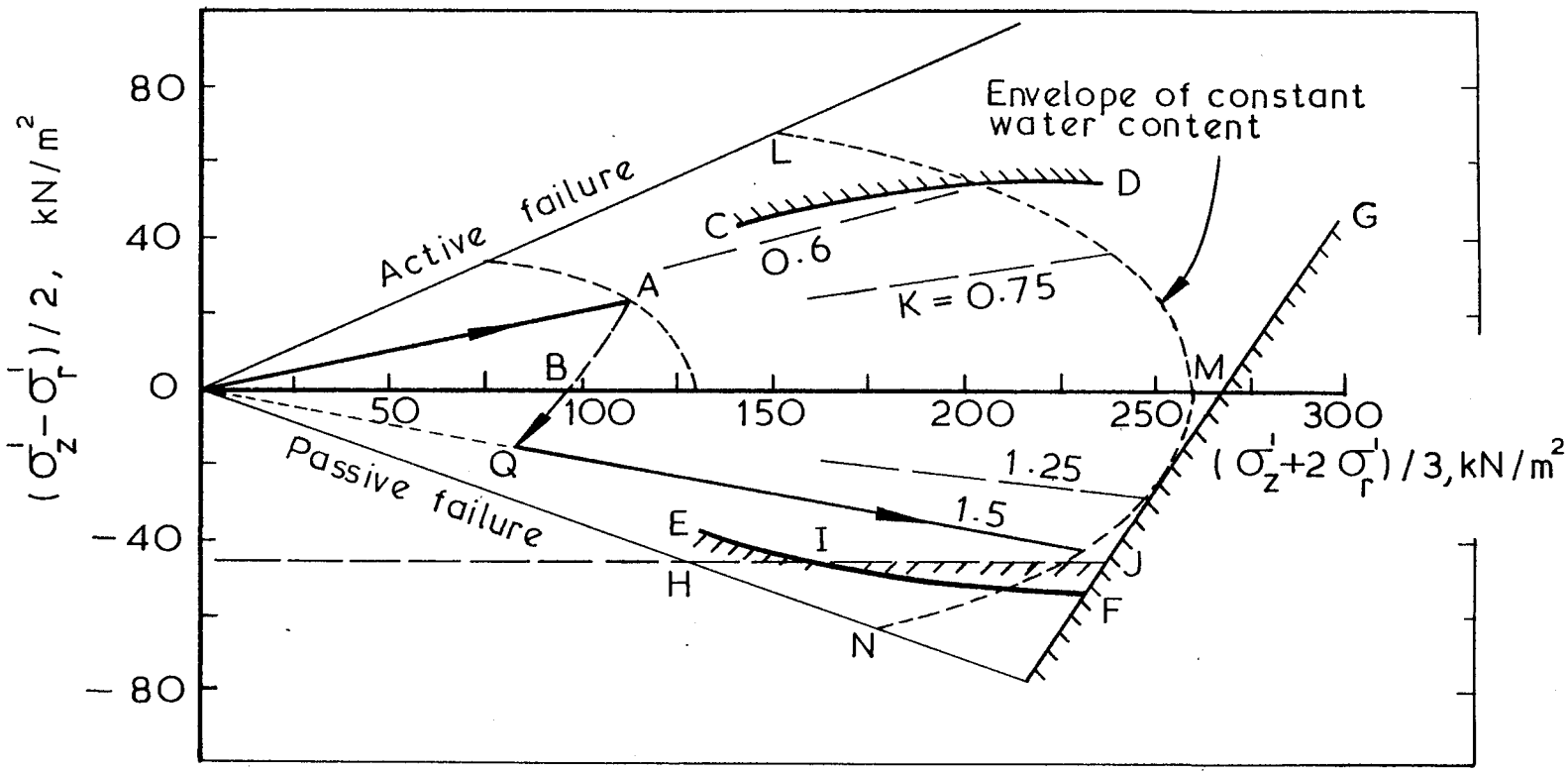


Fig. 4.3

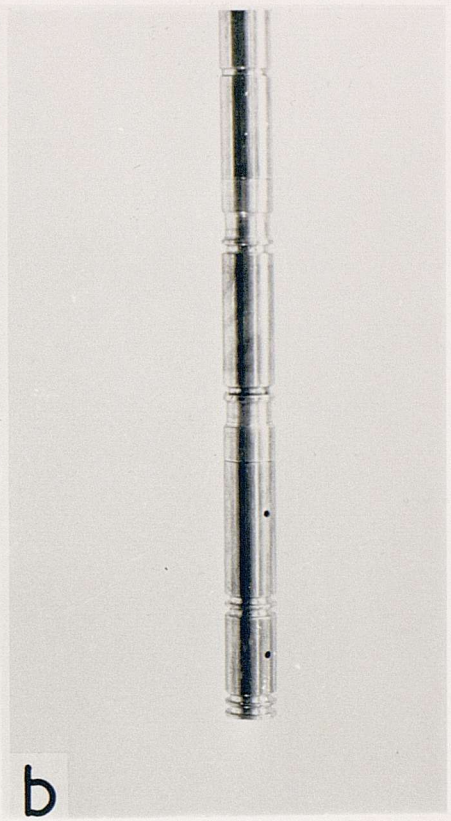
Results of a trial consolidation to establish suitable rates of compression

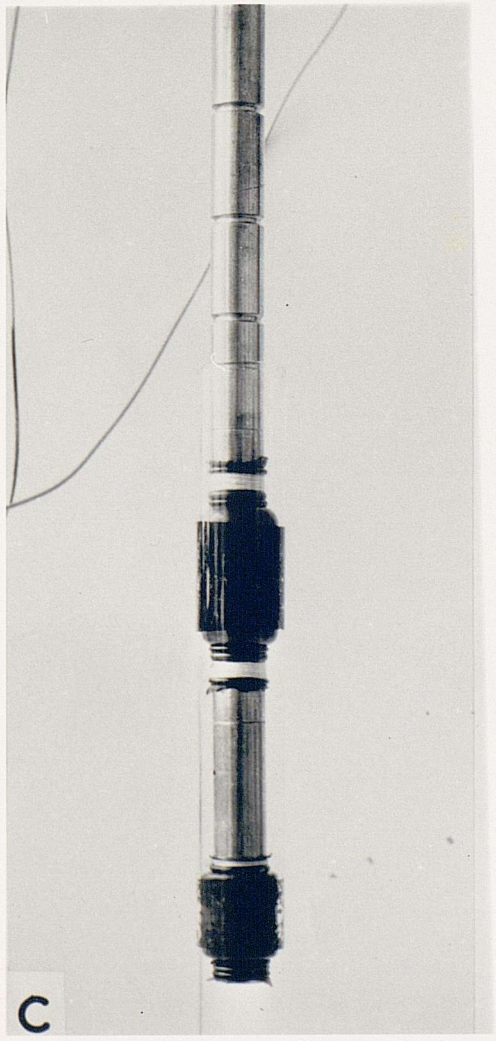


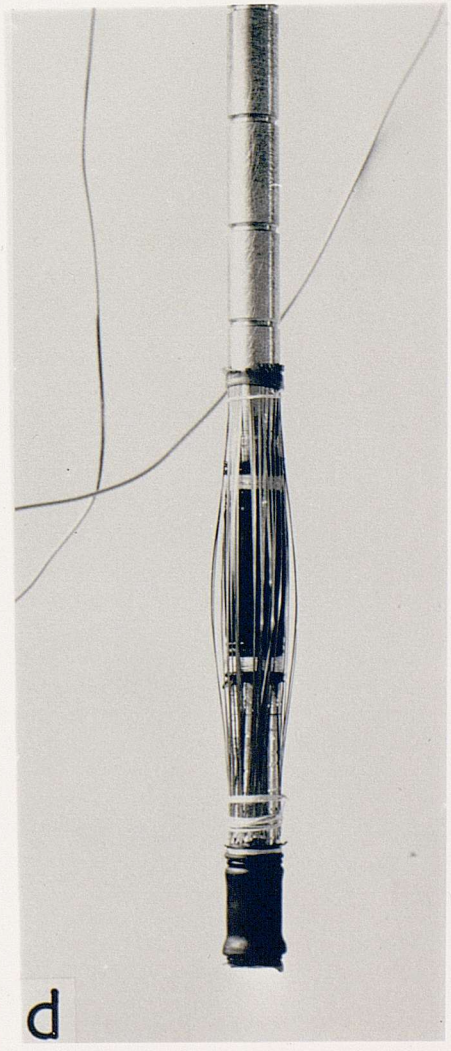
Stress paths available during consolidation of kaolin samples

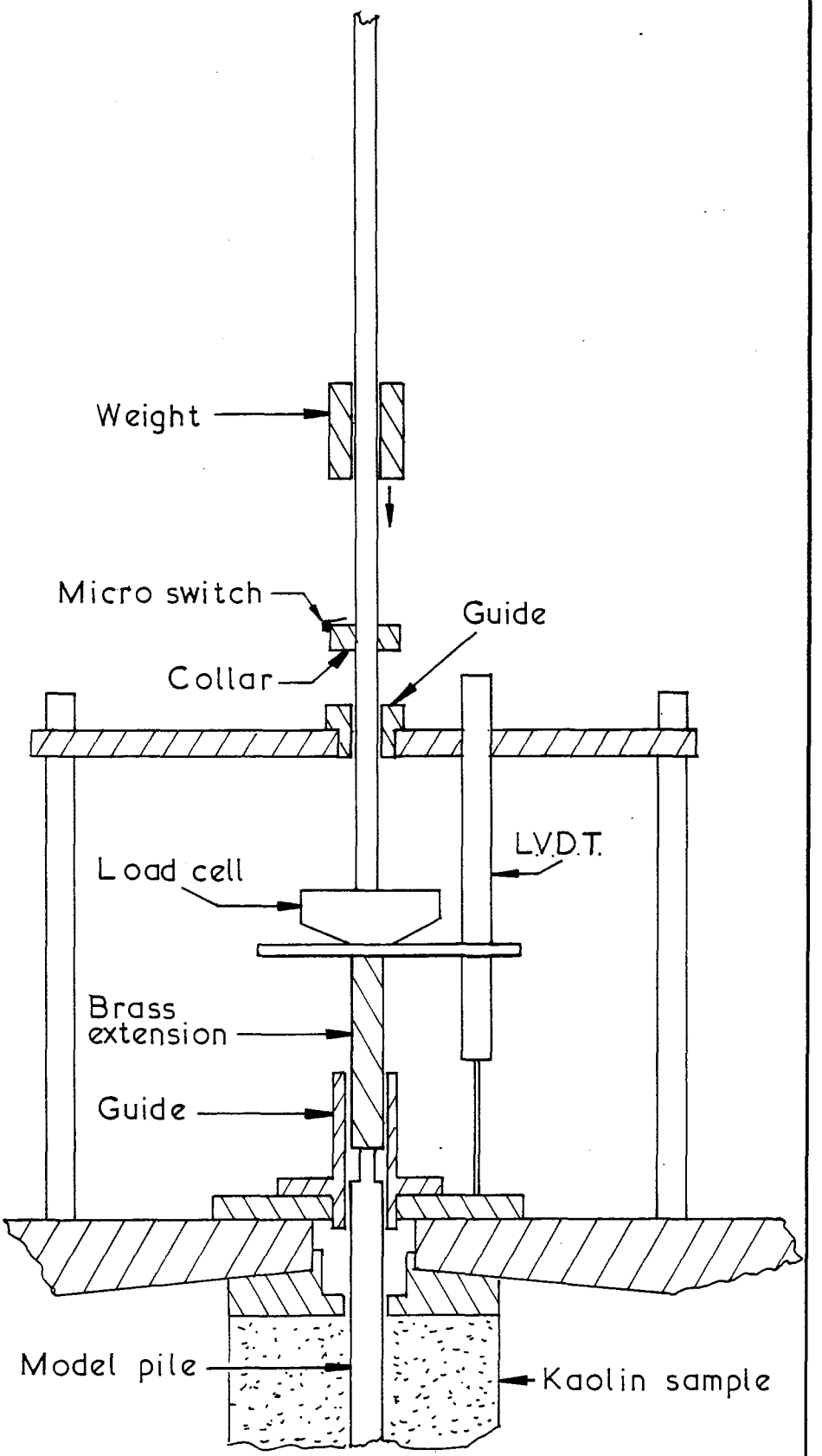
Fig. 4.4


20 mm
a


b

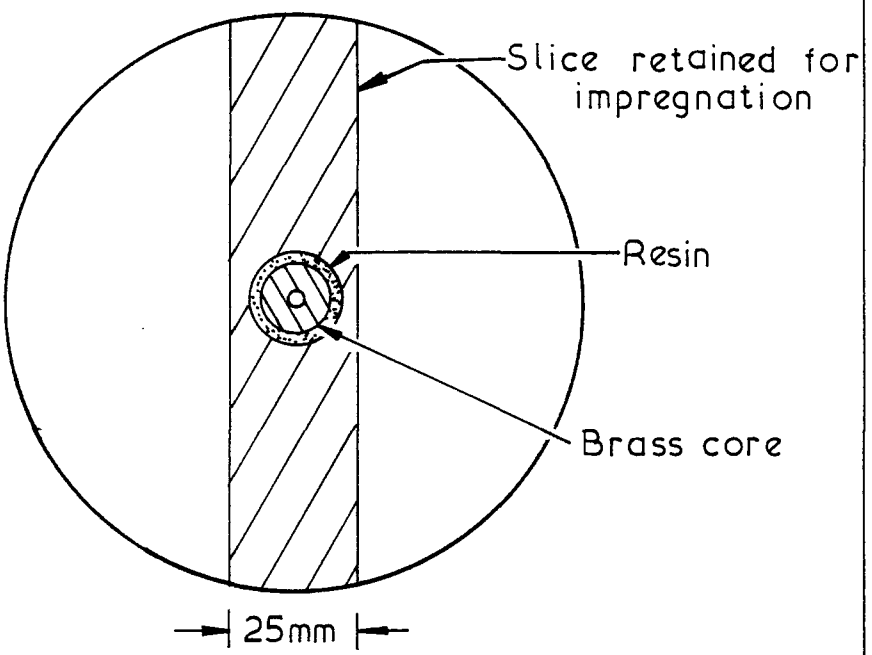

c


d



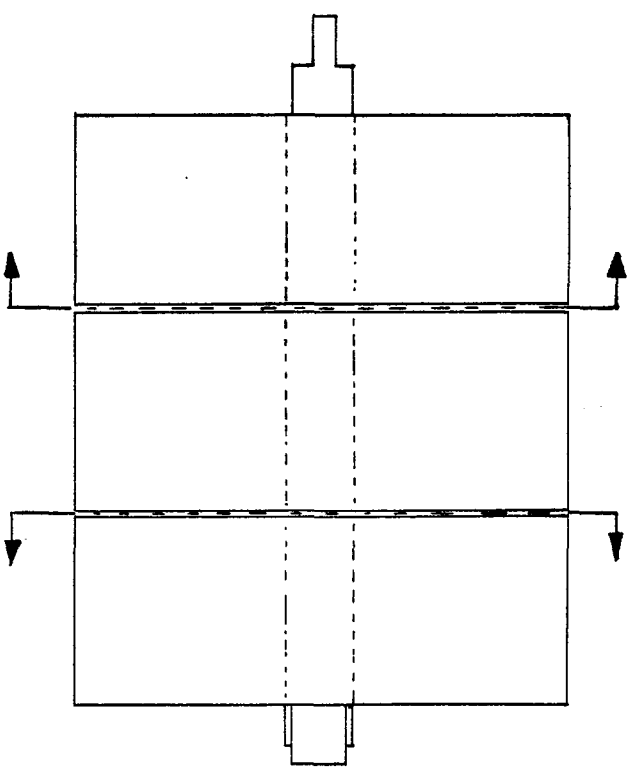
Schematic view of apparatus for driving model piles

Fig. 4.6



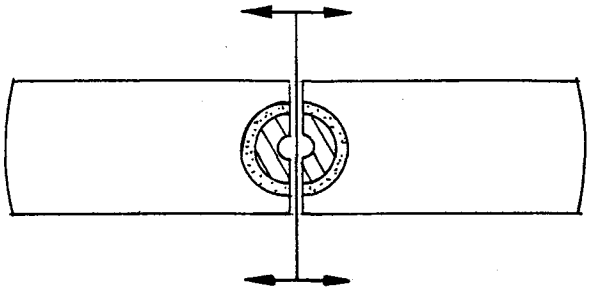
Cross-section through a sample illustrating the trimming prior to impregnation

Fig. 4.7

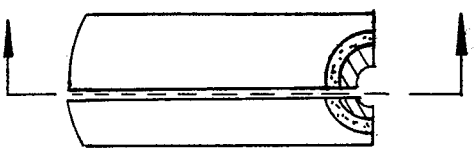


Separating the impregnated sample into three sections

Fig. 4.8(a)

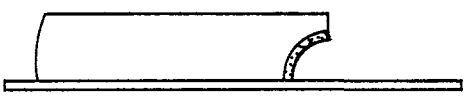


(b)



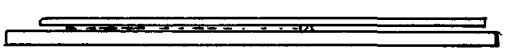
Cut off-centre

(c)



Brass core removed ; cut surface ground , polished and stuck to a microscope slide

(d)



Top surface ground and polished ; cover slip attached

(e)

Illustration of the stages involved in preparing a longitudinal thin section through a pile

Fig 4.8 cont'

APPENDIX 4.1

RESIDUAL SHEAR STRENGTH OF KAOLIN

Introduction

Ring shear tests were performed with J.F. Lupini to examine the residual strength of Speswhite Kaolin, with particular reference to effect of rate of shearing. The results of this work are presented in Lupini (1980), but they are briefly considered below for the sake of completeness.

Direct shear box interface tests were performed, which involved shearing Speswhite Kaolin against flat surfaces of the same epoxy resin as that used to grout the model piles. Although the apparatus was rather crude, the results are of some relevance to the model pile tests and are considered below.

Ring-Shear Tests

The Kaolin was consolidated from a slurry which had a water-content of 132%. The first drained shearing was effected at a normal effective stress of 352.2 kN/m^2, and the residual angle of shearing resistance was found to be 12.3°, at a rate of displacement of 0.015 mm/min (this is about four times faster than the drained loading rate selected for the model pile tests). The normal effective stress was increased to 519 kN/m^2, and the residual angle of shearing resistance was found to lie between 11.3° and 11.8° (at a rate of 0.015 mm/min).

Further testing of the sample was performed to investigate the influence of the rate of shearing on the residual strength of the Kaolin. Rates of displacement between 0.0001 mm/min and 130 mm/min were employed. The tests conducted at displacement rates of up to 3.6 mm/min were continued for a time (> 10 mins) sufficient for any excess pore pressures generated near the residual surface to dissipate. However, the test at 130 mm/min was only continued for 5 minutes because of the loss of clay associated with the large displacements. For this reason, one cannot be sure that the results were not still influenced by excess pore pressures.

The residual shear strengths obtained during shearing at a variety of rates of displacement are shown in Fig. A.4.1.1 where it may be seen that the shear strength increases with the rate of displacement, particularly at

speeds in excess of 0.1 mm/min. On completion of stages conducted at speeds greater than 0.015 mm/min, the sample was allowed to consolidate fully and was then reloaded at a rate of 0.015 mm/min and the response observed. A small peak was observed during the reloading, after which the strength decreased to the residual value determined previously at a rate of 0.015 mm/min. The observed peak strengths are plotted in Fig.A.4.1.1, and the presence of such peaks suggests that the rapid shearing has caused a non-transient change in the structure of the residual shear surface, but that on further slow shearing the surface returns to a residual condition appropriate to the new rate of shearing. The difference between the strengths observed during rapid shearing and the peak values observed on slowly re-shearing the sample represent a transient increase in strength. This will be influenced by viscous forces acting within the clay and also by any excess pore pressures remaining during shearing.

Further information about the effects of rate of shearing on the residual strength in clays may be found in Lupini (1980) and in Appendix 5.3 of this dissertation. The tests described in Appendix 5.3 were performed to investigate the nature of the transient increase in strength of natural soil from Panama.

Direct-shear Interface Tests

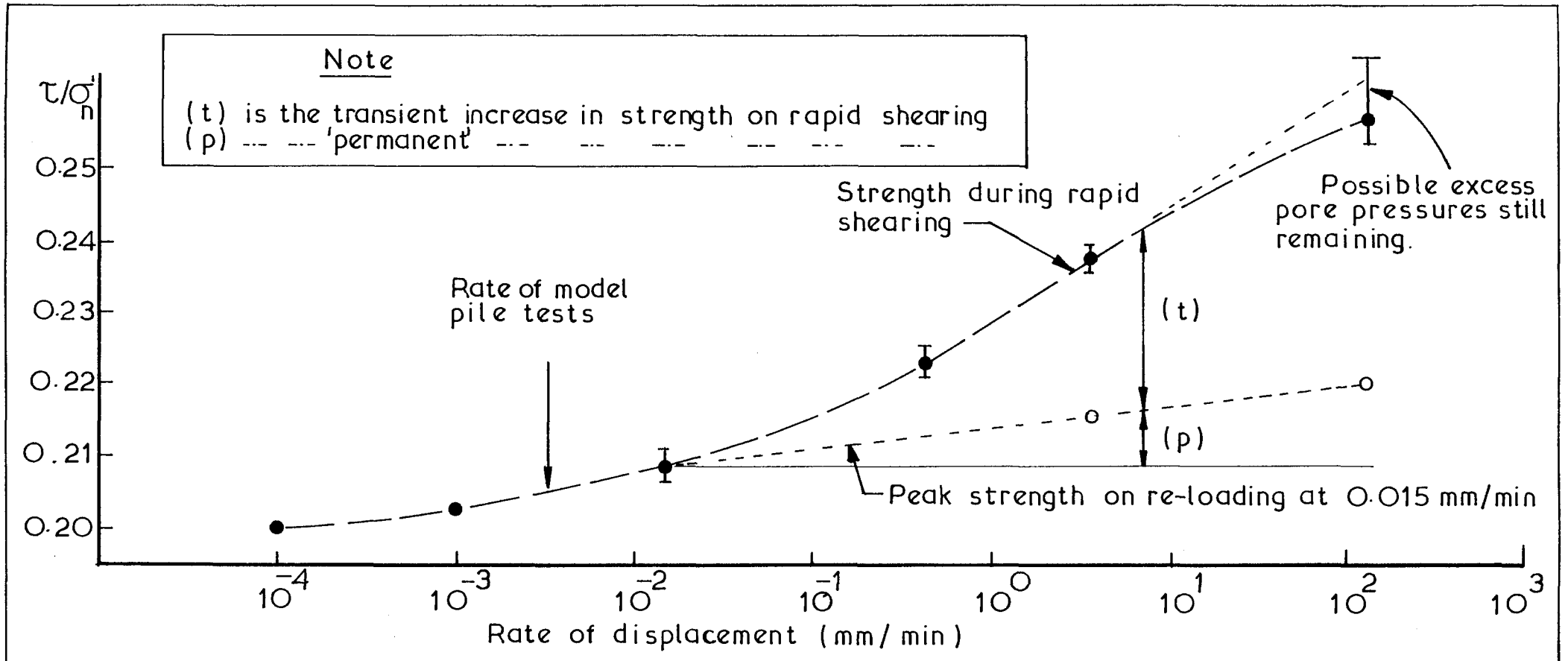
Speswhite Kaolin was sheared against interfaces made from the epoxy resin used in the model pile tests, in direct shear boxes. The Kaolin was consolidated from a slurry against the interface to a normal stress of about 250 kN/m^2, and then sheared at a drained rate of 0.015 mm/min.

A typical result of such tests is shown in Fig. A.4.1.2 where the ratio (τ/σ'_n) is presented as a function of the relative displacement. It may be seen that the peak strength was achieved after a displacement of just under two millimeters, and that residual conditions were achieved, in this case, within about four millimeters. In the various tests performed, the displacements required to reach residual conditions varied between 3.5 and 7 mm, tending to increase with increasing surface roughness. Littleton (1976) presents similar results from interface tests involving Kaolin and an illitic clay being sheared against steel interfaces.

The peak angle of shearing resistance determined in the course of the interface tests varied between 17° and 19°, and was probably influenced by the fact that the Kaolin slurry was consolidated against the interface. The residual angles of shearing resistance varied between 10.5° and 12°,

the higher value corresponding to roughened surfaces. The ring shear tests together with the interface tests suggest that the residual angle of shearing resistance appropriate to the conditions obtaining in the model pile tests is between 11.5° and 12°.

An understanding of the behaviour of soil sheared against rigid interfaces is believed to be of great importance to pile design, and is currently being studied at Imperial College.



Effects of the rate of displacement on the residual strength of Speswhite kaolin ($\sigma'_n = 518.9$ kN/m^2)
(from data presented in Lupini, 1980)

Fig.A 4.1.1

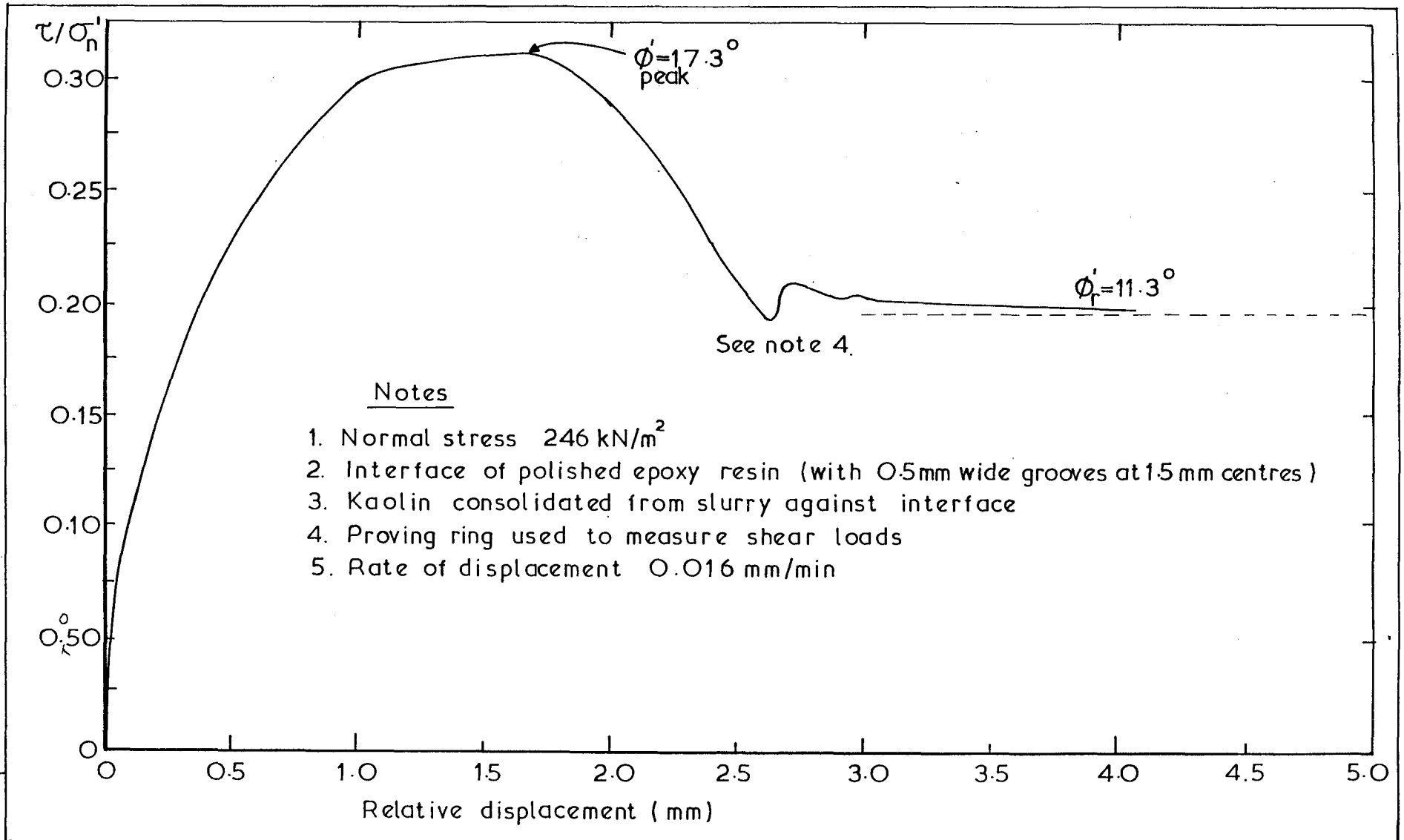


Fig. A. 4.1.2

Typical result from an interface test using Speswhite kaolin

APPENDIX 4.2

SELECTION OF THE RATE OF PILE LOADING

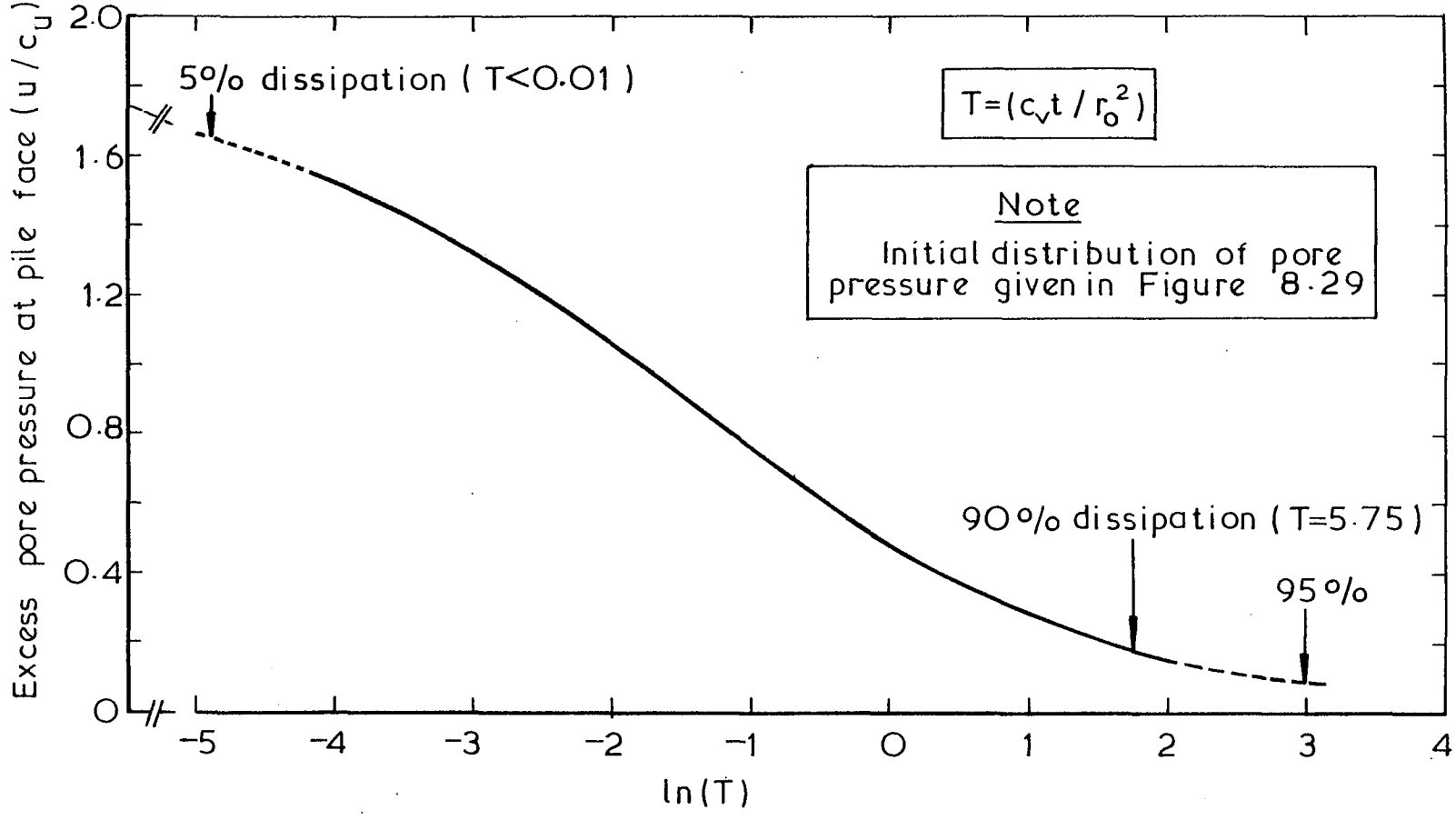
A finite difference program was written in order to analyse the rates of radial consolidation around piles, starting with arbitrary distributions of initial excess pore-water pressures. A description of the program and a check against an available analytical solution are presented in Appendix 9.1.

In Chapter 8, the behaviour of model piles installed without disturbance into Kaolin are analysed by means of Finite Element methods; the Kaolin is represented by a form of the Modified Cam Clay constitutive law (Roscoe and Burland, 1968). In section 8.8, the undrained loading of piles is considered, and it is shown that the greatest excess pore pressures are generated around piles installed into initially isotropically, normally-consolidated clay. The predicted radial distribution of excess pore pressures at peak pile load is shown in Fig. 8.29.

The predicted distribution of excess pore pressures in Fig. 8.29 was used to define the initial conditions for a finite difference radial-consolidation analysis. In the analysis presented here it has been assumed that the coefficient of swelling is equal to that of consolidation. The predicted variation of the excess pore pressure at the pile face, as a function of a dimensionless measure of time ($T = c_v t/r_o^2$) is shown in Fig. A.4.2.1.

In the case of the model pile tests, r_o = 7.5 mm, and c_v is roughly 10 m^2/year or 0.32 mm^2/second. Thus, 90% of the excess pore pressures at the pile face are predicted to have dissipated within 17 minutes (T = 5.75), and 95% within an hour. During pile loading the pore pressures are generated continuously, and so a longer time to failure must be allowed to ensure drained loading. Accordingly, in the model pile tests the time to peak (9 hours) was chosen to be almost 10 times greater than the value predicted above for 95% dissipation of excess pressures at the pile face. In addition to the radial consolidation there was axial consolidation within the sample (90% consolidation in less than 9 hours) which has not been taken into account, and so it is believed that the selected rates of displacement were sufficiently slow to ensure fully drained conditions.

From Fig. A.4.2.1, it may also be seen that more than 5% of the initial excess pore pressures have decayed by T = 0.01. Thus, in order to load one of the model piles in Kaolin under undrained conditions, peak load must be achieved within about a second!



The predicted decay, with time, of the excess pore pressures at the face of a model pile loaded to peak (under undrained conditions) ; K=1·0

Fig. A.4.2.1

CHAPTER 5

EXPERIMENTAL RESULTS - EXCLUDING MICRO-FABRIC STUDIES

5.1 INTRODUCTION

In total, 19 model pile tests were conducted, employing the equipment described in Chapter 3, and the procedures described in Chapter 4. The results obtained from the tests, in terms of the forces, stresses and displacements which were measured, are presented in this chapter. Results from the micro-fabric investigations performed after each test are presented in the following Chapter, No. 6.

Two series of pile tests were performed. The purpose of the first series was to investigate the behaviour, on loading, of piles installed with minimal disturbance, whereas the purpose of the second series was to examine the behaviour of full-displacement piles.

5.2 TESTING PROGRAMME

5.2.1 Introduction

Details of the 19 model pile tests are summarised in Tables 5.1 and 5.2; the former table describes the nature of the tests, and the latter summarises the principal results.

The testing programmes from the two series of tests are considered separately.

5.2.2 Piles Installed with Minimal Disturbance

Tests 1, 2 and 3 were performed using Spestone Kaolin (no longer commercially available), and were intended for practice with the new equipment in advance of the delivery of the Speswhite Kaolin which was used in the other tests. As a result of these first three tests, minor modifications were made to the equipment and to the testing procedures. The results obtained cannot readily be compared with those obtained in the later tests, and are not discussed further.

Test No. 4 was performed using Speswhite Kaolin, prepared using the procedures described in Chapter 4. The purpose of this test was to examine the nature of the micro-fabric disturbance resulting from the proposed drilling and reaming operations. After consolidating the sample in the

hydraulic triaxial cell, the sample was unloaded (by the procedures described in Chapter 4) and a hole was drilled through the centre using the twist drill followed by the reaming tool. Thin sections of the clay beside the hole were then prepared. These served to confirm that the cutting of the hole caused negligible disturbance to the clay micro-fabric (see Fig. 6.2). Further discussion of this test is reserved until Chapter 6.

Twelve pile tests were then performed following the procedures described in Chapter 4. With the exception of test no. 7, the tests were performed using normally-consolidated Kaolin consolidated to a range of initial stress ratios. These twelve tests may conveniently be considered in four groups of tests, although some tests are relevant to more than one group.

(i) Tests 9,10,12 and 13; the Kaolin samples employed were similarly consolidated to a stress ratio ($K = \sigma'_r/\sigma'_z$) of 1.5. The pile loadings were stopped at different stages so that progressive micro-fabric changes within the clay, with pile loading, could be established (see Chapter 6). These four tests served to demonstrate the repeatability of the procedures employed.

(ii) Tests 5,6,8,9,11,16 and 15; the Kaolin samples were all consolidated to different initial stress ratios. The piles were loaded at a constant rate of displacement until eventually residual capacities were achieved, and thin sections were prepared. The tests were performed in order to investigate the effect of the initial stress conditions on the subsequent pile behaviour.

(iii) Test 7; this test was conducted using Kaolin prepared to an over-consolidation ratio of 5, and was performed to determine whether there were any fundamental differences in behaviour between normally-consolidated and over-consolidated samples.

(iv) Tests 7,15 and 17; these tests each incorporated a device for measuring the radial stresses acting on the pile during installation and loading.

5.2.3 Full-displacement Piles

Three tests (No's. 16,18 and 19) were conducted to examine the effects on the pile loading behaviour of installing full-displacement piles by driving and by jacking. The micro-fabric changes induced in the clay beside the piles were also examined.

In test 16, a pile was driven about half way into a sample of Kaolin (using the procedures described in Chapter 4). The sample was then removed and thin sections were prepared (the pile was not loaded).

In tests 18 and 19, model piles were driven and jacked, respectively, through similar prepared Kaolin samples. After allowing full consolidation, the piles were slowly loaded until residual loads were achieved. The loading behaviours were recorded, and thin sections were prepared (they are discussed in Chapter 6).

5.3 RESULTS OBTAINED DURING SAMPLE PREPARATION

5.3.1 Introduction

All of the Kaolin samples were prepared by a two-stage consolidation process. The samples were one-dimensionally consolidated from a high water-content slurry (c. 2 x LL) to a water content of about 52%, before being subject to the main anisotropic consolidation in the hydraulic triaxial cell. In the course of the sample preparation, information about the consolidation behaviour of Speswhite Kaolin was obtained, and this is briefly considered.

5.3.2 One-dimensional Consolidation

A typical graph of voids ratio against the natural logarithm of the mean effective stress, obtained during sample preparation, is presented in Fig. 5.1. It may be seen that in the stress range of 20 to 100 kN/m^2, the slope of the virgin consolidation $\lambda(= - de/d(\ell nP'))$ and the voids ratio at unit pressure $(e_\lambda)_{1\text{-}D}$ had mean values of 0.25 and 2.52 respectively. There was, however, a tendency for λ to decrease with increasing stress level. This phenomenon was also observed during oedometer testing (refer to Chapter 4, section 4.2.2).

5.3.3 Anisotropic Consolidation within the Hydraulic Triaxial Cell

5.3.3.1 Normally-consolidated Samples

The one-dimensionally consolidated samples, at water contents of around 52%, were transferred to the hydraulic triaxial cell where the stress level was approximately doubled. The range of permissible stress paths is shown in Fig. 4.4, and a selection of actual stress paths followed (by the samples used in tests 11,13,14 and 15) are presented in Fig. 5.2. Results obtained from these four samples will be used to illustrate the behaviour of the Kaolin during consolidation.

The consolidation of the samples at stress ratios other than K_o was monitored in terms of the changes in the void ratio and the ratio of total strain increments $(\dot{\varepsilon}_s/\dot{\varepsilon}_v)^T$ with increasing mean effective stress (the use of strain increment vectors to monitor consolidation is discussed in Appendix 5.1). Results obtained during the consolidation of the four samples mentioned above are presented in Figs. 5.3 and 5.4. It may be seen that the approach to normally-consolidated behaviour consistent with the new stress ratios was asymptotic with increasing stress level. However, a doubling of the stress level was found to be sufficient to ensure an adequate approximation to the desired conditions.

5.3.3.2 Over-consolidated Sample

The main testing programme was conducted using normally-consolidated Kaolin samples. However, one test (No. 7) was performed using over-consolidated Kaolin to give an indication of any major differences in behaviour that might be expected between piles installed in normally-, and over-consolidated clays. Another reason for not performing further tests on over-consolidated samples was that finite element studies indicated that progressive failure down the pile might be a problem.

The sample employed was consolidated to a cell pressure of 1000 kN/m^2, whilst the height of the sample was held constant. The sample was then swelled back to a cell pressure of 200 kN/m^2, giving an 'OCR' of 5. The stress paths followed by the sample during consolidation and swelling are shown in Fig. 5.5.

5.4 INSTALLATION OF PILES WITH MINIMAL DISTURBANCE

5.4.1 Introduction

The aim of the installation procedure adopted was to enable a pile to be introduced into a sample of Kaolin, with a minimum of disturbance to either the stress field or the micro-fabric of the clay. The principles underlying the procedures adopted are discussed in Chapter 3, section 3.3, and the experimental details are described in Chapter 4, section 4.4.

In the course of installing the model piles, measurements of the total stresses acting on the clay samples were made. Additionally, the radial stresses acting on the model piles were successfully measured in two tests. The results are presented below.

5.4.2 Results; Excluding Measurements of the Radial Stresses Acting on Piles

5.4.2.1 Introduction

In order to install a model pile, the total radial stress acting on the sample was removed whilst undrained conditions were maintained and the sample height kept constant. A hole was drilled through the sample, and the brass core of the pile grouted in place. Once the newly formed pile was rigid, the radial total stress was re-applied to the sample. Ideally the axial and radial effective stresses within the sample should have been uniform, and should have returned to their original values.

5.4.2.2 Measurements of Total Stress Changes

The axial total stress acting on the sample was monitored as the cell pressure was varied during the three stages.

(i) unloading before installing the pile;

(ii) re-loading to return the radial total stress on the sample to the original cell pressure;

(iii) unloading the sample at the end of the test (again under conditions of zero axial strain).

Measurements of these stresses, corresponding to tests 9,11,14 and 15 are presented in Figs. 5.6a,b,c and d. Results from other tests are presented in Appendix 5.2.

The observed behaviour may be seen to have departed from the ideal. The final stresses acting on the sample after pile installation did not, in general, return to the same values as those obtaining at the end of the main consolidation. The stresses were, however, not 'corrected' for to have done so would have caused axial strains within the sample, and hence relative movement between the soil and the pile in advance of loading the pile. The result was that samples were typically left in a very lightly over-consolidated state and at a slightly higher stress ratio than that which obtained during sample preparation.

On reducing the cell pressure in order to install a pile, the axial total stress should have reduced by the same amount. However, as may be seen in Fig. 5.6, the axial stresses initially reduced at a slower rate than the cell pressure; a possible explanation for this behaviour is the absorption of small quantities of water which could not be removed from the drainage system by the earlier flushing with air (this view is supported by the profiles of water-contents (presented below) which were obtained in the course of the pile installation procedure). After the early non-linear behaviour, the axial total stresses reduced linearly at the same rate as the cell pressure.

On re-loading the sample, the response of the axial stresses to increases in cell pressure was essentially linear until the cell pressure had nearly returned to its former value. The non-linearity observed at this stage may be explained in terms of the expulsion of some of the water absorbed earlier, and by small plastic deformations occurring around the top and bottom of the pile. On unloading the sample after the pile tests, the response was very similar to that obtained on reloading after pile installation, indicating that the processes were largely elastic.

In test 19 (employing a full-displacement jacked pile), the sample was unloaded and re-loaded following the procedures described above, with the exception that no pile was installed until the end of the first unloading, re-loading sequence. The results of measurements made during this process are presented in Fig. 5.7, and these may be seen to be very similar to those presented in Fig. 5.6. This suggests that the behaviour observed in the tests described above was not noticeably affected by the presence of the model pile.

The shapes of the re-loading curves in all tests were similar which suggests that any rigid inclusion effects that there may have been are likely to have been largely independent of the initial stress ratio. Rigid inclusion effects would tend to increase the radial stresses acting on the piles. Measurements of the radial stresses acting on the piles employed in tests 15 and 17 (see section 5.4.4) suggest that after pile installation the radial effective stresses returned to 100% and 107% of the cell pressure, respectively. Thus, it is believed that although the installation procedures caused some disturbance to the stresses within the samples, the effect on the radial stresses acting on the model piles was small, and was largely independent of the initial stress ratio.

5.4.3 Water-content Profiles

The clay removed from the sample during the drilling process was used to obtain a water-content profile through the sample along the line of the forthcoming pile. On extraction of the drill, the 'waste' Kaolin was immediately transferred to a sealed water-content tin. The samples employed weighed only about three grams, and therefore much care was needed in order to obtain accurate results. At first a balance measuring to 5 milli-grams was used. This proved to be insufficiently accurate and was replaced by a balance sensitive to less than 0.5 milli-grams; the results obtained from the latter exhibited much less scatter. Water-content profiles obtained in the course of tests 12,13,14,15 and 17 (using the more accurate balance) are presented in Fig. 5.8. The earlier, less reliable results are presented in Table 5.3, for the sake of completeness.

It may be seen in Fig. 5.8 that, during drilling, the water-contents at the top and the bottom of the samples were higher than in the rest of the sample because of water absorbed from the drainage system. Away from the ends of the samples, however, the water contents were fairly uniform (generally within ± 0.5%). The mean values quoted exclude the higher water-contents at either end. After the pile tests, water-contents at various locations within the samples were determined. In particular, the water contents on the perimeter of the sample at its mid-height were measured. These results are also presented in Fig. 5.8 for comparison with the mean water-contents obtained during pile installation; the values are in close agreement.

5.4.4 Instrumented Model Piles

5.4.4.1 Introduction

Altogether three model piles (used in tests 7,15 and 17) were constructed incorporating devices for measuring the radial stress acting on the pile. As described earlier, the device employed in Test 7 failed to work satisfactorily (because of a leak) and the results are not presented. However, in tests 15 and 17 the devices worked very well during pile installation and it is believed that reliable measurements of the radial stresses acting on the piles after installation were obtained. A diagram of the device is presented in Fig. 3.5, and the installation procedure is described in Chapter 4.

5.4.4.2 Membrane Inflation Pressures

A small excess pressure was required to inflate the membrane so that a length of about 20 mm was in contact with the bore hole. A suitable pressure was determined by repeatedly inflating the membrane in a glass tube of the same diameter as the hole to be drilled through the sample (see Fig. 4.5). The length of membrane in contact with the tube was determined as a function of the inflation pressure the results obtained during the calibration of membrane used in test 15 are shown in Fig. 5.9.

It is evident that the excess pressure applied to the membrane must result in some radial stress on the tube, and similarly on the soil beside the bore hole. At any point on the membrane, the radial stress transmitted to the wall has been assumed to be the difference between the current excess fluid pressure and that required to inflate the membrane so that it just touches the point in question. Thus the variation along the length of the membrane of the excess radial stress acting on the bore hole may be established; this is illustrated in Fig. 5.10. The difference between the excess fluid pressure and the average excess radial stress acting on the wall is taken to be the equivalent inflation pressure. In tests 15 and 17, the total inflation pressures were 37 kN/m^2 and 32 kN/m^2 respectively, and the equivalent inflation pressures were 22 kN/m^2 and 20 kN/m^2.

5.4.4.3 Installation of the Instrumented Pile in Test 15

Fig. 5.11 represents the pressures in the radial stress-measuring device as the total radial stress was re-applied to the sample after pile installation, and also as the stress was removed at the end of the test.

During the initial stages of reapplying cell pressure to the sample, 'corrections' were made to the pressure within the device according to the response of the soil (the reason for the corrections, and the procedures adopted are described in Chapter 3, section 3.4.4.3). The incremental response of the device (before correction) to increases in cell pressure is shown in Fig. 5.12, as a function of the cell pressure. It may be seen that as the cell pressure was increased the 'stiffness' of the system increased, with the result that corrections were not required in the final stages of reapplying the cell pressure.

The radial stress acting on the pile after the reapplication of cell pressure and allowing 15 hours to 'settle', was 247 - 22 = 225 kN/m^2. This value compares with the applied cell pressure of 226 kN/m^2. The closeness of the agreement is probably somewhat fortuitous but does show that the radial stress acting on the pile is very close to the applied cell pressure.

On removing the cell pressure at the end of the pile test, there was no reason to apply corrections to the pressures in the device, and none ~~were~~ was applied. The similarity between the shapes of loading and unloading curves is encouraging.

5.4.4.4 Installation of the Instrumented Pile in Test 17

Test 17 was a repeat of Test 15, and was intended as a check on the measured radial stresses acting on the pile. As described in Chapter 4, section 4.5.3, the whole hydraulic system of the radial stress-measuring device in Test 17 was de-aired by maintaining the system at a pressure of 1000 kN/m^2, and flushing with de-aired water for a period in excess of one month. In Fig. 5.12 it may be seen that the incremental response was better than that obtained in Test 15 (in which only the pressure transducer assembly was de-aired under high pressure). Nevertheless, the finite stiffness of the system still required pressure corrections to be applied in the early stages of reapplying the cell pressure.

The overall response of the device to increases in cell pressure is shown in Fig. 5.13. The final radial stress acting on the device was 262 - 20 = 242 kN/m^2, which is 7% in excess of the cell pressure.

The results from Tests 15 and 17 confirm that the pile installation procedure did not lead to significant rigid inclusion effects (< 10%), and so as a reasonable approximation the radial stress acting on the pile at the start of pile loading may be taken to equal the cell pressure.

5.5 LOADING BEHAVIOUR OF PILES INSTALLED WITH MINIMAL DISTURBANCE

5.5.1 Introduction

After allowing the sample, with the now included pile, to 'rest' for between 15 and 24 hours after the reapplication of the cell pressure, the pile was loaded axially at a constant rate of displacement of about 0.25 mm/hour. This displacement rate resulted in peak load being achieved in about 9 hours, and was sufficiently slow to ensure that the pile loading was drained (see Appendix 4.2).

The testing programme was outlined in section 5.2.2 of the present chapter, and the results will generally be presented in the four groups suggested.

5.5.2 Load-Displacement Behaviour

5.5.2.1 Tests Conducted to Investigate the Development of Micro-Fabric Changes with Pile Loading (Nos. 9,10,12,13)

The samples employed in these tests were all prepared in a similar fashion, and were normally-consolidated to a stress ratio(K) of 1.5. Each sample was consolidated individually from a slurry, and so comparison between the pile loading behaviour obtained during the four tests should provide a useful guide to the reproducibility of the procedures employed. The four tests were each stopped at a different stage of loading, and thin sections were prepared so that the micro-fabric changes could be observed (see Chapter 6).

The observed load-displacement behaviours are presented in Fig. 5.14. It will be seen that the behaviour of all piles is very similar (up to 85% of the peak load, the curves from Tests 9,10 and 12 are almost inseparable) and the curve from Test 9 represents behaviour typical of all the tests taken to residual capacity. Typically at least 100 readings were taken pre-peak and as the scatter between readings was negligible, the individual points are not shown.

There are a number of features to note regarding the shapes of the load-displacement curves. The early behaviour, up to about 50% of the peak load, was apparently elastic and the response was very stiff (back-calculated G/Cu values are presented in Table 5.2); thereafter there was a considerable loss of stiffness. Although the load-displacement behaviour was similar up to about 95% of the peak load, the final displacements to peak load were variable; analyses of thin sections taken at different stages of loading

suggest that this may be the result of an instability phenomenon associated with 'failure'. The post-peak behaviour was brittle, and following post-peak displacements of some 10 mm, residual conditions were achieved and the shear strength mobilised along the shaft remained constant thereafter, at roughly one-half of the peak value.

Observation of thin sections confirm that after 10 mm of post-peak displacement the clay around the pile had formed a thin continuous displacement discontinuity along which the particles were highly oriented (see Fig. 6.8), at a distance of about 0.5 mm from the shaft. This series of tests also demonstrated that the residual surface was not present at peak conditions. Ring shear tests and direct shear interface tests (see Appendix 4.1) suggest that the residual angle of friction appropriate to the model pile tests lies within the range $11.5° < \phi'_r < 12°$. This compares with the peak angle of shearing resistance determined in triaxial compression, of 23°.

Although the results from the micro-fabric investigations are presented and discussed in detail in Chapter 6, several observations are relevant to an interpretation of the pile loading behaviour and are briefly repeated here. It is seen that beyond a distance of about one-half of a pile radius from the shaft, the soil fabric is apparently unaffected by the pile loading. Closer to the pile Riedel shear structures are seen at inclinations of about 15° to the direction of pile penetration, to a distance of up to 5 mm from the shaft; these structures are shown to be associated with peak-conditions, but are obsolete thereafter. The post-peak displacements of the pile appear to be accommodated by very large shear strains confined within a zone less than one millimeter thick, adjacent to the shaft. Eventually a continuous residual shear surface is formed, and this acts as a principal displacement discontinuity.

5.5.2.2 Effects of Initial Stress Ratio on the Pile Load-Displacement Behaviour

Altogether eleven pile loading tests were performed using normally-consolidated samples of Speswhite Kaolin. Test No. 6 was conducted at a much higher stress level than the others and is considered separately. Of the remaining tests, six were subject to post-peak displacements sufficient to cause residual conditions to be achieved.

Fig. 5.15 presents the normalised pre-peak pile load-displacement behaviour obtained from the ten tests conducted at similar stress levels, and it may be seen that the behaviour is similar in all tests. The initial loading

stages were very stiff, with equivalent linear-elastic G/Cu values typically between 150 and 200 (see Table 5.2). There was a tendency (with the exception of Test 5) for the required displacement to achieve peak-conditions to increase with increasing initial stress ratio.

The normalised post-peak behaviour of the tests conducted on normally-consolidated Kaolin are shown in Fig. 5.16. In each case the residual capacity was achieved after a post-peak displacement of about 10 mm, and was roughly one-half of the peak value. The shapes of the post-peak displacement curves are very similar to one another. It should be noted in Fig. 5.16 that even at residual conditions the pile loads continue to decrease slowly with further pile displacement, a consequence of the reducing length of the piles embedded in the clay; the average shear stress along the pile shaft is constant after a displacement of about ten millimeters, however.

Test No. 6 was conducted on Speswhite Kaolin, normally-consolidated to almost twice the stress level employed in the other tests. The load-displacement behaviour (normalised by the cell pressure) is shown in Fig. 5.17 where it is compared with that observed in Test 8 which was conducted at a similar stress ratio, but smaller stresses. The peak load in Test 6 was proportionately smaller than in Test 8, and the pre-peak response was less stiff (in terms of G/Cu). Nevertheless, the post-peak reduction in strength was a similar fraction of the peak load to that measured in the other tests, suggesting that the radial stress acting on the pile at peak was somewhat smaller than might have been expected.

5.5.2.3 Pile Installed in Over-Consolidated Kaolin (OCR 5)

Test No. 7 was conducted as a trial to establish whether there were any differences in behaviour between piles installed in normally-consolidated and over-consolidated clays at similar stress levels. The observed load-displacement behaviour is illustrated in Fig. 5.18 where it may be seen that the post-peak brittleness was again about two, and that the overall shape of the curve was similar to that observed in the tests on normally-consolidated clay. There is no way of ascertaining whether these results were influenced by progressive failure down the pile shaft resulting from local strain softening in the clay, as suggested by finite element analyses. In the discussion of results it will be shown that the radial stress acting on the shaft appears to have increased during the pile loading, which is in contrast to the decrease observed in the tests on normally-consolidated clay.

The pile used in Test No. 7 was fitted with the first prototype device for measuring the radial stress acting on the shaft. Unfortunately a tiny leak developed in the system and so the results obtained are meaningless. Once this was discovered a constant pressure, equal to the cell pressure, was applied to the device in order to minimise the effect on the overall load-displacement behaviour of the pile. Thin sections taken through the device, at the end of the test, showed that clay surrounding the device had been sheared in a similar manner to that observed elsewhere along the pile and that the residual shear surface was continuous along the device (see Appendix 6.2).

5.5.3 Measurements of Radial Stresses Acting on Pile Shafts during Pile Loading

5.5.3.1 Introduction

The piles employed in Tests Nos. 15 and 17 were each equipped with an improved design of radial stress-measuring device which was used to measure the stresses acting on the piles during installation (section 5.4.4) and during loading. Test 17 was conducted under similar conditions to Test 15, and was intended as a check on the repeatability of the results from the radial stress-measuring devices.

5.5.3.2 Test 15

The variations of the pile load and the radial stress acting on the pile, with pile displacement, are shown in Fig. 5.19. The pre-peak behaviour is illustrated in more detail in Fig. 5.20. The figures show that on loading, the radial stress acting on the pile dropped rapidly at first, and then remained fairly constant at about 15% less than the initial value until the peak pile load was achieved. With post-peak displacements the pressure in the device increased initially but then reduced to the value which obtained at peak load conditions. It is considered that the radial stress transducer was best suited to measurements taken at small pile displacements (i.e. pre-peak).

The most significant results from these measurements are that, on loading the pile, the radial stress reduced by about 15% and that there was no significant departure from this value on displacing the pile to residual conditions.

5.5.3.3 Test 17

The radial stress transducer performed well during the pile installation and on loading to roughly 50% of the peak pile load. At this stage, however, problems developed with the shear reinforcement and the test was aborted. The pile was exhumed and this confirmed that some of the reinforcing strips had become detached on shearing (as a result of inadequate resin penetration).

The measured radial stress changes on loading the pile to 50% of its peak capacity are shown in Fig. 5.21, which indicates a similar behaviour to that observed in Test 15.

5.6 A DISCUSSION OF THE RESULTS FROM THE TESTS CONDUCTED ON PILES INSTALLED WITH MINIMAL DISTURBANCE

5.6.1 Variations of the Angles of Shaft Friction and the Radial Effective Stress during Pile Loading

5.6.1.1 Variation of the Radial Effective Stress on Loading to Residual Conditions

It was seen in Fig. 5.16 that the residual pile capacities were generally about half of the peak values. The variation of the ratio of the pile load at peak (F_p) to that at residual conditions (F_r), is shown in Fig. 5.22 as a function of the stress ratio acting in the soil immediately before pile loading. The figure confirms that the ratio of the pile loads (F_p/F_r) has a mean value of 2, which is independent of the initial stress ratio.

This result may be employed to establish a relationship between the angle of 'shaft friction δ', and the radial effective stress, σ'_{rp}, acting on the pile shaft at peak load. With a knowledge of the residual angle of shaft friction (ϕ'_r may be determined by means of Ring shear tests and direct shear interface tests - Appendix 4.1), and the measured residual pile load, it is possible to determine the mean radial effective stress σ'_{rr} acting at residual conditions.

Thus, $$F_r = A_r \cdot \sigma'_{rr} \cdot \tan \phi'_r$$

and hence $$\sigma'_{rr} = F_r/A_r \cdot \tan \phi'_r \qquad (5.1)$$

where

A_r is the surface area of the pile embedded in the clay at residual conditions.

It is shown in Appendix 4.1 that $11.5° \leqq \phi'_r \leqq 12°$; this result has been used to determine the radial effective stresses acting at residual conditions for all the tests taken to large post-peak displacements. The results are presented in Fig. 5.23 where σ'_{rr} is normalised by the cell pressure appropriate to each test, and expressed as a function of the initial stress ratio prior to pile loading. For the piles installed in normally-consolidated Kaolin a reduction in radial stress of between 2% and 27%, depending on the stress ratio, was found. In contrast, the test (No. 7) conducted on Kaolin with an OCR of 5 exhibited an increase in radial stress of up to 15% on loading.

It may be noted that any rigid inclusion effects resulting from the pile installation process would be expected to have increased the radial stresses acting on the piles; the measurements of the radial stresses acting on the piles employed in Tests 15 and 17 suggest that the rigid inclusion effects were small.

5.6.1.2 Determination of the Peak Angles of Shaft Resistance

If the post-peak variation of the radial stresses acting on the piles is assumed to be independent of the initial stress ratio (an argument in support of this assumption is presented in section 5.6.1.3), then it may be inferred that the peak angle of shaft friction is also independent of the intial stress ratio. Thus, from Fig. 5.22

$$\frac{F_p}{F_r} = 2 = \frac{A_p.\sigma'_{rp}.\tan\delta'_p}{A_r.\sigma'_{rr}.\tan\delta'_r}$$

now $\qquad 11.5° \leqq \phi'_r \leqq 12°$

and as a first approximation $A_p/A_r = 1$

$$0.407\left(\frac{\sigma'_{rr}}{\sigma'_{rp}}\right) \leqq \tan\delta'_p \leqq 0.425\left(\frac{\sigma'_{rr}}{\sigma'_{rp}}\right)$$

Thus, if $(\sigma'_{rr}/\sigma'_{rp})$ is independent of K then so too is δ'_p. It may be of interest to note that such a result is a necessary consequence if the soil is assumed to obey an elastic-plastic constitutive law (see Chapter 7).

In order to obtain a rough estimate of δ'_p, let it further be assumed that the radial stresses do not vary post-peak, i.e. $\sigma'_{rr}/\sigma'_{rp} \cong 1$ (this

assumption is consistent with measurements taken in Test 15). Thus $22° \leq \delta'_p \leq 23°$; this compares with a ϕ' value of 23°, measured in triaxial compression.

5.6.1.3 Discussion of the Post-Peak Behaviour

A full account of the micro-fabric changes observed around the model piles is presented in Chapter 6; however, some of the results are discussed here in relation to the post-peak changes in the angles of shaft friction and radial effective stress acting on the model piles.

The micro-fabric studies indicate that once peak conditions are achieved, the major plastic shear deformations within the clay are confined to a region less than half of one pile radius from the shaft. The post-peak pile displacements appear to be confined to a very narrow zone (typically less than 1 mm from the shaft) with the clay beyond this zone suffering no further plastic deformations. The shear strains within the clay immediately adjacent to the pile become enormous and the angle of friction parallel to the shaft locally reduces as a result of particle orientation effects, until eventually a very narrow (c. 10 μ) residual shear surface is formed, along which the clay particles are strongly oriented. The post-peak reductions of the angle of shearing resistance in Kaolin have been studied by means of Ring shear tests and Direct shear interface tests (see Appendix 4.1).

That the post-peak reduction in pile-shaft capacity is caused primarily as a result of a decrease in the angle of shaft friction, rather than a reduction in the radial effective stress is supported by the results from Direct shear interface tests conducted at constant normal effective stress. Littleton (1976), for instance, performed drained interface tests in which a Kaolin and an illitic clay were consolidated against, and then sheared against rigid interfaces. The peak angles of friction were achieved after displacements of about two millimeters, after which the mobilised angles of friction decreased to residual conditions (roughly half of the peak values), as a result of post-peak displacements of between two and five millimeters. These results are similar to those presented in Appendix 4.1. Thin sections prepared after the interface tests referred to in Appendix 4.1 confirmed that residual conditions were associated with the presence of a thin continuous shear surface along which the clay particles were strongly oriented.

The micro-fabric studies performed in association with the model pile tests have shown that the post-peak displacements were accommodated within a very narrow zone of clay adjacent to the pile, and that this zone eventually

reduced to a displacement discontinuity about 10 μ thick. As the pile load reduced with post-peak displacement, the surrounding clay was forced to unload in shear in order to maintain equilibrium. Beyond the narrow zone of clay undergoing 'strain-softening', the unloading presumably occurred in a predominantly elastic fashion. The volume of clay undergoing strain-softening was small in relation to the surrounding 'elastic' material and so it is believed that as the pile tests were fully drained, the post-peak variation of the radial effective stresses acting on the piles was largely controlled by the 'elastic' material. Although small changes in mean effective stress may have been associated with the 'elastic' unloading, they were probably largely independent of the initial stress ratio. Therefore, it is considered reasonable to assume that the post-peak changes in the radial stresses acting on the model piles were both small, and largely independent of the initial stress ratio. The measurements of the radial effective stresses acting against the pile in Test 15 support the assumption that the post-peak variations of the radial effective stresses are small.

5.6.2 Comparison between the Test Results and Predictions Based on Effective Stress Methods of Pile Design

The results from the model pile tests may be compared with predictions based on the Chander-Burland approach to pile design, by evaluating the ratio (τ/σ'_{ro} tan ϕ') for each test; a ratio of unity indicates agreement with the theory (σ'_{ro} is the initial in-situ radial effective stress).

In Fig. 5.24 the above ratios derived from the model tests are plotted as a function of the initial stress ratio. It will be seen that the Chandler-Burland predictions over estimate the strengths of the pile installed (with minimal disturbance) in normally-consolidated Kaolin, but underestimate the strength of the pile installed in over-consolidated Kaolin. There are two probable reasons for the over estimation of the strengths of the piles in the normally-consolidated clay; the first is that the radial effective stresses acting on the piles decrease on loading to values which are less than σ'_{ro} (see Figs. 5.20 and 5.23), and the second is that the peak angle of friction that can be mobilised parallel to the shafts is probably slightly less than ϕ' (see Chapter 7). The under-prediction of the capacity of the pile in over-consolidated Kaolin is thought to be the result of an increase in the radial effective stress on loading, caused by dilation within the clay.

In practice the behaviour of piles is complicated by the effects of the fabric-disturbance and the stress-field disturbance resulting from the

method of pile installation. For instance, the installation of bored piles in over-consolidated clay causes local swelling of the clay adjacent to the pile, with the result that the radial effective stresses acting on the installed piles are less than σ'_{ro}. On loading, however, the radial stresses may increase as a result of dilation, so that the radial stresses acting at peak load may not be significantly different from σ'_{ro}. This may explain why Chandler (1968) obtained such good agreement with field data.

The installation of a displacement pile (i.e. by driving) probably causes the radial effective stress acting on the pile to exceed σ'_{ro}. However, it is thought that the fabric disturbance caused by the installation may result in a decrease in the peak angle of shaft friction that can be mobilised, and the pile loading may also cause a reduction in the radial effective stress acting on the pile. These various influences appear to be somewhat self-compensating which may explain the agreement obtained by Burland (1973) with field data from driven piles in normally-consolidated clays. The behaviour of displacement piles is considered in section 5.7, Chapter 6 and Chapter 9.

5.6.3 Comparison between the Test Results and Predictions Based on Total Stress Design Methods

The load-carrying capacity of piles has conventionally been estimated in terms of total stresses using the equation (Skempton, 1959)

$$\bar{\tau} = \alpha \cdot C_u$$

where C_u is the average undrained shear strength (measured in triaxial compression on vertical test specimens) along the pile length, and α is a factor which allows for the effects of pile installation. Values of α corresponding to the model tests are considered below.

Water content measurements obtained during the installation of the model piles have been used to estimate the undrained shear strength of the clay prior to pile loading; a relationship between undrained triaxial shear strength and water content was determined using the measured slope of the virgin consolidation line, λ, in conjunction with a known undrained shear strength of 40 kN/m^2 at a water content of 50% (from Steenfelt et al, 1981). The undrained shear strengths determined in this manner are presented in Table 5.2, and the values of α appropriate to the various tests were determined by dividing the mean shear stresses acting on the piles by the estimated initial undrained shear strengths. The results are presented in Fig. 5.25, as a

function of the initial stress ratio.

For the normally-consolidated samples, the α values corresponding to peak load conditions increased from 1.2 to 1.6 with increasing initial stress ratio. α values in excess of unity are believed to have been obtained because the installation procedure caused minimal disturbance and the pile loadings were fully drained, which resulted in a local increase in shear strength of the clay adjacent to the pile.

The α value corresponding to the test on over-consolidated Kaolin (Test 7) was 0.8. It is probable that dilation of the clay around the loaded pile led to local swelling and hence to an increase in the water-content of the clay beside the pile. The above α value is somewhat higher that those commonly associated with bored piles; the difference is thought to be largely a result of the swelling which occurs during the installation of field piles.

5.7 TESTS ON FULL-DISPLACEMENT PILES

5.7.1 Introduction

In the model tests described above the piles were installed by a procedure designed to cause a minimum of disturbance to either the stress field or the fabric of the clay. In practice, the installation of piles (particularly full displacement piles) may be expected to cause severe disturbance, and a series of three model pile tests was performed in order to investigate the nature and influence of this disturbance.

In the course of the tests on piles installed with minimal disturbance it was noted that residual conditions were achieved following post-peak displacements of about 10 mm. This observation raised the question of whether or not the clay around full-displacement piles should be expected to be at a residual strength in advance of pile loading. Ring shear tests conducted at a variety of rates of displacement (see Appendices 4.1 and 5.3) have shown that the residual strength is rate dependent, and suggest that the residual shear surfaces become increasingly disordered as the rate of displacement increases. The result of this is that on slowly reloading a shear surface formed at a higher rate of displacement a peak strength is obtained after which the strength decreases to a residual value appropriate to the slower rate of displacement. Thus, even if residual conditions do obtain around displacement piles in advance of loading, the available strength may depend on the method of installation, and the final residual strength will probably be lower than the peak value. The post-peak behaviour may, in fact,

be a useful guide to the mechanisms operating.

Three model tests were conducted on full displacement piles, two involving driven piles (Tests 16 and 18) and the other a jacked pile (Test 19). Test 16 was performed in order to investigate the micro-fabric changes induced in the clay as a result of pile driving and the pile was therefore not loaded after installation. The results of the pile loadings performed in Tests 18 and 19 are compared with those obtained during tests conducted on piles installed with minimal disturbance with similar samples of clay. Thin sections were prepared after all three tests, and are presented in Chapter 6 which also contains a discussion of the behaviour of displacement piles.

5.7.2 Driven Piles

5.7.2.1 Sample Preparation

The Kaolin samples for Tests 16 and 18 were normally-consolidated in the hydraulic triaxial cell to a stress ratio of 0.7. Before pile installation, the samples were unloaded under undrained conditions with the sample heights kept constant in order to introduce the tip of the piles through the top of the cell. The cell pressure was then reapplied before the piles were driven. The details of the stresses employed in these tests and the corresponding water-contents are summarised in Table 5.2.

5.7.2.2 Pile Driving

The procedures employed during the pile driving are described in Chapter 4. The pile driving was monitored so that an estimate of the peak rate of pile penetration following each blow could be obtained. A tracing from a photograph of a typical oscilloscope trace obtained during the driving of the pile in Test 16 is presented in Fig. 5.26. It may be seen that the peak penetration of nearly 3 mm was reached in about 3 milli-seconds, corresponding to a rate of penetration of the order of 1 metre per second. Similar rates were determined from the other traces, and these are of the same order as the rates measured in the field; see, for example, the results from Dolwin, Leonard and Poskitt, 1979. Following each blow of the pile, the pile penetrated further into the clay after which there was some rebound, as may be seen in Fig. 5.26. At low pile penetrations, i.e. one pile diameter, the rebound was equal to about half of the maximum penetration. As the pile penetration increased, however, the rebound reduced to some 10% of the maximum penetration (about 0.2 mm). It is uncertain whether the rebound during the

latter stages of pile driving involved relative slip between the pile and the surrounding clay, or whether it was accommodated by continuous deformation within the clay. It may be noted that the rebound was of the same order as the displacements required to mobilise the peak shaft resistance on slowly loading the pile (see Fig. 5.27).

In Test 16, the pile was only driven to the sample mid-height in order that soil deformation patterns around both the toe and the shaft could be examined by means of thin sections. The pile was not loaded, and the sample was removed after full consolidation had been permitted. As noted earlier, it proved difficult to obtain accurate determinations of the water contents close to the pile without risking damage to the micro-fabric of the clay to be thin-sectioned. The water-content of the sample prior to pile driving was 45.3%. On dismantling the sample the water content at the circumferential boundary was 44.7%, but was only 42.7% at the pile face, i.e. 2.2% lower. This indicates that the undrained shear strength of the clay adjacent to the pile had been increased by about 30% as a result of the consolidation following driving.

In Test 18, the pile was driven through the sample so that the tip entered the cavity in the bottom platen of the hydraulic triaxial cell, thereby eliminating any end-bearing resistance of the pile. As a result of the pile driving 15 cc of water were expelled from the 1250 cc sample. No measurements were made of the excess pore pressures at the pile face, but it may be of interest to note that 90% of the water was expelled in under two hours. The sample was left to consolidate for 36 hours before the pile was loaded (Steenfelt et al (1981) showed that 90% dissipation of excess pore pressures around 19 mm diameter jacked piles in Kaolin occurred in about three hours).

5.7.2.3 Pile Loading

The pile in Test 18 was slowly loaded to residual conditions, using the same procedures as used in the tests on piles installed with minimal disturbance. The recorded behaviour is shown in Fig. 5.27 as a graph of the average shear stress on the pile (normalised by the cell pressure) against pile displacement. The results from Test 19 and Test 11 are also shown in the figure for comparison.

It may be seen that the pre-peak behaviour observed in Test 18 was almost linear and was very similar to the behaviour observed in the early stages of loading the piles installed with minimal disturbance; see for instance the curve in Fig. 5.27 corresponding to Test 11 which was conducted at a

similar initial stress ratio to Tests 18 and 19. The peak pile load in Test 18 occurred at a stress level ($\bar{\tau}/\sigma'_{cell}$) of 0.269 (which is only 65% of the peak value measured in Test 11), and at a displacement of about 0.1 mm (or 1.3% of one pile radius). The post-peak behaviour was very brittle, and residual conditions were achieved following displacements of about 5 mm. The residual mean shear stress acting on the pile was about 18% less than the peak value.

If it is assumed that the residual angle of friction at the pile shaft was between 11.5° and 12°, then it follows that at residual conditions the average radial effective stress acting on the pile was between 4% and 9% in excess of the cell pressure. It should be noted that the radial effective stress acting on the pile after driving and consolidation may well have been greater than this, because stress changes may have occurred during the pile loading to peak conditions. In the course of the pile loading less than 0.2 cc of water was expelled from the sample, which suggests that such excess pore-pressures that may have been generated by the loading were very small and/or highly localised.

5.7.2.4 Sample Removal

Following the test, the sample was removed from the triaxial cell, water content samples were taken, and the specimen impregnated in Carbowax.

The water-content of the sample prior to pile driving was 43.1%. After the pile test the water content on the outer circumferential boundary was 42.9%, whereas closer to the pile, at a distance of between 1 and 1.5 pile radii from the shaft, the water-content was only 41.5%; the latter result implies a 20% increase in the undrained shear strength of the clay compared with the value in advance of pile driving.

5.7.2.5 Comments

The tests on displacement piles were performed to examine the micro-fabric changes in the clay around the piles, and to compare the pile load-displacement behaviour of driven and jacked piles with observations made on piles installed with minimal disturbances. It is believed that micro-fabric changes induced in the Kaolin as a result of pile driving had a significant effect on the subsequent loading behaviour, and for this reason the main discussion of the tests on displacement piles is presented in Chapter 6 following the results from the thin-section studies. However, the peak and residual loads are briefly compared below with predictions based on total

stress design methods.

On the basis of the initial water-content of 43.1%, the undrained shear strength of the sample prior to pile installation is estimated to have been about 80 kN/m^2. Thus, at peak pile load the equivalent α value $\bar{\tau}/C_{u,0}$) was only 0.85, and at residual conditions α was 0.66. The peak α value was, therefore, less than unity despite the local increase in undrained shear strength of more than 20%! This result is considered to be a consequence of the fabric disturbance caused by the pile driving, and is considered in detail in Chapter 6.

5.7.3 Jacked Pile

5.7.3.1 Sample Preparation

The sample for Test 19 was consolidated at a stress ratio of 0.7 to a water-content of 45.9%, following the same procedures as used in the foregoing tests.

5.7.3.2 Pile Jacking

The solid pile was jacked into the Kaolin at an average rate of about 4 mm/min. Unfortunately a follower attached to the pile interfered with the pile-guide, and so the measurements of the pile load during jacking were unreliable and are not reproduced here. On dissipation of the excess pore-pressures generated during the pile installation 16.7 cc of water were expelled from the sample, 90% of which again occurred within two hours.

The sample was left overnight to consolidate before the pile was loaded.

5.7.3.3 Pile Loading

The pile was loaded under fully drained conditions in a similar manner to the earlier tests. Once again, less than 0.2 cc of water was expelled from the sample during the loading process. The average shear stress on the pile (normalised by the cell pressure) is shown in Fig. 5.27 as a function of the pile displacement. It may be seen that the pre-peak behaviour was similar to that observed in Test 18 and in the early stages of Test 11. The peak was less pronounced than in the case of the driven pile, and a reduction in strength of about 10% occurred on loading from peak to residual conditions (this compares with the 18% measured in Test 18). The peak normalised shear stress acting on the jacked pile was roughly 12% less

than on the driven pile, whereas the difference between the residual values was only 4%. The results obtained at residual conditions suggest that the final radial stress acting on the pile was up to 5% greater than the cell pressure.

5.7.3.4 Sample Removal

After the test, the water-content of the Kaolin at the outer circumferential boundary was 45.9% which is the same as the water-content of the sample prior to pile jacking. At a distance of one pile radius from the shaft the water-content was only 44.2%, representing a local increase in undrained shear strength of about 20%. The water-content of the clay immediately adjacent to the pile may have been even lower but was not measured for fear of damaging the micro-fabric of the clay to be thin-sectioned.

5.7.3.5 Comments

The main discussion of test results is presented in Chapter 6 following the presentation of the micro-fabric observations. However, the pile loads are briefly compared below with predictions based on total stress design methods.

The initial water-content of the sample was 45.9% which corresponds to an undrained shear strength of about 60 kN/m^2. The α value corresponding to the peak pile load was, therefore, 0.7, and the residual α value was 0.63. Thus, the peak 'α' value was less than unity despite the local decrease in the water-content and increase in undrained shear strength, caused by the pile installation.

Table 5.1: Summary of Model Pile Tests

Test No.	Type of Kaolin	Method of Pile Installation	Stage at which Test Stopped	Pile Instrumented	Comments
1	Spestone	'Wished-in-Place'	Pile installed	No	Trials with equipment and techniques
2	"	" "	Residual pile load	"	
3		" "	"	"	"
4	Speswhite	" "	Hole drilled in sample	"	To examine fabric disturbance caused by drilling
5	"	" "	Residual pile load	"	Full Test
6	"	" "	"	"	"
7	"	" "	"	Yes	OCR = 5
8	"	" "	"	"	-
9	"	" "	"	"	-
10	"	" "	Immediately post-peak	"	To examine development of micro-fabric changes
11	"	" "	Residual pile load	"	-
12	"	" "	Immediately pre-peak	"	To examine development of micro-fabric changes
13	"	" "	70% of peak load	"	"
14	"	" "	Residual pile load	"	
15	"	" "	"	Yes	To measure radial stresses on pile after installation and driving loading
16	"	Driven	Pile installed	No	To examine fabric changes induced by driving
17	"	'Wished-in-Place'	~60% of peak load	Yes	As Test 15
18	"	Driven	Residual pile load	No	To examine loading behaviour of driven pile
19	"	Jacked	"	"	To examine loading behaviour of jacked pile

Table 5.2: Summary of the Results from the Model Pile Tests

Test	4	5	6	7	8	9	10	11	12	13	14	15	16	17	18	19
OCR	1	1	1	5	1	1	1	1	1	1	1	1	1	1	1	1
K_{consol}	0.70	0.67	1.25	0.73	1.16	1.49	1.50	0.6	1.51	1.51	0.96	0.81	0.7	0.80	0.7	0.7
K_{test}	0.75	0.75	1.31	0.81	1.29	1.47	1.50	0.74	1.50	1.50	1.11	0.97	0.78	0.98	0.77	0.77
σ_{cell} (kN/m^2)	~250	200	596	205	258	265	260	210	258	260	260	225	225	225	250	175
$\omega_{consolidation}$ %	42.9	450	39.6	387	46.1	45.5	46.5	44.3	45.9	46.2	44.5	44.5	45.3	45.3	43.1	45.9
$C_{u_{estimated}}$ (kN/m^2)	85	67	118	130	60	64	58	72	61	59	71	71	66	66	80	60
F_{max} (N)	N/A	429	1030	66 2	501	597	615	515	568	427	619	551	N/A	N/A	385	286
τ_{peak} (kN/m^2)	N/A	82.8	164	104.5	78.2	96.7	98.9	88.1	92.0	N/A	99.5	89.3	N/A	N/A	67.3	42
$F_{residual}$ (N)	N/A	215	570	330	255	287	N/A	250	N/A	N/A	304	285	N/A	N/A	293	243
$\tau_{residual}$ (kN/m^2)	N/A	41.5	90.8	51.5	40.9	46.5	N/A	42.8	N/A	N/A	48.9	46.2	N/A	N/A	55.5	37.5
$\tau_{peak}/\tau_{residual}$	N/A	2.00	1.81	2.03	1.91	2.08	N/A	2.06	N/A	N/A	2.03	1.93	N/A	N/A	1.21	1.12
Pile length (at peak) (mm)	N/A	110	133	134	136	131	132	124	131	130	132	131	N/A	132	125	141
Diameter of Residual Shear Surface mm	N/A	15.8	15.5	15.9	15.9	15.4	N/A	16.1	N/A	N/A	16.2	15.9	N/A	N/A	> 16 < 17	155
ω close to pile at end of test % (distance from pile at which measurement made (mm))	N/A N/A	44.9 (25)	390 (10)	383 (5)	463 (10)	44.3 (5)	45.7 (10)	43.5 (10)	45.6 (10)	-	44.3 (15)	44.7 (20)	42.7 (5)	43.0 (5)	41.5 (10)	44.2 (7.5)
$\sigma'_{r_{residual}}/\sigma_{cell}$ $\delta'_r = 12°$	N/A	0.98	0.66	1.18	0.76	0.83	N/A	0.96	N/A	N/A	0.88	0.97	N/A	N/A	1.04	1.00
$\delta'_r = 11.5°$	N/A	1.02	0.69	1.23	0.79	0.86	N/A	1.00	N/A	N/A	0.92	1.01	N/A	N/A	1.09	1.05
Volume of water expelled from sample as a result of pile loading (cc)	N/A	-	-	-	-	2.7	2.9	6.3	3.6	2.6	5.5	8.5	N/A	5.6	0.2	0.2
$(G/C_{u,o})$ Early stage of pile loading	N/A	185	60	66	194	204	210	194	207	205	176	150	N/A	155	187	203

N/A non applicable

Table 5.3: Water Content Profiles Measured During Pile Installation

Test No.	5	6	7	8	9	10	11
Top of Sample	-	42.2	39.9	48.5	46.7	49.1	43.3
	-	-	38.4	-	48.6	47.7	42.6
	-	-	39.1	46.4	45.3	37.4	43.5
	44.5	39.5	-	45.7	45.7	46.9	42.5
	-	-	38.9	46.5	44.3	46.0	43.3
	-	39.2	-	46.1	45.4	47.8	44.3
	-	-	38.6	46.1	46.0	47.1	43.4
	43.5	-	39.8	-	-	-	44.7
Bottom of Sample	-	39.5	40.4	-	48.3	48.6	45.1

NOTE: These results were obtained using a relatively insensitive balance, and are less accurate than those presented in Fig. 5.8 for tests 12, 13, 14, 15 and 17; see section 5.4.3.

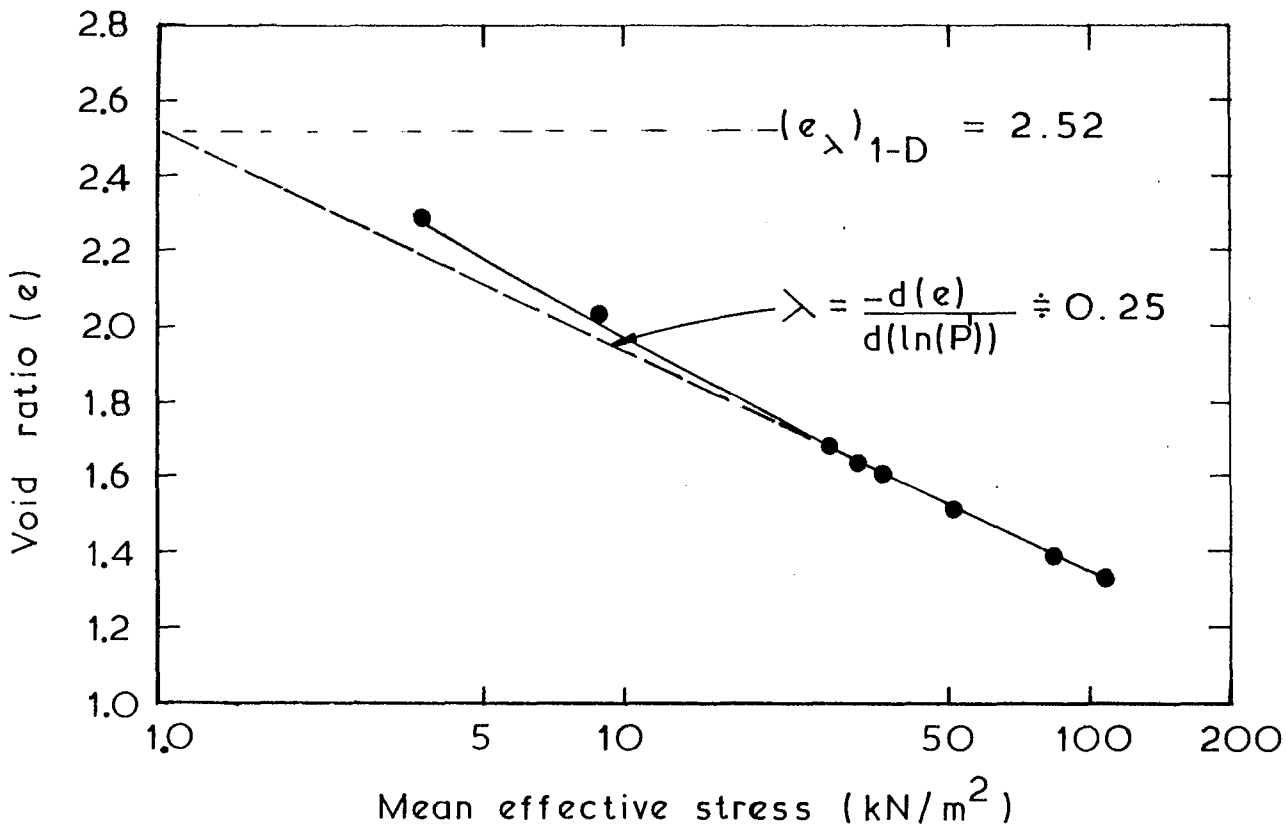


Fig. 5.1

Variation of voids ratio with mean effective stress
One-dimensional consolidation

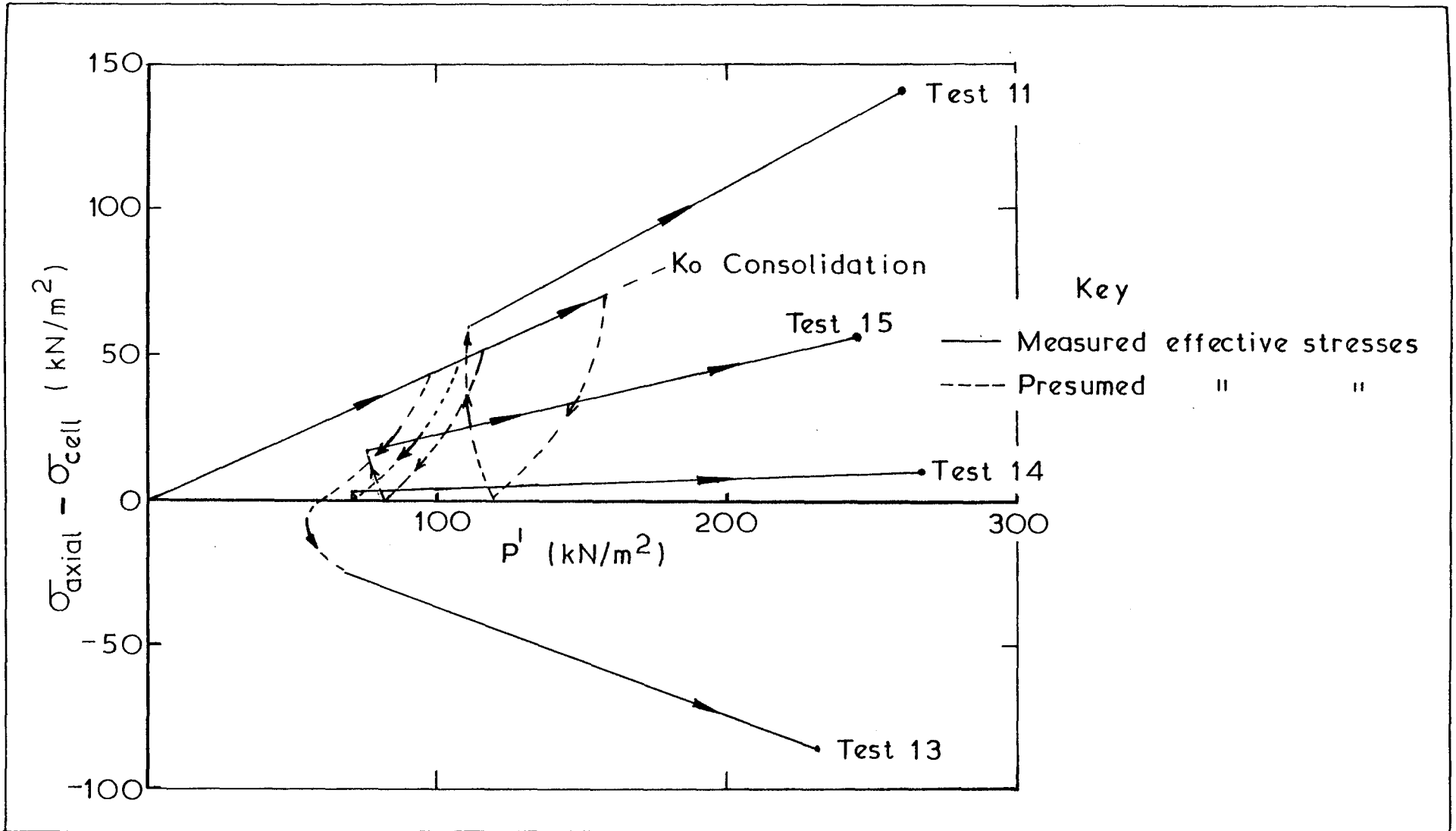


Fig. 5.2

A selection of effective stress paths followed during consolidation

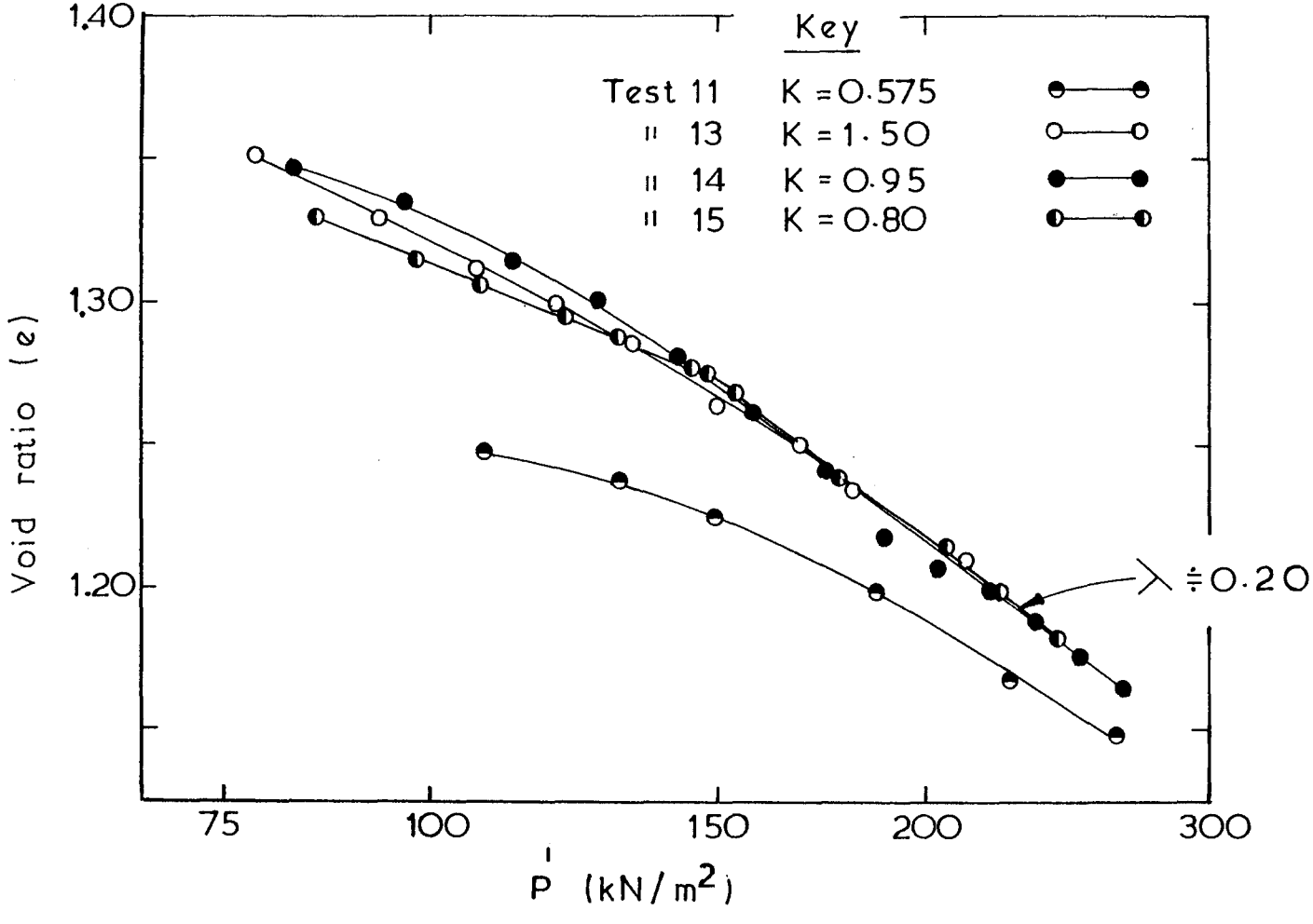


Fig. 5.3

A selection of paths in e-P' space followed during consolidation in the hydraulic triaxial cell

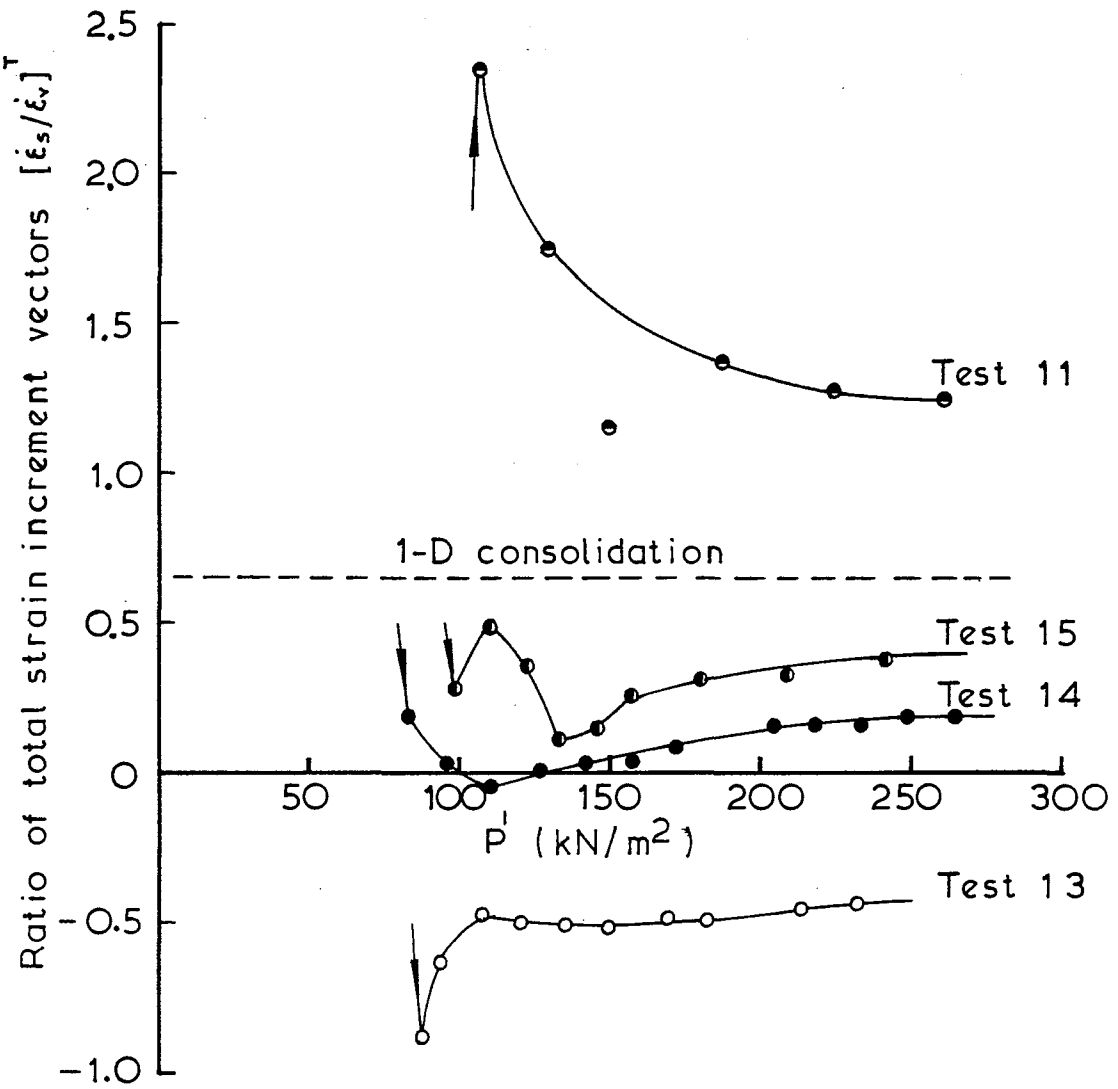


Fig. 5.4 Variation of total strain-increment vectors during the consolidation of a selection of samples

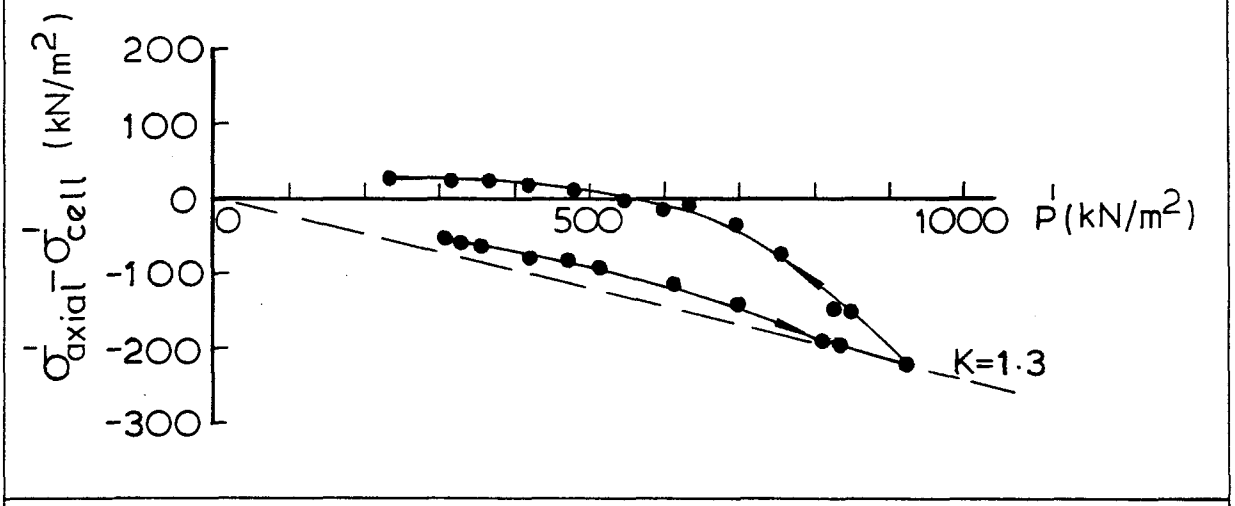
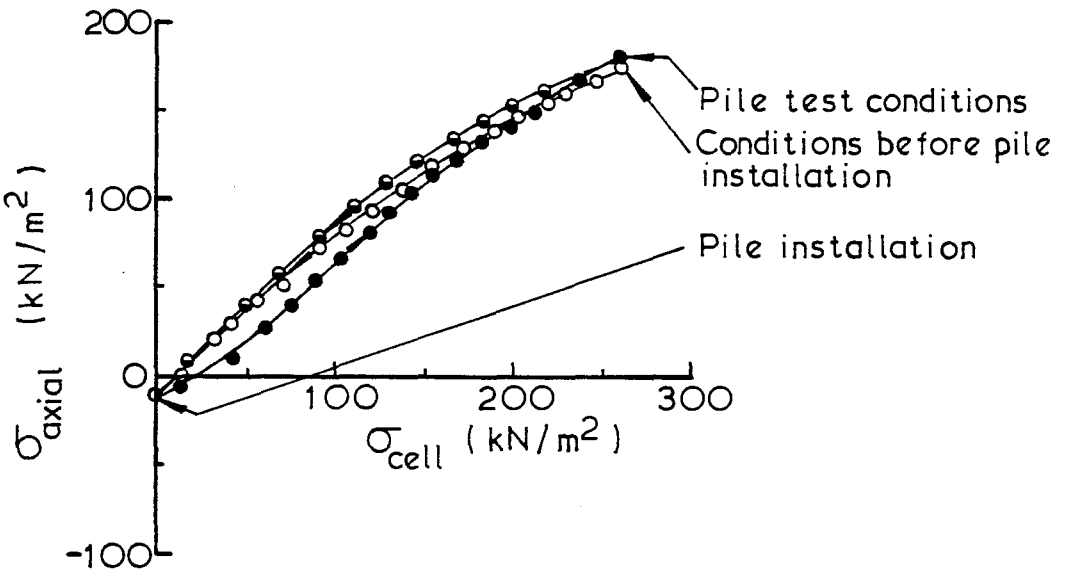
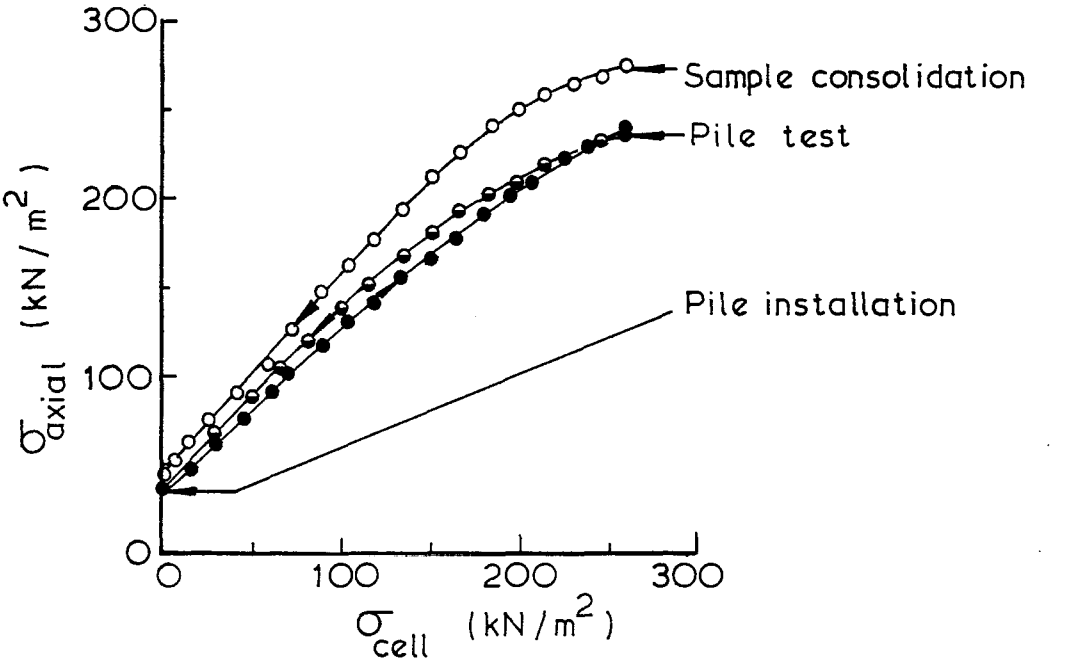


Fig. 5.5 Stress paths followed during consolidation and swelling in the preparation of an overconsolidated sample (Test 7)



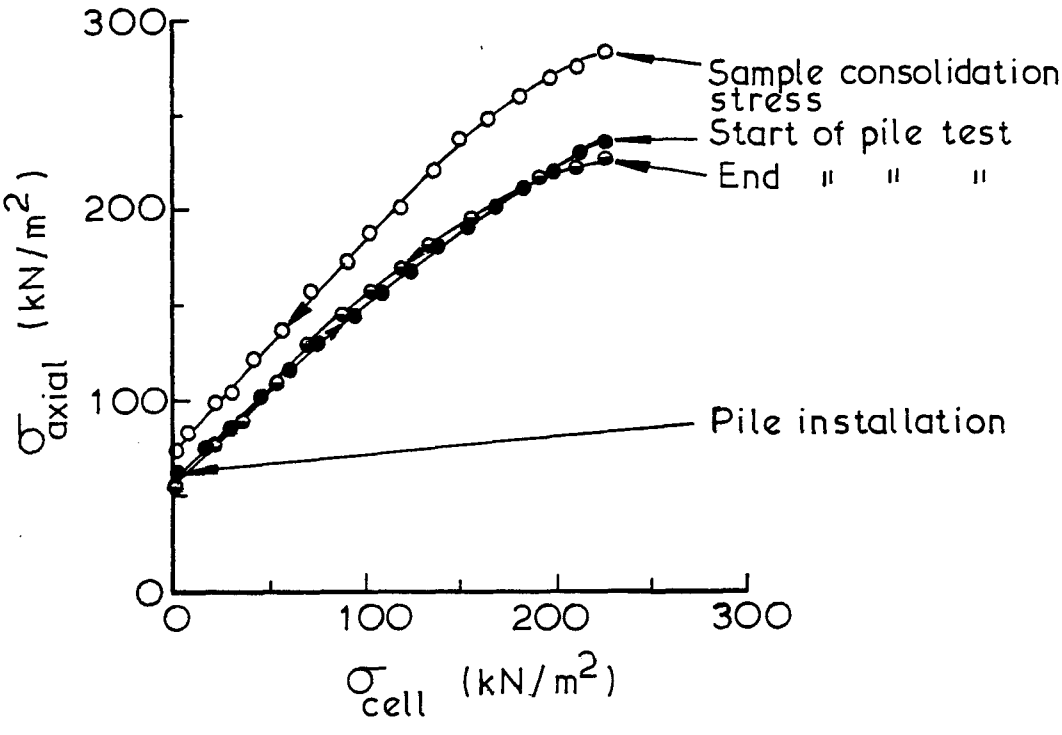
(a) Pile test 9; Consolidation stress ratio, K=1·5



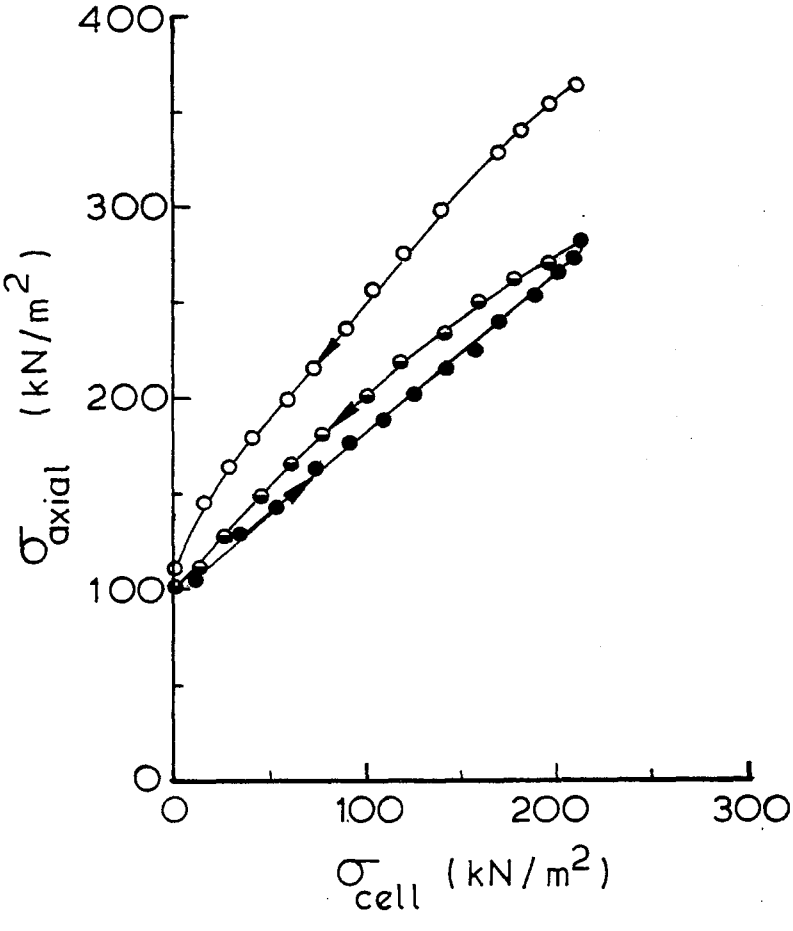
(b) Pile test 14; Consolidation stress ratio, K=0·95

Fig. 5.6 Total stress changes before and after pile installation

/ continued over-leaf

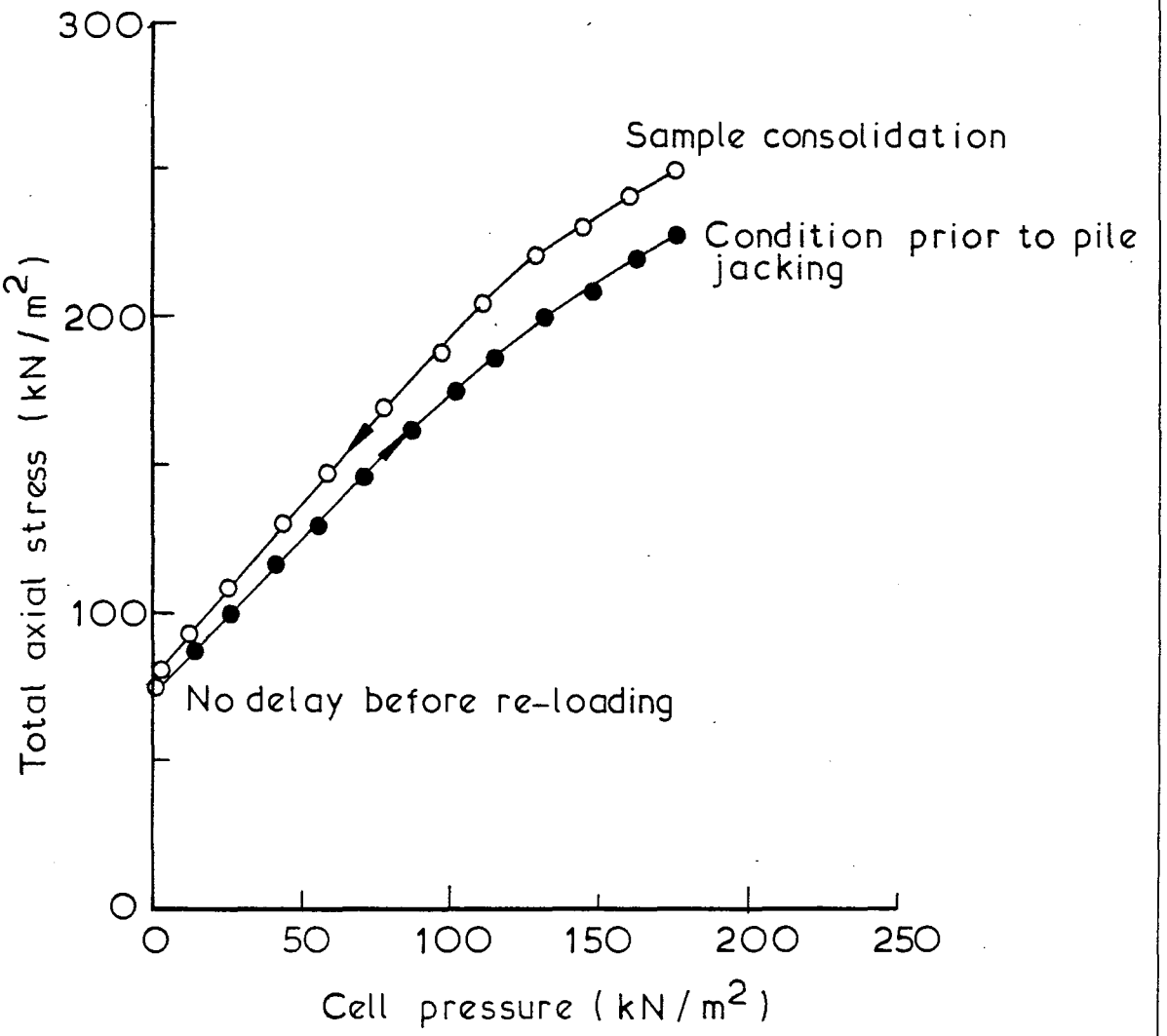


(c) Pile test 15 ; Consolidation stress ratio, K=0·8



(d) Pile test 11; Consolidation stress ratio, K=0·575

Fig. 5 · 6 continued



Total stress changes occurring during the unloading and re-loading of the sample from Test No. 19, before pile installation

Fig. 5.7

Sample 12	Sample 13	Sample 14	Sample 15	Sample 17
Top	Top	Top	Top	Top
46.2	48.5	45.9	45.3	46.6
46.7	47.2	45.4	44.0	45.7
45.0 ?	45.6	46.0 ?	44.5	45.6
45.9	45.7	44.8	44.5	45.3
45.2	47.1 ?	44.3	44.5	45.3
45.9	46.2	44.5	44.7	46.0?
45.2	46.4	44.6	44.0	45.3
45.9	46.8	44.1	44.4	45.1
46.3	46.5	45.1	44.3	44.9
46.7	47.1	46.2	44.4	45.3
Bottom	Bottom	Bottom	Bottom	Bottom
Mean 45.7	Mean 46.2	Mean 44.7	Mean 44.5	Mean 45.3
Post-test 45.9 *	Post-test N/A	Post-test 44.5 *	Post-test 45.0*	Post-test 45.5 *

Water content profiles obtained during pile installation

[*see text]

Fig. 5.8

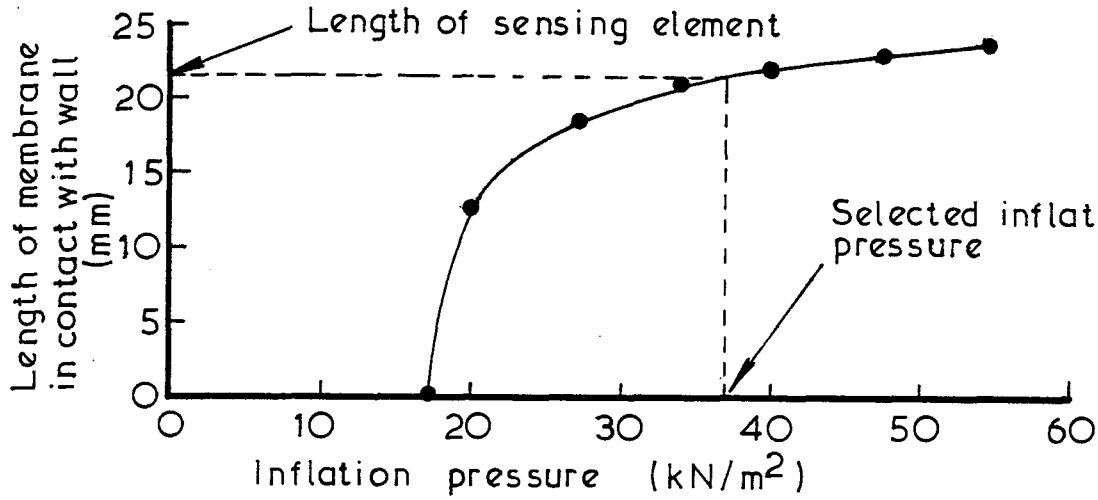
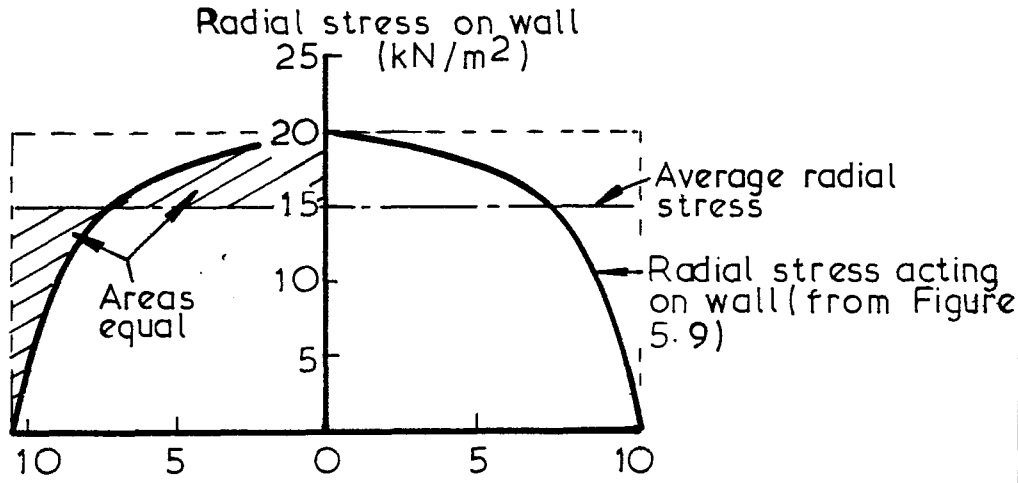


Fig. 5.9 Inflation characteristic of membrane employed in test 15.



Inflation pressure	= 37	kN/m^2
Average radial stress	= 15	"
Equivalent inflation pressure	= 22	"

Fig. 5.10 Determination of equivalent inflation pressure for Test 15

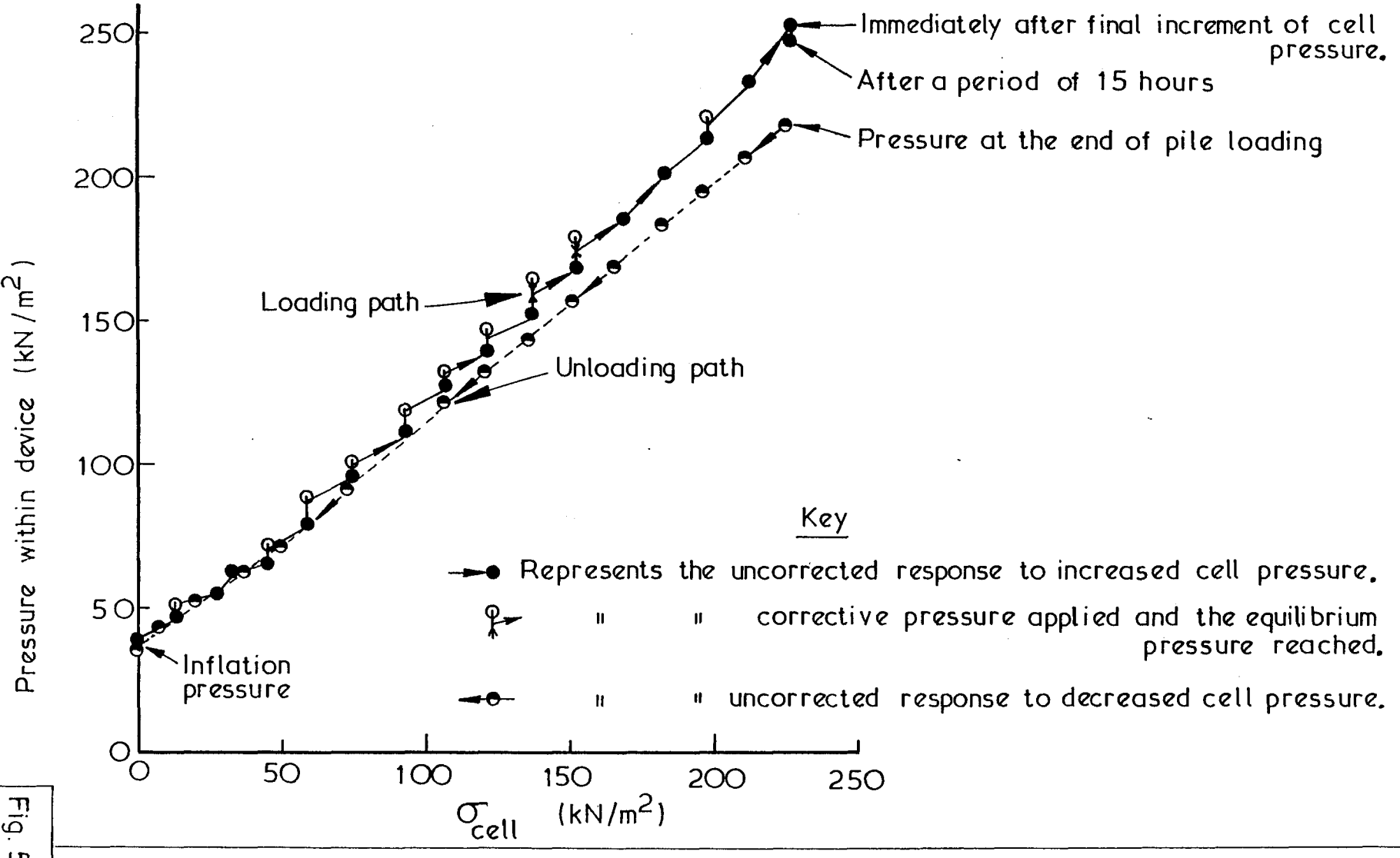


Fig. 5.11

Response of radial stress measuring device to changes in cell pressure (Test 15)

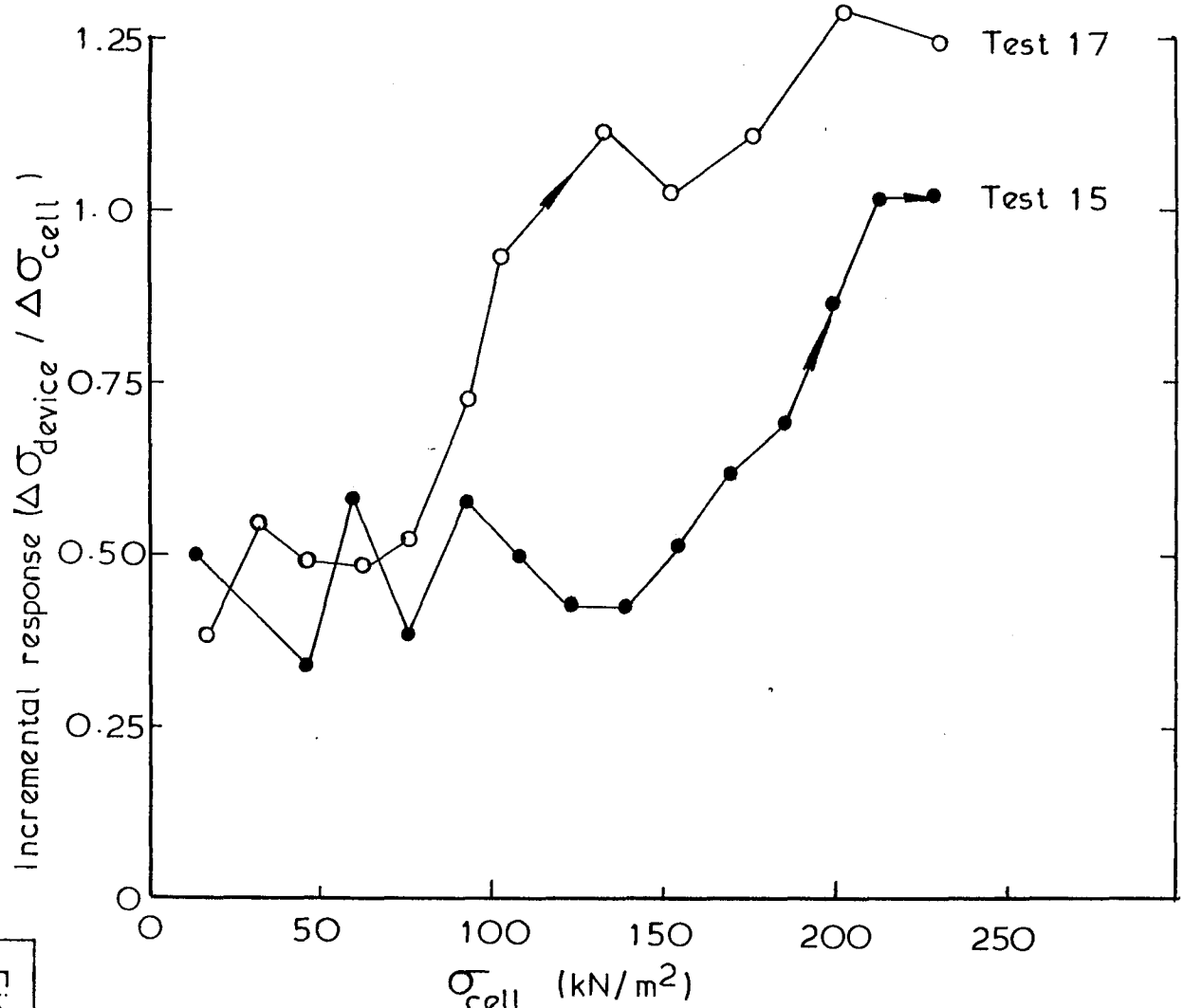
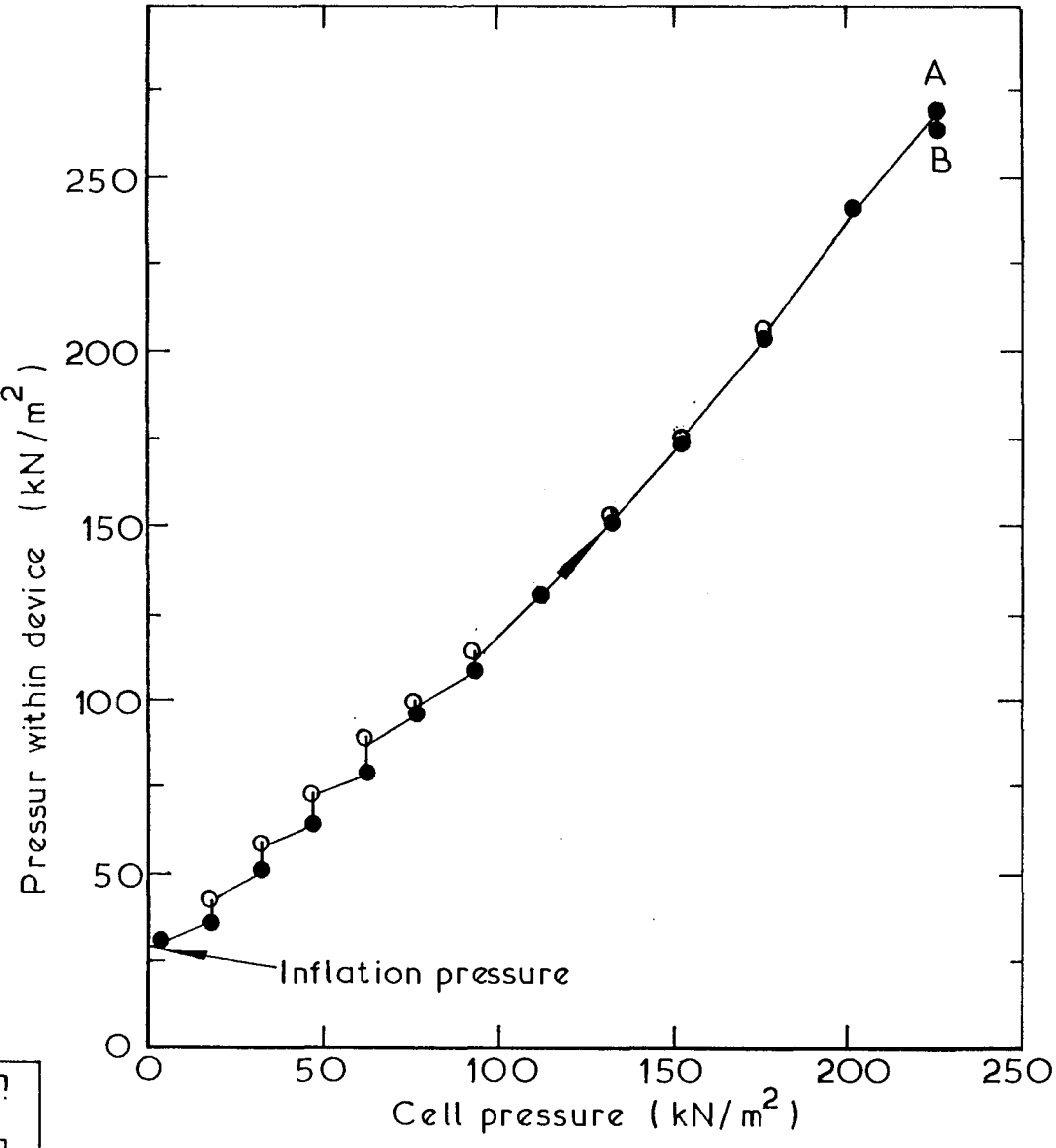


Fig. 5.12 Incremental responses of radial stress measuring devices employed in Tests 15 and 17.



Key

Point A – immediately after final increment of cell pressure

Point B – after 15 hours 'settling'

→● represents uncorrected response

→○ " final corrective pressure applied and the equilibrium pressure reached

Fig. 5.13

Response of radial stress-measuring device to increases in cell pressure (Test 17)

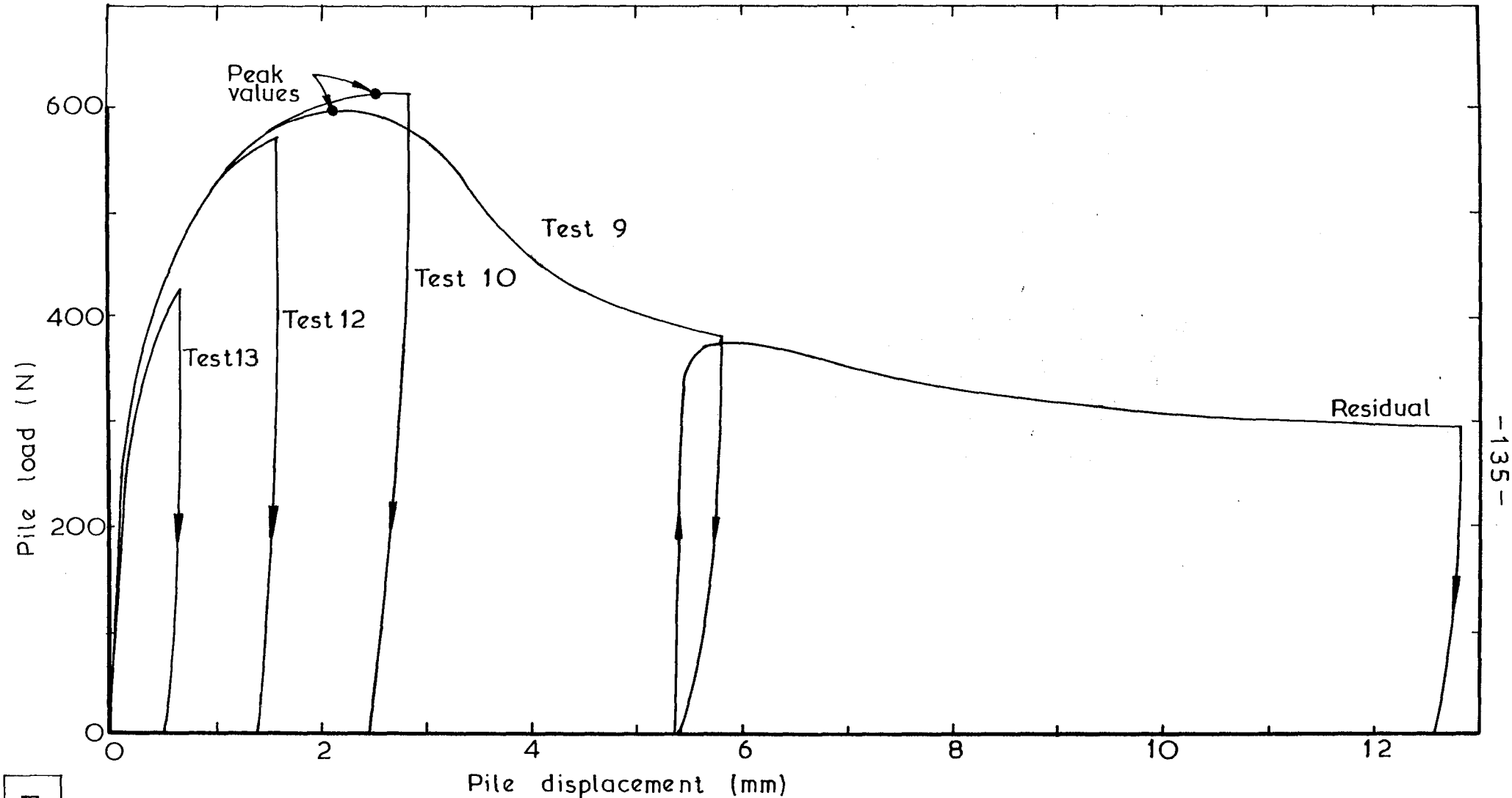


Fig. 5.14

Load-displacement curves for four similar tests stopped at different stages.

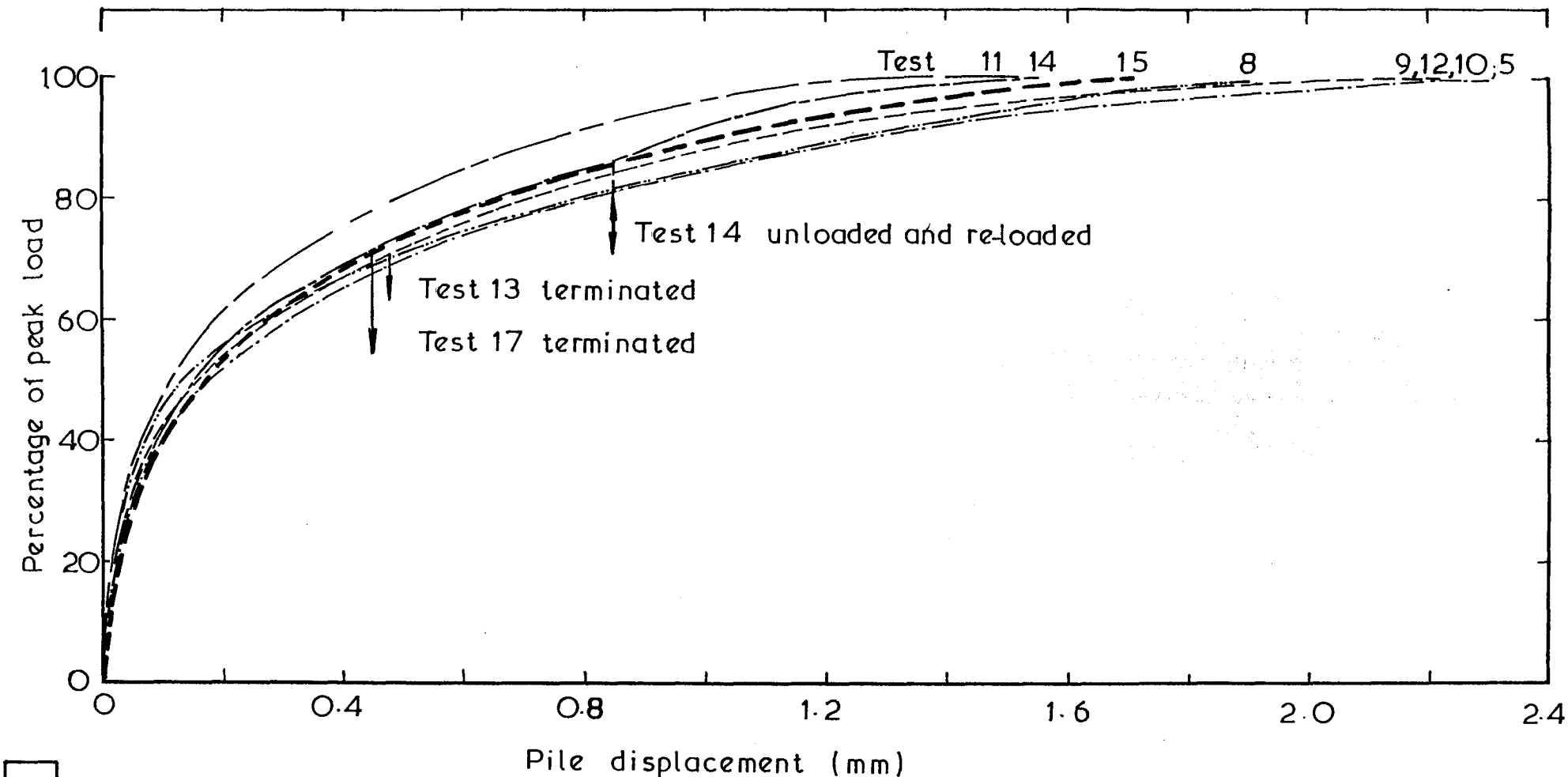


Fig. 5.15

Normalized pre-peak load-displacement behaviour during tests on normally consolidated kaolin at cell pressures of between 200 – 265 kN/m^2

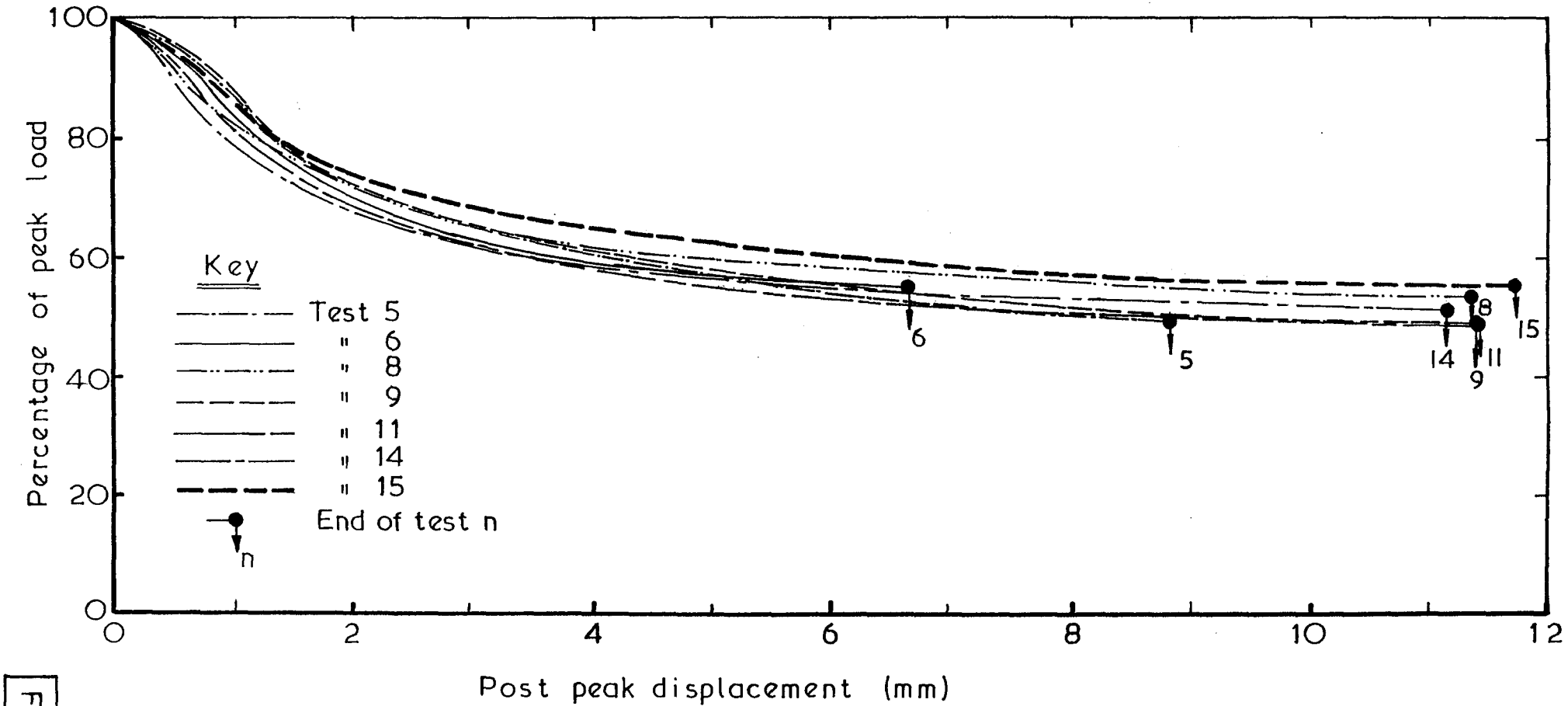
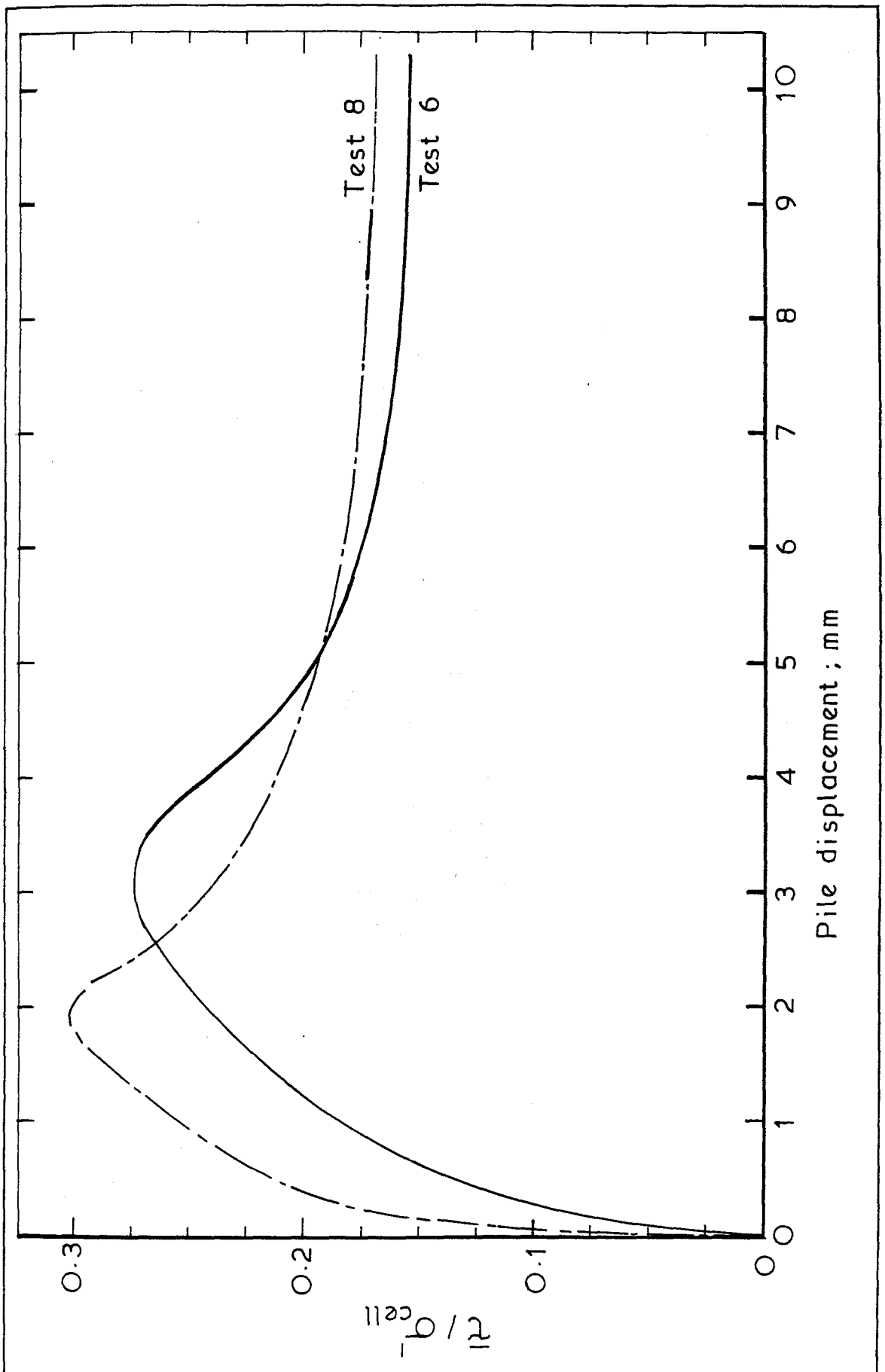


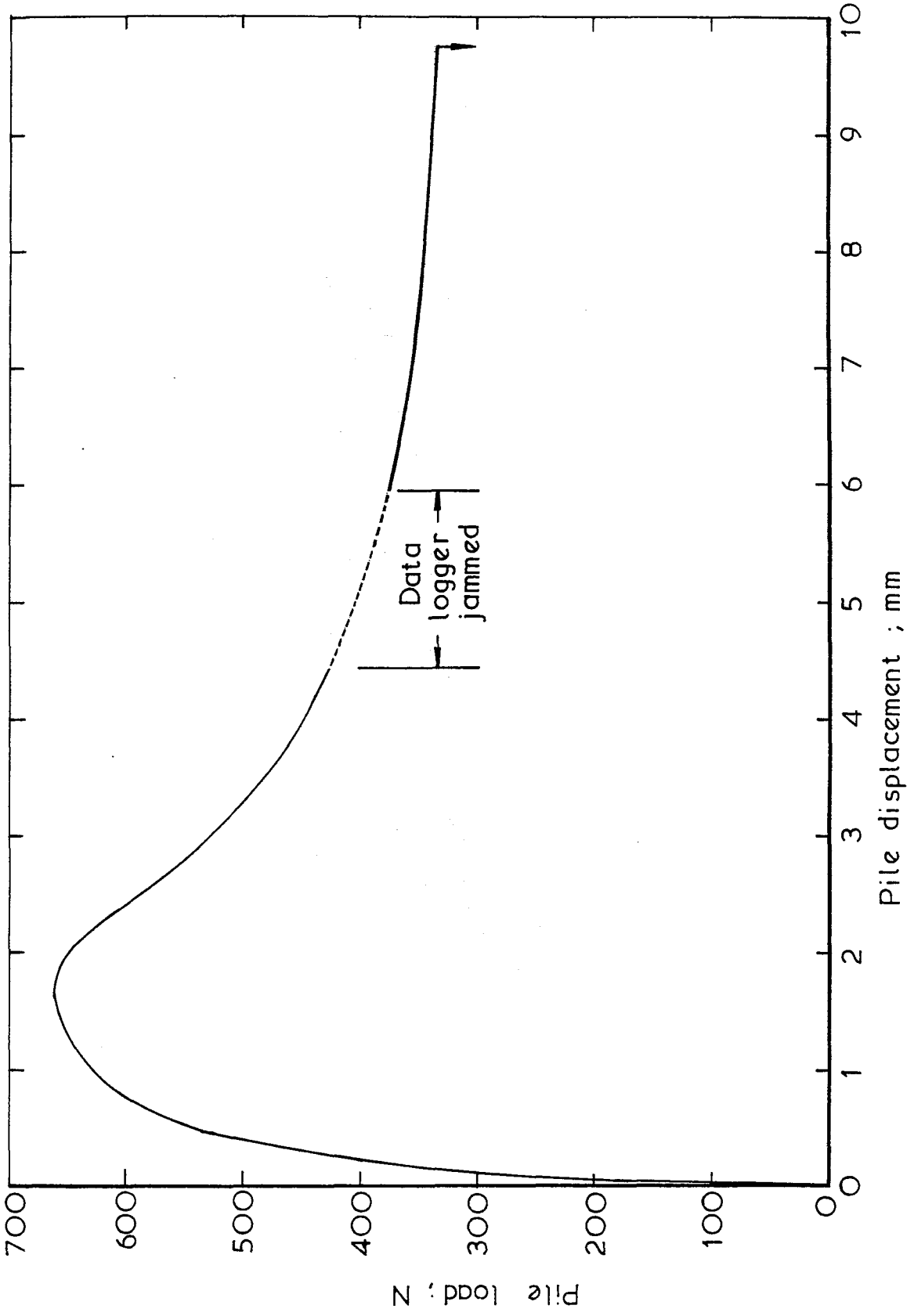
Fig. 5.16

Normalized post-peak load-displacement behaviour during tests on normally-consolidated kaolin.



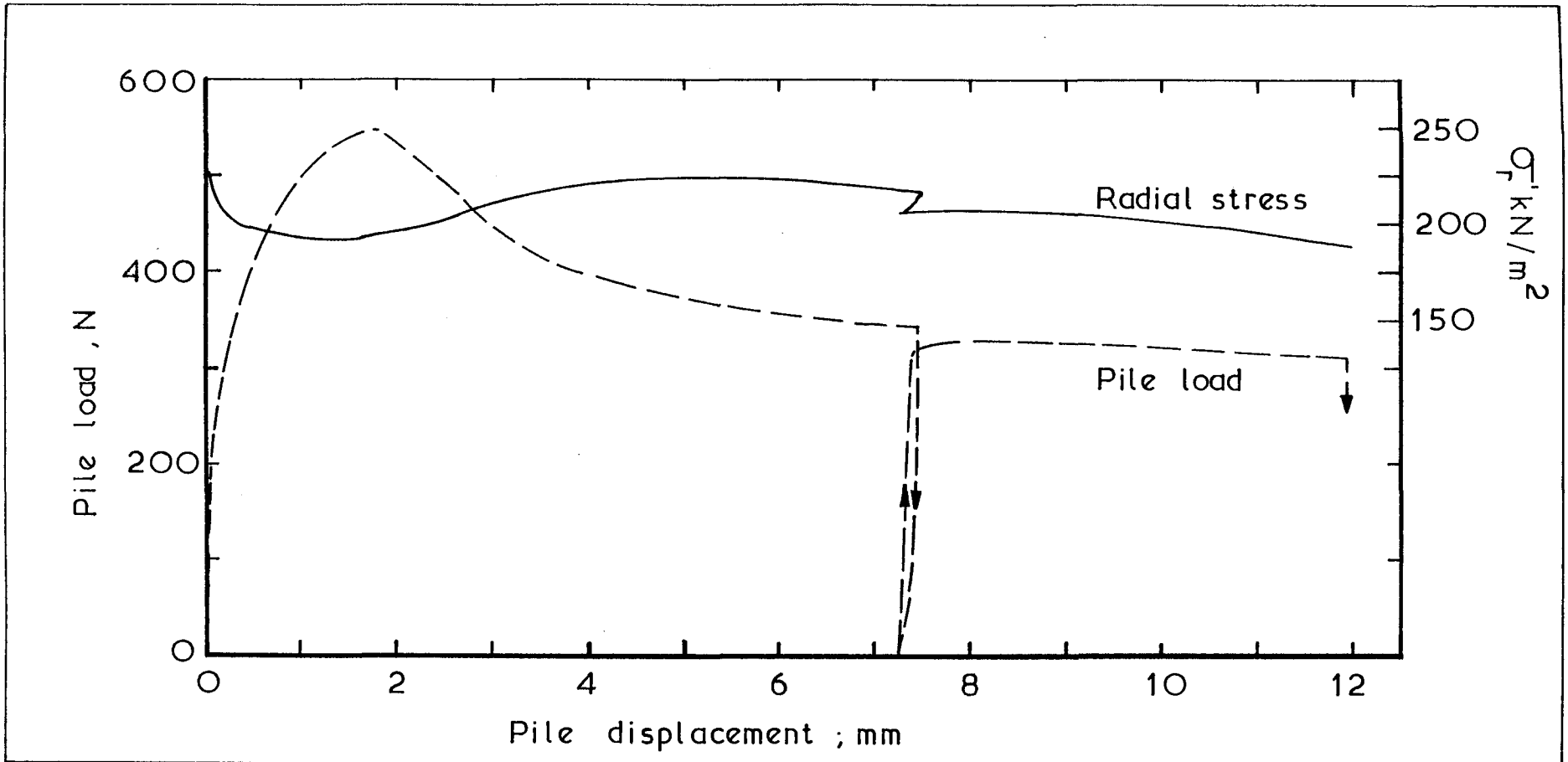
A comparison between the pile loading behaviours observed during Tests 6 and 8.

Fig. 5·17



Pile load-displacement behaviour observed during Test 7, performed on over-consolidated kaolin

Fig. 5 · 18



Variation of pile load and radial stress with pile displacement ; Test 15

Fig.5.19

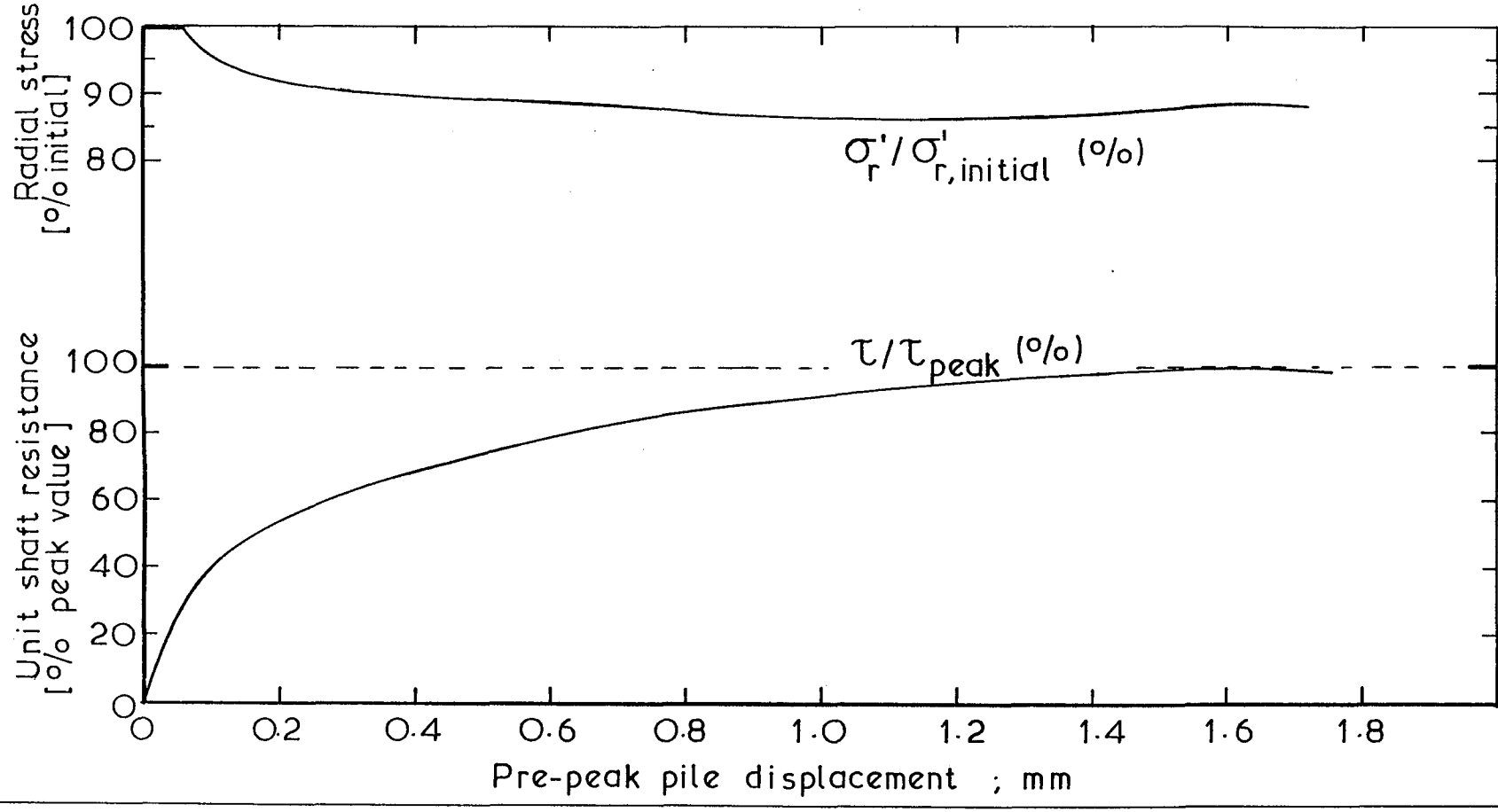
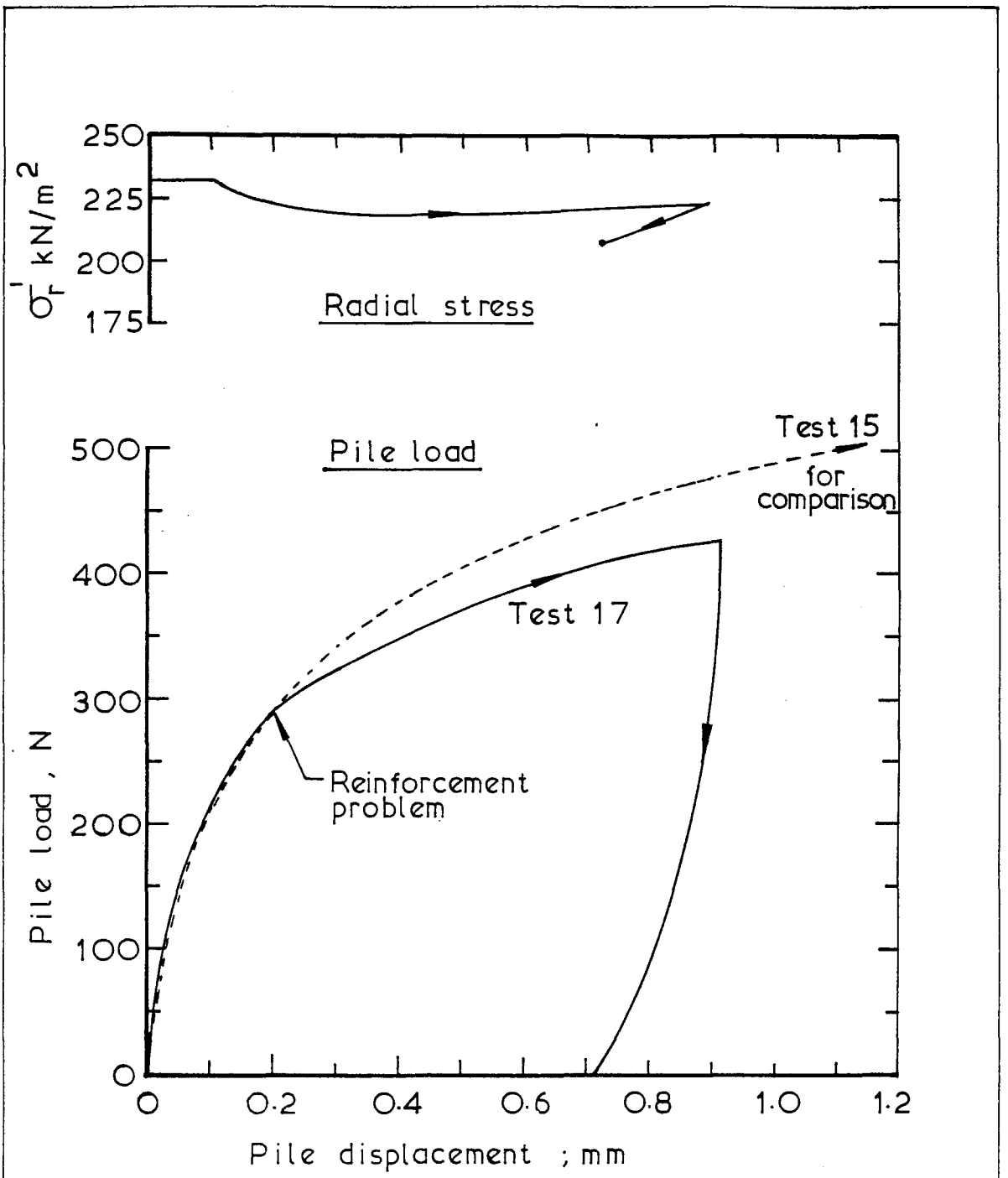


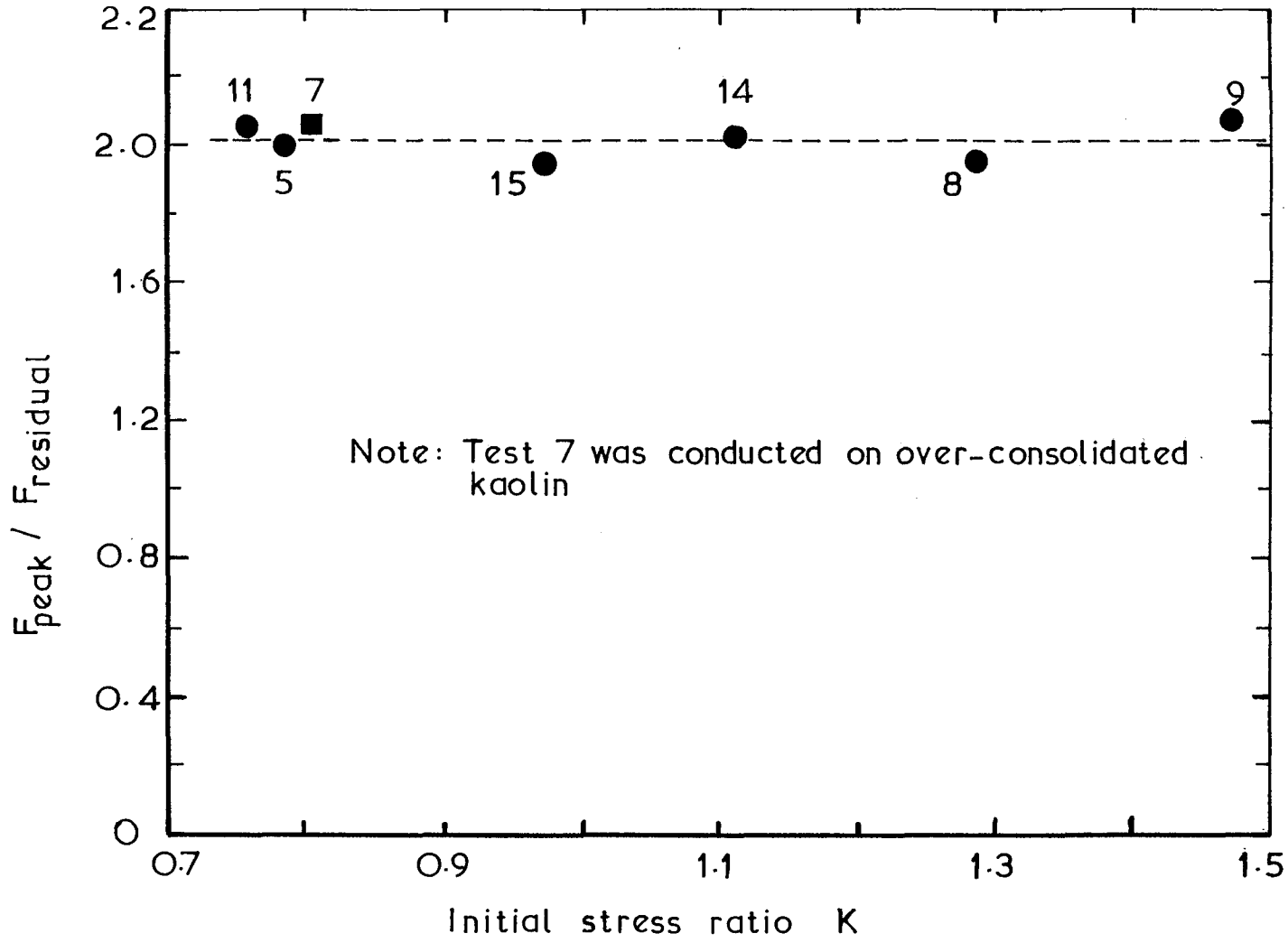
Fig. 5.20

Pre-peak variation of unit shaft resistance and radial stress with pile displacement
Test 15



Variation with pile displacement of the pile load and the radial stress; Test 17

Fig 5 · 21



Variation of the pile load ratio F_{peak} / $F_{residual}$ with the initial stress ratio, K

Fig. 5·22

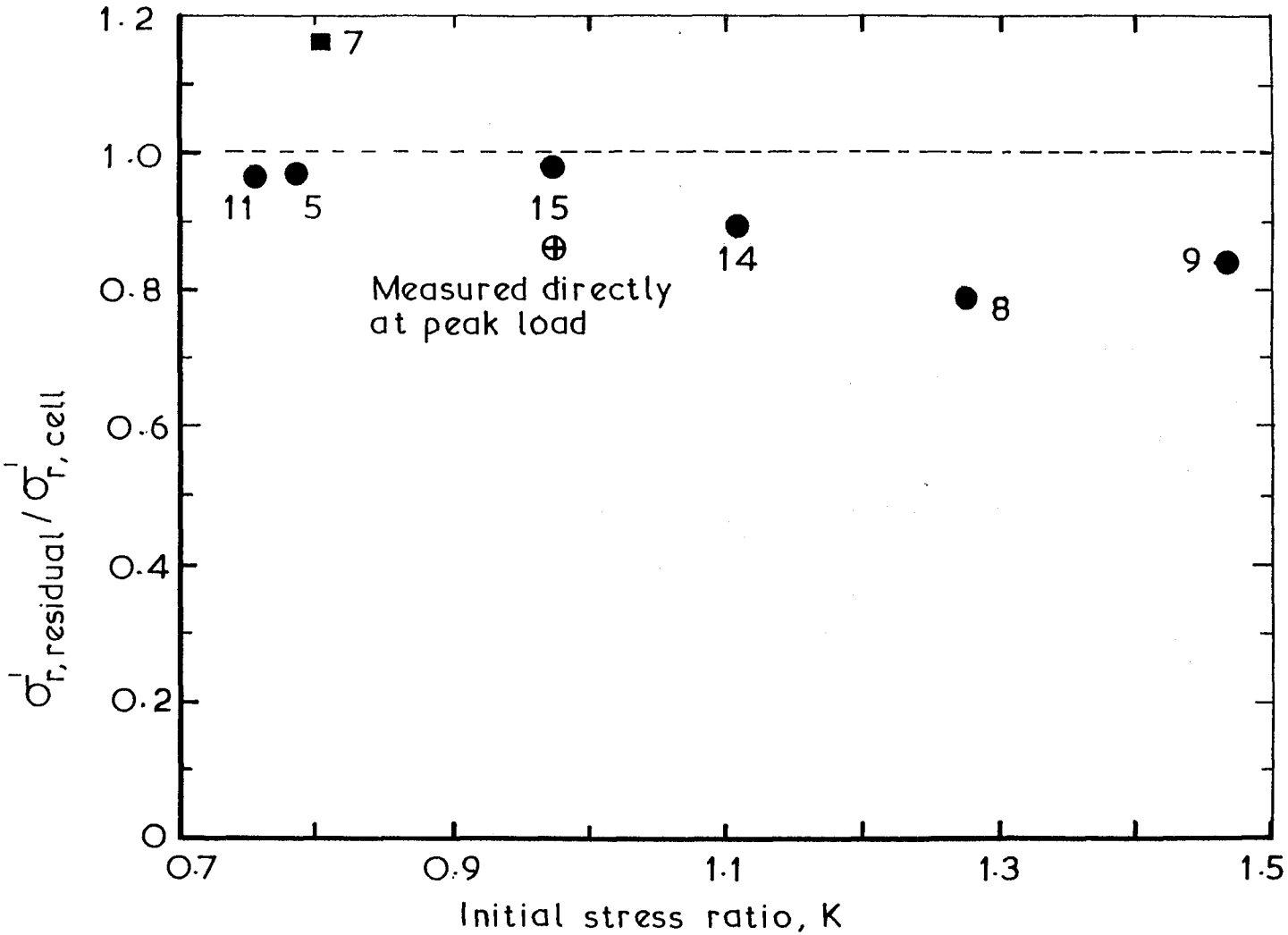
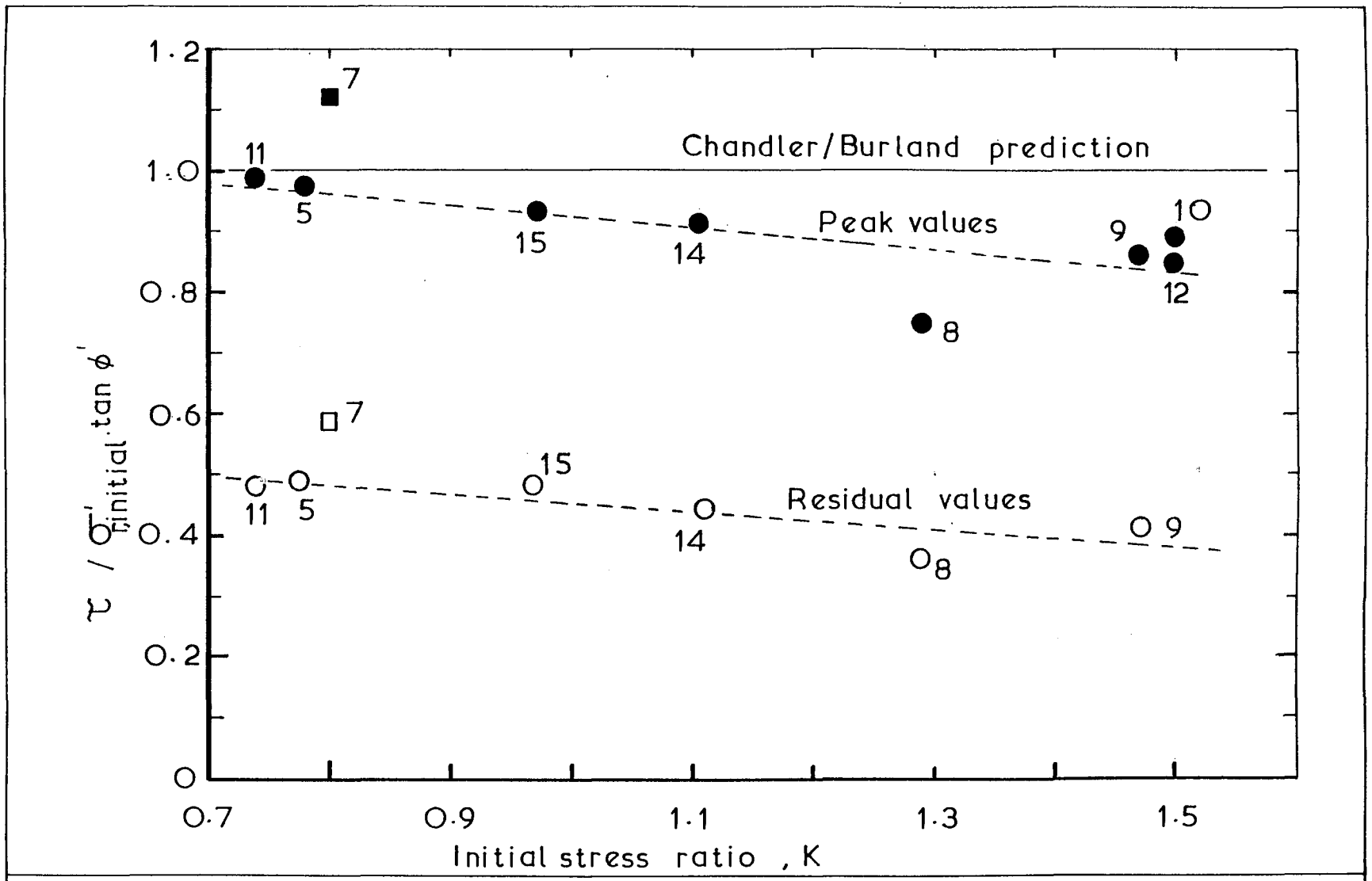


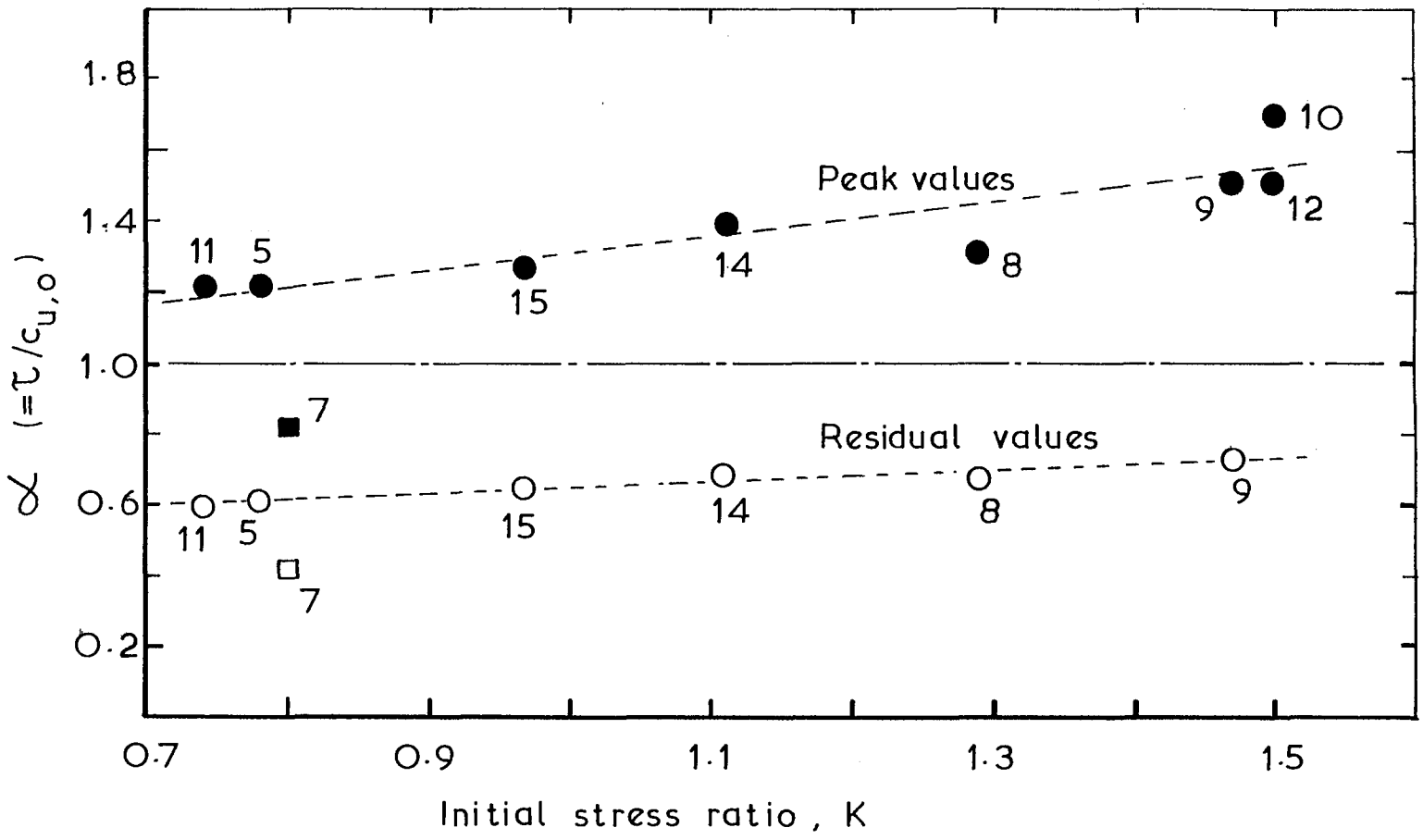
Fig. 5.23

Variation of back-calculated radial stress ratio $\sigma'_{r,residual} / \sigma'_{r,cell}$ with initial stress ratio, K, applied to the sample.



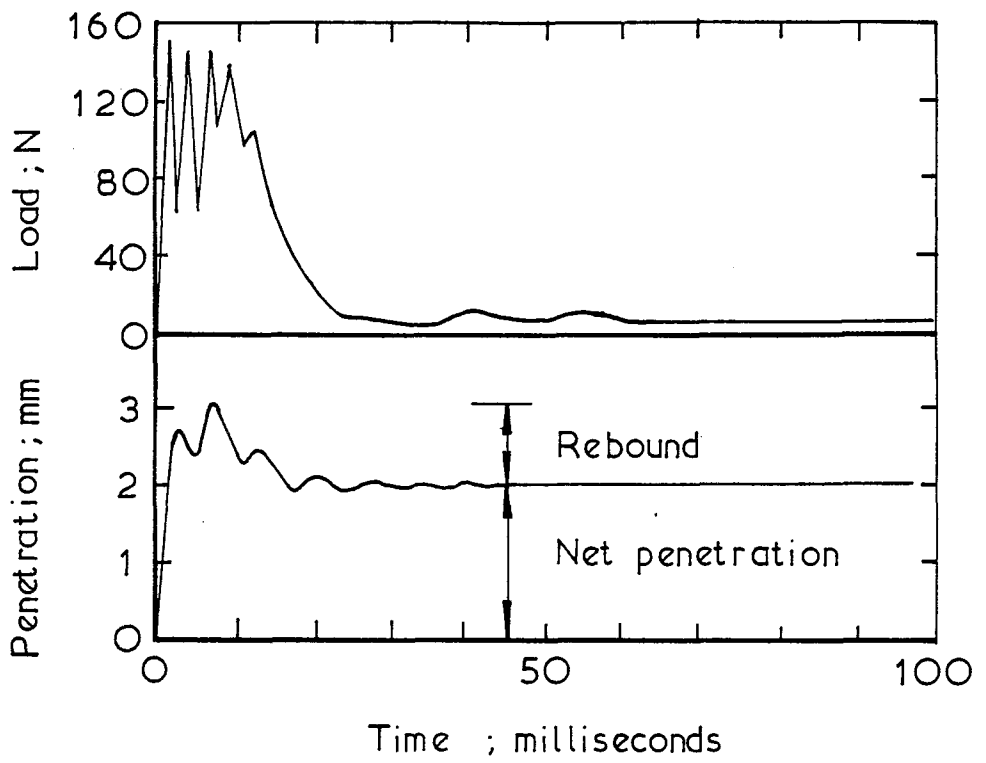
Model pile test results compared with the Chandler / Burland predictions

Fig. 5.24



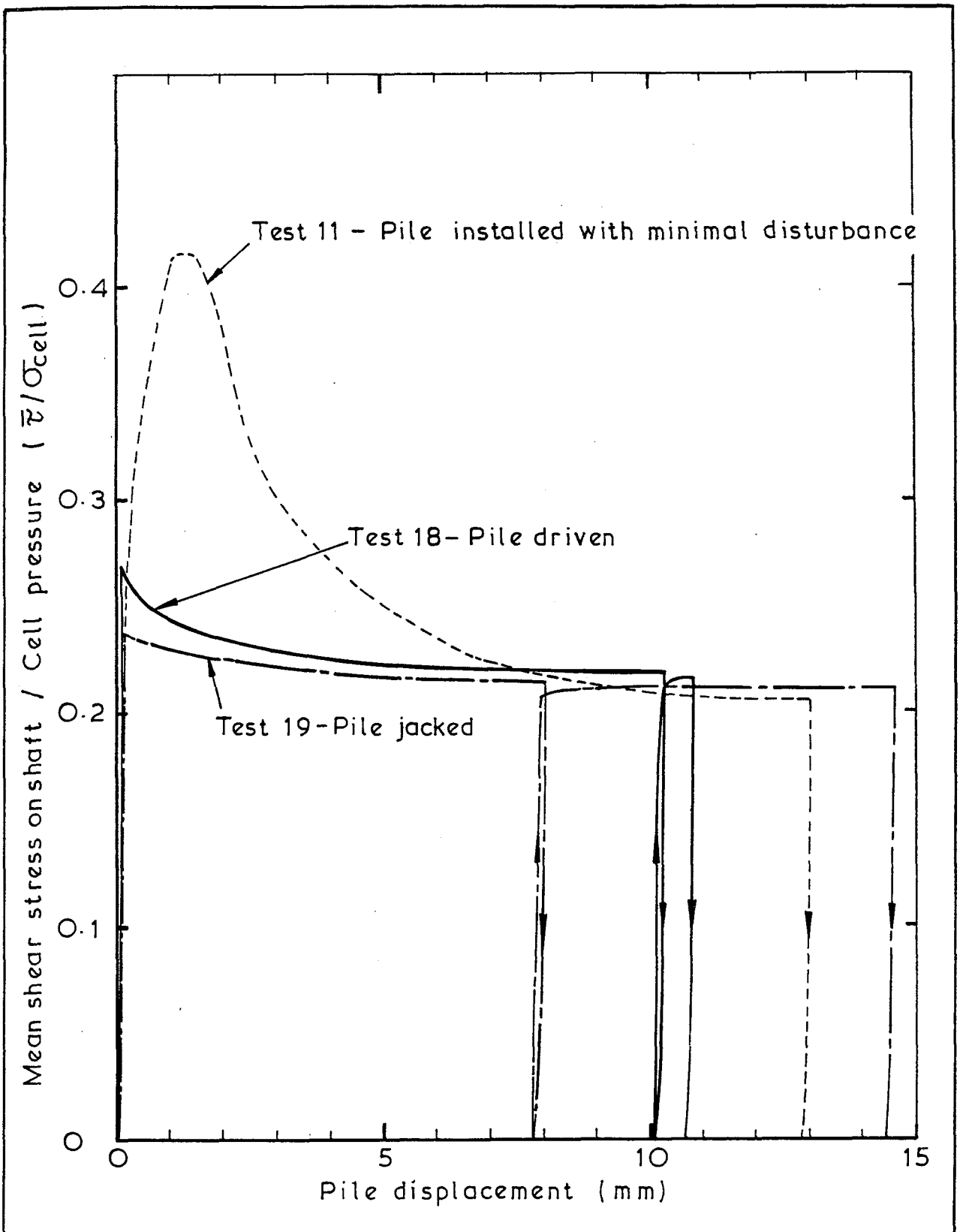
Variation of α with initial stress ratio

Fig. 5·25



Oscilloscope traces representing the pile load and displacement as functions of time, following a hammer blow during the pile driving in Test 16. Current pile embedment is about 30 mm

Fig. 5.26



Load-displacement behaviour of piles installed by different methods.

Fig. 5·27

APPENDIX 5.1

THE USE OF STRAIN INCREMENT VECTORS TO MONITOR CONSOLIDATION

Two convenient invariant measures of volumetric and shear strain, ε_v and ε_s respectively, may be defined in terms of the three principal strains ε_1, ε_2, ε_3 as follows;

$$\varepsilon_v = \varepsilon_1 + \varepsilon_2 + \varepsilon_3$$

$$\varepsilon_s = \frac{\sqrt{2}}{3}\left[(\varepsilon_1 - \varepsilon_2)^2 + (\varepsilon_2 - \varepsilon_3)^2 + (\varepsilon_3 - \varepsilon_1)^2\right]^{\frac{1}{2}}$$

In triaxial space, $\varepsilon_2 = \varepsilon_3$ or $\varepsilon_2 = \varepsilon_1$, so the above quantities reduce to;

$$\varepsilon_v = \varepsilon_1 + 2\varepsilon_3 \text{ or } \varepsilon_3 + 2\varepsilon_1$$

and

$$\varepsilon_s = \frac{2}{3}(\varepsilon_1 - \varepsilon_3)$$

For a triaxial sample of length L, and volume v, the incremental values of ε_v and ε_s (i.e. $\dot{\varepsilon}_v$ and $\dot{\varepsilon}_s$) reduce to

$$\dot{\varepsilon}_v = \dot{\varepsilon}_{axial} + 2\,\dot{\varepsilon}_{lateral}$$

so

$$\dot{\varepsilon}_{lateral} = (\dot{\varepsilon}_v - \dot{\varepsilon}_{axial})/2$$

as

$$\dot{\varepsilon}_s = \frac{2}{3}(\dot{\varepsilon}_1 - \dot{\varepsilon}_3)$$

$$\dot{\varepsilon}_s = \frac{2}{3}\left|\dot{\varepsilon}_{axial} - \dot{\varepsilon}_{lateral}\right| = \frac{2}{3}\left|\dot{\varepsilon}_{axial} - (\dot{\varepsilon}_v - \dot{\varepsilon}_{axial})/2\right|$$

$\therefore$

$$\dot{\varepsilon}_s = \left|\dot{\varepsilon}_{axial} - \dot{\varepsilon}_v/3\right|$$

For the present purposes it is convenient to define $\dot{\varepsilon}_s$ as $(\dot{\varepsilon}_{axial} - \dot{\varepsilon}_v/3)$ rather than as its modulus, and the quantity is no longer invariant as its sign will depend on whether the sample is subject to triaxial compression or extension.

Now $\dot{\varepsilon}_v = \dot{V}/v_o$, and $\dot{\varepsilon}_{axial} = \dot{L}/L_o$

so $$\left(\frac{\dot{\varepsilon}_s}{\dot{\varepsilon}_v}\right) = \left(\frac{\dot{\varepsilon}_{axial} - \dot{\varepsilon}_v/3}{\dot{\varepsilon}_v}\right) = \left(\frac{\dot{L}/L_o}{\dot{V}/v_o} - \frac{1}{3}\right)$$

While a sample of clay is undergoing virgin consolidation at a constant stress ratio, the plastic strain increment vectors lie at a fixed orientation with respect to the consolidation stress vector. The relative inclinations depend on the flow rule, the plastic strain increment vector being normal to the yield surface if the plastic potential and the yield surface are co-incident. The direction of the strain increment vector may be determined from the ratio of plastic shear, to plastic volumetric strain increments $(\dot{\varepsilon}_s/\dot{\varepsilon}_v)^P$. Experimentally, the ratio of the total strain increments (elastic and plastic components combined) is much easier to determine, and for this reason it was used to monitor the consolidation. If the clay were to obey the 'Modified Cam Clay' constitutive law, then the total and plastic strain increment ratios would be related by the expression

$$\left(\frac{\dot{\varepsilon}_s}{\dot{\varepsilon}_v}\right)^T = (1 - \kappa/\lambda) \left(\frac{\dot{\varepsilon}_s}{\dot{\varepsilon}_v}\right)^P$$

and are, therefore, in a constant proportion to one another (provided that κ/λ does not change).

If a sample of clay which behaves in a normally consolidated fashion at one stress ratio is then consolidated at a new stress ratio, the direction of the strain increment vectors will change, asymptotically approaching a constant value corresponding to the new stress ratio. This behaviour was observed during the consolidation of Kaolin samples in the hydraulic triaxial cell. In Fig. A.5.1.1, the ratio of total strain increments is plotted against mean effective stress for four samples which were consolidated initially under K_o condition, and then at a stress ratio, K, of 1.5. One of the samples was initially consolidated to a lower water content than the other three before being transferred to the triaxial cell, and the effect of this on the subsequent response may be seen in Fig. A.5.1.1. In all cases, however, the ratio of the total strain increments tended asymptotically to a constant value, and the samples were all behaving in a normally-consolidated fashion at the new stress ratio when the desired stress level was achieved. This illustrates that a doubling of the stress level was sufficient largely to obliterate the effects of the earlier stress history.

The values of the asymptotic ratios of total strain increments from various tests are plotted as a function of the consolidation stress ratio in Fig. A.5.1.2. Also shown in the figure are experimental results compiled by Lewin (1970) from work performed, using Spestone Kaolin, by Thurairajah, Poorooshasb, Balasubramaniam and Parry and Amerasinghe (1975). Predictions based on Modified Cam Clay are also presented for comparison.

The results obtained during the current investigation are in good agreement with those quoted by other workers. However, predictions based on Modified Cam Clay are in only fair agreement with the experimental results. The value of K_o determined from the experimental results (corresponding to $(\dot{\varepsilon}_s/\dot{\varepsilon}_v)^T = 2/3$) is 0.65 ± 0.01, which is in excellent agreement with direct measurements; Yong (1979) measured K_o = 0.64 ± 0.01 for Speswhite Kaolin, and Parry and Nadarajah (1974) measured K_o = 0.66 for Spestone Kaolin. In contrast, Modified Cam Clay predicts $K_o \sim 0.74$ which is clearly an overestimate. This is not a surprising result, and is in common with predictions based on the majority of currently available constitutive laws which do not use a value of K_o as one of the basic parameters.

The experimentally determined ratio of total strain increments is a very sensitive quantity being affected by changes in increment sizes, temperature and other factors, but has proved to be a most useful quantity to observe during consolidation, and the author is grateful to Dr. Antonio Gens for suggesting its use.

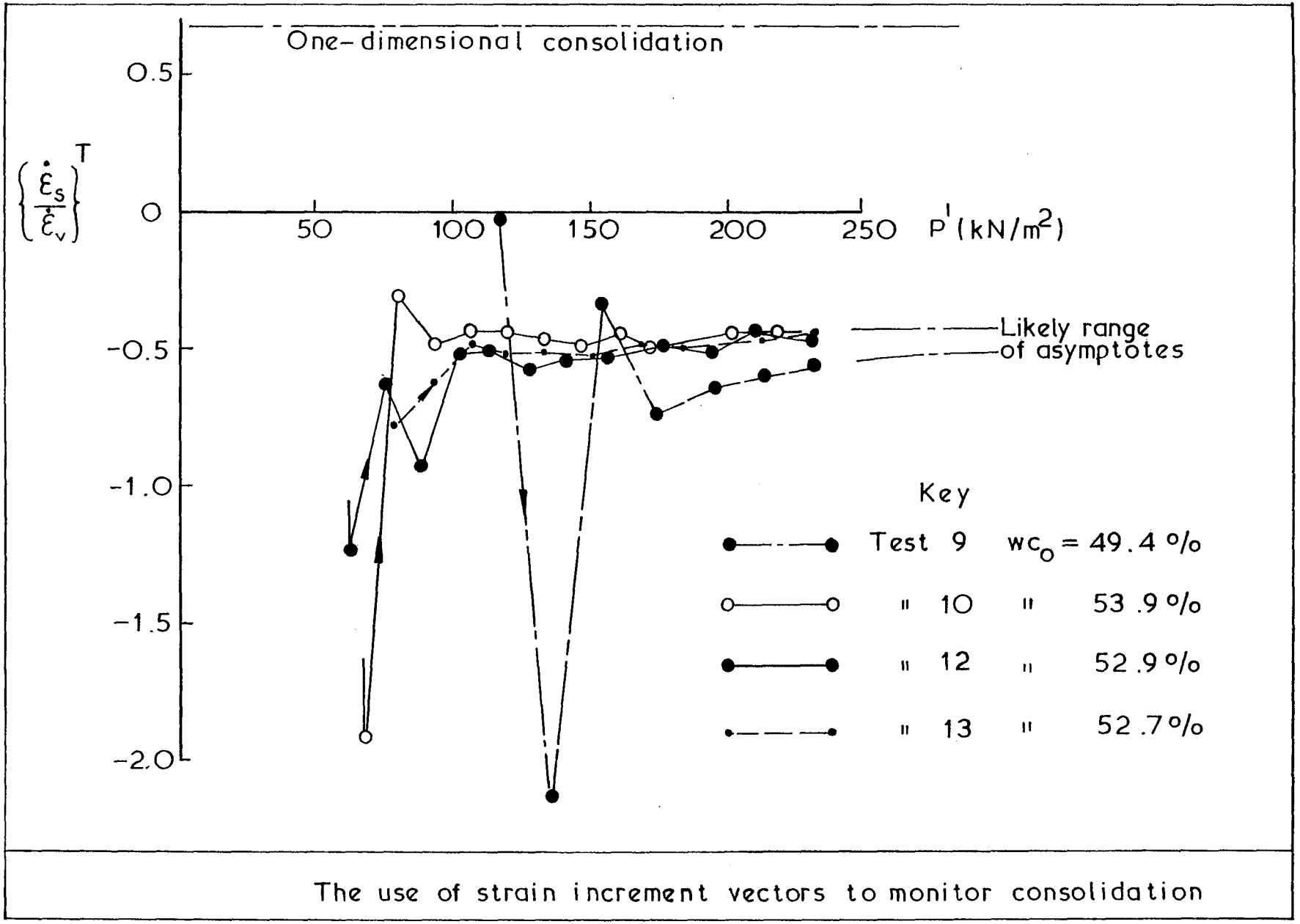


Fig. A. 5. 1. 1

The use of strain increment vectors to monitor consolidation

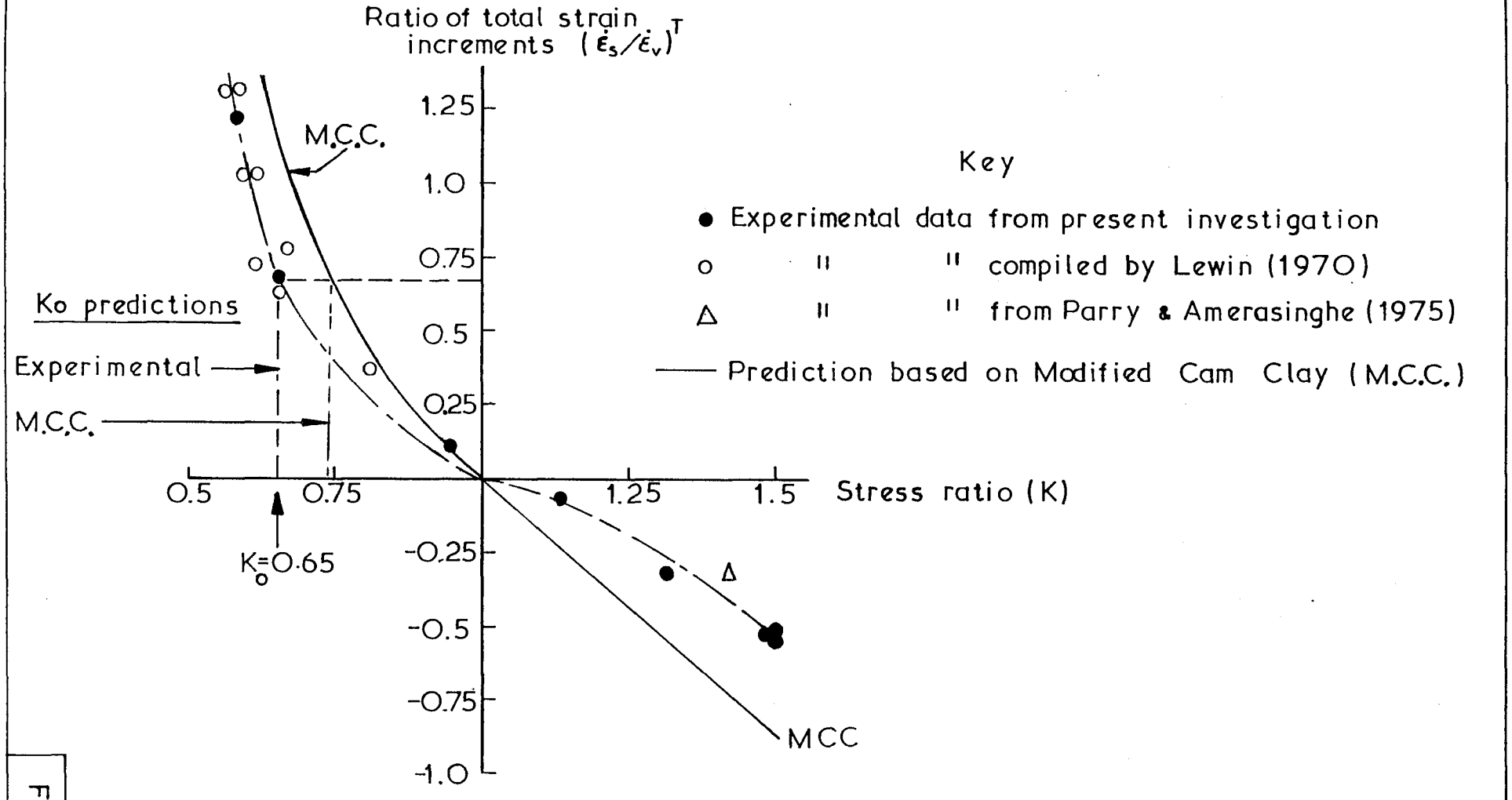


Fig. A.5.1.2

Variation of the ratio of total strain increments with consolidation stress ratio (K)

APPENDIX 5.2

TOTAL STRESS CHANGES MEASURED DURING PILE INSTALLATION

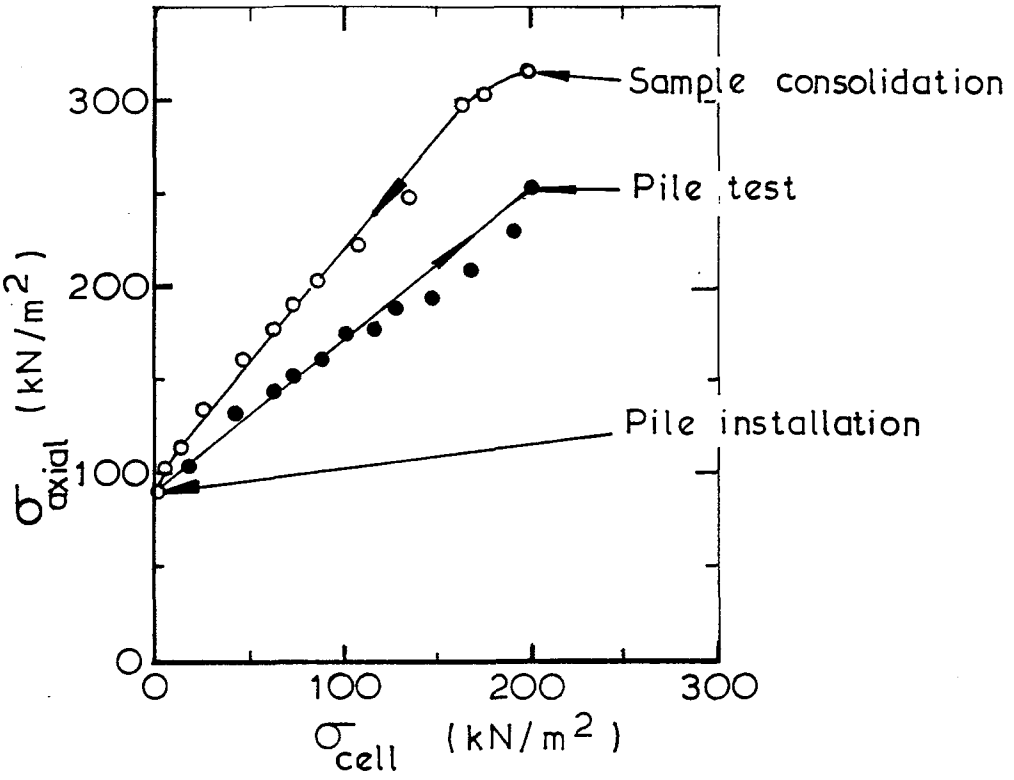
The variation of the axial total stresses acting on the Kaolin samples during the installation of the model piles in tests 5, 6, 8, 10, 12 and 13 are illustrated below in Figures A.5.2a, b, c, d, e and f respectively.

Key

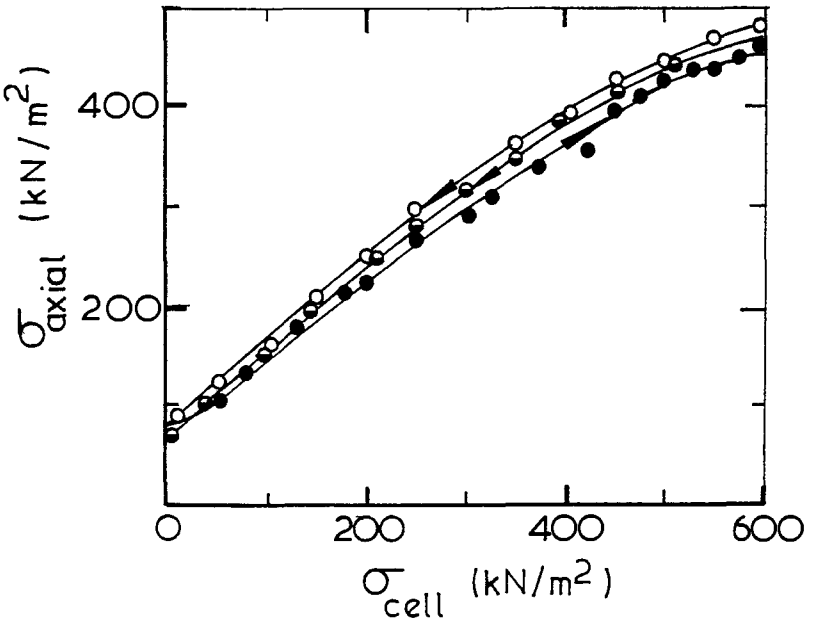
o—o Represents unloading path before pile installation

●—● " reloading " after " "

o—o " unloading " " " test



(a) Pile test 5



(b) Pile test 6

Fig.A.5.2 Total stress changes before and after pile installation.

/continued over-leaf

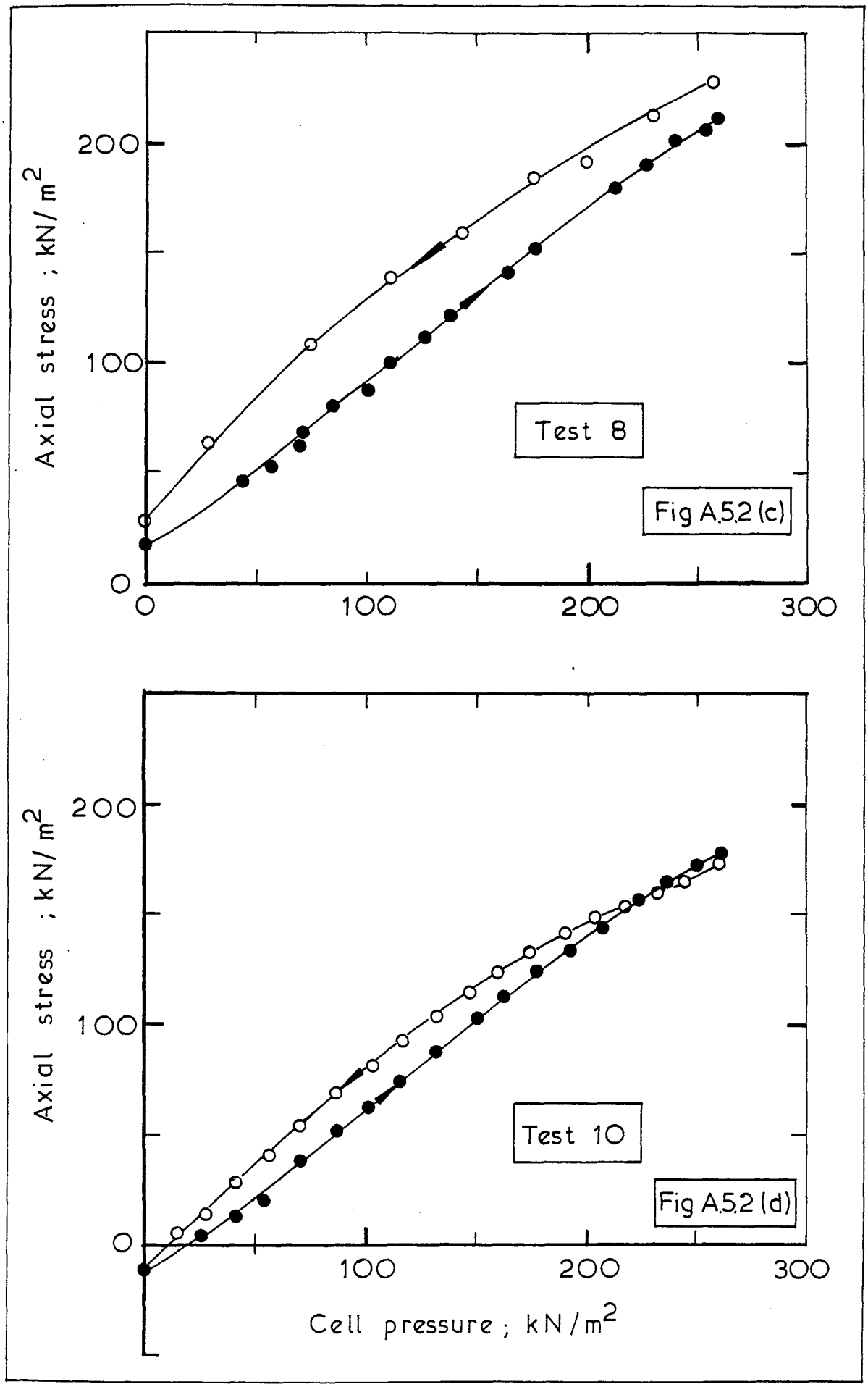


Fig.A.5.2 cont'd

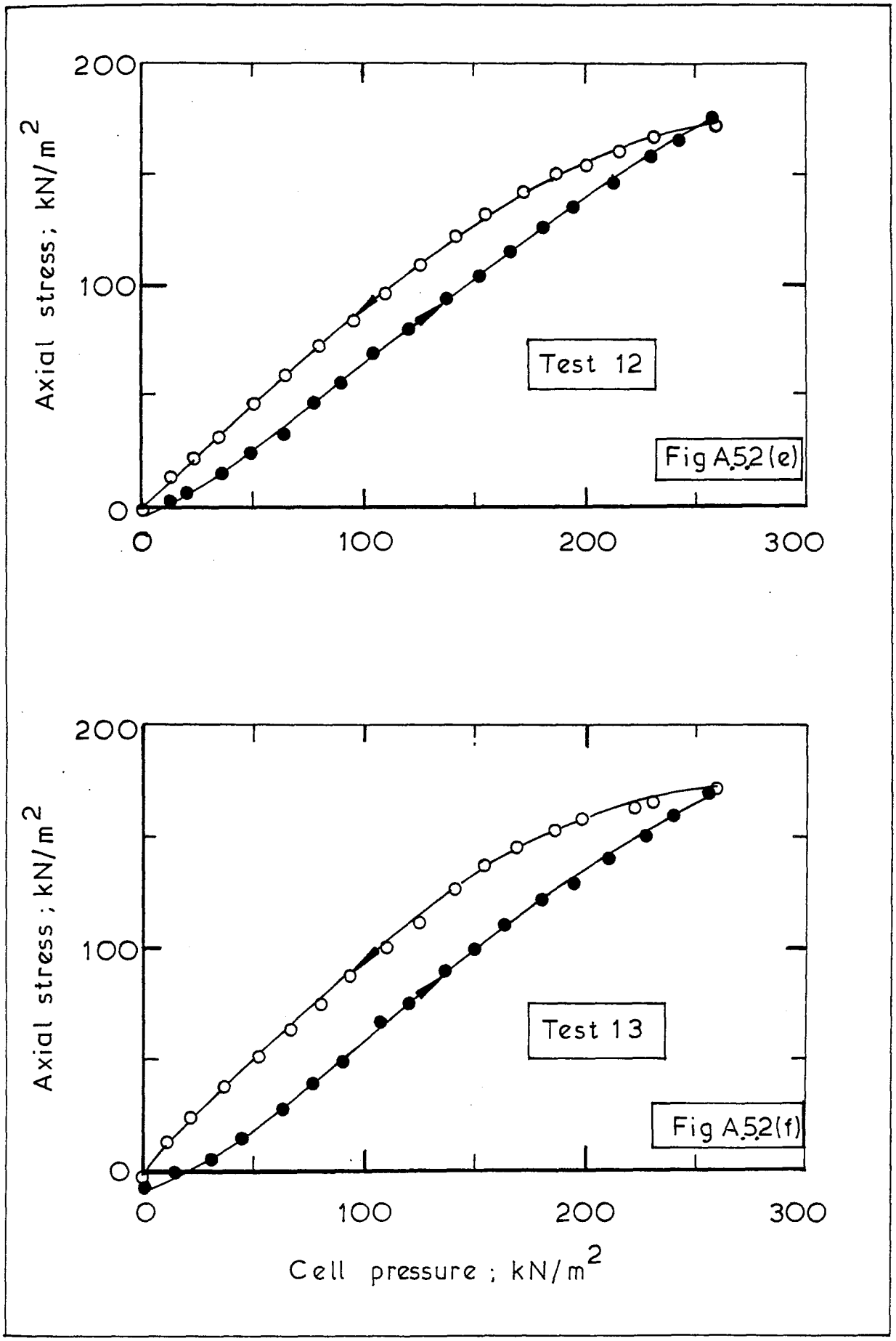


Fig. A.5.2 cont'd

APPENDIX 5.3

FAST RING SHEAR TESTS

A.5.3 Aim of Present Study

A short series of tests was performed to investigate the response of pre-existing shear surfaces to rapid rates of shear displacement. In particular, it was hoped to establish whether for the two soils considered, there was a consistent increase in the shear stress required to initiate slip with increasing rate of shearing. If such a positive, rate-dependent threshold strength effect could be demonstrated then it was hoped to be able to take this into account when assessing the stability of a particular slope which may be subject to earthquake loadings (the stability of the slope in question was judged to be determined by the strength of numerous pre-existing shear surfaces within it).

The rates of displacement employed were selected in relation to the problem of earthquake loadings, and the study concentrated on the behaviour of the shear surface at small post-slip displacements. Nevertheless, some interesting phenomena were encountered at larger displacements and are briefly reported here because it is believed that they may be of relevance to an understanding of the behaviour of soil around driven piles.

A.5.3.1 Previous Observations of Rate Effects on Pre-existing Shear Surfaces

Lupini (1980) performed a comprehensive literature survey relating to determinations of residual strength, and this included a summary of investigations into rate-effects; the reader is therefore referred to Lupini. The vast majority of ring-shear and reversal shear box tests appear to have been performed at rates of displacement less than one millimeter per minute, and for a wide range of speeds below this value the observed changes in the residual strength are typically less than 4%. One exception quoted by Lupini is the work of Bucher (1975) who performed ring shear tests on a clay of medium plasticity and noted a 24% increase in strength if the speed was varied between 0.0145 to 14.6 mm/minute.

Lupini performed ring shear tests on four clays (Happisburgh Till, London Clay, Speswhite Kaolin, and a Fiji Clay) at rates of up to

177 mm/minute and identified three rate dependent effects.

(i) a transient increase in strength (possibly due to viscous forces)

(ii) the effect of pore pressure generation

(iii) a non-transient increase in the residual strength

In Lupini's testing the monitoring of all loads was performed manually using proving rings with dial gauges or load cells monitored on a manual Wheatstone bridge. Thus Lupini was unable to monitor the short term behaviour on fast loading.

The sample was then slowly sheared to peak strength, and then the rate was increased to 0.1 mm/min and the sample was sheared until residual conditions were achieved (the residual strength was measured at a displacement rate of 0.0006 mm/min). The sample was then unloaded in shear and allowed to consolidate fully prior to performing a fast test stage. After the fast test, the sample was again unloaded in shear and was allowed to consolidate fully before slowly re-shearing to residual conditions. In order to investigate further the nature of the rate effects, various 'probes' were conducted during the testing. These probes were conducted by re-shearing the sample at a different rate from that immediately preceding, and monitoring the instantaneous response. The probes were conducted either after allowing the sample to fully consolidate after the previous stage, or immediately afterwards so that pore pressure effects could be investigated.

Once testing had been completed at the first normal stress level, the sample was unloaded in shear and then subjected to a new normal stress, so that the stress level dependence of the various effects could be ascertained. After a further series of tests, the sample was removed and the shear surface examined.

A.5.3.2 Present Study

The three effects identified by Lupini (1980) were observed in the study and are illustrated in Fig. A.5.3.1. The threshold (or transient) increases in strength observed in this study are presented for the record. Although it is well appreciated that the measurements of the non-transient increases in residual strength are scanty (because they were not the object of the testing) they are presented in order to reinforce the observations

made by Lupini (1980) on other clays, and to suggest that the subject is worthy of further research by others because it may well have a bearing on the behaviour of driven piles and cone-penetrometers, for instance.

A.5.3.2.1 Experimental Method

Apparatus

The ring shear machine employed was that described by Bishop et al (1971) and used by Lupini (1980). However, it was modified for these tests in order to permit the electronic monitoring of the various forces and displacements involved. The logging of the fast tests was performed with the aid of an Ultra-violet recording-oscilloscope, and a Solartron D.T.U. was used for the slower stages.

Procedure

Soil passing through a 0.425 mm sieve was mixed with distilled water and allowed to hydrate for several days. The soil was placed in the ring shear apparatus at a water content close to the plastic limit, and consolidated in stages to the maximum available normal stress (1000 kN/m^2). The sample was then swelled back to its first operating stress (either 100 kN/m^2 or 300 kN/m^2).

A.5.3.2.2 Test Material No. 1

Soil

Weathered Tuff - from Panama

Atterberg limits: LL = 58; PL = 41; PI = 17

It should be noted that the soil used for determining the index properties was prepared in the same manner as the soil tested, and therefore does not represent conditions on the shear surface itself where local degradation may lead to an increased plasticity index (see Heley and MacIver, 1971).

The angles of shearing resistance at peak and at residual conditions (at 0.0006 mm/min) were determined as follows:

$\phi'_{peak} = 33°$

$\phi'_{residual} = 9°$ $(\sigma'_n = 300\ kN/m^2)$

$\phi'_{residual} = 11.2°$ $(\sigma'_n = 100\ kN/m^2)$

Results

The first series of tests was conducted at a normal stress level of 300 kN/m^2. The sample was sheared to its peak strength at a rate of 0.007 mm/min and then the rate was increased to 0.1 mm/min in order to achieve residual conditions; this was accomplished after 600 millimeters of relative displacement. The sample was unloaded in shear and allowed to fully consolidate before performing the first fast testing stage, which was monitored using the recording oscilloscope. The testing rates selected were 10 mm/min and 100 mm/min. After each stage, the sample was unloaded in shear and allowed to consolidate before reloading very slowly to establish whether there had been any non-transient increase in the 'residual' shear strength. The sample was then slowly sheared until stable residual conditions were achieved, before conducting the next stage.

Fig. A.5.3.2 illustrates a loading curve obtained at a displacement rate of 100 mm/min, and a normal stress level of 300 kN/m^2. It may be seen that the shear stress at which slip occurred is significantly higher than the original residual strength, and that the strength continues to increase with further displacement, until the surfaces have been sheared for some 100 millimeters. After unloading in shear, and allowing full consolidation, the sample was reloaded at a rate of less than 0.1 mm/min whereupon it may be seen that the stress required to cause slip is well in excess of the original residual strength. This latter effect is not a consequence of the rate at which the 'probe' was performed, but rather suggests that there has been a structural change within the shear surface, i.e. the particles are not so strongly aligned parallel to one another. This view is supported by the observation that the gain in strength increases with increasing rapid displacement, until a new equilibrium level is achieved at that higher rate.

The behaviour followed on re-shearing to residual at a rate of 0.1 mm/min is illustrated in Fig. A.5.3.3, following a fast stage at 100 mm/min and a normal stress of 100 mm/min. It may be seen that the strength decreases with displacement, eventually reaching the slow stable residual strength after a displacement of about 100 millimeters, which is of the same order as the displacement required to achieve the equilibrium higher strength at the fast displacement rate.

The immediate (transient) increases in shear strength on loading fast are illustrated in Fig. A.5.3.4 where it may be seen that at displacement rates of 100 mm/min, the 'viscous' component of strength is sizeable.

Results are presented corresponding to the two normal stress levels employed, and to a number of displacement rates.

The permanent (or non-transient) increases in strength as a result of rapid shearing are shown in Fig. A.5.3.5. As mentioned above, these values were established by means of slow 'probes' conducted after permitting full consolidation. It is of interest to note that at displacement rates of 100 mm/min, the strengths increased by about 80% (after displacements of 100 millimeters), whereas at rates of below about 1 mm/min, the gain in strength is negligible. This behaviour suggests that there is perhaps a critical rate of displacement below which the shear surface is not disrupted by the shearing. This critical strength would be expected to depend on the soil tested and, as suggested by Lupini (1980), may depend on the values of the angles of inter-particle friction (ϕ'_μ), and the angle of shearing resistance for constant volume shearing (ϕ'_{cv}).

A.5.3.2.3 Test Material No. 2

Soil: Mechanically degraded Tuff (from Panama)

Atterberg Limits: LL = 50; PL = 36; PI = 14

(See note concerning Atterberg Limits in the description of the Weathered Tuff.)

The angles of shearing resistance at slow rates were established as;

$\phi'_{peak} = 44°$

$\phi'_{residual} = 17.5°$ (ϕ'_n = 300 kN/m^2)

$\phi'_{residual} = 23°$ (ϕ'_n = 100 kN/m^2)

Sample preparation

The parent rock was subjected to six cycles of wetting and drying, after which the soil was mechanically ground. The soil was then put through a 0.425 mm sieve, and mixed with distilled water and allowed to hydrate.

Comments

In this series of tests, attention was concentrated on investigating the nature of the threshold strength effect and little information about the permanent increases in strength was obtained. Many more shearing stages were performed, but, in order to minimise the additional loss of soil the displacements at each stage had to be restricted to consider only the immediately post-slip behaviour. As the non-transient gains in strength increase with displacement, the measured values are lower than the equilibrium values.

Results

The threshold, or transient, increases in shearing resistance are illustrated in Fig. A.5.3.6, and are of a similar magnitude to those observed for the weathered soil. As remarked earlier, the measured non-transient increases in strength do not represent the equilibrium values, and are hence shown in Table A.5.3, together with the corresponding displacements. Despite the relatively small displacements (in relation to the 1200 mm required to develop residual conditions initially) the gains in strength are significant.

Implications

The investigation of the threshold effect was conducted with the behaviour of slopes subject to earthquake loading in mind, and after an encouraging start is receiving further attention at Imperial College.

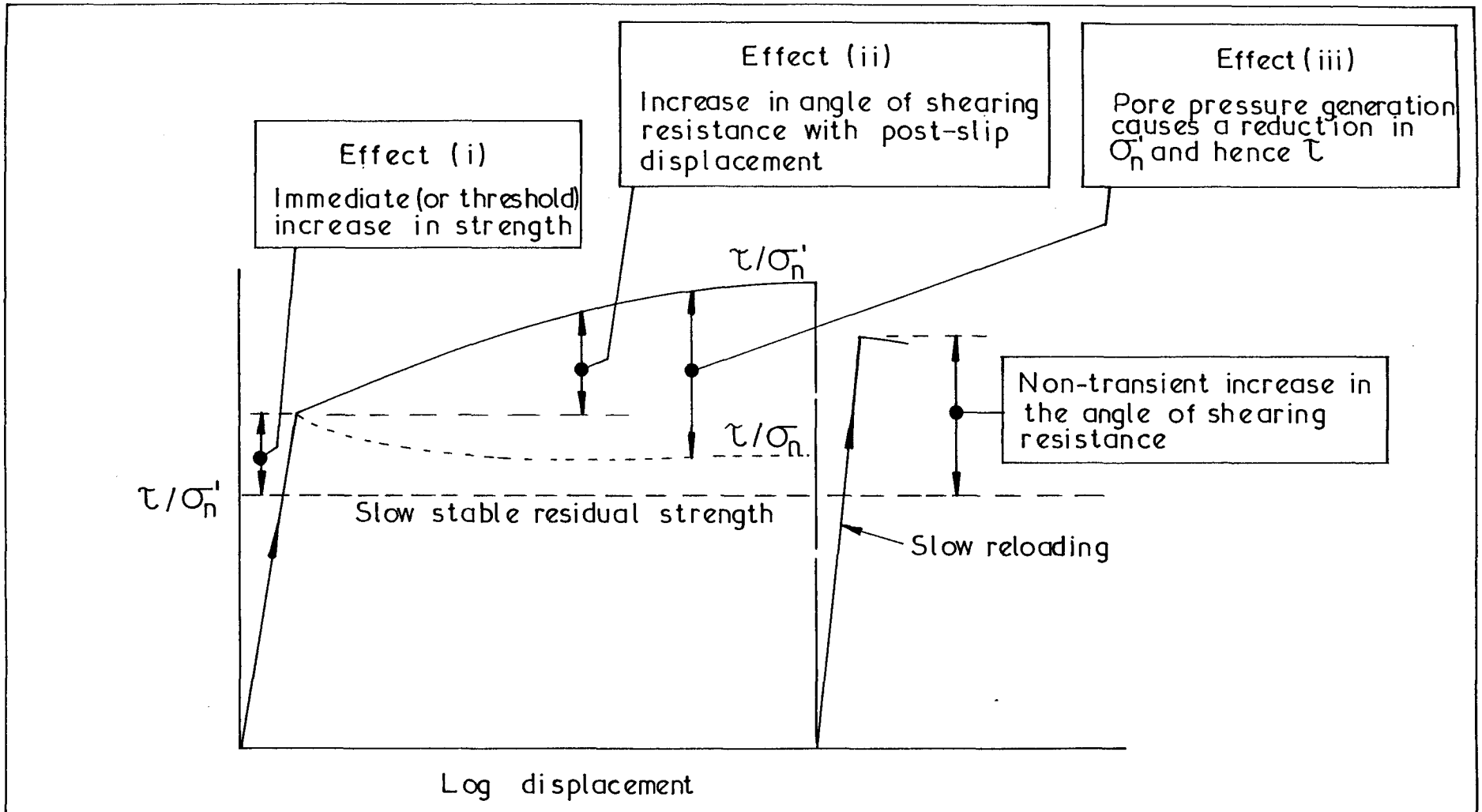
The tests reported above, and those performed by Lupini, involved soil-soil shearing. It is very likely indeed that similar phenomena would be observed if soil were to be sheared against a rigid interface. The major difference anticipated is that much smaller relative displacements would be required to achieve equilibrium conditions at a given rate of displacement.

The presence of such viscous (or transient) components of strength may well have a bearing on the interpretation of data from cone-

penetrometers, and will influence the behaviour of piles during jacking or driving.

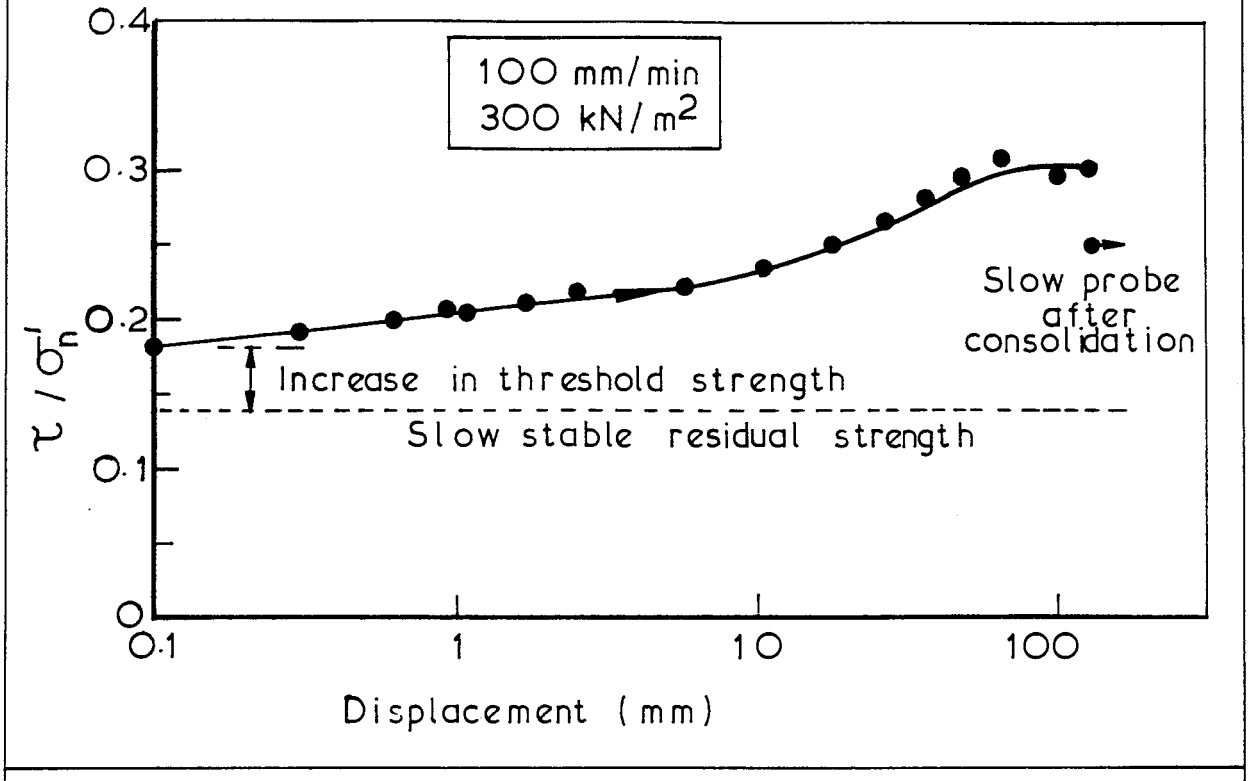
The non-transient increase in strength caused by rapid shearing is believed to have very important implications for the behaviour of displacement piles (see Chapters 5 and 9). It has been observed that a shear surface forms parallel to a driven pile as a result of installation. The strength of this surface will be influenced by the effective stress level, and the rate of displacement during driving. It is well known that the residual strength tends to increase with decreasing effective normal stress; as the effective stress level beside a pile on driving is likely to be small, the strength of the shear surface is likely to be relatively large. Similarly, the high rates of displacement will cause a non-transient increase in the angle of friction that can be mobilised.

Thus, despite the fact that a shear surface has formed parallel to the pile, its peak mobilised angle of shearing resistance may be considerably higher than that which would be measured by means of a drained (and necessarily slow) interface shear test conducted at the effective stress level assumed to exist beside the pile after full consolidation. This possibly explains only the simple effective stress method proposed by Burland (1973) for driven piles works well although the angle of shaft friction is taken to be ϕ'_{peak}. However, the presence of both the rigid interface and the pre-existing shear surface will cause the ultimate, slow, residual strength to be achieved after small post-peak displacements. This will render long, compressible, piles very prone to progressive failure. It is shown, in Chapter 9, that for long piles the assumption that the angle of shaft friction equals the angle of friction measured in drained interface tests gives very good results with field data.



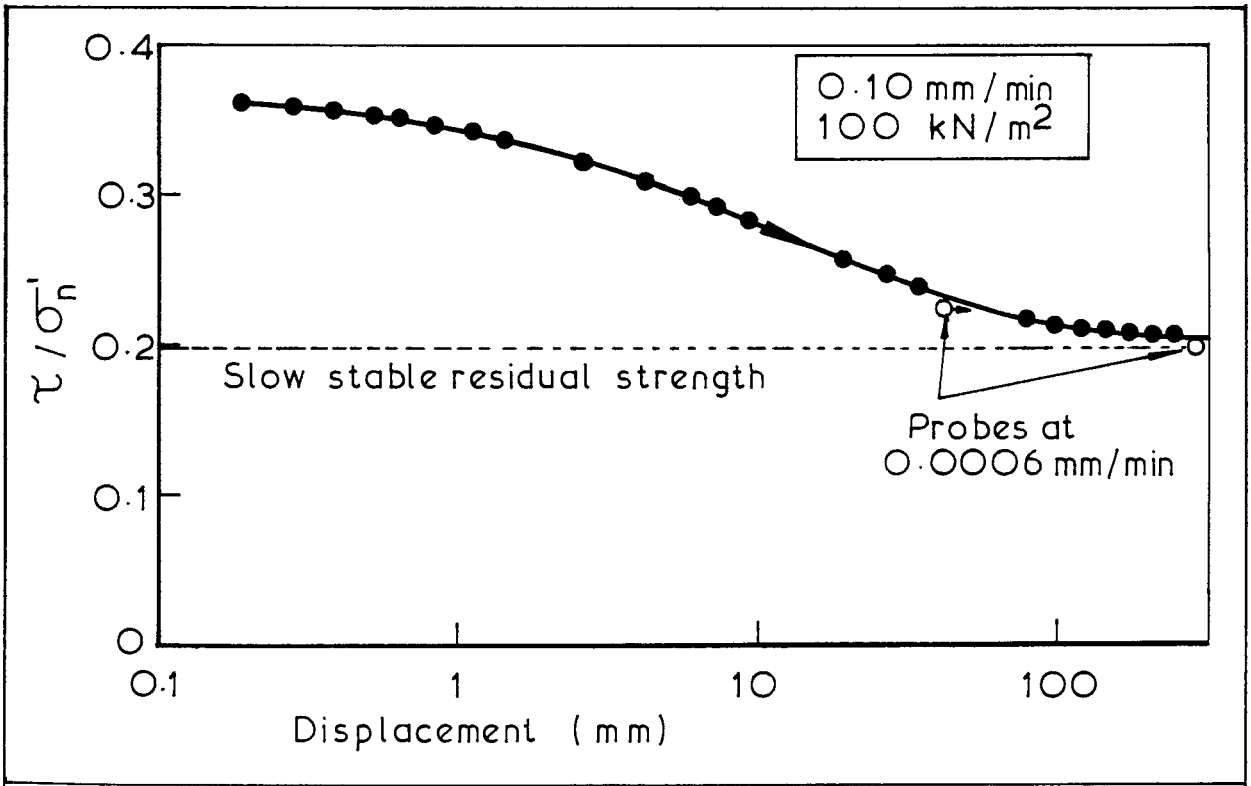
Summary of the rate-dependent phenomena observed

A.5.3.1



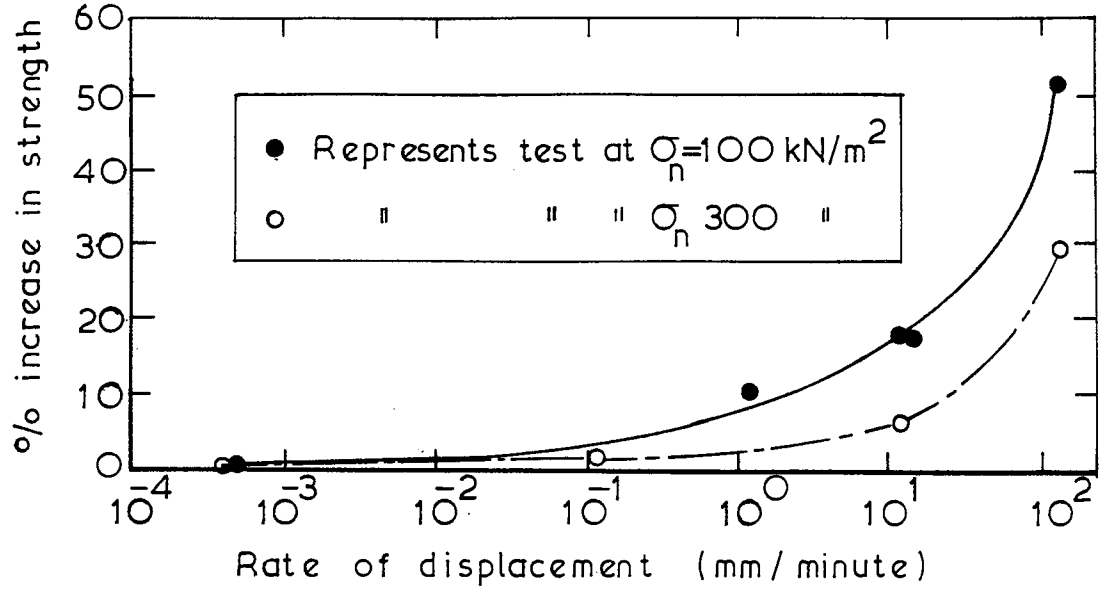
Fast loading test on weathered Tuff

Fig.A.5.3,2



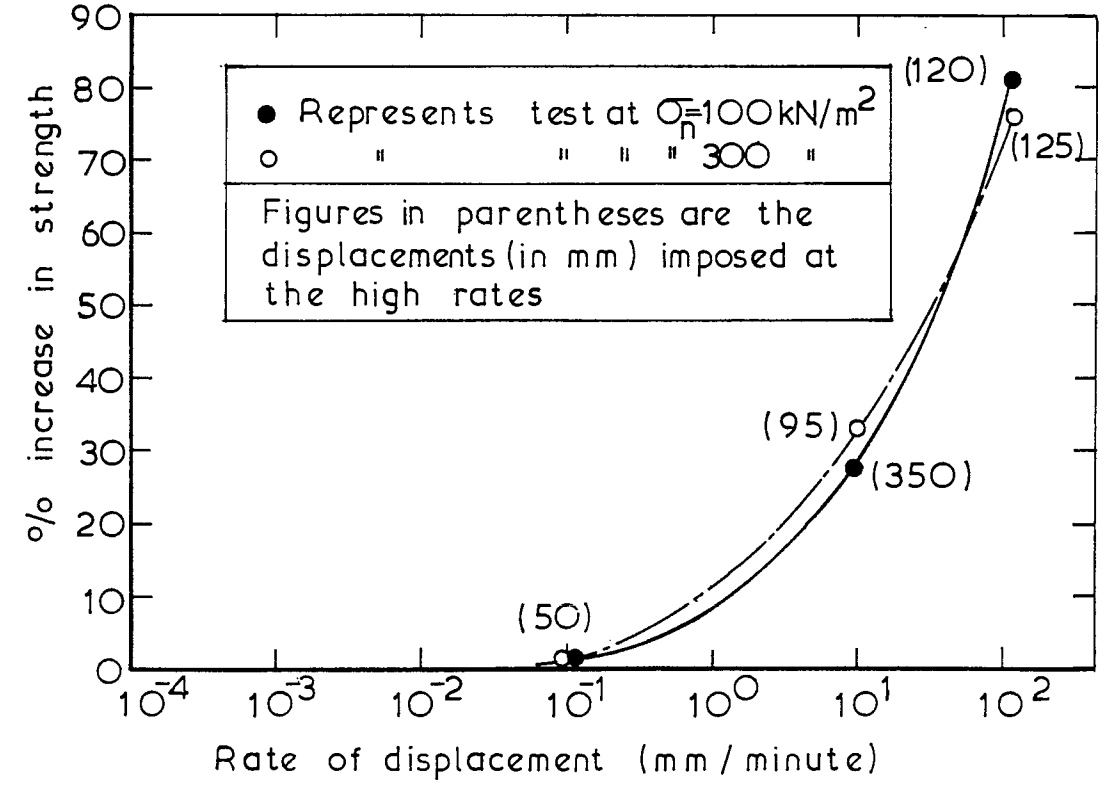
Slow loading following fast test (at 100 mm/min) on weathered Tuff

Fig.A.5.3,3



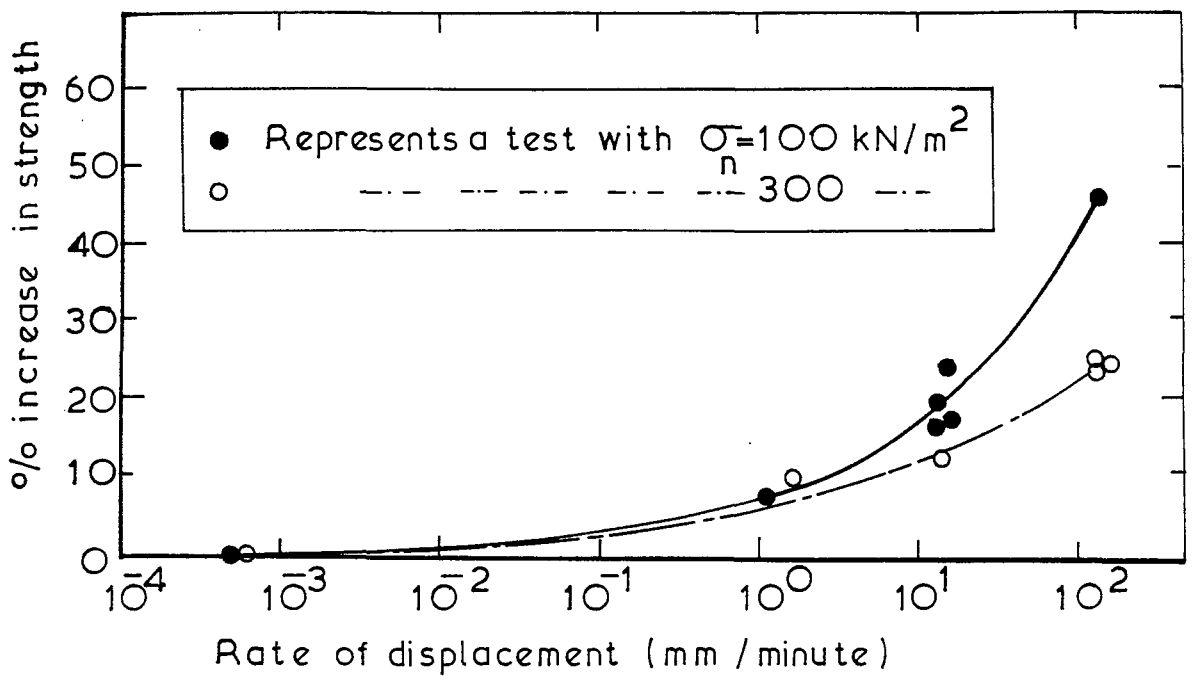
Fast tests on weathered Tuff. Immediate (Threshold) increase in strength expressed as a percentage of the slow residual strength for various rates of displacement

Fig. A .5 .3, 4



Slow probes following fast tests at the rates indicated, on weathered Tuff. Increase in strength (non-transient) expressed as percentage of the final slow stable residual strength

Fig. A.5.3, 5



Fast tests on mechanically degraded Tuff. Immediate (threshold) increase in strength expressed as a percentage of the slow residual at the corresponding normal stress

Fig A.5·3, 6

TABLE A.5·3

σ_n = 100 kN/m^2		
Rate of displacement (mm/minute)	Total displacement (mm)	% increase in non-transient strength
10	290	55
σ_n = 300 kN/m^2		
10	17	18
100	76	29
100	130	33

CHAPTER 6

MICROFABRIC INVESTIGATIONS

6.1 INTRODUCTION

The micro-structure of a soil may conveniently be regarded as having two components. The first, termed the 'original fabric', will depend on the mode of deposition of the soil and may either be random or, more probably, may exhibit a planar preferred orientation. If the soil is then subjected to further shear strains it may exhibit an additional 'shear-induced' fabric. A shear-induced fabric usually consists of domains in which the fabric is homogeneous, separated by kinematic discontinuities. As noted by Morgenstern and Tchalenko (1967,d) it is convenient to use three types of terminology to describe shear-induced fabric; kinematic, sequential and mechanistic.

Kinematic terminology describes the structural features present in the soil which are a function of the modes of deformation. The classification of kinematic discontinuities summarised by Houlsby and Wroth (1980) is convenient but it should be appreciated that the terms 'continuity', 'strain discontinuity', 'velocity discontinuity' and 'rupture' depend on the scale at which the soil fabric is viewed. For instance a velocity discontinuity defined at one magnification may be reduced to a system of strain discontinuities at a greater magnification and may be viewed in terms of slip between individual particles (or group of particles) at a still greater magnification.

The sequential terminology describes the order of appearance in time of the kinematic discontinuities and other features of the fabric. The notation which is commonly used in structural geology, and was employed by Morgenstern and Tchalenko (1967,d) will be adopted here. Thus, S_1 is the first structure to be observed, S_2 the second, and so on. Where a structure such as S_3 appears to be reducible to a set of sub-structures, the notation S_{3a}, S_{3b} will be used. The original fabric features caused by deposition will be called S_1.

The mechanistic terminology such as that described by Morgenstern and Tchalenko (1967,c) (and largely introduced by Skempton (1966)) was intended to relate a particular kinematic discontinuity to the orientation and magnitude of the stresses acting upon it. In practice, the stresses in

the vicinity of such discontinuities are often very difficult to measure. Nevertheless, the terminology is convenient for describing characteristic types of structures, encountered in a variety of circumstances. The term 'principal displacement shear'(Skempton, 1966) will be restricted to describe a continuous displacement discontinuity which extends for the length of, and is parallel to, the pile shaft. Further mechanistic terms employed in the text will be used in the same sense as defined by Morgenstern and Tchalenko (1967,c) unless otherwise stated.

Two distinct series of tests were performed in the present study. The first was intended to examine the nature and development of micro-fabric changes in the clay caused by the loading of piles installed with minimal disturbance (by the technique described in Chapter 4). Within this series, a set of five tests was conducted to observe the development of micro-fabric changes within the clay beside loaded piles. Further tests were performed at different initial stress ratios in order to examine the effect of the initial stress conditions.

The second series of tests, on the other hand, was performed to investigate the nature of the fabric disturbance caused by the installation of full-displacement piles, and to relate this disturbance to the subsequent pile loading behaviour. The results are compared with field observations.

The micro-fabric of the clay around the piles was studied by viewing thin sections of the material under crossed nicols, as described in Chapter 4. The reader is also referred to Chapter 2, section 4 for a discussion of earlier work concerning thin section studies. In the following, several photographs of thin sections are presented, and these are usually accompanied by schematic interpretations of the photographs. In general, these interpretive figures have been constructed from at least two photographs (taken under different orientations of polarised light) and possibly different magnifications, although in several cases only one of the set is presented here.

6.2 DEVELOPMENT, WITH PILE DISPLACEMENT, OF MICRO-FABRIC CHANGES WITHIN THE CLAY ADJACENT TO LOADED MODEL PILES INSTALLED WITH MINIMAL DISTURBANCE

6.2.1 Introduction

A series of five tests was performed to investigate the sequence of development of shear structures in the kaolin surrounding model piles installed with minimal disturbance (using the techniques described in

Chapter 4). The first test was conducted to demonstrate that the drilling and reaming process involved in the pile installation process caused minimal fabric disturbance. The other four tests were each stopped at different stages of pile loading (see Fig. 6.1) and thin sections were then prepared. The kaolin for these tests was normally-consolidated to a stress ratio (σ'_r/σ'_z) of 1.5 because earlier tests had shown that the shear structures were most easily distinguishable at high initial stress ratios.

Tchalenko (1967), and Morgenstern and Tchalenko (1967,d) present the results of an analogous series of tests performed within a direct-shear box. Reference will be made to the many similarities between the work of Tchalenko, and the results from the model pile tests.

6.2.2 Fabric Disturbance Caused by the Drilling Operation

Test No. 4 was conducted to examine the fabric disturbance caused to the clay sample by the drilling and reaming operations performed in the course of installing 'wished-in-place' piles (see Chapter 4).

Photographs, taken under crossed nicols, of a cross-section and a longitudinal thin section taken through the sample, are shown in Figs. 6.2(a) and (b) respectively. Fig. 6.2(c) is a schematic diagram constructed from the longitudinal section. It may be seen from these figures that the shrinkage cracks which form on cooling the impregnated sample (see Chapter 2) lie parallel to the original horizontal bedding fabric, S_1. The slight disturbance caused by the drilling and reaming process may be seen as the light area bordering the hole. In the cross-section small zones of disturbance, probably caused by the reaming tool, may be seen as short lines tangential to the hole. The orientation of the polarised light was selected to show the maximum disturbance. If comparison be made between the above results and those obtained after pile loading (see, for instance, Fig. 6.12) it will be seen that the fabric disturbance caused by the drilling operation is negligible.

6.2.3 Test Stopped at 70% of Peak Load

Test 13 was terminated at about 70% of the peak load, after a displacement of about 0.5 mm.

A photograph and a diagrammatic interpretation of a longitudinal thin section through the sample are shown in Figs. 6.3(a) and (b). The original bedding fabric, S_1, does not appear to have suffered permanent deformation within the clay beyond a distance of about 0.25 mm from the pile.

The light band immediately adjacent to the pile suggests that there has been plastic straining within this region. In Fig. 6.3(b) a number of sites from which penetrative, S_2, structures may grow, are indicated. These 'nuclei' may be analogous to Griffith cracks.

In summary, it would appear that by this stage of loading there has been some very localised plastic shear straining within the clay, but that penetrative discontinuities have not yet started to propagate although a number of 'nuclei' are present.

There is no direct analogy between these results and those described by Morgenstern and Tchalenko (1967,d) because the non-uniformities in the direct shear box caused large, penetrative, discontinuities to propagate from a very early stage.

6.2.4 Test Stopped at 95% of Peak Load

Test No. 12 was stopped just pre-peak; thin sections were then prepared.

A photograph of a longitudinal thin section taken from the sample is shown in Fig. 6.4(a), and a schematic view of the photograph is presented in Fig. 6.4(b). There are at least four penetrative discontinuities, S_2, ('Riedel' structures) visible, each at an early stage of development. Because of the axi-symmetric nature of the problem, these structures presumably form as cones. The Riedels probably initiate at the sites of earlier 'nuclei', and in the immediate vicinity of the pile they propagate at about 6° to the pile axis. This angle increases to roughly 15° at a distance of less than one millimeter from the shaft, and thereafter remains constant. It is interesting to observe that the uppermost structure has already degenerated into a small kink band, S_{2b}.

It is unfortunate that the original bedding fabric was slightly inclined, and not horizontal. This is thought to be the result of the kaolin slurry having been a little too 'dry', with the result that tilted bedding structures remained after pouring the slurry into the consolidation tube. This phenomenon is unlikely to have affected the loading behaviour of the pile (see Tchalenko, 1967) but nevertheless more care was taken after this test to produce nearly horizontal bedding fabric, so as to avoid unnecessary complication of the micrographs. As a result of the above inclination of the bedding fabric, it is difficult to analyse the plastic deformations within the soil.

From Figs. 6.4(a) and (b), it would seem to be a reasonable approximation to model the clay around the pile as a continuum, up to this stage of loading.

6.2.5 Test Stopped Immediately Post-peak

Test No. 10 was stopped immediately post-peak at a total displacement of 2.85 mm, and unloaded (the permanent displacement was 2.45 mm).

Photographs of a longitudinal thin section and a cross-section are shown in Figs. 6.5(a) and (b), and an interpretive diagram of the longitudinal section is presented in Fig. 6.5(c). It is evident that a considerable growth of the penetrative, S_2, discontinuities is associated with peak conditions. A similar result was found by Tchalenko (e.g. Morgenstern and Tchalenko (1967,d)) using the direct shear box. There is no evidence to suggest the presence of a continuous principal displacement shear surface at this stage.

The families of shear structures visible in the longitudinal sections are now considered. Reference is made to two different longitudinal sections through the same sample in order to illustrate particular features. The longitudinal section represented by Figs. 6.5(a) and (c) is relatively simple, and forms a useful introduction.

The penetrative discontinuities (S_2) propagate at fairly regular intervals of between 10 mm and 15 mm down the length of the pile, although the 'nuclei' for such structures (of the type seen in Test 12) may be present at more frequent intervals. The propagation of such structures will tend to release locally stored strain energy and this probably has the effect of inhibiting the growth of nearby 'nuclei'. Thus, the Riedel structures propagate randomly in time, but at spacings which may be influenced by the presence of other shear structures. The phenomenon has analogies with the formation of shrinkage cracks in concrete around reinforcing steel.

The family of S_2 structures start close to the pile as S_{2a} structures but are observed to degenerate, at a distance of between one and two millimeters from the pile, into reverse kink bands, S_{2b} structures (see Morgenstern and Tchalenko (1967,d) for definition of normal and reverse kink bands). The kink bands represent an unstable mode of deformation, and may be regarded as a region of material undergoing simple shear deformation separated from the surrounding soil by two, almost parallel, strain discontinuities. In the present series of tests, the kink bands were observed to grow to a width of about one millimeter, and to propagate at a constant

angle of about 12° to the direction of pile loading. The rotation of the S_1 (original bedding) fabric within the kink band was observed to be such that the kink band boundary (at roughly 12° to the direction of loading) bisected the angle formed by the S_1 directions on either side of it. Further rotation of the S_1 fabric within the kink band would imply compression normal to the plane of preferred particle orientation, and hence the rotation is restricted. Thus the kink bands could sustain a relative displacement of nearly one millimeter before becoming inoperative. The kink bands terminated at a distance of about five and a half millimeters from the pile, where the average shear stress, τ_{rz}, was only 60% of the value at the pile face. It will be shown in section 6.2.6 that even in the case of a pile taken to a very much larger displacement, the kind band penetration did not increase beyond this value. It would therefore seem that the kink band mode of deformation on planes inclined to the pile axis has become incapable of accommodating further pile displacements, and a new mode of deformation is required.

As the system of S_2 structures becomes inoperative, a new family of relief structures (S_3) forms close to the pile, starting near the pile-ward end of existing S_{2a} structures. Although some S_3 structures are present in the longitudinal section represented in Figs. 6 .5(a) and (c), the polarisation direction for the photograph was selected to illustrate the S_2 structures and so the S_3 structures, which lie at a different inclination to the pile axis and are smaller than the S_2 structures, are indistinct. The photograph in Fig. 6.6(a) (which is a composite from several micrographs) was prepared to illustrate the shear fabric close to the pile, and a schematic view of the photograph is presented in Fig. 6.6(b). These are now considered.

The new generation of relief shear structures begin with S_{3a} thrust shears which lie at angles of between 12° and 15° to the upward vertical. Although these thrust shears may help to dissipate energy and to redistribute stresses in the vicinity of S_2 structures, they too are oriented in the wrong directions to be able to accommodate significant displacements. The result appears to be the creation of the family of en-echalon displacement discontinuities which lie sub-parallel to, and very close to (typically < 1 mm), the pile shaft. Thus, at last, a kinematically acceptable deformation mode has been established, and further pile displacements are largely accommodated within the thin band of S_{3b} structures which extends to be continuous along the length of the pile. Such deformations will lead to very high local shear strains and will enhance the local degree of preferred particle

orientation. It will be seen in section 6.2.6 that after large post-peak displacements, the S_{3b} structures may coalesce with sections of S_{2a} structures to form a continuous displacement shear S_4.

The family of S_3 relief structures formed around the pile is rather different from that occurring in the shear box where the structures are free to weave either side of the centre-line (see Morgenstern and Tchalenko (1967,d)). This is prevented by the surface of the pile, and so in this case the S_3 structures are subject to a greater restraint.

An interesting feature of these photographs is that it is possible to estimate the magnitude of the plastic deformations occurring within the clay by following the deformation of the initial bedding fabric, S_1. In this respect the shrinkage cracks (where present), which generally occur parallel to the bedding, are useful markers; it may be seen for example in Fig. 6.5(a) that the shrinkage cracks follow the abrupt changes in inclination of the S_1 fabric within the kink bands. It is assumed that before pile loading the fabric, S_1, was at a constant inclination (unfortunately not quite horizontal) right up to the pile, and therefore observed deviations from this original line may be attributed to plastic shear strains caused by the pile loading. The shrinkage of the specimen on cooling is ignored because axial contraction close to the pile will have been limited by the presence of the pile. The derived plastic deformations within the clay at locations A, B and C in Fig. 6.5(a) are presented in Fig. 6.7. It may be seen that the kink bands at sections A and C are associated with strain discontinuities on both faces, and that the presence of kink bands tends to reduce the shear strains in the soil that is immediately adjacent; comparison may be made with section B which was scarcely affected by penetrative discontinuities. From section B it may be seen that in general the majority of the plastic vertical deformation occurs within 4 to 5 millimeters from the pile (i.e. within about 60% of one pile radius from the shaft), and that shear strains of the order of 100% occur close to the pile. It is interesting to note that this simple, approximate, technique can account for about 2.1 millimeters of the 2.4 millimeters of permanent deformation measured in the course of the model pile test.

6.2.6 Test Pile Displaced to Residual Conditions

The pile employed in Test 9 was loaded to a post-peak displacement of just over 10 millimeters by which stage residual conditions were achieved (see Fig. 6.1). Photographs of a longitudinal thin section viewed under two

orientations of polarised light (at 45° to one another) are shown in Figs. 6.8(a) and (b), and a schematic representation is shown in Fig. 6.8(c). A more detailed view of the region marked x-x in Fig. 6.8(c) is presented in Fig. 6.9 and a cross-section is shown in Fig. 6.10.

The most significant difference between the micro-fabric structures present at this stage, and those present immediately post-peak is the existence now of a thin (circa 10 microns) continuous principal displacement discontinuity, S_4. This structure forms parallel to the pile shaft, and at a distance of about 0.5 millimeters from it; large relative displacements parallel to the direction of pile loading are kinematically admissible. The formation of the principal displacement discontinuity appears to involve the coalescence of S_{3b} relief structures which are sub-parallel to the shaft, and extensions of the S_{2a} Riedel structures adjacent to the pile. With the large post-peak pile displacements, the particles on either side of the principal displacement discontinuity are subject to a high degree of preferred orientation sub-parallel to the direction of pile displacement, and so the strength of the shear surface drops to its residual value appropriate to the current stress level and rate of displacement.

In order to determine how much of the permanent pile displacement was accommodated by plastic deformations within the clay, rather than slip on the principal displacement shear, a similar exercise to that presented for conditions immediately post-peak was conducted using Figs. 6.8(a),(b) and (c), and the results are presented in Fig. 6.11. It may be seen that a permanent pile displacement of about 2 millimeters was again accommodated without the 'assistance' of the principal displacement shear. This suggests that the pre-peak pile displacements are largely accommodated by plastic straining within the clay, whereas the post-peak displacements involve shearing within a very thin zone close to the pile.

Further evidence for this view may be obtained by comparing the shear structures (e.g. S_{2a}) close to the pile at residual conditions with those immediately post-peak (see Figs. 6.8 and 6.5 respectively). It may be seen that the S_{2a} structures appear to be undisturbed even after the very large post-peak displacements. Thus it is believed that the post-peak displacements are accommodated within a very narrow zone (< 0.5 millimeters) close to the pile, and that the resulting local shear strains are enormous which is why residual conditions are achieved very rapidly (in comparison with results from a reversal direct shear box, or a ring shear device).

6.2.7 Comments

In order to attempt to establish the nature of the various micro-fabric features observed around the loaded piles, it is first necessary to determine the stress field in the soil at various stages during the loading. Unfortunately it is impossible to measure all of the stress components close to the pile, and it is also impossible to establish the stresses uniquely from measurements of the radial stress and the shear stress acting on the pile face. Morgenstern and Tchalenko (1967,d) argued that the direction of propagation of the S_2 structures suggested that simple shear conditions act in the centre of the shear box, and a similar interpretation may, therefore, be true for conditions around a pile. However, there appears to be little point in continuing that discussion at this stage.

In Chapter 8, the model pile tests are analysed by finite element methods, employing Modified Cam Clay as the soil constitutive law. An interpretation of the observations from the micro-fabric studies is presented in section 8.6.

6.3 THE EFFECT OF THE INITIAL STRESS RATIO ON THE MICRO-FABRIC CHANGES INDUCED IN THE CLAY SURROUNDING LOADED PILES

6.3.1 Introduction

As discussed earlier, model pile tests were performed to investigate the influence on the pile loading behaviour of the initial stress ratio in the soil. The tests were generally continued until residual conditions were achieved, after which thin sections were prepared and the micro-fabric changes examined.

The observations of the effect of the initial stress ratio on micro-fabric changes induced in the clay around loaded piles was performed with the aim of providing additional information about the nature of the load transfer mechanism involved. In Chapter 8, the observed micro-fabric changes are considered in relation to stress changes predicted (by means of elasto-plastic finite element analyses) around loaded piles installed in clays consolidated to different initial stress ratios.

In order to demonstrate the nature of the variation of micro-fabric changes with stress ratio,observations obtained from three tests (9,11,14) are presented. Test No. 9 (which has already been considered in relation to the development of micro-fabric changes with pile displacement) was conducted at the highest stress ratio (1.5), Test No. 11 at the minimum stress ratio

(0.74), and Test No. 14 was conducted at an intermediate stress ratio (1.1). The results are now considered.

6.3.2 Test Conducted at an Initial Stress Ratio of 1.5

The sequence of development of micro-fabric changes in pile tests conducted at an initial stress ratio of 1.5 have been discussed in section 6.2, and Figs. 6.8, 6.9 and 6.10 illustrate the micro-fabric features present when residual conditions are achieved.

It may be recalled that typically, penetrative discontinuities, S_{2a}, initiated at intervals of between 10 and 15 millimeters down the length of the pile, and at angles of between 6° and 10° to the pile shaft, although the inclination increased to around 15° beyond 1 millimeter from the pile. At a distance of between 2 and 3 millimeters from the shaft, the S_{2a} structures degenerated into kink bands (S_{2b} structures) which propagated at a fairly constant inclination of about 12°, to a distance of between 5 and 6 millimeters from the pile. The kink bands were well defined structures which could accommodate relative displacements of up to about one millimeter. When the pile displacements became so large that the kinking mechanism could not accommodate further displacements, relief structures, S_3, were generated close to the pile. The S_{3a} structures were inclined to the pile axis, but the S_{3b} structures formed sub-parallel to the pile and represented a kinematically acceptable mode of deformation. At large displacements these structures coalesced with components of the S_{2a} structures to form a thin, continuous, principal displacement shear, S_4, close to the pile.

The micro-fabric features found after tests conducted at the other stress ratios will be compared with these results.

6.3.3 Test Conducted at an Initial Stress Ratio of 1.11

Two photographs and a corresponding diagram of a longitudinal thin section taken after Test 14 are presented in Figs. 6.12(a), (b) and (c) respectively. It may be seen that there are several micro-fabric features in common with those already presented for the tests at a stress ratio of 1.5, but that there are also some important differences.

Riedel structures, S_{2a}, inclined at about 16° to the direction of loading are present at roughly 10 millimeter intervals down the length of the shaft, and extend to a distance of about 2 millimeters from the pile before degenerating into kink bands, S_{2b}. These structures propagate at 13° (which is very similar to the angles measured after Tests 9 and 10) to the

direction of loading, but only extend to about 4 millimeters from the shaft. The kink bands in Test 14 are less well defined structures than those encountered in Tests 9 and 10, and are narrower, but more numerous.

Relief structures (thrust shears S_{3a}, and S_{3b} structures) of a similar form to those found after Test 9 may be seen, as may the principal displacement shear, S_4, which formed at a distance of about 0.5 millimeters from the shaft.

The radial distribution of plastic deformation within the clay is considered by observing the deformed shape of the bedding plane marked A-A in Fig. 6.12(c); the result is illustrated in Fig. 6.14 where it is compared with results similarly obtained from Tests 9 and 11.

6.3.4 Test Conducted at an Initial Stress Ratio of 0.74

A photograph and a corresponding schematic view (assembled from this and other photographs) of a longitudinal thin section taken after Test No. 11 are presented in Figs. 6.13(a) and (b). It may readily be seen that there are significant differences between the micro-fabric around this pile and that around the pile following Test No. 9.

Riedel structures, S_{2a}, propagated at between 10° and 15° to the direction of loading but extended only to a distance of about 1.5 millimeters from the shaft. The Riedel are much more closely spaced than previously observed; the stronger structures are present at roughly 4 millimeter intervals, whereas the minor ones are even more frequent. The S_{2a} structures do not appear to have degenerated into discrete S_{2b} structures, but rather into a region of diffused shear structures. Nevertheless, the envelope of the diffused S_{2b} structures may clearly be seen in contrast to the apparently undisturbed clay at a distance 2 millimeters from the shaft. The radial distribution of plastic deformations within the clay is shown in Fig. 6.14.

A family of S_3 Relief structures is also present, although because of the very concentrated nature of the shear deformations in this case, the structures are very fine and are difficult to resolve in the above photograph. Once again a very thin principal displacement shear formed parallel to the shaft, at a distance of between 0.5 and 1.0 millimeters from it.

6.3.5 Comparison between the Observed Modes of Deformation

Riedel shears, S_{2a} structures

In each of three tests considered, the Riedel shears propagated at angles of between 10° and 16° to the direction of pile loading, with no obvious dependence on the initial stress ratio. The spacings and the penetration of these structures, on the other hand, varied considerably with the initial stress ratio. In Test 9 (K = 1.5) the S_{2a} structures were observed to form at intervals of between 10 and 15 millimeters down the length of the pile and to propagate to a distance of 3 millimeters from the shaft whereas the corresponding dimensions for Test 14 (K = 1.11) are 10 millimeters and 2 millimeters, and for Test 11 (K = 0.74) are 4 to 6 millimeters and 1.5 millimeters respectively. Thus the S_{2a} structures became shorter, and more closely spaced as the initial stress ratio decreased, although the direction of propagation was largely unaffected.

S_{2b} structures

In Test No. 9 (K = 1.5) the S_{2b} structures which resulted from the degeneration of the Riedels formed as distinct kink bands which propagated at an angle of about 12° to the direction of loading, and extended to a distance of 5.5 millimeters from the shaft. In Test 14 (K = 1.11) kink bands were also formed and they were inclined at a similar angle (13°) to the direction of loading. However, structures were less sharply defined than those in Test 9 and, being more numerous, tended to merge into one another; they only penetrated to a distance of 4 millimeters from the pile. Following this trend, the S_{2b} structures in Test 11 (K = 0.74) merged into one another to such an extent that individual structures could not be distinguished, and the envelope of these structures extended to a distance of only about 2 millimeters from the pile.

S_3 and S_4 structures

Relief shear structures (thrust shears S_{3a}, and S_{3b} structures) appear to have formed in a similar manner in the three tests although the S_{3b} structures were difficult to resolve in Test 11 (K = 0.74). In all tests, residual conditions were associated with the presence of a narrow, continuous, principal displacement shear surface (S_4) which was parallel to the pile shaft and at a distance of about 0.5 millimeters from the pile face. In all cases the S_2 structures (which are associated with peak conditions) appeared to be unaffected by the large post-peak displacements

required to reach residual conditions.

Radial distribution of plastic deformations within the clay

The profiles derived by considering the deformed shape of bedding planes (S_1 structures) are shown in Fig. 6.14 for the three tests. Only deformations beyond the principal displacement shears are considered, and the sections were selected to avoid the influence of intersecting S_2 structures as far as possible.

It may be seen that the maximum plastic deformations beyond the S_4 structures were between 1.9 and 2.6 millimeters. These values are of the same order as the plastic components of the displacements to peak, but very much smaller than the overall pile displacements of about 12 millimeters. The distributions of the plastic deformations are all very similar in the three cases, although it appears that the deformations around the pile in Test 14 (K = 1.11) were the least localised.

6.4 TEST CONDUCTED ON A PILE INSTALLED IN OVER-CONSOLIDATED KAOLIN

6.4.1 Introduction

Although, for reasons discussed earlier, the experimental programme was largely confined to testing normally-consolidated soils, one test (No. 7) was performed with over-consolidated kaolin in order to see whether there were any fundamental differences in behaviour. Thus, after the test thin sections were prepared.

The kaolin for Test No. 7 had an over-consolidation ratio of 5, and a stress ratio, K, of 0.8, having been consolidated and swelled back under conditions of zero axial strain.

6.4.2 Observed Micro-fabric Changes

Two photographs of a longitudinal thin section through the sample are presented in Figs. 6.15(a) and (b). The shear structures are very similar to those that might be expected from a test conducted on normally-consolidated clay at a stress ratio of less than unity. The major Riedel structures, S_{2a}, formed at intervals of roughly 11 millimeters down the length of the pile and penetrated, at inclinations of between 10° and 16°, to a distance of nearly 2 millimeters from the pile. The S_{2b} structures were merged into one another and extended to a maximum of 3 millimeters from the pile. A continuous principal displacement shear, S_4, formed at a

distance of just over 0.5 millimeters from the pile.

In this test, a device was employed to measure the radial stress acting on the side of the pile. After the test, thin sections were prepared from the clay immediately adjacent to the device, and results are presented in Appendix 6.2.

6.4.3 Comments

The micro-fabric changes observed after this test are remarkably similar to those which might have been expected had the test been performed at a similar stress ratio in normally-consolidated kaolin. This perhaps suggests that by the time that the S_{2a} structures are formed, the relationship between the stresses in the clay adjacent to the pile is relatively independent of the initial OCR.

6.5 Summary of Micro-fabric Features Observed as a Result of Loading Piles installed with Minimal Disturbance

One of the main purposes in performing the micro-fabric studies described above was to obtain information about the deformations within the clay so that a comparison with theoretical predictions might be made. The main features observed are summarised below, and are compared with some theoretical predictions in Chapter 8.

(1) The Riedel (S_{2a}) structures propagate at between 10° and 16° to the direction of pile loading, irrespective of the initial stress ratio.

(2) The spacing and penetration of these structures increase with increasing initial stress ratio.

(3) The kink bands (S_{2b}) are inclined at 12° to 13° to the direction of pile loading, irrespective of the initial stress ratio (where the individual structures can be resolved).

(4) The penetration of the S_{2b} structures increases with increasing initial stress ratio.

(5) The radial distribution of plastic vertical deformations within the clay are similar in all cases.

(6) Following post-peak displacements of about 10 millimeters, a continuous displacement discontinuity, S_4, is formed parallel to the pile.

6.6 TESTS TO EXAMINE FABRIC DISTURBANCE CAUSED BY INSTALLING AND LOADING DISPLACEMENT PILES

6.6.1 Introduction

Following the series of tests performed to examine the behaviour, on loading, of model piles installed with minimal disturbance into kaolin samples, an additional set of three tests was conducted with full-displacement piles. The object of this latter series was to provide information about the nature and influence of fabric disturbance caused by driving or jacking displacement piles.

In the first test, a solid model pile was driven into a sample of kaolin (which was subject to confining stresses). After allowing the sample to consolidate fully, it was removed, trimmed, and the clay around the pile impregnated with Carbowax so that thin sections could be prepared. This test enabled the soil deformation patterns and fabric changes caused by the installation process to be examined. In the second test, a pile was driven into a kaolin sample and, after allowing full consolidation to occur, the pile was slowly loaded until residual conditions were reached. Thin sections were then prepared. A third test was performed in which a similar pile was jacked into a clay sample, and the above process was repeated. The experimental details involved in these tests are described in Chapter 4, and the results obtained ~~driving~~ during the pile loading are presented in Chapter 5.

The results from the micro-fabric studies are presented below, and are later discussed in relation to the field observations presented by Tomlinson (1970,b).

6.6.2 Pile Driven into Clay Sample, but not Loaded

6.6.2.1 Introduction

The pile employed in Test 16 was driven to a depth of about six pile diameters into a sample of normally-consolidated kaolin, leaving a similar depth of soil between the pile tip and the base of the sample. The aim of the test was to examine the nature of the soil deformations beside and beneath the driven pile.

The thin sections prepared from the kaolin sample were examined and photographed under polarised light. As previously observed, the general deformation pattern was highlighted by the presence of shrinkage cracks which formed in the directions of the locally distorted bedding planes, whereas regions of intense shear straining were characterised by a high degree of preferred particle orientation which was detected by the polarised light.

Radial deformations within the clay could not be established for lack of suitable vertical markers,and it is suggested that the use of radiographic techniques in conjunction with thin-section methods would provide a very powerful combination for examining soil deformations.

6.6.2.2 General Description of Deformations around the Pile

Two photographs (taken under different orientations of polarised light) of a longitudinal thin section prepared from the base of the pile (which was not driven 'through' the sample) are presented in Fig. 6.16(a) and (b), and a schematic representation is shown in Fig. 6.16(c).

It will be seen that beneath the pile the soil is failing in a 'punching-shear' mode, as might be expected in a normally-consolidated clay.

At a distance in excess of about one pile radius from the shaft (in Zone C), the clay fabric appears to have been largely unaffected by the driving process. However, the lack of suitable reference points within the clay mass means that it is not possible to determine the radial movements which occurred as a result of the pile installation. The measured distance (in terms of pile radii) between the pile and the region of apparently undistorted clay is in good agreement with field observations around piles with much greater diameters (e.g. Cummings et al., 1950; Tomlinson, 1970(a)).

Closer to the pile, in Zone B, the clay has been strongly deformed, as is evident from the curvature of the shrinkage cracks and from the orientation of the S_1 fabric (viewed under polarised light). The original bedding was roughly horizontal (Zone C, below the level of the pile tip) and appears light in Fig. 6.16(a). However, between Zone C and the pile shaft, the clay fabric is rotated through some 90°, with the clay beside the pile again appearing light. The light transmitted through the thin-section is in extinction when the bedding direction has rotated through 45° from the horizontal, and is back in full illumination after a further 45° rotation; this explains the progressive change in tone of the photograph in Fig. 6.16(a) from light to dark and back to light again with radial distance from the pile shaft.

Zone A is closest to the pile and extends to a distance of about two millimeters (or about 25% of one pile radius) from the pile, and the boundary between Zones A and B appears to be a displacement discontinuity (see Fig. 6.16(a)). The clay within Zone A may be seen (particularly in Fig. 6.17) to contain numerous shear surfaces inclined at small inclinations to the direction of pile penetration.

6.6.2.3 Deformations around the Pile Shaft

Fig. 6.18(a) and (b) are photographs of a longitudinal thin section from the top of the pile shaft. For a distance of two or three pile diameters from the top of the sample there is a progressive development of the deformation pattern within the clay, whereas below that level the pattern is independent of depth until the toe of the pile is approached.

During the preparation of the thin-section, some kaolin was lost from Zone A near the top of the pile. In the lower half of the photographs, however, it may be seen that Zone A contains countless shear surfaces which are oriented at a small inclination to the direction of pile penetration, and probably have shear strengths close to the residual strength (appropriate to the rate of pile penetration, and effective stress level operating during driving).

Examination of the deformed bedding planes (with the accompanying shrinkage cracks) suggests that the boundary between Zones A and B is a displacement discontinuity. Close to this boundary Riedel structures may be seen within Zone B, inclined at between 10° and 15° to the direction of pile penetration. The boundary between Zones B and C, on the other hand, appears to be a strain discontinuity.

6.6.2.4 Soil Deformations beneath the Advancing Pile Tip

The pattern of deformed bedding planes around the pile in Figs. 6.16(a),(b) and (c) may be used to establish the progressive deformation of a single, originally undistorted, bedding plane as a pile tip advances towards, and then passes through the original elevation of the plane. The main advantage of using thin section techniques for this purpose is that observations of the clay very close to the pile shaft may be obtained. However, as remarked earlier, the lack of reference points in the vertical plane means that it is not possible to establish the trajectories of individual particles, and so attention must be restricted to the deformation of identifiable planes. As stated earlier, the use of thin section techniques combined with radiographic techniques would be much more powerful.

From Fig. 6.16 it would appear that deformations within Zone C are small compared with those in Zones A and B. This is confirmed by measurements presented by Randolph, Steenfelt and Wroth (1979), and by Steenfelt et al. (1981). In order to examine (in an approximate fashion) the deformation of

an arbitrary bedding plane, it will be assumed below that the boundary between Zones B and C is a line of zero vertical and zero radial displacement.

As noted in section 6.6.2.3, the displacement field around the lower half of the pile shaft appears to be independent of depth and so it is reasonable to assume (as did Randolph et al., 1979) that all soil particles in a given line parallel to the pile axis, undergo a similar displacement path. With the aid of this assumption, it is possible to establish the progressively deformed shape of an originally horizontal plane of particles as the pile tip approaches and passes that level. The results of such an exercise are shown in Fig. 6.19. The 'dead' soil beneath the blunt pile tip acts as if it were part of the pile itself, and this cone of soil influences the deformation of the soil below. It may be seen in Fig. 6.19 that as the pile tip advances, the soil ahead of it is deformed, with severe distortions occurring in Zone B. Eventually, as the pile tip reaches the deformed plane of particles, the soil immediately beneath the tip is swept across the tip and into Zone A. As this soil is forced across the pile tip, it is subject to large shear strains, as is evident from the high degree of preferred particle orientation parallel to the tip of the cone (see Fig. 6.16(b)). This strongly oriented clay is subsequently forced into Zone A, which contains innumerable shear surfaces inclined at small angles to the direction of pile penetration. The inclination of these shear surfaces decreases with axial distance along the shaft from the pile tip, becoming almost vertical at a distance of some three pile diameters from the tip. Away from the ends of the pile, the pile penetration appears to be accommodated by slip within Zone A.

6.6.2.5 Comments

It is clear from the longitudinal thin sections that the driving of a full-displacement pile has resulted in a narrow zone of clay (about 25% of one pile radius) within which the particles are strongly oriented sub-parallel to the direction of pile penetration. The shear strength of this zone probably corresponds to the residual strength appropriate to the rates of penetration and effective stress levels obtaining during driving (see Appendices 4.1 and 5.3). The presence of such a zone might be expected to influence the subsequent loading behaviour of the pile.

6.6.3 Pile Driven, and Slowly Loaded to Residual Conditions

6.6.3.1 Introduction

The purpose of this test (No. 18) was to relate the load-displacement behaviour of the pile to fabric changes induced in the clay as a result of driving. The pile was driven into the kaolin sample (with peak velocities of the order of one metre per second) in the same manner as that employed in Test 16. In the present case, however, the pile was driven until the tip entered the cavity in the bottom platen. After allowing the kaolin to consolidate fully, the pile was slowly loaded until a constant, residual, load was achieved, after which thin sections were prepared. Further details of the method of pile installation and of the pile test results may be found in Chapters 4 and 5 respectively.

6.6.3.2 Fabric Changes Adjacent to the Pile Shaft

Figs. 6.20(a) and (b) present low magnification photographs of a longitudinal thin section and a cross-section through the sample, respectively. The boundary between the apparently undistorted clay(Zone C) and the more obviously distorted clay (in Zones B and A) lies at a distance of about one pile radius from the shaft. The most severely deformed clay in Zone A extends to a distance of about one and a half millimeters (or roughly 20% of one pile radius) from the shaft. Zone A may be seen in the cross-section as a set of numerous concentric shear surfaces. It is of interest to note that no evidence was found from the thin sections to suggest that radial cracks were formed in the clay during the pile tests (some workers, e.g. Massarsch and Broms (1977), postulate that the clay surrounding a driven pile is subject to hydraulic fracturing during installation).

A more detailed view of the clay close to the pile may be seen in Fig. 6.21 which includes two photographs,(a) and (b), (taken under different orientations of polarised light) and an interpretive diagram in Fig. 6.21(c). At the boundary between Zones A and B, faint Riedel structures may be seen, inclined at between 12° and 15° to the direction of pile penetration. The fabric within Zones A and B may be seen at a higher magnification in Fig. 6.22(a) and (b). Although the pile had achieved a residual capacity before the thin sections were prepared, it may be seen in Fig. 6.22(b) that there is no obvious, single, principal displacement shear. Rather, it would seem that the pile displacements were accommodated by slip on combinations of the many shear surfaces present.

6.6.3.3 Comments

It was shown in section 6.6.2 that the clay adjacent to a driven pile is strongly oriented sub-parallel to the direction of pile penetration. In view of the large displacements involved, it was suggested that the strength of this shear zone probably corresponds to residual conditions (appropriate to the rate of penetration and the effective stresses acting during driving). On slowly loading a similar pile, brittle post-peak behaviour was encountered, after which residual conditions were again achieved. The reasons for the brittle behaviour are now considered.

Experimental work to study the influence of rate of displacement on residual strength has been performed (see Appendices 4.1 and 5.3, and also Lupini, 1981). The results suggest that the degree of orientation of clay particles beside a residual shear surface decreases with increasing rate of displacement. On slowly reloading a shear surface that has been subject to rapid displacements, the peak strength corresponds to the relatively disordered state of the particles beside the shear surface, but the strength decreases with further displacement as the particles become more strongly aligned parallel to the direction of displacement.

By an analogous argument,it would be expected that the residual strength of the shear zone (Zone A) beside a driven pile would be relatively high in view of the rapid displacements and low effective stresses operating during driving. On slowly loading the pile (in the model tests this was performed at a rate some seven orders of magnitude slower than the peak rate of penetration during driving), peak load would occur when the strength of the shear zone is exceeded; thereafter the pile capacity would be expected to decrease with further pile displacement as the clay particles within the shear zone became more strongly aligned parallel to the direction of movement. Following this argument, if the pile were to be loaded slowly to residual conditions and then unloaded and later reloaded, the new peak strength should correspond to the strength obtained immediately prior to unloading, and not to the original peak value. This behaviour was indeed observed (see Fig. 5.27).

6.6.4 Pile Jacked, and then Slowly Loaded to Residual Conditions

6.6.4.1 Introduction

The pile (in Test 19) was jacked through the sample at an average rate of about 4 millimeter/minute, until the tip of the pile entered the cavity in the bottom platen. The sample was then left overnight to ensure

complete consolidation before the pile was slowly loaded ($5x10^{-3}$ mm/min) to residual conditions. The pile load-displacement behaviour exhibited some brittleness, but this was much less than that observed in the case of the driven pile (see Fig. 5.27). For further details of the installation procedure and the results of the load testing see Chapters 4 and 5 respectively.

6.6.4.2 Micro-fabric Changes Beside the Pile

As might be expected, the thin sections show that the final micro-fabric changes were intermediate in nature between those observed following the tests on the driven piles, and those observed after any of the earlier series of tests conducted on piles installed with minimal disturbance.

Two photographs of a longitudinal thin section taken from the top of the jacked and loaded pile are shown in Figs. 6.23(a) and (b) and two photographs and a schematic representation of a thin section taken from the centre of the sample are presented in Figs. 6.24(a),(b) and (c).

By comparing the two sets of figures it will be seen that the general shearing pattern was established by a depth of about one pile diameter from the top of the sample; there is no evidence to suggest pile wobble during installation. In general, the clay appears to have been severely disturbed to a distance of roughly one pile radius from the shaft, which is similar to the distance measured following the tests on driven piles, but twice that measured after the tests on piles installed with minimal disturbance.

Close to the pile, Riedel structures may be seen. They penetrate to a distance of some two millimeters from the shaft, at intervals of between 5 and 10 millimeters down the pile, and at inclinations of between 20° and 35° to the direction of penetration. The inclinations suggest that they may have formed around the toe of the pile and were left as relic structures along the shaft. It may be of interest to note that these structures were not encountered so close to the driven piles, probably because the shear zone (Zone A) extended to a distance of nearly two millimeters from the shaft and would have destroyed all traces of them.

Very close to the pile a single, continuous, principal displacement shear structure may be seen running parallel to the shaft. It is unfortunate that during the preparation of the thin sections, a little clay was lost in places from the edge of the pile. However, wherever the clay is intact, the principal displacement shear may be seen at a distance of between 0.1 and 0.5 millimeters from the shaft.

6.6.4.3 Comments

It is suggested that during jacking the large relative displacements between the pile and the clay were accommodated primarily by slip on this thin shear surface, which had a shear strength determined by the rate of penetration and the effective stress level. On slowly loading the pile, the peak load was achieved when the shear strength of this discontinuity was exceeded. With post-peak displacement (three orders of magnitude slower than during jacking) the clay particles on the shear surface probably become more highly ordered, resulting in the observed post-peak brittleness.

The experimental observations concerning jacked and driven piles are now discussed with reference to field observations reported by Tomlinson (1970,b) and by Butterfield and Johnson (1973).

6.7 DISCUSSION OF THE BEHAVIOUR OF DISPLACEMENT PILES

6.7.1 Summary of the Results from the Model Tests on Displacement Piles

One of the most interesting aspects of this study has been the demonstration (see Fig. 5.27) that the peak capacities of both jacked and driven piles are less than those of piles installed with minimal disturbance into similarly consolidated samples of kaolin. This result was observed despite the measured decrease in water content of the clay beside the displacement piles as a result of installation and consolidation. Examinations of the thin sections taken at the pile-clay interface suggest that the clay adjacent to the displacement piles was severely disturbed during the installation, and that shear surfaces were formed parallel to the direction of pile movement.

On slowly loading the displacement piles, the pre-peak behaviour was very similar to that of the piles installed with minimal disturbance, until peak conditions were abruptly reached by the displacement piles (see Fig. 5.27 once again). These piles presumably 'failed' when the peak angles of friction on the shear surfaces generated by pile installation were mobilised. As the rate of pile penetration during driving was much faster than that during jacking, it would be expected (from the work presented in Appendices 4.1 and 5.3, and by Lupini, 1981) that the peak angle of shaft friction around the driven piles would be greater than around the jacked piles. The peak normalised capacity of the driven pile was indeed observed to be more than 10% higher than that of the jacked pile.

In all the pile tests, it was observed that following post-peak displacements of between 5 and 10 millimeters, constant residual conditions were achieved. As the final displacement rate was the same for all tests, it seems reasonable to assume that the residual angles of shaft friction were the same too. Taking this angle of friction to be 11.5° it may be shown that for a given cell pressure the radial stresses acting at residual conditions were 10% greater for the driven pile than for one installed with minimal disturbance. The radial stresses acting on the jacked pile were intermediate in value (6% greater). It should be remembered that the boundary conditions acting on the kaolin samples were not ideal for the conduct of tests on displacement piles, and so the above values should be taken as being indicative of a trend, rather than as precise results.

The micro-fabric studies suggest that the principal displacement shear induced in the soil around the jacked pile was very narrow and continuous, whereas around the driven pile no obvious single shear surface could be found, and the pile displacement appears to have been accommodated by simultaneous slip on numerous parallel shear surfaces within Zone A.

6.7.2 Field Tests on Jacked and Driven Piles in London Clay

6.7.2.1 Introduction

Tomlinson (1970,b) presented the results of several field tests performed on straight, closed-ended, steel piles which were either driven, or jacked into London Clay. After testing,some of the piles were exhumed in order to examine the nature of the disturbance to the clay caused by the pile installation.

Butterfield and Johnston (1973) jacked an instrumented pile into London Clay, and measured the local shear stresses and radial total stresses acting on the pile during jacking.

The results from both sets of tests are discussed below.

6.7.2.2 Comparison between the Behaviour of Jacked and Driven Piles

Of the nineteen test piles discussed by Tomlinson (1970,b) twelve were installed into London Clay which was not covered by overburden. These tests were conducted in pairs of similar piles; in each case one pile was installed by jacking and the other by driving. After allowing the soil around the piles to consolidate for 28 days, the piles were tested, and later re-tested three months, and one year after installation. The early stages of the pile tests were load-controlled but displacement-controlled

loadings were used to examine the post-peak behaviour.

Of the six pairs of piles mentioned above, the two pairs JP5, DP5 and JP6, DP6 had the greatest penetration, and results from tests on them will be used for illustration in the discussion below, although similar results were obtained with the shorter piles. The piles were constructed from 168 mm OD mild steel seamless tubes, and the four piles considered were installed to a depth of some five and a half metres (or some thirty two times the pile diameter). The piles were strain-gauged so that the load distribution along the piles could be measured.

The load-displacement behaviour of the jacked piles JP5, JP6 and the driven piles DP5, DP6 are illustrated in Fig. 6.25, and it may be seen that there are some obvious differences in behaviour between the two types of pile. The driven piles exhibited a marked peak on first loading, after which the shaft capacity reduced by 30% to a value which did not change with further displacement (the quoted reduction in capacity is the average value from the six tests (DP1 to DP6) conducted on driven piles). In contrast, the jacked piles exhibited a much less pronounced peak which was typically about 6% in excess of the residual capacity. The residual capacities of similar pairs of driven and jacked piles were generally within 5% of each other, the driven piles being the stronger.

Tomlinson noted that the forces required to jack the piles into position exceeded those required to bring the piles to peak load after 28 days consolidation. Thus, during installation the mean α value was 0.6, whereas on loading the values varied between 0.5 and 0.6. Although the shear strength of a shear surface in London Clay increases with rate of displacement (see Lupini, 1981), Tomlinson's observations suggest that the radial effective stresses acting on the piles during jacking were not significantly different from those acting during pile loading.

If Figs. 5.27 and 6.25 are compared, it will be seen that the shapes of the load-displacement curves for the corresponding field and the laboratory pile tests have several features in common. The deformations required to achieve peak load would be expected to depend on the pile diameter, and it may be seen that the normalised displacements to peak measured during the field tests and the laboratory tests, are similar (1.5% and 0.7%). These two values would not be expected to be identical in view of the differences between the clays and their stress histories prior to pile installation.

On the basis of the micro-fabric studies, however, it is suggested that the majority of post-peak displacements occur in a very narrow zone close to the pile, and so the displacements to achieve residual conditions would not be expected to be significantly influenced by the pile diameter (provided, of course, that it is much greater than the particle sizes involved). In the field tests displacements of 20 to 25 mm were required, compared with the 10 mm required in the laboratory.

After the field tests, Tomlinson (1970,b) exhumed one jacked pile and three of the driven piles. In all cases, a gap had developed between the pile and the clay for the first four pile diameters from the ground surface (presumably as a result of pile wobble). Over the lower portion of the pile, however, a thin skin of clay between 1 and 6 mm thick remained strongly adhering to the pile. The outer surface of this skin was apparently very smooth and slickenslided, whereas the surface in contact with the pile had a matt appearance and carried the pattern of the steel. This strongly suggests that the slip between the pile and the clay was occurring on the slickenslided surface of adherent skin, and not at the pile-clay interface. Tomlinson had electron-micrographs prepared from the clay on the slicken-slided surfaces of both the driven and jacked piles, and showed that the clay particles were very strongly aligned at a very small angle to the pile axis. Thin sections prepared after the laboratory tests show similar results.

Tomlinson suggested that these slickenslided surfaces must be at residual strength, and measured the residual angle of friction to be 10° (using a direct shear box).

6.7.2.3 Stresses Acting on a Continuously Jacked Pile in London Clay

Butterfield and Johnston (1973) reported the results obtained during the jacking of an instrumented model pile (100 mm diameter) into London Clay. The instrumentation incorporated enabled measurements of local shear stresses and radial total stresses acting on the pile shaft to be obtained at various locations down the pile.

The radial total stresses were seen to be very strongly influenced by the initial undrained shear strength, Cu, in the adjacent soil. Away from the top and the bottom of the pile the radial stresses were generally about 4 x Cu, and the local values of $\alpha(\bar{\tau}/Cu)$ lay between 0.7 and 0.8 during installation.

Employing 200 simultaneous local measurements of shear and total radial stresses, the authors determined values for the angles of interface friction . More than 70% of the values fell in the range 10° ± 3°, and the authors argued that an appreciable, and essentially constant proportion of the total radial stress was effective across the interface. Although it is very unfortunate that this assumption could not be confirmed by measurements of local pore pressures, it is supported by Tomlinson's observation that on loading a jacked pile a month after installation, the peak load was less than the jacking force.

It would, therefore, appear from both sets of field tests that on loading the jacked piles in London Clay, the peak angle of shaft friction was not much greater than the residual value of around 10°, and was certainly much smaller than the angle of shearing resistance that might be determined by means of a triaxial test.

6.7.3 Conclusions

It has been demonstrated that the installation of a displacemnt pile into a plastic clay may cause severe disturbance to the micro-fabric of the clay adjacent to the pile. The large relative displacements between the pile and the clay are accommodated by slip within a narrow shear zone, and locally the clay particles are re-oriented to lie sub-parallel to the direction of pile penetration. When the pile is loaded, its shaft capacity is limited by the presence of this shear zone.

Both the laboratory and the field tests indicate that the peak capacities of driven piles exceed those of otherwise similar jacked piles, whereas the residual capacities are very similar. It is suggested that the greater peak strengths of driven piles result from rate effects experienced during installation by the clay in the shear zones beside the piles (see Appendix 5.3 for example), and possibly also from the reverse shear that may occur on pile rebound following each blow during driving.

If a displacement pile is slowly loaded beyond peak conditions, the clay particles within the shear zone become more strongly aligned in the direction of pile displacement, and the mobilised angle of friction tends rapidly towards a residual value appropriate to that particular rate of displacement. If the pile is unloaded and later re-loaded, the new peak angle of shaft friction will equal the residual value unless some form of cementing or other ageing process occurs in the meantime.

It is suggested that when estimating the capacities of long, and therefore compressible, piles a reasonable lower bound to the angle of shaft friction may be obtained from the results of direct shear tests in which the soil is sheared, under drained conditions, against a rigid interface made from the pile material; this idea is considered further in Chapter 9. The major obstacle to the development of a general effective stress method of pile design is now the shortage of reliable measurements of radial effective stresses acting on piles as a result of both installation and loading.

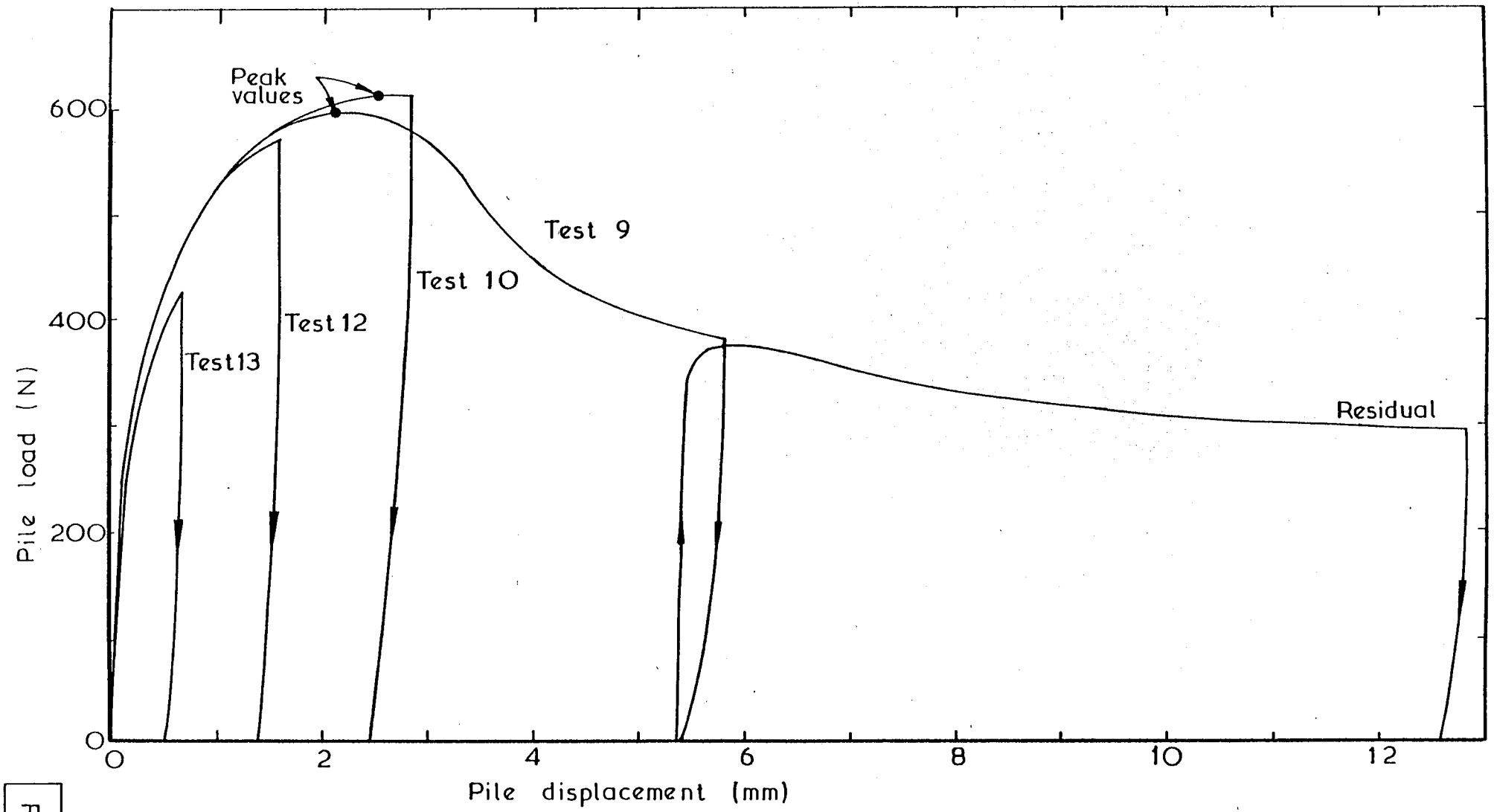


Fig.6.1

Load-displacement curves for four similar tests stopped at different stages.

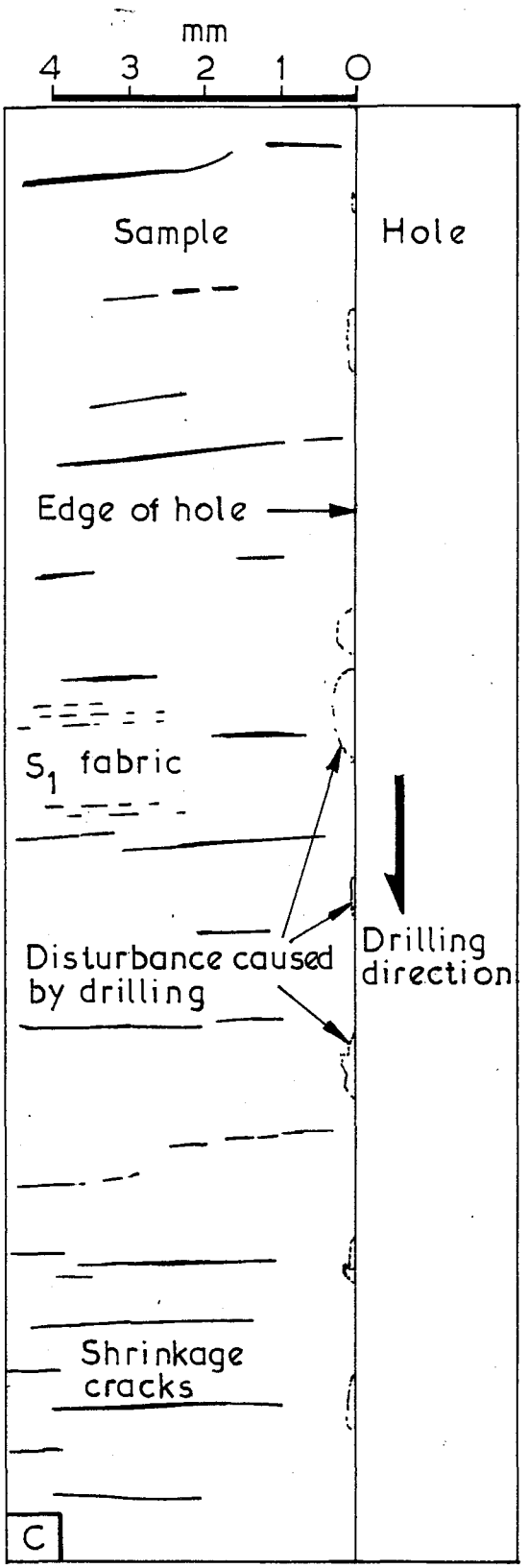


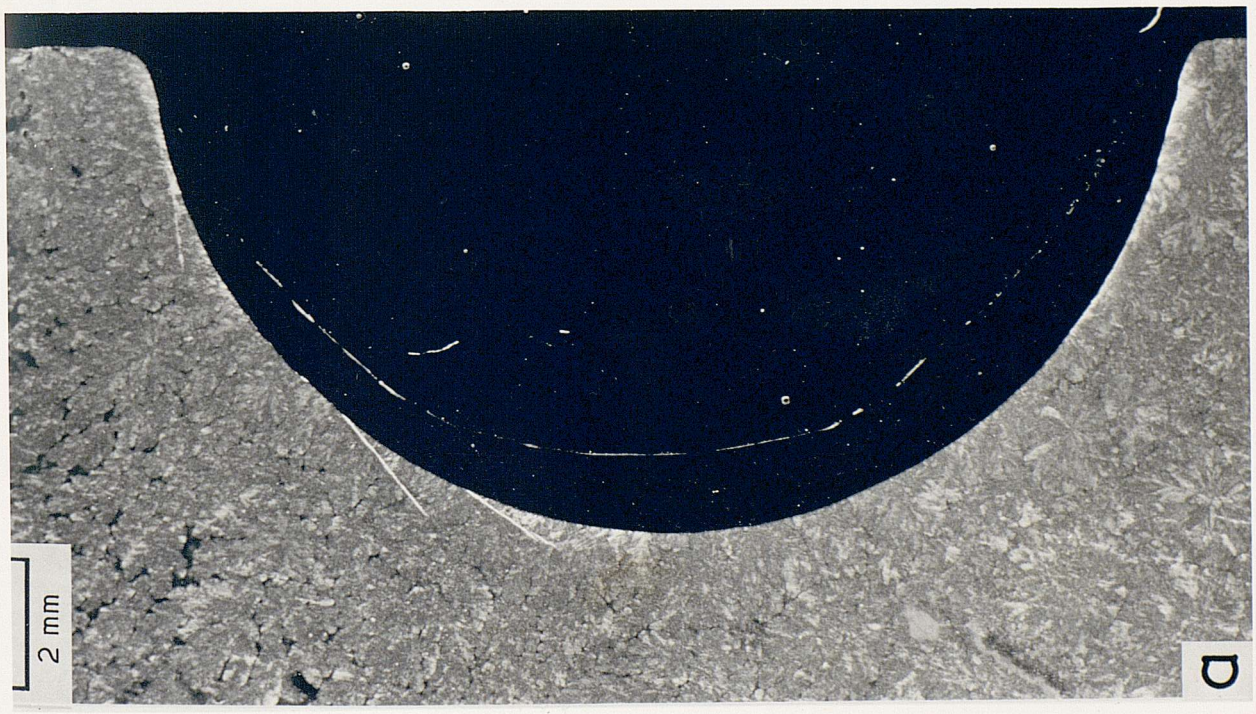
Figure 6.2 Thin sections of the sample from Test No.4 -hole drilled through the centre.

(a) Photograph of cross-section

(b) —·— ·-· longitudinal section

(c) Interpretation of the longitudinal section


2 mm
b


2 mm
a

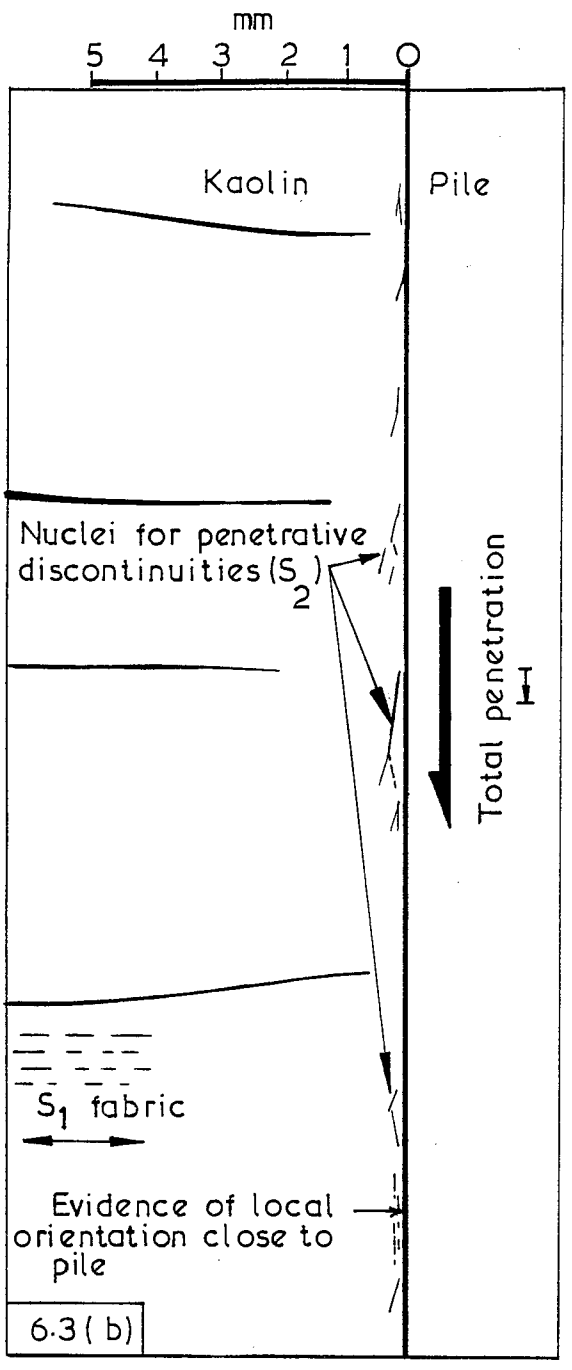


Figure 6.3 Longitudinal thin section after Test No.13

(a) Photograph

(b) Interpretation

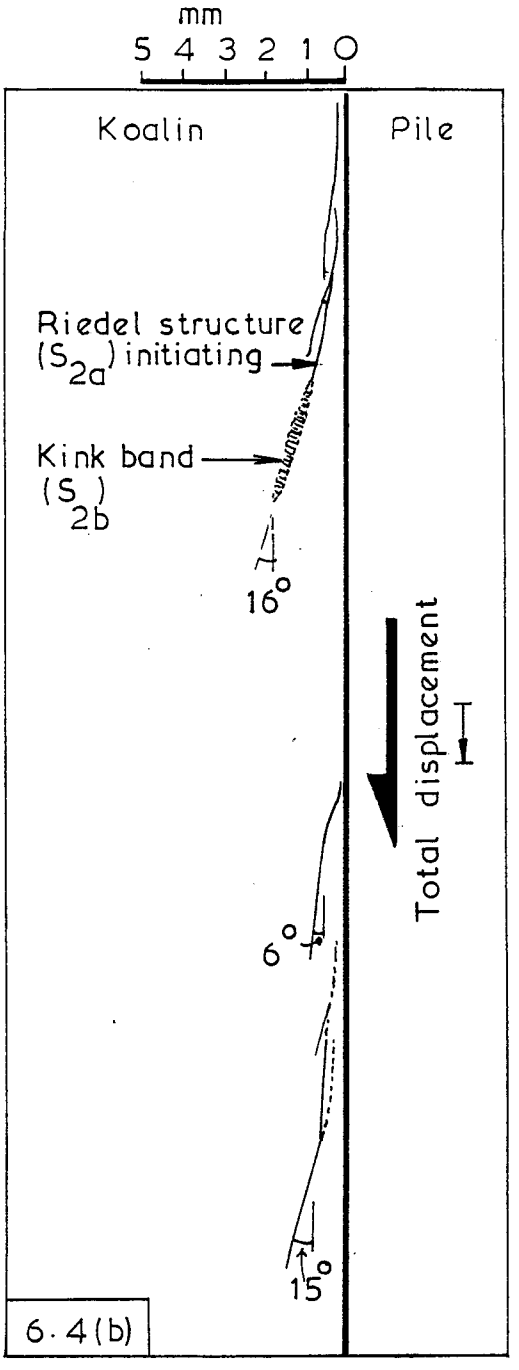


Figure 6.4 Longitudinal thin section after Test No. 12

(a) Photograph

(b) Interpretation



6.3(a)



6.4(a)

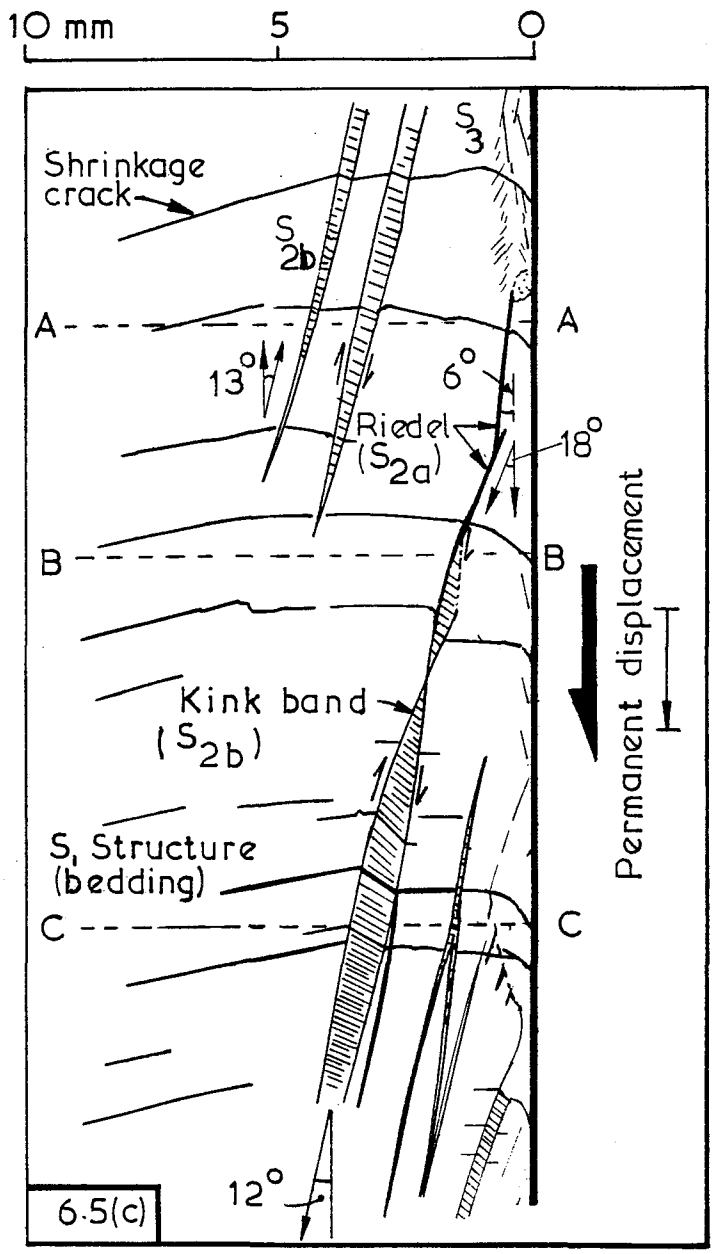
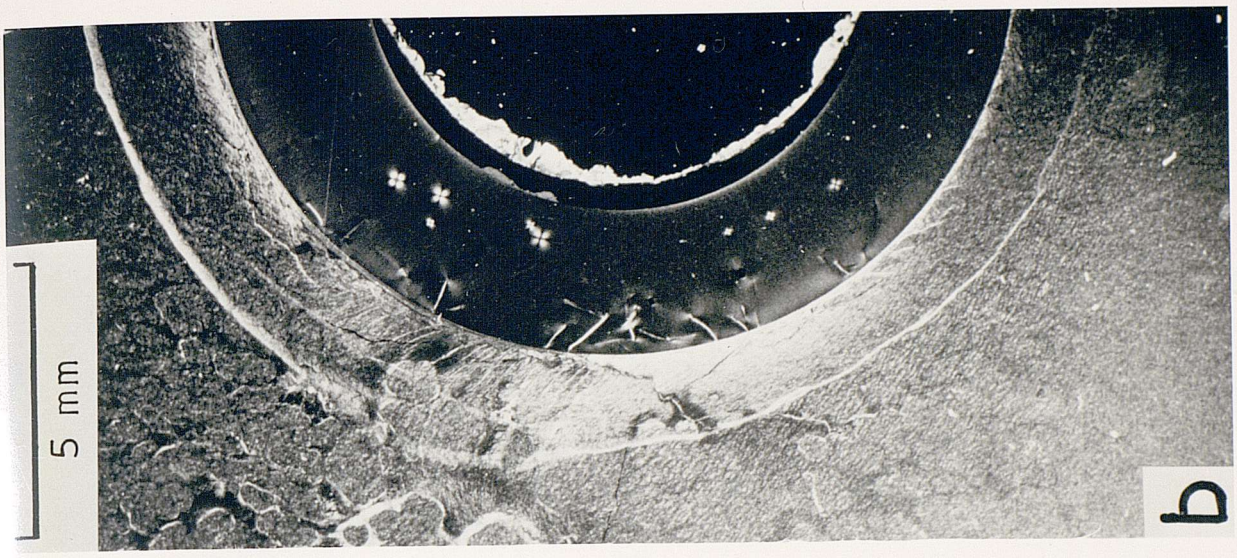


Figure 6.5 Thin sections following Test 10

(a) Photograph of longitudinal section

(b) —·— ·—· cross- ·—· —·—

(c) Interpretation of longitudinal section



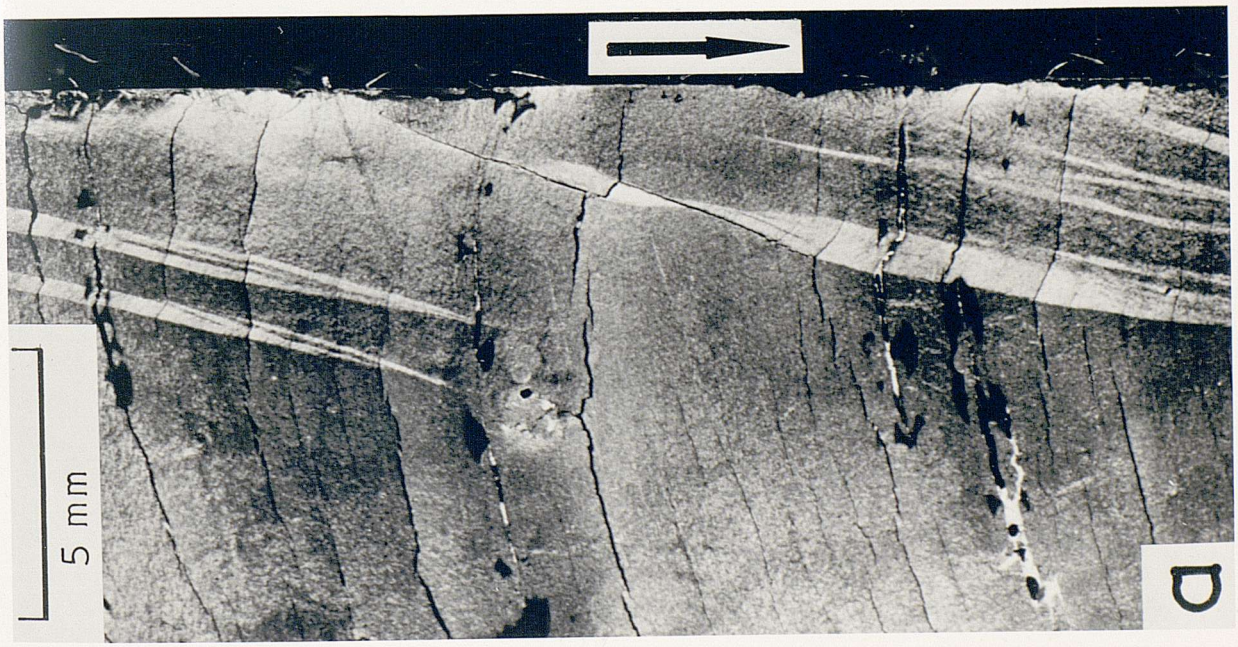
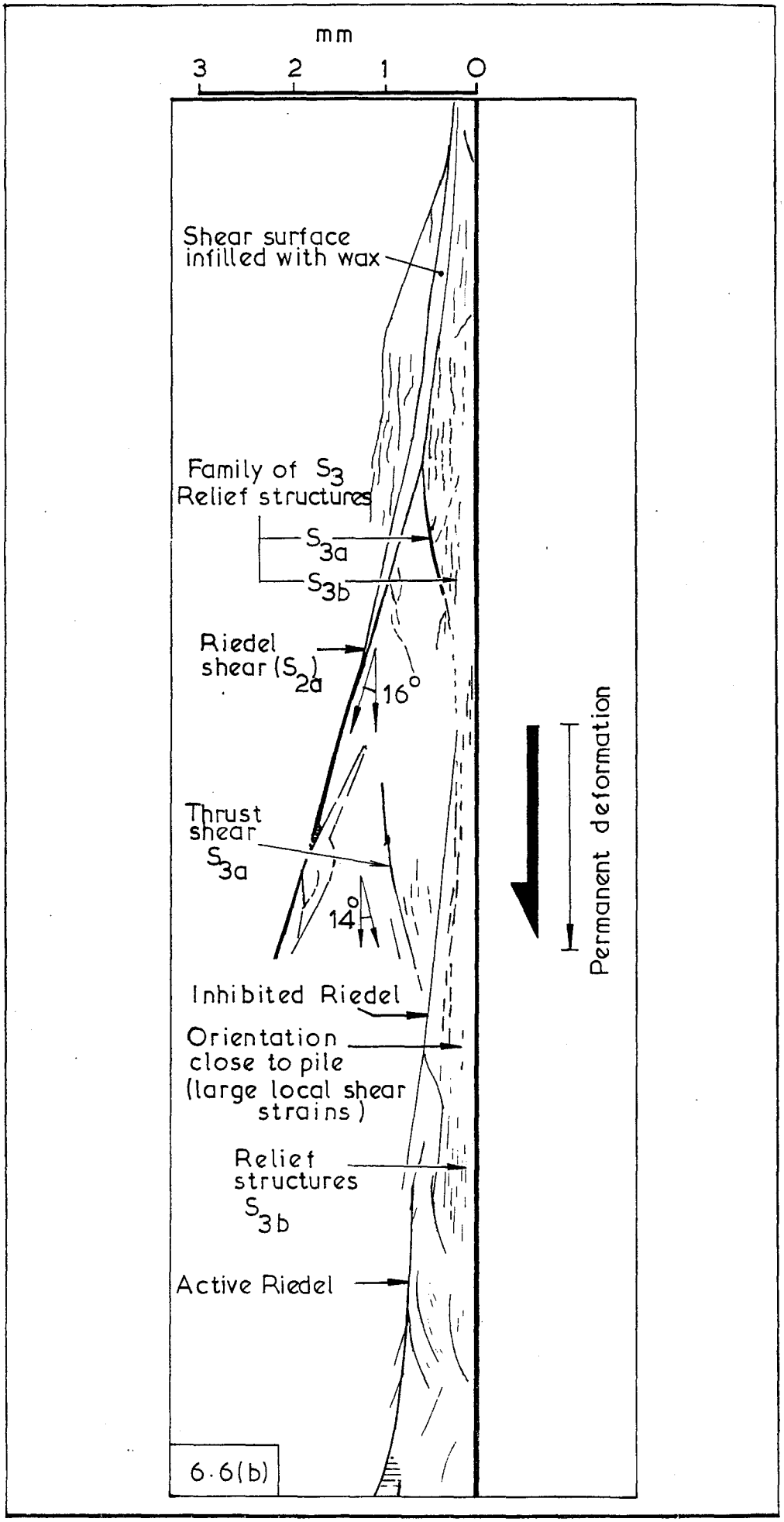
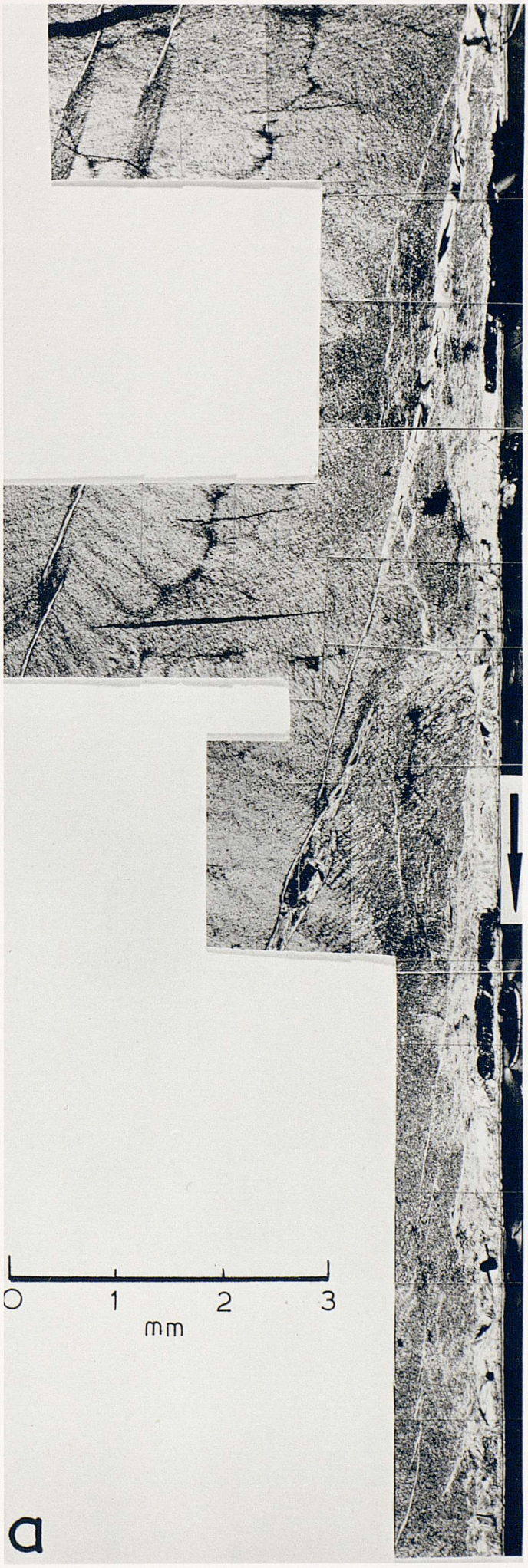
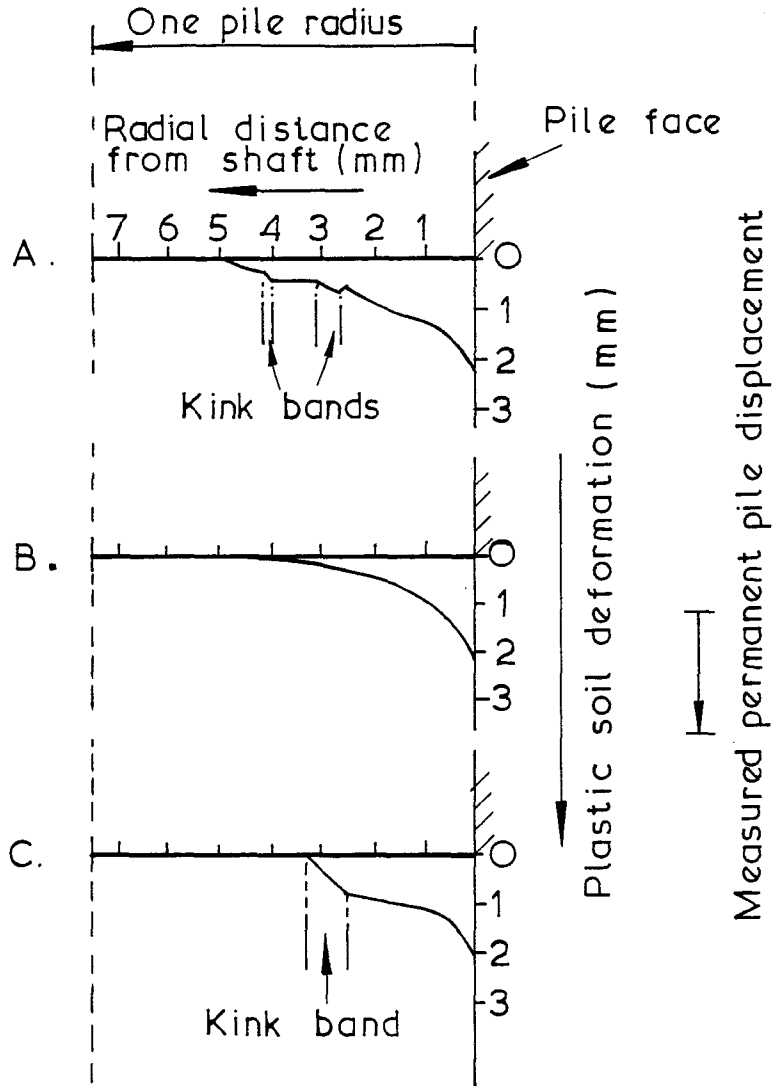


Fig. 6.5


mm
3
2
1
0
Shear surface infilled with wax
Family of S_3 Relief structures
S_{3a}
S_{3b}
Riedel shear (S_{2a})
16°
Thrust shear S_{3a}
14°
Inhibited Riedel
Orientation close to pile (large local shear strains)
Relief structures S_{3b}
Active Riedel
Permanent deformation
6·6(b)


0
1
2
3
mm
a



Sections A, B, and C correspond to those shown in Figure 6.5 (c)

Permanent deformations within the clay around a pile loaded to peak (Test 10, K=1.5)

Fig. 6.7

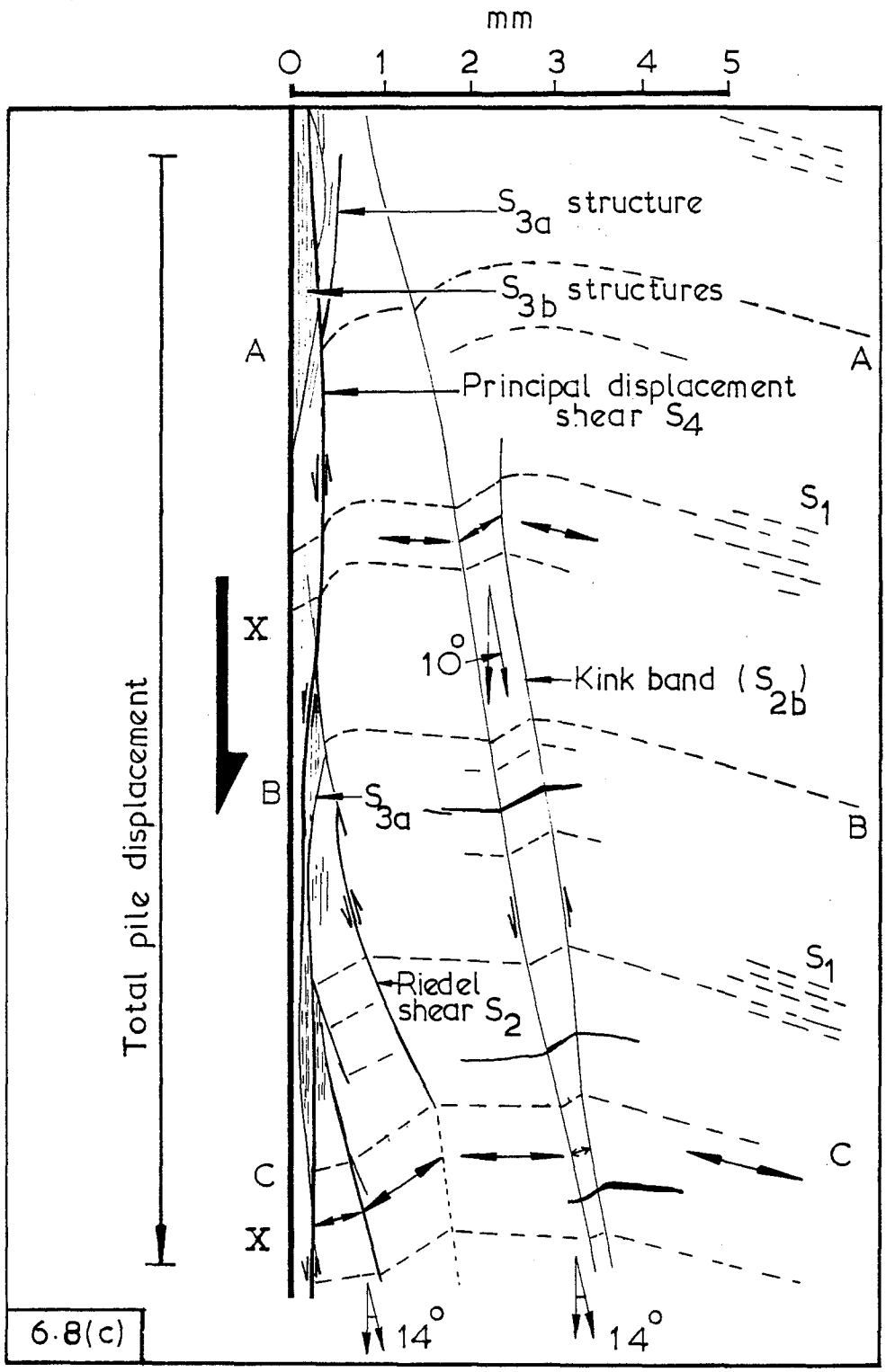
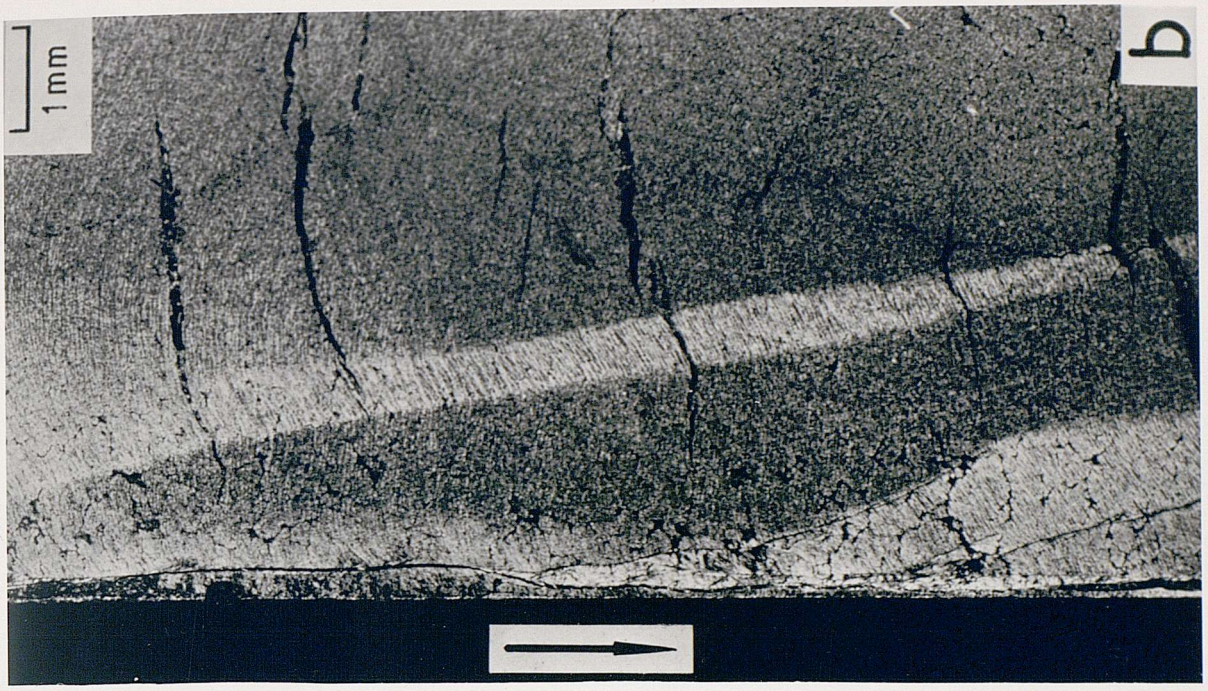


Figure 6.8 Longitudinal thin section following Test 9

(a) Photograph

(b) Photograph with plane of polarisation rotated through 45°

(c) Interpretation



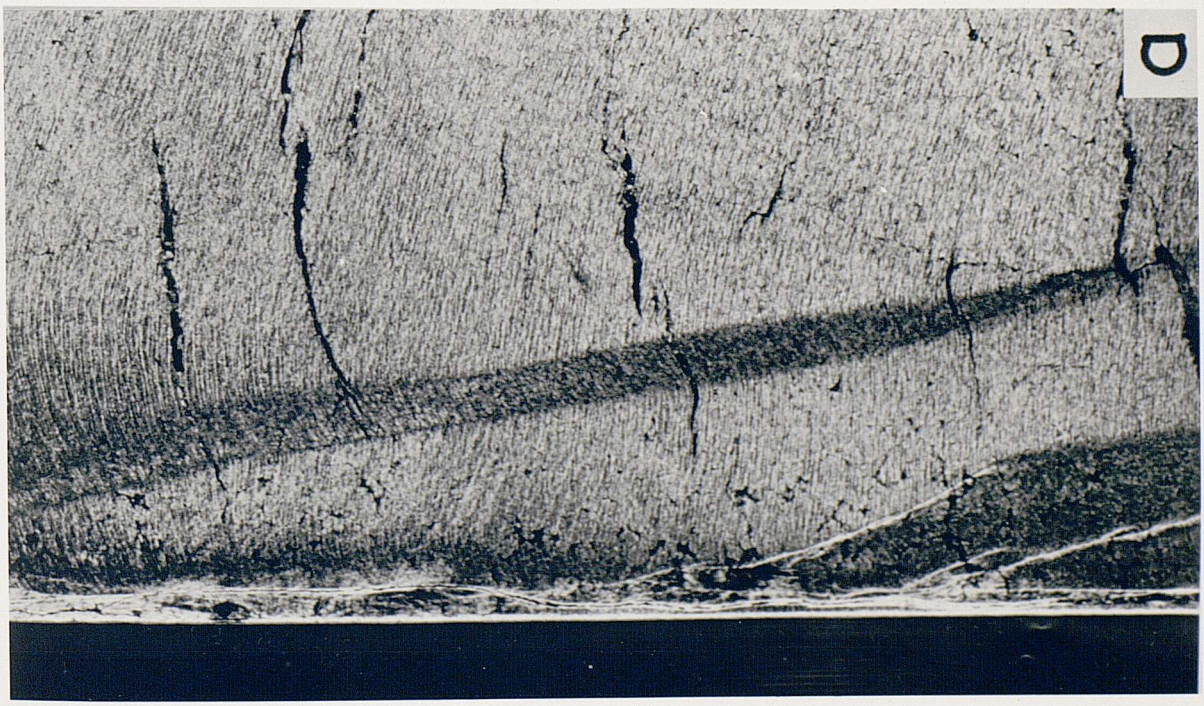


Fig. 6.8

Figure 6.9 (facing)

Composite longitudinal section following Test No. 9

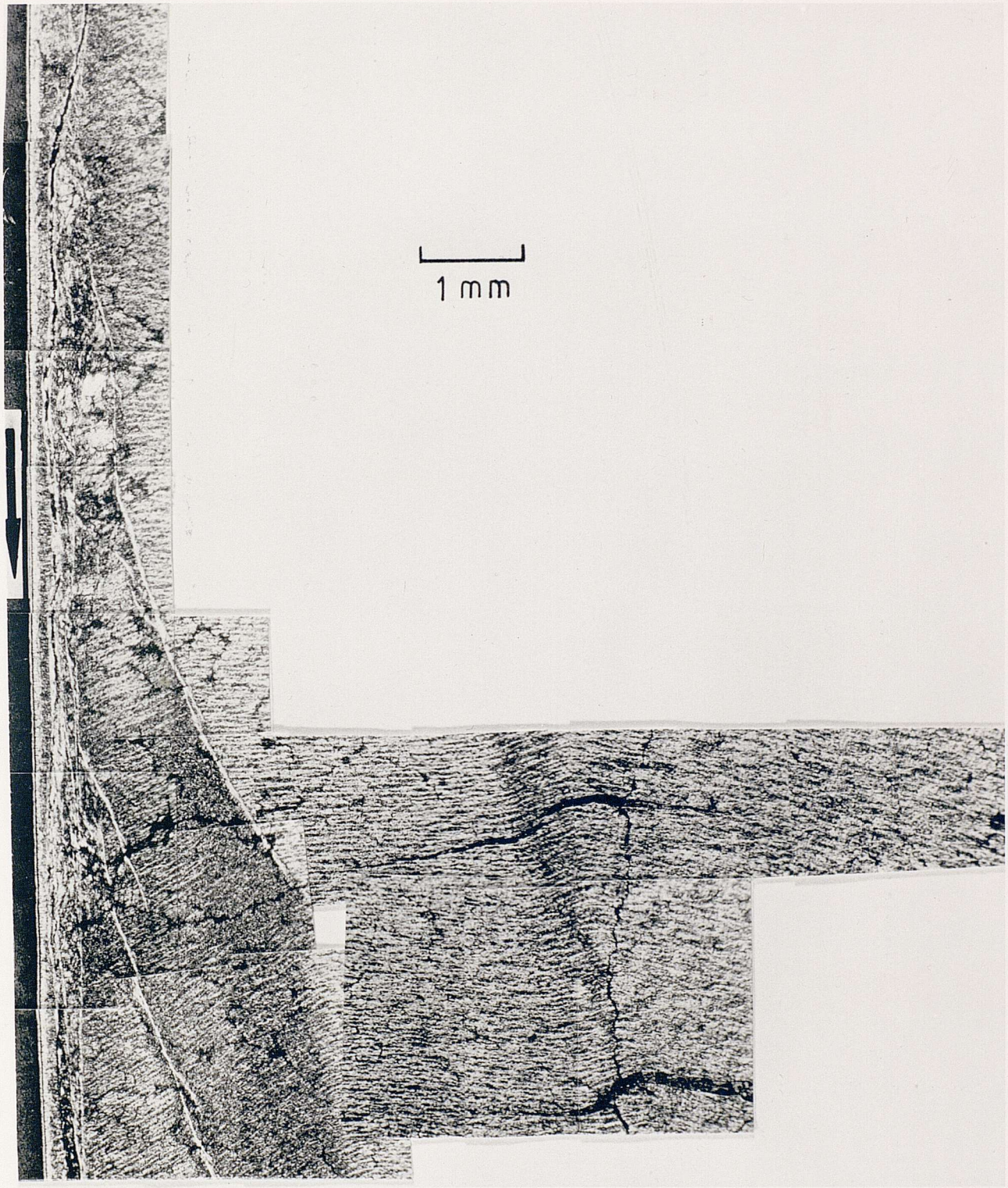
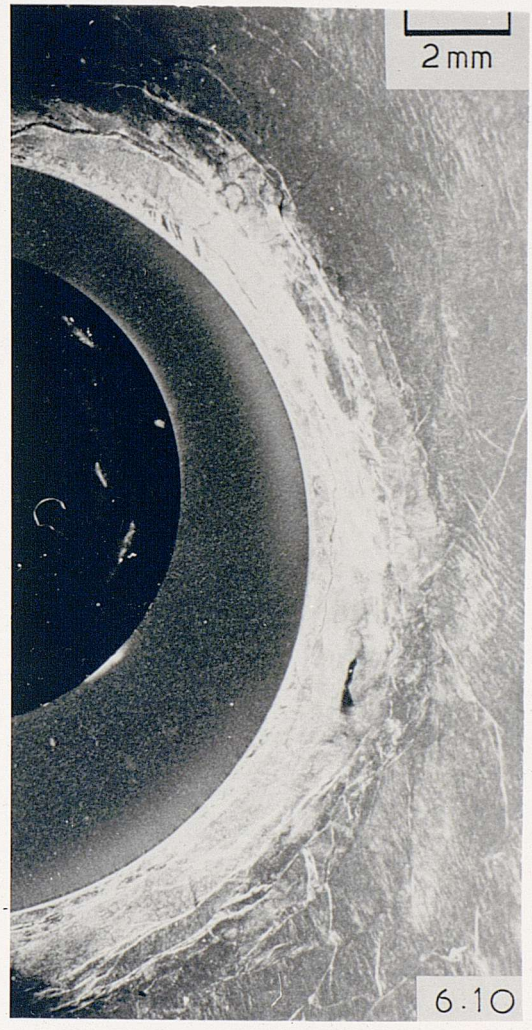
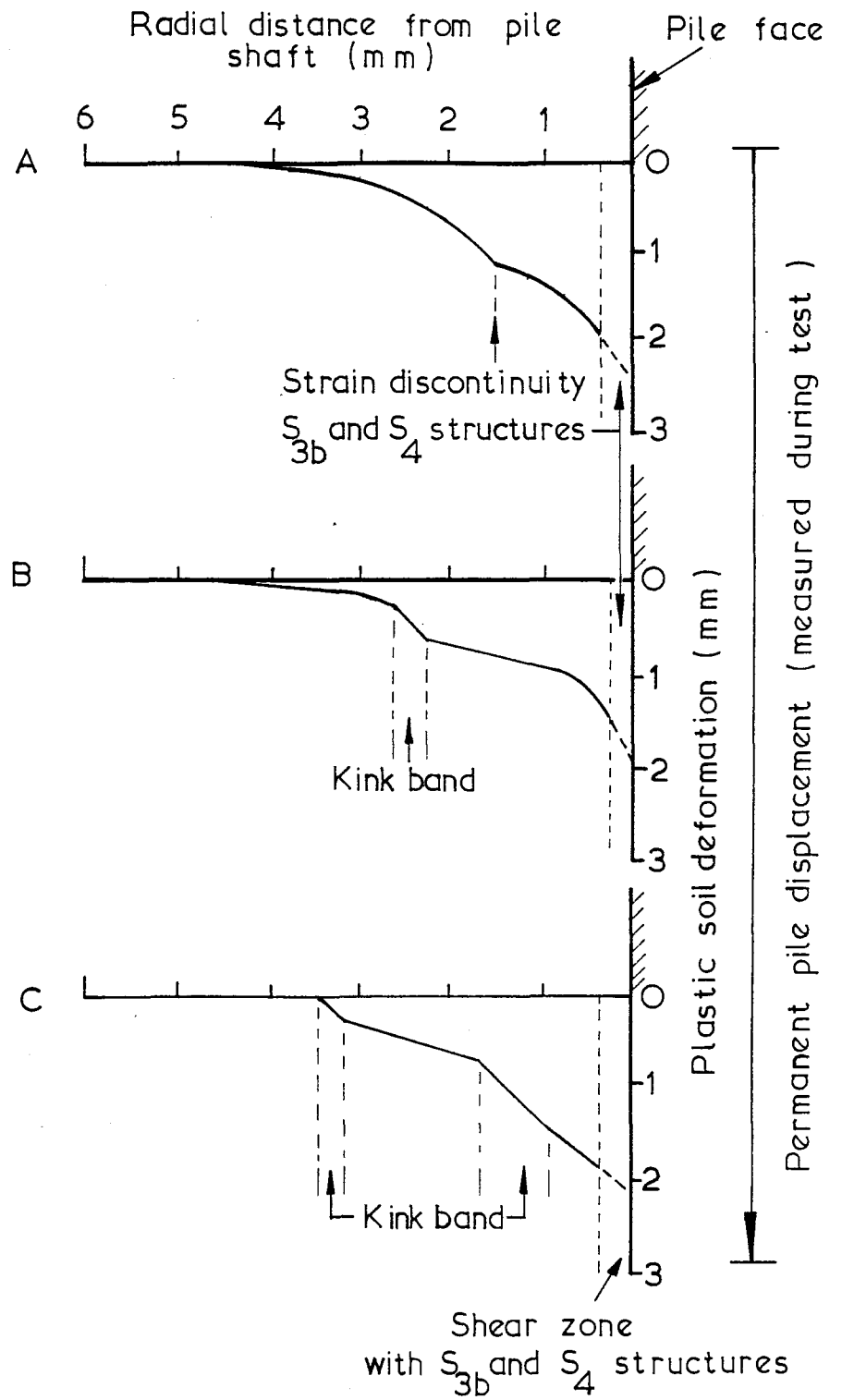


Fig. 6·9

Figure 6.10 (facing)

A cross-section prepared following Test No.9


2 mm
6.10



Sections A B and C correspond to Figure 6.8

Permanent deformations within the clay surrounding a pile loaded to residual conditions (Test 9, K=1.5)

Fig 6.11

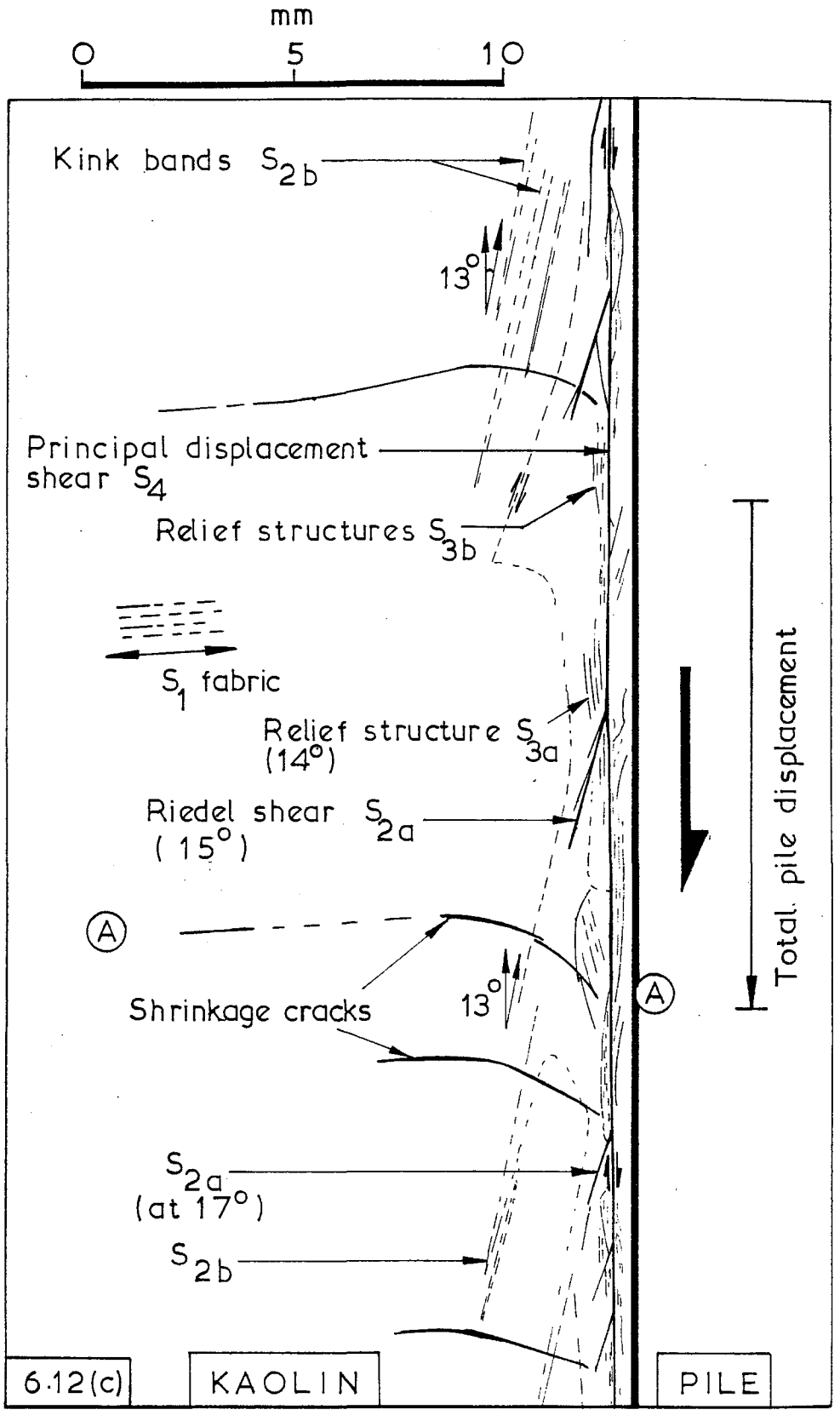


Figure 6·12 Longitudinal thin sections following Test No. 14

(a) Photograph of longitudinal section

(b) " " " " with plane of polarisation rotated 45°

(c) Interpretive diagram

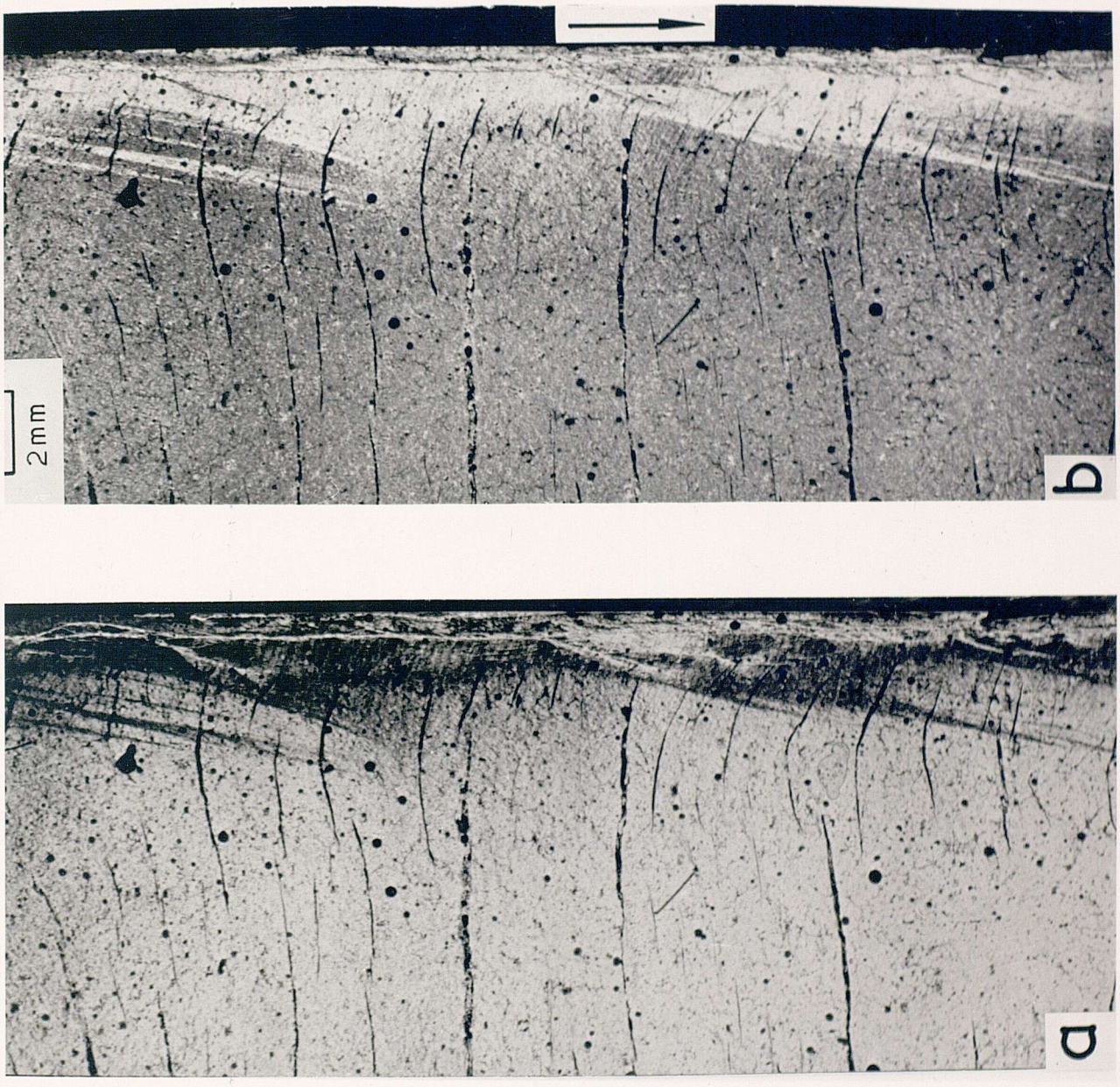


Fig. 6.12

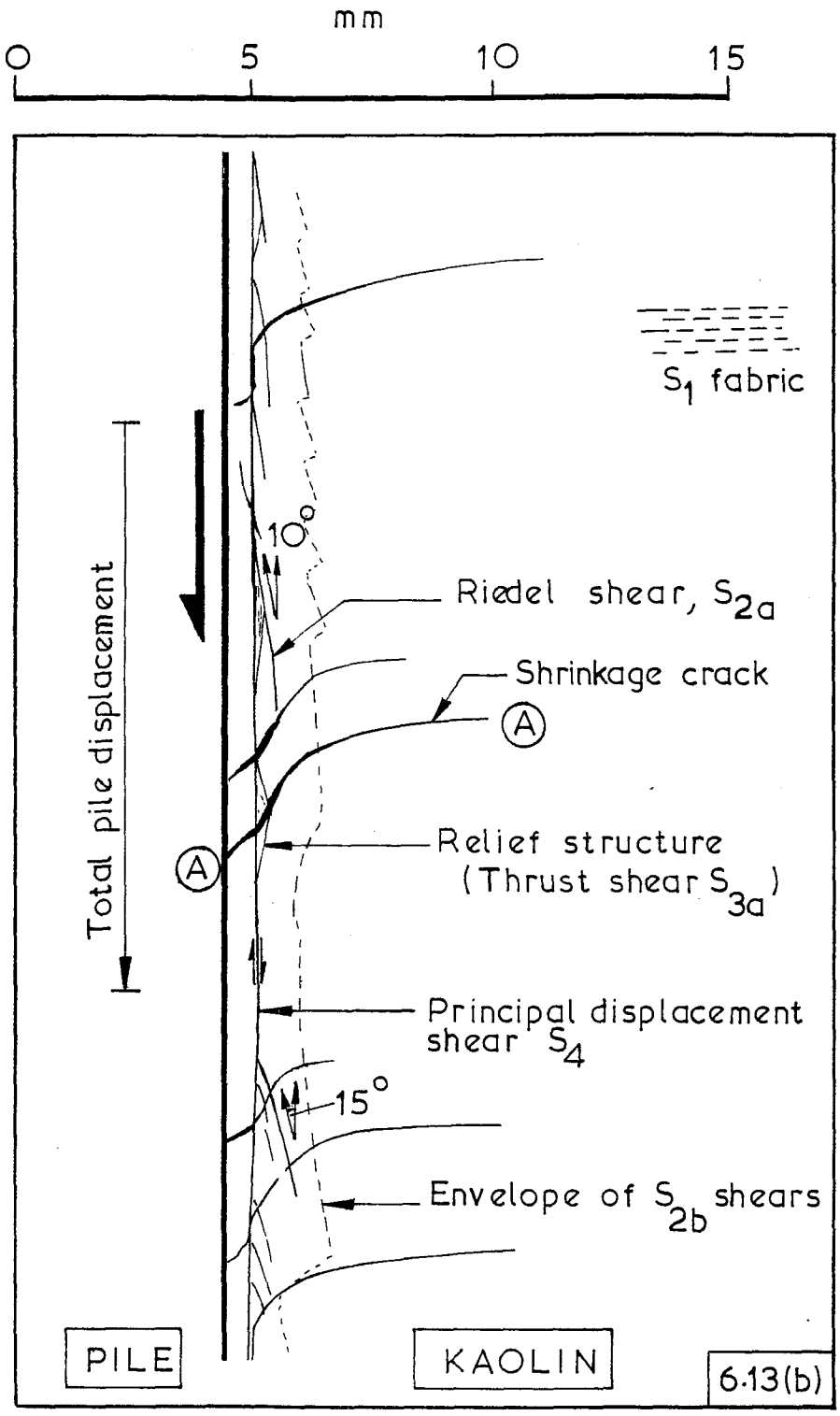


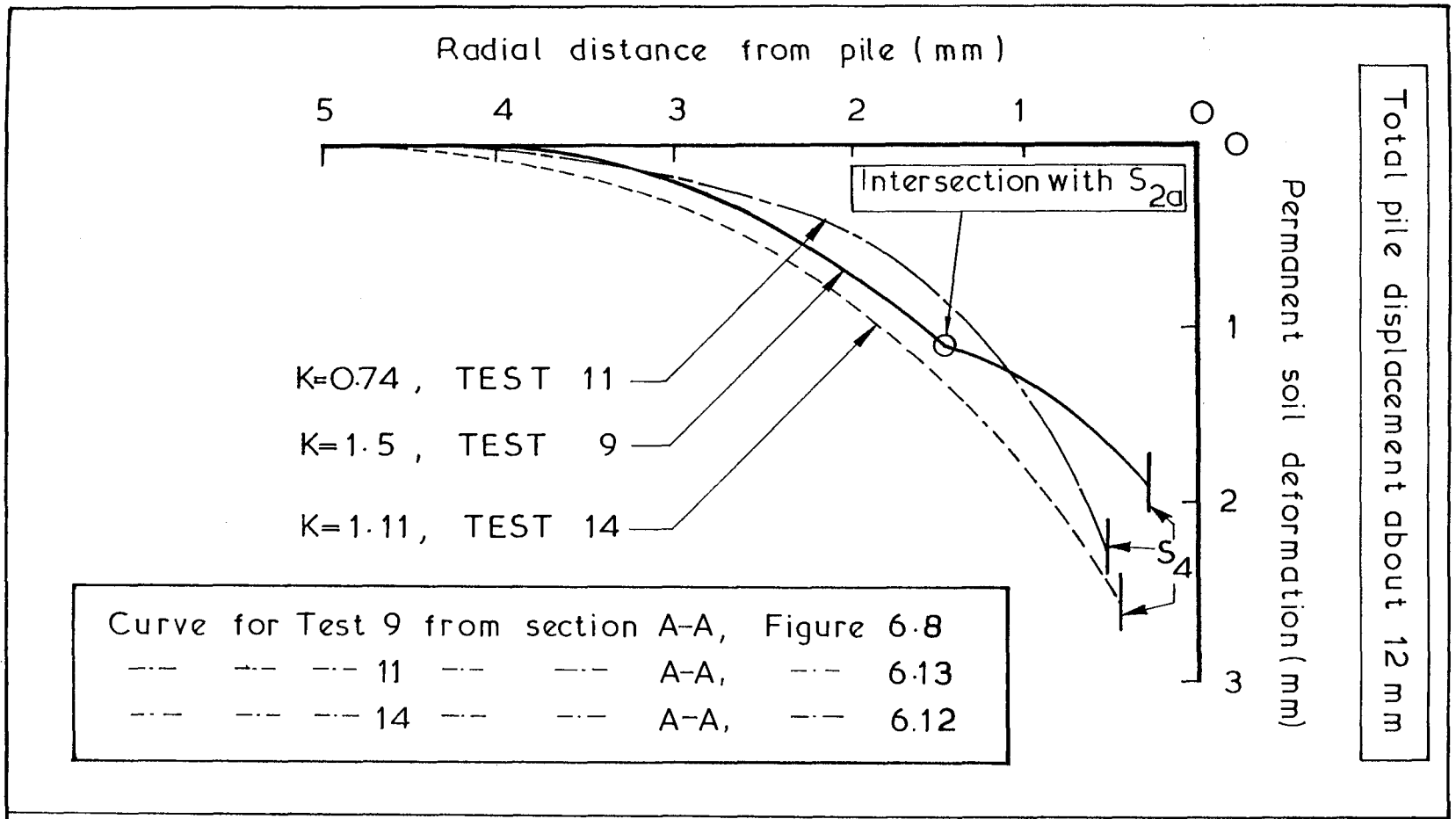
Figure 6.13 Longitudinal thin section prepared after Test No. 11

(a) Photograph

(b) Interpretive diagram



Fig. 6.13



Comparison between soil deformation profiles around the piles from Tests 9, 11 and 14 beyond the principal displacement shears, S_4

Figure 6·15 (facing)

Longitudinal thin section prepared after Test No 7 , conducted on over-consolidated kaolin



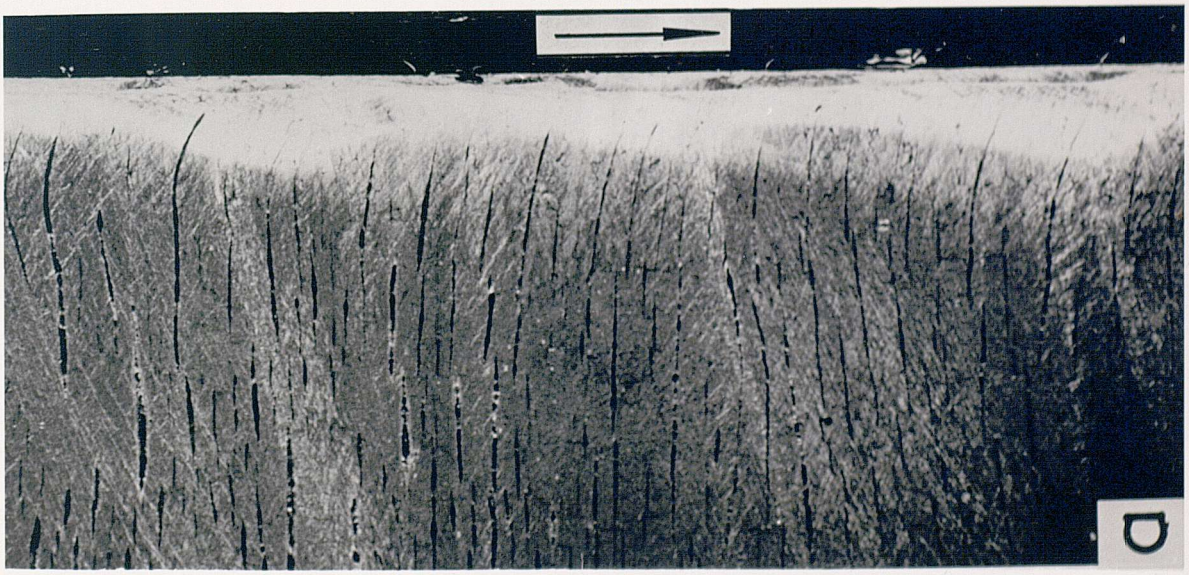


Fig. 6.15

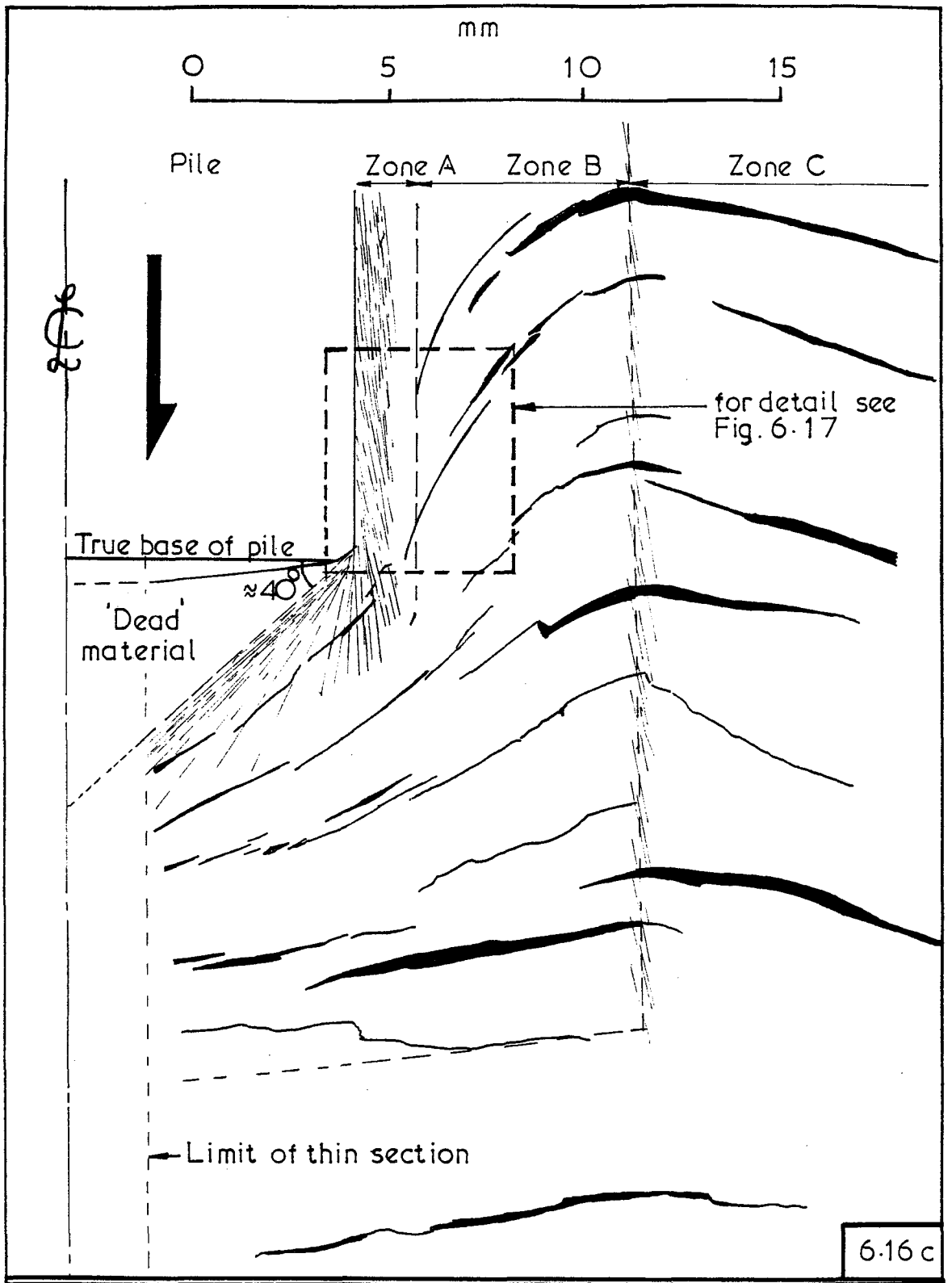
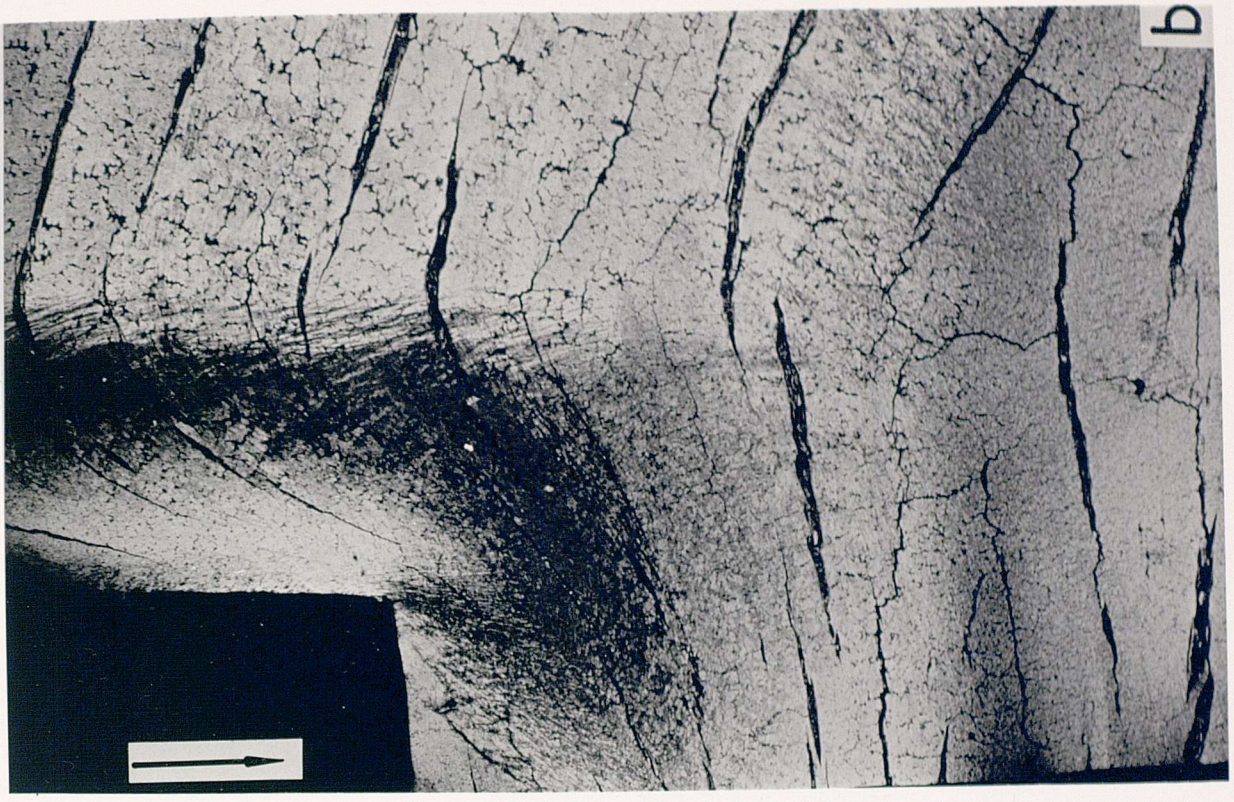


Figure 6·16 Longitudinal thin section prepared from the base of a driven pile (Test No 16)

(a) Photograph

(b) Photograph with plane of polarised light rotated through 45°

(c) Interpretive diagram



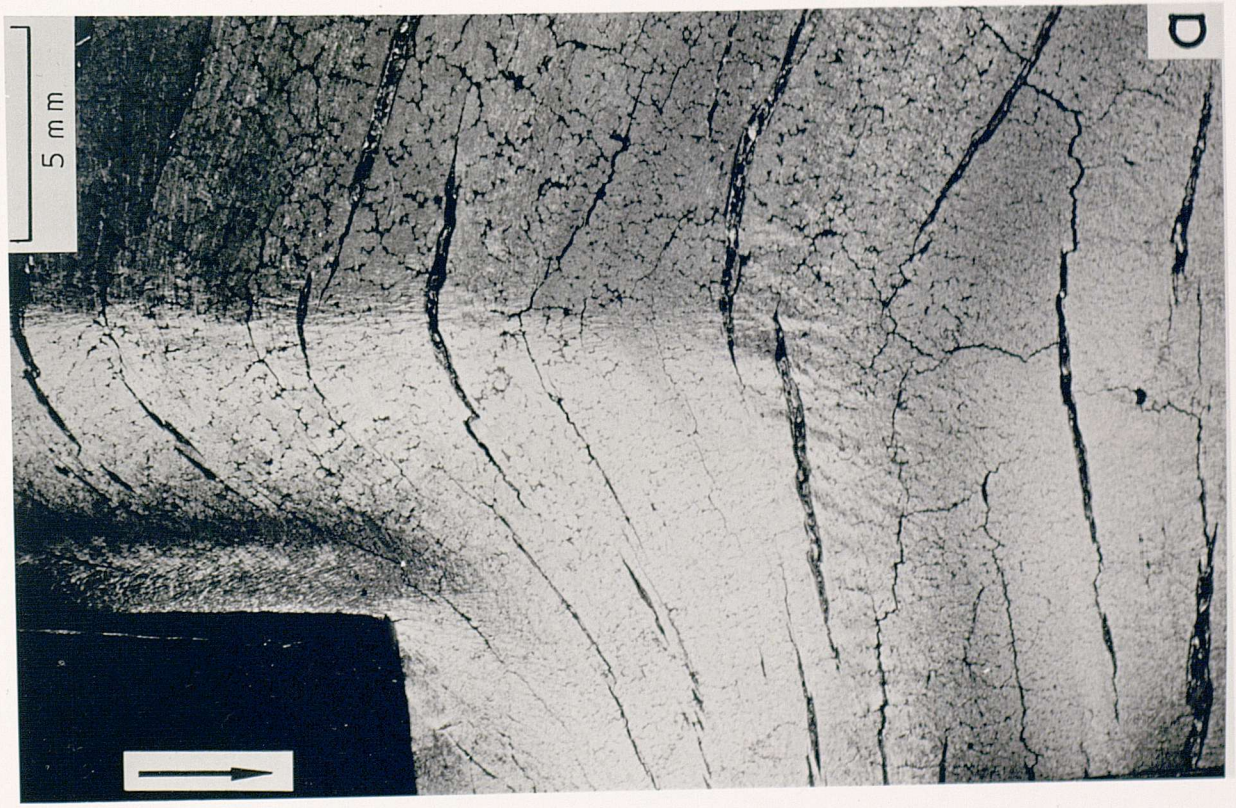


Fig. 6.16

Figure 6.17 (facing) Detailed view of the micro-fabric within Zone A, close to the tip of the driven pile in Test 16 (also see Figure 6.16)

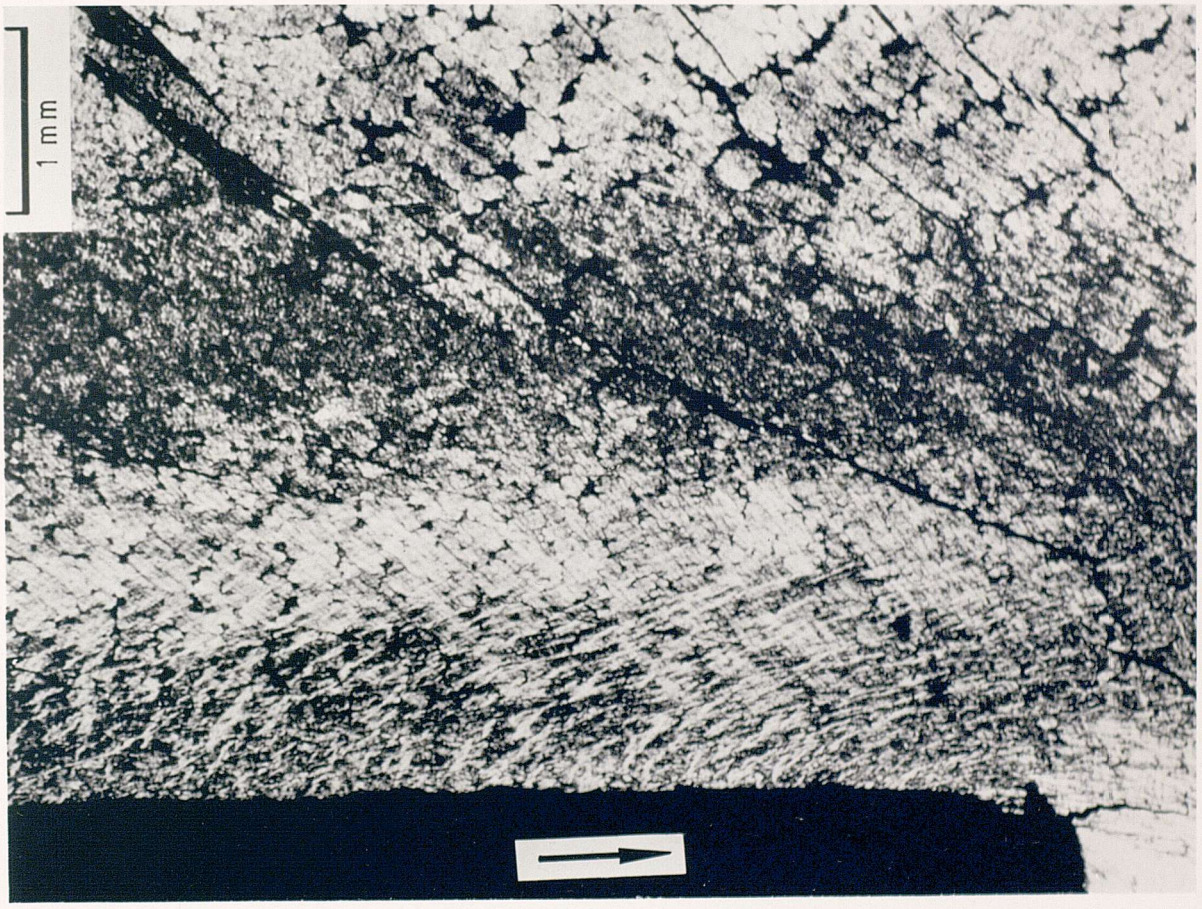
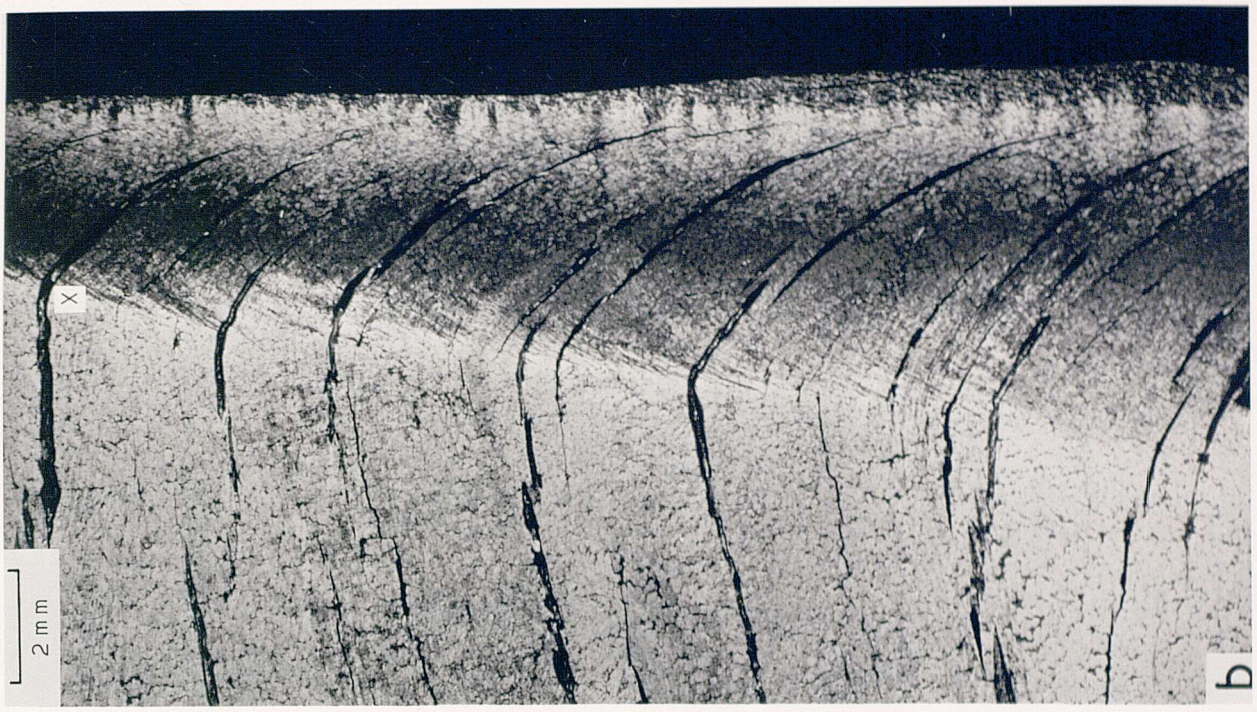


Fig. 6.17

Figure 6.18 (facing)

Longitudinal thin section from the top of the driven pile in Test 16

Note: Photographs (a) and (b) are at different magnifications, but the points marked [x] are common to both.



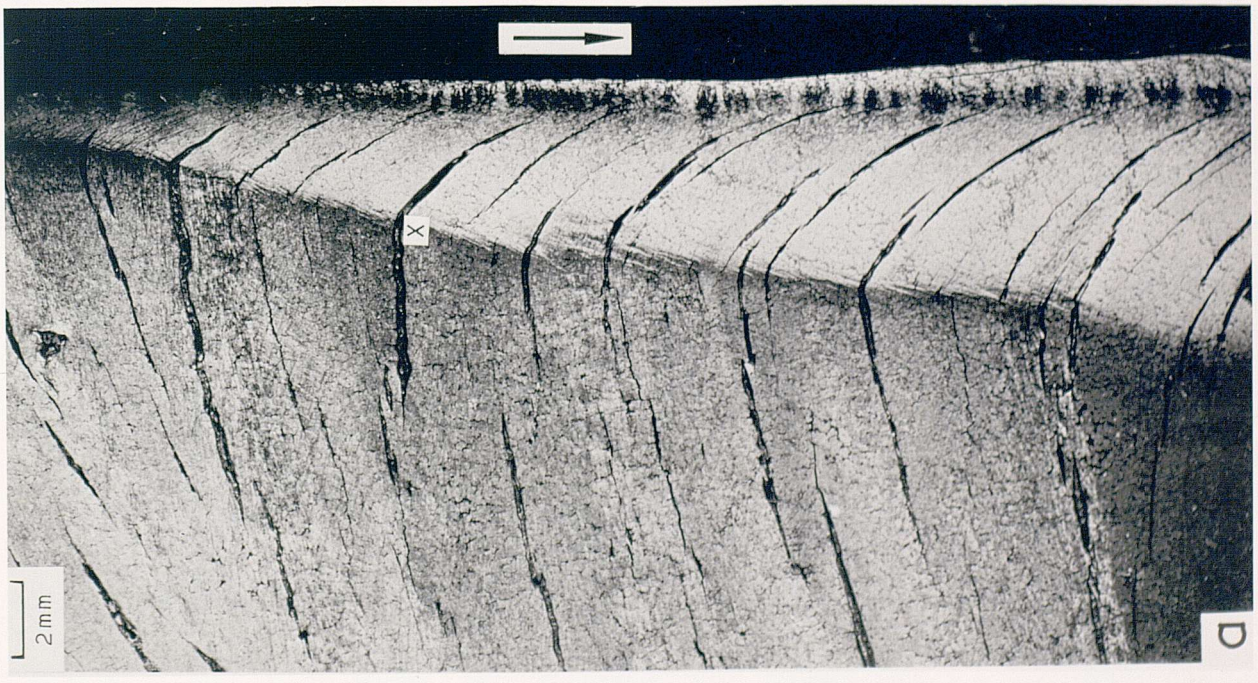
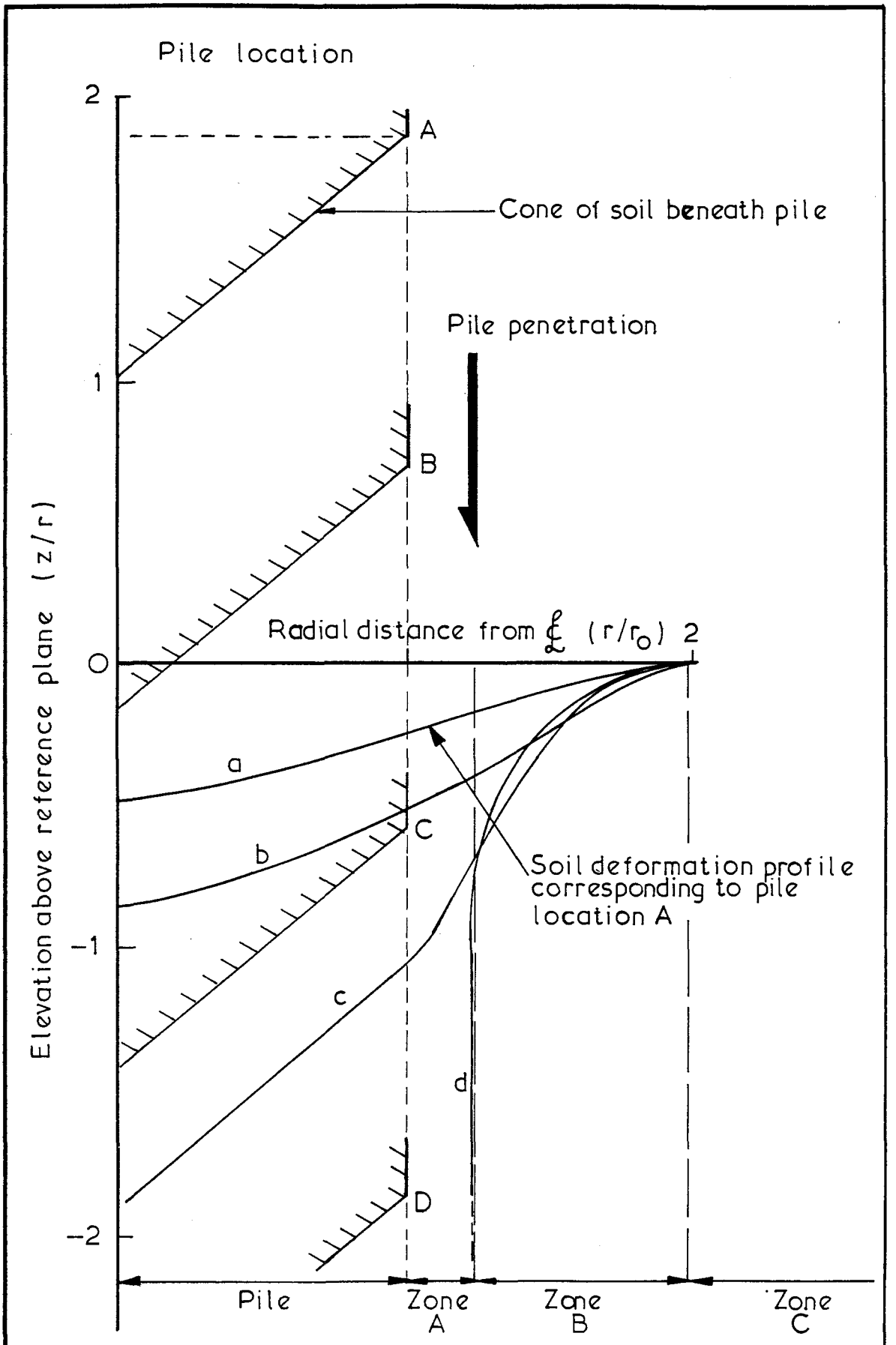


Fig. 6. 18



Deformation of an originally horizontal plane of particles with the approach of the pile tip.

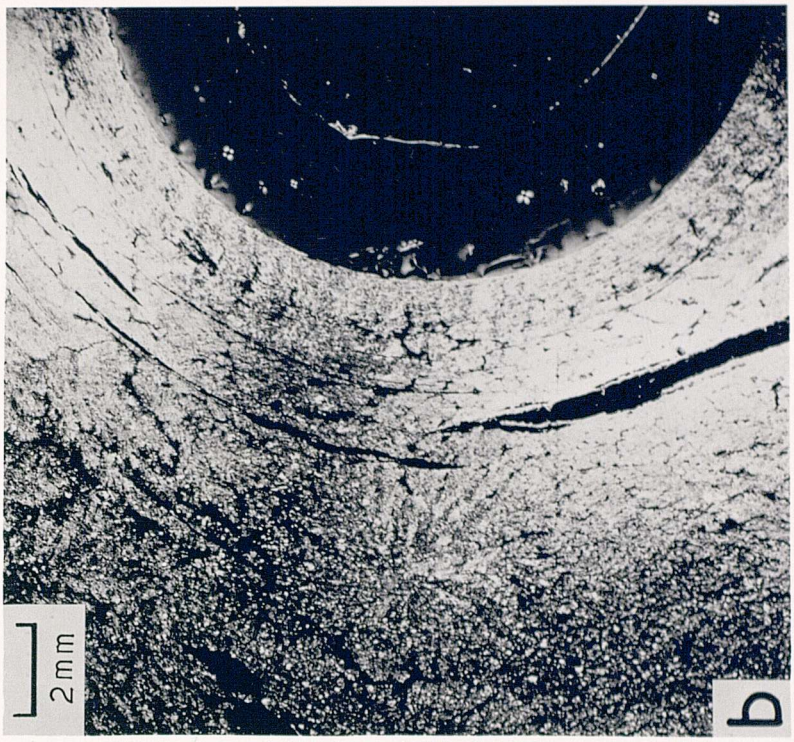
Fig. 6.19

Figure 6.20 (facing)

Thin sections prepared following Test 18

(a) Longitudinal section

(b) Cross section



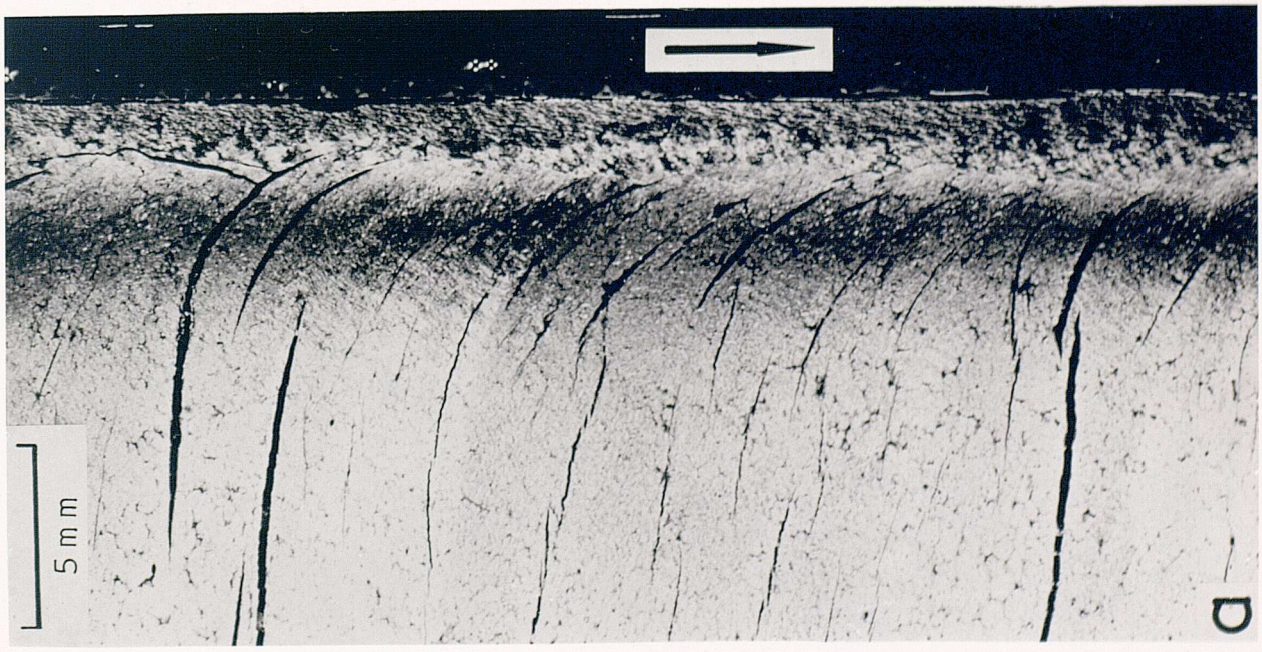


Fig. 6.20

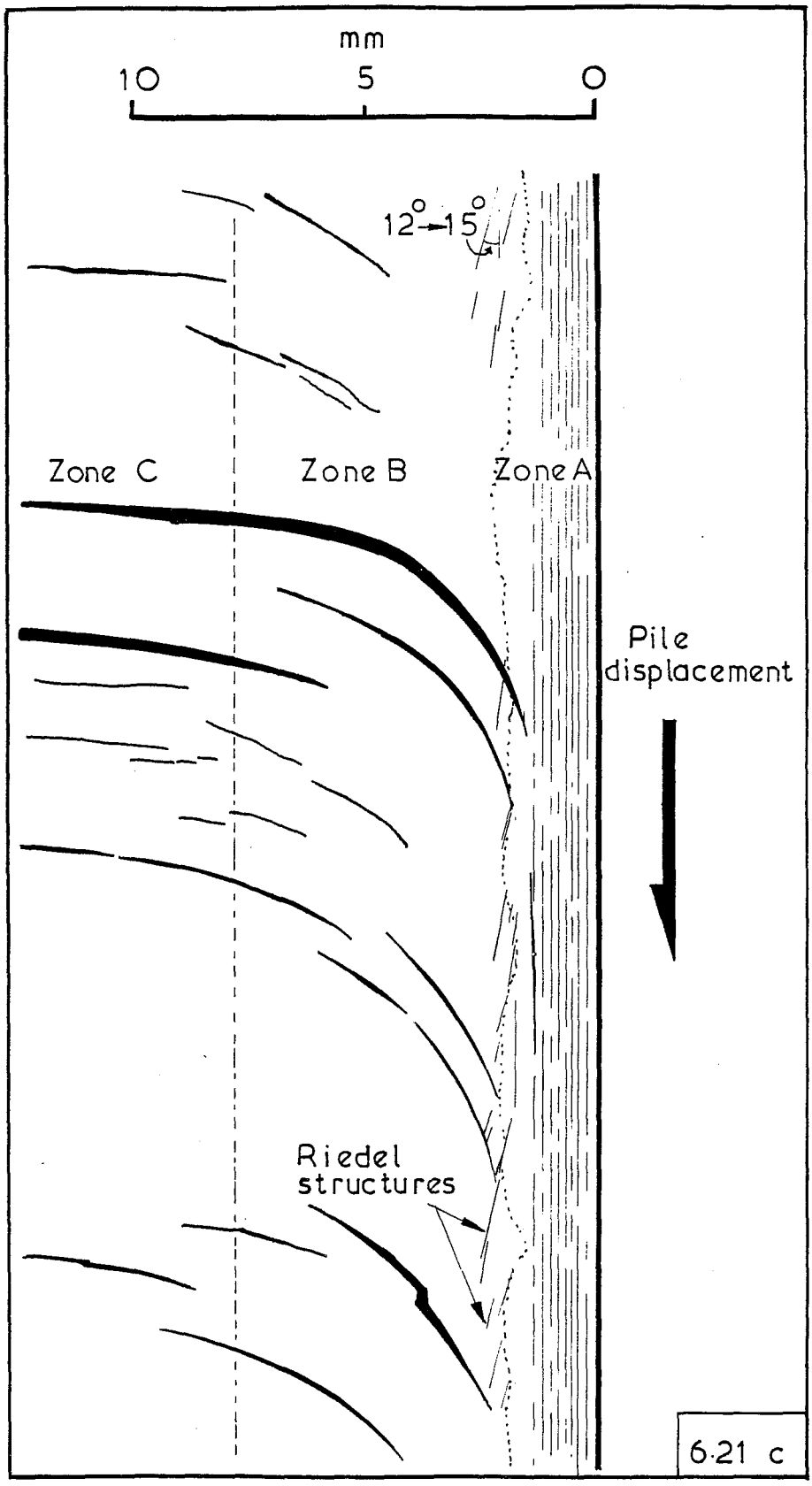
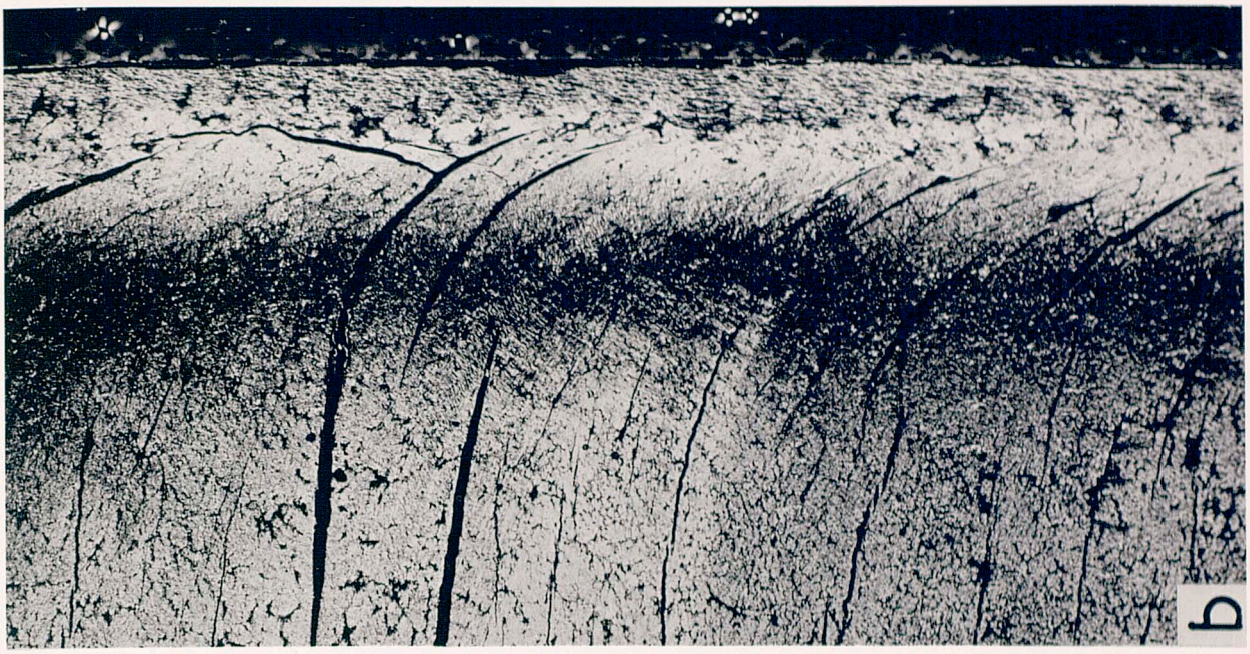


Figure 6.21 Longitudinal thin section from Test No. 18.
(a) Photograph
(b) —·—
(c) Interpretive diagram



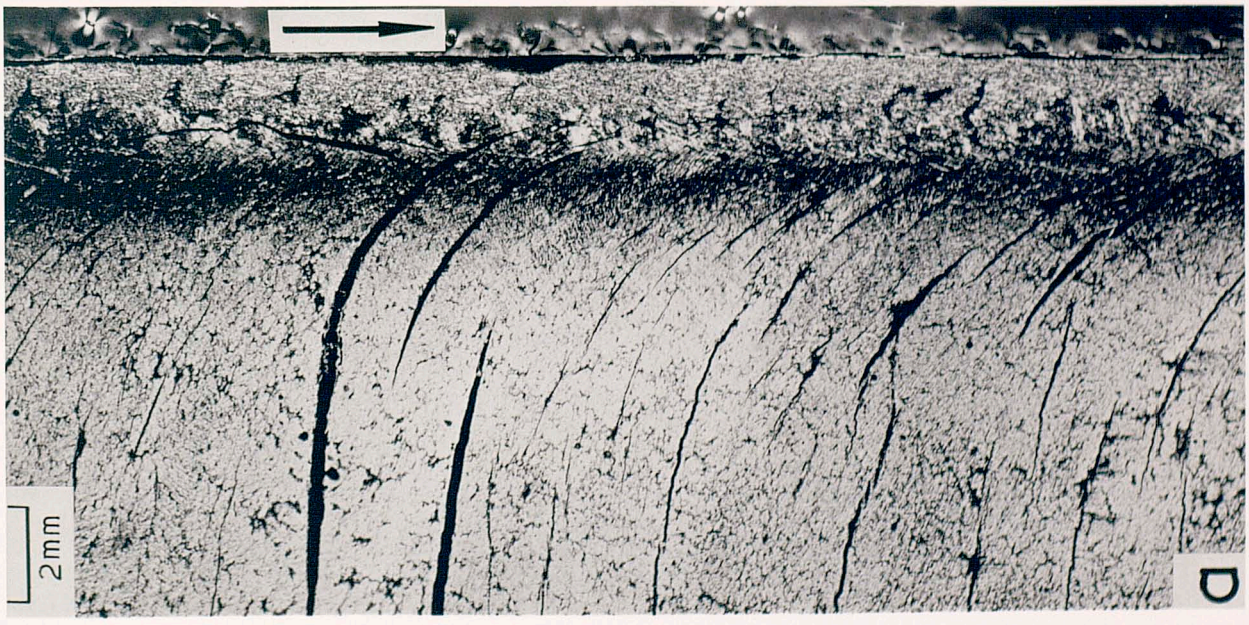
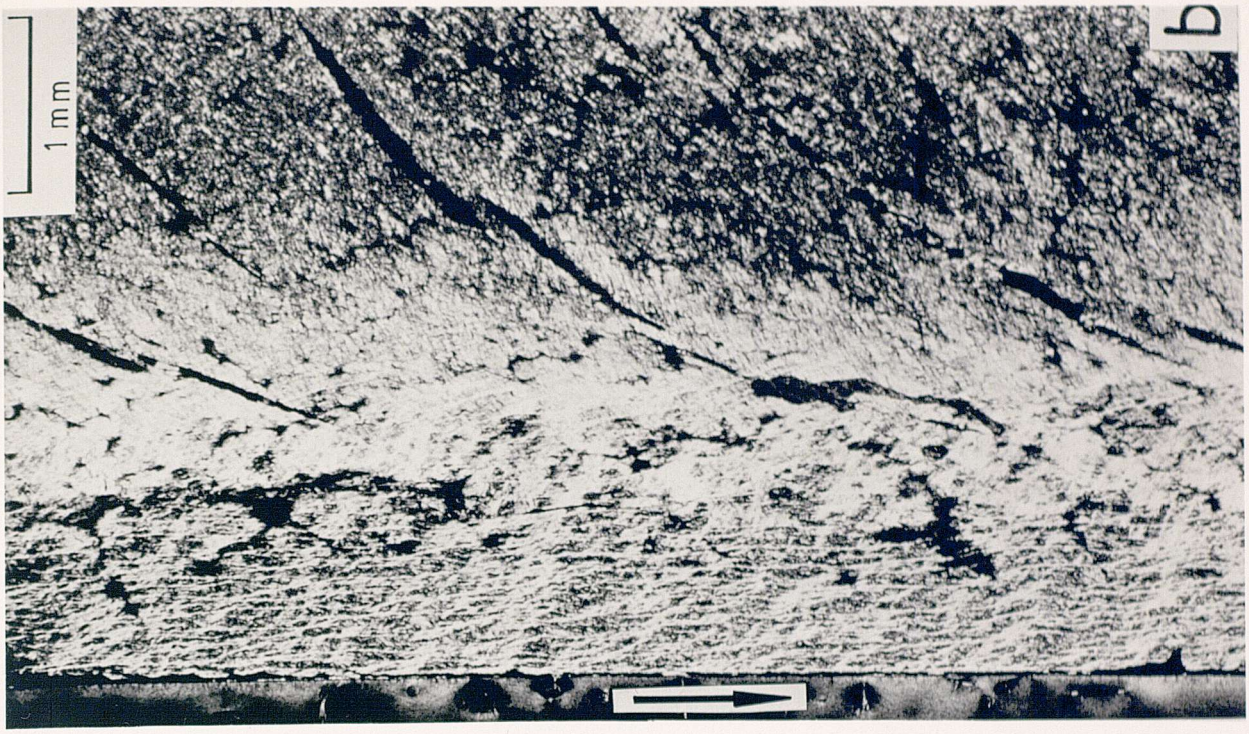


Fig. 6 · 21

Figures 6.22 (a) and (b) — facing

Detailed views of the micro-fabric within Zones A and B, adjacent to the driven pile from Test 18



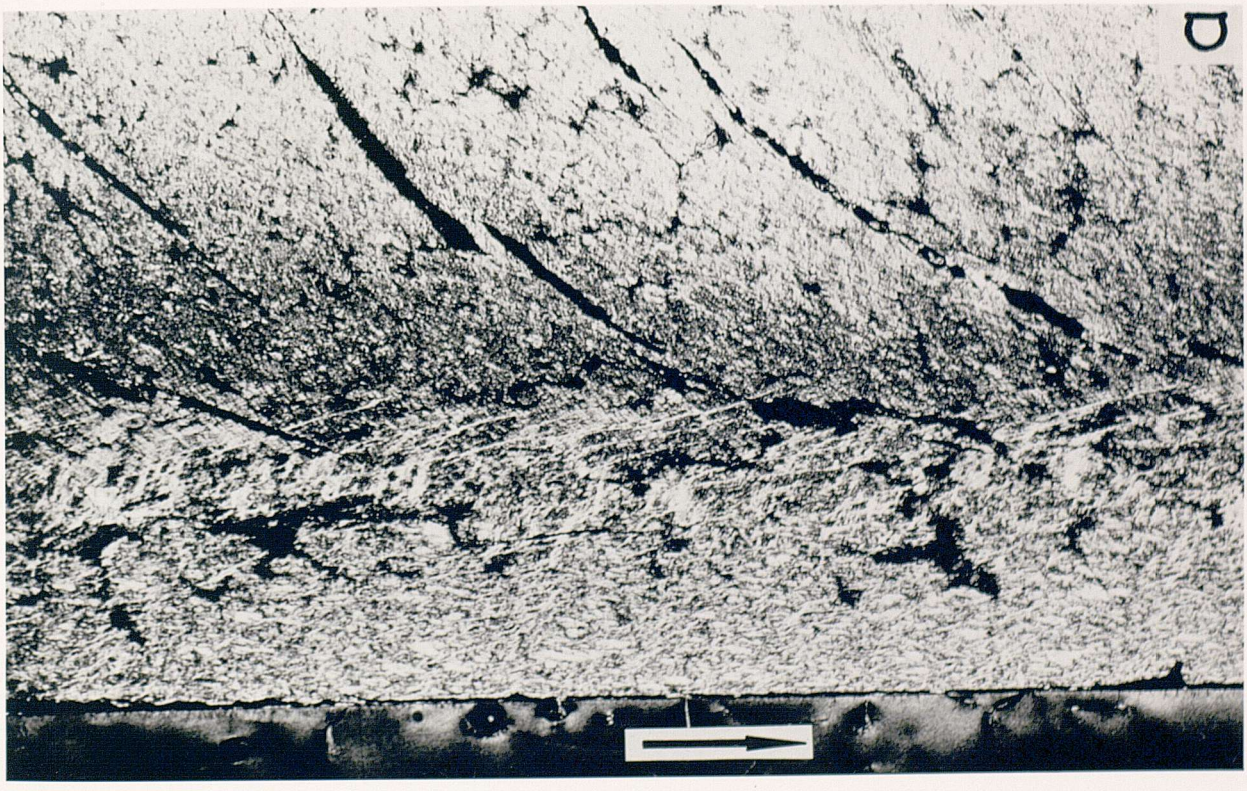
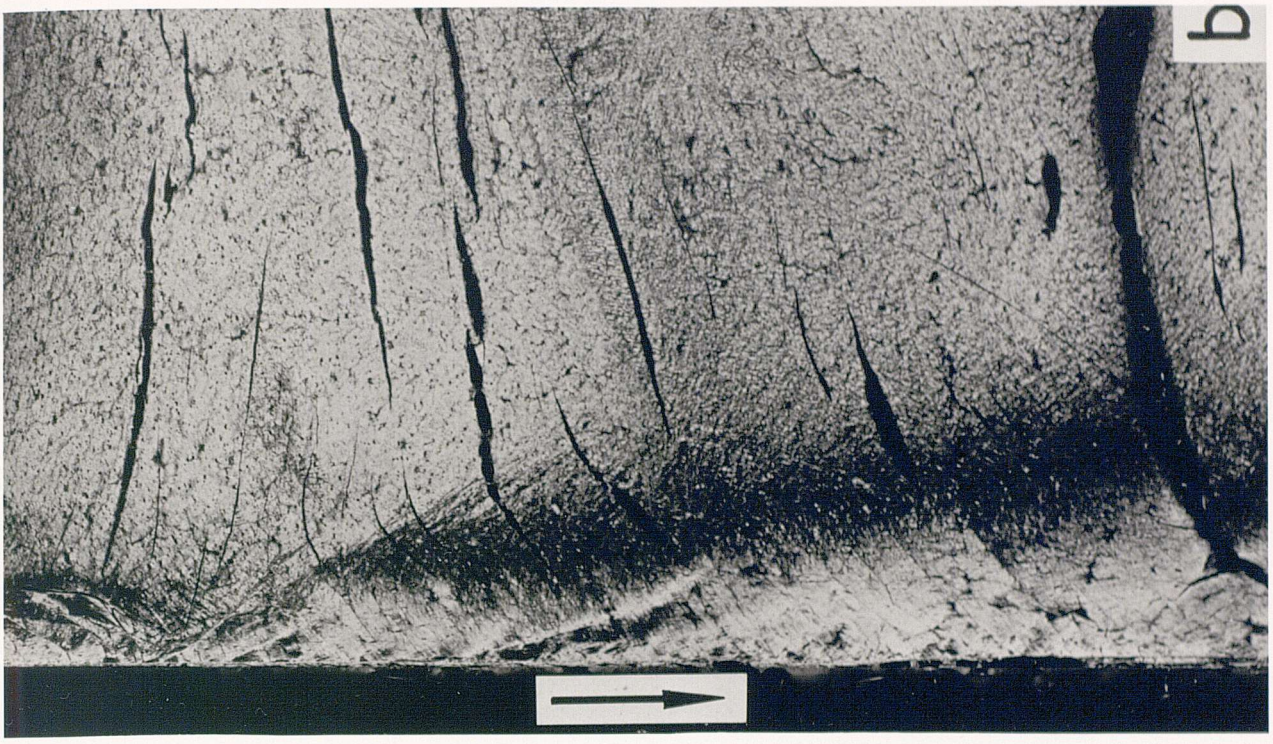


Fig. 6. 22

Figures 6.23 (a) and (b) — facing

Longitudinal thin sections through the top of the pile from Test 19 (photographs taken under different orientations of polarized light).



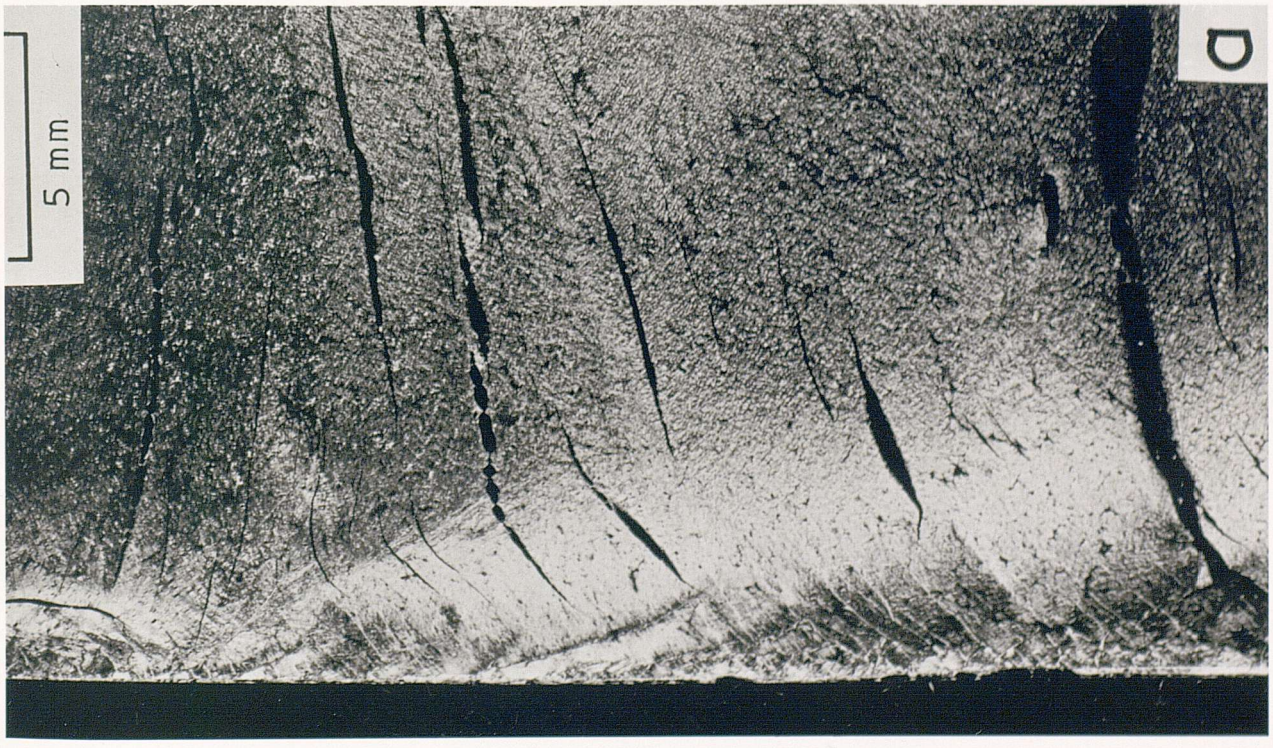


Fig. 6-23

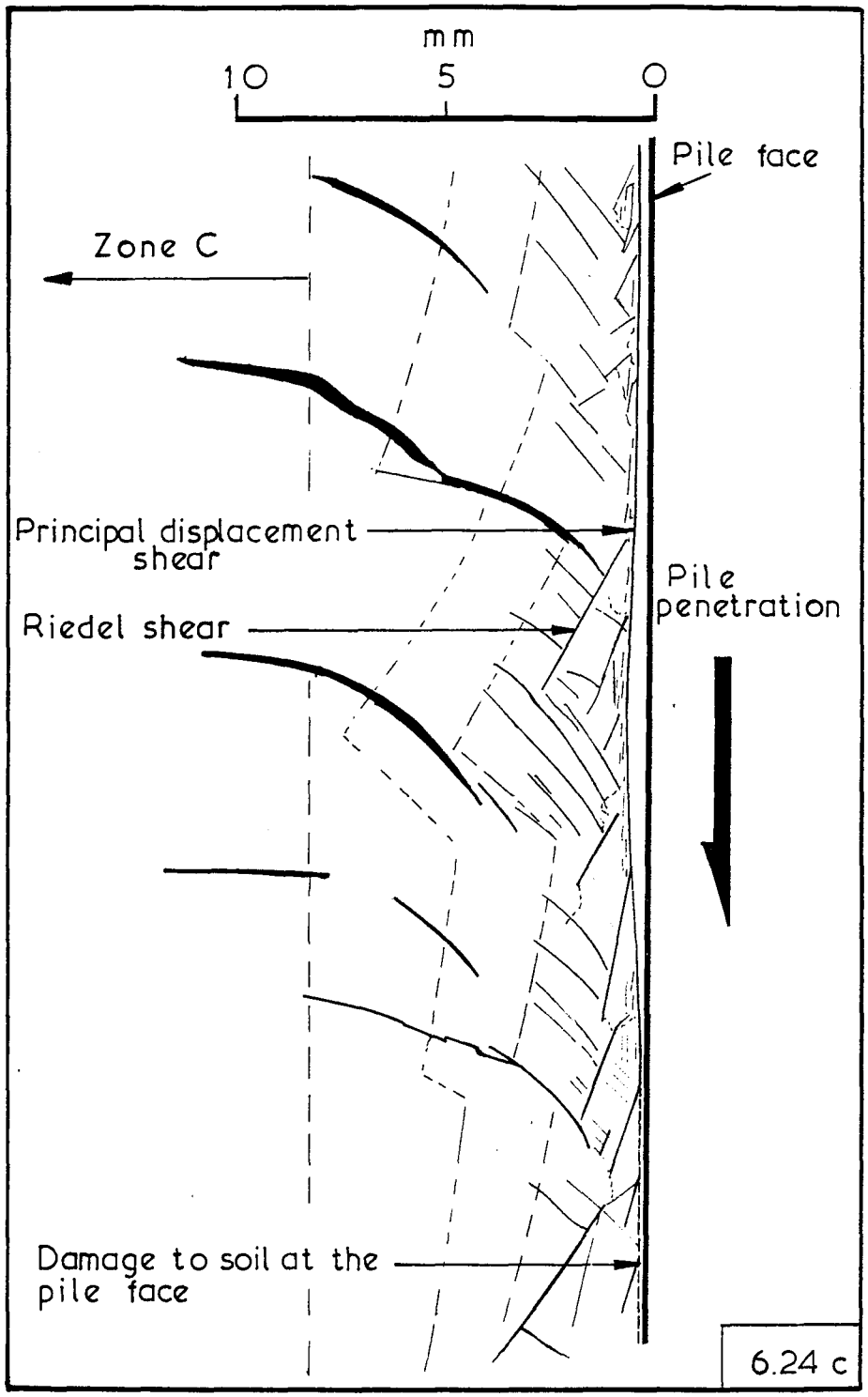


Figure 6.24 Longitudinal thin section through the middle of the jacked and loaded pile of Test 19

(a) Photograph
(b) —"—
(c) Interpretation



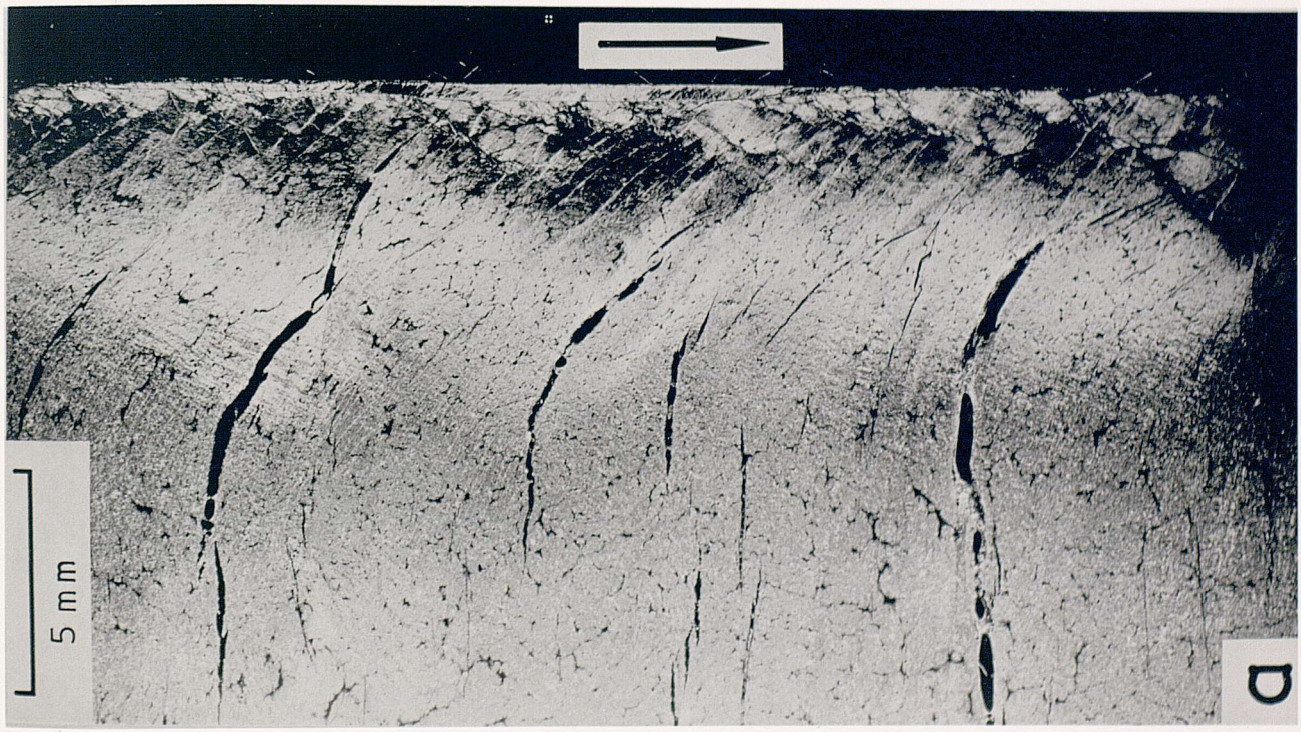
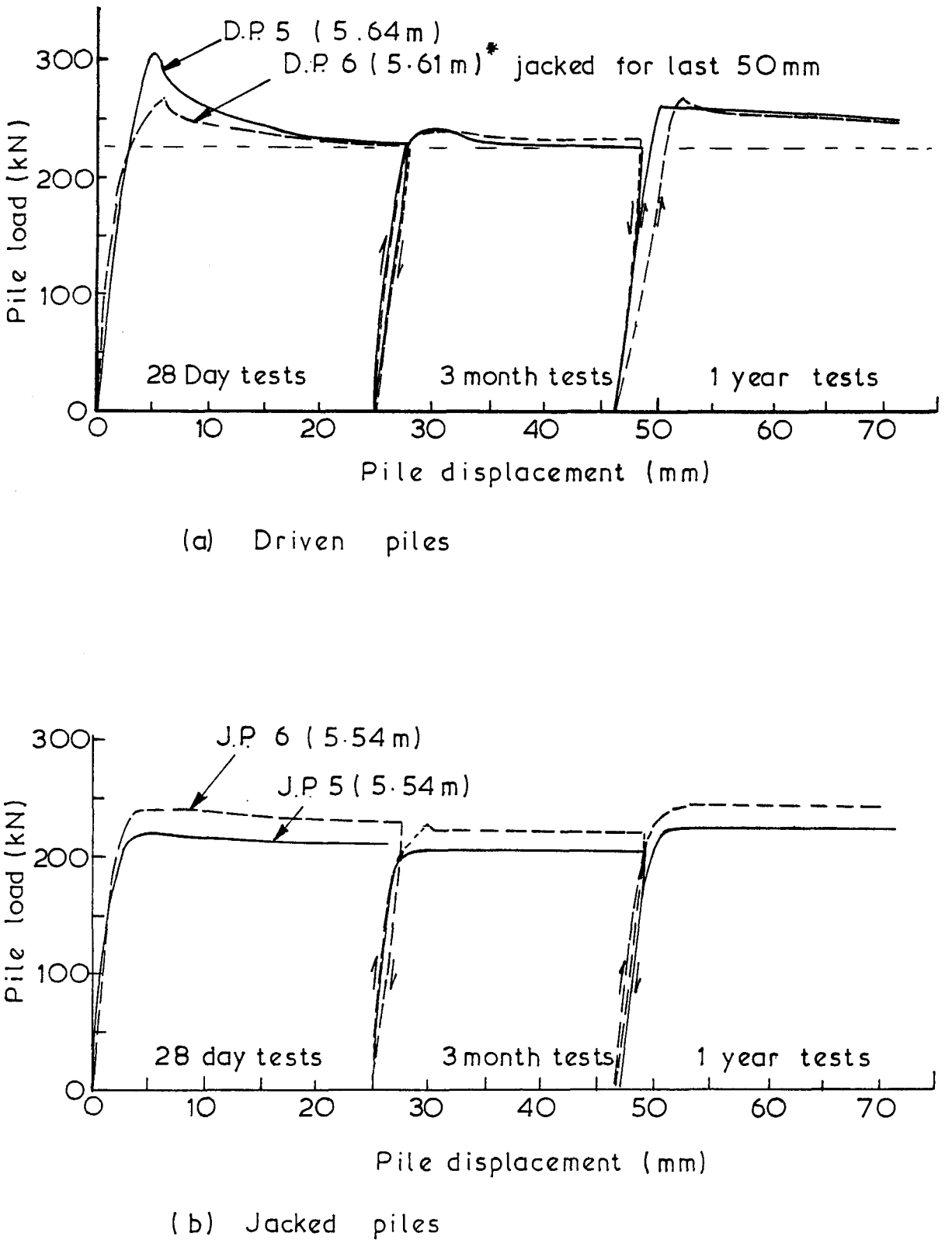


Fig.6. 24



Behaviour of driven and jacked piles in London Clay – from Tomlinson, 1970(b)

Fig. 6·25

APPENDIX 6.1

END EFFECTS IN THE MODEL PILE TESTS

A.6.1.1 Introduction

The stresses acting in the clay adjacent to one of the loaded model piles are likely to be locally perturbed at the pile entry and exit as a result of the geometry of the apparatus. In general, the influence of 'end effects' is difficult to establish and thin section observations provide a means whereby regions of atypical shearing behaviour may be identified. The technique is not suitable for quantifying the effects of local perturbations; these were estimated by means of Finite element modelling of the pile tests (described in Chapter 8).

In the following discussion, conditions around the pile employed in Test 14 (K = 1.11) are considered. Reference will be made to photographs of longitudinal thin sections taken from the top, middle and the base of the pile. A location plan for the photographs is shown in Fig. A.6.1.1.

A.6.1.2 Top of the Pile

During the installation of the model pile , the annular gap between the brass core and the Kaolin sample was grouted with epoxy resin to the top of the sample (or as nearly as possible). As the pile was loaded a gap was left between the top of the pile and the top platen.
Fig. A.6.1.2(a) is a photograph taken from the top of the pile used in Test 14, after the pile had been displaced by a total of 13 millimeters.

Comparison between the relic S_2 shear structures left in the clay at the top of the sample, and those nearer the centre indicates very little difference in behaviour although the structures at the top are somewhat more closely spaced than those lower down. Thus, at least until peak conditions, end effects at the top of the pile are likely to have had very little influence on the pile behaviour.

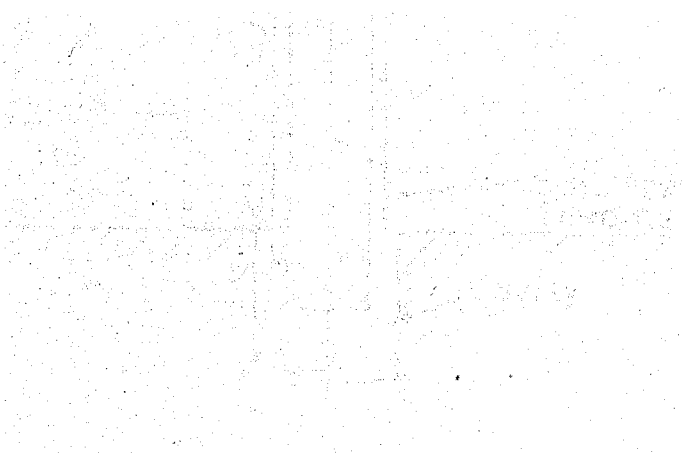
The thin sections provide little information about the post-peak behaviour because the clay deformations have become so localised. The clay left radially unsupported in the absence of the pile appears, from the thin sections, to have deformed inwards. However, as this was not

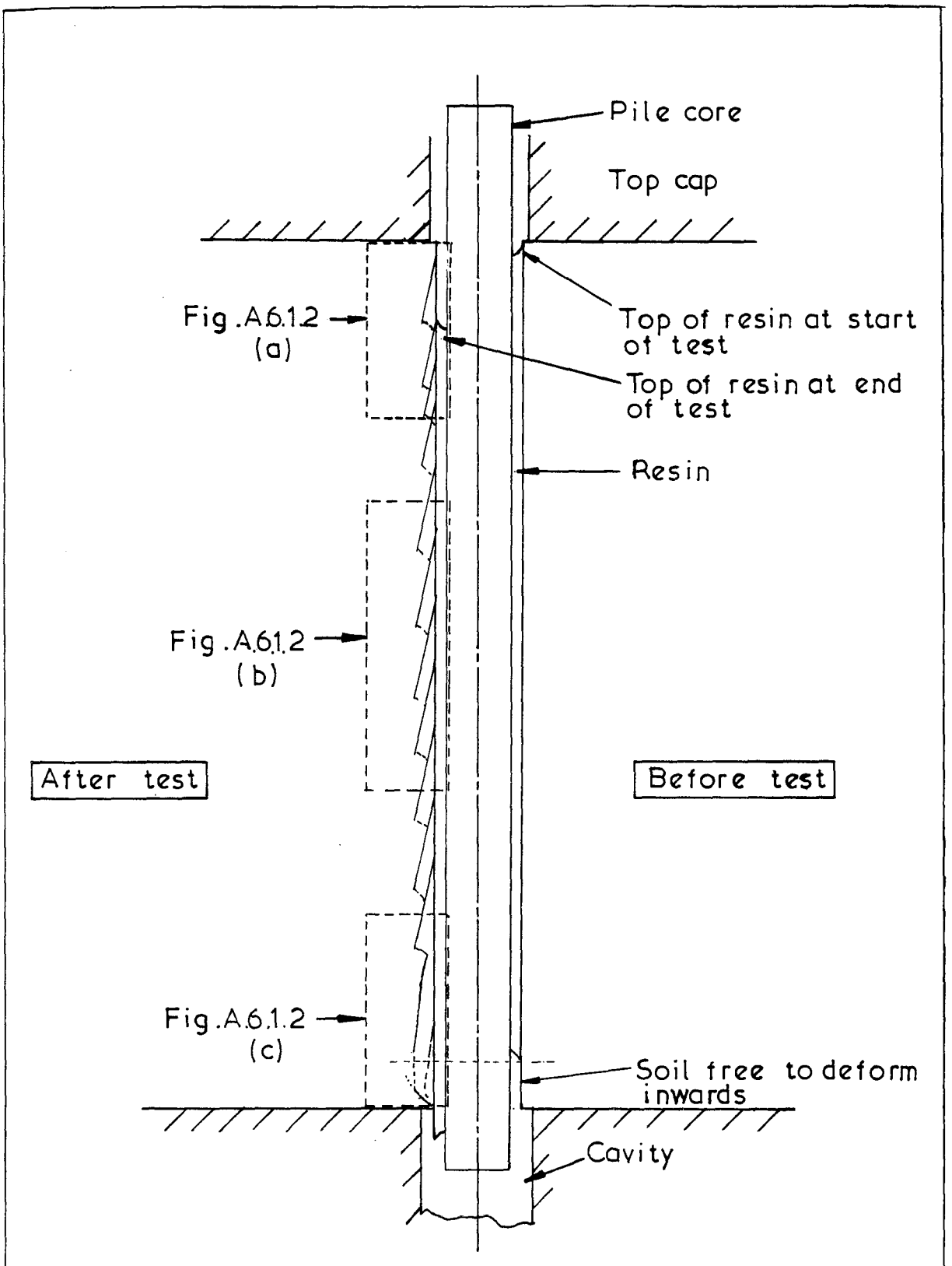
observed during the course of the pile test, it is thought that at least some of this movement occurred during the impregnation process.

A.6.1.3 Base of the Pile

A photograph of a longitudinal thin section taken from the bottom of the sample is presented in Fig. A.6.1.2(c) and the region represented is shown in relation to the rest of the pile, in Fig. A.6.1.1.

The photograph indicates that atypical shearing behaviour extended for a distance of about 25 millimeters from the bottom platen. However, most of the structures seen were formed at around peak pile load conditions, when the base of the shaft (seen in the photograph) was about 11 millimeters above the bottom platen. The atypical structures were induced by the local increase in axial stress resulting from the absence of shear restraint on the circumferential boundaries of the clay sample, and because the bore-hole beneath the pile was initially unsupported. Bearing in mind the position of the pile at peak load, it may be seen that the length of pile influenced by this atypical behaviour is of the order of 15 millimeters, or around 10% of the pile length. The finite element modelling suggests that the shear distribution along the pile is very uniform, except for a few millimeters at the top and bottom, and that these end-effects have little influence on the pile behaviour when normally-consolidated Kaolin is tested.





Location plan for photographs of thin sections taken from Test 14.

Fig. A.6.1.1

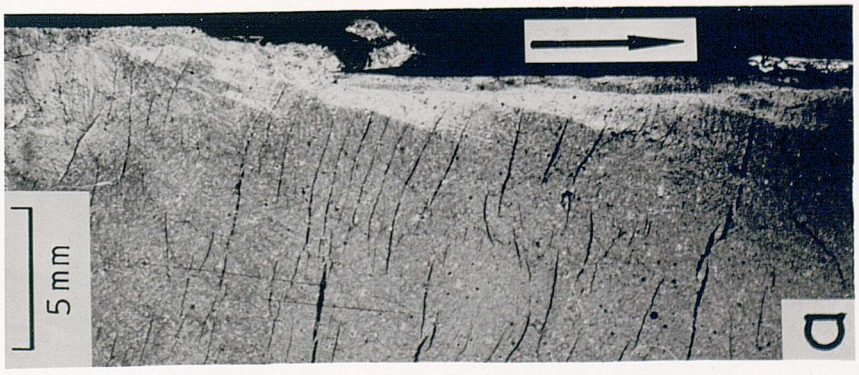
Figure A.6.1.2 – (facing)

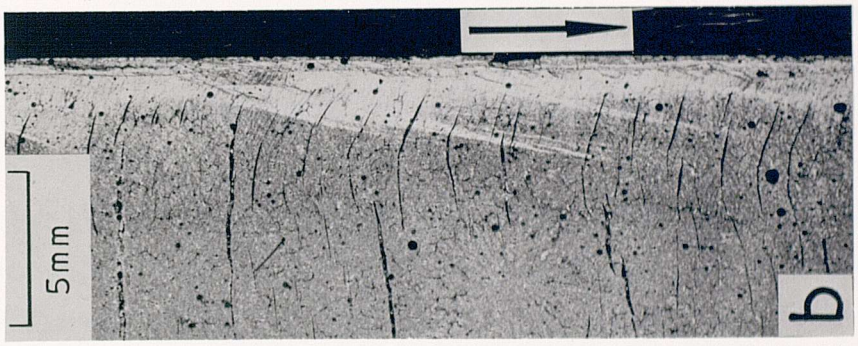
Longitudinal thin sections taken from different elevations along the model pile used in Test 14

(a) Top of pile

(b) Middle of pile (for reference)

(c) Base of pile





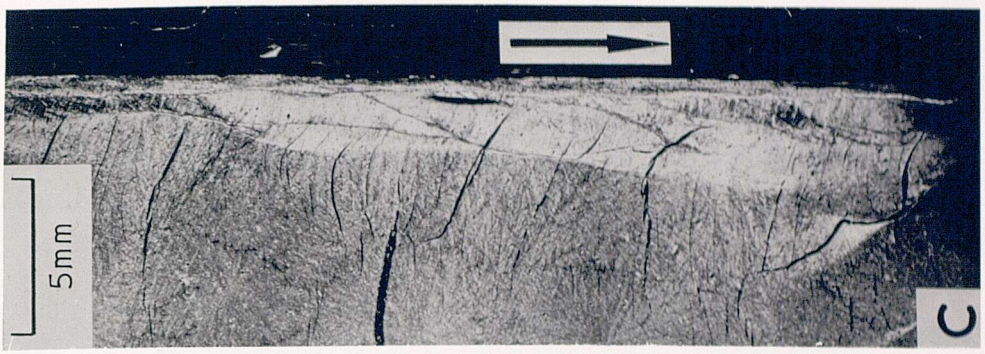


Fig. A.6.1.2

APPENDIX 6.2

MICRO-FABRIC CHANGES AROUND THE RADIAL-STRESS MEASURING DEVICES

A.6.2.1 Introduction

Devices for measuring the radial stresses acting against model piles installed with minimal disturbance were incorporated in three tests (Nos. 7,15 and 17). Following Tests 7 and 15, thin sections were prepared so that the micro-fabric changes in the clay beside the measuring devices could be compared with those occurring at other locations along the piles.

A.6.2.2 Test 7

The Kaolin in this test was over-consolidated with an OCR of 5. The radial stress device developed a leak during operation and it was not possible to obtain reliable measurements of the radial stresses. However the leak was very small and the test was continued, with the pressure in the device being kept at the cell pressure so as not to affect the overall pile behaviour much.

A photograph of a longitudinal thin section prepared from the clay surrounding the radial stress measuring device is shown in Fig. A.6.2.1(a), together with a schematic view in Fig. A.6.2.1(b). Photographs of a longitudinal thin section taken from higher up the pile are shown in Chapter 6, Figs. 6.15(a) and (b).

It may be seen that the principal displacement shear, S_4, is continuous along the radial stress measuring device, even where some clay was lost during preparation of the thin section. However, there is a deviation in the line of this structure at the top of the cavity, altnough this is thought to have occurred as a result of the impregnation process (close to the pile shaft shrinkage of the impregnated clay was prevented by the rigid resin and core, whereas the clay adjacent to the cavity was unsupported). The pattern of S_{2b} shear structures is similar to that seen beside the pile in Figs. 6.15, and so it is concluded that the behaviour of the clay adjacent to the radial stress-measuring device was similar to that occurring elsewhere along the pile.

A.6.2.3 Test 15

This test was performed on Kaolin normally-consolidated to a stress ratio close to unity. An improved design of radial stress-measuring device was employed, and it worked satisfactorily during the test.

Photographs of longitudinal thin sections taken through the radial stress-measuring device are presented in Figs. A.6.2.2,3 and 4. The top of the device is shown in 3a and the base in 4a; schematic views of the two longitudinal sections are shown in Figs. 3(b) and 4(b) respectively. For comparison, a photograph and a corresponding schematic view of a longitudinal thin section taken from the top of the same pile are presented in Figs. A.6.2.2(a) and (b). In all of the photographs, the direction of polarisation of the light was selected to highlight the micro-structural features close to the pile (i.e. S_4, S_{2a} structures), rather than the more diffused S_{2b} structures.

In the thin section of the bottom of measuring-device, some clay was lost during preparation of the thin section, and this was largely replaced with Carbowax, as may be seen in Figs. A.6.2.4(a) and (b). If the three thin sections are compared, it may be seen that the patterns of the structures beside the measuring-device are similar to those occurring elsewhere along the pile. Thus, it is believed that the shear-reinforcement around the measuring device performed satisfactorily during this test, and that the measured radial stresses represent a close approximation to those acting on the pile during the test.

Figure A.6.2. 1

1(a) (facing) Photograph of longitudinal section through the radial stress measuring device from Test 7

1(b) (overleaf) Interpretation of 1(a)

Figure A.6.2. 2

2(a) (facing) Photograph of longitudinal section through top of pile in Test 15

2(b) (overleaf) Interpretation of 2(a)

Figure A.6.2. 3

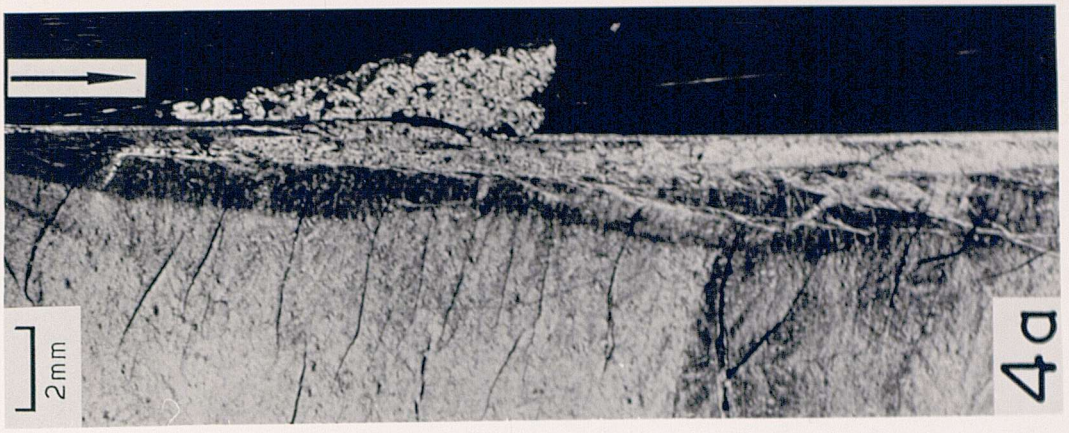
3(a) (facing) Photograph of longitudinal section through top of Radial stress measuring device from Test 15

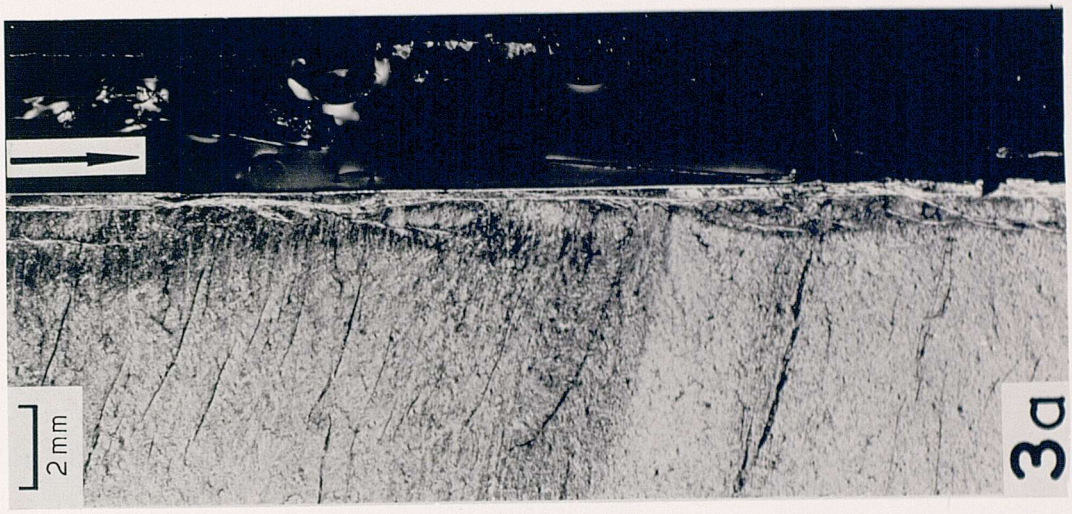
3(b) (overleaf) Interpretation of 3(a)

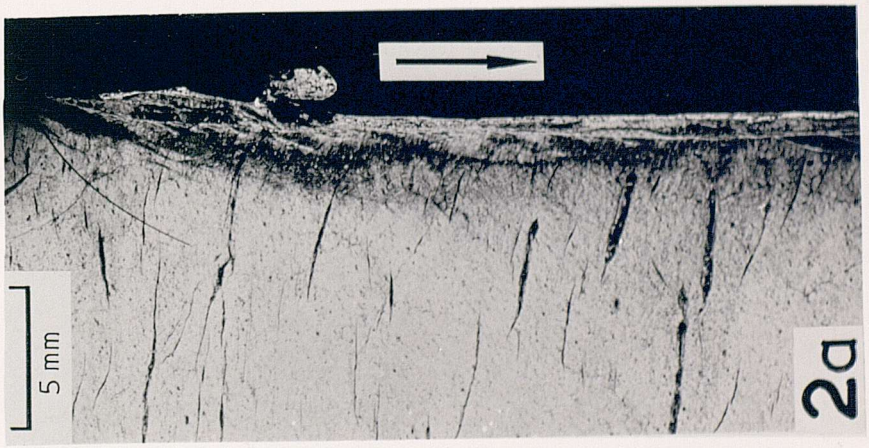
Figure A.6.2. 4

4(a) (facing) Photograph of longitudinal section through base of radial stress measuring device from Test 15

4(b) (overleaf) Interpretation of 4(a)







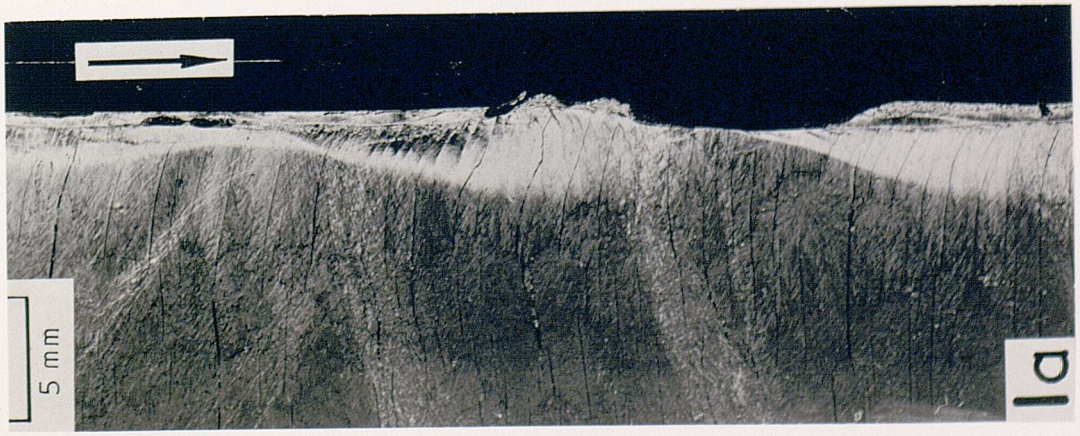
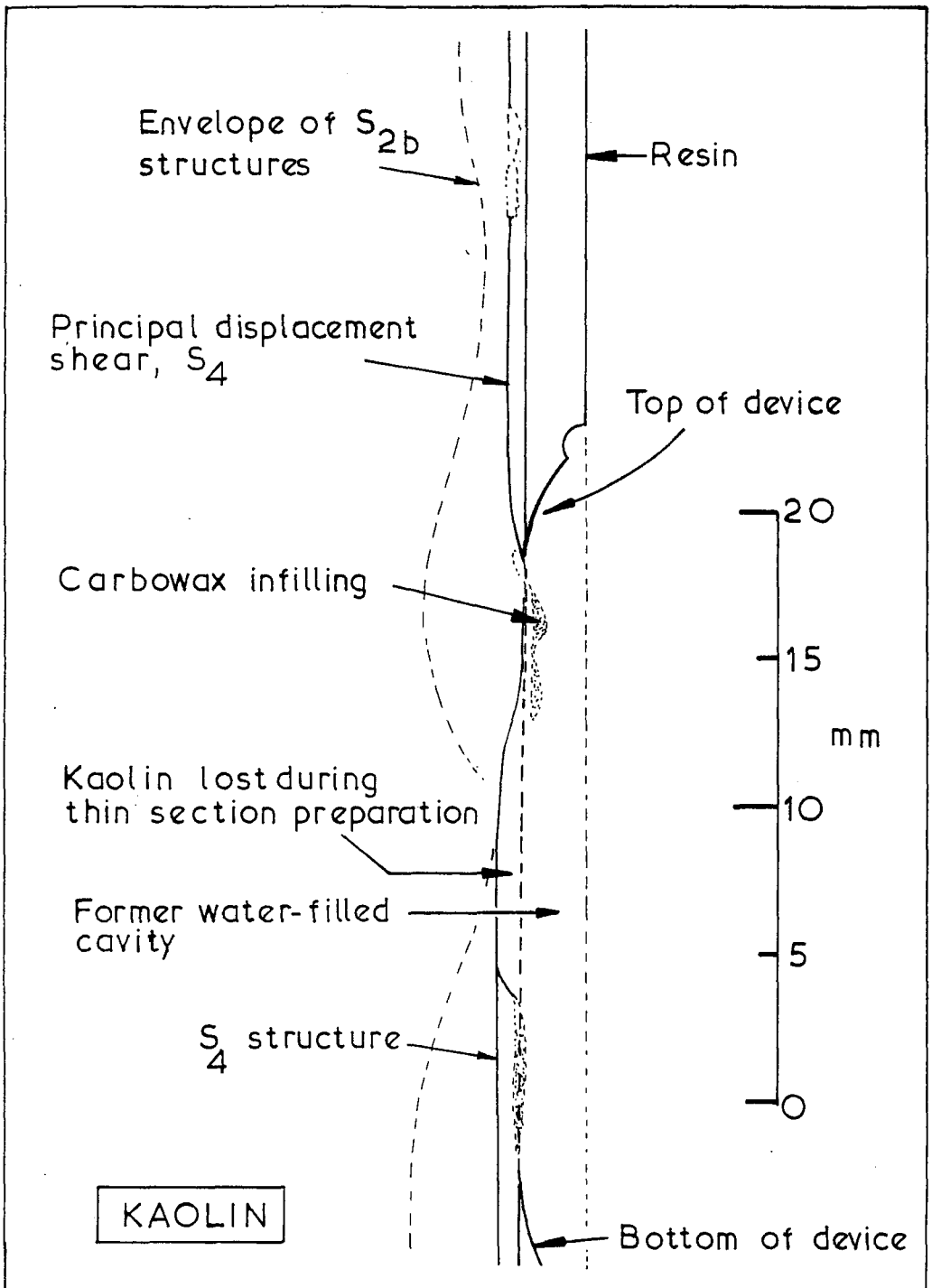
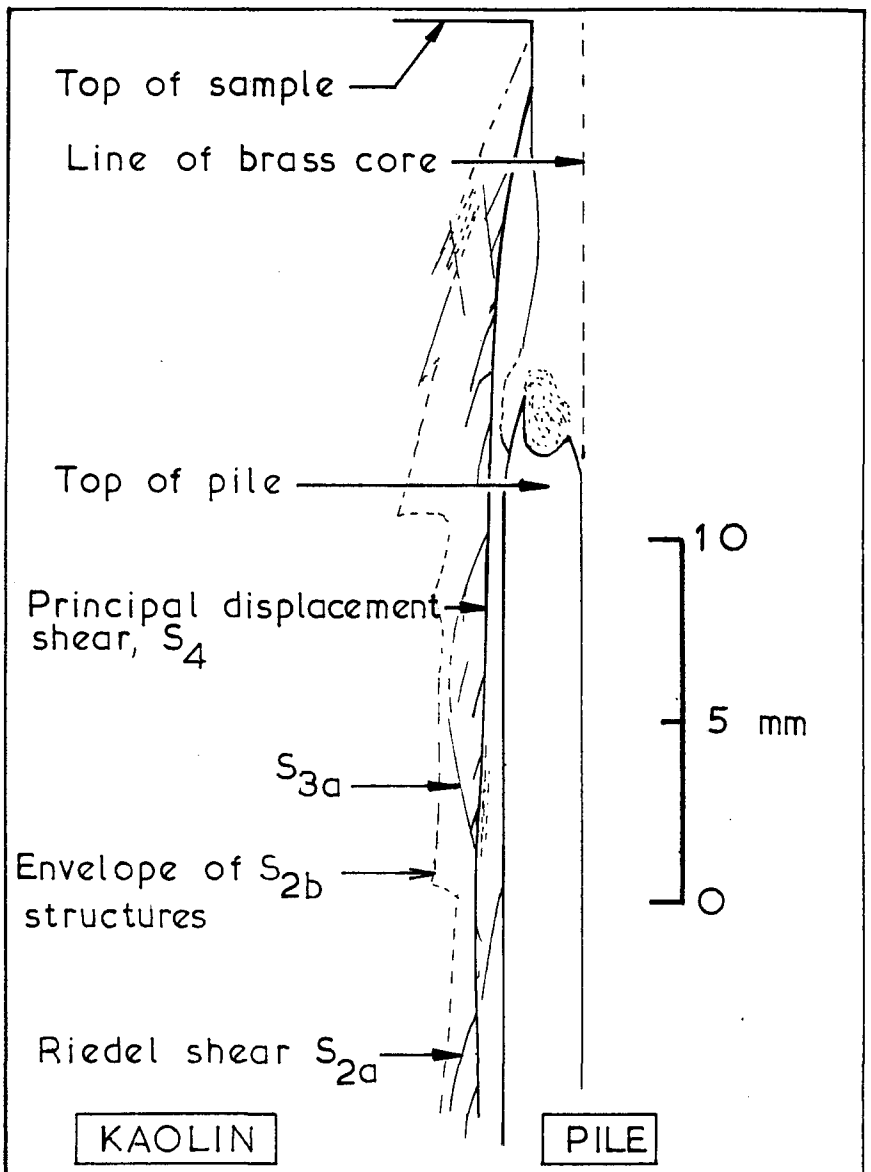


Fig: A.6.2.1



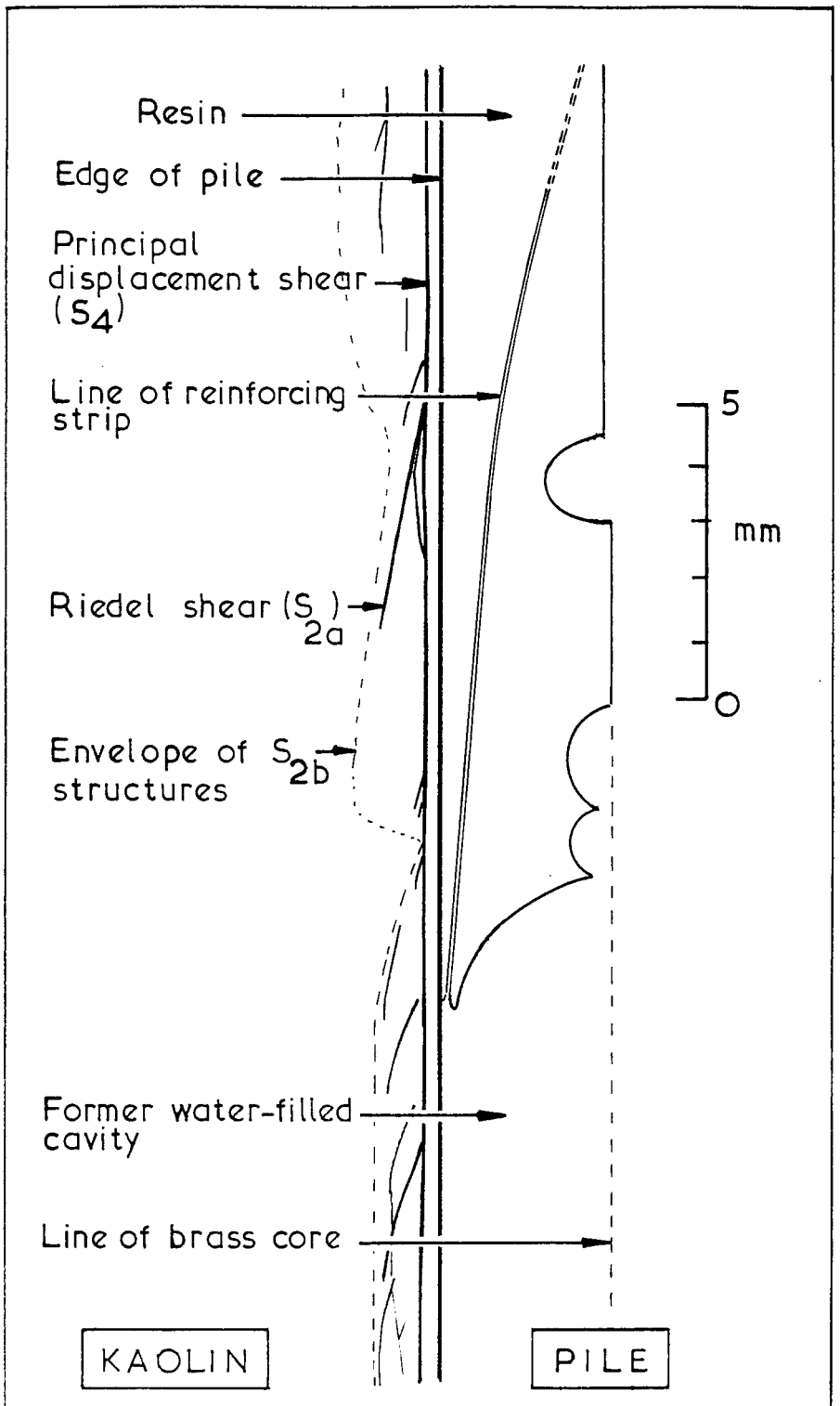
Micro-fabric in the kaolin surrounding the radial stress measuring device from Test 7

Fig. A.6.2.1 (b)



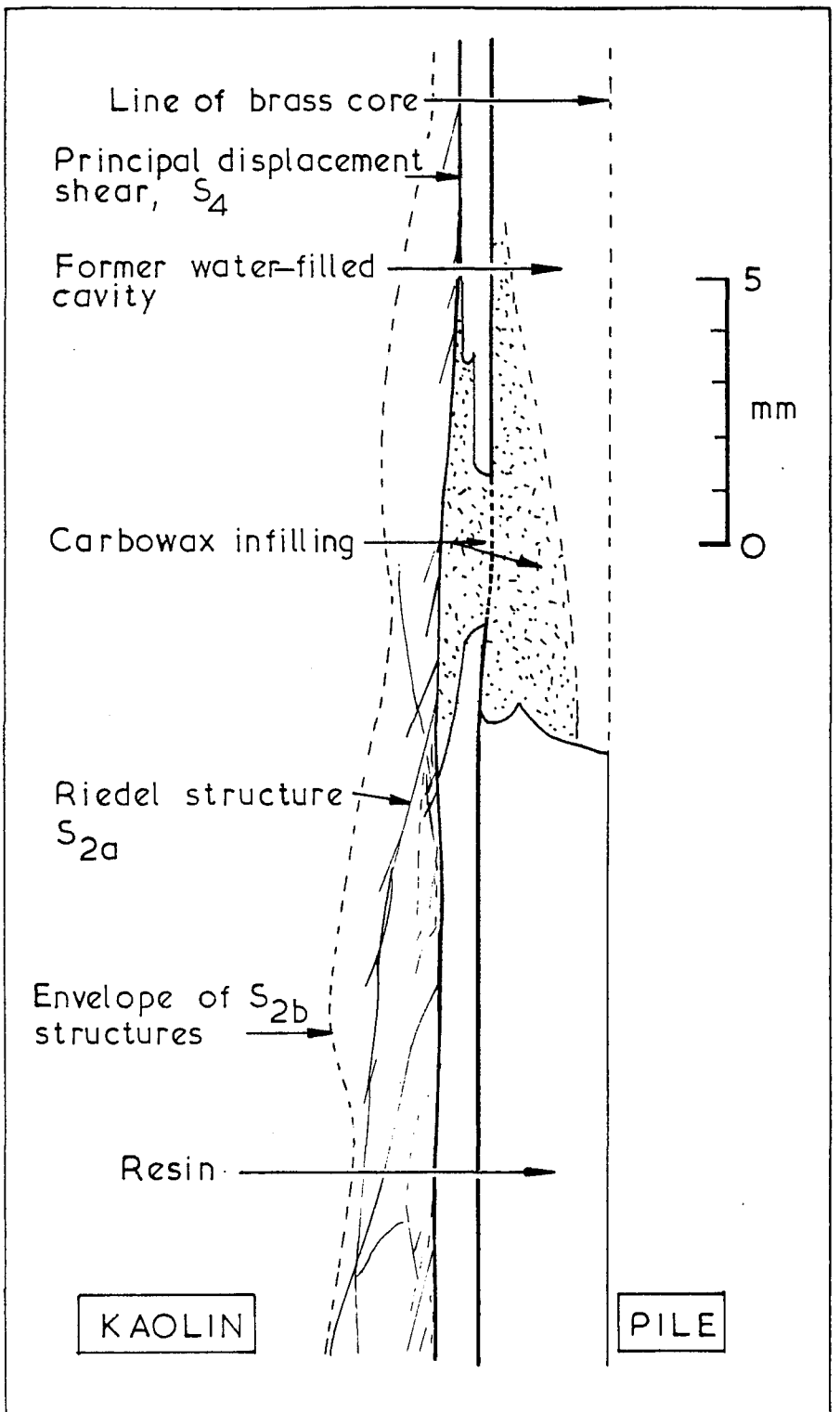
Schematic view of longitudinal thin – section through top of pile from Test 15

Fig. A.6.2.2 (b)



Schematic view of longitudinal thin-section through top of the radial stress-measuring device from Test 15

Fig.A.6.2.3 (b)



Schematic view of longitudinal thin-section through bottom of the radial stress – measuring device from Test 15

Fig.A.6.2.4(b)

CHAPTER 7

FINITE ELEMENT ANALYSES

7.1 INTRODUCTION

The series of model pile tests (described in Chapters 3,4,5 and 6) which was conducted on piles installed with minimal disturbance provides information about the load-displacement behaviour of the piles, the effect of initial stress conditions, and about the micro-fabric changes that are induced in the clay simply as a result of loading the piles. Although measurements or estimates of the shear and radial stresses acting on the loaded piles were obtained, no direct information could be obtained about principal stress rotations and changes in the other components of stress in the clay adjacent to the piles.

In the theoretical work presented below the pile-soil load transfer mechanism is examined, and the predictions obtained are compared with the experimental results. The analyses are later extended to consider the influence of more realistic pile installation procedures, and predictions are compared with available field data.

The behaviour of the soil close to a loaded pile is predominately displacement controlled and, provided that there is no relative slip between the pile and the soil, kinematic continuity requires that the total axial strain in the soil adjacent to the pile is the same as that of the pile itself (zero if the pile is axially rigid). The radial displacement of the soil at the interface is the same as that of the pile itself (zero if the pile is radially rigid) and, in the latter case, this implies that the total hoop strain is locally zero too. On drained shearing, most soils tend either to dilate or to contract and so, in order to satisfy the kinematic boundary constraints, complex stress changes may be required close to the pile. For this reason the results of analyses of this problem will be strongly influenced by the kinematic aspects of the chosen soil constitutive law.

Analyses of the stress conditions in the soil adjacent to a loaded pile, assuming the soil to be isotropic elastic, lead to the predictions that both the local radial and axial stresses remain approximately constant during pile loading. If the soil were to remain elastic until some form of strength

criterion such as Mohr-Coulomb were satisfied, then the situation depicted in Fig. 7.1 would obtain. The peak angle of shaft resistance, δ', which is indicated in this figure is dependent on the c'-ϕ' parameters of the soil, and the initial stress ratio, K, in the soil. The predicted variation of the ratio $\tan \delta'/\tan \phi'$ with K (for the parameters appropriate to the Kaolin employed in the experimental investigation) is shown in Fig. 7.2. Comparison with the experimental results, which are also indicated in the figure, demonstrates the inadequacies of the predictions. Similar conclusions arise whether the clay is assumed to be linear or non-linear isotropic elastic; see Lopez 1980. This result occurs because the volumetric and the shear strains are not coupled.

In order to provide a more realistic model of the soil behaviour, analyses have been performed assuming the soil to be a work-hardening elasto-plastic material, behaving in accordance with a form of the Modified Cam Clay constitutive law (see Roscoe and Burland, 1968). Work at Cambridge and elsewhere has shown that theoretical models of this type provide a useful description of the behaviour of many normally consolidated and lightly over-consolidated soils (and of Kaolin in particular!). It should be borne in mind, however, that the Modified Cam Clay constitutive law is based on data obtained from triaxial compression tests, and the extension of the model to consider complex stress paths in three-dimensional stress space is as yet largely unsupported by laboratory data. This implies that although very valuable information about trends in behaviour may be obtained with this relatively simple model, the results should not be applied directly to design without the confirmation of appropriate stress or strain path testing (see Wood, 1980).

The soil behaviour predicted by the Modified Cam Clay constitutive laws is in general highly non-linear and for this reason an incremental finite element formulation has been employed in the analyses of pile loading behaviour. In the remainder of this chapter the theoretical procedures, the soil constitutive models and the finite element meshes employed are described. In Chapter 8 the response of the soil beside model piles installed with minimal disturbance is analysed and the predictions are compared with experimental results presented in Chapters 5 and 6. In Chapter 9 the analyses are extended to consider the behaviour of displacement piles, and the predictions are compared with field observations.

7.2 FINITE ELEMENT PROGRAM

The computer program employed is a finite element package (I.C.F.E.P.) developed at Imperial College (largely by Dr. D.M. Potts, whose assistance is gratefully acknowledged), and it was executed on the Imperial College CDC Cyber 174 and 7200 machines. The program is capable of solving problems involving non-linear material properties, but as yet facilities for performing consolidation analyses and for considering large deformations are not available.

For the analyses described below, eight-noded iso-parametric elements of the 'Serendipity' family are employed, using reduced integration in preference to 'exact' integration because the former typically produces better conditioned results when considering undrained conditions. The program incorporates an automatic mesh generator, and the global stiffness matrices are assembled by the direct-stiffness approach. A re-numbering routine is used to reduce the storage requirements.

Both load (point or distributed) and displacement boundary conditions may be specified in order to solve boundary value problems. A particularly useful feature of the program is the facility to 'tie together' two or more nodes, anywhere in the mesh, such that selected components of displacement are identical. The tying is achieved by giving the same degree of freedom number to all of the tied components of displacement, the magnitudes of which are evaluated in the course of the analysis. An application of this feature is discussed later.

Because of the highly non-linear nature of the predicted soil behaviour, the pile displacements are applied incrementally. The solution routine employs an accelerated form of the initial stress approach, and typically fifty increments of pile displacement are employed, with an average of six iterations per increment. After every fifth increment data ~~is~~ are stored on file to enable the analysis to be restarted from that stage if necessary.

7.3 MESH GEOMETRIES EMPLOYED

7.3.1 Introduction

The aims of both the experimental work described in Chapters 3 to 6, and the finite element analysis are to examine the behaviour of soil close to a short element of a very long rigid pile, well away from the influences of both the tip and the ground surface. A simplified mesh geometry (employing tied degrees of freedom) is employed to model the idealised behaviour, and a

much larger mesh is used to examine the stress conditions within the experimental apparatus, thus enabling an estimate of how well the experimental conditions approximate to the ideal to be obtained.

7.3.2 Mesh to Analyse the Ideal Behaviour

The mesh, illustrated in Fig. 7.3, was employed to model the behaviour of the soil around a short segment of a very long pile. The dimensions of the mesh were selected for ease of comparison with the experimental conditions but no loss of generality is implied as the predicted results are independent of assumed scale.

The mesh consists of a horizontal disc of soil having a thickness of 5 mm, and an external radius of 345 mm. The modelled pile of 7.5 mm radius is coaxial with the disc. As indicated in Fig. 7.3, the disc has been divided into twenty, eight-noded, iso-parametric elements. Immmediately adjacent to the pile shaft, the elements have a width of only 0.25 mm (or 3% of the pile radius). To model the loading of the pile, axial displacements were imposed over the boundary AF. On the outer circumference of the disc, region CD, zero displacement boundary conditions were imposed. Parametric studies (Appendix 7.1) were performed varying the numbers of elements, the element sizes and the radial distance to the boundary CD in order to verify that the mesh shown in Fig.7.3 accurately models the problem under consideration. Along the boundaries AC and FD the displacements were tied, such that at any radius, r, the displacements both vertically and radially at corresponding nodes on AC and FD were forced to be identical. As a result, a vertical line such as EB in Fig. 7.3 remained vertical during loading. The magnitudes of both the vertical and radial displacements of this line are clearly unknown at the outset of the calculation and are determined by the analysis. This tying of displacements was achieved in the finite element analysis by giving the same degree of freedom number to nodes at the same radius along AC and FD. This also resulted in a smaller stiffness matrix and essentially reduced the problem to a one-dimensional situation in which all variables were a function of radius only. Initial stresses specified at the start of the analysis were chosen to represent the stresses believed to exist around the model piles immediately prior to loading.

Pile displacements were applied incrementally and the finite element equations solved using an accelerated form of the initial stress approach employing reduced integration. A parametric study was performed to ensure that the increment sizes were sufficiently small to provide accurate

predictions (see Appendix 7.2).

7.3.3 Mesh to Analyse the Experimental Conditions

In order to investigate how well conditions within the Kaolin samples during model pile tests approximated to the idealised situation under consideration, finite element analyses of the tests were performed. The mesh shown in Fig. 7.4 was used to represent the experimental conditions, and consists of 196, eight-noded iso-parametric elements. Immediately adjacent to the pile shaft, the elements have a width of only 1 mm, and so the closest Gauss-point is less than 0.25 mm away. The top and bottom platens of the test apparatus were modelled as being rough and rigid by imposing zero vertical and radial displacements along the boundaries AB and CD. Pile loading was simulated by imposing increments of axial displacement along the boundary region EF, and the radial rigidity of the pile was modelled by preventing radial movement of the boundary. Over the remaining boundaries of the sample the stresses were set to the values applying immediately after pile installation, and the same stresses were input as initial stresses in the soil.

7.4 SOIL CONSTITUTIVE MODELS

7.4.1 Introduction

The soil is modelled as an elasto-plastic continuum, and has been assumed to behave in accordance with various forms of the 'Modified Cam Clay' constitutive law (Roscoe and Burland, 1968). The analyses presented are largely restricted to piles installed in normally-consolidated or lightly over-consolidated clays, and so details of the shapes of the plastic potentials and the yield surfaces on the 'dry' side of the critical state are not relevant. On the 'wet' side both associated and non-associated plasticity has been considered, and the influences on the predicted pile behaviour of the shapes of the plastic potential and the yield surface in the deviatoric plane are examined below.

When considering the loading behaviour of displacement piles, it is assumed that the presence of pre-existing shear surfaces parallel to the pile (see Chapter 6) does not influence the behaviour of the surrounding soil, and that slip on the discontinuity is initiated only when a critical angle of friction is mobilised.

7.4.2 Constitutive Model in 'Triaxial' Stress Space

7.4.2.1 Introduction

The Modified Cam Clay constitutive law (Roscoe and Burland, 1968) was developed with the aid of experimental data obtained from static 'triaxial' compression tests performed on Spestone Kaolin. Before possible extensions of the model to consider more generalised stress conditions are presented, some important features of the original model are briefly reviewed.

7.4.2.2 Consolidation Behaviour

It was assumed that the clay, when subject to isotropic consolidation, follows a trajectory in $v - \ell n\ P'$ space given by the virgin consolidation line; see Fig. 7.5(a).

Thus
$$v = v_1 - \lambda \ell n\ P' \tag{7.1}$$

$$v = v_s - \kappa \ell n\ P' \tag{7.2}$$

where

v is the specific volume

P' is the mean effective stress $= (\sigma_1' + \sigma_2' + \sigma_3')/3$ (7.3)

λ is the slope of the virgin consolidation line

κ is the slope of the swelling line

v_1 is the virgin consolidation specific volume at unit P'

v_s is the specific volume at unit P', on the swelling line

λ, κ, and v_1 are properties of a particular clay, whereas the value of v_s is different for each swelling line. The volume change along each swelling line is recoverable, or elastic, whereas much of the volume change along the virgin consolidation line is irrecoverable, or plastic.

7.4.2.3 Yield Function and Plastic Potential

It was assumed that the plasticity is, in the terms of classical plasticity, 'associated'; in other words the yield function and the plastic potential were assumed to be coincident. An assumption regarding the nature

of the dissipation of energy within the clay led to the definition of a flow rule from which the equation of the Stable State Boundary Surface (S.S.B.S.) was derived.

The equation of the S.S.B.S. may be written as

$$F_o = q^2 - M^2 p'^2 \left(\frac{P'_o}{P'} - 1\right) = 0 \qquad (7.4)$$

where

q is $\sigma'_1 - \sigma'_3 = \sigma'_z - \sigma'_r$

M is a clay parameter representing the slope of the critical state line in q-P' space

P'_o is the value of P' at the intersection of the current swelling line and the virgin consolidation line (see Fig. 7.5(b)). P'_o is employed as a hardening parameter.

The yield surface plots as an ellipse above each swelling line.

It was assumed that when the clay is subject to an increasing deviatoric stress it behaves in an elastic manner (whilst $F < 0$) until the yield surface is reached ($F = 0$), at which point strain hardening/softening plastic behaviour occurs.

Roscoe and Burland (1968) extended the model to consider more generalised stress space by assuming that the S.S.B.S. describes a surface of revolution about the space diagonal.

7.4.3 Constitutive Models in Generalised Stress Space

7.4.3.1 Introduction

In order to describe the stress state at any point in a body, it is necessary to specify six independent quantities. One possibility is to employ six components of stress referred to a given system of axes. However, the magnitudes of these stresses will depend on the choice of axes. Often a more convenient approach is to specify three stress parameters which are independent of the choice of references axes and which are unique for a given state of stress, and three quantitites to specify orientations. Such

stress parameters are termed invariant quantities and are employed below.

Three convenient invariant quantities P', J and θ are represented in Fig. 7.6, where the simple geometrical relationship between the invariants may be seen in three-dimensional stress space.

P' is the mean effective stress defined by eqn. (7.3)

J is the second invariant of the deviatoric stress tensor, and is defined by

$$J^2 = \frac{1}{6}\left((\sigma'_1 - \sigma'_2)^2 + (\sigma'_2 - \sigma'_3)^2 + (\sigma'_3 - \sigma'_1)^2\right) \tag{7.5}$$

$$= \frac{1}{2} \text{ trace } \underset{\sim}{S}^2 \tag{7.6}$$

(in which $\underset{\sim}{S}$ is the deviatoric stress tensor $(\underset{\sim}{\sigma} - P.\underset{\sim}{1})$)

and

θ is the Lode angle. This quantity expresses the magnitude of the intermediate principal stress as a function of the major and minor principal stresses, and is an equivalent of Bishop's parameter

$$b\left(= \frac{\sigma'_2 - \sigma'_3}{\sigma'_1 - \sigma'_3}\right)$$

θ may be defined formally as

$$\theta = -\frac{1}{3}\sin^{-1}\left(\frac{3\sqrt{3}}{2} \cdot \frac{\det \underset{\sim}{S}}{J^3}\right) \tag{7.7}$$

The Lode angle is related to b by the expression given below (and derived in Appendix 7.3);

$$\theta = \tan^{-1}\left((2b-1)/\sqrt{3}\right) \tag{7.8}$$

Thus $\theta = -30°$ corresponds to triaxial compression $(b = 0)$

$\theta = +30°$ corresponds to triaxial extension $(b = 1)$

$\theta = 0°$ corresponds to $\sigma'_2 = \left(\frac{\sigma'_1+\sigma'_3}{2}\right)$ or $(b = \frac{1}{2})$

7.4.3.2 General Expressions for the Yield Function and the Plastic Potential

The equation derived by Roscoe and Burland (1968) for the yield function of Modified Cam Clay (in triaxial stress space) may be rewritten in a dimensionless form as

$$F = \left(\frac{q}{MP'}\right)^2 - \left(\frac{P'_o}{P'} - 1\right) = 0 \qquad (7.9)$$

Clearly, the quantity (q/MP') is a normalised measure of the current level of deviatoric stress. It has been found convenient to replace this quantity by S, which takes the value of zero on the isotropic stress axis, and unity at the critical state.

The yield function may thus be rewritten as

$$F = S^2 - \left(\frac{P_o}{P} - 1\right) = 0 \qquad (7.10)$$

S may be related to the invariant quantities introduced earlier. Thus in triaxial stress space

$$S = \frac{q}{MP'} = \frac{J}{MP'} \cdot (2 \cos (\pm 30°))$$

($q = 2J \cos \theta$, see Appendix 7.4)

In general, the value of M will depend on the magnitude of the intermediate principal stress and it proves useful to define a further quantity, $g(\theta)$, (see Fig. 7.7) such that

$$g(\theta) = M(\theta)/2 \cos \theta \qquad (7.11)$$

and thus

$$S = \frac{J}{P'} \left(\frac{2 \cos \theta}{M(\theta)}\right)$$

becomes

$$S = \frac{J}{P' g(\theta)} \qquad (7.12)$$

If the yield function is assumed to be a surface of revolution about the space diagonal (as in the extended Von Mises criterion), then $g(\theta)$ is constant and takes the value

$$g(\theta) = \left(M_{\theta=-30°} \right)/\sqrt{3} = \text{constant} \qquad (7.13)$$

It should be noted that the above assumption implies that ϕ' varies significantly with the value of the intermediate principal stress; this is demonstrated in Appendix 7.5.

It has been found experimentally that for the majority of clays ϕ' values are relatively insensitive to the Lode angle. Typically, ϕ' may change 1° or 2° between triaxial compression and plane strain. It would, therefore, seem more appropriate to represent the shape of the yield function in the deviatoric plane as a Mohr Coulomb hexagon (ϕ' constant), rather than as a circle ($g(\theta)$ being constant).

The expression for $g(\theta)$ appropriate to a Mohr Coulomb hexagon is derived in Appendix 7.5;

$$g(\theta) = \sin \phi' / (\cos \theta + \frac{1}{\sqrt{3}} \sin \theta \sin \phi') \qquad (7.14)$$

Finite element analyses of piling problems were initially performed assuming the yield function to describe a surface of revolution, and later the more realistic assumption of ϕ' constant was employed. It was found that the stress paths predicted on the basis of the second assumption were far more difficult to interpret than those based on the first, and so calculations using both will be discussed.

The plastic strain increment vectors are normal to a plastic potential surface which need not necessarily coincide with the yield function. The plastic potential was taken to be of the same general form as the yield function;

$$Q = S^2 - \left(\frac{p'_o}{p'} - 1\right) = 0 \qquad (7.15)$$

However, the function $g(\theta)$ for the plastic potential was not necessarily the same as that for the corresponding yield function. Potts and Gens (1983) discuss the application of a versatile family of plastic potential surfaces defined by the expression

$$g(\theta) = X/(1 + Y \sin 3\theta)^Z \qquad (7.16)$$

where Y and Z are material properties, and the parameter X is varied such that when the soil is yielding, the current plastic potential and the yield surface coincide at the current state of stress. This is illustrated in Figs. 7.8(a) and (b). In the deviatoric plane the two surfaces do not, in general, coincide except at the current stress state, where the local derivatives $\partial F/\partial\theta$ and $\partial Q/\partial\theta$ are still unequal. However, at the current state of stress the yield function and the plastic potential are of the same form and the projections of the surfaces in the J-P' plane are coincident.

The values of the parameters Y and Z are best established from experimental data concerning the shape of the plastic potential in the deviatoric plane. Typically, however, such data are not available and the parameters may be selected to represent a variety of convex surfaces passing through pre-determined end points (as may be determined by triaxial compression, triaxial extension or plane strain tests for instance).

The function in eqn. (7.16) exhibits six-fold symmetry in the deviatoric plane, and has smooth corners at $\theta = \pm n\pi/3$. It has been shown by Potts and Gens (1983) that in circumstances where one of the components of direct plastic strain increment is zero, and the volumetric plastic strain increment is also zero then the final Lode angle is dependent only on the shape of the plastic potential in the deviatoric plane. A simple consequence of this is that the Lode angle at failure may be pre-selected by judicious choice of the shape of the plastic potential.

Thus, the selected yield functions and plastic potentials differ only in their shapes in the deviatoric plane and are, in general, non-associated. However, if the constants Y and Z are set to zero and unity respectively then the shape of the plastic potential in the deviatoric plane reduces to a circle. If, in addition, $g(\theta)$ corresponding to the yield function is defined by eqn. (7.13), associated conditions are obtained with $X = M/\sqrt{3}$.

7.4.3.3 Elastic Behaviour

If the soil is subject to unloading and reloading of the mean effective stress, then the response is assumed to be determined by eqn. (7.2). This gives an elastic bulk modulus, K_B, of

$$K_B = v.P'/\kappa \qquad (7.17)$$

This implies that the bulk modulus is a function of both the current stress level and the specific volume. In the original formulation of Modified Cam Clay, elastic shear strains were neglected; however, this neglect results in unrealistic predictions when purely elastic behaviour is considered. In the constitutive laws employed in the current study, a constant value of the elastic shear modulus, G, has been adopted. Such an assumption is conservative (in the sense of energy dissipation), but suffers from the implied variation of Poisson's ratio with stress level. However, this was considered preferable to assuming a stress level dependent shear modulus, as this would imply a violation of the Second Law of Thermodynamics (see Zytynski et al, 1977).

Thus, in order to specify a particular soil model in the analyses described below, values of the following seven parameters (which may be determined by laboratory testing) are required: G, M or ϕ', λ, κ, V_1, Y and Z.

7.4.4 Discussion of Some Implications of the Chosen Soil Models

Before presenting the results of predictions based on the constitutive models presented above, it is pertinent to examine some of the implications and limitations of the models. If an element of soil which is initially normally consolidated or lightly over-consolidated (i.e. wet of critical) is sheared, then peak conditions are assumed to occur as the state of stress approaches the critical state. Once the critical state has been reached, the model is unable to predict any shear stress reduction with further shear strain, and so the residual strength behaviour observed in the model pile tests cannot be simulated. Once peak conditions have been achieved the model necessarily predicts no further change in volume. The model also assumes, in accordance with classical plasticity theory, that the directions of the principal axes of stresses and plastic strain increments are always coincident.

These last two assumptions which are incorporated into the model, in combination with the kinematic constraints encountered in the pile problem lead to the following observations:

(1) At peak conditions the directions of the principal strain increments are inclined at $\pm$ 45° to the pile axis as a result of the kinematic restraints and the condition of no volume change at the critical state.

Because the stress and plastic strain increment directions have been assumed coincident, the principal stresses are also inclined at ± 45° to the pile axis. This, in turn, implies that the peak angle of shaft friction, δ', that can be mobilised is given by;

$$\delta'_{peak} = \tan^{-1} (\sin \phi') \qquad (7.18)$$

where ϕ' is the angle of shearing resistance mobilised at the critical state.

This result is independent of the initial stress ratio in the soil, and is supported by the experimental observations presented in Chapter 5. It should be noted that the predicted angle of shaft friction does not depend on whether the soil is assumed to obey associated or non-associated plasticity.

(2) As remarked earlier, it has been shown by Potts and Gens (1983) that in circumstances of kinematic restraint such as those encountered close to a pile at peak conditions, the Lode angle at peak is dependent only on the shape of the plastic potential in the deviatoric plane. For example, if the shape of the plastic potential in the deviatoric plane is specified as being circular, then peak conditions will be associated with a Lode angle of $\theta = 0°$ (or $b = 0.5$).

7.4.5 Parameters Selected for the Soil Models Employed

Two soil models (A and B) were used in the finite element studies to represent the Kaolin employed in the model pile tests. In both soil models, the parameters M or ϕ', λ, κ and v_1 were selected on the basis of conventional laboratory test data, and G was determined from the initial slope of the load-displacement curve obtained during a model pile test. The yield surface employed in Model A describes a circle in the deviatoric plane, whereas that of Model B describes a Mohr-Coulomb

hexagon. The plastic potential employed in Model A also describes a circle in the deviatoric plane, whereas the plastic potential employed in Model B is represented by a more general shape (defined by eqn. (7.16)). The values of Y and Z were selected to ensure that plastic potential is always convex, and that the Lode angle at peak conditions corresponds to a 'b' value of 0.35 (θ = -9.8°).

Thus, the soil parameters may be summarised as;

(a) Soil Model 'A'

$M = 0.9$, $\lambda = 0.25$, $\kappa = 0.05$, $v_1 = 3.65$, $G = 18{,}000\ kN/m^2$,

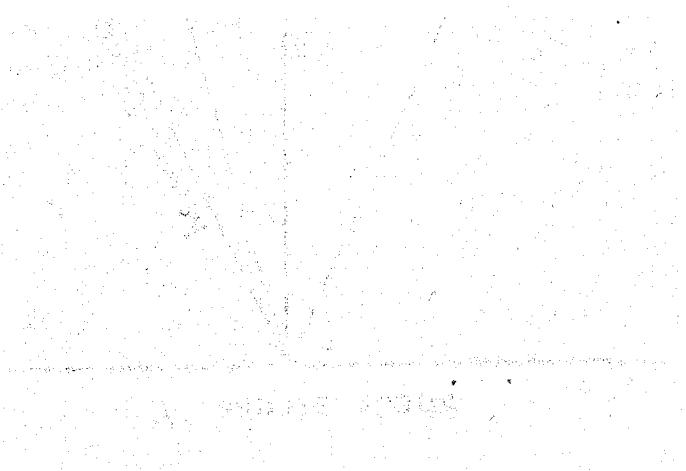
$Y = 0.0$ and $Z = 1.0$.

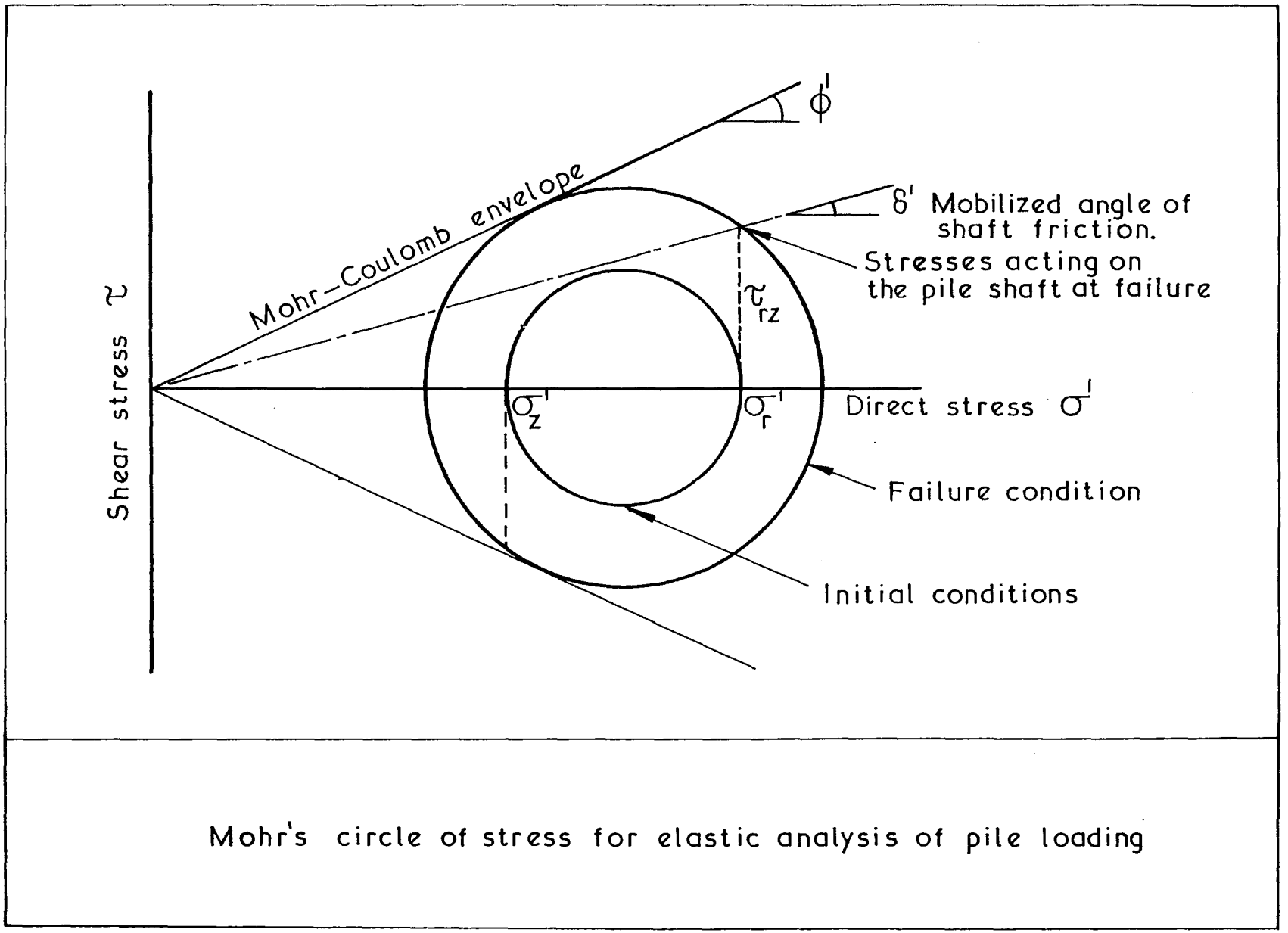
(b) Soil Model 'B'

$\phi' = 23°$, $\lambda = 0.25$, $\kappa = 0.05$, $v_1 = 3.65$, $G = 18{,}000\ kN/m^2$,

$Y = 0.2535$ and $Z = 0.229$

In Chapter 9, analyses are extended to consider displacement piles in both London Clay and in Boston Blue Clay. The selected soil parameters are discussed in Chapter 9.





Mohr's circle of stress for elastic analysis of pile loading

Fig. 7.1

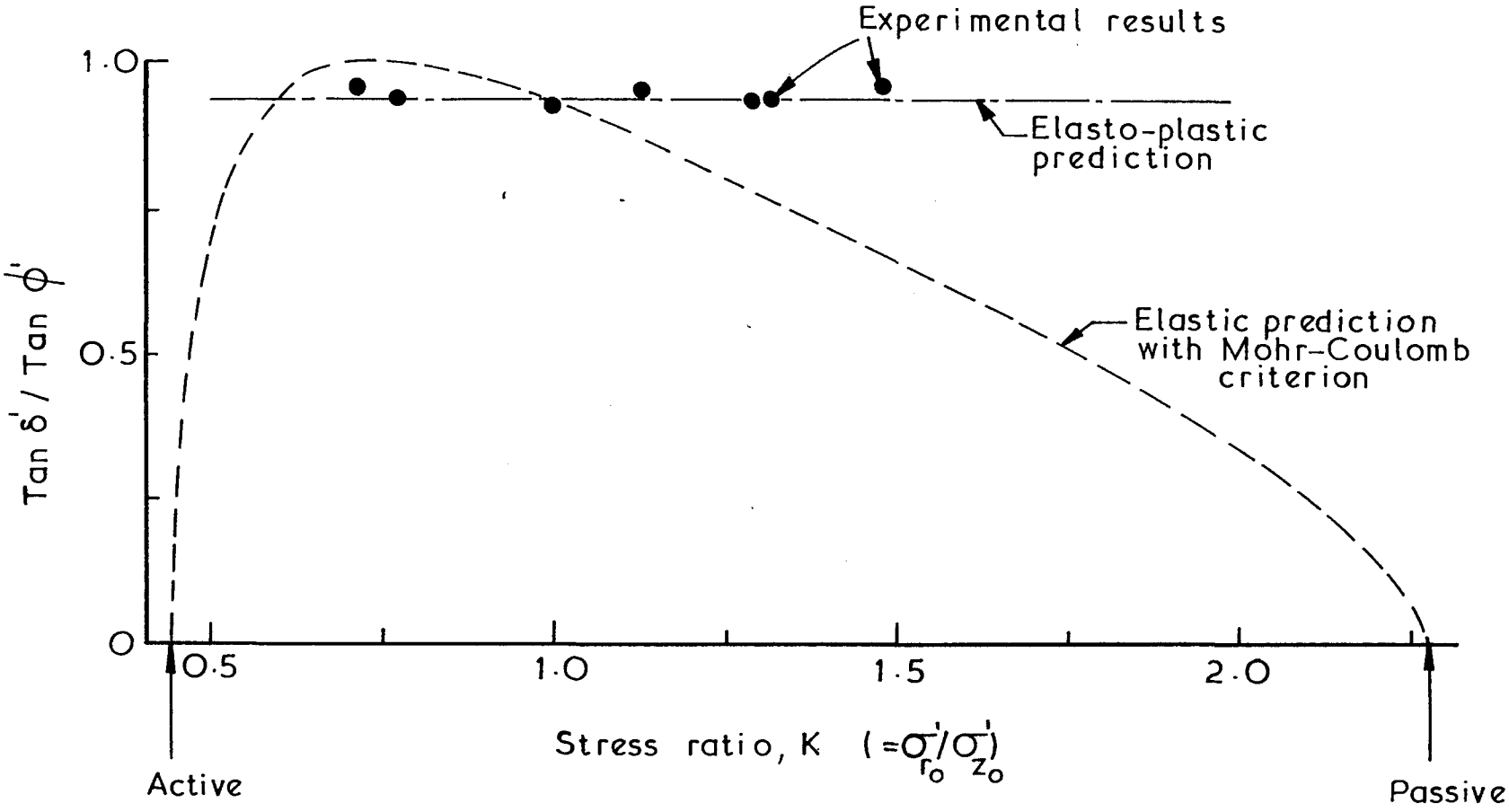
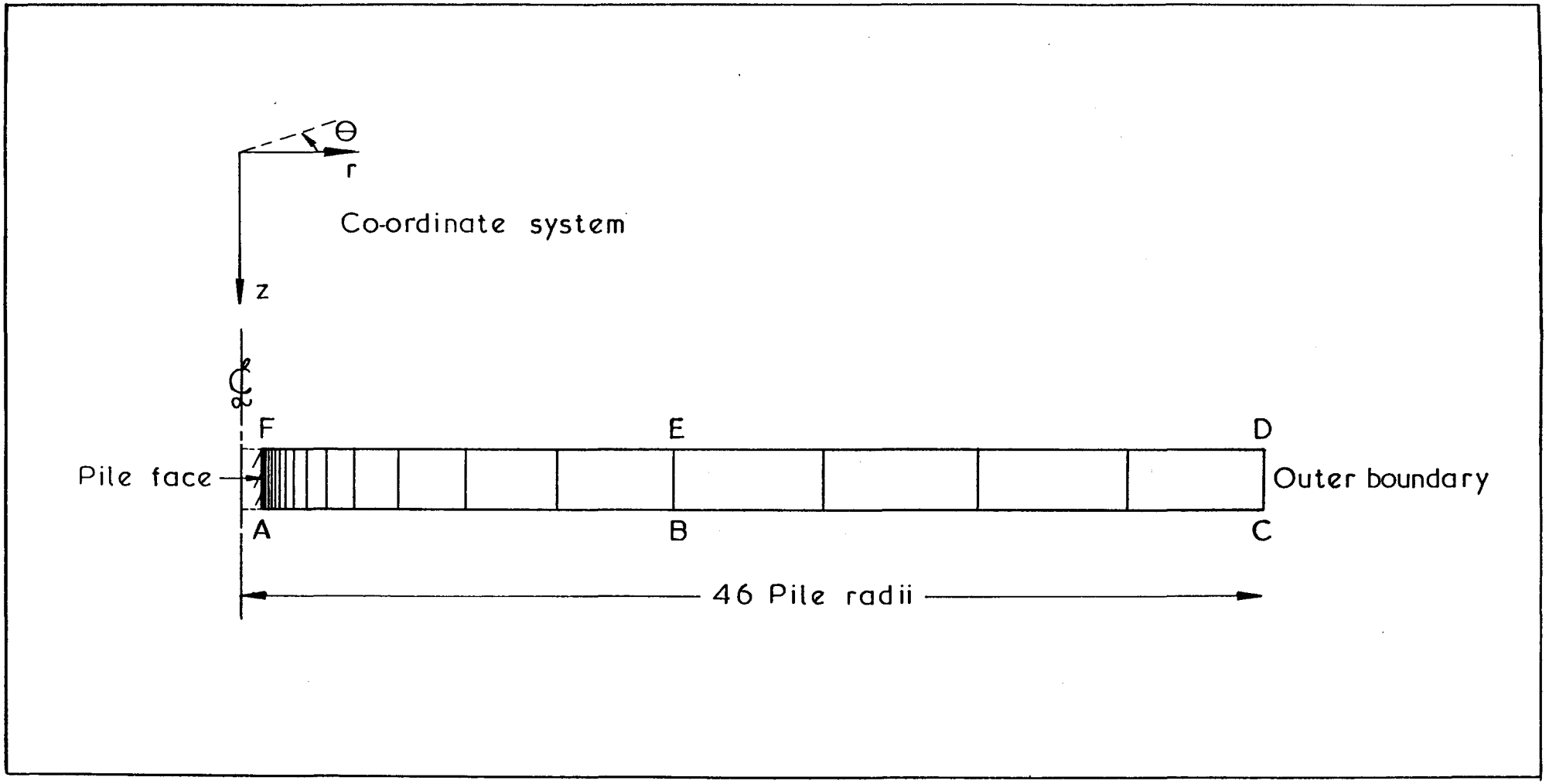


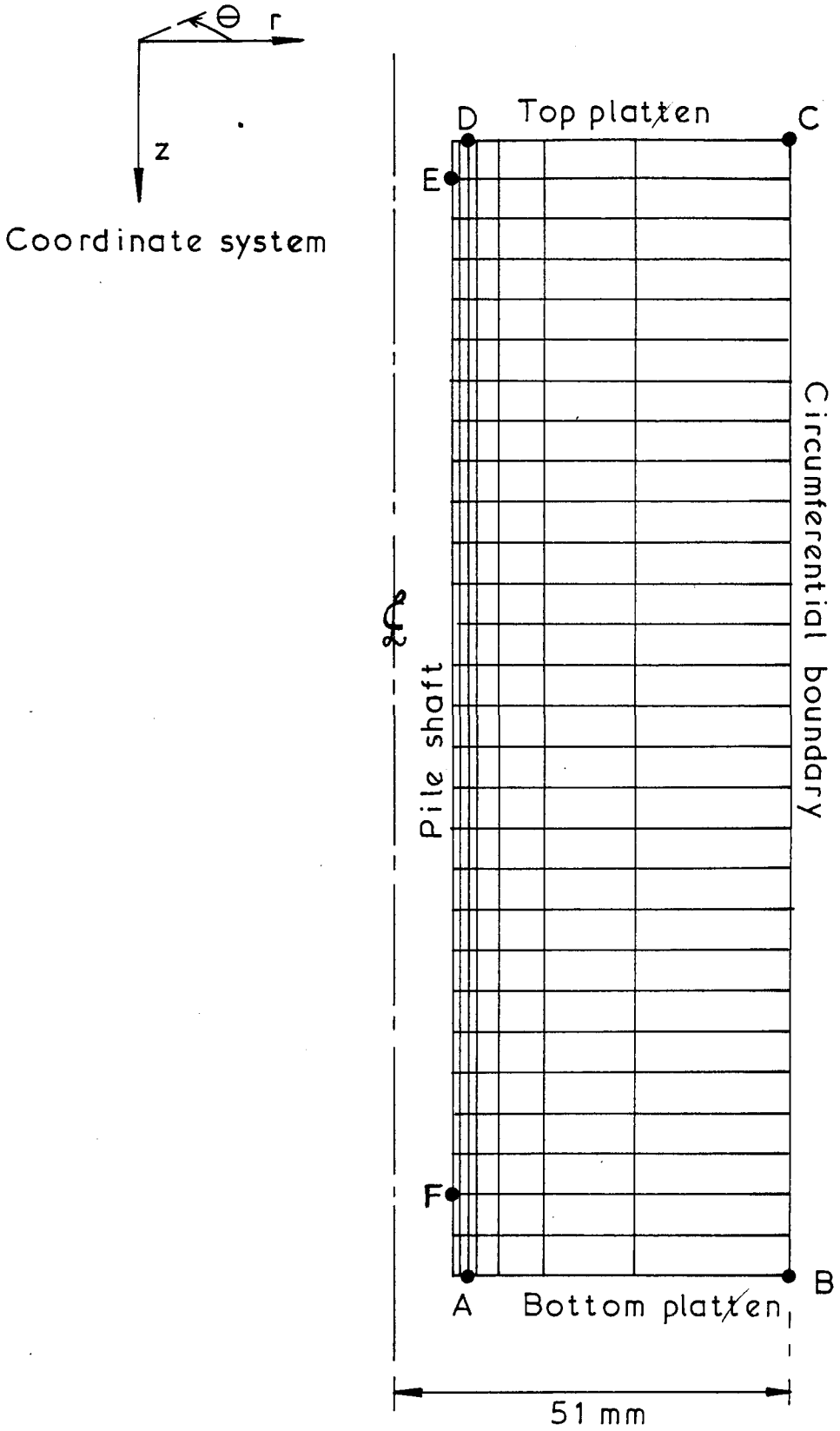
Fig. 7.2

Variation of $\tan\delta' / \tan\phi'$ with initial stress ratio, K



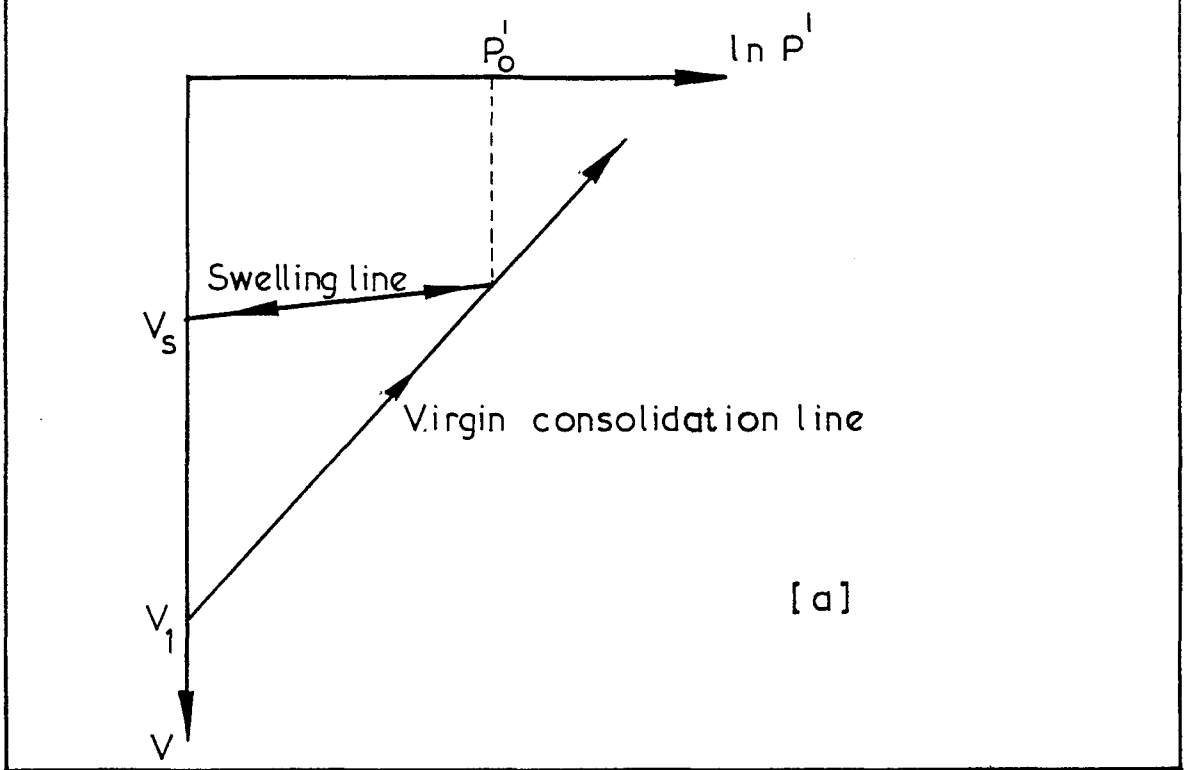
Finite element mesh for simulation of a short segment of a long pile in an infinite soil mass.

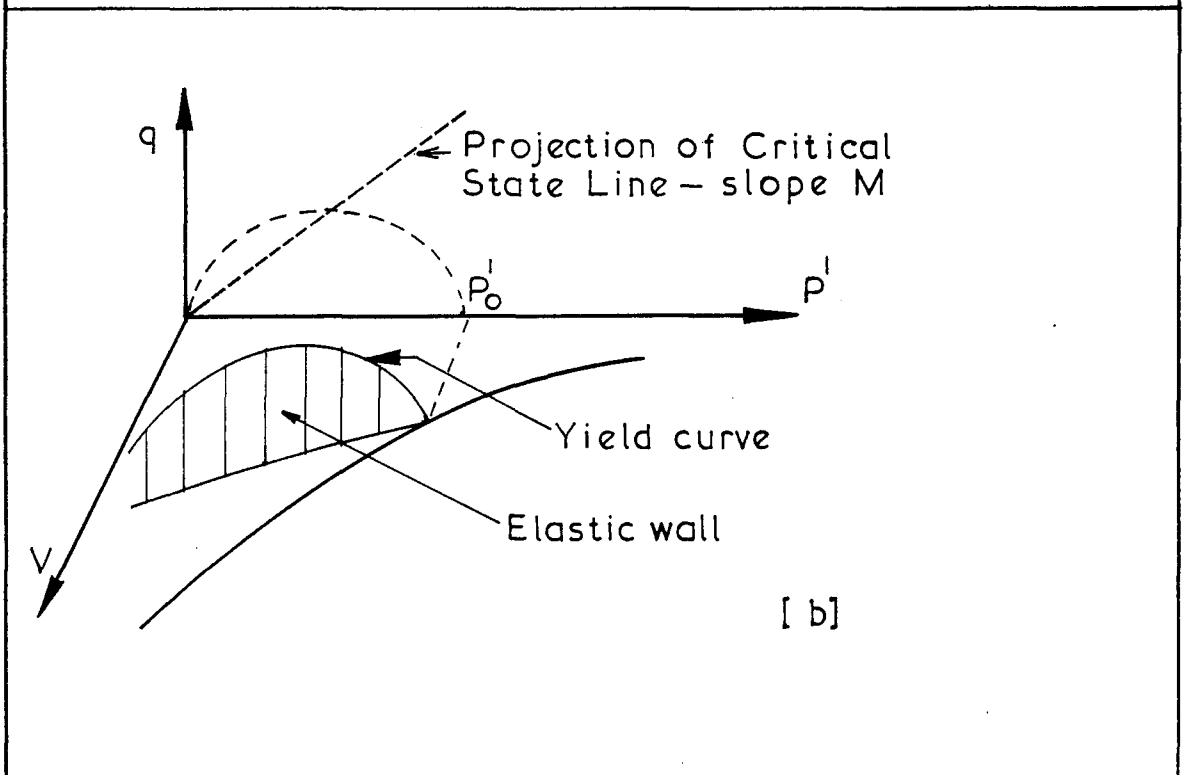
Fig. 7.3



Finite element mesh for simulation of model pile tests

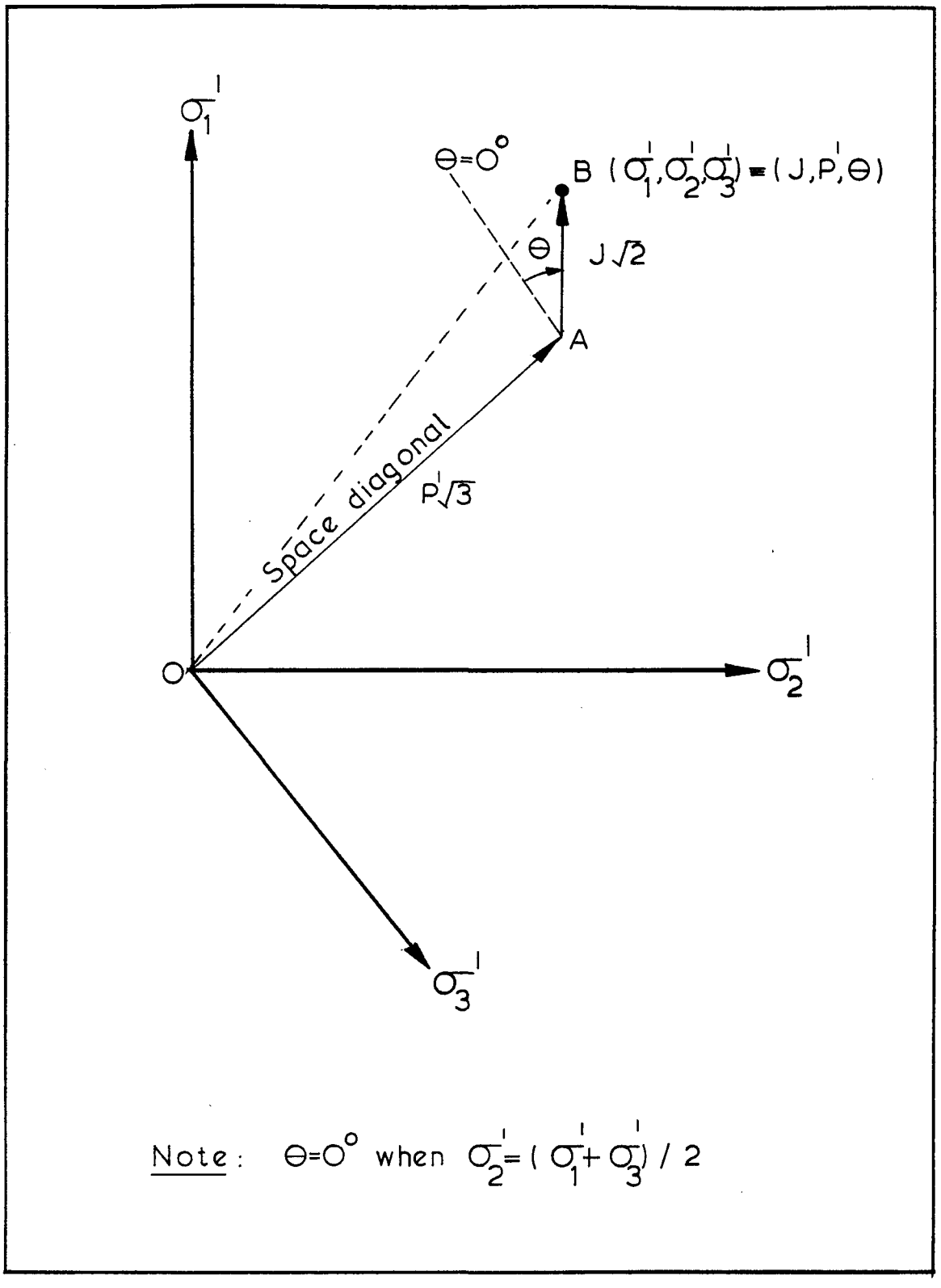
Fig. 7 . 4





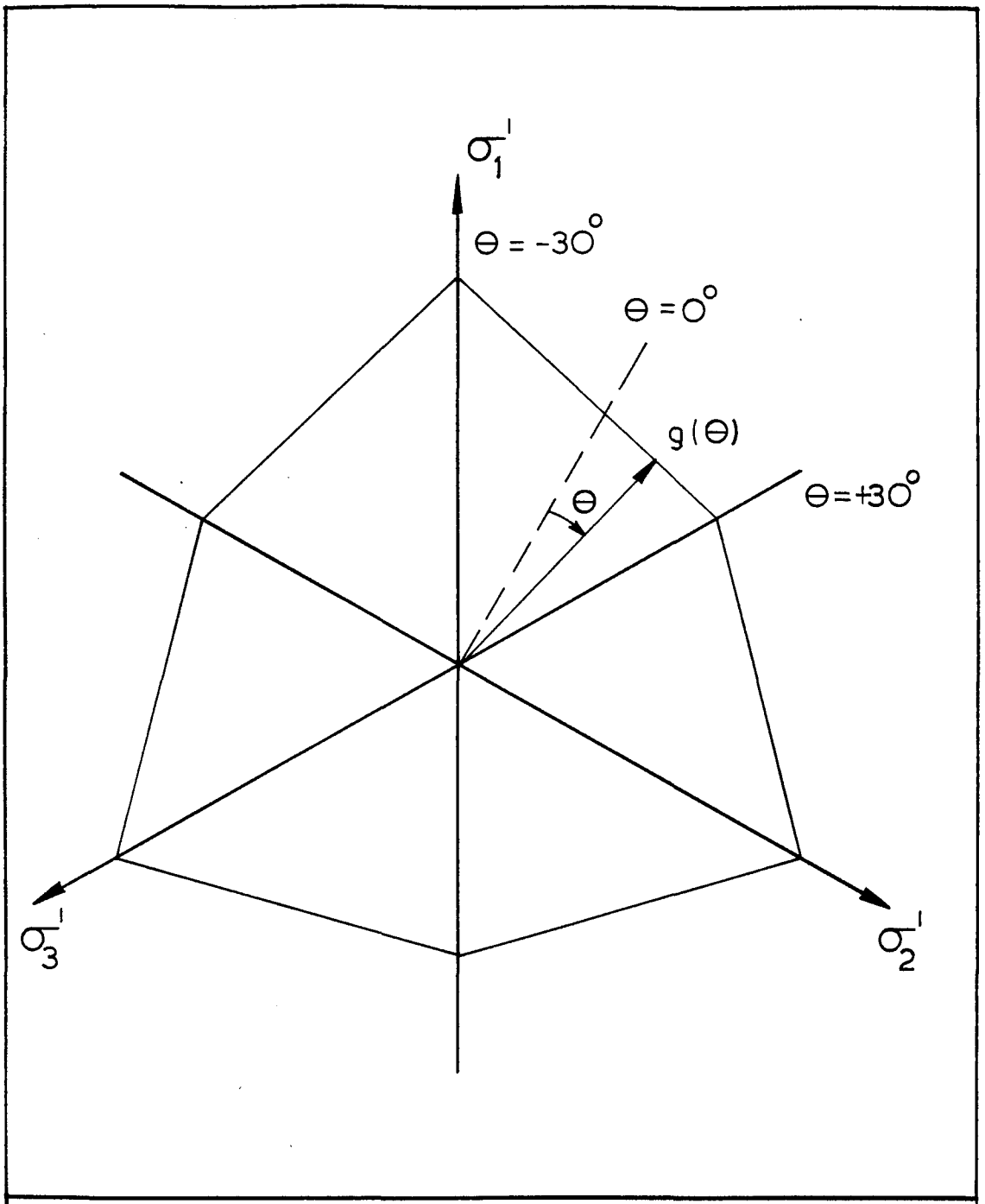
Essential details of Critical State Model

Fig. 7.5



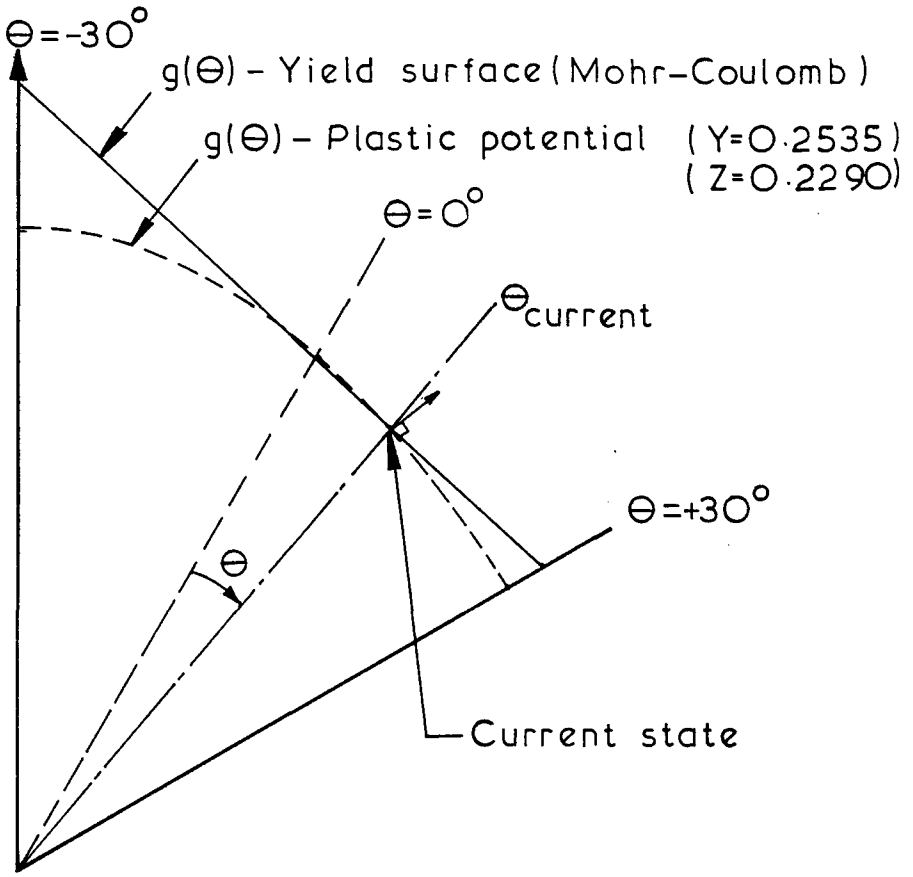
Representation of stress invariants J, P', and θ in three-dimensional stress space

Fig. 7 · 6

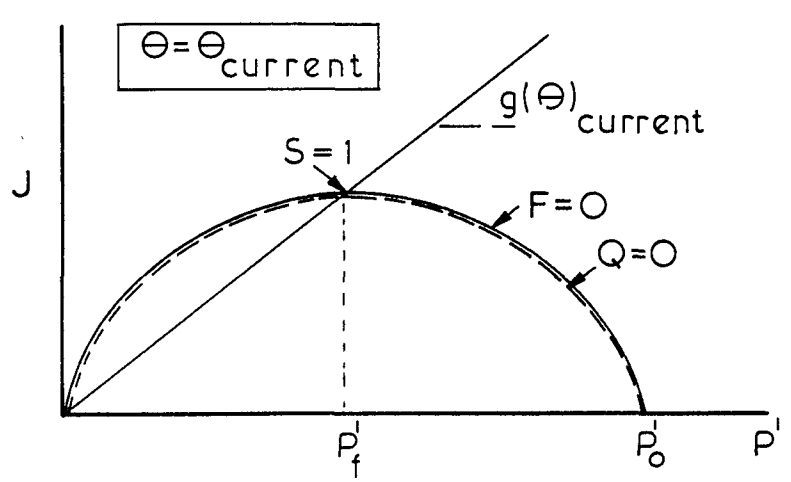


Variation of $g(\Theta)$ in the deviatoric plane

Fig. 7.7



(a) Relationship between Yield function and Plastic potential (variation of g(Θ)) in the deviatoric plane



(b) Yield function and Plastic potential in the J-P' plane

Fig. 7.8

APPENDIX 7.1

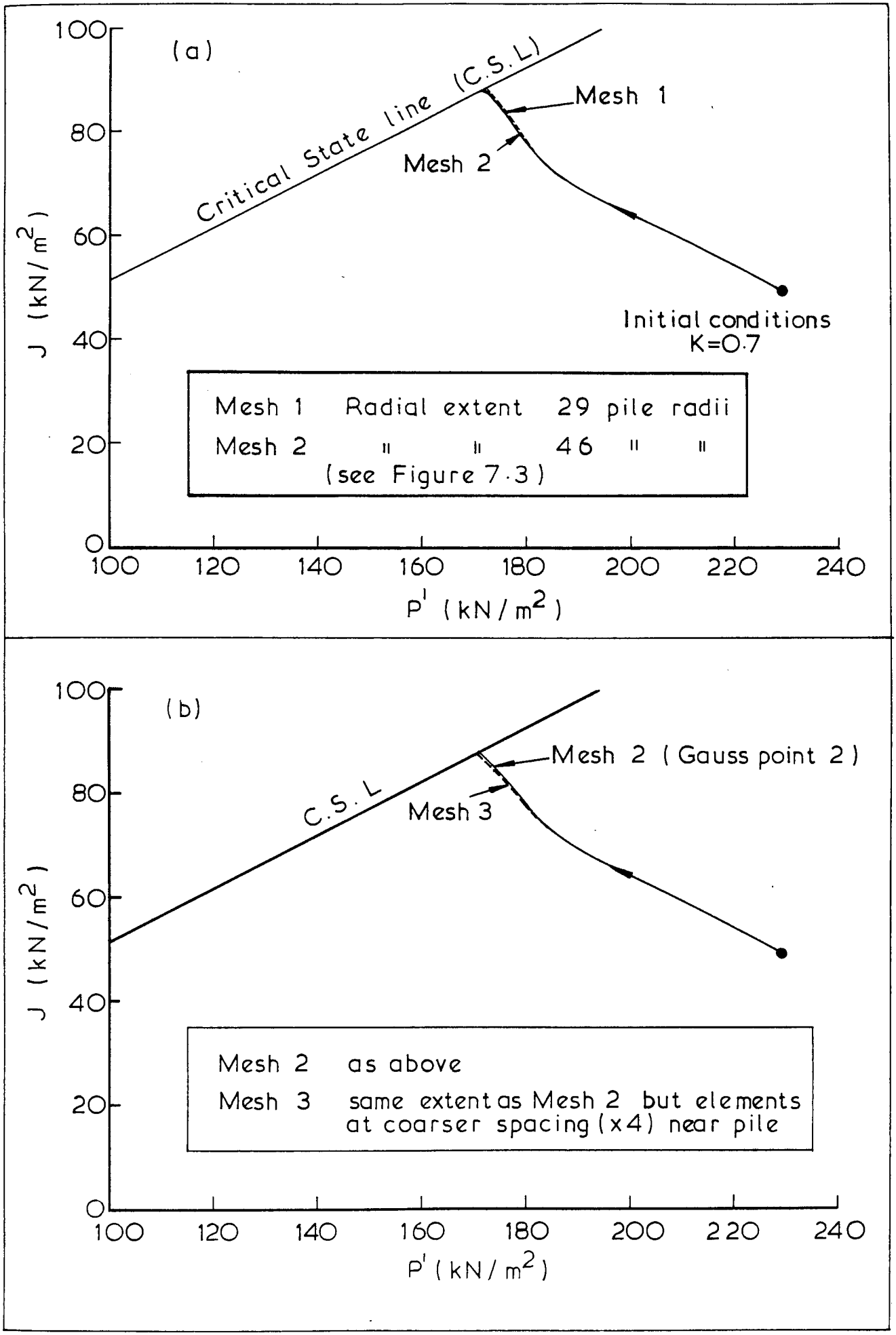
DETERMINATION OF APPROPRIATE MESH GEOMETRY

As described in section 7.3.2, a simple mesh was employed to analyse the conditions in the soil surrounding a short segment of a very long pile. The element sizes and the radial distance to the outer circumferential boundary were established with the aid of a parametric study.

Results obtained using three of the meshes investigated in the parametric study are considered below; the drained loading of a rigid pile installed without disturbance into Kaolin normally-consolidated to a stress ratio, K, of 0.7 is simulated. The predicted stress paths (in terms of J and P') followed by the elements of soil immediately adjacent to the piles are compared in Figs. A.7.1 (a) and (b).

The mesh finally adopted (No. 2) is illustrated in Fig. 7.3. The ratio of the outer radius of the mesh to the radius of the pile is 46, and the mesh is divided into 20 eight-noded isoparametric elements. Immediately adjacent to the pile shaft, the elements have a width of only 3% of the pile radius. Mesh No. 1 was selected to have identical elements to a distance of 10 pile radii from the pile, but the outer boundary was located at a distance of only 29 pile radii (compared with 46). In Fig. A.7.1 (a) the stress paths followed by the Gauss points closest to the piles (for meshes 1 and 2) are compared, and it will be seen that the results are almost identical. This suggests that that radial extent of Mesh No. 2 is sufficient to provide accurate predictions.

Mesh No. 3 has the same overall dimensions as Mesh No. 2 but, up to a distance of more than ten pile radii from the shaft, the elements were four times larger. Because of the differences in element sizes close to the piles, predictions based on the Gauss point closest to the pile in Mesh No. 3 are compared with those based on the Gauss point second closest to the pile in Mesh No. 2. The corresponding stress paths are illustrated in Fig. A.7.1 (b), where it will be seen that the paths are very similar. This suggests that further reducing the sizes of the elements closest to the piles would have little influence on the accuracy of prediction.



Stress path followed by soil adjacent to the pile during drained loading—effects of Mesh geometry.

Fig. A.7.1

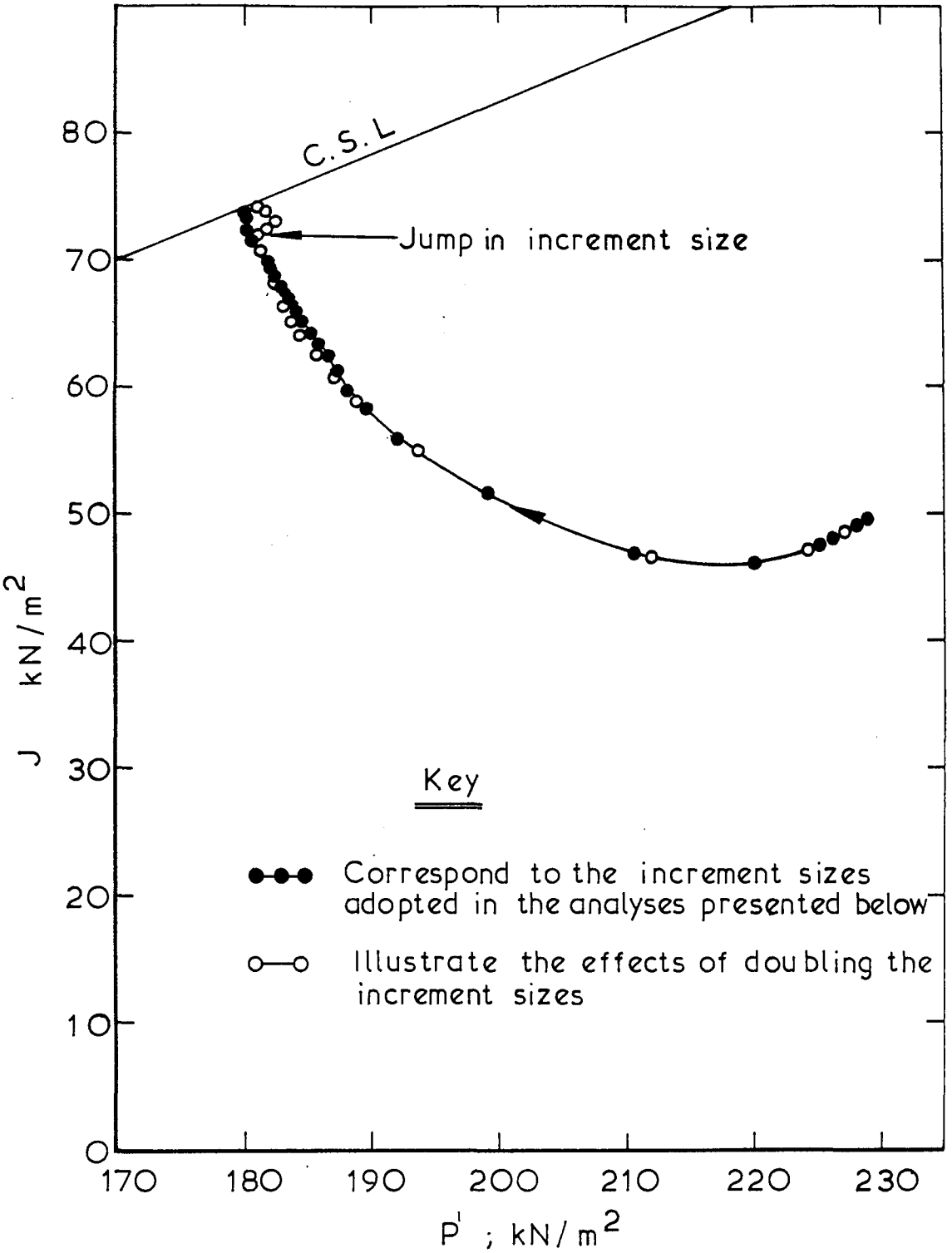
APPENDIX 7.2

SELECTION OF INCREMENT SIZES

As described in section 7.3.2, the pile loading was simulated by imposing increments of vertical displacement over the boundary AF (see Fig. 7.3). Appropriate increment sizes depend on the current stiffness of the pile-soil system, and in the early stages of loading small increments are required, especially if transitions from elastic to elasto-plastic behaviour are involved. However, once elasto-plastic conditions are established in the soil close to the pile, larger displacement increments may be tolerated.

Because of the highly non-linear nature of this problem, no hard and fast rules for selecting increment sizes can be given. However, with experience of a particular type of problem, sensible ranges are soon established. Data were saved after every fifth increment so that the analyses could be restarted at a variety of stages if necessary. On changing increment sizes, checks were made to ensure that no abrupt changes in stress conditions were predicted. If such changes were encountered then the proposed increment sizes were reduced.

Fig. A.7.2 presents a comparison between a stress path predicted using the increment sizes finally selected for the main analyses, and a stress path predicted using increment sizes of double the magnitude. It will be seen that there is very little difference between the predictions, which suggests that little would be gained by employing even smaller increments.



An illustration of the effects of doubling the sizes of the increments of pile displacement; K=0·7, Model B employed.

Fig. A.7·2

APPENDIX 7.3

RELATIONSHIP BETWEEN THE LODE ANGLE, θ, AND BISHOP's PARAMETER, b

Fig. A.7.3 represents a projection in $(\sigma_1', \sigma_2', \sigma_3')$ stress space down the space diagonal. The stresses at an arbitrary point A are considered.

Resolving parallel to the θ = 0° direction

$$\sigma_1' \cos 30° - \sigma_3' \cos 30° = x \qquad \text{(A.7.3.1)}$$

$$\therefore \quad x = (\sigma_1' - \sigma_3')\sqrt{3}/2 \qquad \text{(A.7.3.2)}$$

Resolving perpendicular to the θ = 0° direction

$$-\sigma_1' \sin 30° - \sigma_3' \sin 30° + \sigma_2' = y \qquad \text{(A.7.3.3)}$$

$$\therefore \quad y = \sigma_2' - (\sigma_1' + \sigma_3')/2 \qquad \text{(A.7.3.4)}$$

Thus

$$\frac{y}{x} = \tan\theta = \frac{2\sigma_2' - (\sigma_1' + \sigma_3')}{\sqrt{3}\,(\sigma_1' - \sigma_2')} \qquad \text{(A.7.3.5)}$$

Substituting

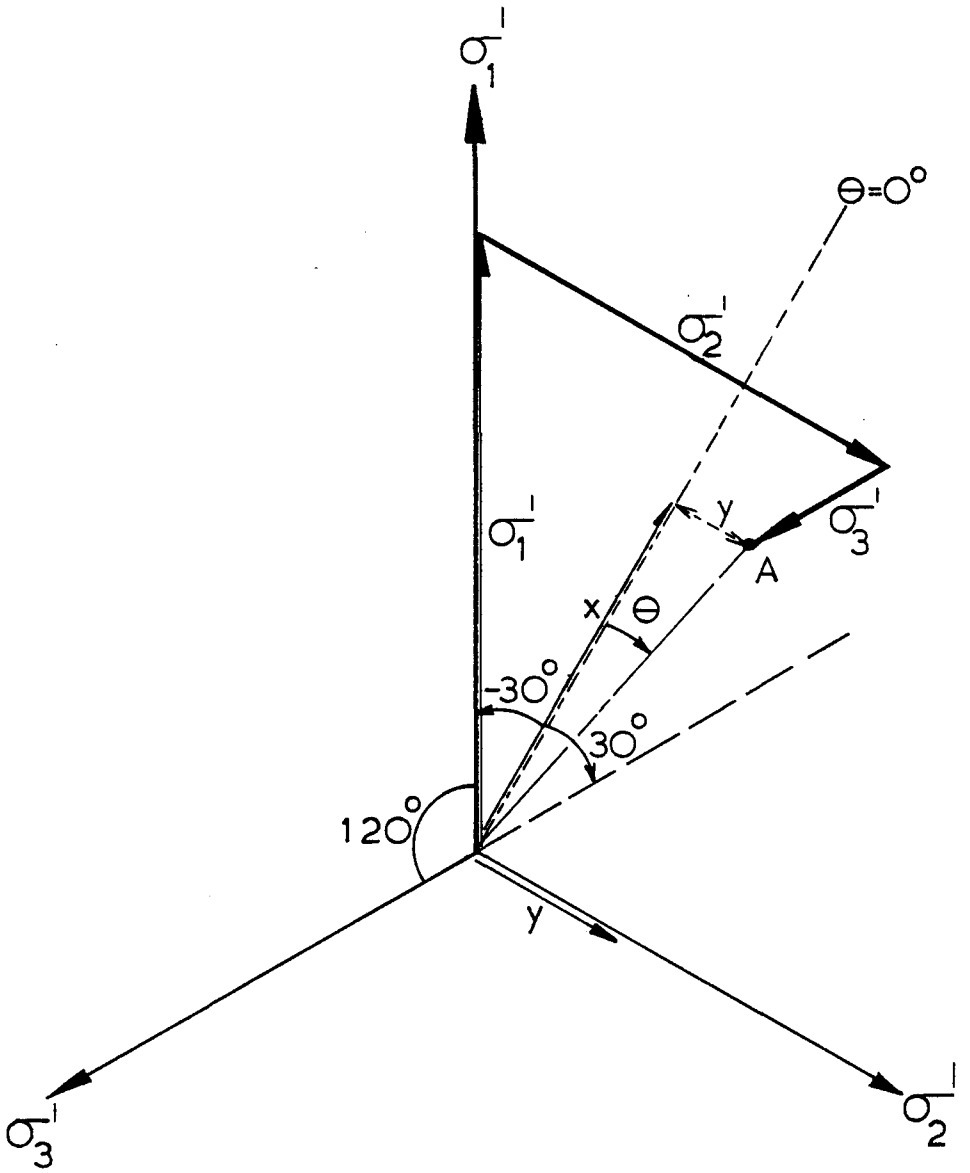
$$b = (\sigma_2' - \sigma_3')/(\sigma_1' - \sigma_3')$$

leads to

$$\tan\theta = (2b - 1)/\sqrt{3} \qquad \text{(A.7.3.6)}$$

or

$$\theta = \tan^{-1}((2b - 1)/\sqrt{3}) \qquad \text{(A.7.3.7)}$$



Geometric representation of the Lode angle (θ) in the deviatoric plane

Fig. A.7.3

APPENDIX 7.4

THE RELATIONSHIP BETWEEN q, J and θ

By definition,

$$J^2 = \frac{1}{6}((\sigma_1' - \sigma_2')^2 + (\sigma_2' - \sigma_3')^2 + (\sigma_3' - \sigma_1')^2) \qquad (A.7.4.1)$$

Substituting

$$b = (\sigma_2' - \sigma_3')/(\sigma_1' - \sigma_3') \qquad (A.7.4.2)$$

leads to

$$J = \frac{\sigma_1' - \sigma_3'}{\sqrt{3}} (b^2 - b + 1)^{\frac{1}{2}} \qquad (A.7.4.3)$$

Thus,

$$q = \sigma_1' - \sigma_3' = \frac{J\sqrt{3}}{(b^2-b+1)^{\frac{1}{2}}} \qquad (A.7.4.4)$$

From eqn. (A.7.3.6),

$$\tan \theta = (2b - 1)/\sqrt{3}$$

substitution into (A.7.4.4) leads to

$$q = 2J \cos \theta \qquad (A.7.4.5)$$

At failure,

$$C_u = \frac{\sigma_1' - \sigma_3'}{2} = \frac{q_f}{2}$$

so

$$C_u = J_f \cos \theta_f \qquad (A.7.4.6)$$

APPENDIX 7.5

RELATIONSHIP BETWEEN $g(\theta)$, θ and ϕ'

$$M = q/P' = \frac{3(\sigma_1' - \sigma_3')}{(\sigma_1' + \sigma_2' + \sigma_3')} \qquad (A.7.5.1)$$

from eqn. (7.11) $$g(\theta) = M/2 \cos\theta \qquad (A.7.5.2)$$

by definition $$b = (\sigma_2' - \sigma_3')/(\sigma_1' - \sigma_3') \qquad (A.7.5.3)$$

and $$\sin\phi' = (\sigma_1' - \sigma_3')/(\sigma_1' + \sigma_3') \qquad (A.7.5.4)$$

Substituting eqns. (A.7.5.2,3,4 into (A.7.5.1) leads to

$$g(\theta)\cos\theta = \frac{3\sin\phi'}{3 + \sin\phi'(2b-1)} \qquad (A.7.5.5)$$

Substituting eqn. (A.7.3.6) into (A.7.5.5),

$$g(\theta) = \frac{\sin\phi'}{\cos\theta + \frac{\sin\phi'\sin\theta}{\sqrt{3}}} \qquad (A.7.5.6)$$

Thus, eqn. (A.7.5.6) may be employed to represent a Mohr-Coulomb yield criterion, assuming a constant value of ϕ' in the deviatoric plane.

Expressing ϕ' in terms of $g(\theta)$,

$$\phi' = \sin^{-1}\left[\frac{g(\theta)\cos\theta}{1 - \frac{g(\theta)\sin\theta}{\sqrt{3}}}\right] \qquad (A.7.5.7)$$

Thus, if $g(\theta)$ is chosen to be constant in order to represent the yield function as a surface of revolution in the deviatoric plane, then a significant variation of ϕ' with θ is implied. This variation is demonstrated in Table A.7.5.1.

Table A.7.5.1

$g(\theta)$	0.4457	0.5680	0.6920
$\phi'(\theta = -30°)$	20°	25°	30°
$\phi'(\theta = 0°)$	26.5°	34.6°	43.8°
$\phi'(\theta = -30°)$	26.9°	36.04°	48.5°

The variations in ϕ' implied by selecting constant values of $g(\theta)$.

CHAPTER 8

THEORETICAL ANALYSES OF MODEL PILE TESTS

8.1 INTRODUCTION

The model tests conducted using piles installed with minimal disturbance into Kaolin samples (see Chapter 5) are analysed theoretically in this chapter. The Kaolin is assumed to behave in an elasto-plastic manner in accordance with a form of the Modified Cam Clay constitutive law, as described in Chapter 7.

Finite element analyses performed to compare the stresses acting on the model piles in the laboratory apparatus with those which would act on long rigid piles installed in an infinite mass of clay, are first considered. It is shown that for normally-consolidated clays, the laboratory apparatus provides a good approximation to the ideal conditions. Computer predictions are then compared with measurements obtained from the model pile tests, and it is shown that there is very encouraging agreement. It will be recalled that the model tests provide information about the variation, with pile displacement, of the average shear stresses and the radial stresses acting on the model piles; the micro-fabric studies enable the deformations within the clay adjacent to the piles to be recorded.

Predictions of quantities not amenable to measurement during the model pile tests are considered with some confidence and useful information is obtained concerning the load transfer mechanism and the role of the kinematic restraints. In Chapter 9, the finite element analyses are extended to consider the behaviour of displacement piles.

8.2 STRESS CONDITIONS WITHIN THE EXPERIMENTAL APPARATUS

8.2.1 Introduction

The stresses acting within the clay samples during the model pile loading tests are considered, with particular reference to the uniformity of the shear stresses and the radial stresses acting on the pile shafts. The predicted stresses within the test apparatus are compared with those predicted for the ideal case of a short element of a long rigid pile embedded in a clay mass of vast extent, in order to establish how well the model pile tests represent the ideal.

8.2.2 Stress Distribution Around the Model Piles

The predictions presented below were obtained using soil Model 'A' (see Chapter 7), in conjunction with the Finite Element mesh representing the experimental conditions (see Fig. 7.4).

The case of a pile installed in a Kaolin sample normally-consolidated to a stress ratio, K, of 1.5 (σ'_{zo} = 173 kN/m^2 and σ'_{ro} = 260 kN/m^2), and loaded to 85% of the peak load is first considered. The predicted distributions throughout the sample of the shear stress (τ_{rz}), the radial stress (σ'_r) and the axial stress (σ'_z) are presented in Figs. 8.1, 8.2 and 8.3. Within the sample a localised stress concentration is predicted near the toe of the pile, and it may be seen in Fig. 8.3(a) that, as discussed in Chapter 4, the average effective axial stress varies slightly down the length of the pile. This is a consequence of the lack of shear reinforcement on the circumferential boundary of the sample, which means that the pile load is supported in the form of an increase in the axial stress at the base of the sample, and a decrease at the top. Nevertheless, because of the work-hardening, contractant, behaviour of the clay the stresses in the clay close to the pile are remarkably uniform with depth, although it should be noted that the uniformity would not necessarily be expected in tests employing heavily over-consolidated clays.

8.2.3 A Comparison between the Stresses Predicted in the Clay adjacent to an Experimental Model Pile and those adjacent to an Element of a Long Pile installed in Kaolin of Vast Extent

In order to examine how well the experimental apparatus models the idealised situation under consideration, analyses performed using the Finite Element mesh illustrated in Fig. 7.4 are compared with analyses based on the idealised mesh of Fig. 7.3. The predicted radial variations of the stress components σ'_r, σ'_θ, σ'_z and τ_{rz} are compared in Fig. 8.4, for the case of a pile installed in Kaolin normally consolidated to a stress ratio, K, of 0.7, and loaded to 90% of the peak capacity. The close agreement between the two sets of stress predictions close to the pile is most encouraging, as this is the region of greatest importance. At larger distances from the pile there is some discrepancy between the two sets of predictions of τ_{rz} and σ'_z. This is a consequence of the lack of shear restraint on the outer circumferential boundary of the sample in the experimental apparatus. In principle this could be rectified by the provision of shear reinforcement, although the latter was not considered essential for this particular investigation as the

stresses in the clay close to the pile do not appear to be adversely affected by its absence.

8.2.4 Discussion

Examples are presented above of Finite Element analyses performed to investigate how closely the stresses acting on the experimental model piles are likely to approximate the ideal case of a long pile installed in clay of vast extent. It is shown that the stresses acting on the model piles are remarkably uniform with depth, and that the apparatus enables an adequate approximation to the ideal to be obtained. Analyses performed using the idealised mesh are considered in detail below, and comparisons are made between these predictions and the measurements obtained during the experimental investigation.

8.3 EFFECTS OF INITIAL STRESS CONDITIONS ON THE DRAINED LOADING BEHAVIOUR OF PILES

8.3.1 Introduction

The analyses discussed below were performed using the idealised mesh of Fig. 7.3, in conjunction with soil Models A and B to represent the Kaolin employed in the model pile tests. It will be recalled that in Model A the shape of the yield surface in the deviatoric plane is a circle whereas in Model B it is a Mohr-Coulomb hexagon. As discussed in Chapter 7, Model B is considered to represent a closer approximation to the true soil behaviour than Model A. However, the physical interpretation of predictions based on Model A is simpler and so analyses employing both models are presented. It is assumed that prior to pile loading the stresses are uniform throughout the sample, and that the initial principal stresses are in the ratios $\sigma'_r = \sigma'_\theta = K\sigma'_z$. Values of K in the range 0.5 to 2.0 are considered, and in all cases the initial stresses are selected such that the same initial specific volume is always employed.

In section 8.4 predictions based on soil Model B are compared with measurements of stresses obtained during the model tests, and in section 8.6 predictions of deformations within the clay are compared with the results of micro-fabric studies.

8.3.2 Stress Changes Occurring on Drained Loading

The effective stress paths followed by elements of clay adjacent to loaded piles are presented in Figs. 8.5 and 8.6; the pile loadings are

fully drained and a variety of initial stress ratios are considered. The stress paths illustrated in Fig. 8.5 correspond to analyses based on soil Model A, whereas those in Fig. 8.6 correspond to Model B. In both cases the values of J and P' have been normalised by $C_{u,o}$, the undrained shear strength in triaxial compression before pile installation. As the installation technique employed in the model tests caused minimal disturbance, this value of $C_{u,o}$ is also the undrained shear strength prior to loading. The initial specific volumes are selected to be equal in all cases, and so the values of $C_{u,o}$ are equal too (the values of $g(\theta)$ in triaxial compression are the same for both models).

In Fig. 8.5 all of the initial stress states lie on the curve AB which represents the intersection of an undrained plane (constant specific volume) with the Stable State Boundary Surface (S.S.B.S.). Curve AB also represents the effective stress path which would be followed during an undrained test performed on an isotropically normally consolidated sample of clay at the same specific volume. A measure of the initial undrained shear strength is provided by J_A, the value of J at A, the critical state. It is shown in Appendix 7.4 that $C_{u,o}$ and J are related by the expression

$$C_{u,o} = J_A . \cos \theta_A$$

where θ_A is the Lode angle at A.

The conditions illustrated in Fig. 8.6 are rather more complex. The curves BC, BD and BE represent the intersection of an undrained plane with the S.S.B.S. for triaxial compression ($\theta = 30°$), triaxial extension ($\theta = +30°$) and for b = 0.35 ($\theta = - 9.8°$) respectively. As noted in Chapter 7, the Lode angle corresponding to the peak shaft resistance may be calculated from a knowledge of the shape of the plastic potential in the deviatoric plane; in Model A the final Lode angle is 0°, whereas in Model B the value is -9.8°.

For initial stress ratios not exceeding unity, the predicted effective stress paths travel continuously to the left, reaching the critical state after a considerable reduction in the mean effective stress, and a change in the Lode angle. Where the initial stress ratio exceeds unity, the loading is first associated with an increase in the mean effective stress, but this is followed by a considerable reduction as the critical state is approached. It may be recalled that had the clay been modelled as an isotropic elastic material then no decrease in mean effective stress would

have been predicted. It may be of interest to note that as a result of the predicted changes of Lode angle and reduction in mean effective stress on loading, the analyses indicate that even on drained loading the peak shaft resistance will generally not be much greater than, and may indeed be less than, the initial undrained shear strength in triaxial compression; in the case of K = 0.5, and employing soil Model B, the peak shaft resistance is predicted to be 10% less than $C_{u,o}$.

The variation of several components of stress and strain with pile displacement are presented in Figs. 8.7a,b and c and 8.8a,b and c, for an element of clay immediately adjacent to the pile shaft. Figs. 8.7 and 8.8 correspond to initial stress ratios of 0.7 and 1.5 respectively and both analyses are based on soil Model B; equivalent analyses based on Model A exhibited similar trends. Inspection of Figs. 8.7 and 8.8 indicates that in both cases there is a net reduction in the radial effective stress acting on the pile, and that in the initial stages of loading the stress measure, S, remains almost constant with the clay behaving in a predominantly elastic fashion despite the fact that the clay is assumed to be normally-consolidated. In order to sustain the increase in τ_{rz} during the stage of loading considerable rotation of the principal stresses occurs (ψ is the inclination of the major principal stress with respect to the vertical direction). As a result of the assumptions incorporated into the soil model, the major principal stress is inclined at 45° to the vertical when peak conditions are achieved, and the final radial stress (σ'_r) and the axial stress (σ'_z) are equal. As discussed in Chapter 7, the maximum value of the ratio (τ_{rz}/σ'_r) is sin ϕ', where ϕ' is the angle of shearing resistance of the clay corresponding to the final Lode angle. These points are illustrated in Fig. 8.9 which represents a Mohr's circle of stresses in the r-z plane, at peak conditions. Stress characteristic directions are indicated in this figure, and are discussed in some detail in section 8.6.4. Additional aspects of the stress changes occurring during drained pile loading are examined below in section 8.4, where the predictions are compared with experimental results.

8.4 COMPARISON BETWEEN THEORETICAL PREDICTIONS OF STRESS CHANGES AND EXPERIMENTAL RESULTS

8.4.1 Introduction

The analyses employing Modified Cam Clay as the constitutive law treat the clay as a continuum, and peak conditions are assumed to coincide with the critical state. Micro-fabric studies (see Chapter 6) suggest that

the shear strains in the clay adjacent to a pile loaded almost to peak conditions are very high, and that the effect of these shear strains is to cause the clay particles to become aligned sub-parallel to the direction of shear. As a result the peak mobilized angle of shaft friction decreases with continuing pile displacement until eventually residual conditions are achieved. Although the theoretical analyses presented below predict very high local shear strains (see Figs. 8.7(a) and 8.8(a) for instance) the constitutive models are unable to consider the above form of displacement-softening behaviour, with the result that only the pre-peak behaviour of the piles is analysed.

8.4.2 Comparison between Predicted and Observed Pile Loading Behaviour

Measurements of the variation of the average shear stress and the radial stress acting on the shaft of a pile during a model test (No. 15) are compared with the corresponding computer predictions in Figs. 8.10 and 8.11. For the purposes of the Finite Element analysis, the initial stress ratio is taken to be unity and soil Model B is adopted.

In Fig. 8.10 it may be seen that the predicted and observed variations of the mean shear stress acting on the pile, with pile displacement, are in good agreement. Similarly, in Fig. 8.11, it is evident that the analysis predicts similar decreases in the radial effective stress to those measured during the test. Such agreement is very encouraging, especially as only one soil parameter (the elastic shear modulus G) of the seven employed was selected with reference to other pile test results. A parametric study was performed to examine the influence on pile loading behaviour of the various soil parameters. For the sake of brevity these results are not included here, particularly as they are similar to those obtained in the course of a comparable study performed in relation to displacement piles. Results of this second parametric study are presented in Chapter 9.

8.4.3 Conditions obtaining at Peak Load

8.4.3.1 Angle of Shaft Resistance

As a direct consequence of the assumptions inherent in the soil models employed, and of the boundary conditions at the pile face, the peak mobilized angle of shaft resistance is predicted to be $\tan^{-1}(\sin \phi')$, irrespective of the initial stress ratio (as discussed in Chapter 7). This prediction is in agreement with the results of the model pile tests conducted

on piles installed with minimal disturbance. The angle of shaft resistance derived from the model tests is 22°, which compares with a predicted value of about 21°, (taking $\phi' = 23°$).

8.4.3.2 Changes in the Radial Effective Stress

Fig. 8.12 presents a comparison between theoretically and experimentally deduced variations of the radial effective stress at peak (expressed as a percentage of the initial value) with initial stress ratio. The observed tendency for the greater reductions in radial effective stress to occur in the tests with the larger initial stress ratios is correctly predicted, although in general the predictions tend to under estimate the final radial stresses.

8.4.4 A Comparison between the observed Pile Capacities and Predictions based on Conventional Pile Design Methods

The commonly adopted practice for the design of piles is to relate the unit shaft resistance to the undrained shear strength, in triaxial compression, of the clay prior to pile installation, by means of the empirical relation (Skempton, 1959)

$$\tau_{max} = \alpha \cdot c_{u,o}$$

Results from the numerical analyses have been used to establish equivalent α values corresponding to the model test conditions. The predicted α values, and those derived from the experimental results, are presented in Fig. 8.13. For the stress ratios employed in the tests, the α values are successfully predicted as being in excess of unity, although the predictions underestimate the experimental values. One reason for this difference may be that in these analyses ϕ' is assumed to be independent of Lodes' angle whereas for Kaolin, ϕ' (plane strain) is greater than ϕ' (triaxial compression) by between 1° and 2°.

The effective stress approach to pile design suggested by Chandler (1968) and by Burland (1973) is based on the equation

$$\tau_{max} = \sigma'_r \cdot \tan \delta' + C'_a$$

The value of the adhesion intercept, C'_a is generally taken to be zero on account of the remoulding assumed to occur during pile installation. As a first approximation both authors assumed that the radial effective stress at peak load is equal to the initial value prior to pile installation

($\sigma_{r,o}'$) and δ' was taken to be ϕ' (triaxial compression). The predicted variations of the ratio ($\tau_{max}/\sigma'_{r,o} \cdot \tan\phi'$) with initial stress ratio, K, is shown in Fig. 8.14, together with the results from the experimental investigation. In the present case C_a' is taken to be zero because the Kaolin is normally consolidated. It is seen that the simple effective stress design method over estimates the pile capacities, whereas the Finite Element analyses tend to slightly under-predict the observed results. The latter is a result of both the earlier mentioned under estimation of the radial stresses acting at peak, and the assumption that ϕ' (plane strain) is equal to ϕ'(triaxial compression). This point is illustrated in Fig. 8.14 in which an additional prediction based on ϕ' being 25° is included; the radial stress is assumed to be equal to that predicted by the original analysis (using soil Model B).

8.4.5 Comments

The analyses presented above employing a form of the Modified Cam Clay constitutive law to model the soil behaviour have provided predictions which are in encouraging agreement with results from the model pile tests.

Assumptions embodied in the constitutive model led directly to the prediction that the peak mobilized angle of shaft resistance around piles installed with minimal disturbance into normally-consolidated clay is independent of the initial stress conditions and is given by $\delta' = \tan^{-1}(\sin\phi')$. This predicts that $\delta'_{max} = 21.3°$, which compares with $\delta' \cong 22°$ derived from the experimental data.

The predicted variation of the radial stress acting on a pile shaft, with pile displacement, (for K = 1.0) is in good agreement with measurements. The analyses also predict the observed result that, within the range of stress ratios covered by the model tests, the reduction in the radial stress on loading to peak increases with increasing initial stress ratio. However, the analyses tend to over estimate the reductions and hence to under estimate the pile capacities.

The analyses illustrate that on drained loading the clay adjacent to the pile consolidates with the result that the predicted α values are in excess of unity; however, they are smaller than the values established experimentally. The soil model employed is not able to predict displacement-softening caused by particle orientation effects and so only the pre-peak pile behaviour is modelled.

In the following sections, the deformations within the clay are considered, and comparisons are made with the results derived from the micro-fabric studies.

8.5 DEFORMATION BEHAVIOUR OF THE SOIL SURROUNDING LOADED PILES

8.5.1 Kinematic Restraints

The behaviour of the soil close to the pile shaft is dominated by the local kinematic restraints. It is assumed that there is no relative slip between the pile and the clay, which implies that the total axial strain (ε_z^T) in the soil adjacent to the pile is the same as that of the pile itself (i.e. zero if the pile is rigid). In the analyses of the behaviour of a short section of an infinitely long pile, symmetry dictates that the total axial strain at any radius is zero.

The pile is assumed to be rigid radially which implies that the radial displacement of the soil at the interface ($u(r = r_o)$) is always zero, which in turn implies that the local total hoop strain $\{\varepsilon_\theta^{T_o} = u/r\}_{r=r_o}$ is zero too. The restraints on the local radial strains $\{\varepsilon_r^T = \frac{du}{dr}\Big|_{r=r_o}\}$ and the radial stresses are determined by the behaviour of the surrounding soil.

On loading a pile, the surrounding soil is subject to increased shear strains. The normally consolidated clay considered here typically responds by exhibiting plastic compressive volumetric strains; the magnitudes of the individual components of plastic strain increment depend on the current stress state and the shape of the plastic potential. In order to satisfy the kinematic restraints compensating elastic strains are generally required which, in the case of normally-consolidated clay necessitate the changes in the mean effective stress (P') discussed earlier. This process has analogies with the compensating elastic strains (with associated changes in the mean effective stress) required during the undrained shearing of normally consolidated clays.

The deformation behaviour of clay surrounding loaded piles is considered in more detail below.

8.5.2 Strains within the Clay Adjacent to a Loaded Pile

The behaviour of an element of clay adjacent to a pile installed in Kaolin normally-consolidated to a stress ratio, K, of 1.5 is considered. The analysis is based on the Finite Element mesh illustrated in Fig. 7.3, in conjunction with soil Model B.

Fig. 8.15 represents the predicted variation of the shear stress, τ_{rz} (normalised by the initial undrained shear strength in triaxial compression, $c_{u,o}$) and the shear strain, γ_{rz}, with pile displacement. It may be seen that initially the shear strains are almost entirely elastic, whereas at a later stage of loading (i.e. increment 11) the shear strains are predominantly plastic in nature.

Fig. 8.16 illustrates the Mohr's circles of total, plastic and elastic strain increments in the r-z plane as a result of the first increment of pile displacement. The major principal stress is still almost horizontal, and the plastic strain increments are very much smaller than the elastic components. In this and the subsequent figures, the magnitudes of the strain increments have all been arbitrarily normalised by the half of the current elastic shear strain increment ($\dot{\gamma}^{e}_{rz}/2$) in order to facilitate comparison. It may be noted that the axial total strain increment $\dot{\varepsilon}^{T}_{z}$ is zero as required by the boundary conditions.

The strain increments corresponding to a shaft resistance of 40% of the peak value (increment 6) are illustrated in Fig. 8.17. The major principal stress is predicted to have rotated through 21° in total and at this stage the elastic and plastic components of strain increment are of similar magnitude. It may be seen that the elastic and plastic components of axial strain increment are equal in magnitude and opposite in sign, as dictated by the kinematic restraints. The total radial strain increment, on the other hand, is compressive. The planes of zero extension (both plastic and total) are illustrated in Fig. 8.17. The velocity characteristics are normal to the planes of zero plastic extension.

Once 70% of the shaft capacity has been mobilized (increment 11), at a displacement of 2.4% of the pile radius, the shear strains are predominantly plastic. The strain increments are illustrated in Fig. 8.18, where it may be seen that the elastic strain increments are very small compared with the plastic components. The major principal stress is predicted to have rotated through 40° of the eventual 45°. The velocity characteristics α and β are inclined at 11.4° above, and 90.1° below the horizontal.

Thus, in the early stages of loading (up to 20% of the peak shaft resistance) the soil behaviour is predominantly elastic. From this stage until 70% of the peak load is mobilized the elastic and plastic shear strains are of comparable magnitude. Eventually as the Lode angle approaches its

ultimate value, the plastic strain increments conform more closely to the kinematic restraints and the magnitudes of the required compensating elastic strain increments become smaller. It may be of interest to note that at peak shaft capacity, the accumulated total radial strain within the clay at the pile face is 2.7% (compressive).

Although only the results from the analysis corresponding to K = 1.5 are presented here, similar overall behaviour is predicted in analyses starting with different initial stress ratios.

8.5.3 Radial Distribution of Shear Strains and Axial Displacements

The radial distribution of the total shear strain, γ^T_{rz}, is first considered for the case of a loaded pile installed in initially isotropically normally-consolidated Kaolin. Once again, the analysis is performed using soil Model B. Fig. 8.19 presents the predicted radial variations of γ^T_{rz} corresponding to various stages in the pile loading. It will be seen that as the ultimate unit shaft resistance is approached, very large shear strains are predicted in the immediate vicinity of the pile shaft. These strains are, however, very localised and at a distance of one pile radius from the shaft the shear strains are typically less than 10% of the peak value, whereas the shear stress has only decreased by 50%. At distances greater than about one pile radius from the shaft, the shear strains remain predominantly elastic throughout the pile loading.

The curve labelled 'c' in Fig. 8.19 corresponds to a pile load of 85% of the ultimate value, and a displacement of 5.6% of one pile radius. The equivalent shear strain distribution for an isotropic linear elastic material around a pile at the same load and displacement is included for comparison.

In order to examine the influence of the initial stress ratio on the deformation behaviour of the clay beside a loaded pile, three examples corresponding to initial stress ratios of 0.7, 1.0 and 1.5 are compared. The predicted radial distributions of the shear strains, γ^T_{rz}, are shown in Fig. 8.20; the piles are at their ultimate capacities and have a common displacement. The distributions are very similar, although the shear strains around the pile in initially isotropically consolidated clay are somewhat less localised.

The corresponding predictions of the axial displacements within the clay around the piles are illustrated in Fig. 8.21. In section 8.6 these

predictions are compared with the deformations measured (in the course of the micro-fabric studies) around the experimental model piles.

8.5.4 Zero Extension Lines

In order to examine an hypothesis that the Riedel structures (S_2) observed around the models piles (Chapter 6) are velocity characteristics, the predicted directions of zero plastic and zero total extension are considered.

In section 8.5.2, Mohr's circles of elastic, plastic and total strain increments were discussed for the various stages in the loading of a pile installed in Kaolin normally-consolidated to a stress ratio, K, of 1.5. The planes of zero extension are illustrated in Figs. 8.17 and 8.18; lines of zero extension are normal to the indicated planes. Velocity characteristics are lines of zero plastic extension and lie at angles of $\pm(45\text{-}v/2)°$ to the direction of the major principal strain increment: the angle of dilation, v, is defined as $v = -\sin^{-1}((\dot{\varepsilon}_1 + \dot{\varepsilon}_3)/\dot{\varepsilon}_1 - \dot{\varepsilon}_3))$ after Bent Hansen (1958), (employing the compression positive convention). As coincidence of the axes of stress and of plastic strain increment is assumed, the velocity characteristics lie at $\psi \pm(45\text{-}v/2)°$ to the vertical.

The initial inclination of the velocity characteristics in the clay adjacent to a loaded pile depends on the ratio of the horizontal to vertical effective stresses to which the clay has been consolidated. Eventually, however, as the critical state is approached, the direction of the major principal strain rate is constrained by the boundary conditions to lie at 45° to the downward vertical, and the angle of dilation tends towards zero. By this stage the two velocity characteristic directions are parallel to, and normal to, the pile axis.

An example of the predicted variation of the velocity characteristic directions with increasing pile load is presented in Fig. 8.22, for Kaolin normally consolidated to an initial stress ratio of 1.5. Mohr's circles of strain increments during the pile loading are considered in section 8.5.2. Once the pile load exceeds about 65% of its ultimate value (at a displacement of 2% of one pile radius), the α velocity characteristics may be seen to lie almost parallel to the pile axis. The predicted radial distribution of velocity characteristic directions, corresponding to the ultimate pile load, is presented in Fig. 8.23. The α characteristics may be seen to remain almost vertical to a distance of more than one pile radius from the shaft. As only the α characteristics may reasonably be compared with the Riedel (S_2)

directions (it may be recalled that these structures are associated with peak conditions and propagate at angles of between 10° and 15° to the pile axis), it would appear that the Riedels do not correspond to velocity characteristics. The nature of the Riedel structures is considered further in section 8.6, below.

8.6 COMPARISON BETWEEN THE PREDICTED SOIL DEFORMATION BEHAVIOUR ADJACENT TO LOADED PILES, AND OBSERVATIONS OBTAINED BY MEANS OF MICRO-FABRIC STUDIES

8.6.1 Introduction

Clay deformations observed with the aid of micro-fabric studies represent the plastic (or permanent) components of deformation. In order to compare theoretical predictions with observations, it is therefore necessary to consider the predicted plastic components of deformation rather than the total values.

There are three major features observed in the course of the micro-fabric studies with which theoretical predictions may be compared;

(i) close to the pile the plastic shear strains are extremely large, leading eventually to the formation of a continuous displacement discontinuity surface, S_4, running parallel to the pile shaft;

(ii) the observed distortions of the original bedding fabric, S_1, close to the pile give good indications of the radial variation of the plastic axial displacements within the clay. A variety of initial stress conditions may be considered;

(iii) the Riedel, S_2, shear structures are straight and propagate typically at angles of between 10° and 15° to the pile axis, irrespective of the initial stress ratio within the clay. However, the radial distance from the pile to which the Riedel structures propagate increases with increasing initial stress ratio.

It should be appreciated that the comparisons proposed above represent a severe test of the relatively simple constitutive law which assumes the clay to behave as a continuum. It may, therefore, be more reasonable to expect agreement between trends in behaviour, rather than

between absolute values. The three main features of the micro-fabric observations are now considered in turn.

8.6.2 Shear Strains in the Clay Adjacent to Loaded Piles

It has been shown in Chapter 6 that as a pile installed with minimal disturbance is loaded to peak conditions, the local shear strains beside the pile become very large. With increasing pile displacement, further clay deformations are concentrated into a narrow zone beside the pile. Eventually a continuous displacement discontinuity is formed along which the clay particles are strongly oriented, and the strength falls towards a residual value.

Fig. 8.20 represents the predicted radial distributions of shear strain beside three piles installed in clay consolidated to different initial stress ratios. It will be seen that the shear strains close to the pile are very large and increase rapidly with additional pile displacement. As the constitutive model for the clay does not incorporate any allowance for strain softening no post-peak brittleness is predicted. However, it is evident that if the model were to incorporate even very gradual strain softening, then the post-peak brittleness could be predicted.

8.6.3 Radial Distribution of Axial Displacements

The permanent axial deformations within the clay may be estimated from the thin sections by observing the distorted profiles of the originally straight bedding planes; examples are presented in Figs. 6.8, 6.12 and 6.15. Fig. 6.15 compares the permanent deformations around three piles installed in Kaolin normally consolidated to initial stress ratio of 0.74, 1.11 and 1.5, and loaded to residual conditions. The axial deformation patterns within the clay beyond the residual surfaces are similar in all three cases, although the deformations around the pile in Test 14 ($K = 1.11$) are the least localised. The permanent deformations around the piles do not extend beyond four millimeters (or just over one pile radius) from the shaft, unless the particular bedding plane considered is intersected by a Kink band in which case the local deformation pattern is distorted (see Fig. 6.12 for instance).

The predicted soil deformation patterns around piles installed in Kaolin normally consolidated to stress ratios of 0.7, 1.0 and 1.5 are illustrated in Figs. 8.21(a),(b) and (c); pile displacements are common

and have a value of 2.4 millimeters. In each of the above figures the observed deformations are also indicated for comparison. It will be seen that there is very encouraging agreement between the predictions and the observations.

8.6.4 Riedel Structures

Thin section analyses (Chapter 6) showed that if local deviations within Kink bands are ignored, the Riedel structures, S_2, propagate at an almost constant angle, typically between 10° and 15°, to the pile axis. This angle does not appear to vary appreciably with radial distance from the pile shaft (see Fig. 6.16 for example), and is also virtually independent of the initial stress ratio within the soil. On the other hand, the radial extent of the structures is sensitive to the initial stress ratio; for instance it may be seen in Fig. 6.17 that Riedel structures only penetrated two millimeters beyond the pile in Kaolin consolidated to a stress ratio of 0.7, whereas they propagated to a distance of more than five millimeters from the piles installed in Kaolin consolidated to a stress ratio of 1.5 (see Fig. 6.5).

Before attempting to predict the inclinations and penetrations of the Riedel structures, it is first necessary to identify the structures in terms of either stresses or strains that can be predicted by the computer analyses. Two simple hypotheses are that the Riedel structures may be identified with either velocity or stress characteristics. The former hypothesis was examined in section 8.5.4 where it was shown that the Riedel structures are not the same as velocity characteristics. The possibility that the Riedels may be equivalent to stress characteristics is now examined.

The relationship between the inclinations of stress characteristics and the principal stresses is illustrated in Fig. 8.9. The stress characteristics are inclined at $\psi \pm (45\text{-}\phi'_c/2)$ to the vertical, where ψ is the inclination to the vertical of the major principal stress, and ϕ'_c is the current mobilised angle of shearing resistance. The predicted variation of the inclinations of the two stress characteristics, α and β, and the major principal stress, ψ, with pile displacement are presented in Fig. 8.24 for an element of clay adjacent to a pile installed in Kaolin consolidated to an initial stress ratio of 1.5. It may be seen that the α characteristic (which bears the greater similarity to the Riedel structures) rotates rapidly with pile displacement from an initial inclination of around 50° to the

vertical to a final value of 11.5°; this final value is achieved once the pile load exceeds some 65% of its ultimate value. It may be noted that the final inclinations of the α characteristics are always 11.5°, irrespective of the initial stress ratio because the final value of ψ is always 45° and $\alpha° = \psi - (45-\phi'/2) = \phi'/2 = 11.5°$. The above arguments lend support to the hypothesis that the Riedel structures coincide with stress characteristics.

The next task is to examine the predicted radial variation of the stress characteristic directions. Fig. 8.25 illustrates the angle of inclination of the α stress characteristics around three piles (K = 0.7, 1.0 and 1.5) as a function of the radial distance from the piles. The piles are each considered at their ultimate loads, and it may be seen that in all cases the inclinations of the characteristics are almost constant to a distance of nearly one-half of a pile radius from the shaft. This prediction is consistent with the observations that the Riedel structures are more or less straight (in the vertical plane).

Finally the penetration of the Riedel structures is briefly considered. The first obvious constraint is the rapid radial variation of the level of deviatioric stress. Fig. 8.26 illustrates the predicted radial variation of the invariant stress measure, S. It will be seen that S decreases rapidly from unity at the face of each of the piles to around 0.5 at a distance of one pile radius from the shafts. It seems probable that the maximum Riedel penetration will be limited to about one pile radius. Fig. 8.25 presents the predicted radial variation of the α stress characteristic inclinations, corresponding to the three initial stress ratios considered above. Although the observed Riedel penetrations are not predicted it will be seen that in the example corresponding to K = 0.7, the α characteristics become vertical (and hence non-penetrative) at a distance of less than one pile radius from the shaft. It is probably not worth pursuing the analogy between stress characteristics and Riedel structures any further. However, it is believed that the adoption of this hypothesis has been of assistance in explaining some of the features observed during the micro-fabric studies.

8.7 DISCUSSION OF THE WORK RELATED TO NON-DISPLACEMENT PILES

8.7.1 Introduction

The behaviour of the soil surrounding loaded piles is subject to severe kinematic constraints. The effects of the constraints are not well understood, and for this reason three independent, although complementary, approaches have been adopted;

(i) drained tests conducted on model piles installed with minimal disturance into normally-consolidated Kaolin;

(ii) micro-fabric studies following these tests;

(iii) finite element analyses based on elasto-plastic constitutive laws to model the clay.

The results from these approaches have been presented above, and the inter-relationships between them are now considered in pairs and are summarised in Table 8.1. The intention behind the experimental work has been to provide a wide variety of data against which to compare theoretical predictions. If analyses are developed that are capable of correctly predicting quantitites which can be measured and observed, then presumably simultaneous predictions of quantities less amenable to measurement are likely to be fairly reliable. The analyses may similarly be extended with some confidence to consider related problems such as the behaviour on undrained pile loading.

8.7.2 Model Pile Tests and Micro-fabric Results

As far as direct interpretation of model test results is concerned, the most important result from the micro-fabric studies is that the shear strains in the soil beside the pile become very large and that eventually a smooth continuous displacement shear, S_4, (along which the clay particles are strongly aligned) is formed adjacent to the pile shaft. These results suggest that particle orientation effects are largely, if not entirely, responsible for the measured post-peak brittleness.

The observation that the inclination of the Riedel structures is largely independent of the initial stress ratio suggests a connection with the result that the peak angle of shaft friction also appears to be independent of the initial stress ratio.

The micro-fabric studies confirmed that the idealised pile installation procedure did, in fact, cause negligible fabric disturbance.

8.7.3 Model Pile Tests and Theoretical Predictions

It has been shown in section 8.4 that the theoretical analyses employing a form of Modified Cam Clay as the soil constitutive law are capable of predicting the main features of the pre-peak behaviour observed during the model pile tests. These are

(i) the peak angle of shaft friction (δ') is independent of the initial stress ratio;

(ii) the radial effective stress acting on a pile varies during loading. The predicted variation of radial stress with pile displacement is in reasonable agreement with measurements, and the observed tendency for the reduction in radial stress during pile loading to increase with increasing initial stress ratio is also predicted;

(iii) the α values corresponding to peak load are successfully predicted to be in excess of unity, although the strength is underestimated.

8.7.4 Micro-fabric Studies and Theoretical Predictions

As remarked above, the constitutive law employed is incapable of considering strain softening at critical state conditions, and so the existence of the continuous displacement surface could not be predicted. However, the analyses did predict very large shear strains in the soil adjacent to the pile as peak conditions were approached. It was successfully predicted that at peak conditions, the deflected form of originally horizontal planes is largely independent of the initial stress conditions.

The hypothesis that the Riedel structures are similar to stress characteristics is supported by the theoretical prediction that at peak pile load, the α stress characteristics lie at an angle of $11\frac{1}{2}°$ to the vertical, this value being independent of the initial stress ratio. The analyses also indicate that this inclination remains constant for a distance of nearly one-half of a pile radius from the shaft; this is consistent with the observation that the Riedel structures are almost straight in the vertical plane, and lie at angles of between 10° and 15° to the vertical.

8.7.5 Conclusions

It has been shown that finite element analyses employing a form of Modified Cam Clay as the constitutive law, are capable of predicting main features observed during the experimental investigation. Having illustrated the validity of the theoretical approach in the analysis of a relatively simple problem, one may have some confidence in extending the scope of the analysis to consider undrained pile loading, and also the behaviour of displacement piles.

8.8 UNDRAINED LOADING OF PILES

8.8.1 Introduction

The analyses presented above have shown that the use of a form of the Modified Cam Clay constitutive law can lead to good agreement between the theoretical predictions and experimental results, for drained pile loadings. The theoretical analyses are now extended to consider the soil response to undrained pile loading. No attempt was made to perform undrained pile loading tests in the laboratory (this would have necessitated loading the piles to peak load within a few seconds), and so there are no experimental data to compare against the computer predictions.

8.8.2 Undrained Loading

In order to investigate the soil response to rapid pile loading the parametric study to consider the effects of the initial stress ratio has been repeated, enforcing undrained (almost constant volume) conditions. The total and effective stress paths (for an element of soil adjacent to the pile shaft) derived from this study are shown in Figs. 8.27 and 8.28). The results presented in Fig. 8.27 are based on the assumption that the shapes of both the yield function and plastic potential surfaces are circular in the deviatoric plane (i.e. soil Model A), whereas the predictions in Fig. 8.28 are based on the assumption of a constant value for ϕ' and with $b = 0.35$ imposed at peak conditions. In both cases the initial effective stresses prior to pile loading are consistent with the specific volume employed in the investigation of drained loadings. Because the yield surfaces in Models A and B are coincident at triaxial compression, the initial undrained shear strengths in triaxial compression are also equal.

In Fig. 8.27 the portions of the curve BA to the left of each of the initial stress states represents the effective stress paths followed.

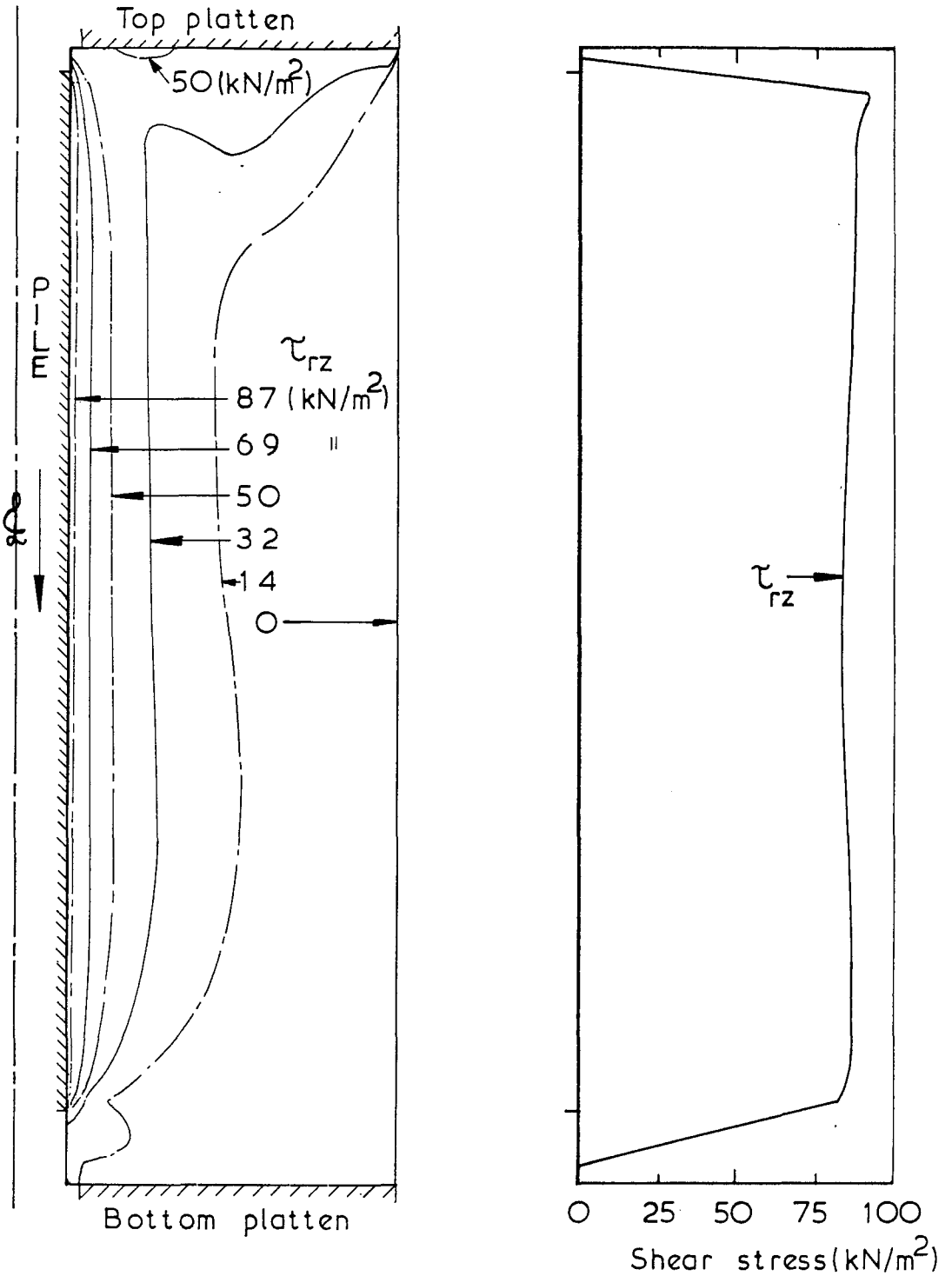
The pore pressures generated during the loading are represented by the horizontal distances between the effective and total stress paths. The greatest pore pressure generation is predicted in the case of initially isotropic clay, whereas negative pore pressures are predicted around a pile installed in clay consolidated to a stress ratio of 0.5.

The adoption of a Mohr Coulomb hexagon for the shape of the yield surface in the deviatoric plane has the effect of making interpretation less straightforward because the effective stress paths now depend on the initial stress ratio ($g(\theta)$ now changes during the loading, whereas a constant value was adopted in soil Model A). The greater complexity may be seen in Fig. 8.28, where the effective stress paths are represented by solid lines, and the total stress paths by dashed lines. When the initial stress ratio (K) exceeds unity, the mean total stress increases initially and is accompanied by a large localised excess pore pressure. In the cases where the initial stress ratio is less than unity the total stress path travels continuously in the direction of decreasing mean stress. It may be seen in Fig. 8.28 that when the initial stress ratio is 0.7, small negative pore pressures are generated initially, but net positive pore pressures are predicted at peak load. However, in the case of the initial stress ratio having a value of 0.5, substantial negative pore pressures ($-0.34\ C_{u,0}$) still remain at peak. The prediction of negative pore pressures during the shearing of a normally consolidated clay may at first seem rather surprising. It is, however, a direct consequence of the kinematic boundary conditions of the problem which, in conjunction with a realistic constitutive soil model, causes a reduction in the total mean stress that outweighs any pore pressures generated as a result of shear alone.

When the initial stress ratio is unity, the predicted total stress path remains almost vertical and this condition leads to the prediction of the greatest excess pore pressures beside the pile. In Fig. 8.29 the predicted radial distribution of excess pore pressures is illustrated for four stages during the pile loading. The results indicate that the generation of excess pore pressures beside the pile is small (less than 20% of the peak value) until about 50% of the pile capacity is mobilised, and even at peak load the pore pressures are fairly localised, having decreased to less than 10% of the peak value at a distance of one pile diameter from the shaft. This suggests that the excess pore pressures would tend to dissipate rapidly; the dissipation of excess pore pressures around the model piles is considered in Appendix 4.3, employing the finite difference program described in Appendix 9.1.

Table 8.1: Interrelationship between the Results of Experimental and Theoretical Approaches to examining the Pile Load-Transfer Mechanism

Source of Experimental Data		Theoretical Approach
Model Pile Loading Tests (Piles installed with minimal disturbance)	Micro-fabric Studies	Finite element analyses (assuming the clay to obey a form of elasto-plastic constitutive law).
1. (a) $\delta'_{Peak} \neq f(K)$		Predicted as a consequence of the constitutive law.
(b) $\delta' = 22°$ ($\phi' = 23°$)		$\delta' = \sin^{-1}(\tan\phi') = 21°$
2. Radial effective stress decreases during loading		Predicted as a consequence of compensating elastic strains required to conform with the kinematic boundary conditions.
3. $1.6 > \alpha_{peak} > 1$ ($1.5 \geq K \geq 0.74$)	Negligible micro-fabric disturbance on installation	Predicted $\alpha > 1$ for drained pile loadings.
4. Shapes of the load-displacement curves		
(a) Pre-peak		Reasonably well predicted
(b) Post-peak softening	The result of particle orientation effects caused by the very high local shear strains.	Analyses predict very high local shear strains but are incapable of predicting strain softening.
(c) Residual conditions	Eventual formation of a continuous displacement discontinuity, S_4, along which the clay particles are strongly oriented.	
5.	Deflected form of bedding planes only slightly dependent on K	The deformed shapes are well predicted.
6.	Riedel structures are straight (in the vertical plane) and lie at angles of between 10° and 15° to the pile axis, independently of K.	Analyses support the hypothesis that Riedels are similar to stress characteristics.

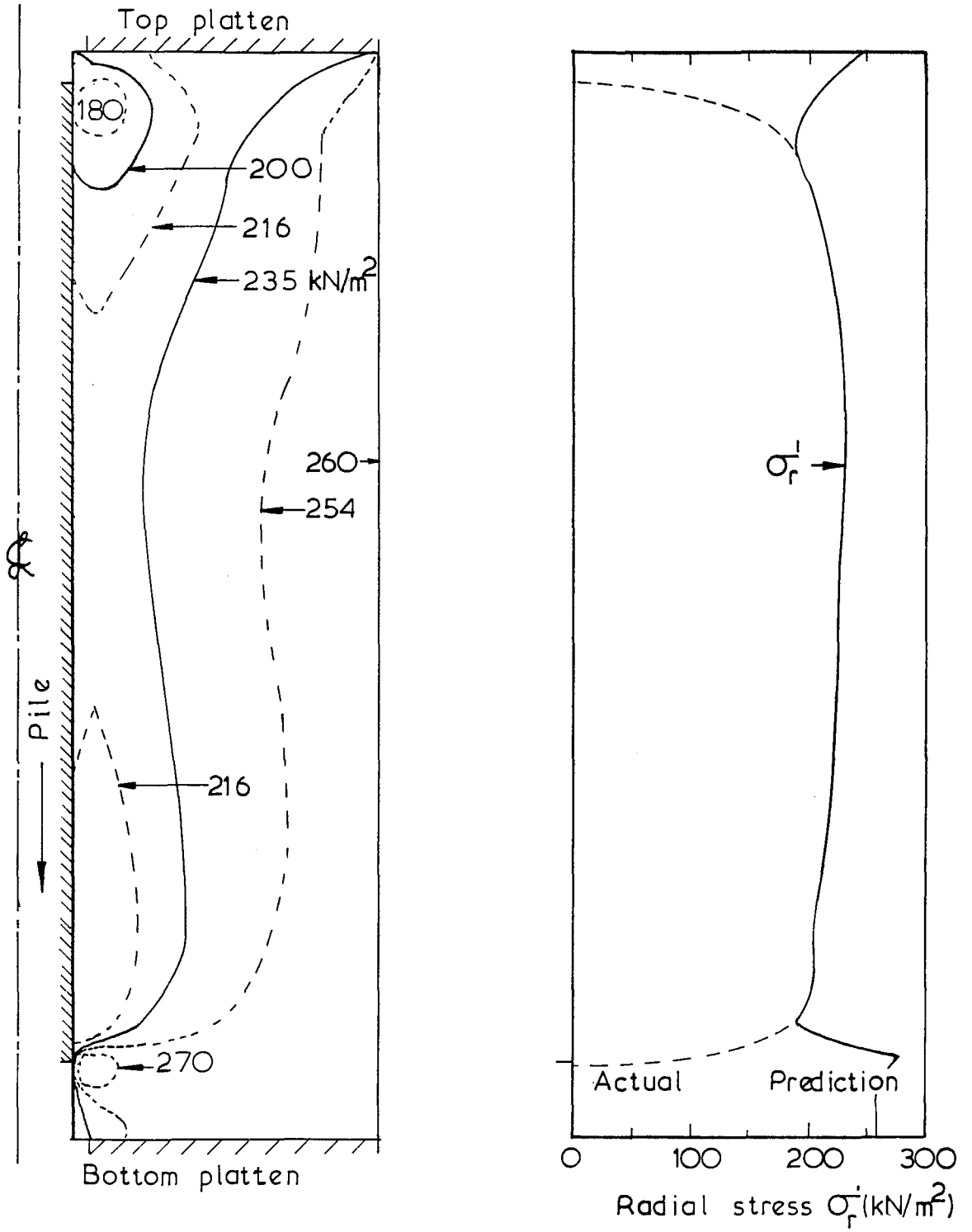


(a) Contours of shear stress τ_{rz}

(b) Variation of shear stress τ_{rz} down the length of the pile

Distribution of the shear stress (τ_{rz}) within a kaolin sample surrounding a model pile subjected to 85% of the peak load. Initial consolidation stress ratio K=1·5

Fig. 8·1

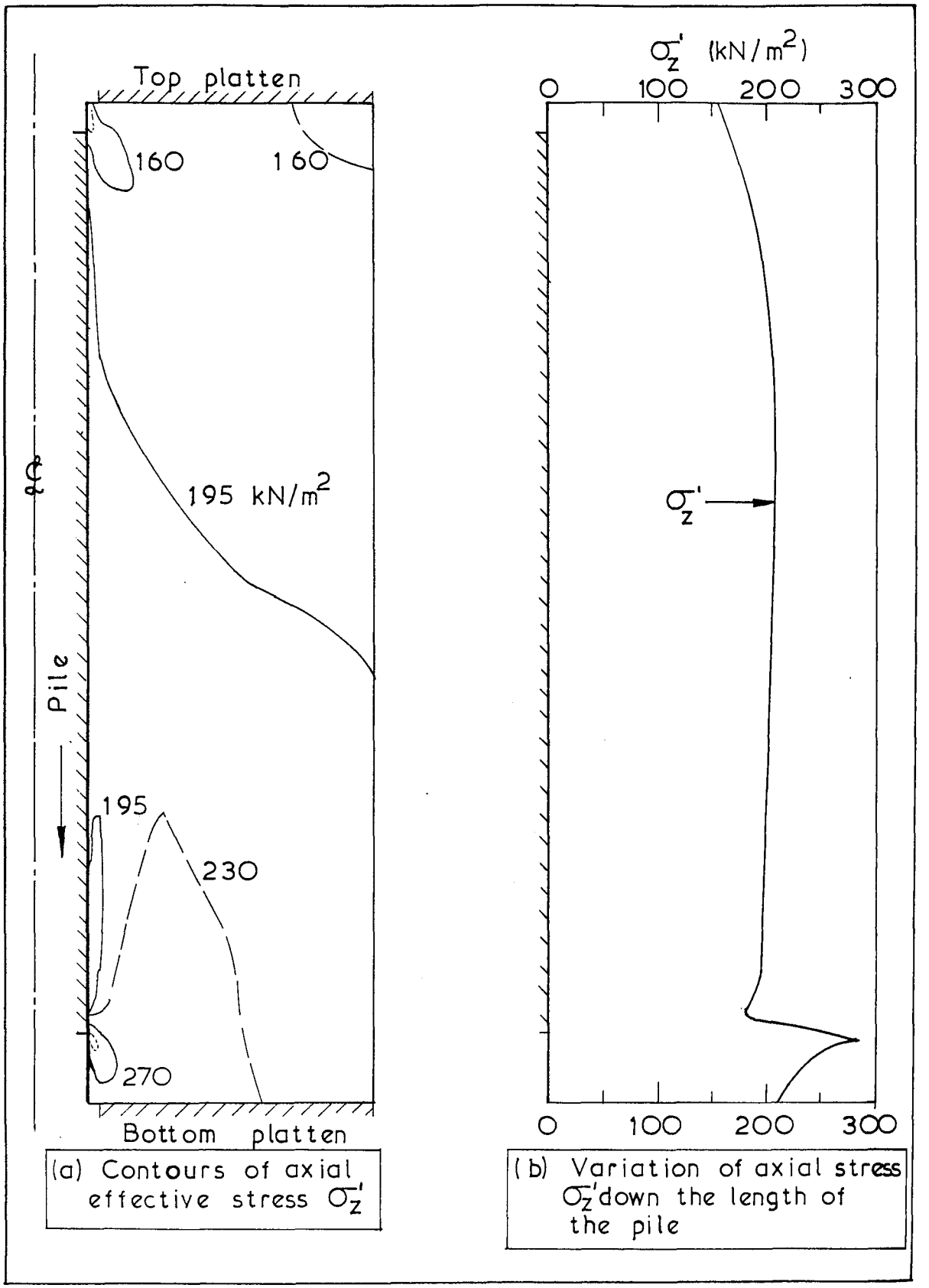


(a) Contours of radial effective stress

(b) Variation of radial effective stress down the length of the pile.

Distribution of radial effective stress within a kaolin sample surrounding a model pile. Pile load is 85% of peak. Initial consolidation stress ratio K=1·5.

Fig. 8·2



Distribution of axial effective stress within the kaolin sample. Pile load is 85% of peak. Initial stress ratio K=1·5

Fig. 8·3

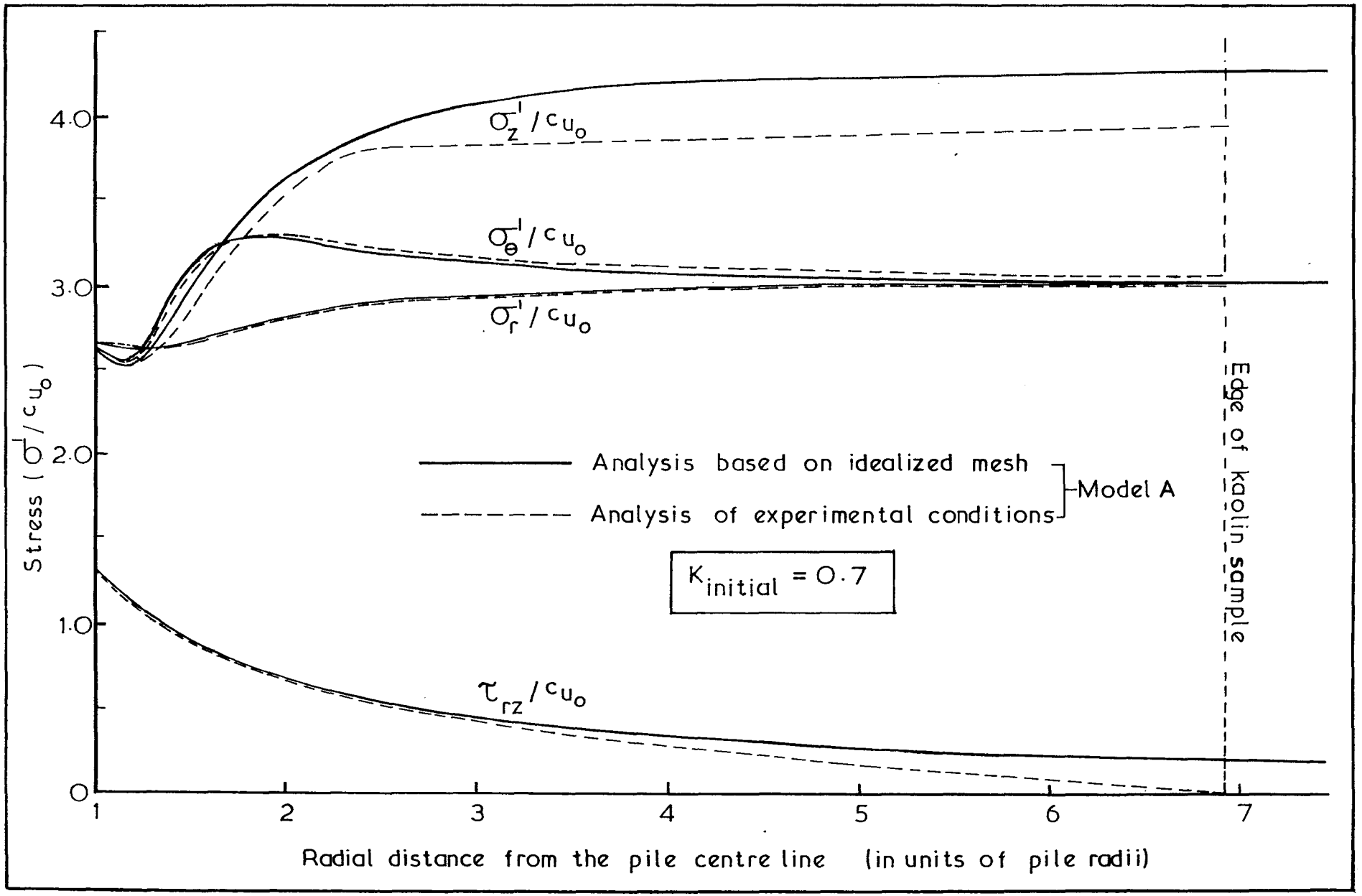
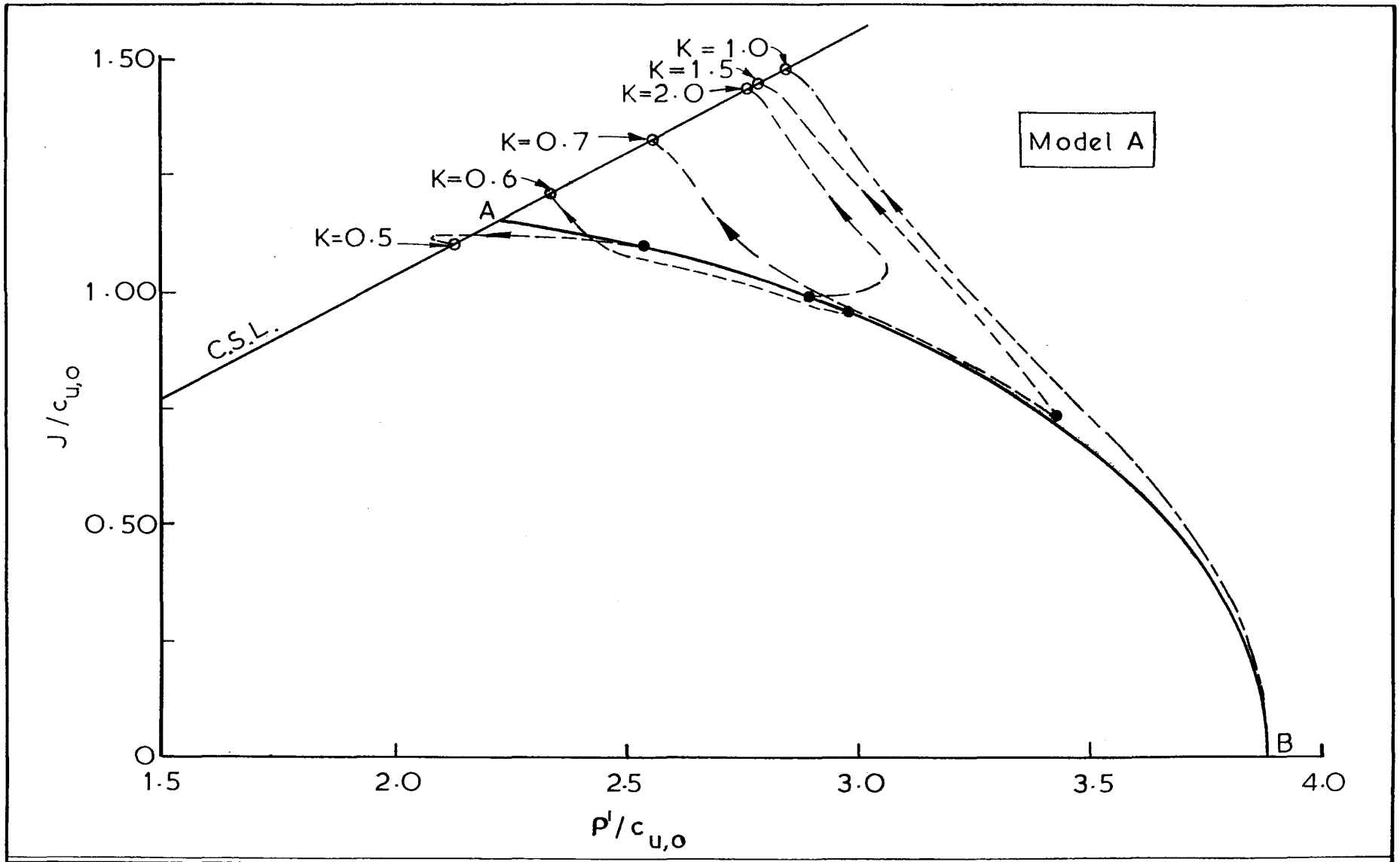
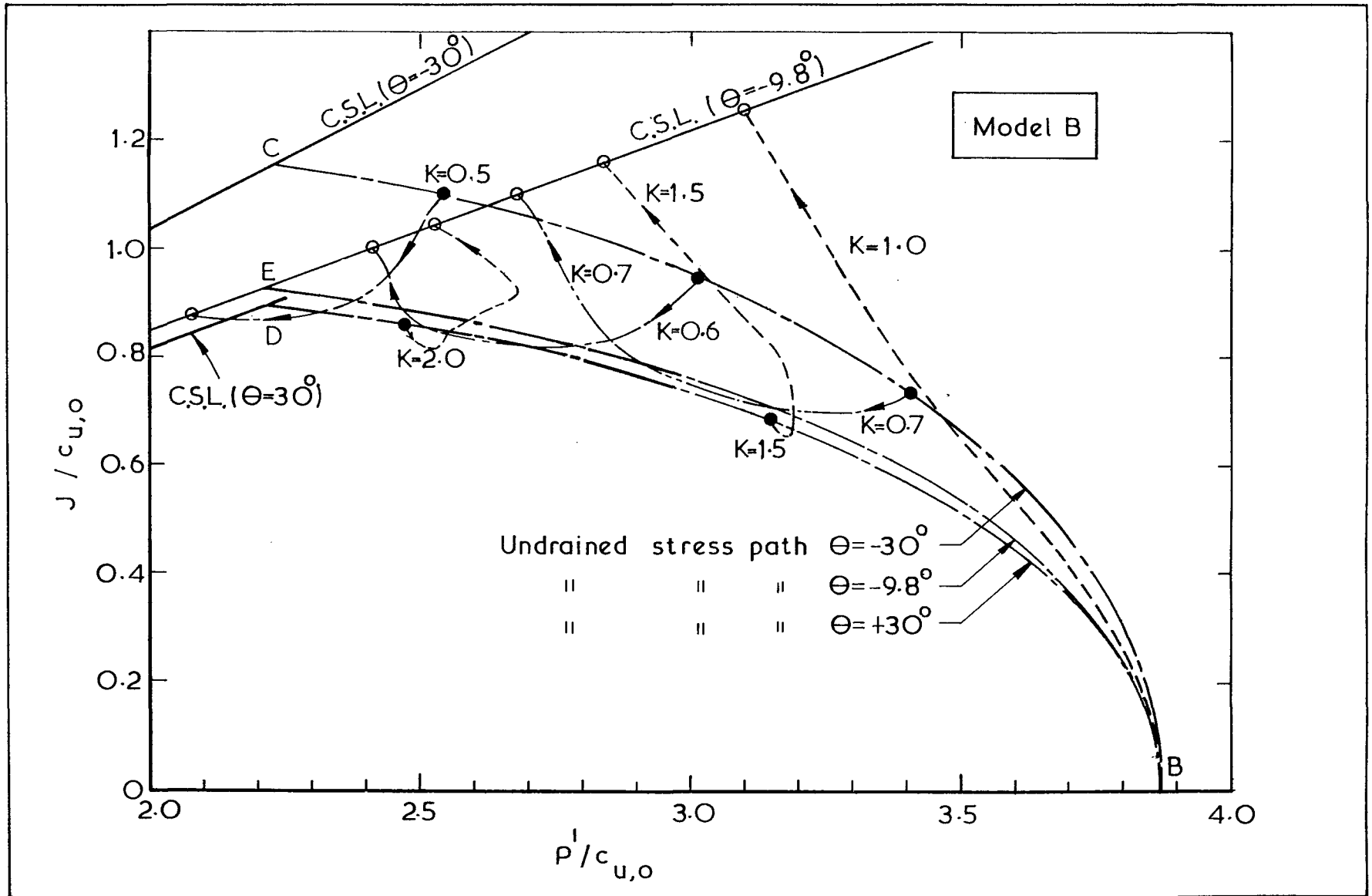


Fig. 8.4 Predicted radial distribution of stress using the ideal and model test meshes



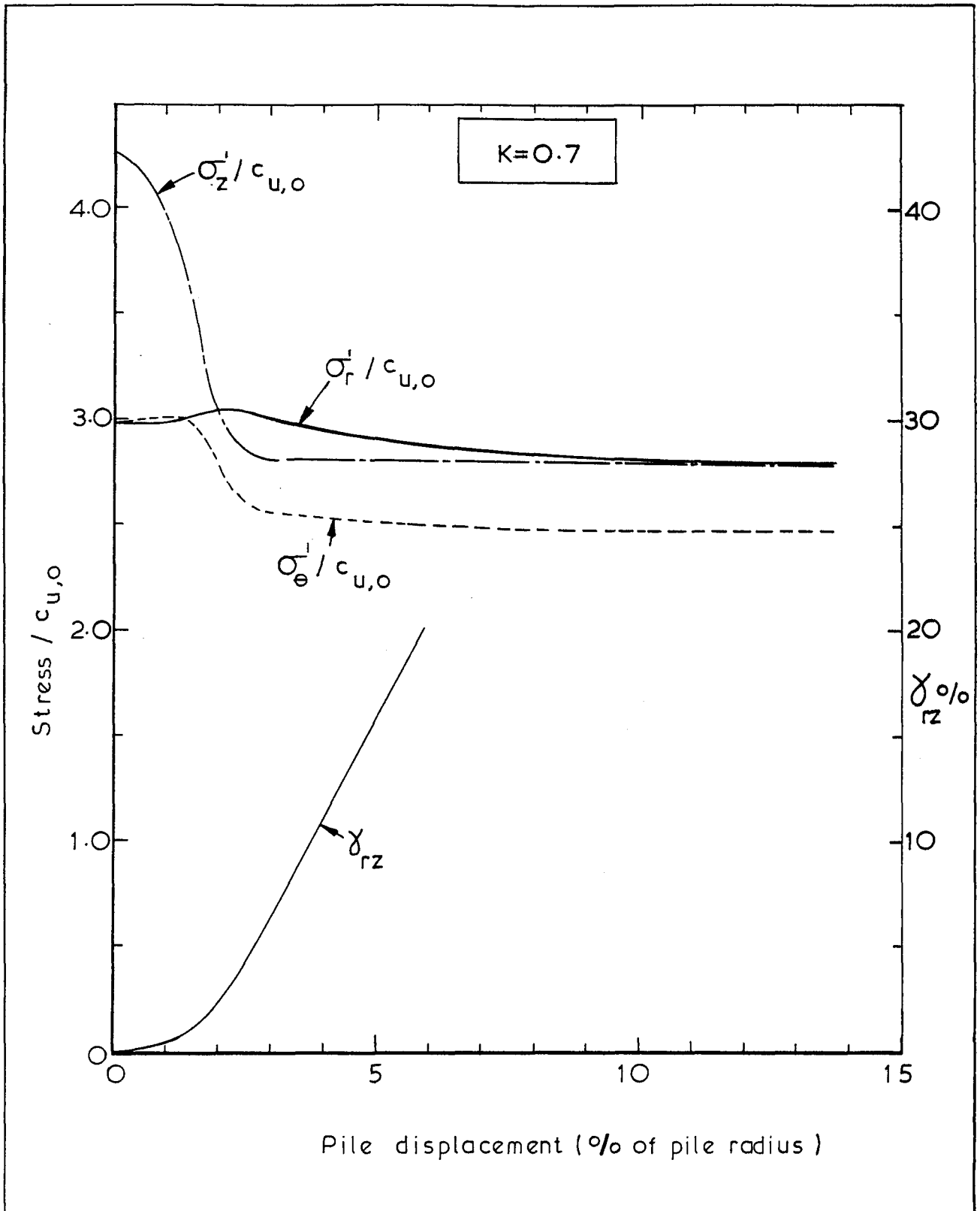
Stress paths followed during drained pile loading (based on soil Model A)

Fig. 8·5



Stress paths followed during drained pile loading (based on soil Model B)

Fig. 8.6



Variation with pile displacement of various components of stress and strain in the clay adjacent to the pile shaft. Predictions are based on soil Model B. K=0·7, drained loading.

Fig. 8·7(a)

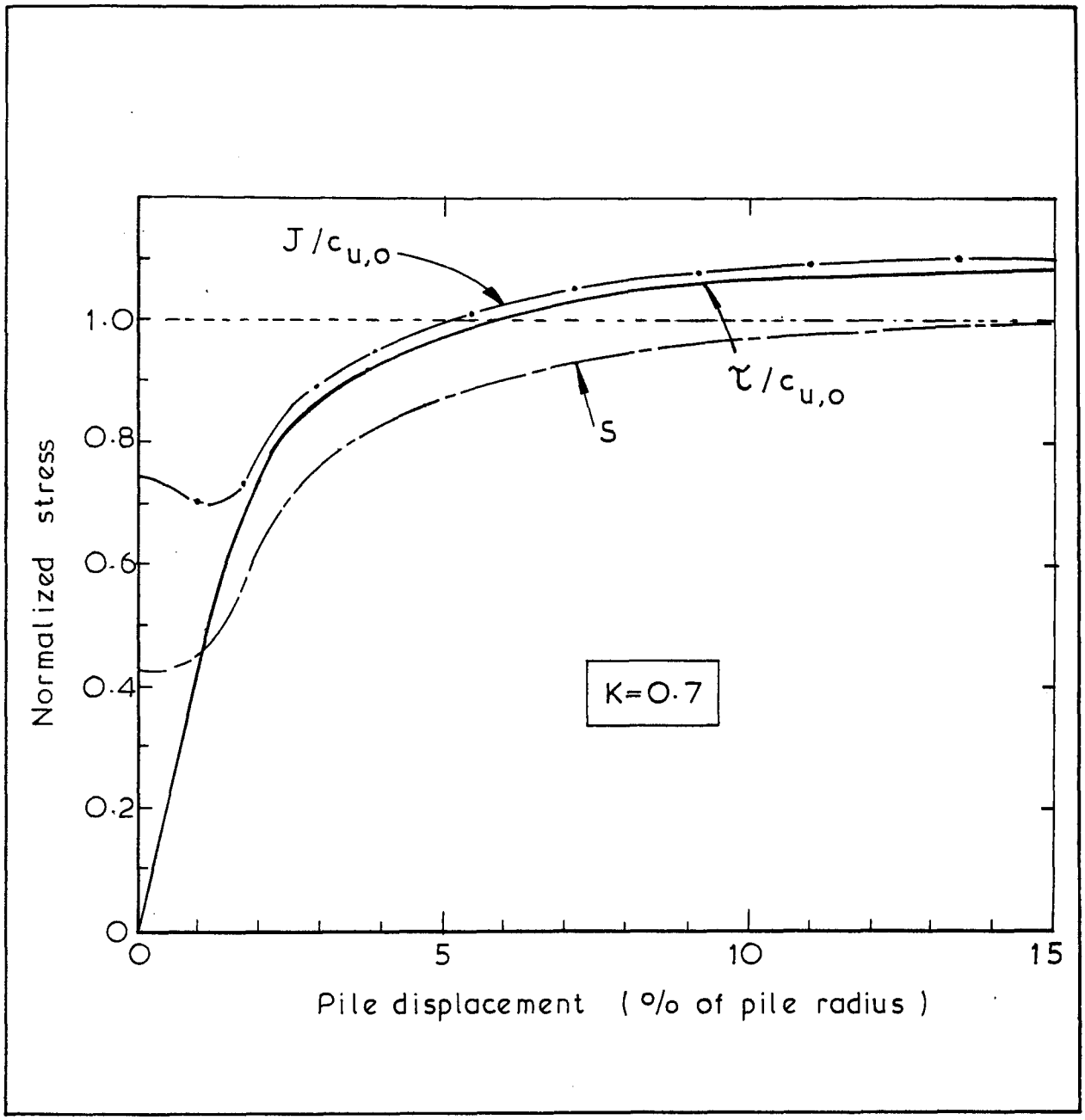

J /c u,o
τ /c u,o
S
K=0.7
Normalized stress
1.0
0.8
0.6
0.4
0.2
0
0
5
10
15
Pile displacement (% of pile radius)

Fig. 8.7(b)

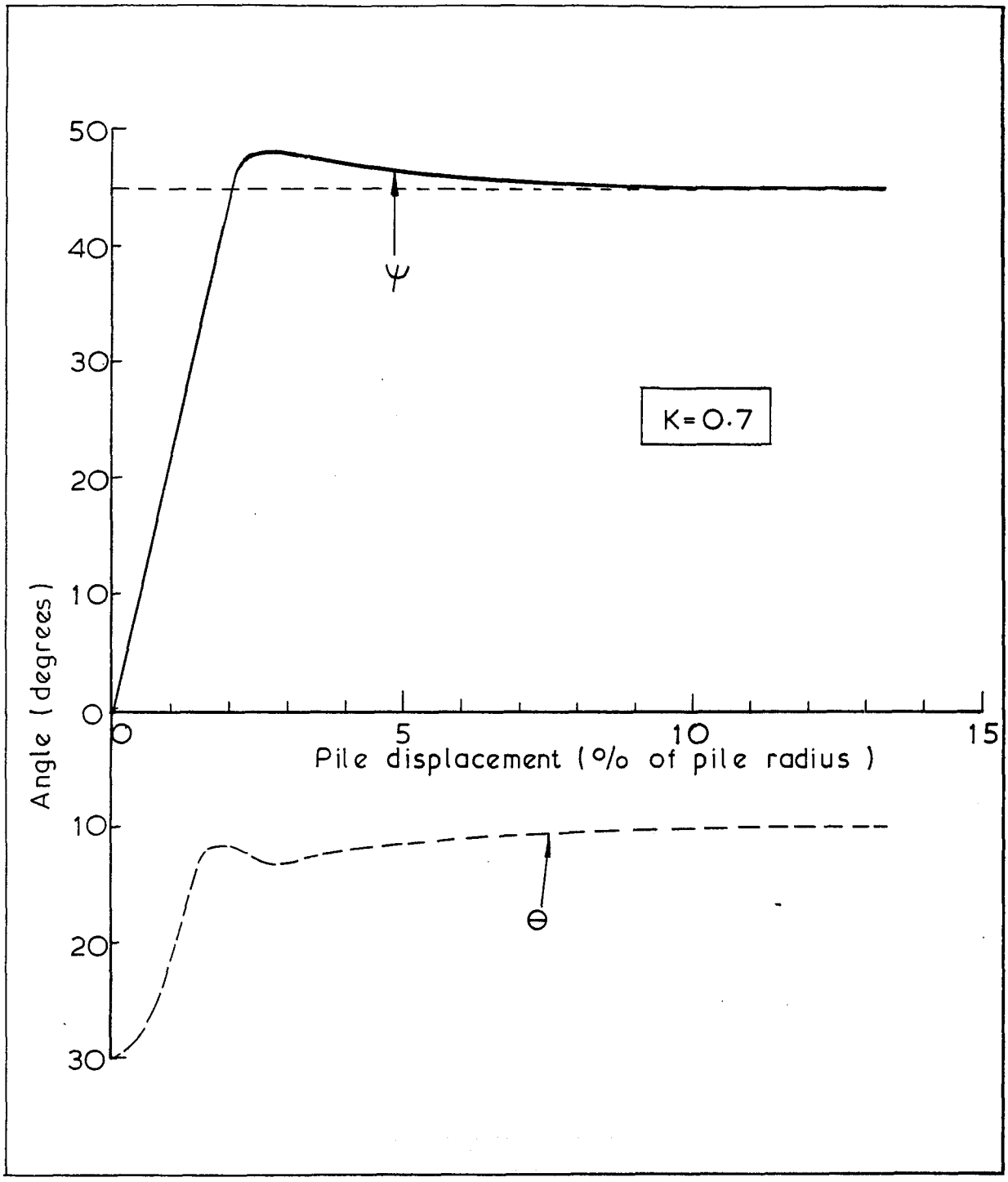
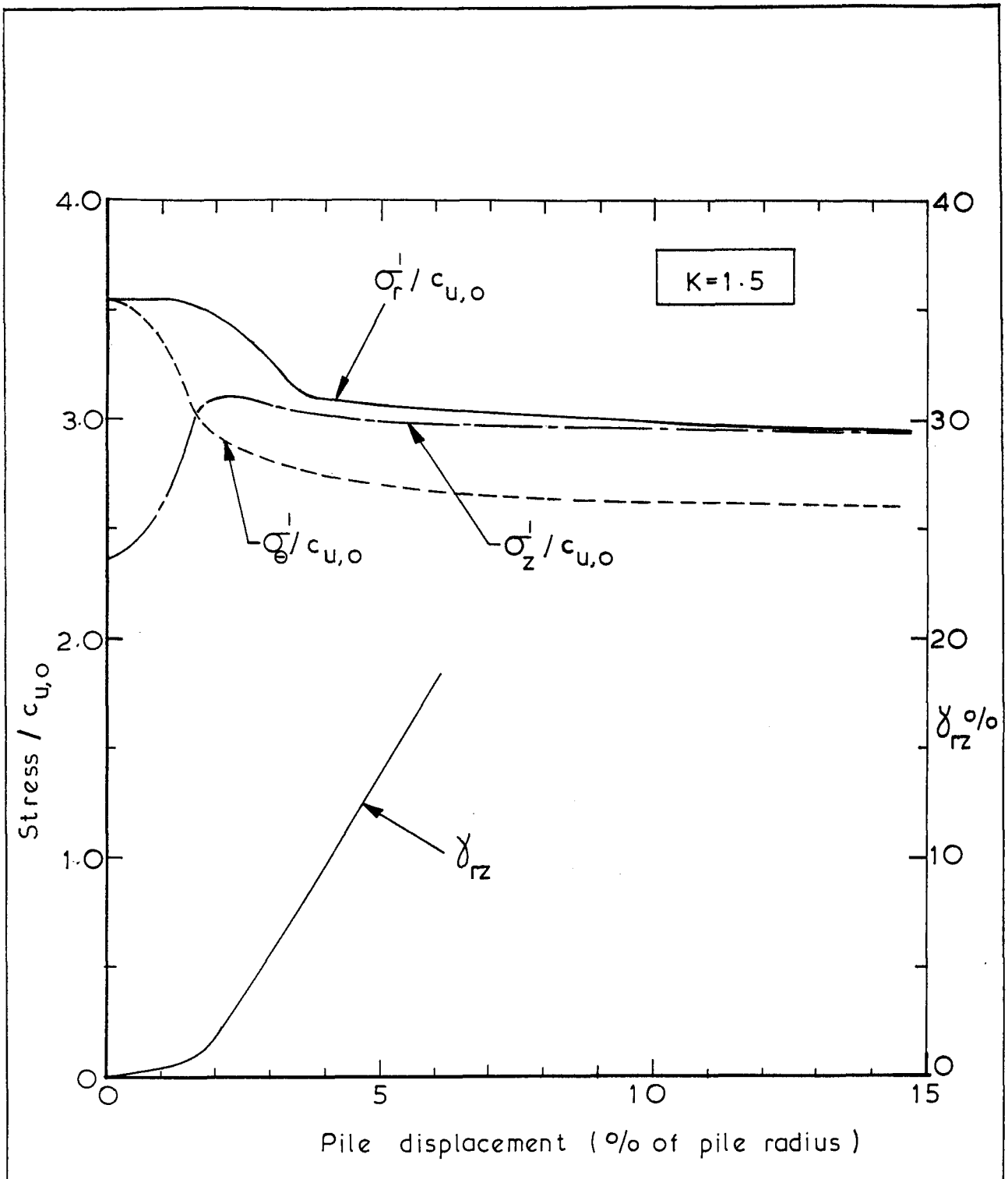

50
40
30
20
10
0
10
20
30
Angle (degrees)
ψ
K = 0.7
0
5
10
15
Pile displacement (% of pile radius)
θ

Fig. 8.7 (c)



Variation with pile displacement of various components of stress and strain in the clay adjacent to the pile shaft. Predictions are based on soil Model B. K-1·5, drained loading.

Fig. 8·8 (a)

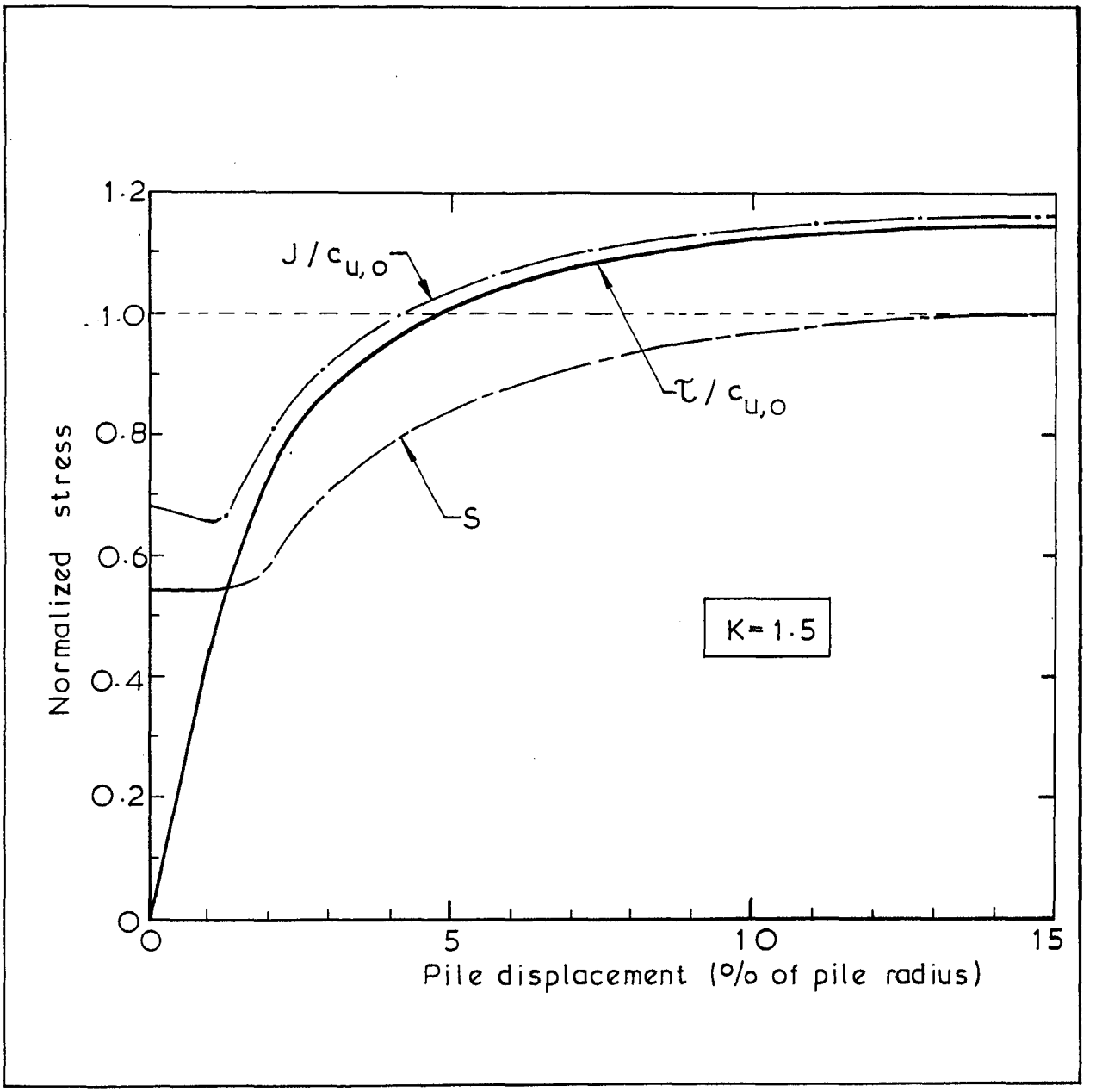

1·2
1·0
0·8
0·6
0·4
0·2
0
Normalized stress
J / $c_{u,o}$
τ / $c_{u,o}$
S
K = 1·5
0
5
10
15
Pile displacement (% of pile radius)

Fig. 8·8(b)

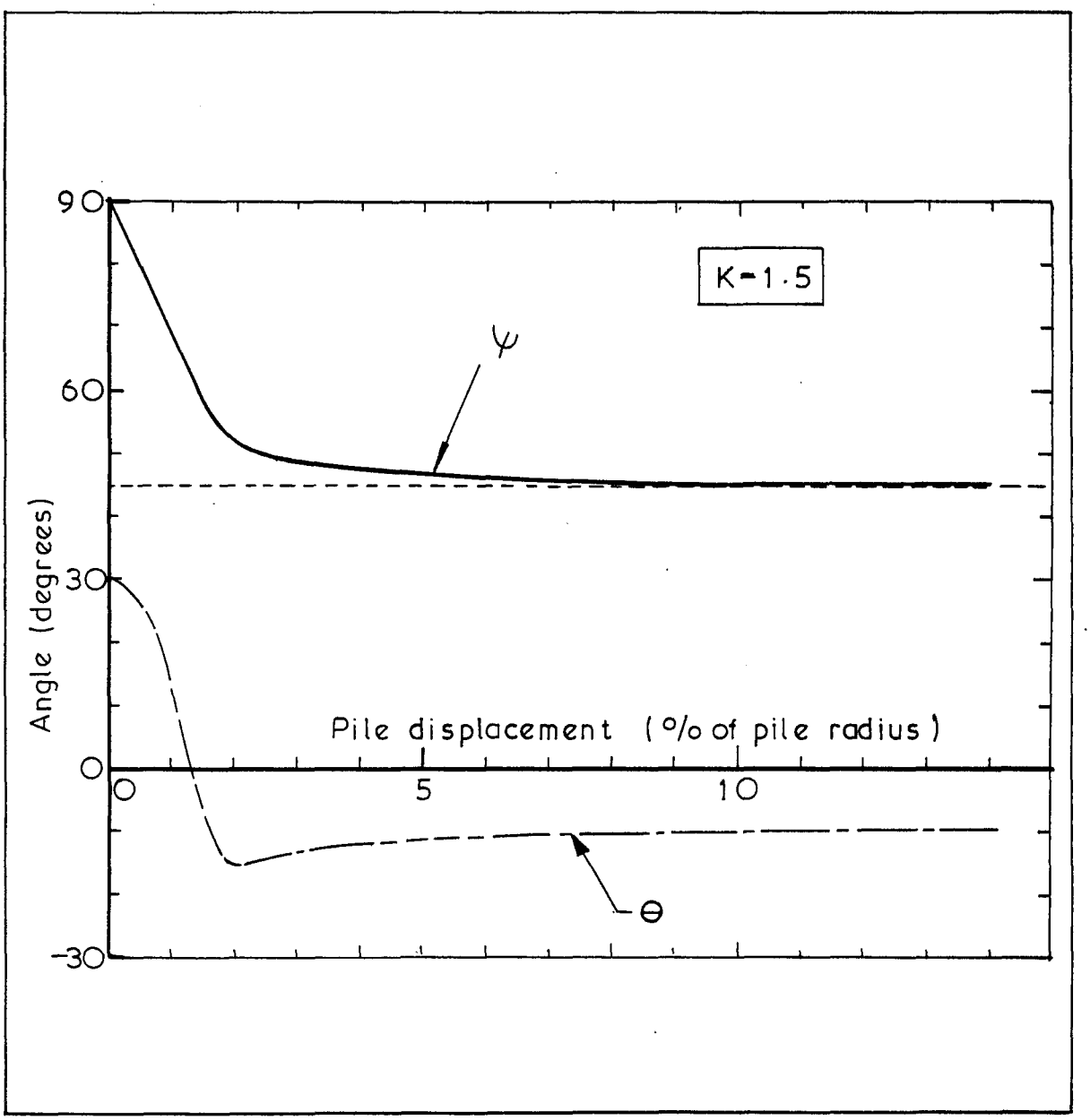

90
60
30
0
-30
Angle (degrees)
K=1·5
ψ
Pile displacement (% of pile radius)
0
5
10
θ

Fig 8.8(c)

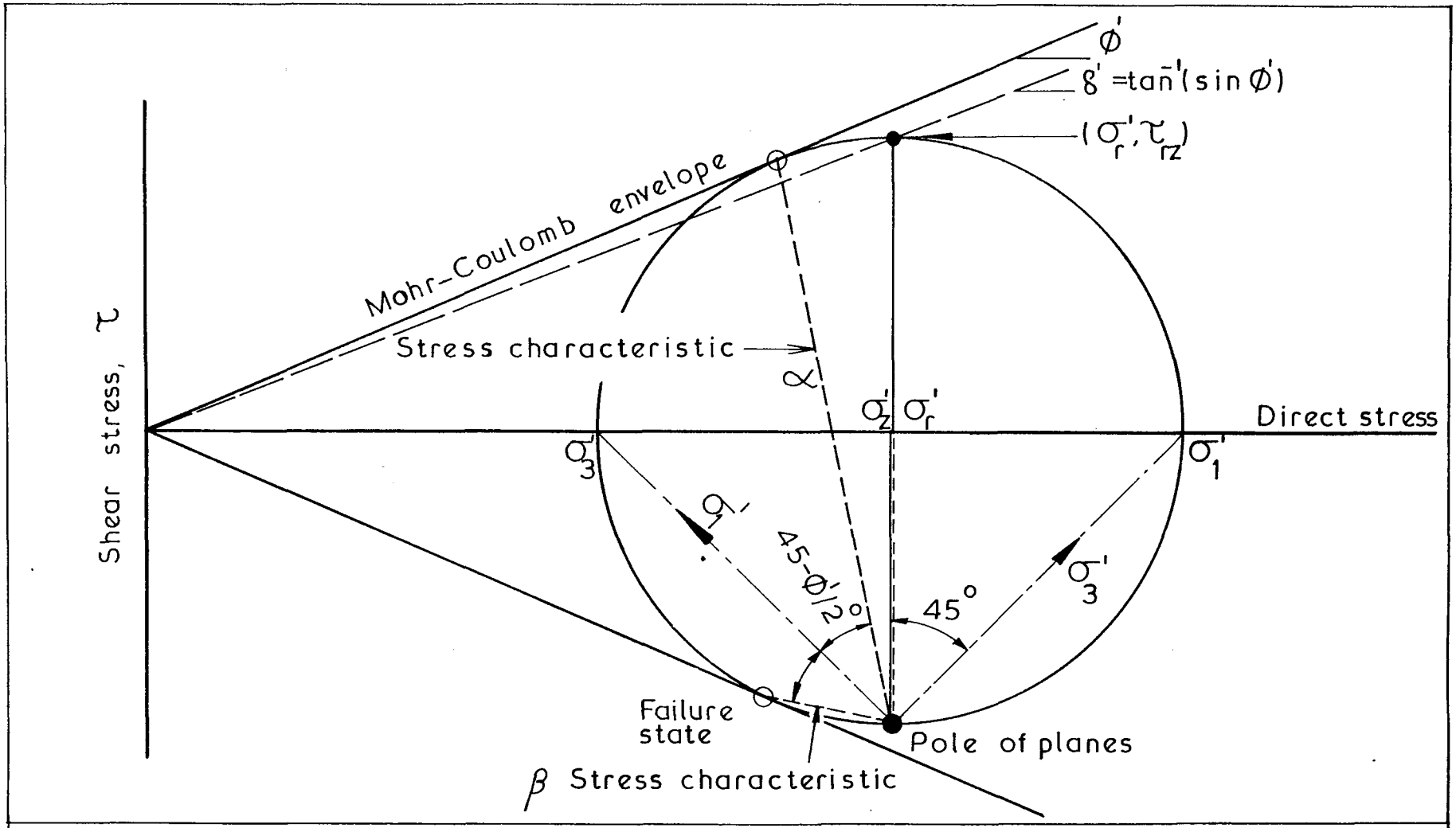
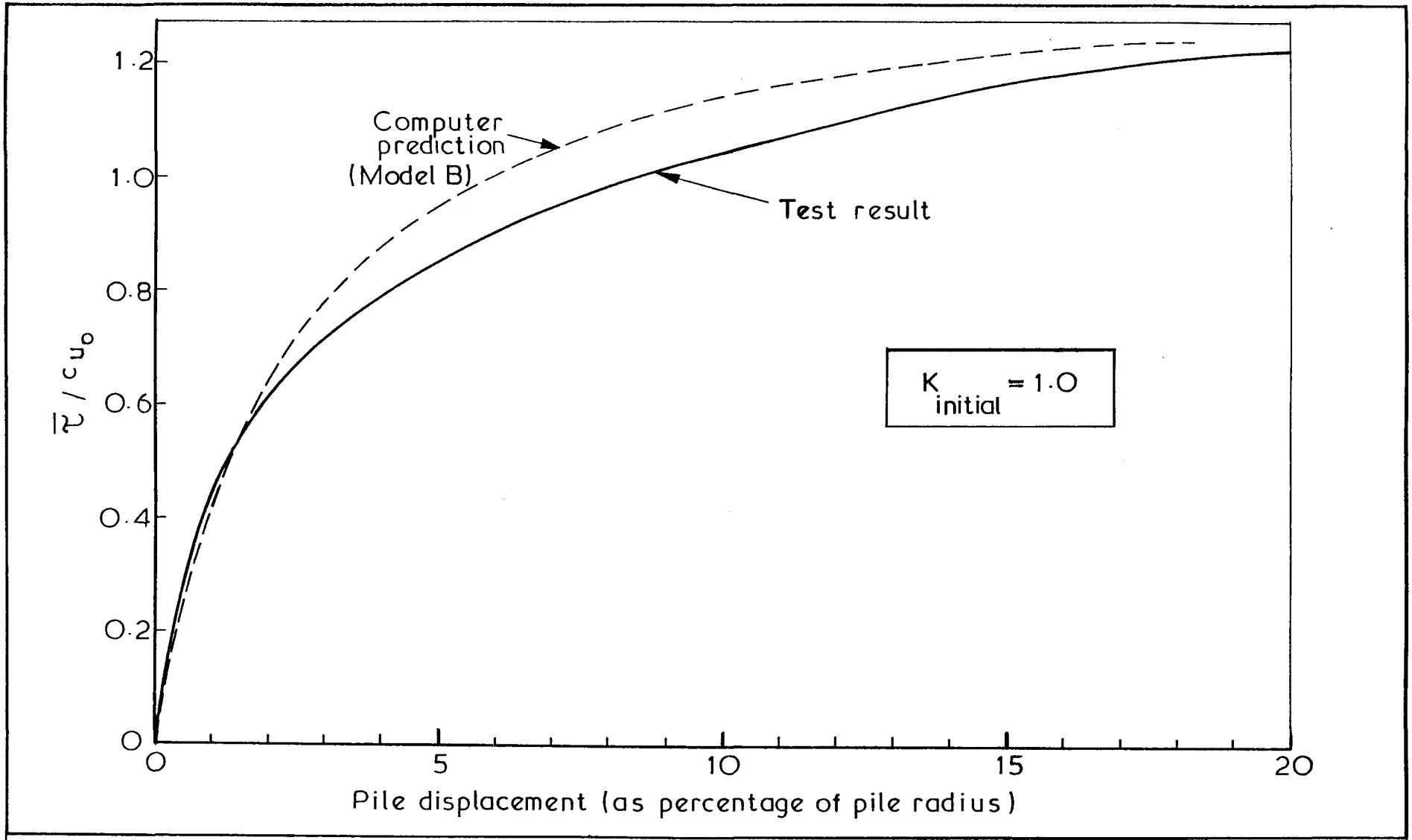


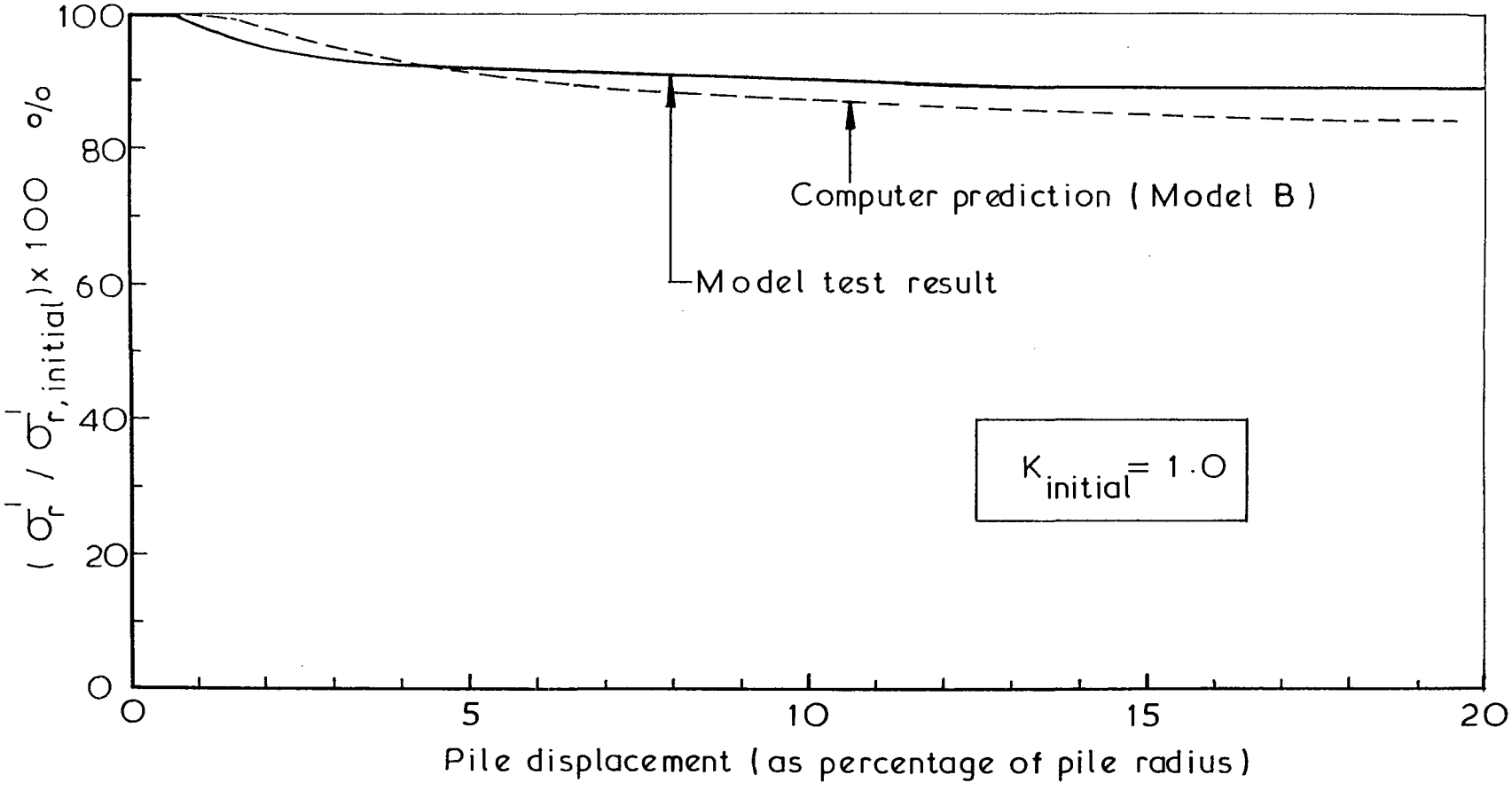
Fig. 8.9

Mohr's circle of stress (in the r-z plane) for an element of soil adjacent to a pile loaded to peak



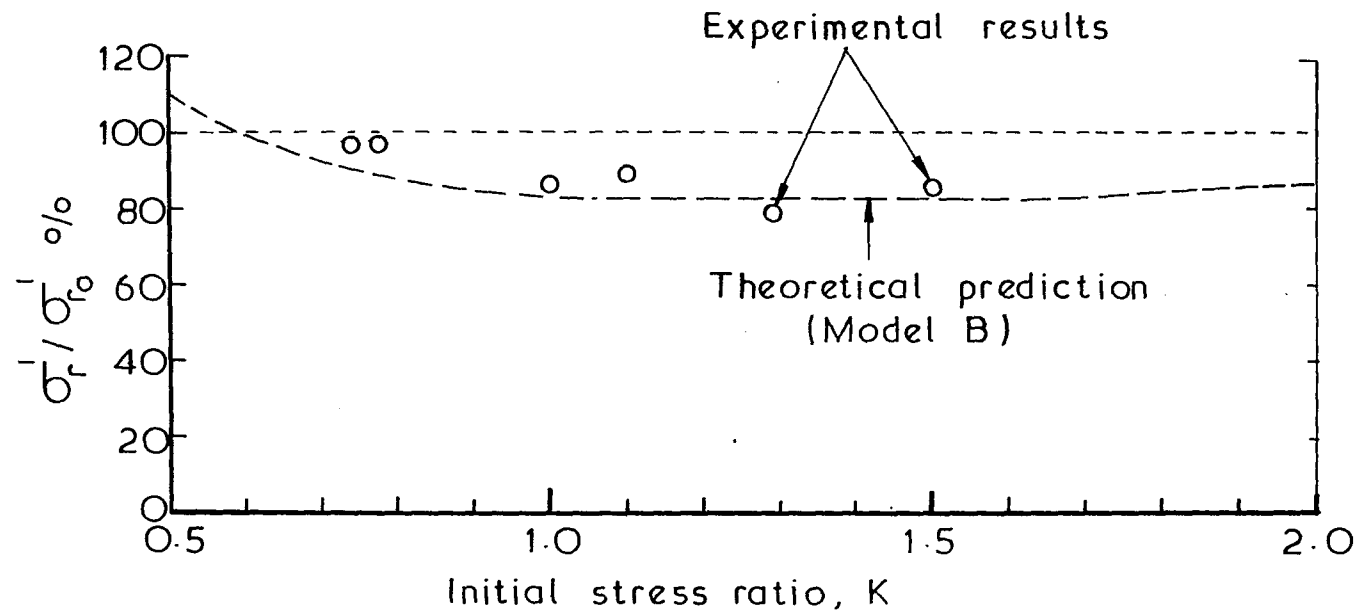
Variation of shear stress (normalized by $c u_o$) with pile displacement — comparison between computer predictions and experimental results.

Fig. 8.10



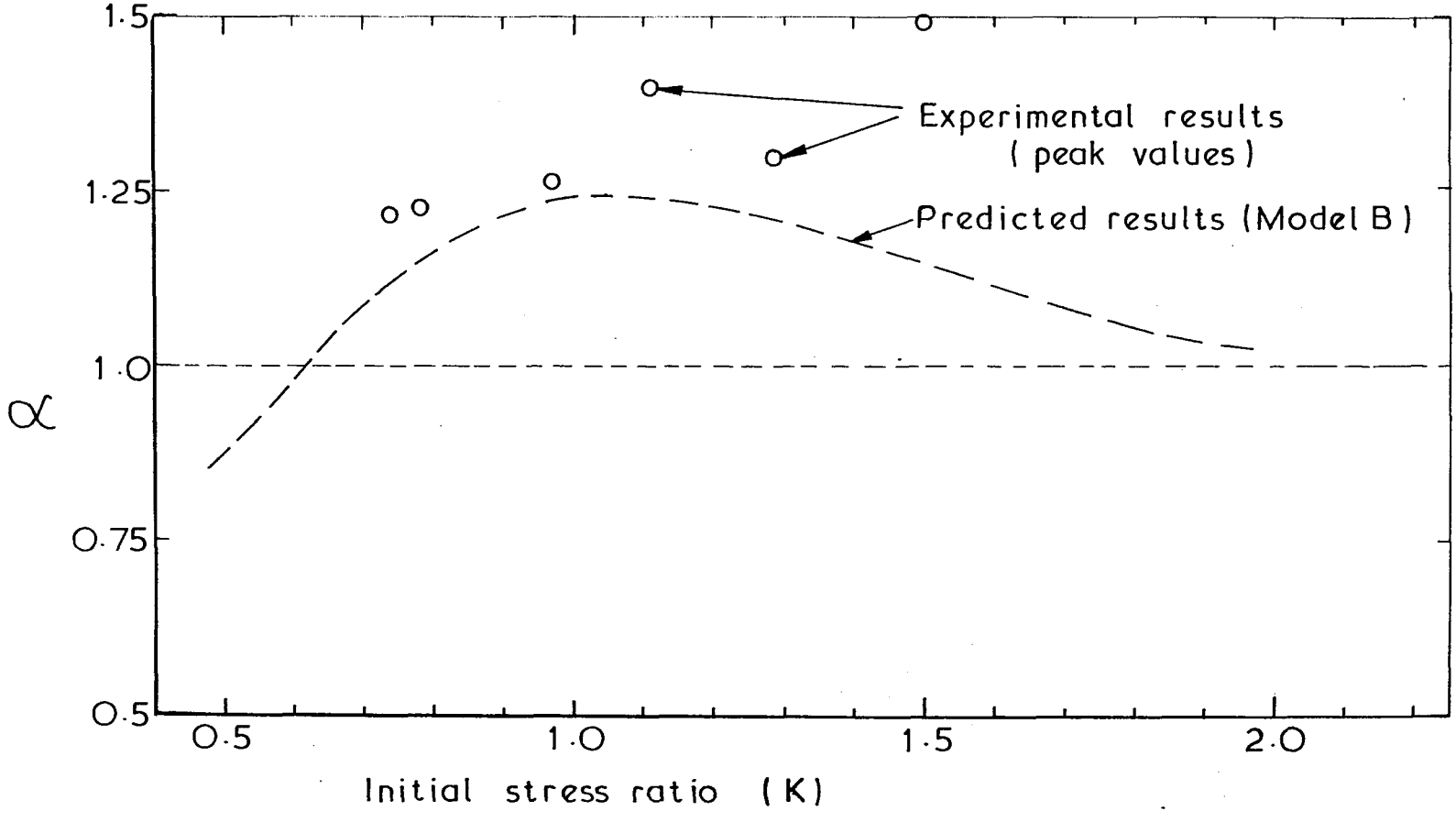
Variation of radial stress with pile displacement — comparison between computer predictions and experimental results

Fig. 8.11



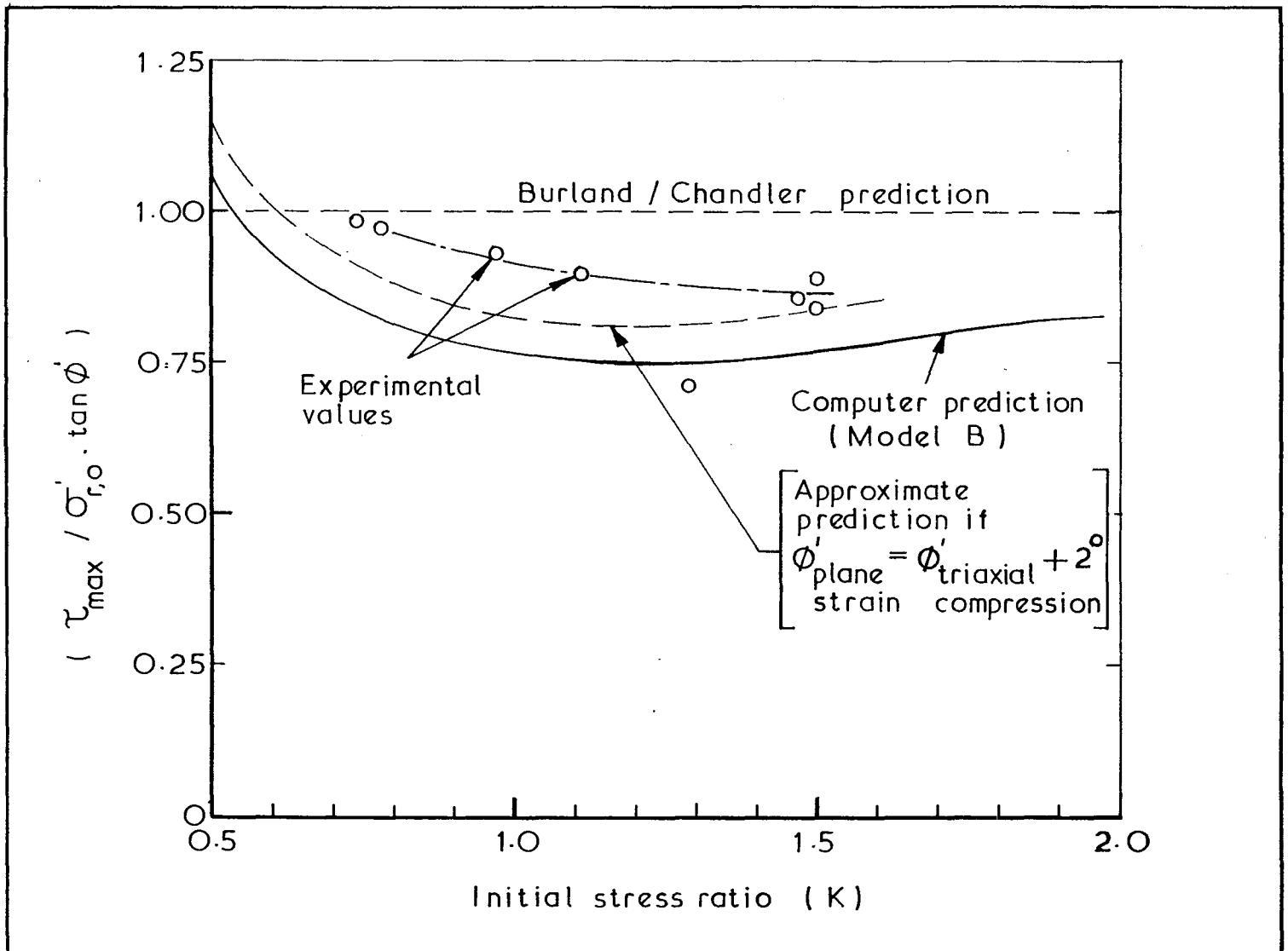
Theoretical and experimental variations of the radial stress σ_r' acting at peak load, with initial stress ratio. (Drained loading)

Fig. 8·12



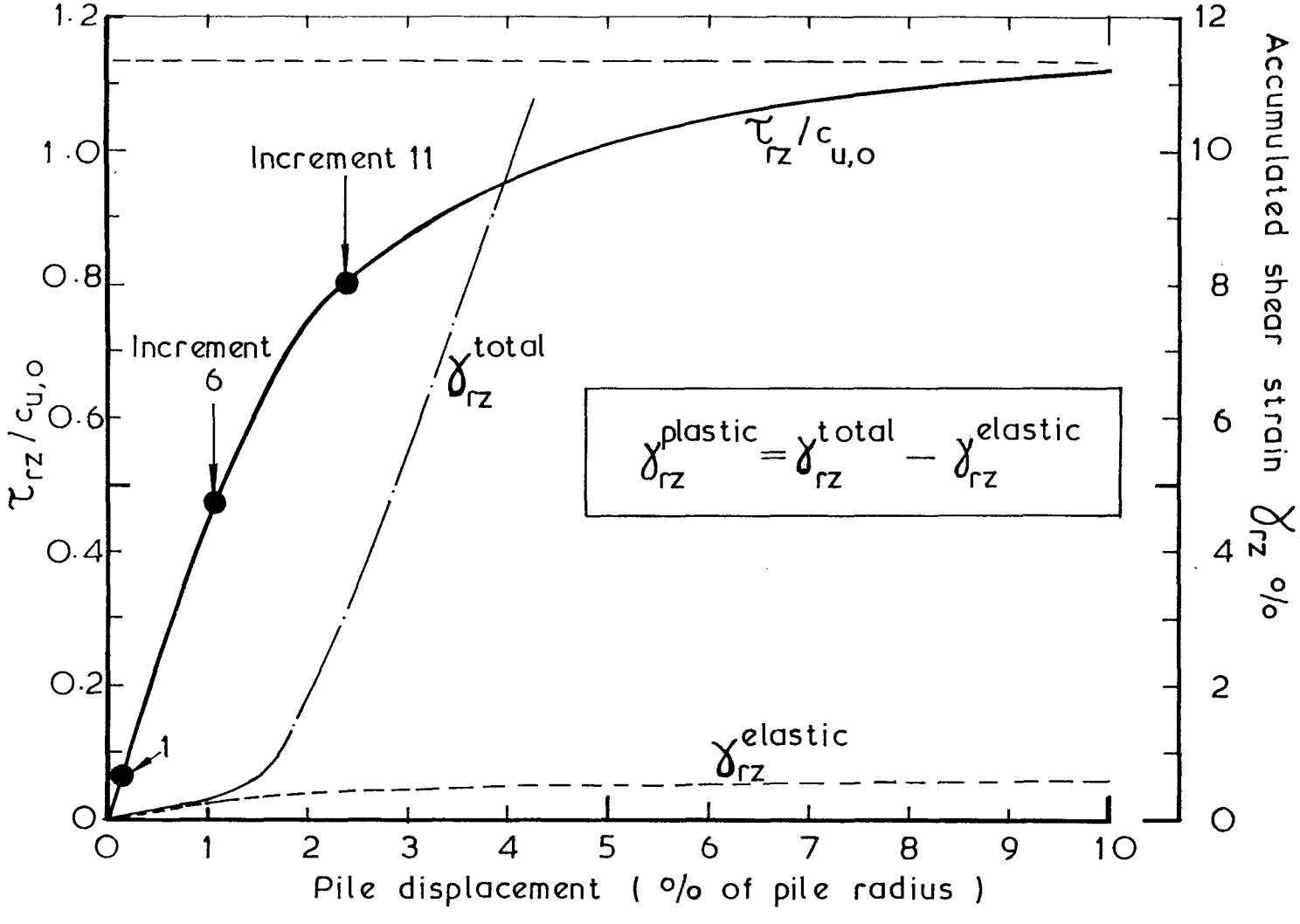
Variation of α with stress ratio, K

Fig. 8.13



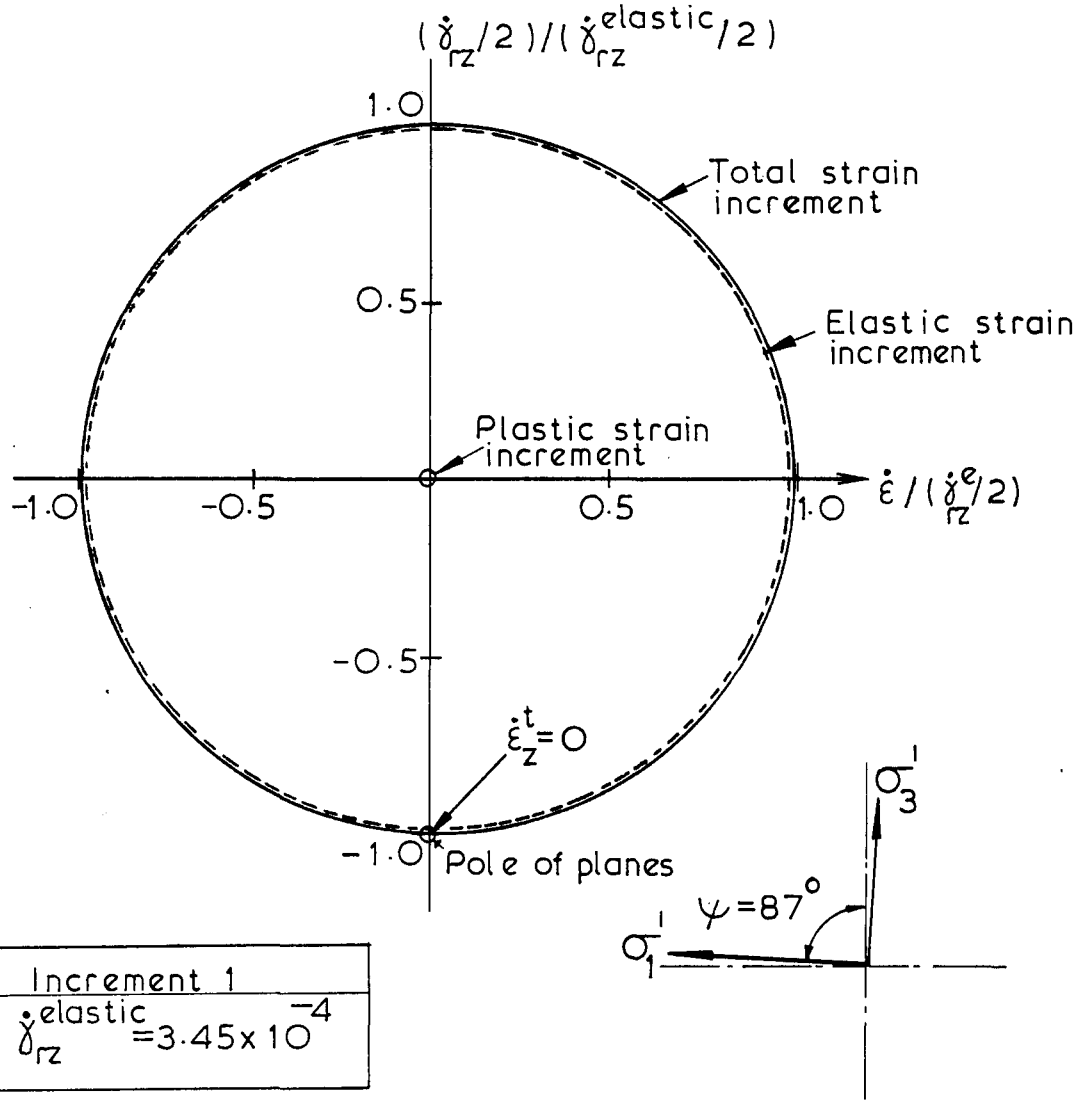
Variation of $\tau_{max} / \sigma'_{r,o} . \tan\phi'$ with stress ratio, K

Fig. 8.14



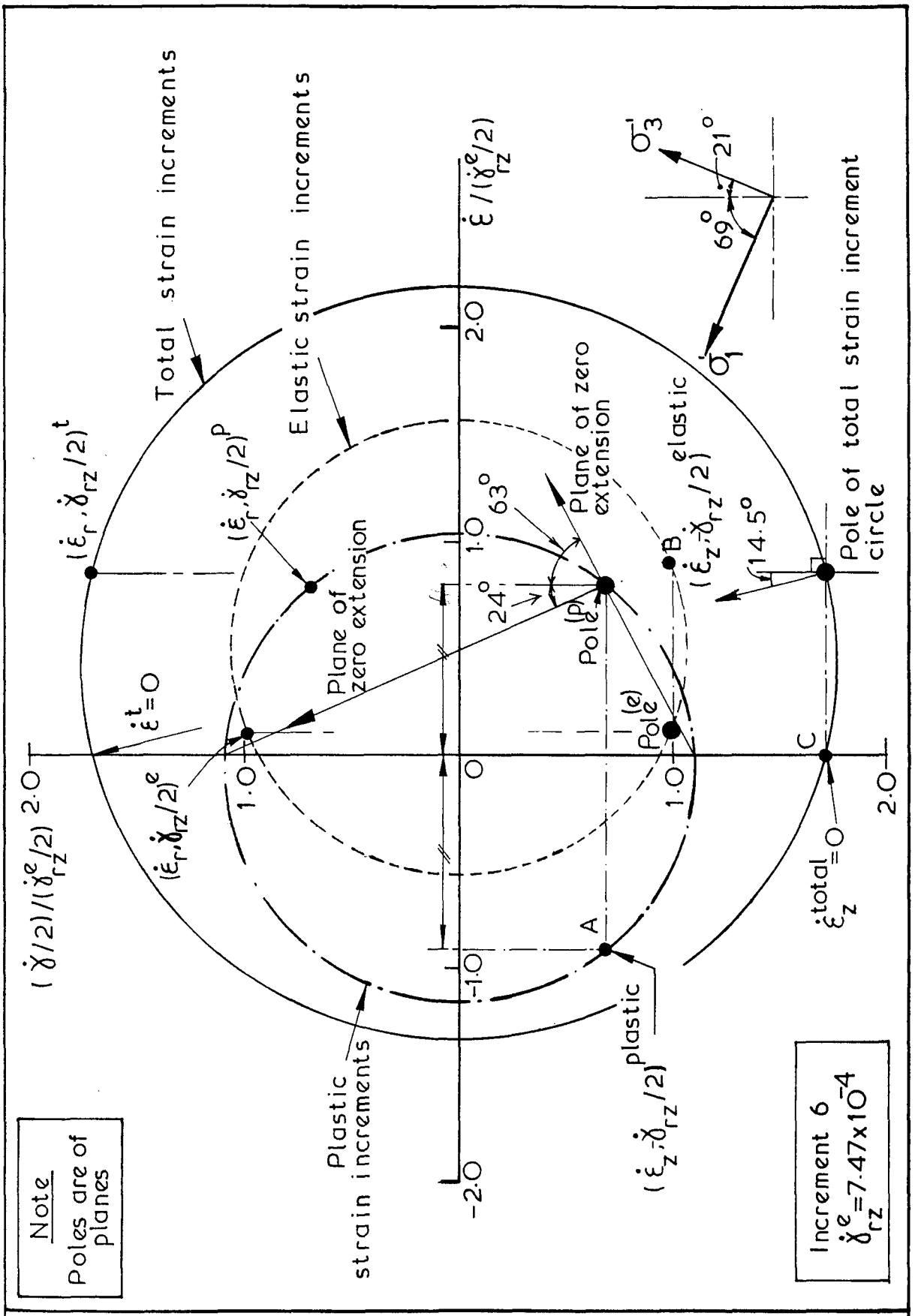
Variation of shear stess and accumulated shear strain within the clay adjacent to the pile shaft, with pile displacement. K=1·5, drained loading.

Fig.8.15



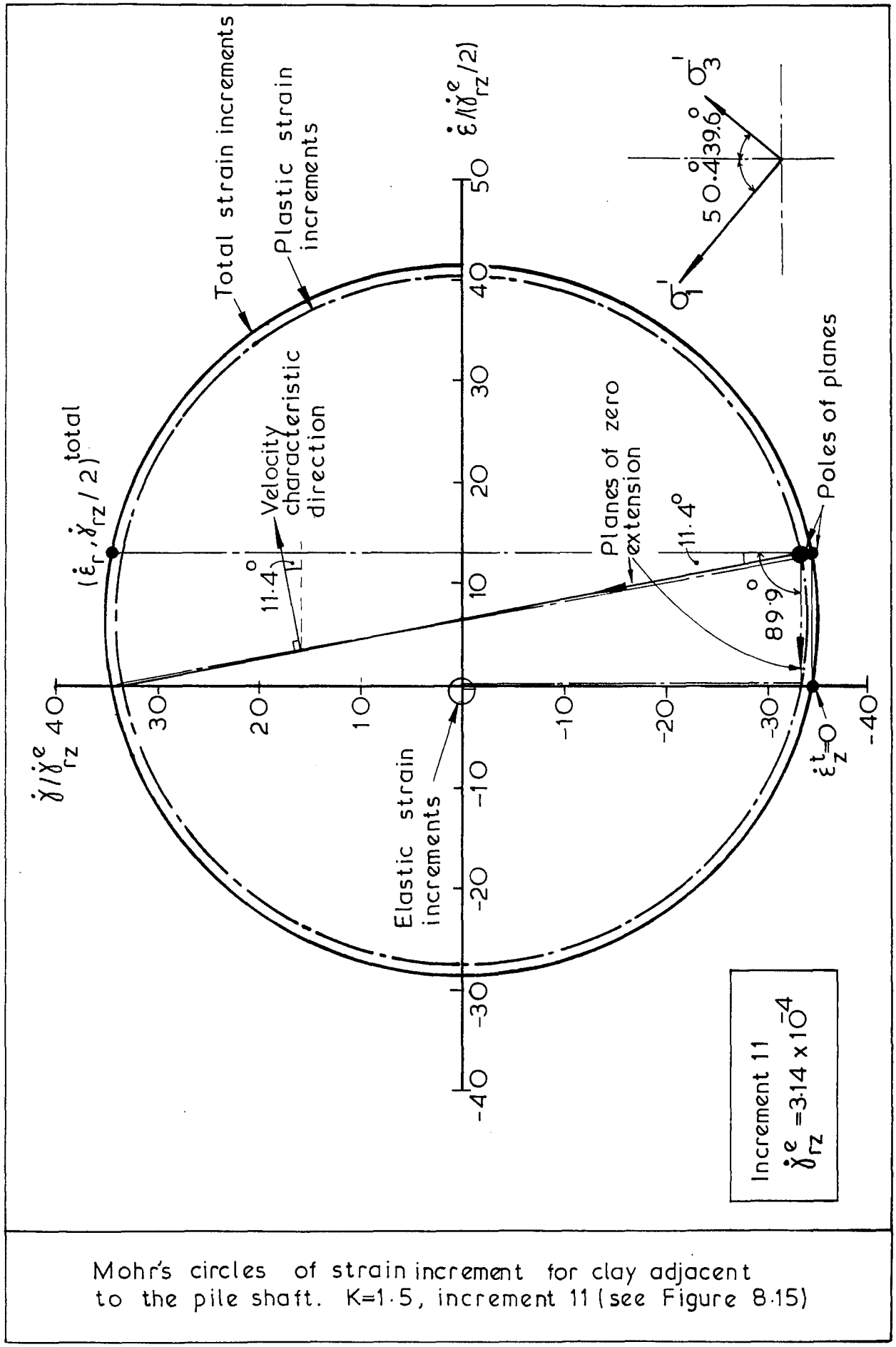
Mohr's circles of strain increment for clay adjacent to the pile shaft. K=1·5, increment 1 .(See Figure 8·15)

Fig. 8·16



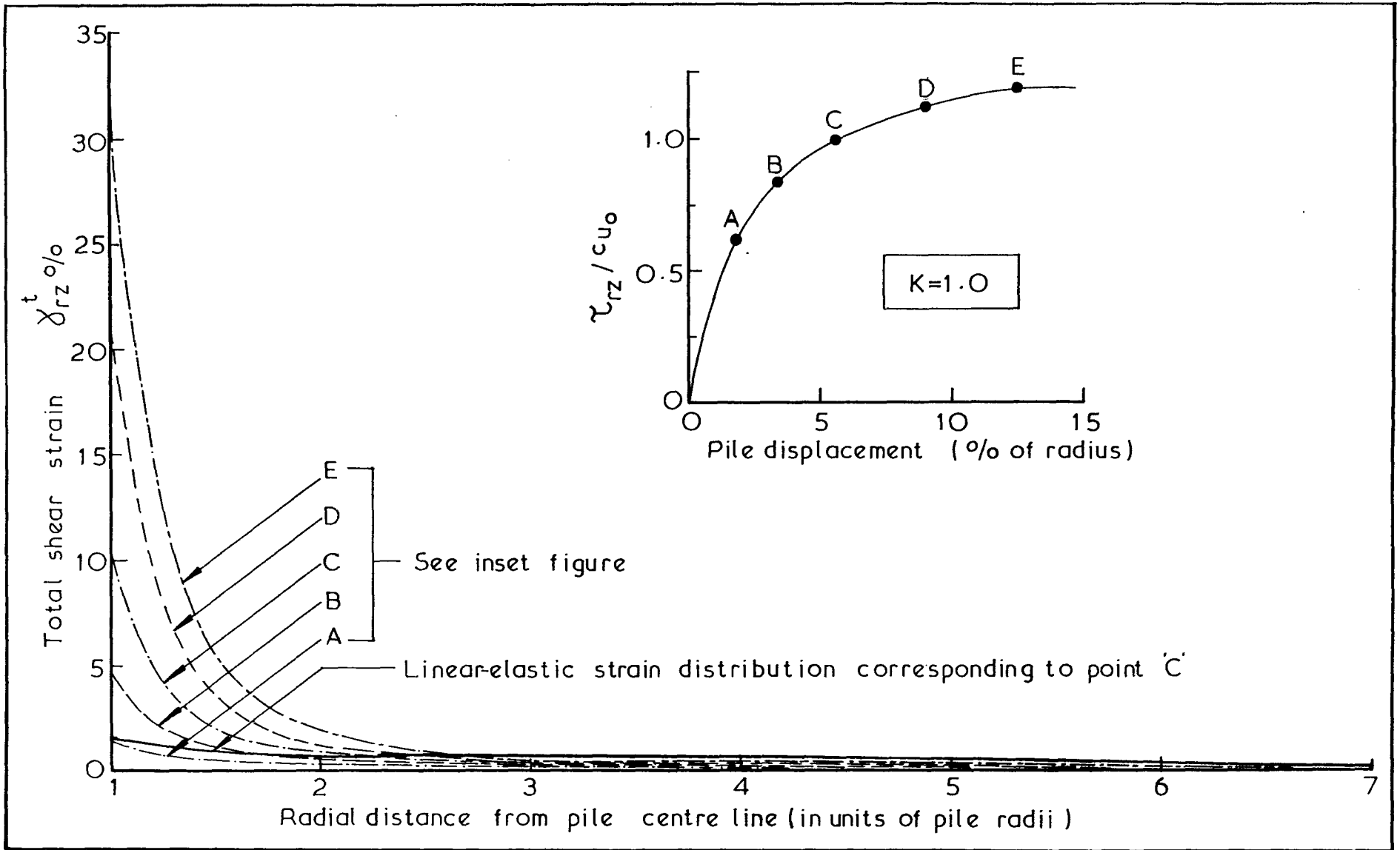
Mohr's circles of strain increment for clay immediately adjacent to the pile shaft. K=1·5 , increment 6. (see Fig. 8·15)

Fig. 8·17



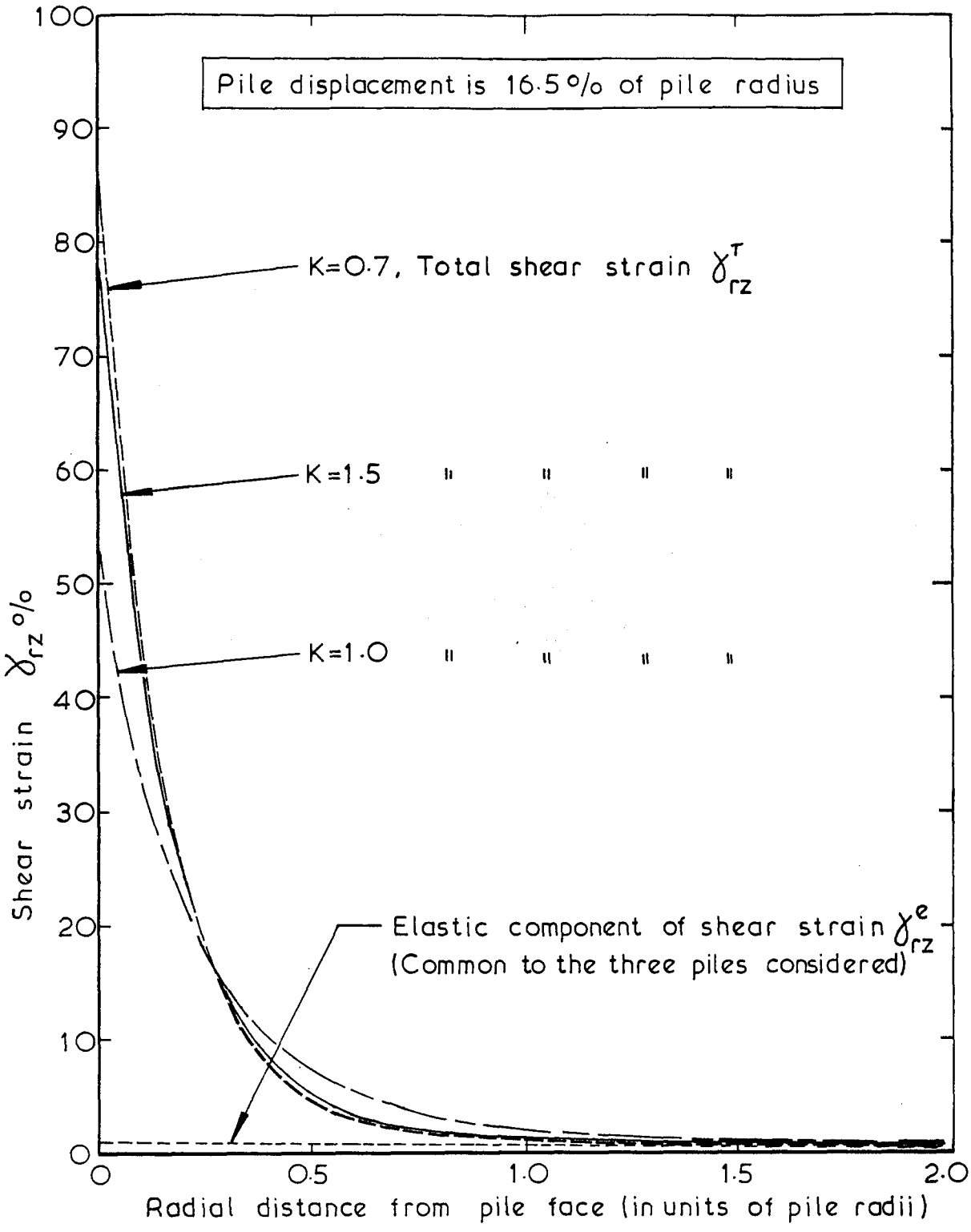
Mohr's circles of strain increment for clay adjacent to the pile shaft. K=1·5, increment 11 (see Figure 8.15)

Fig.8.18



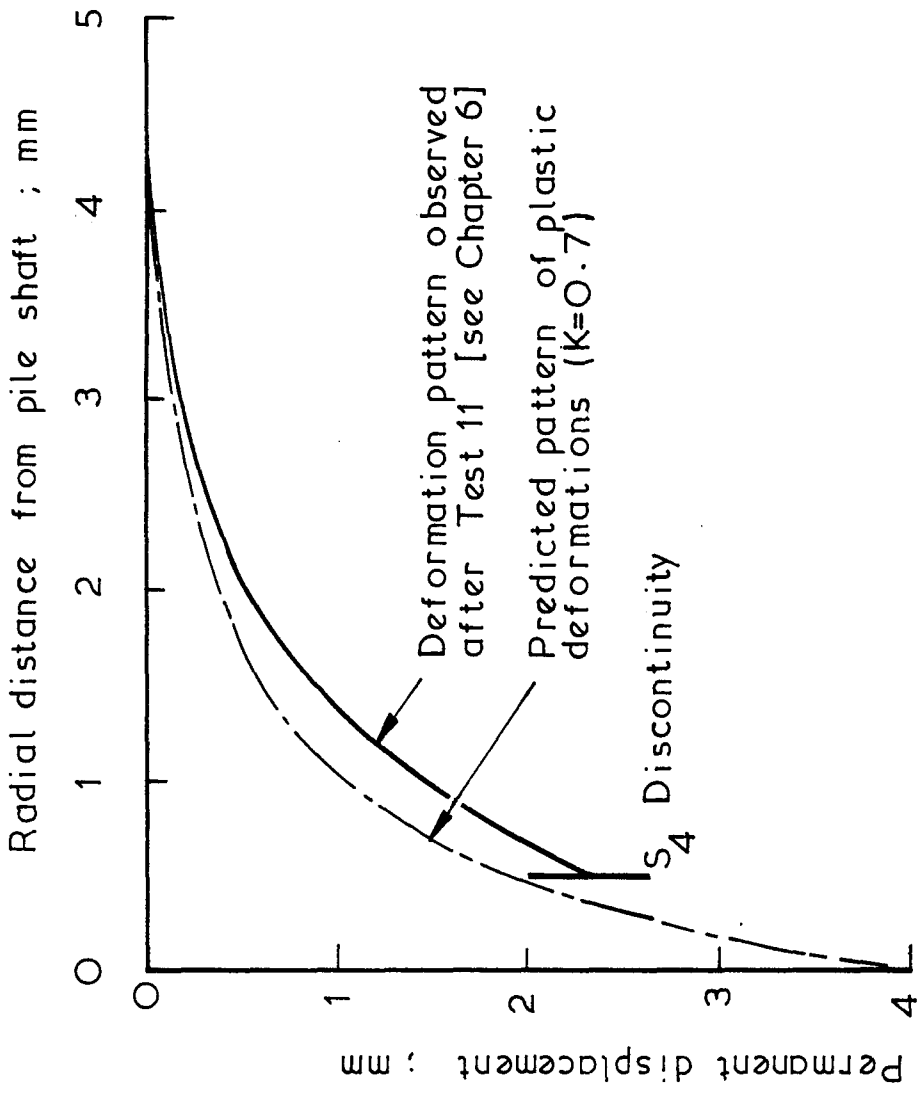
Radial distribution of shear strain γ^t_{rz} at various stages of pile loading (fully drained)

Fig.8.19



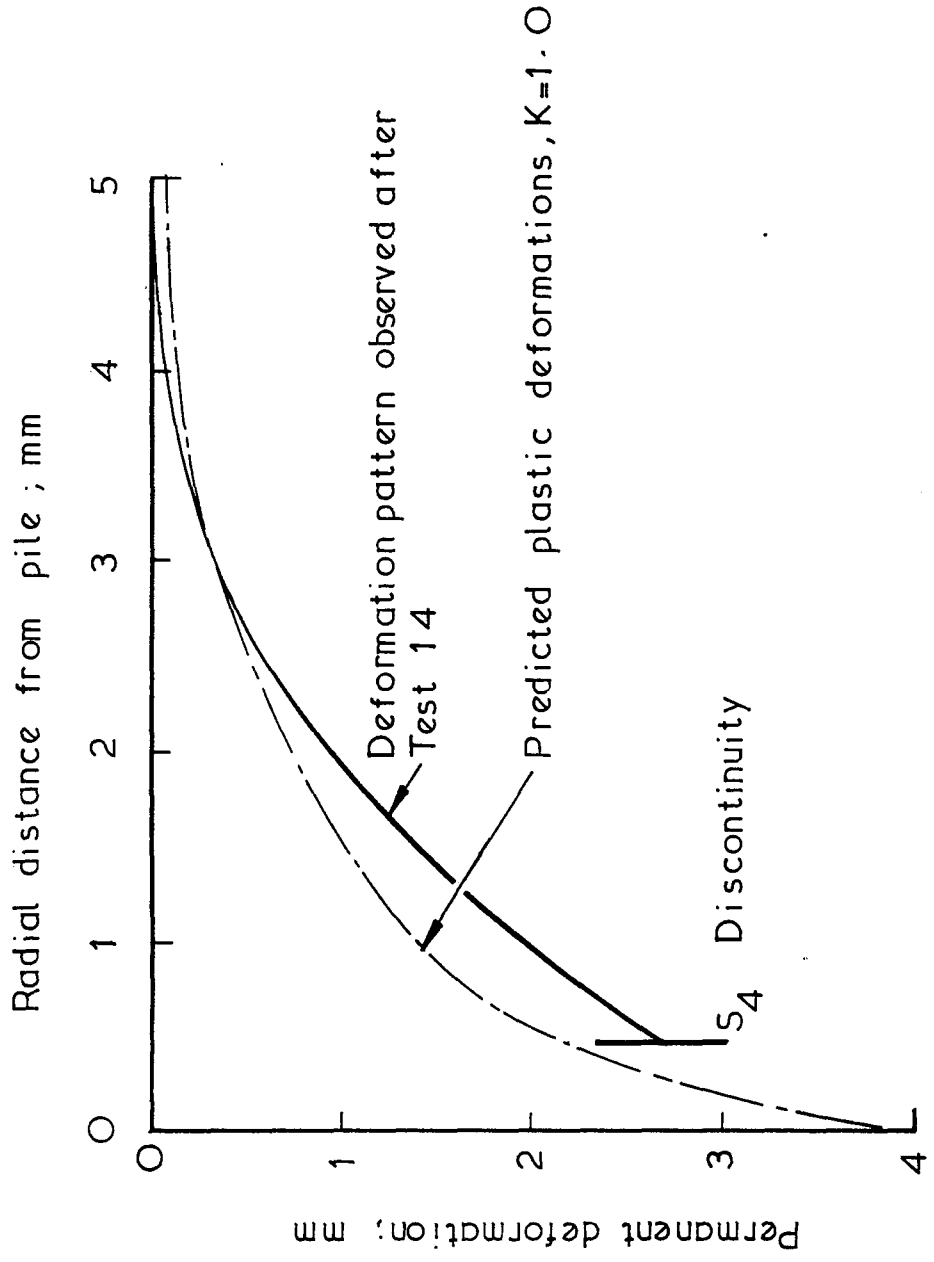
Radial distribution of the shear strain γ_{rz}, for piles installed in clay consolidated to different stress ratios. The piles are at peak load, and at a common displacement.

Fig. 8.20



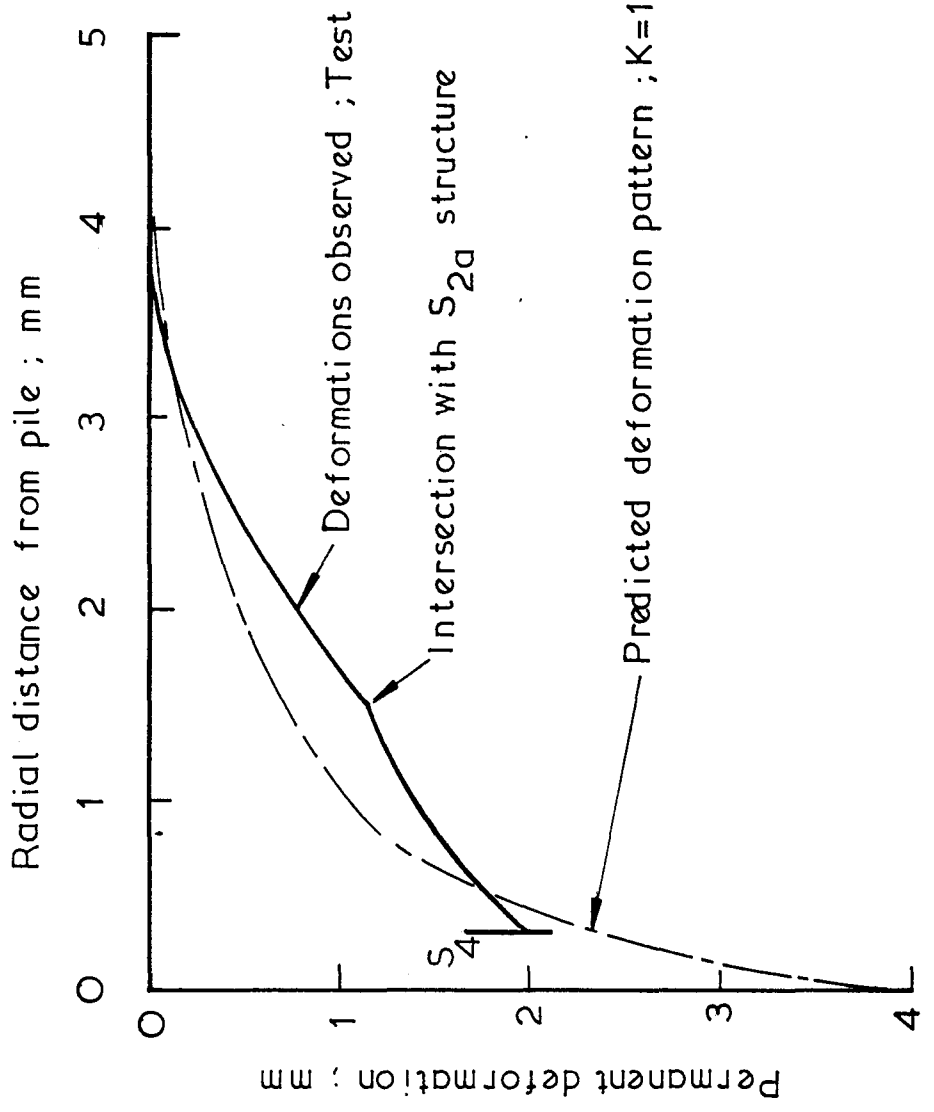
Comparison between predicted and observed axial deformations adjacent to a pile in clay; K~0·7

Fig. 8·21(a)



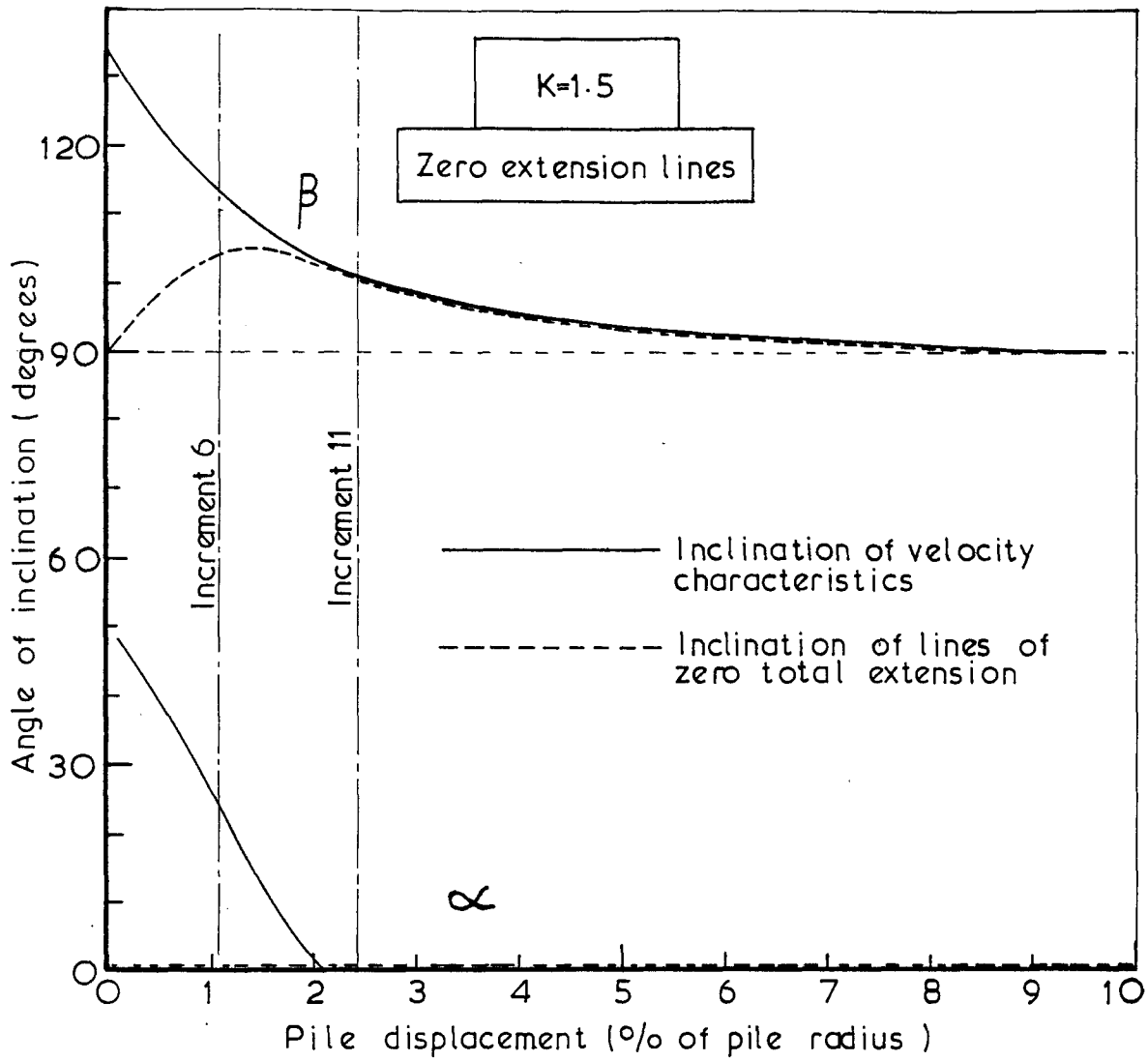
Comparison between predicted and observed axial deformations adjacent to a pile in clay ; K ~ 1·0

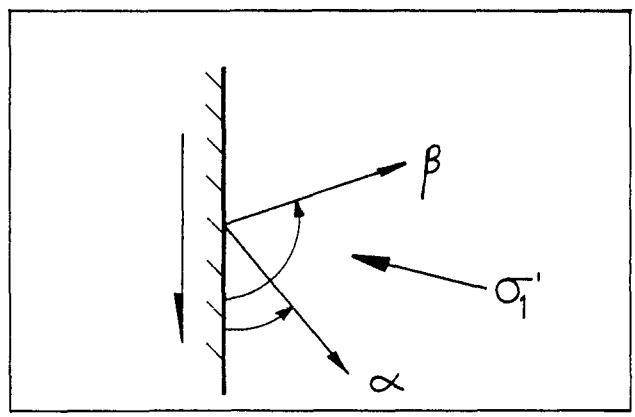
Fig. 8·21(b)



Comparison between predicted and observed axial deformations adjacent to a pile in clay ; K= 1·5

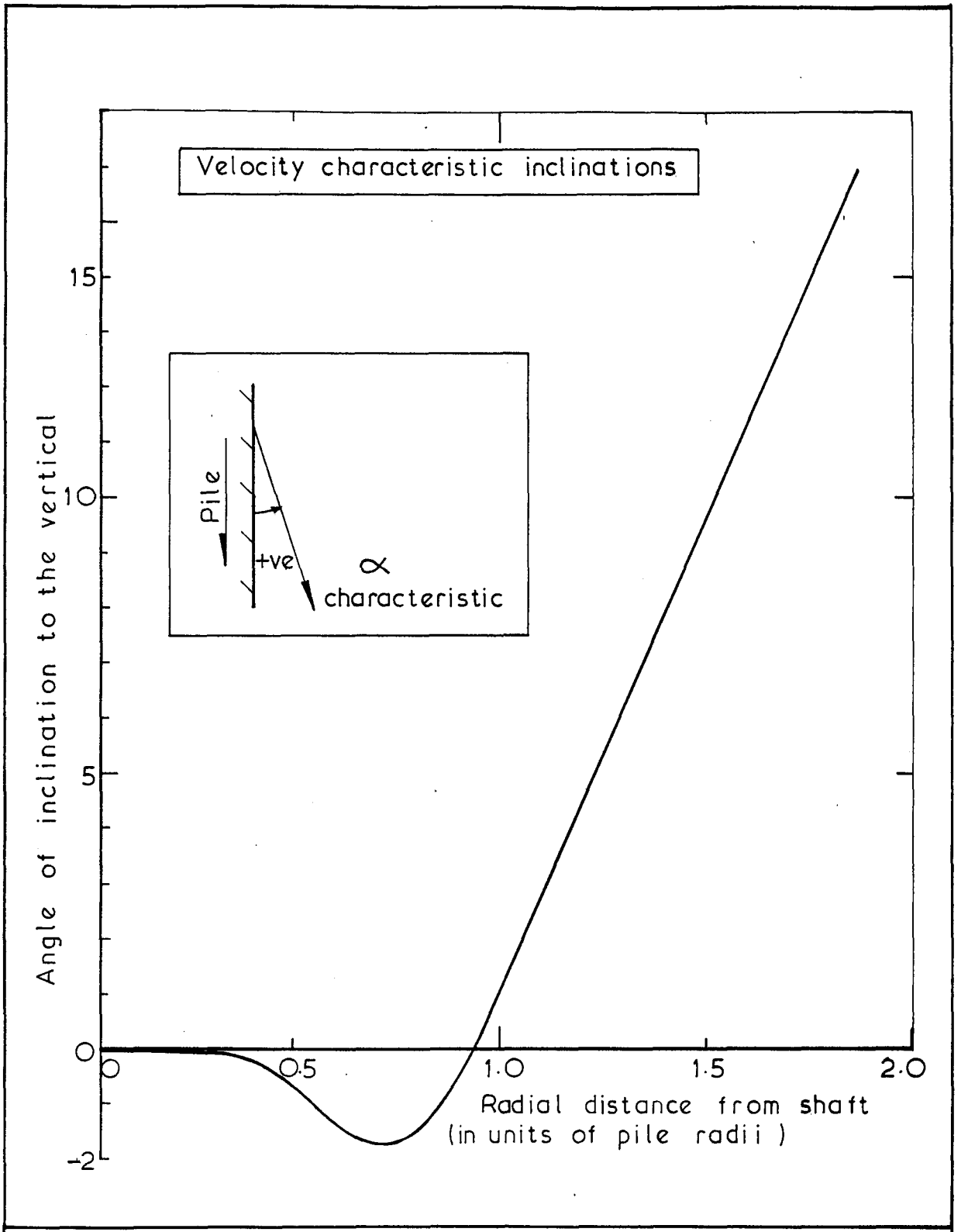
Fig.8·21 (c)





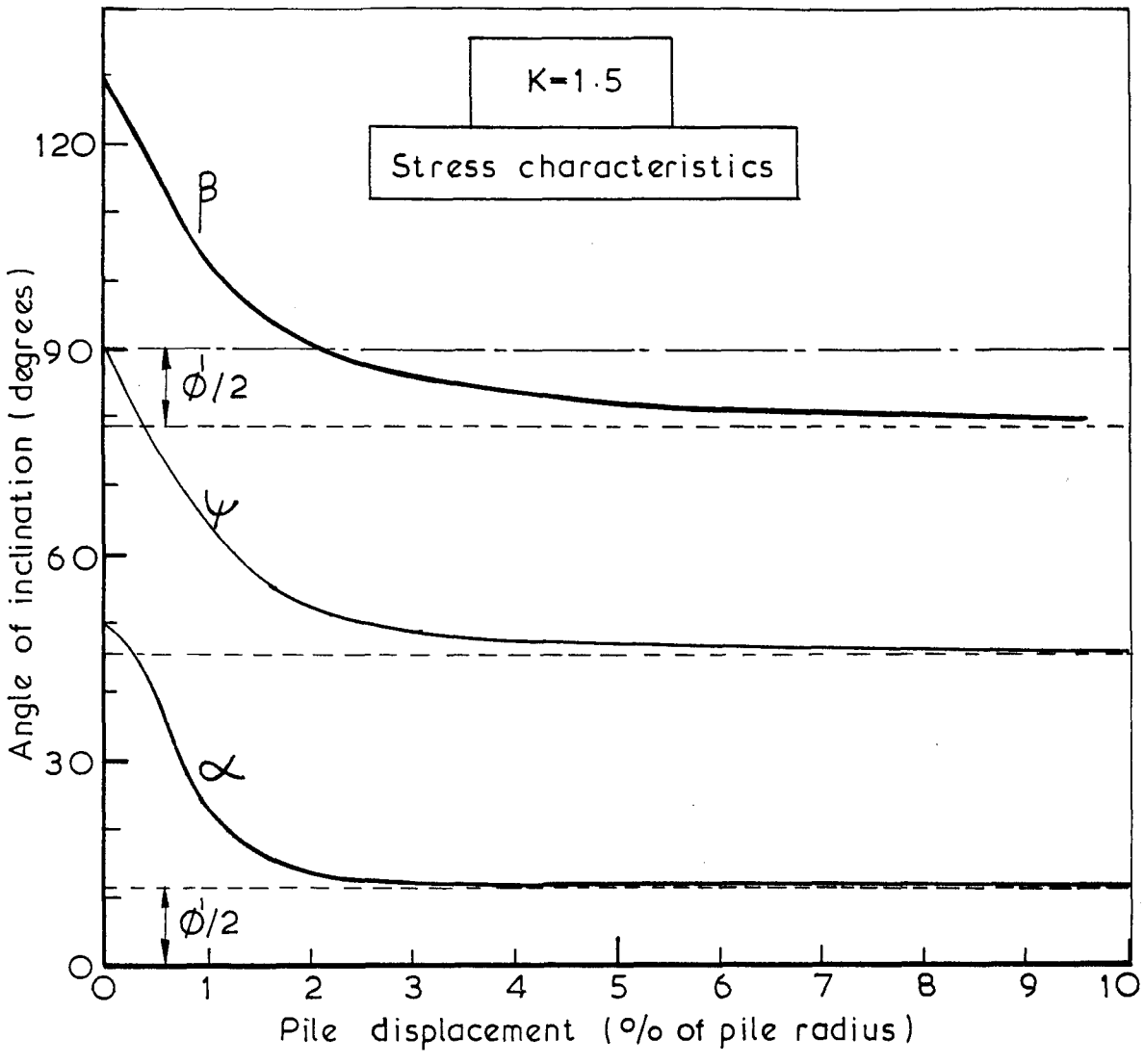
Predicted variation of the inclination of velocity characteristics and lines of zero total extension with pile displacement, for clay adjacent to the pile. K=1.5

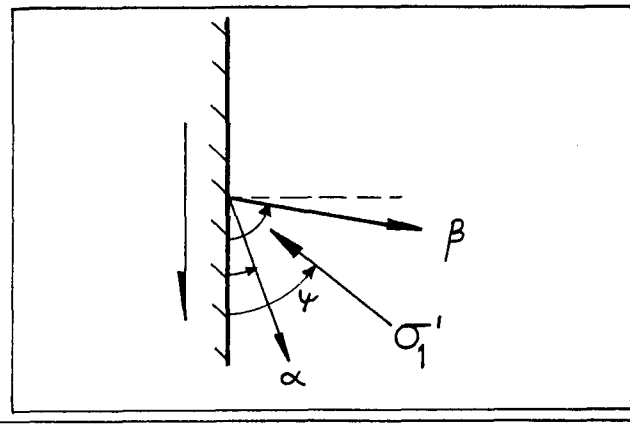
Fig.8.22



Variation of the inclination to the vertical of ∝ velocity characteristics with radial distance from the pile shaft. The pile is loaded to the maximum value; K=1.5

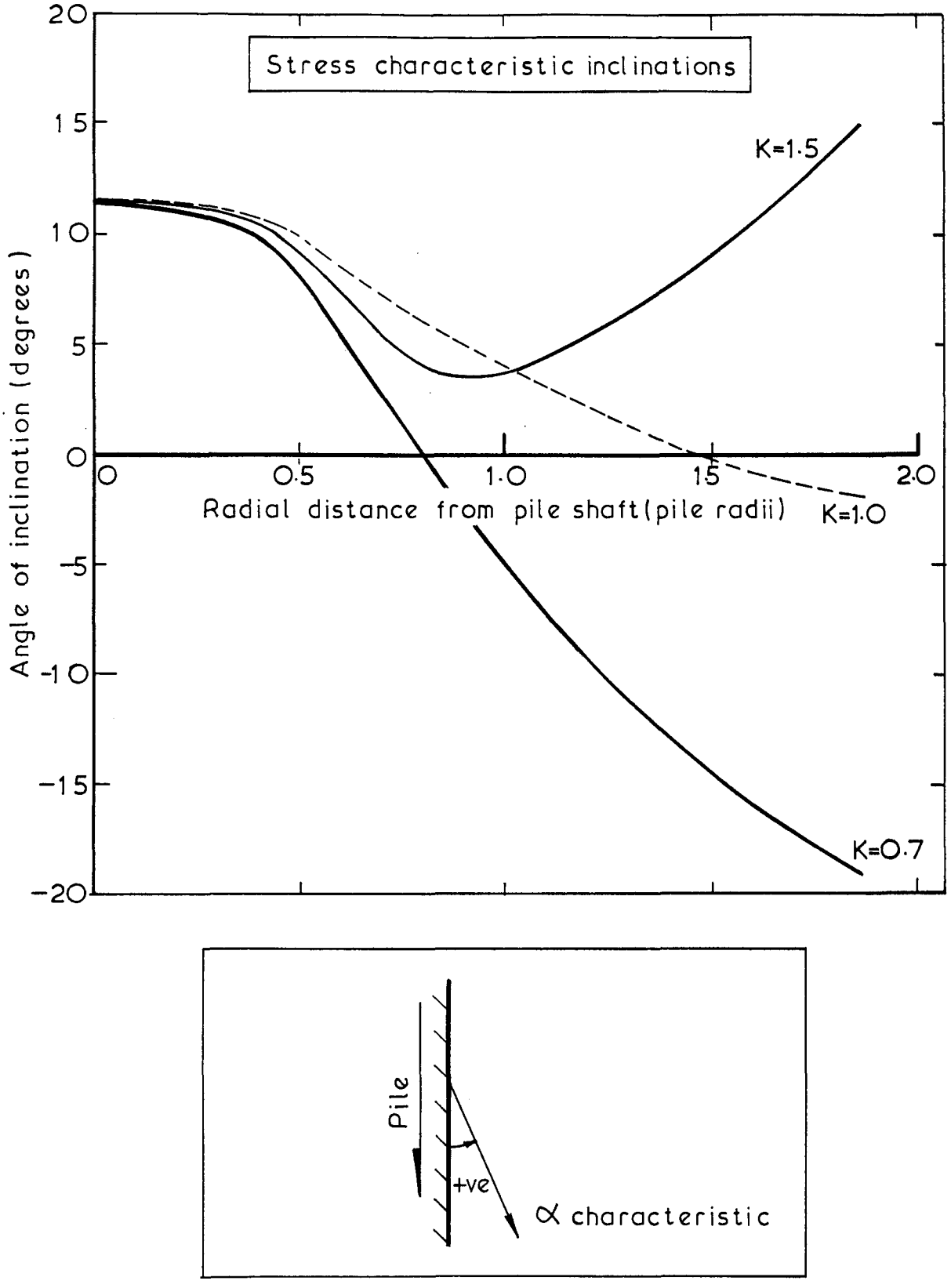
Fig. 8.23





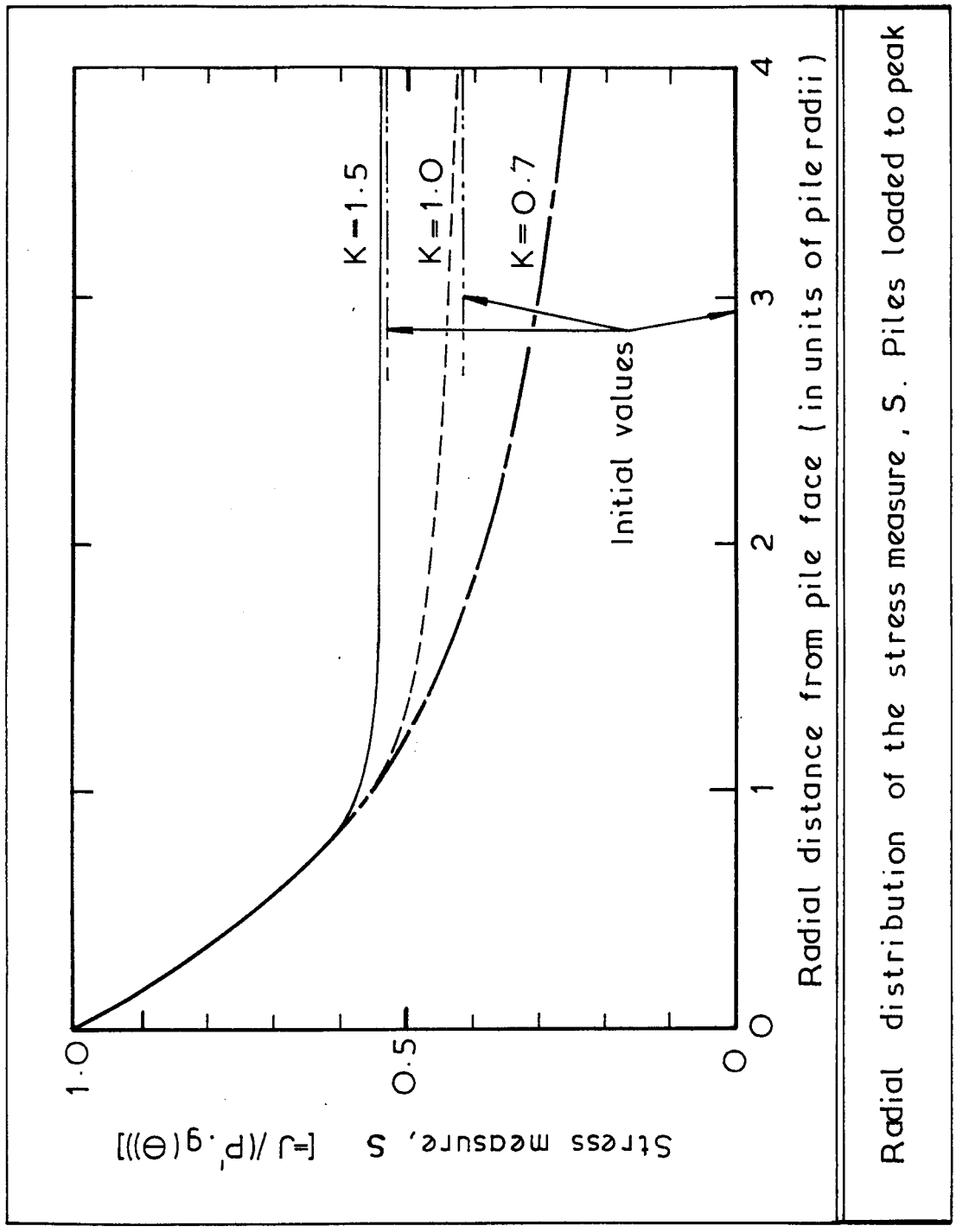
Predicted variation of stress characteristic directions with pile displacement, for an element of clay adjacent to the pile.
K 1·5, Soil Model B. Refer to Figure 8·15.

Fig. 8.24



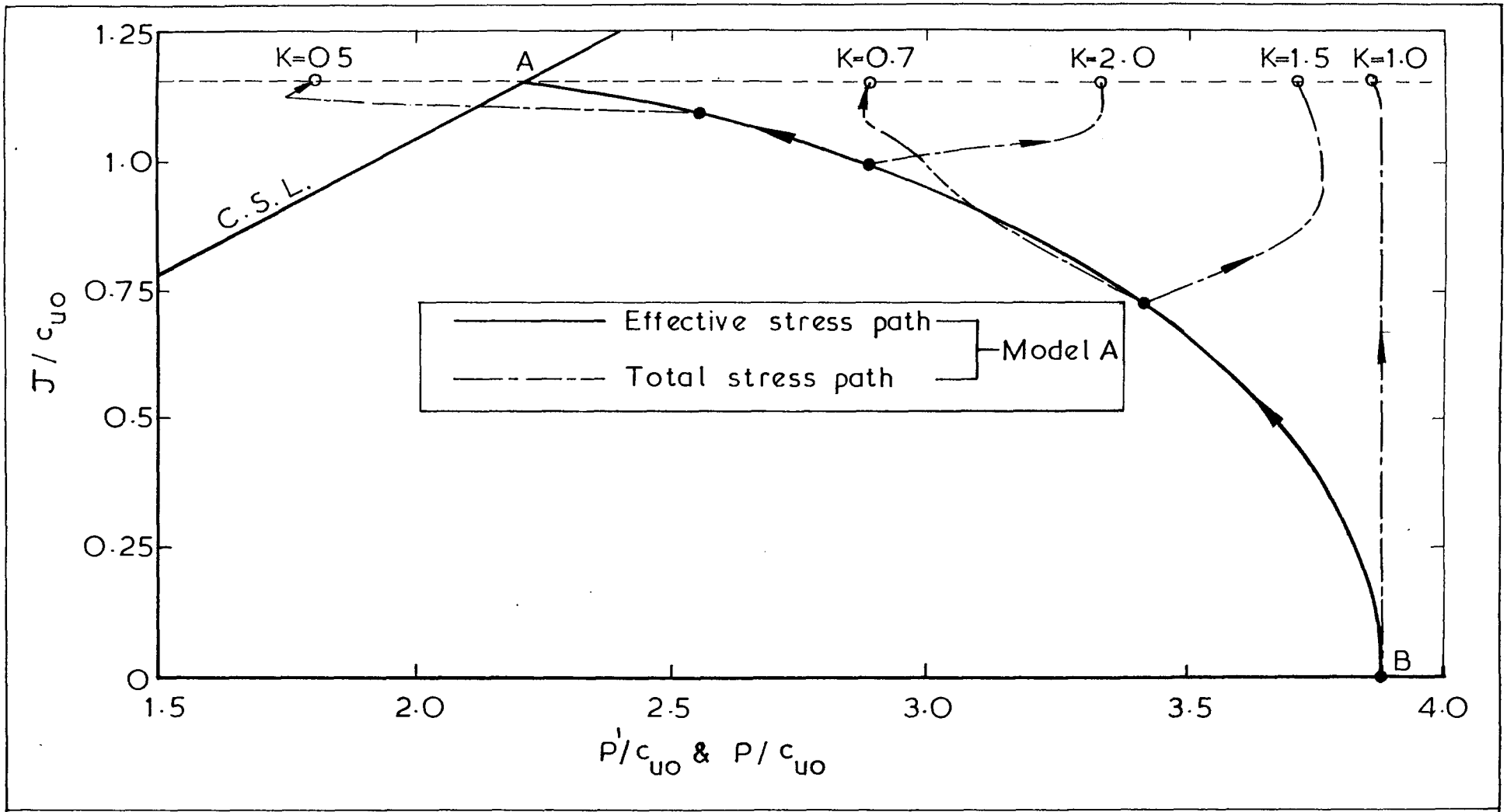
Variation of the inclinations of α stress characteristics with radial distance from the pile shaft. Pile loaded to peak.

Fig.8·25



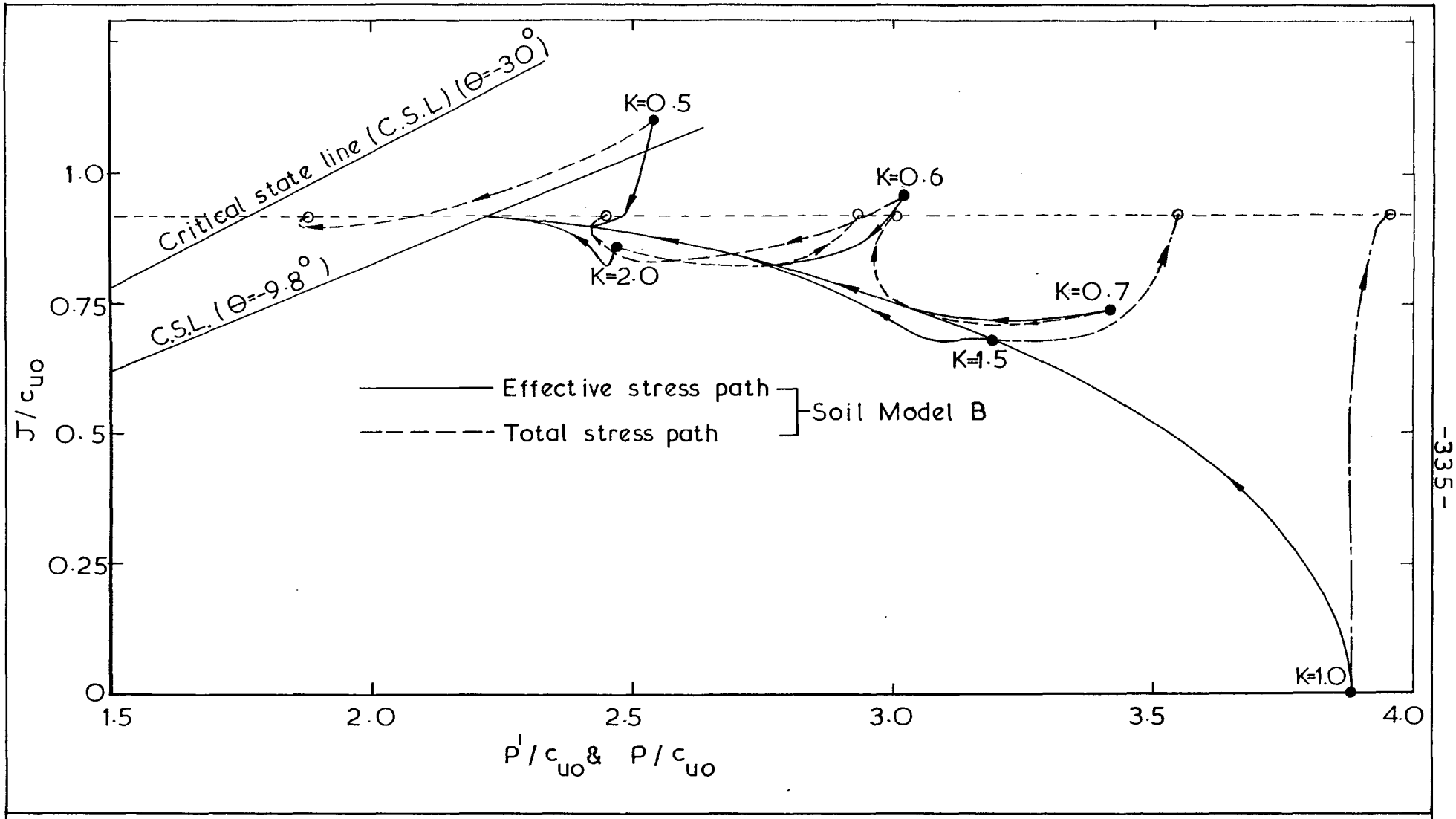
Radial distribution of the stress measure, S. Piles loaded to peak

Fig. 8.26



Stress paths followed during undrained loading; using soil Model A. Stresses normalized by the undrained shear strength in triaxial compression.

Fig. 8·27



Stress paths followed during undrained loading ; using soil Model B .
(Stresses normalized by the undrained shear strength in triaxial compression)

Fig.8.28

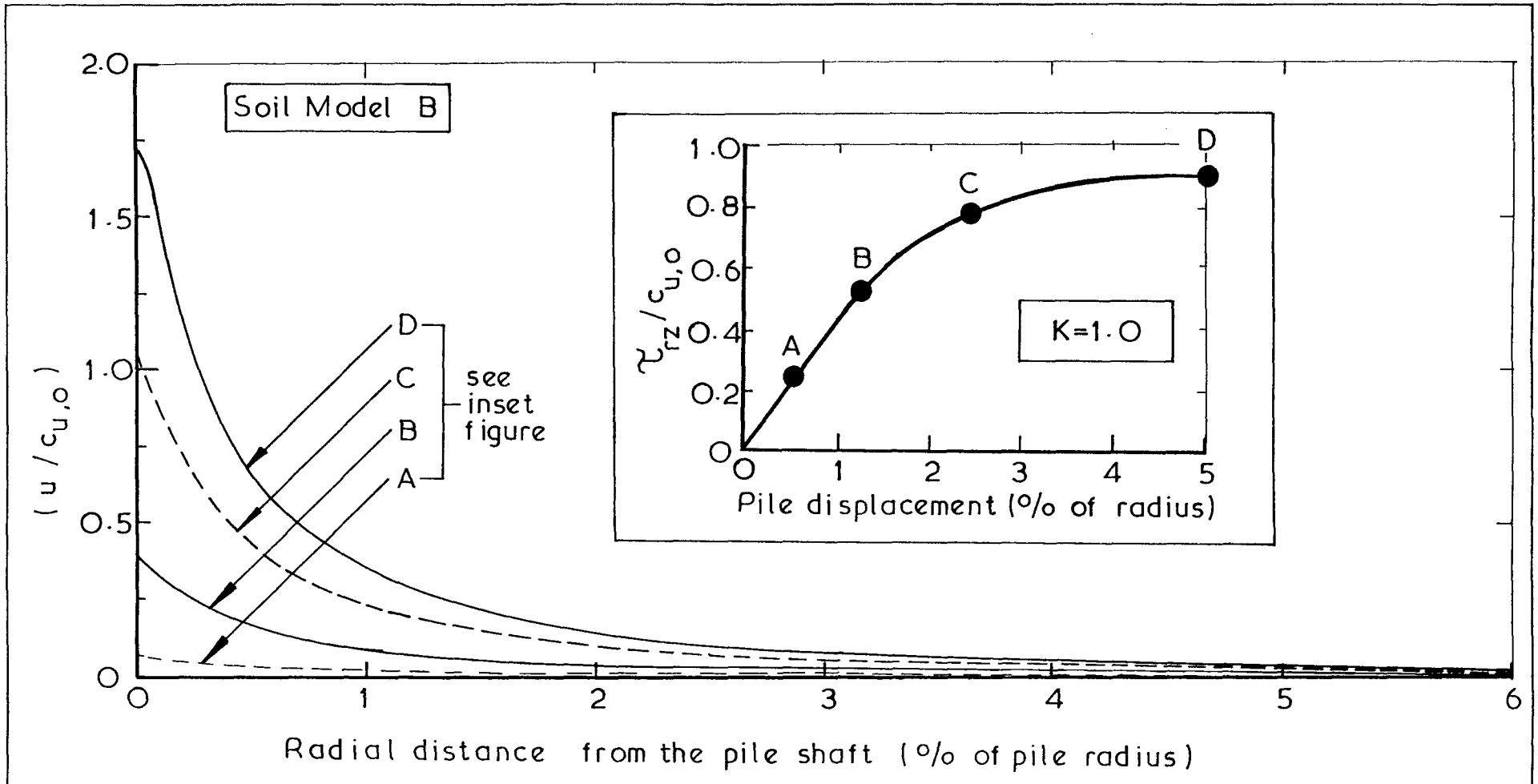


Fig.8. Radial distribution of pore pressures (normalized by the initial undrained shear strength in triaxial compression) at various stages during undrained loading. K=1·0

CHAPTER 9

DISPLACEMENT PILES

9.1 INTRODUCTION

In order to employ effective stress methods to analyse the loading behaviour of displacement piles, it is first necessary to be able to predict the state of stress acting in the clay surrounding the piles following installation and consolidation. These stresses will depend on the type of pile installed, i.e. full or partial displacement, the method of installation, and the nature of the clay. No attempt is made to model the details of the installation and consolidation processes; rather, it is believed that in the case of low-displacement piles some simple assumptions may be made regarding the stress state prior to pile loading, and the stresses around full-displacement piles are selected on the basis of work performed by Randolph and Wroth (e.g. 1979).

Tubular steel piles, such as those used extensively offshore, cause relatively little displacement of the soil provided that they do not plug during driving (there remains considerable doubt within the industry about whether, and under what circumstances, tubular steel piles do plug during installation). Carter, Randolph and Wroth (1980) have analysed the stress state in the clay surrounding low-displacement piles, modelling the installation as the expansion of a cylindrical cavity and employing the Modified Cam Clay constitutive law. Their results suggest that the stresses in the clay adjacent to low displacement piles are greater than the initial in-situ values. However, as far as the author is aware, these predictions have not yet been verified by field measurements. For the present, it might be advisable to adopt a more conservative approach and to assume that the pile installation/consolidation does not affect the stresses in the ground. The stresses in the clay surrounding the pile may, therefore, be taken as

$$\sigma'_r = \sigma'_\theta = K_o \sigma'_z$$

These conditions are the same as those employed in the first series of model pile tests described in Chapters 3, 4 and 5, and considered analytically in Chapter 8 (for normally-consolidated clays). The behaviour of low-displacement

piles is considered below in section 9.4.

The installation of full-displacement piles may be expected to have a more pronounced effect on the local soil stresses. A number of workers (e.g. Butterfield and Bannerjee (1970), and Randolph, Carter and Wroth (1979)) have modelled the pile installation as the expansion of a cylindrical cavity. Although predicted pore pressure changes during pile installation are in fair agreement with field measurements, the predicted radial effective stresses acting on the pile after consolidation are yet to be verified. More recently Baligh and Levadoux (1980) have modelled the related problem of the installation of cone piezometers by means of a strain path method. Although the approach appears to be most promising, field verification of the results are yet to be published.

In the work performed at Cambridge by Randolph and Wroth, the installation of a displacement pile is modelled as the plane strain expansion of a cylindrical cavity. The analyses employ the finite element method to obtain numerical predictions, and the clay is assumed to obey the 'Modified Cam Clay' constitutive law. One of the most important predictions arising from this research is that after pile installation and subsequent consolidation, the clay adjacent to the pile is in a normally-consolidated state irrespective of its initial in-situ overconsolidation ratio. The analyses also predict that immediately adjacent to the pile shaft $\sigma'_r = K_{o_{NC}} . \sigma'_z$, and $\sigma'_\theta = \sigma'_z$ where $K_{o_{NC}}$ is the 'at rest' coefficient of earth pressure associated with a one-dimensionally normally-consolidated clay. It should be noted that zero vertical total strain is assumed throughout the cavity expansion analysis. As this is equivalent to assuming that no heave occurs, the predicted stress changes are likely to represent an upper-bound to those actually occurring.

In order to examine the loading behaviour of full displacement piles, the results of two of the analyses presented by Randolph et al (1979) and Wroth et al (1980) have been employed to provide initial stress conditions in numerical computations employing the finite element mesh illustrated in Fig. 7.3. The cases selected are those of a pile installed in normally-consolidated Boston Blue Clay, and of a pile installed in London Clay having an initial overconsolidation ratio of eight. In the cavity expansion analyses the clays were assumed to obey a form of the Modified Cam Clay model in which both the yield function and the plastic potential exhibit rotational symmetry in the deviatoric plane. In the first analyses of pile

loading the same form of the constitutive law has been adopted for the sake of consistency; however, the analyses are later extended to consider the effect of employing a constitutive model in which the yield surface describes a Mohr-Coulomb hexagon, and the plastic potential a circle, in the deviatoric plane.

It is important to note that in the analyses of pile loading presented below it is assumed that the soil around the driven piles is intact in advance of pile loading, i.e. no account is taken of residual shear surfaces which might have been induced as a result of the pile installation procedure (see Chapter 6). The possible influence of such surfaces is considered in section 9.5.5.

9.2 THE LOADING BEHAVIOUR OF FULL-DISPLACEMENT PILES

9.2.1 Introduction

The behaviour on loading of piles installed in normally-consolidated Boston Blue Clay and in over-consolidated London Clay is considered for both drained and undrained conditions. The stresses induced by pile installation are taken from Randolph et al (1979) and from Wroth et al (1980), and both the yield functions and the plastic potentials are assumed to be surfaces of revolution.

9.2.2 Piles in Normally-consolidated Boston Blue Clay

The soil parameters (see Chapter 7) are assigned the following values to represent Boston Blue Clay;

$$M = 1.2,\ \lambda = 0.15,\ \kappa = 0.03,\ G = 12000\ kN/m^2,\ V_1 = 2.827,$$
$$Y = 0,\ \text{and}\ Z = 1.0$$

Except where stated to the contrary, the stresses represented in the following diagrams are normalised by $C_{u,i}$, the undrained shear strength (at a Lode angle, $\theta = 0°$) of the clay adjacent to the pile immediately in advance of pile loading.

Fig. 9.1(a) is a schematic representation of the total and effective stress paths followed by an element of clay adjacent to the pile during the cavity expansion and the subsequent consolidation (data taken from Randolph et al (1979)). Pile loading is simulated by imposing increments of shaft displacement, and the analyses are first performed to represent drained conditions. The predicted stress path for the above element of soil is

shown in Fig. 9.1(b) as the dashed line BC_1. Inspection of this figure indicates that the stress path followed during loading travels continuously in the direction of decreasing mean effective stress. The variation with pile displacement of the quantitites σ'_r, σ'_θ, σ'_z, τ_{rz}, J, γ_{rz} and ψ are illustrated in Fig. 9.2 for the same element of clay. Although it is predicted that the final shear stress acting on the shaft, τ_{rz}, is some 30% in excess of $C_{u,i}$, the decrease in the radial effective stress of roughly 40% should be noted.

The analysis is repeated to simulate undrained loading conditions. The total and effective stress paths followed by an element of clay adjacent to the shaft are presented in Fig. 9.1(b), and the corresponding variation with pile displacement of the quantities σ'_r, σ'_θ, σ'_z, τ_{rz}, J, u, γ_{rz} and ψ are shown in Fig. 9.3; u is the excess pore pressure generated on pile loading. It may be noted that the analysis predicts that on loading to peak the radial effective stress decreases by about 50%, whereas the radial total stress (σ'_r + u) decreases by only 17%. Excess pore pressures equal in magnitude to the undrained shear strength (at $\theta \simeq 0°$) of the clay beside the pile prior to loading, are predicted to be generated.

The predicted radial distribution of excess pore pressures at various stages during the pile loading are indicated in Fig. 9.4. For comparison, the predicted pore pressures generated during pile installation (taken from Randolph et al, 1979) are also indicated. The pore pressures have been normalised by $C_{u,o}$, the undrained shear strength of the clay in triaxial compression, prior to pile installation. It may be observed that the excess pore pressures generated on loading are much smaller, and are more localised, than those predicted to be generated during pile installation. If pile 'failure' were to be associated with slip along a shear surface created during pile installation then the peak excess pore pressures generated on loading would be even more localised. The differences between the distributions of excess pore pressures generated during installation and during loading suggest that the latter may dissipate more rapidly than the former. This subject is considered in the following section.

9.2.3 Dissipation of Excess Pore Pressures Around Loaded Piles

A finite difference program has been written to enable the rate of dissipation of excess pore pressures generated around piles to be estimated. It is assumed that the soil skeleton deforms elastically and the program, which is described in Appendix 9.1, can consider arbitrary distributions of

the initial excess pore pressures. Randolph and Wroth (1979) present an analytical solution for the dissipation of an initially logarithmic distribution of excess pore pressures; it is shown in Appendix 9.1 that predictions based on the finite difference program are in excellent agreement. Carter et al (1979) showed that the predicted rate of dissipation of excess pore pressures is relatively insensitive to the choice of soil constitutive model, and so it is believed that the finite difference program is capable of providing reasonable estimates of consolidation times for arbitrary distributions of initial excess pore pressures.

Reconsider the example presented in section 9.2.2 of the excess pore pressures generated around a pile installed in normally-consolidated Boston Blue Clay (also refer to Fig. 9.4). The predicted variations of excess pore pressures at the pile face with a dimensionless measure of time ($T = C_v t/R^2$) are illustrated in Fig. 9.5; the dissipation of excess pressures generated during installation and on loading to peak is considered. By comparing the times for either 50% or for 90% dissipation of excess pore pressures at the pile face, it may be seen that the pressures generated on loading to peak dissipate almost an order of magnitude faster than the installation pressures.

Randolph et al (1979) present an example of the predicted times for the dissipation of excess pore pressures at the face of a 0.2 m radius pile driven into clay with a coefficient of consolidation of 3 m^2/year. Times for 50% and 90% dissipation of excess pore pressures at the pile face were estimated at 1 week and 20 weeks respectively. Extending this example to consider the dissipation of pore pressures generated on loading to peak, the times for 50% and 90% dissipation at the pile face are of the order of 17 hours and 2 weeks respectively. For the loading to be considered undrained (i.e. less than 5% dissipation of excess pore pressures at the face), the loading time would need to be of the order of half an hour. Such results suggest that on land, where piles are often loaded at a rate determined by the speed of construction of the structure to be supported, the loadings will often be almost fully drained. Even pile loading tests will tend to be partially drained.

Offshore, piles of up to 2 m diameter are being employed. Taking the example of a 2 m diameter pile driven into a Glacial Till having a coefficient of consolidation of 1 m^2/yr, the times for 10%, 50% and 90% dissipation of excess pore pressures generated at the pile face as a result

of pile loading are 6 days, 3 months and more than 3 years, respectively. Such results suggest that storm loadings will be completely undrained phenomena, whereas the pore pressures generated by the dead-load of the structure may have dissipated significantly before the onset of the first winter storms; pressures induced by driving will dissipate far more slowly.

The rapidity with which the excess pore pressures dissipate has important implications for model pile testing in the laboratory. For the loading of a 15 millimeter diameter model pile installed in Kaolin to be considered truly undrained, the loading to peak would need to be accomplished within less than one second! With such rapid loadings, strain rates of the order of 100% per second might be expected; these would tend to complicate interpretation of the results!

9.2.4 Pile Installed in Over-consolidated London Clay

On the basis of Wroth et al (1980) the following soil parameters have been selected to represent London Clay; $M = 0.984$, $\lambda = 0.161$, $\kappa = 0.062$, $V_1 = 2.759$, $G = 6750\ kN/m^2$, $Y = 0.0$ and $Z = 1.0$.

The radial variation of the principal effective stresses σ'_r, σ'_θ and σ'_z, and the undrained shear strength of the clay following pile driving and the subsequent consolidation are taken from Wroth et al (1980) for the case of a full displacement pile driven into London Clay having an initial over-consolidation ratio of eight. As noted earlier, Wroth et al predict that after driving and consolidation, the clay at the pile face is normally-consolidated.

Pile loading is again simulated by applying increments of shaft displacement, and the analysis is performed to represent drained conditions. The stress paths followed by the clay adjacent to the pile during driving and consolidation are illustrated schematically in Fig. 9.6, and the predicted stress path on loading is represented by the dashed line BC_1.

The variations with pile displacement of the quantities σ'_r, σ'_θ, σ'_z, τ_{rz}, J, γ_{rz} and for an element of clay adjacent to the pile shaft are shown in Fig. 9.7. The rapid rotation of the principal stresses may be noted; 90% of the overall rotation has occurred once 80% of the pile capacity has been mobilised.

The predicted radial variations of the total shear strain, γ_{rz}, are presented in Fig. 9.8 for various stages of loading. It is evident that as the pile load approaches the peak capacity, very large shear strains are

predicted in the immediate vicinity of the pile. If the clay were to exhibit even gradual strain softening (such as might result from particle orientation effects) then the post-peak behaviour would be brittle and progressive failure would be predicted for compressible piles. It should be remembered that in the current analysis it is still assumed that the clay beside the pile is intact after pile driving (see section 9.5.5 for a discussion of the possible effects of shear surfaces formed during pile installation).

9.2.5 Simplified Analyses of Pile Loading

The work of Randolph and Wroth suggests that the stress state of the clay adjacent to a displacement pile may readily be predicted from a knowledge of the initial in situ undrained shear strength and the 'Cam Clay' parameters representative of the particular clay. However, prediction of the radial variation of the stress state in the surrounding clay typically requires full cavity expansion and consolidation analyses. The question naturally arises as to whether this radial variation in conditions has an important bearing on the subsequent loading behaviour. Could a reasonable approximation be made by ignoring the radial variation and setting the stresses everywhere to equal those predicted to exist adjacent to the pile face? This subject is addressed below.

The earlier analyses of the loading behaviour of displacement piles in normally-consolidated Boston Blue Clay and in over-consolidated London Clay are repeated, but the radial variation of the stress state prior to loading is ignored; the stress state is set everywhere to that predicted to exist in the clay immediately adjacent to the shaft.

The simplified analysis predicts that for a loaded pile in normally-consolidated Boston Blue Clay, the element of clay adjacent to the shaft will follow the effective stress path shown as BC_2 in Fig. 9.1. It may be seen that there is very good agreement between this stress path and that obtained (BC_1) starting from the 'correct' initial stress distribution.

A similar simplified analysis performed to consider the behaviour of a pile in over-consolidated London Clay predicts that the stress path followed by the clay adjacent to the pile will be as shown as the path BC_2 in Fig. 9.6. The correspondence between this stress path and that predicted using the 'correct' initial stress distribution is not as good as that obtained above for the pile in normally-consolidated clay, although the approximate prediction is at least conservative. In both sets of analyses,

the variations with pile displacement of σ'_r, σ'_θ, σ'_z, τ_{rz} and γ_{rz} for the element of clay beside the pile predicted on the basis of the simplified initial stress distribution are also in good agreement with the corresponding 'correct' analyses.

The agreement between the predictions of drained pile loading behaviour based on the simplified and the 'correct' analyses is very convenient and it highlights the importance of correctly predicting the stresses acting in the clay immediately adjacent to a displacement pile prior to loading. For the present these stresses may be predicted on the basis of the work presented by Randolph et al (1979). The above results also mean that useful parametric studies of pile loading behaviour may be performed without the need to conduct numerous costly cavity expansion and consolidation analyses; parametric studies are described in section 9.3.

9.2.6 Undrained Pile Loading

The kinematic constraints acting on the soil adjacent to a pile loaded under undrained conditions are very severe and completely dictate the soil response and pile loading. The constraints are;

(i) $(\dot{\varepsilon}_z^T)_{r=r_o} = 0$ because of the assumption of no slip at the pile/soil interface.

(ii) $(\dot{u}^T)_{r=r_o} = 0$ because the pile is assumed to be rigid radially.

(iii) $(\dot{\varepsilon}_\theta^T)_{r=r_o} = 0$ because $(\dot{u}^T)_{r=r_o} = 0$; $\dot{\varepsilon}_\theta^T = \frac{\dot{u}^T}{r} = 0$

(iv) $\dot{\varepsilon}_r^T + \dot{\varepsilon}_\theta^T + \dot{\varepsilon}_z^T = 0$ undrained conditions imposed.

(v) $\dot{\varepsilon}_z^T = 0$ by symmetry if a short segment of a very long pile is considered.

u is the local radial displacement

The above constraints impose a further restriction on the permissible radial displacements within the soil surrounding the pile;

$$\dot{\varepsilon}_r^T = -\frac{d\dot{u}^T}{dr}$$

$$\dot{\varepsilon}_\theta^T = \frac{\dot{u}^T}{r}$$

$$\dot{\varepsilon}_z^T = 0 \qquad \text{from (v)}$$

Combining these conditions and substituting into (iv) leads to

$$-\frac{d\dot{u}^T}{dr} + \frac{\dot{u}^T}{r} = 0$$

Thus

$$\frac{d\dot{u}^T}{\dot{u}^T} = \frac{dr}{r}$$

$$\ell n\left(\frac{\dot{u}^T_{r=r}}{\dot{u}^T_{r=r_o}}\right) = \ell n\left(\frac{r}{r_o}\right)$$

and hence

$$\dot{u}^T_{r=r} = \dot{u}^T_{r=r_o}\left(\frac{r}{r_o}\right)$$

As

$$\dot{u}^T_{r=r_o} = 0 \quad \text{from (ii)},$$

(vi) $$\dot{u}^T = 0 \quad \text{everywhere.}$$

Consequently (vii) $$\dot{\varepsilon}_r^T = 0 \quad \text{everywhere}$$

(viii) $$\dot{\varepsilon}_\theta^T = 0 \quad \text{everywhere}$$

A consequence of these constraints is that the soil everywhere is being deformed in undrained simple shear, and if the behaviour of a single

element of the soil can be established then this may be used to determine the overall response using the equilibrium equation

$$\tau_{rz}(r) = \tau_{rz}(r_o) \cdot (\frac{r_o}{r})$$

and integrating the predicted shear strains with respect to radius.

The behaviour of an element of soil in undrained simple shear may be estimated by using the Modified Cam Clay constitutive law in conjunction with a computer code. However, if only the final stress conditions at the pile interface are required then these may be evaluated directly from a knowledge of the initial stresses acting on the shaft following driving and consolidation. This is considered further in Appendix 9.2.

Thus it is possible to determine the undrained failure conditions without performing numerical analyses. However, drained conditions are far more complex, and no such simple relations have been found to establish conditions at peak. In the remainder of this chapter attention is largely restricted to drained loading behaviour, although in practice pile loadings will generally be partially drained (as discussed in section 9.2.3) and the actual behaviour will tend to lie between the bounds of fully drained and undrained conditions.

Noting that the soil around a pile loaded under undrained conditions behaves in undrained simple shear, Randolph and Wroth (1981) proposed that the simple shear apparatus be used to establish the constant volume behaviour of soils; these results would then be used in pile design. The validity of such a procedure is considered in section 9.6.

9.3 PARAMETRIC STUDIES

9.3.1 Introduction

It has been shown in section 9.2 that when the loading behaviour of piles is considered, a useful simplification may be made in which it is assumed that there is no radial variation of the stresses in the soil prior to loading. The values of the stresses assumed may be those predicted on the basis of cavity expansion and consolidation analyses (Randolph et al, 1979).

Parametric studies have been performed to consider the influence on the predicted pile loading behaviour of the following factors:

(i) the assumed shape of the yield surface in the deviatoric plane;

(ii) small deviations of the initial stresses at the pile face, prior to loading, from the values predicted on the basis of Randolph et al (1979);

(iii) the various soil parameters employed in describing the constitutive model.

9.3.2 Shape of the Yield Surface in the Deviatoric Plane

In order to ensure compatibility with the cavity expansion analyses presented by Randolph et al (1979), the analyses presented in the previous sections have adopted a surface of revolution for the yield surface. As illustrated in Table A.7.1 the use of such an assumption leads to a considerable variation in the angle of shearing resistance, ϕ', with the Lode angle.

Three analyses are presented in order to demonstrate the influence of the shape of the yield surface in the deviatoric plane on the predicted behaviour of the soil adjacent to a loaded pile. The same initial stress conditions are adopted in the three analyses, and it is assumed that there is no initial radial variation in stress. The parameters λ, κ, v_1 and G are assigned values used earlier to represent London Clay, and in the three examples the plastic potential has been taken to be a surface of revolution. The effect of this latter assumption, as discussed earlier, is to ensure that the critical state is reached at a Lode angle of zero. In two of the analyses surfaces of revolution are also adopted for the shape of the yield function; in one analysis M has been selected as 0.732 and in the other 0.984. These M values correspond to ϕ' values of 19° and 25° respectively in triaxial compression, and to 25° and 34.6° at a Lode angle of zero. In the third analysis a Mohr-Coulomb hexagon has been adopted for the shape of the yield surface in the deviatoric plane, and ϕ' is chosen to be 25°. The initial stresses are the same in all three examples, and the values have been selected such that in the case of the clay assumed to have a constant ϕ' of 25°, the initial undrained shear strength at a Lode angle of zero is 100 kN/m^2.

The stress paths predicted to be followed by the clay adjacent to the pile faces are illustrated in Figs. 9.9(a) and (b). In the former, the stresses are normalised by the undrained shear strength (100 kN/m^2) of the clay exhibiting a constant $\phi' = 25°$, whereas in the latter the three stress paths are each normalised by the respective initial undrained shear strengths at a Lode angle of zero.

Comparing predictions based on the two models employing constant values of M, the following points may be noted.

(i) as may be seen in Fig. 9.9(a), stress paths (b) and (c), the predicted peak values of J are markedly different whereas the final values of P' are similar (having reduced by about 15%). As a result of the similarity in P' values, the peak values of J and also τ_{rz} are directly proportional to M;

(ii) reductions in σ'_r of about 38% are predicted in both cases.

The stress path predicted by the analysis employing a Mohr-Coulomb hexagon for the yield function is indicated by the path (a) in Figs. 9.9(a) and (b). It is predicted that P' reduces by about 20%, and that σ'_r reduces by 42%. These reductions are greater than those predicted by the models having constant values of M. Similarly, the final values of both J and τ_{rz} are smaller in the analyses assuming a constant value of ϕ'.

These observations suggest that analyses based on soil models which assume the yield function to be a surface of revolution may lead to slightly unconservative predictions. Nevertheless, the final strengths predicted by the two analyses having the same value of ϕ' at a Lode angle of zero (curves (a) and (b) in Fig. 9.9(a)) differ by only 10%, and this is within the range of uncertainty in the selection of soil parameters. The use of a surface of revolution for the yield function therefore appears to be a reasonable approximation provided that the predicted shaft capacities are adjusted to correspond to the correct value of M at peak.

The stress paths followed by an element of clay adjacent to a full-displacement pile loaded under drained and undrained conditions are illustrated in Fig. 9.10. The yield surface is taken to be a Mohr-Coulomb hexagon in the deviatoric plane, and $\phi' = 25°$; the plastic potential is again a surface of revolution. The simplified initial stress distribution has been

adopted, and K_o is assumed to be 1-sin ϕ' (see section 9.3.3.3). The variation with pile displacement of various components of stress and strain are illustrated in Fig. 9.11, where it will be seen that the stress measure, S, remains constant during the early stages of loading and then increases monotonically to reach the ultimate value of unity at the Critical State.

9.3.3 The Effects of Deviations of the Stress Conditions (around Displacement Piles) from the Values Predicted on the Basis of Cavity Expansion Analyses

9.3.3.1 Introduction

The aim of this parametric study is to examine whether there are any particular features of the stress state predicted to exist in the clay around an unloaded displacement pile, to which the subsequent loading behaviour might be particularly sensitive. It may be helpful to repeat the main features of stress state predicted by Randolph et al (1979) to exist in the clay adjacent to a displacement pile following installation and consolidation;

(i) $\sigma'_\theta = \sigma'_z = K_{o_{NC}} . \sigma'_r$

where K_{ONC} is the 'at-rest' coefficient of earth pressure associated with one-dimensionally, normally-consolidated clay;

(ii) the clay immediately adjacent to the pile is in a normally-consolidated state, irrespective of the initial in situ overconsolidation ratio.

In the following analyses a Mohr-Coulomb hexagon is adopted for the shape of the yield surface in the deviatoric plane, and ϕ' is 25°. The soil parameters λ, κ, v_1 and G are assigned the values employed earlier to represent London Clay, and the magnitudes of the stresses are selected such that prior to loading, the undrained shear strength of the clay, at a Lode angle of zero, is 100 kN/m^2.

In section 9.3.3.2, below, the effects of departures from normally-consolidated conditions immediately adjacent to the pile are considered,

and in section 9.3.3.3 the influence of the assumed value of K_o is examined (K_o predicted by Modified Cam Clay is much larger than 1-sinϕ').

9.3.3.2 Departures from Normally-Consolidated Conditions Adjacent to Displacement Piles

The results of two analyses assuming OCR's (defined in Chapter 7 as P'_o/P') of 1.5 and 2.0 are presented, and compared with the analysis assuming normally-consolidated conditions (see section 9.3.2). The relative locations of the three initial stress conditions in the plane corresponding to a constant water-content are illustrated in Fig. 9.12.

The results of the pile loading analyses are presented in the form of stress paths (solid lines in Fig. 9.13), and of graphs of the variation of the local radial stresses with pile displacement (Fig. 9.14). Whilst there are evidently differences between the predictions corresponding to the various initial degrees of overconsolidation, the values of $J/C_{u,i}$ and $\sigma'_r/C_{u,i}$ at peak load are very similar in all three cases. Thus the stresses acting on the pile shaft at peak are little affected by the local OCR, as long as the correct undrained shear strength after pile driving and consolidation has been established. For comparison, the stress paths predicted by analyses adopting a constant value of M (selected such that $\phi' = 25°$ at $\theta = 0°$) are also shown in Fig. 9.13.

9.3.3.3 Influence of the Initial Stress Ratio

Randolph et al (1979) suggest that the stresses in the clay at the face of a displacement pile prior to loading are in the ratios

$$\sigma'_\theta = \sigma'_z = K_{o_{NC}} \cdot \sigma'_r$$

where $K_{o_{NC}}$ is the 'at-rest' coefficient of earth pressure corresponding to normally-consolidated conditions. The value of $K_{o_{NC}}$ predicted by the Modified Cam Clay (M.C.C.) is in general too high; in the present example of London Clay MCC predicts $K_o = 0.715$, whereas Jaky would suggest 0.577 for $\phi' = 25°$. Analyses have been performed in which the value of K_o is varied, but the initial stress levels are adjusted such that the initial undrained shear strength remains constant (see Potts and Martins, 1982(a)). The results suggest that the ultimate values of J, τ_{rz} and σ'_r are relatively insensitive to K_o, provided that the initial undrained shear strength is correctly established. The initial shapes of the loading stress paths are

somewhat more sensitive to the value of K_o selected.

In conclusion the studies have shown that it is important to correctly predict the undrained shear strength of the clay beside the pile after installation and consolidation. However, small departures from the conditions outlined by Randolph et al (1979) are relatively unimportant.

9.3.4 Effect of Changes in the Parameters Describing the Soil Model on the Behaviour of Full-Displacement Piles

9.3.4.1 Introduction

A limited parametric study has been performed in order to investigate the influence of the quantities ϕ', $G/C_{u,i}$, λ and κ on pile behaviour. In the analyses described below, the yield function is assumed to describe a Mohr-Coulomb hexagon in the deviatoric plane whereas the plastic potential is taken to be a surface of revolution. The initial stresses are prescribed in the ratios

$$\sigma'_z = \sigma'_\theta = K_{o_{NC}} \sigma'_r = (1 - \sin \phi') \sigma'_r$$

and there is no initial radial variation in the stresses. The stress levels are selected in each case such that the initial undrained shear strength $C_{u,i}$ at a Lode angle of zero is 100 kN/m^2.

9.3.4.2 Angle of Shearing Resistance, ϕ'

The value of ϕ' is varied between 20° and 35° whilst the values of $G/C_{u,i}$, λ, κ and v_l are maintained at 120, 0.15, 0.03 and 2.83 respectively (appropriate to the Boston Blue Clay described in section 9.2). It may be seen in Fig. 9.15 that the resulting curves of shear stress acting on the shaft against pile displacement are little different despite the changes in ϕ'. Fig. 9.16 demonstrates that for a given value of $C_{u,i}$ there is a tendency for τ_{max} to decrease with increasing ϕ'! The reduction in the radial stress on loading to peak changes from 34% to 45% as ϕ' is increased from 20° to 35°. For drained loadings τ_{max} does not exceed $C_{u,i}$ by more than 20%, and is, of course, equal to $C_{u,i}$ on undrained loading.

9.3.4.3 $G/C_{u,i}$

The predicted stress paths corresponding to both drained and undrained loading are presented in Fig. 9.17 for a variety of values of

$G/C_{u,i}$. At the start of loading the clay beside the pile is in a state of triaxial compression, whereas on loading, the Lode angle of the clay beside the piles rapidly tends towards zero; this rotation of the stress state in the deviatoric plane results in a decrease in the value of $g(\theta)$, and hence initially in $J/C_{u,i}$.

In the case of drained loadings, the ultimate strength increases slightly with decreasing $G/C_{u,i}$, but the overall variation is less than 10% and so the correct prediction of $G/C_{u,i}$ is considered relatively unimportant in the estimation of shaft resistance. However, the same is certainly not true when considering shaft load-displacement behaviour as can be seen in Fig. 9.18. Until about 70% of $C_{u,i}$ is mobilised the load-displacement behaviour for drained and undrained loadings is very similar, and the slope is directly proportional to $G/C_{u,i}$. Evidently an accurate assessment of $G/C_{u,i}$ is important when estimating settlements.

9.3.4.4 λ and κ

As discussed earlier, the response of the clay around a loaded pile is dominated by the kinematic boundary conditions. The kinematic constraints necessitate a balance between elastic and plastic components of strain and so it seems reasonable to expect that the response will be influenced by the values of λ and κ. In the analysis presented below different values of λ and κ are adopted and the initial undrained shear strength, $C_{u,i}$, at a Lode angle of zero, is again set to be 100 kN/m^2.

It may be seen in Fig. 9.19 that the effect of increasing λ is to slightly reduce the available strength on drained loading; a change in λ from 0.09 to 0.24 results in an 8% reduction in the drained shaft resistance. A high value of λ tends to increase the plastic strains which in turn require greater compensating elastic strains to satisfy the kinematic restraints, and thus the drained stress path is constrained further towards the undrained stress path. Changes in κ have a slightly smaller effect.

It would appear that in practice the likely errors in the determination of λ and κ are unlikely to cause serious error in the prediction of pile capacities, provided that the undrained shear strength of the clay adjacent to the unloaded pile is correctly established.

9.3.5 Comments

The work presented on loaded full-displacement piles has considered the surrounding soil to be intact, i.e. no account is taken of discontinuity surfaces that might be induced in the soil as a result of the installation. It has been shown that if this were true then the pile capacities in drained and undrained loading would be directly related to the undrained shear strength in the soil adjacent to the pile prior to loading, and otherwise relatively independent of the soil parameters. The slope of the load-displacement curve was shown to be directly related to the $G/C_{u,i}$ values in the early stages of loading. As peak conditions are approached the shear strains near the pile become locally very large and predominantly plastic. Pore pressures generated during undrained loading are similarly localised and it has been shown that these may be expected to dissipate roughly an order of magnitude faster than those generated during pile installation.

The dominating influence of the kinematic restraints in forcing the drained and undrained stress paths for elements adjacent to driven piles to be so similar is the reason why the undrained strength after installation is such an important quantity. As this in turn is directly related to the initial in situ undrained shear strength, it suggests an explanation in terms of effective stresses of why total stress design methods have been as successful as they have, despite the fact that in practice many pile loadings are probably almost fully drained.

9.4 LOW-DISPLACEMENT PILES

9.4.1 Introduction

Carter, Randolph and Wroth (1980) present an analysis of the stress changes occurring around an unplugged, open-ended pipe pile as it is driven into clay which is then allowed to consolidate. It was assumed that a volume of clay equal to that of the pile wall embedded is displaced radially outwards, and the problem was analysed as the expansion of a cylindrical cavity. The results obtained suggest that stress changes in the clay surrounding the pile are significant, although they are far more localised than those predicted to occur around full-displacement piles.

As the above predictions have not yet been validated in the field, it has been decided to adopt a more conservative approach. In the following analyses, it is assumed that the installation of a low-displacement pile has a negligible influence on the stress state of the clay. Attention is restricted to piles installed into normally-consolidated clay, although the main conclusions are valid even if the clay around the pile is lightly over-consolidated immediately prior to loading. It must again be emphasised that no account is taken of the local fabric disturbance which may occur adjacent to the pile shaft during installation.

9.4.2 Drained and Undrained Pile Loadings

On the basis of the assumptions outlined above, the stresses within the clay surrounding an unloaded pile are given by

$$\sigma'_r = \sigma'_\theta = K_{o_{NC}} \sigma'_z \cong (1-\sin\phi')\,\sigma'_z$$

In the analyses presented below the clay parameters are assigned the following values; $G/C_u = 120$, $\lambda = 0.15$, $\kappa = 0.03$, $v_1 = 2.83$ and $\phi' = 25°$. The yield surface is assumed to describe a Mohr-Coulomb hexagon in the deviatoric plane, and the plastic potential is a surface of revolution.

The stress paths followed by an element of clay adjacent to the pile shaft are presented in Fig. 9.20 for both drained and undrained loadings. In the early stages of loading the stress paths are very similar, but they diverge as peak conditions are approached, although the drained capacity exceeds the undrained capacity by less than 10%. Comparison between the total and effective stress paths for the undrained loading reveals that

negative excess pore pressures may be generated initially despite the fact that the clay is normally-consolidated. As discussed in Chapter 8, this phenomenon is an unusual consequence of the kinematic constraints imposed. The variations with pile displacement, of several components of stress and strain, are illustrated in Fig. 9.21. It may be seen that on loading to peak, σ'_z reduces at around 40%, whereas σ'_r decreases only slightly. The peak value of τ_{rz} is a little greater than the initial undrained shear strength at a Lode angle of zero.

A study of the effects of ϕ' on the pile capacity, for a given value of the initial undrained shear strength, reveals a similar trend to that encountered in the analyses of full-displacement piles; the results are compared in Fig. 9.16. Curves of unit shaft friction against pile movement for a 'full'-displacement pile and a 'zero' displacement pile are compared in Fig. 9.22. Although the curves are very similar, it should be remembered that $C_{u,i}$ in the clay adjacent to the full-displacement pile will be of the order of 1.6 times greater than that adjacent to the 'zero'-displacement pile.

9.5 DISCUSSION OF RESULTS

9.5.1 Introduction

The predicted variations of the stresses acting on piles during loading are compared with the limited field and laboratory data available. It is unfortunate that there are few published measurements of the radial stresses, shear stresses or even pore pressures acting on the faces of loaded piles, and even fewer simultaneous measurements of all three quantities. It should be recalled that the analyses above have all assumed the soil beside the pile to be intact prior to loading. The possible influence of shear surfaces created during pile installation is considered separately in section 9.5.5.

9.5.2 Pore Pressure Generation

The most common measurements of pore pressures generated around piles are obtained by means of piezometers located some distance from the pile face. Typical measurements range between 0.2 and 0.5 times the initial in situ undrained shear strength in triaxial compression, $C_{u,o}$ (e.g. Lo and Stermac (1964), and Clark and Meyerhof (1972,a), and Meyerhof (1976)). On the other hand, measurements obtained at the pile face are usually higher, and values up to 1.5 $C_{u,o}$ have been recorded along piles in sensitive clays (e.g. Roy, Blanchet, Tavernas and La Rochelle (1981), Puech and

Jezequel (1980), and Massarch, Broms and Sundquist (1975)). The field results are summarised in Chapter 2, Table 2.1.

The theoretical predictions presented above (taking no account of the possible influence of shear surfaces induced parallel to the piles during installation) indicate that peak excess pore pressures ranging between 0.25 and 1.8 times the initial undrained shear strength of the clay (in triaxial compression) may be anticipated; the lower limit corresponds to low displacement piles and the higher to full displacement piles. Of course, if the pile were to 'fail' along a pre-existing shear surface then the peak excess pore pressures would be smaller.

It may be of interest to note that Roy et al (1981) measured excess pore pressures of up to 1.5 $C_{u,o}$ at the face of a pile, whereas no change in pore pressure was recorded at a distance of only one pile diameter from the face. In contrast, pore pressure increases were recorded at distances of up to twenty pile radii from the shaft during the driving of the same pile. This confirms the prediction that pore pressures generated as a result of pile loading are very localised in relation to those generated during pile installation. The measurements taken by Roy et al (1981) also confirm the view that pore pressures recorded at a short distance from a loaded pile are probably considerably smaller than those obtaining at the pile face (care must, therefore, be taken when interpreting field measurements).

9.5.3 Changes in Radial Stresses Acting on Loaded Piles

Direct measurements of the radial total stresses acting on loaded displacement piles are scarce; simultaneous measurements of pore pressures are even more rare.

Clark and Meyerhof (1972,a), in their tests on a 75 mm diameter model pile, measured decreases in the radial effective of between 0.1 and 0.3 times the initial undrained shear strength, at a distance of one pile radius from the shaft. It should be noted that the stress changes at the pile face may have been significantly larger. For comparison theoretical analyses of a full displacement pile installed in normally-consolidated Boston Blue Clay suggest that at a distance of one pile radius from the shaft, a decrease in the radial effective stress of around 0.19 $C_{u,o}$ might be expected, whereas at the pile face a decrease of 0.5 $C_{u,o}$ is predicted when the mobilised α value is 1.2; see Fig. 9.23.

Puech and Jezequel (1980) report measurements of changes in the radial total stresses and the pore pressures acting on the face of a 275 mm diameter pile during loading (the soil was a silty clay having a P.I. of 28). The results indicate that both the radial total stresses and the pore pressures increased during loading, in such a manner that the radial effective stresses reduced by around 23% of the effective overburden pressure. It is most unfortunate that the accompanying soil data is very limited and does not include measurements of either the initial undrained shear strengths or the c', ϕ' parameters of the clay. It is, therefore, not reasonable to attempt a more sophisticated interpretation of otherwise interesting results.

Butterfield and Johnston (1973) present measurements of the radial total stresses and the local shear stresses acting on the shaft of a continuously jacked pile in London Clay. It is unfortunate that measurements of excess pore pressures could not be taken, although the authors argue that the rate of pile penetration was such that the excess pore pressures around the shaft were decaying significantly during the jacking. If this is correct then the radial effective stresses acting on the shaft away from the influence of the toe were between 4.5 and 5 times the initial local undrained shear strength, and the mobilised angle of shaft friction was around 10°. Such values for the radial effective stress are somewhat greater than the predicted value of just under 4 $C_{u,o}$; however, the analysis takes no account of the possible presence of a shear surface parallel to the shaft, as suggested by the low angle of shaft friction. The influence of shear surfaces parallel to loaded piles is considered in section 9.5.5.

9.5.4 Pile Capacities

9.5.4.1 Introduction

The most convenient way to compare predicted pile capacities with field observations is to consider the respective values of the α and β parameters which are commonly employed in pile design. In predicting theoretical values for α and β it is assumed, for the present, that the pile behaviour is unaffected by the presence of shear surfaces which may have been formed during pile installation.

9.5.4.2 Full-displacement Piles

In order to derive typical predictions for α and β values, the analyses described earlier employing clay parameters ϕ' = 25°, λ = 0.15,

κ = 0.03 etc. are reconsidered. Wroth et al (1980) predict that after driving and consolidation, the clay beside the shaft of a full-displacement pile is normally-consolidated and has an undrained shear strength of roughly 1.6 times the initial value, irrespective of the initial O.C.R. Analyses presented earlier in this chapter have shown that pile loading behaviour is strongly dependent on the state of stress in the clay immediately adjacent to the pile before loading, and so it follows that the predicted α values are almost independent of the initial O.C.R.

In the analyses presented earlier, the stresses acting on the pile shaft have been expressed in terms of the undrained shear strength of the clay, at a Lode angle of zero, after installation and consolidation. Before proceeding, this value will be related to the initial in situ undrained shear strength in triaxial compression, $C_{u,o}$;

$$C_{u(\theta = 0°)} = \left(\frac{3-\sin \phi'}{3}\right). \; C_{u(\theta = -30°)} \qquad \text{at same water content}$$

Thus

$$C_{u,i} = C_{u(\theta=0°)} \cong 1.6 \times \left(\frac{3-\sin 25}{3}\right) \; C_{u,o}$$

(before loading)

$$= 1.38 \; C_{u,o} \qquad (9.1)$$

Analyses have typically shown that the final value of $\tau_{rz}/C_{u,i}$ is around 1.2 on drained loading, and 1.0 on undrained loading.

Thus, in the former case, $\tau_{rz\,(max)} = 1.2 \times 1.38 \; C_{u,o} = 1.66 \; C_{u,o}$

hence $\alpha = 1.66$

On undrained loading, $\alpha = 1.38$

As noted above these α values are largely independent of O.C.R., but vary a little with the clay type.

β values may similarly be derived.

Thus

$$\beta = \tau_{rz\,(max)}/\sigma_{v,o'} = \frac{\tau_{rz}/C_{u,o}}{\sigma_{v,o'}/C_{u,o}} = \frac{\alpha}{(\sigma_{v,o'}/C_{u,o})} = \alpha.\left(\frac{C_{u,o}}{\sigma_{v,o'}}\right)$$

Values of $(\sigma_{v,o'}/C_{u,o})$ are not well predicted by the Modified Cam Clay model for heavily over-consolidated clays, and in the example presented below, only a normally-consolidated clay is considered.

A typical value of $C_{u,o}/\sigma_{v,o'}$, for normally-consolidated clay, might be 0.22 (if necessary a rough estimate may be derived from Skempton's relation $C_{u/p'} = 0.13 + 0.0037\ PI$).

This leads to $\beta \cong \alpha \times 0.22$

for drained loading $\beta \cong 0.37$

and for undrained loading, $\beta \cong 0.30$

The predicted values of α and β are compared with field and laboratory measurements in section 9.5.4.4.

9.5.4.3 Low-displacement Piles

In order to be conservative, it is assumed that the strength of the clay beside the pile is not increased by the installation process; thus $C_{u(\theta=0°)} = 0.86.C_{u,o}$ for a clay with $\phi' = 25°$. Only normally-consolidated clay is considered.

Referring to Fig. 9.20, it may be seen that

$J_{max}/C_{u,o}$ $(\theta = 0°)$ = 1.05 on drained loading, and 1.0 on undrained loading

At peak, $\theta = 0°$ and so $J = \tau_{rz}$

Thus, on drained loading $\alpha = 0.9$ and $\beta = 0.2$

and on undrained loading, $\alpha = 0.86$ and $\beta = 0.19$

The predicted α and β values are summarised in Table 9.1.

9.5.4.4 Comparison with Field and Laboratory Measurements

Kraft, Focht and Amerasinghe (1981) present a recent compilation of α, β and λ values derived from good quality test data. Both closed and open-ended piles are considered, in both normally- and over-consolidated clays. The results suggest that whilst for short piles (< 30 m long) α values in excess of unit are sometimes measured, longer piles are typically

associated with α values between 0.5 and 1.0. The A.P.I. Method 2 (1980) recommends a maximum value for α of unity for plastic normally-consolidated clays, and values as low as 0.5 for less plastic clays (the permissible α value decreases with increasing $C_{u,o}$).

β values are less amenable to comparison because the corresponding values of ϕ' and initial OCR are not quoted. Nevertheless, it may be noted that whereas for shallow piles, β values may range between 0.2 and 0.6 (both normally- and over-consolidated clays are included), longer piles are associated with β values between 0.1 and 0.2.

It would appear that pile capacities predicted on the basis of cavity expansion theory followed by the loading analyses presented above, are far from being conservative. A partial explanation may be that the effects of fabric disturbance caused by pile installation are ignored in the analyses presented earlier (evidence for such fabric disturbance may be found in Tomlinson (1970) and in Chapter 6 of this thesis. In section 9.5.5, the analyses of pile loading behaviour are reviewed in order to consider the possible influence of shear surfaces parallel to the pile shaft. Randolph and Wroth (1981) suggest that the most appropriate way to consider pile loading is on the basis of undrained simple shear tests. The validity of such an approach is also discussed below.

9.5.5 The Possible Influence of Fabric Disturbance Caused During Pile Installation

9.5.5.1 Introduction

There is now a significant amount of evidence to suggest that during the installation of a displacement pile in clay, considerable micro-fabric disturbance may occur to the clay adjacent to the pile. In some instances this disturbance may result in the formation of a continuous displacement discontinuity surface parallel to the shaft. Some of the evidence is briefly reviewed below.

Tomlinson (1970) reports the results of field tests on jacked and driven piles in London Clay. On completion of the tests, Tomlinson exhumed one jacked and one driven pile; he found that a thin skin of clay remained adhering to the piles, and that the surface of this skin was slickenslided. Scanning electron micrographs made of the skins showed that the clay particles were strongly oriented parallel to the axes of the piles. Tomlinson suggested that the slickenslided surfaces were probably at residual conditions

(Tomlinson's work is also discussed in some detail in Chapter 6).

Flaate(1972) measured the undrained shear strength of the clay (by U.U. and vane tests) around a driven pile before and after pile installation. He found that close to the pile, the undrained shear strengths after driving and consolidation were typically between 20% and 60% greater than those before installation. However, during the pile loading test, which was conducted 5½ years after installation, the equivalent α value was found to be only 0.6. Thus the average unit shaft friction was only about 60% of the initial average undrained shear strength, or 40% of the measured undrained shear strength at the pile face before pile loading. One explanation for this observation is that on pile loading, the clay 'fails' prematurely on a pre-existing shear surface parallel to the pile.

Butterfield and Johnston (1973) determined an approximate value for the mobilised effective angle of shaft friction acting on a continuously jacked pile in London Clay. The angle was about 10°, which is much lower than the intact angle of shearing resistance, ϕ', but similar to the residual angle of friction determined by Tomlinson (1970) using a direct shear box, for instance.

In Chapters 5 and 6 of this thesis, the results of laboratory tests on driven and jacked piles are presented. Fig. 5.27 illustrates the load-displacement behaviour exhibited by three piles installed by different methods; one pile was installed with minimal disturbance, one was jacked, and the other was driven. On the basis of the shapes of the pile load-displacement curves and the micro-fabric observations, it is argued in Chapter 6 that the behaviour of the driven and the jacked piles is consistent with the formation during pile installation, of a thin zone of re-oriented clay parallel to the pile. The peak angle of shearing resistance which can be mobilised on such a shear surface will depend on several factors which include the relative velocity between the pile and the clay, and the normal effective stress acting on the shear surface, during pile installation. However, if after allowing the clay beside the pile to consolidate, the pile is slowly loaded beyond peak conditions then the pile capacity will tend to decrease as the angle of friction which can be mobilised on the shear surface falls to a residual value consistent with the new rate of pile displacement and the higher effective stresses. If the pile were to be unloaded, and then reloaded some time later, the pile behaviour would be far less brittle than that observed on first-time loading, and the new peak shaft resistance would be similar to the former residual value. This behaviour was observed during

the laboratory model tests, and has been reported by Tomlinson (1970) and by Kraft, Cox and Verner (1981).

9.5.5.2 Theoretical Analyses of Pile Loading Incorporating Allowances for the Presence of Pre-existing Shear Surfaces

Typical analyses for the drained and undrained loading of a displacement pile are briefly considered in order to examine the required angles of shearing resistance on surfaces parallel to the pile shaft, at various stages during loading. In the discussion below it is assumed that if a pre-existing shear surface is present around a loaded pile, then 'failure' will occur when the maximum available angle of friction on the surface is mobilised. It is further assumed that the continuum analyses of stress changes within the clay during pile loading are valid until slip is predicted across the shear surface.

Fig. 9.24 presents the predicted variations of the radial stress (σ'_r), the shear stress (τ_{rz}) and the tangent of the mobilised angle of shaft friction (tan δ'), with pile displacement during the drained loading of a full-displacement pile. The stresses induced by pile installation have been selected on the basis of cavity expansion theory (although radial variations of stress have been ignored), and the clay is characterised by the parameters $\phi' = 25°$, $\lambda = 0.15$, $\kappa = 0.03$, and $G/C_u = 120$. In Fig. 9.24, the stresses are normalised by the undrained shear strength (at $\theta = 0°$) of the clay beside the pile before loading, $C_{u,i}$. By way of an example, assume that the peak value of tan δ' (i.e. τ_{rz}/σ'_r) which can be withstood by a shear surface parallel to the pile is 0.2. The maximum value of $\tau_{rz}/C_{u,i}$ is then 0.78, which corresponds to an α value of 1.08 (i.e. 0.78 x 1.6 x 0.86 - see eqn. (9.1)).

Fig. 9.25 presents the predicted variation of the maximum available α value with the peak angle of friction, δ', which can be mobilised on planes parallel to the pile shaft. Both drained and undrained loadings are considered, and it may be of interest to note that if the maximum available value of ϕ' is less than about 15°, the drained and undrained pile capacities are very similar. This prediction is consistent with field observations reported by Eide, Hutchinson and Landva (1961).

For a plastic clay having an angle of shearing resistance, ϕ', of say, 25°, a typical residual angle of friction as established by means of a ring shear apparatus might be 12°. However, the peak angle of friction which

could be mobilised around a driven pile would be expected to be higher, i.e. 16-18° (for reasons discussed earlier), and so from Fig. 9.25 it may be seen that α values in excess of unity are predicted. Such values are greater than those typically determined from field tests, and suggests that the stresses predicted (Randolph et al, 1979) to exist around driven piles prior to loading are perhaps too large. It has been suggested by Wood (1981) that when modelling the installation of a pile, the necessary soil constitutive data might best be obtained by performing strain-path tests, using a True Triaxial Cell. There is great need at present for reliable field measurements of the radial effective stresses acting on displacement piles during installation, consolidation, and on subsequent loading.

An alternative approach to the modelling of conditions during pile loading has been proposed by Randolph and Wroth (1981). This is briefly discussed below in section 9.6.

9.6 THE POSSIBLE USE OF THE SIMPLE SHEAR TEST IN PILE DESIGN

9.6.1 Introduction

Observing that the soil adjacent to a loaded pile is deformed in a manner similar to simple shear, Randolph and Wroth (1981) proposed that the results from constant volume simple shear tests should be used in pile design. The main advantage enjoyed by such an approach compared with conventional methods based on triaxial compression testing, is that the soil element under test is subjected to a strain path which is apparently similar to the one expected in practice. However, there are a number of reasons why it is considered that the direct use of such results may not be appropriate to pile design; these are discussed below.

9.6.2 Undrained Pile Loading

It has been demonstrated in section 9.2.6 that if a pile is loaded under undrained conditions, the kinematic constraints ensure that the radial total strain is zero, and that the soil deforms initially under conditions of undrained simple shear. In principle, the simple shear test conforms with these restraints.

Randolph and Wroth (1981) refer to the simple shear test data reported by Ladd and Edgers (1972). Tests performed on initially intact clays (particularly sensitive ones) indicate considerable stress-path softening at large strains. Although the tests suggest that the angle of friction

mobilised parallel to the direction of shearing finally reaches the angle of shearing resistance, ϕ', for the intact clay, the normal effective stress appears to reduce by up to 80%! Employing the conventional interpretation of constant volume simple shear tests, these reductions in the normal effective stress imply the generation, under undrained conditions, of excess pore pressures of up to 0.8 times the initial normal stress. Now, it is predicted (e.g. Randolph et al, 1979) that the radial effective stress acting on a full displacement pile after driving and consolidation will be between 4 and 5 times the initial in-situ undrained shear strength. Thus the generation of excess pore pressures of between 3.2 $C_{u,o}$ (i.e. 0.8 x 4 $C_{u,o}$) and 4 $C_{u,o}$ (i.e. 0.8 x 5 $C_{u,o}$) is implied during loading. Such values are considerably greater than any excess pressures reported to date.

However, to employ directly the results of simple shear tests performed on intact clays is to ignore the likely presence of low strength shear surfaces formed parallel to the pile during installation (see, for example, Tomlinson (1970) and Chapter 6 of the present thesis). In practice, the presence of such pre-existing shear surfaces will modify the undrained loading behaviour of the clay, and slip on the shear surfaces will occur once the mobilised angle of shaft friction equals the available angle of friction on the shear surfaces. Thereafter, it is anticipated that the mobilised angle of shearing resistance will decrease towards a residual value. This discontinuum behaviour could not adequately be modelled in a conventional simple shear apparatus.

9.6.3 Drained Loading of Piles

The analyses presented in section 9.2.3 suggest that the pore pressures generated on pile loading are likely to dissipate roughly an order of magnitude faster than those generated on driving, and so many pile loadings are likely to be at least partially drained.

Radial strains may occur in the clay adjacent to a pile loaded under drained conditions, and it is believed that the dramatic reductions in the radial effective stress implied by the constant volume simple shear tests would not be observed because of the influence of the surrounding clay. The presence of pre-existing shear surfaces would also tend to limit the possible reductions in the radial effective stresses.

The influence of pre-existing shear surfaces on pile loading behaviour is demonstrated by comparing the results from Test 9 with those

from Test 18 (see Chapter 5). Test 9 was performed on a model pile installed with a minimum of stress-field or micro-fabric disturbance into a sample of Kaolin normally-consolidated to a stress ratio of 1.5. In Test 18, a model pile was driven into Kaolin normally-consolidated to a stress ratio of 0.7. On the basis of cavity expansion theory (e.g. Randolph et al, 1979) it is estimated that after consolidation, the radial stress acting in the clay adjacent to the pile is the major principal stress, and the local stress ratio σ'_r/σ'_z is $1/K_o \cong 1.5$. Thus, in both tests the stress conditions obtaining around the piles before loading were such that the radial stress was the major principal stress, and the initial stress ratio was around 1.5; the hoop stresses were not the same. However, a major difference between these two tests was the presence, before pile loading, of pre-existing shear surfaces parallel to the driven pile. It may be seen in Fig. 5.27, however, that the loading behaviour of the driven pile was very different from that of the piles installed without disturbance (the load-displacement behaviour observed in all tests conducted on piles installed with minimal disturbance were similar). It is suggested that the presence of the pre-existing shear surfaces around the driven pile is the simplest explanation for the differences observed.

9.7 A SIMPLE METHOD FOR DETERMINING LOWER BOUNDS TO THE CAPACITIES OF LONG DRIVEN PILES

9.7.1 Introduction

It is well established, on the basis of field measurements, that the values of the design parameters α,β and λ used to predict the capacities of long piles are significantly smaller than those applicable to shorter piles (see Meyerhof (1976), Vijayvergija and Focht (1972), and Kraft, Focht and Amerasinghe (1981)).

Kraft et al (1981) suggest that the major cause of the apparent decrease in load carrying capacity with pile length is progressive failure, and introduce a dimensionless coefficient, π_3, to describe the relative compressibility of the pile with respect to the soil ($\pi_3 = Df_{max} L^2/AEU^*$ where D = pile diameter, L = pile length, A = cross-sectional area of the pile, E is the pile modulus, f_{max} = the peak pile-soil friction, and U* is the relative pile-soil movement at which f_{max} is developed). Kraft et al established a reasonable correlation between λ values and the values of π_3. Unfortunately, neither of the parameters f_{max} nor U* is easy to determine directly.

In order to establish the ultimate capacity of a long pile by means of an effective stress approach, it is necessary to be able to predict the axial variations of both the radial effective stress and the angle of friction parallel to the pile. The determination of values for these quantities, appropriate to a long pile, is considered in the light of results from the model pile tests, the micro-fabric studies, and the theoretical analyses presented earlier.

9.7.2 Ultimate Angle of Shaft Friction

It was suggested earlier that the peak angle of shaft friction which can be mobilised around a driven pile corresponds to the residual strength appropriate to the effective stress level and the rate of displacement encountered during installation. If the pile is subsequently loaded, the mobilised angle of shaft friction will increase to this peak value, and then fall to a residual angle of friction appropriate to the slower rate of displacement and the higher effective stress level. One way of establishing an appropriate lower limit to the angle of shaft friction would be to perform slow direct shear interface tests, under drained conditions, between the soil under consideration and a flat interface made from the pile material. In this context, there are two important points to note;

(i) the residual angle of friction measured in soil-soil shear (using a ring shear apparatus, for example) may not represent a lower bound to the soil-interface friction, especially in the case of a low plasticity clay sheared against a smooth interface (see the results appropriate to Happisburg Till, in Table 9.2);

(ii) when selecting an appropriate surface roughness for the interface, it should be borne in mind that the face of the pile will be abraded by being driven through tens of metres of soil. It is probably advisable to err on the side of excessive smoothness when preparing an interface for testing.

9.7.3 Ultimate Value of the Radial Effective Stress

Analyses of the loading behaviour of both full- and low-displacement piles have been presented earlier in this Chapter. It has been shown that during the loading of a full-displacement pile, the radial effective stress may decrease by as much as 40% from the value obtaining prior to pile loading,

with the result that the final radial stress may not be very much greater than the initial in situ horizontal stress, for normally or lightly over-consolidated deposits. It has also been suggested that the use of cavity expansion theory in conjunction with the Modified Cam Clay constitutive law may tend to overestimate the radial stresses acting on a full displacement pile after installation and consolidation. A conservative approach to estimating the radial effective stresses acting on a full-displacement pile loaded to residual conditions might, therefore, be to assume that the final radial stress is equal to the initial in situ value.

In the study of the loading behaviour of low-displacement piles it has been assumed that radial effective stress acting on such a pile after driving and consolidation is not significantly different from the initial in situ horizontal effective stress. The parametric study performed to consider the loading behaviour of piles installed in clays having ϕ' values between 20° and 35° predicts only small changes in the radial effective stress during loading (see Fig. 9.26). This prediction is supported by the results of the two model pile tests (No.5 and No. 11) conducted on one-dimensionally normally-consolidated Kaolin. It is, therefore, considered that the final radial effective stress acting on a low-displacement pile loaded to residual conditions may reasonably be assumed to equal the initial in situ horizontal effective stress (for piles installed in normally or lightly over-consolidated, insensitive clays).

Typically, in conditions where long piles (> 50 m, say) are employed, a large proportion of the pile length will be surrounded by either normally- or lightly over-consolidated clay (examples of typical profiles of OCR with depth, for various platform sites in the North Sea, are presented by Semple and Gemeinhardt (1981)). In the forthcoming discussion the radial effective stresses acting on a long loaded pile are assumed to be given by

$$\underset{(\text{final})}{\sigma'_r} = \underset{\text{N.C.}}{K_o} \cdot \sigma'_{z,o} = (1-\sin\phi')\,\sigma'_{z,o} \qquad (9.2)$$

9.7.4 Evaluation of the Shaft Resistance

Methods for estimating the magnitudes of both the radial effective stresses acting on an element of a pile loaded to residual conditions, and the ultimate angle of shaft friction have been discussed above. The shaft resistance of long compressible piles is now considered.

As a result of the strain softening behaviour of the clay, long compressible piles will typically exhibit progressive failure. Thus the clay adjacent to the top of the pile may have reached residual conditions before the tip has reached peak conditions. A lower bound to the shaft resistance of the pile may be obtained by assuming residual conditions to obtain along the length of the pile.

At some arbitrary depth below the ground,

$$\tau_{(residual)} = \sigma'_{r\ (residual)} \cdot \tan \delta'_r$$

Using eqn. (9.2),

$$\tau_{residual} \cong (1 - \sin \phi') \sigma'_{z,o} \tan \delta'_r \qquad (9.3)$$

$$= \mu \sigma'_z \qquad (9.4)$$

where

$$\mu = (1 - \sin \phi') \tan \delta'_r \qquad (9.5)$$

μ is analogous to the β value often used in determining the capacity of rigid piles. The pile shaft resistance, R, is given by

$$R = \pi D \int_0^L \mu(z)\, \sigma'_z\, dz$$

$$= \pi D \int_0^L \mu(z).\, \gamma'(z).z\, dz \qquad (9.6)$$

The soil parameters required to establish a lower bound to the pile capacity are, therefore, γ', ϕ' and δ'_r. These parameters are readily measured in the laboratory, and it is a significant advantage that undisturbed soil samples are not required for the determination of either ϕ' or δ'_r.

9.7.5 Comparison between Predictions and Field Measurements

9.7.5.1 Introduction

Generally, it is not possible to perform direct comparisons between predictions based on the method outlined above and the published results of field tests conducted on long piles, because values of ϕ' are often not

quoted and drained interface tests do not appear to have been performed. Thus, a more general method of comparison must be adopted.

Table 9.2 presents measured values of ϕ', and δ'_r for a selection of clays. These values are used in conjunction with the method outlined in section 9.6.4 to determine typical lower bounds to the shaft resistance of compressible piles. In order to facilitate the comparison with field measurements (see Kraft et al (1981) for a recent compilation of field data), the predictions are translated into equivalent α, β and λ values. It is important to note that this translation process requires additional assumptions to be made; these would not be necessary when using the new method for design.

9.7.5.2 Derivation of Equivalent α Values

$$\bar{\tau} = (\mu.\overline{\sigma_{z,o'}}) = \alpha_{(equivalent)} \cdot \overline{C_{u,o}} \qquad (9.7)$$

If the clay is assumed to be one-dimensionally, normally-consolidated prior to loading, then the initial undrained shear strength, $C_{u,o}$, may be related to the effective overburden stress by means of Skempton's approximation. Thus,

$$\frac{C_{u,o}}{\sigma_{z,o'}} = (0.11 + 0.0037.PI)$$

Thus from eqn. (9.7),

$$\alpha_{equivalent} = \frac{\mu.\sigma'_{z,o}}{\overline{C_{u,o}}} \cong \left(\frac{\mu}{0.11 + 0.0037.PI}\right)$$

or

$$\alpha_{equivalent} = \left\{\frac{(1-\sin\phi')\tan\delta'_r}{0.11 + 0.0037.PI}\right\} \qquad (9.8)$$

If several layers of soil having different values of γ', ϕ', δ' and PI are encountered then the $\alpha_{equivalent}$ must be established as a weighted average of the contributions from each layer.

Equivalent α values appropriate to the clays considered in Table 9.2 are presented in Table 9.3, and are compared with field data in section 9.7.5.5.

9.7.5.3 Derivation of Equivalent β Values

Values of μ are equivalent to limiting values of β. Thus

$$\beta_{equivalent} = (1 - \sin \phi') \tan \delta_r' \qquad (9.9)$$

9.7.5.4 Derivation of Equivalent λ Values

$$\bar{\tau} = (\mu.\overline{\sigma_{z,o'}}) = \lambda_{equivalent} \cdot (\overline{\sigma}_{z,o'} + 2\,\overline{C_{u,o}})$$

so,

$$\lambda_{equivalent} \cong \mu/(1 + 2\,(\frac{C_{u,o}}{\sigma'_{z,o}}))$$

$$\cong \frac{(1-\sin \phi') \tan \delta_r'}{1.22 + 0.0074.PI} \qquad (9.10)$$

If several layers of soils are encountered, then $\lambda_{equivalent}$ must be established as a weighted average of the contributions from the various layers.

9.7.5.5 Comparisons between Predicted Values of α, β and λ with Field Test Results

Laboratory measurements of the parameters ϕ', δ_r' and PI for various clays are summarised in Table 9.2. These values are used to derive equivalent lower bounds to the parameters α, β and λ, which are presented in Table 9.3. This selection of lower bound values is compared in Figs. 9.27, 9.28, 9.29 and 9.30 with the field data compiled by Kraft et al (1981). It may be seen that the range of lower bound values predicted by the new method are in very good agreement with the available field data. Fig. 9.30, which is based on a figure by Kraft et al, illustrates that the pile compressibility, rather than the pile length as such, is most important in determining how closely the pile capacity tends towards the lower bound.

In conclusion, it is suggested that the method outlined above can provide a quick and relatively cheap method of establishing a lower bound to the capacities of long piles in clay, and it has the advantage of not being empirical. It is strongly recommended that drained interface shear tests

(either direct shear box or an improved method) should be performed routinely as part of the site investigation for pile foundations (particularly where long piles are anticipated).

Table 9.1: Predicted Values of α and β assuming the Clay to be Intact; $\phi' = 25°$.

Pile Type	α_{peak}		β_{peak}	
	Drained Loading	Undrained Loading	Drained Loading	Undrained Loading
Full displacement				
OCR = 1	1.66	1.38	0.37	0.30
OCR > 1	1.66	1.38	-	-
'Zero' Displacement				
OCR = 1	0.9	0.86	0.2	0.19

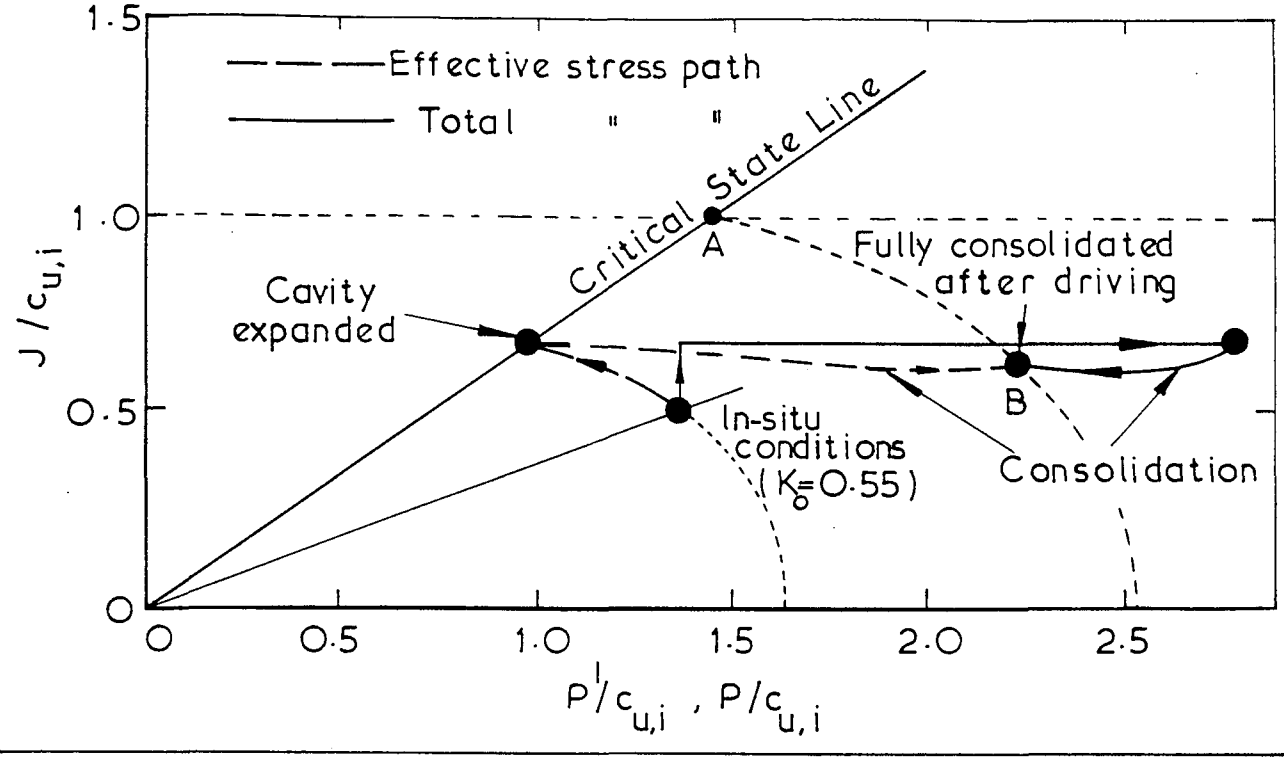
Table 9.2: Properties of a Selection of Clays

Clay	PI	$\phi'_{Triaxial}$	$\delta'_{Residual}$	Interface Material	Source of Data
Speswhite Kaolin (Clay > 82%)	36	23°	11.5°	Smooth epoxy resin	This thesis
Kaolinite	53	-	11.5°	Smooth steel	Littleton (1976)
Illite from Kimmeridge	33	-	11.5	" "	" "
Illite	20.4	24.4°	13°	Rough steel	Clarke and Meyerhof I. (1972)
	"	"	11.5°	Normal finish	
	"	"	9°	Smooth steel	" "
London Clay	46	25°	10	Clay/clay	Tomlinson (1970)
Happisburg Clay	13	30°	16°-18°	Smooth resin	Lemos (1982) (Private communication)
	"	"	30°	Rough resin	
	"	"	30°	Clay/clay	Lupini (1981)

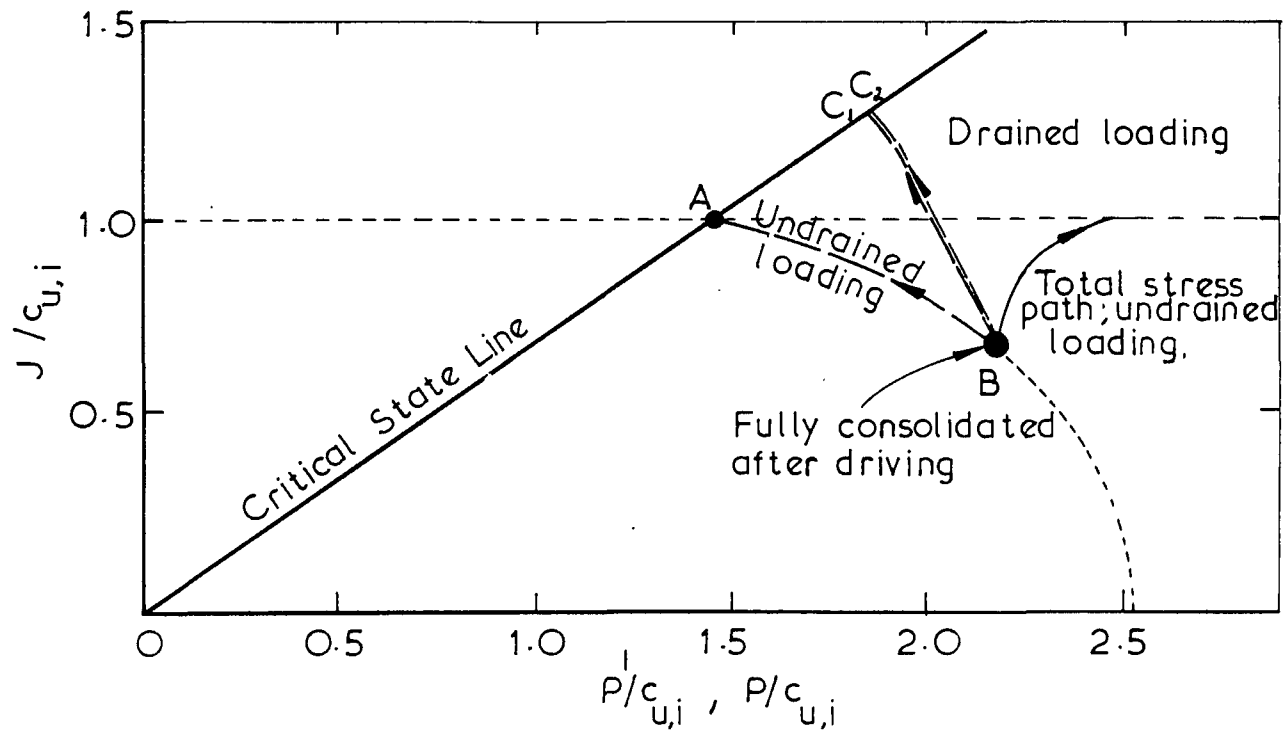
Table 9.3: Predicted Lower Bounds for the Coefficients α, μ or β_{min}, and λ.

Present No.*	$\phi'_{Triaxial}$	$\delta'_{Residual}$	α_{min}	$\mu = \beta_{min}$	λ_{min}
1	23°	11.5°	0.51	0.124	0.087
2	(23°)	"	0.405	0.124	0.077
3	(23°)	"	0.534	0.124	0.085
4	24.4°	13°	0.728	0.135	0.098
5	"	11.5°	0.641	0.119	0.087
6	"	9°	0.501	0.093	0.068
7	25°	10°	0.364	0.102	0.065
8	30°	16°	0.900	0.143	0.107
9	30°	30°	1.77!	0.280	0.208

*See Table 9.2



(a) Total and effective stress paths followed during driving and subsequent consolidation.



(b) Total and effective stress paths followed on undrained and and drained loading of a pile driven into normally-consolidated Boston Blue Clay; soil adjacent to pile

Fig.9·1

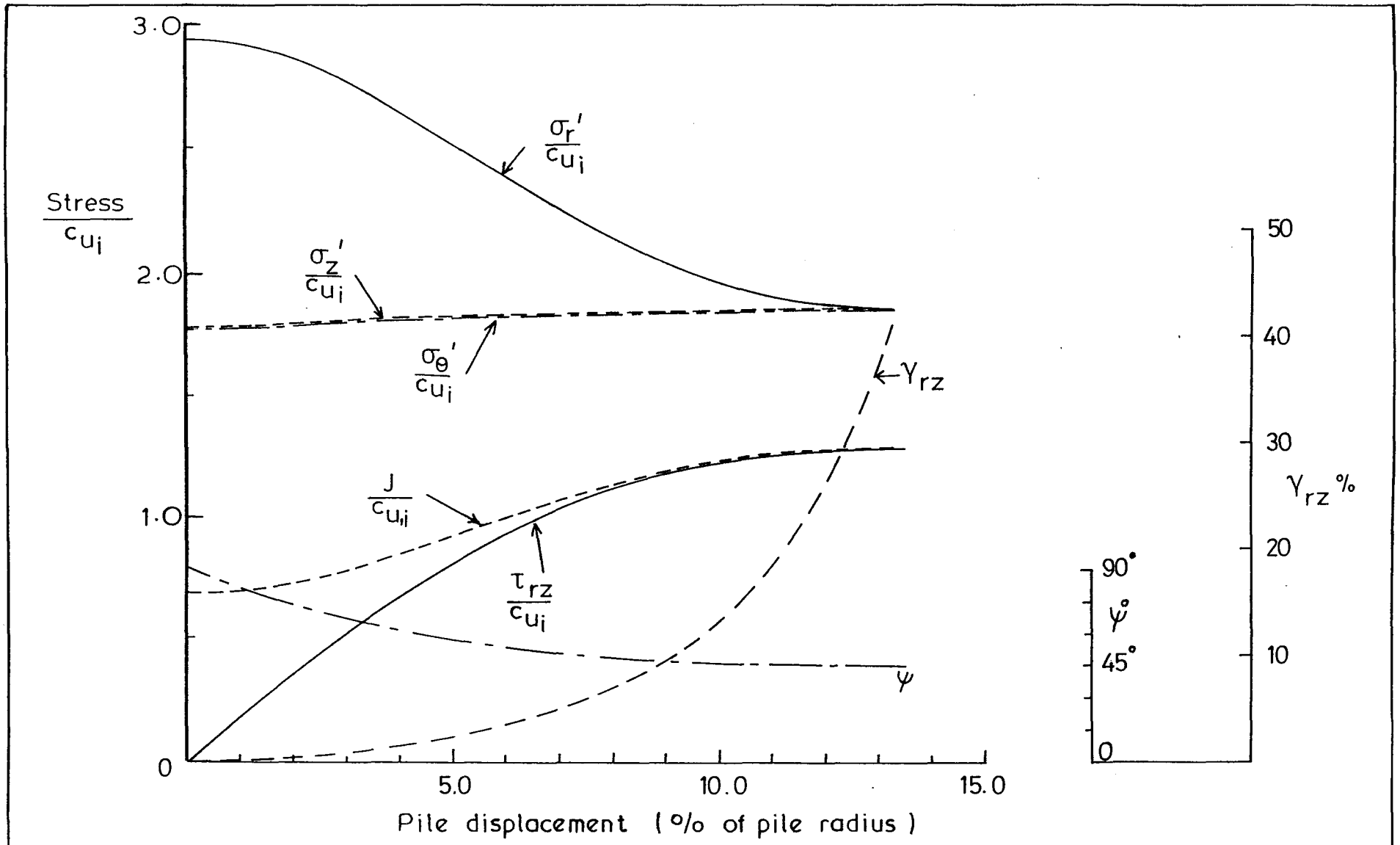


Fig.9.2

Variation of stresses adjacent to a pile installed in normally consolidated Boston Blue Clay on drained loading

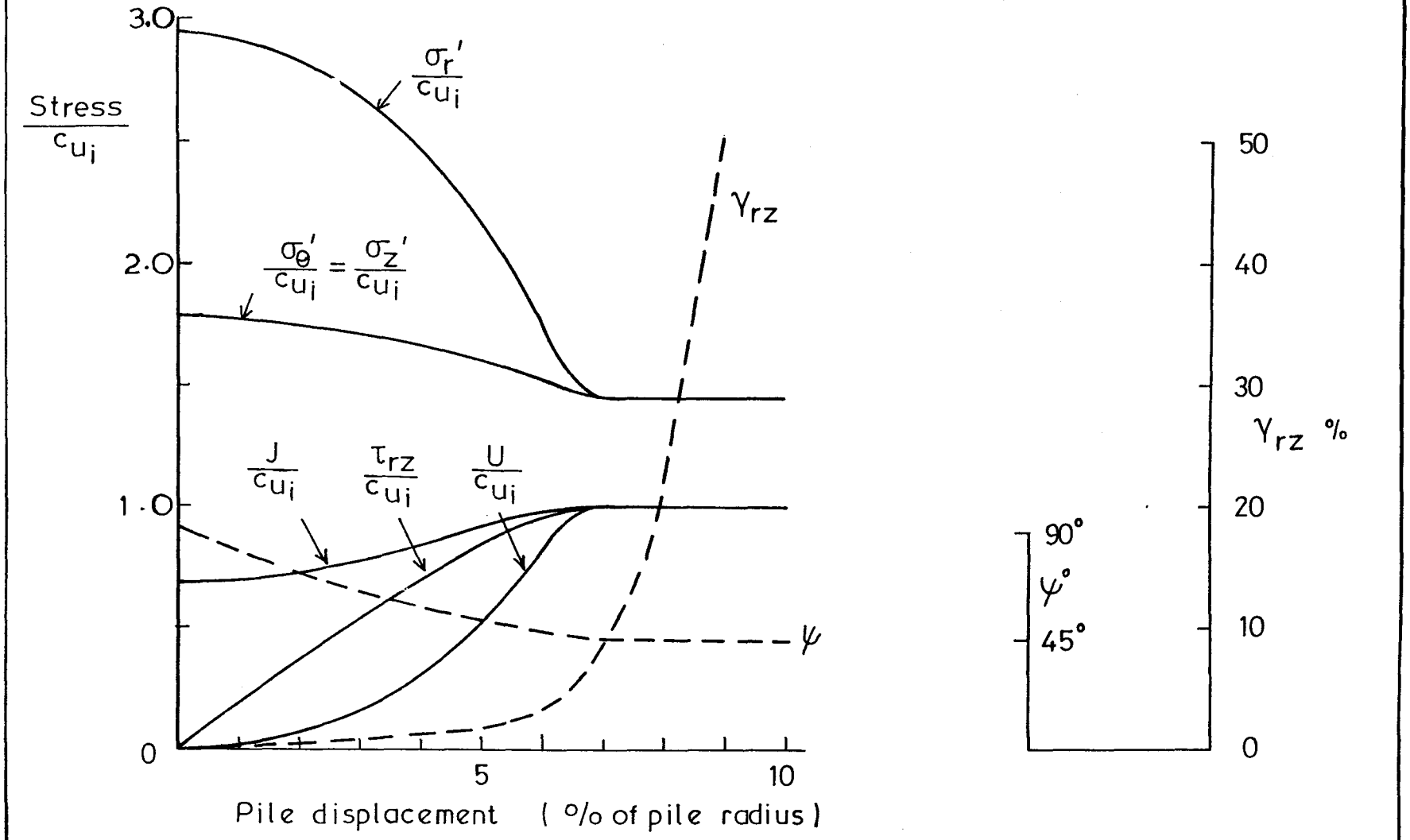
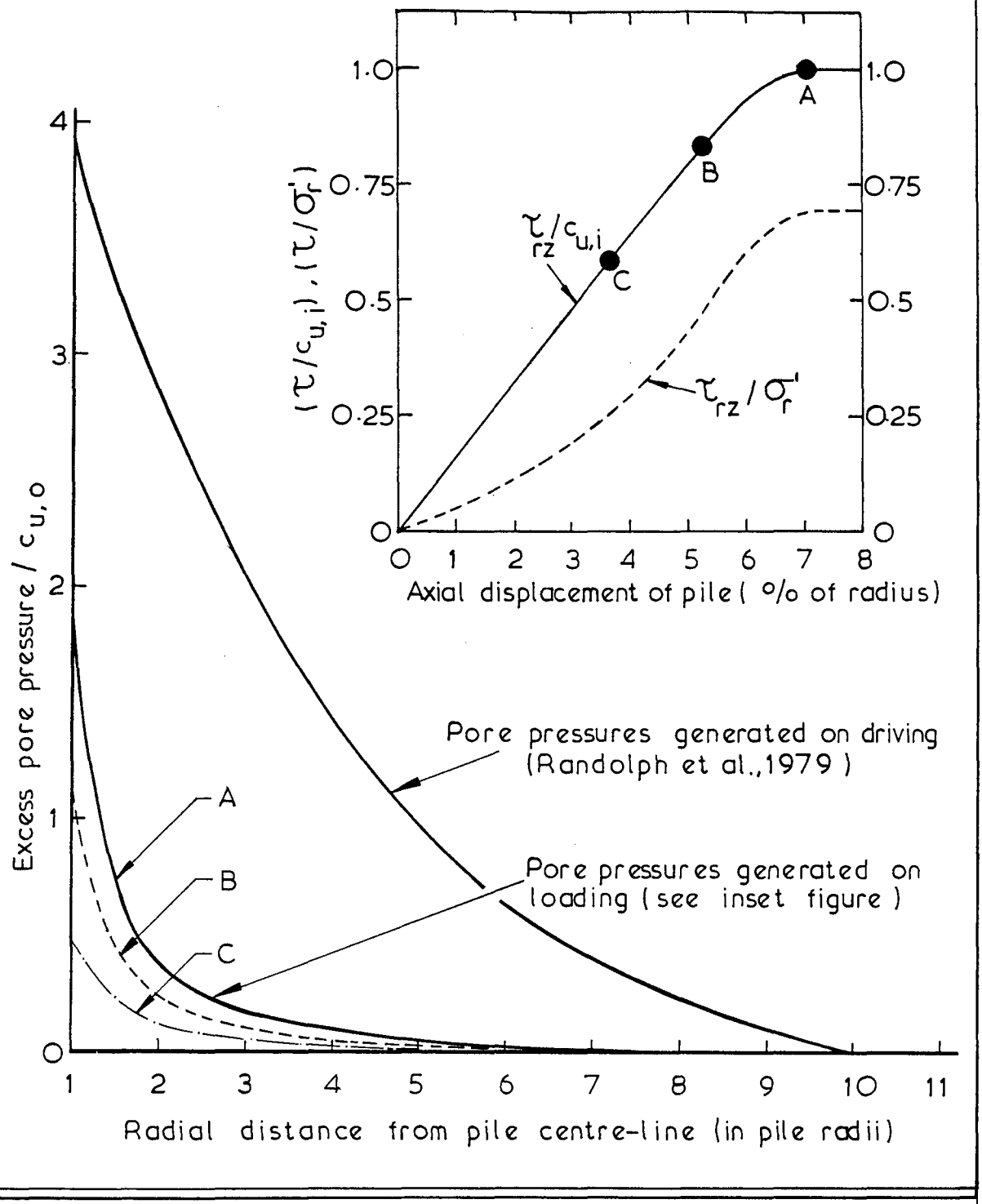


Fig. 9.3

Variation of stresses adjacent to a pile installed in normally consolidated Boston Blue Clay on undrained loading



Radial distribution of excess pore pressures around a driven pile

Fig. 9.4

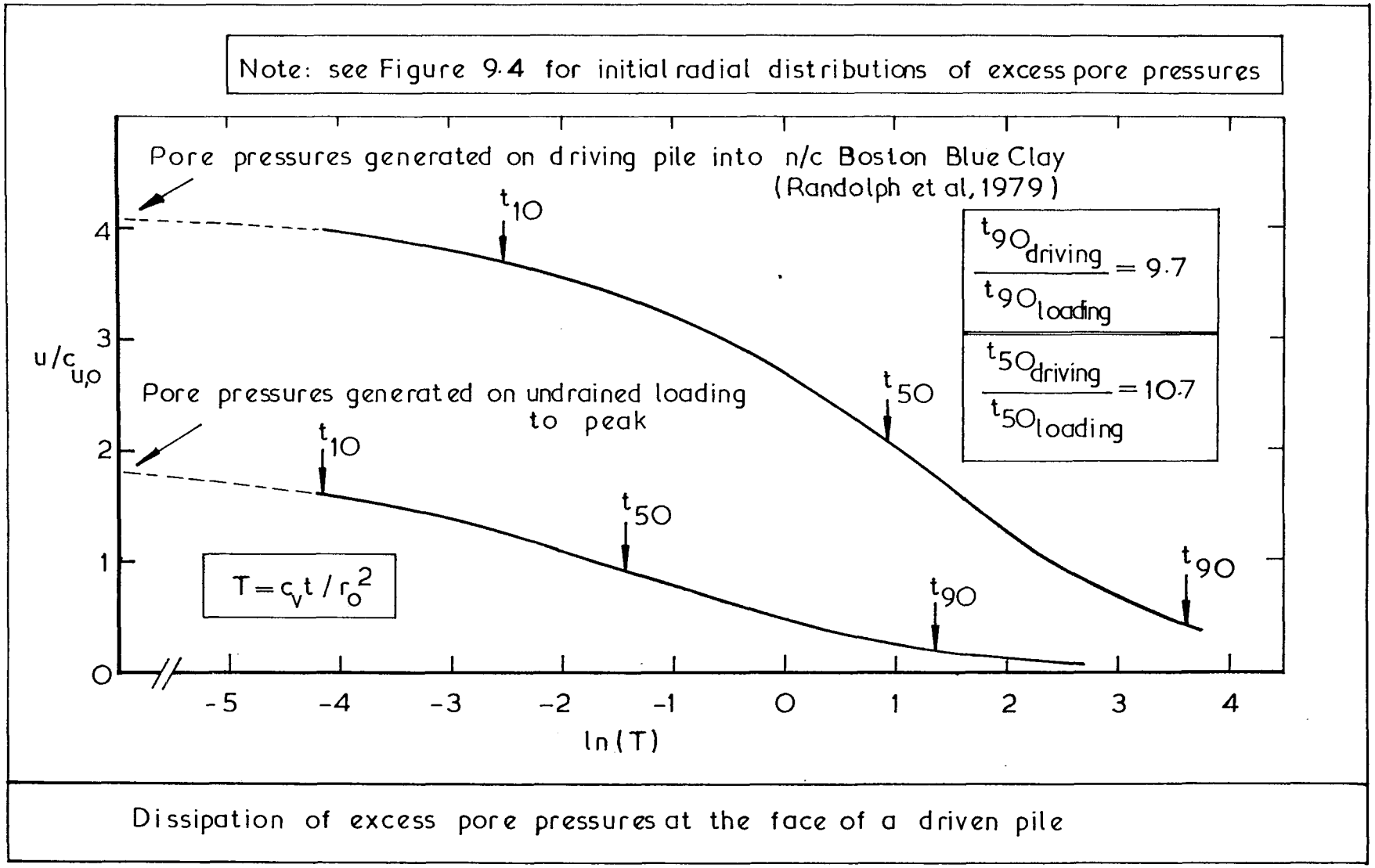
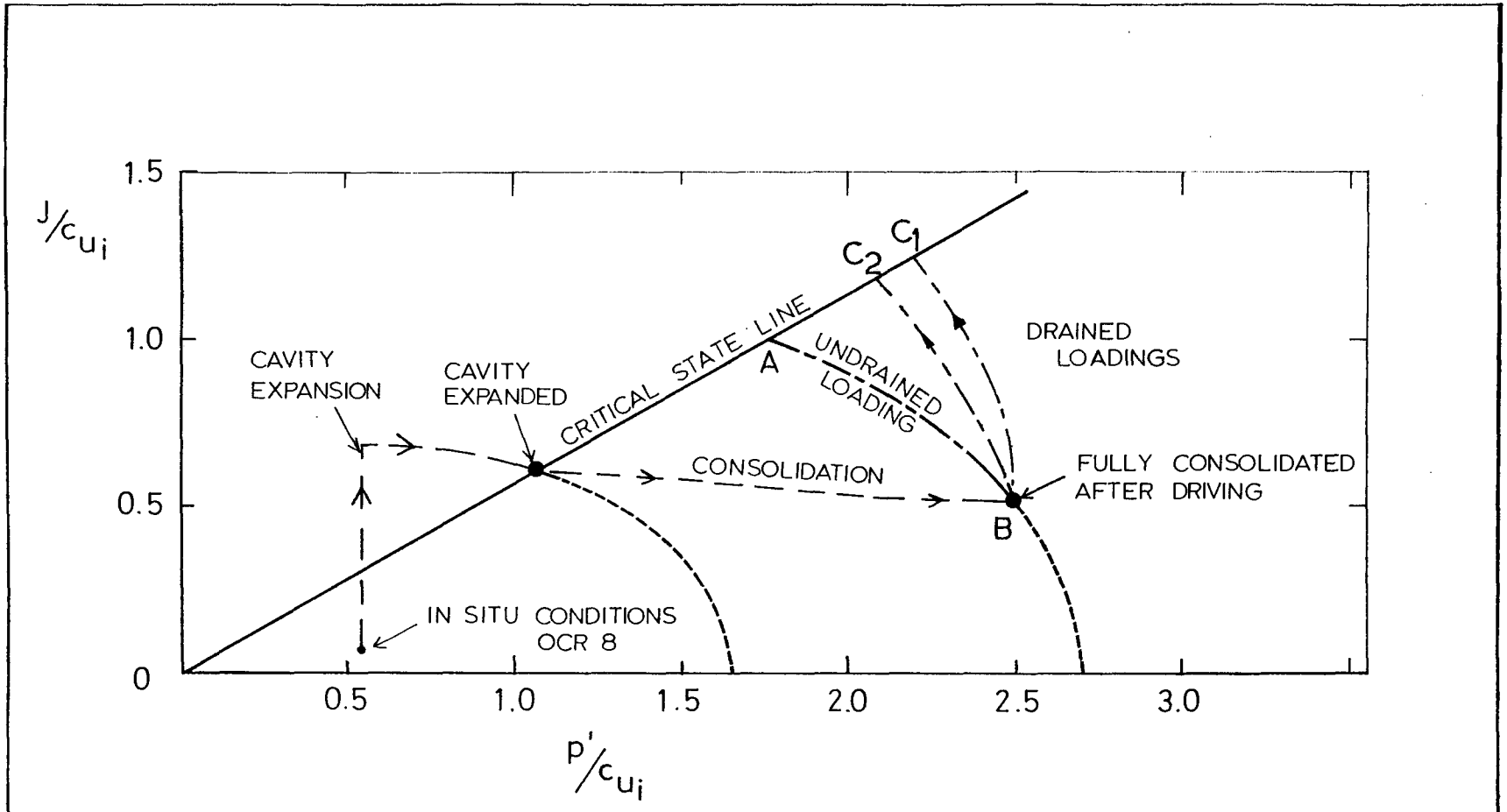


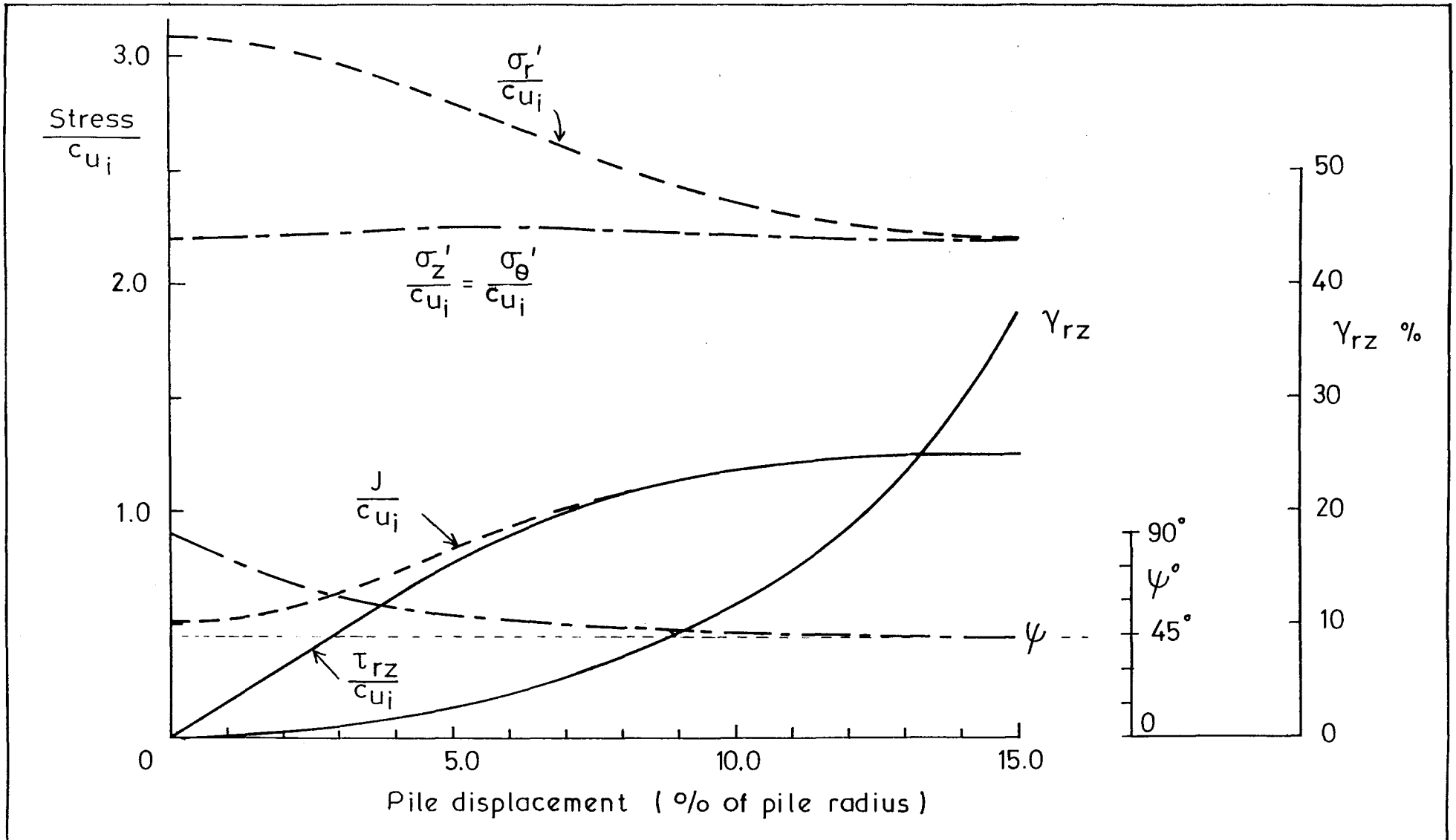
Fig. 9.5

Dissipation of excess pore pressures at the face of a driven pile



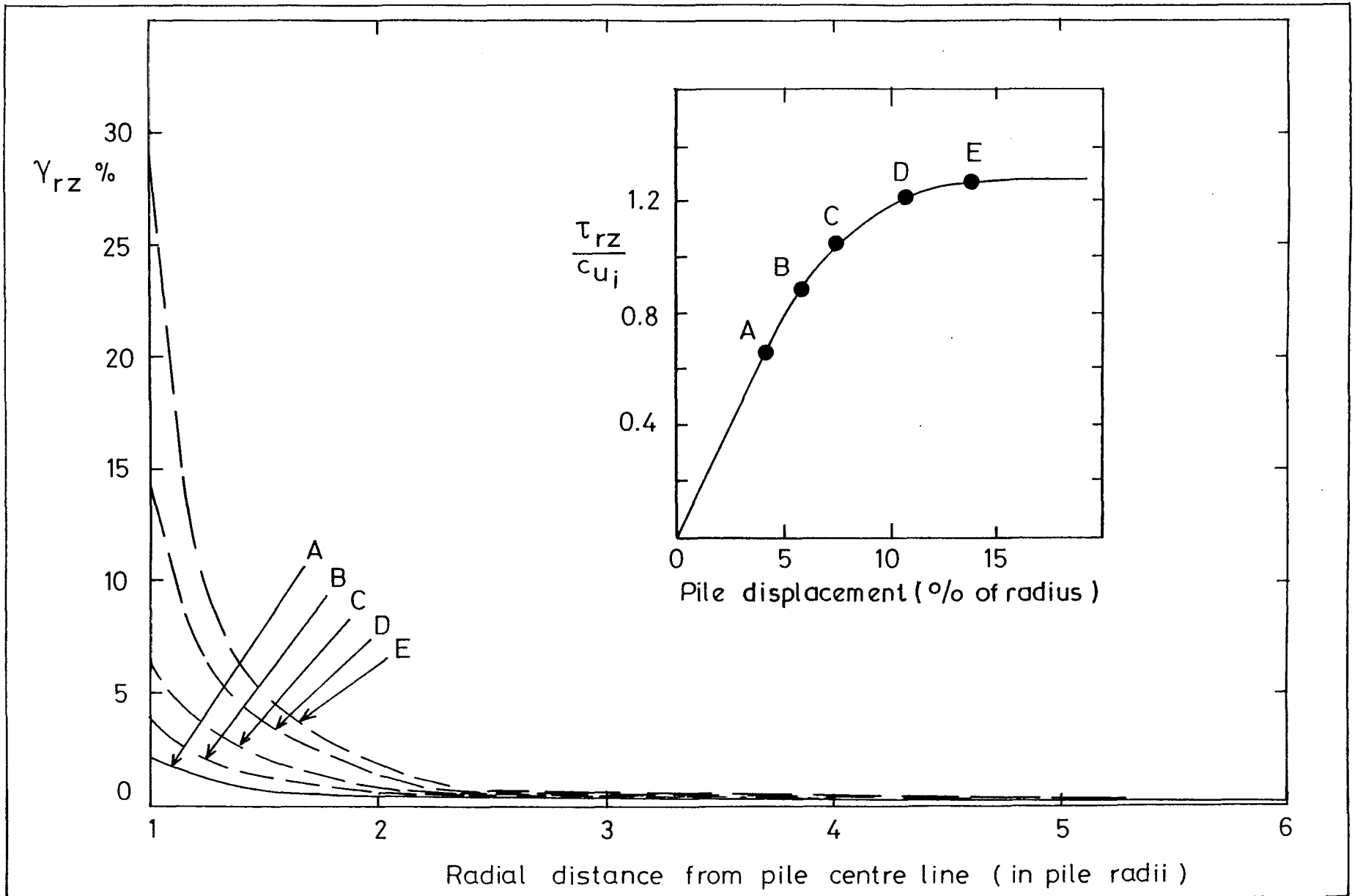
Stress paths followed by an element of clay adjacent to a pile driven into overconsolidated London Clay, allowed to consolidate, and then loaded

Fig. 9.6



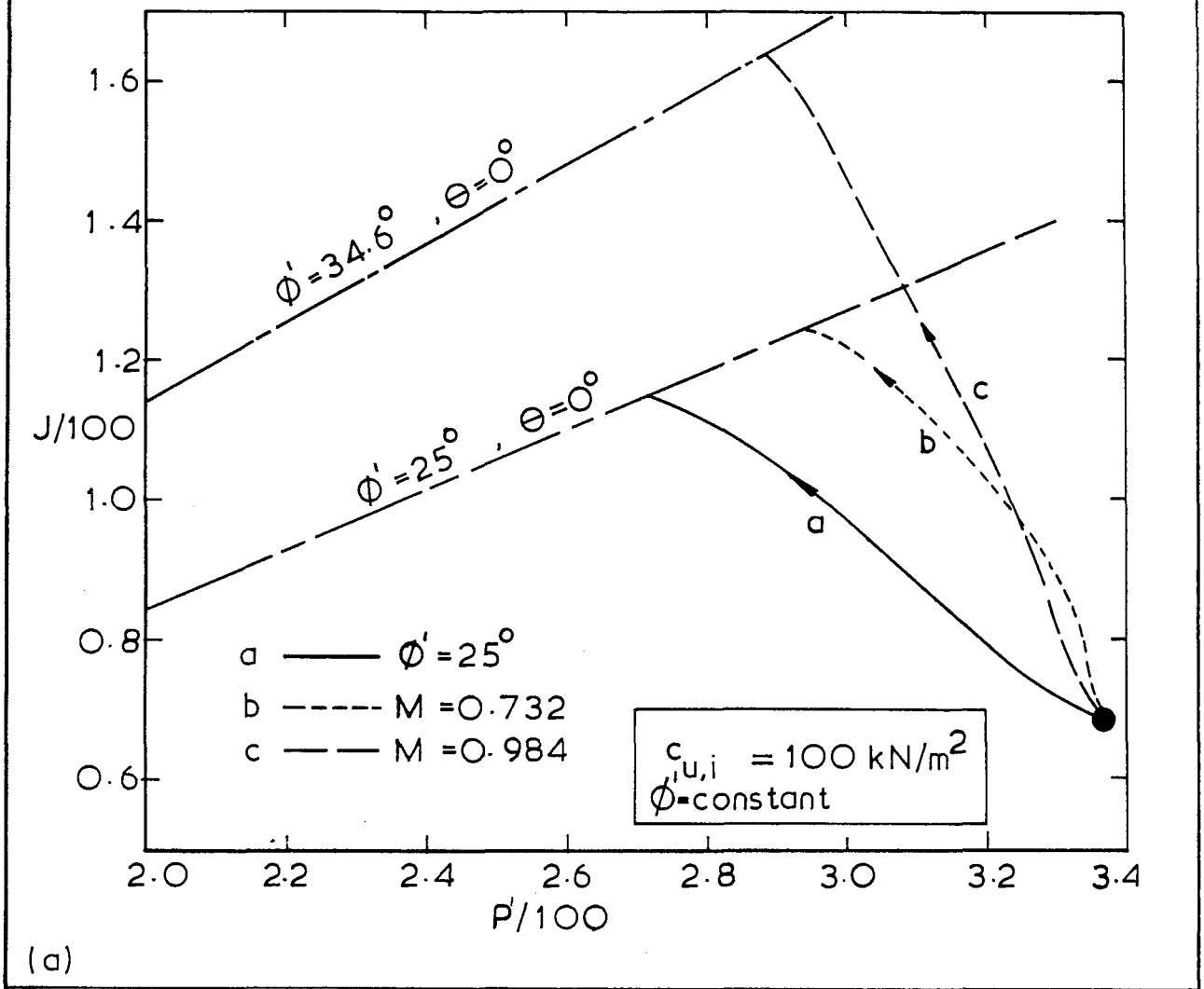
Variation of stresses adjacent to a pile driven into overconsolidated London Clay, on drained loading

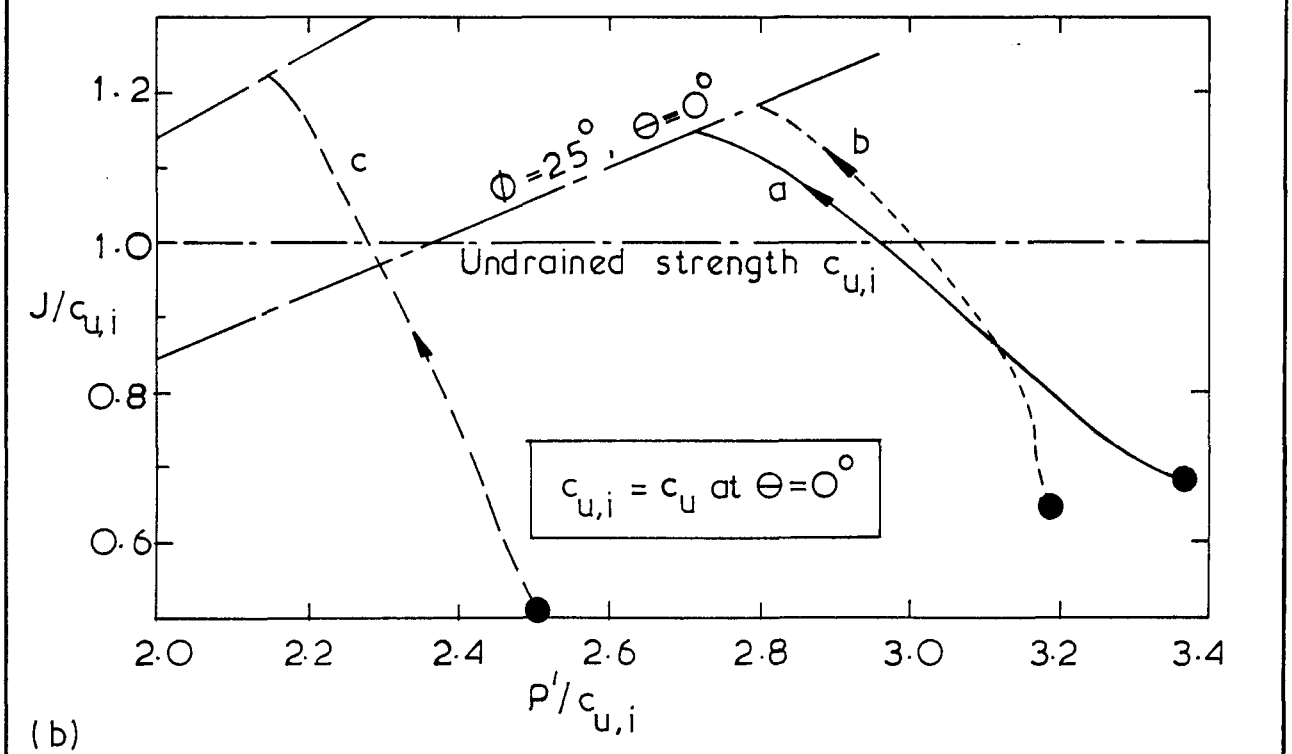
Fig. 9.7



Driven pile in overconsolidated London Clay; radial distribution of shear strains on loading

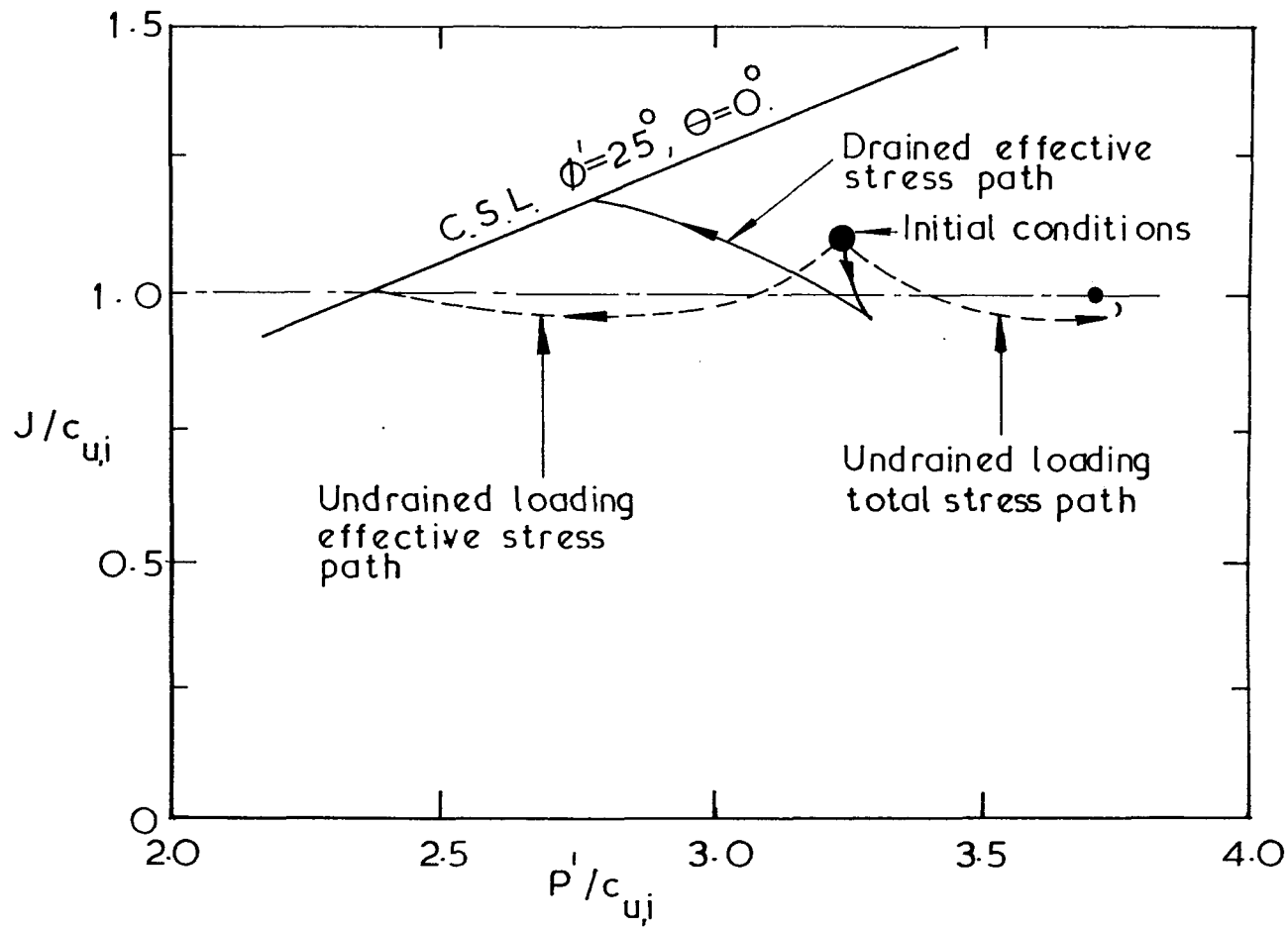
Fig. 9.8





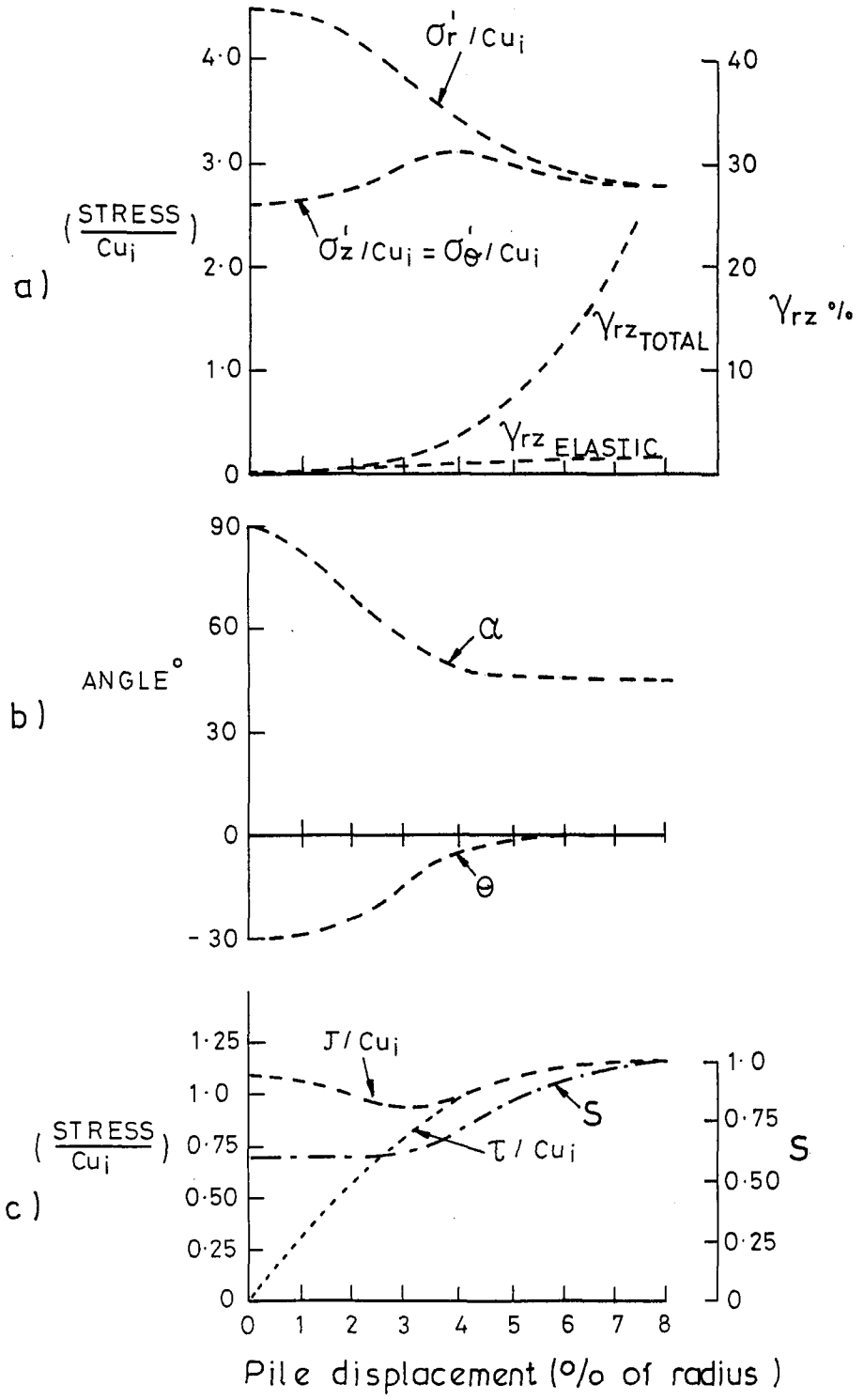
Stress paths followed on drained loading, as a function of the shape of the yield curve in the deviatoric plane. All loadings start from same stresses. In Figure (b) the stresses are normalised by the value of $c_{u,i}$ appropriate to each case.

Fig. 9·9



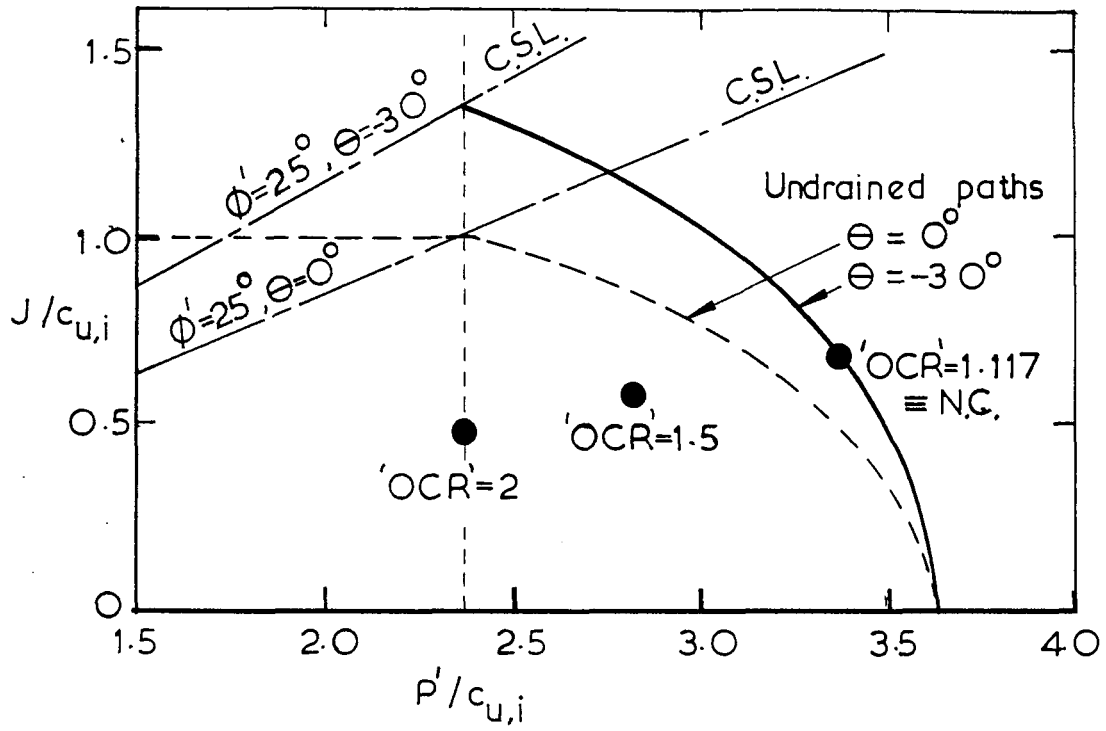
Stress paths followed by an element of soil adjacent to a driven pile on drained and undrained loading

Fig. 9.10



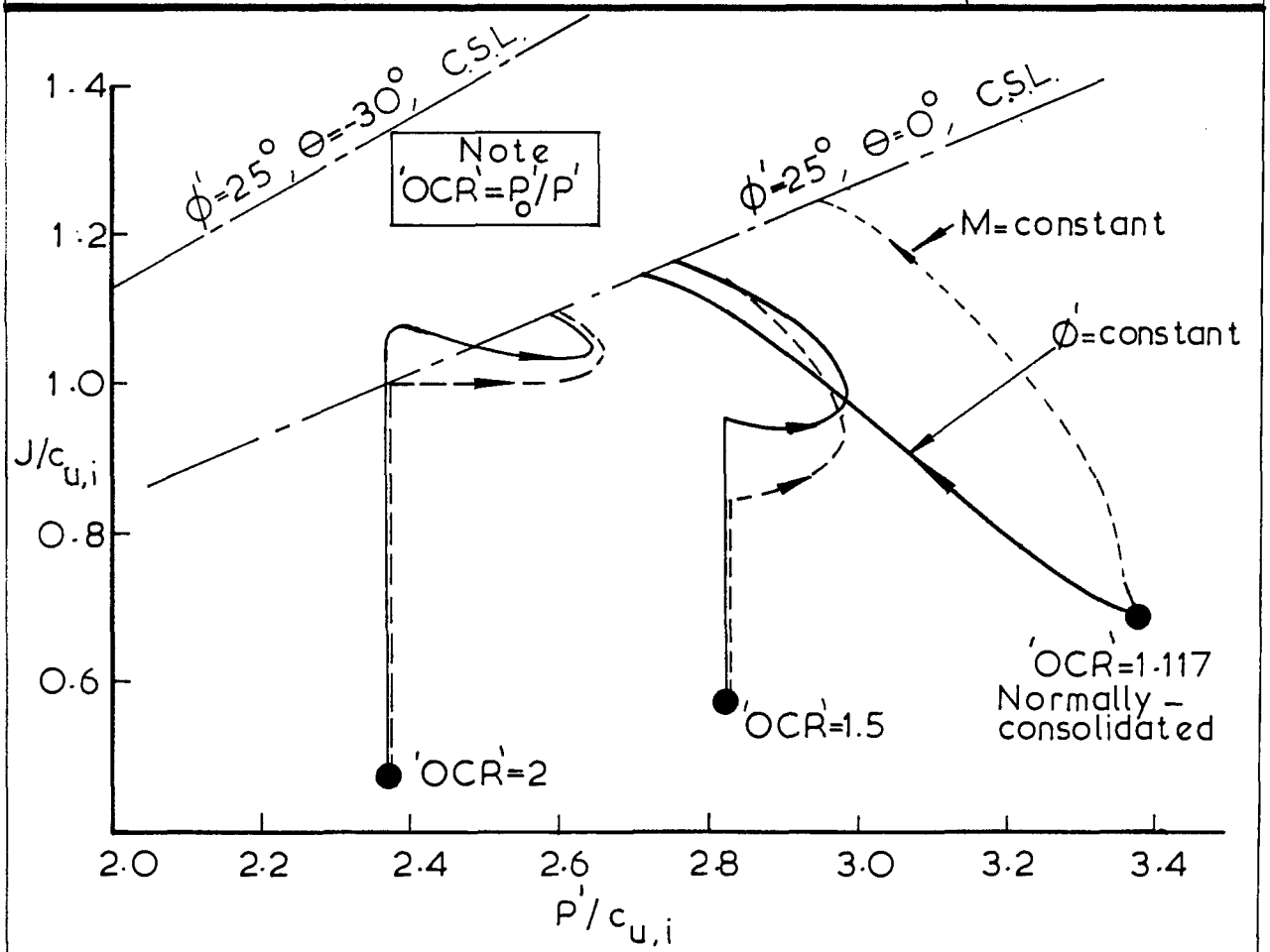
Variation with pile displacement of various components of stress and strain adjacent to a full displacement pile loaded under drained conditions.

Fig. 9.11



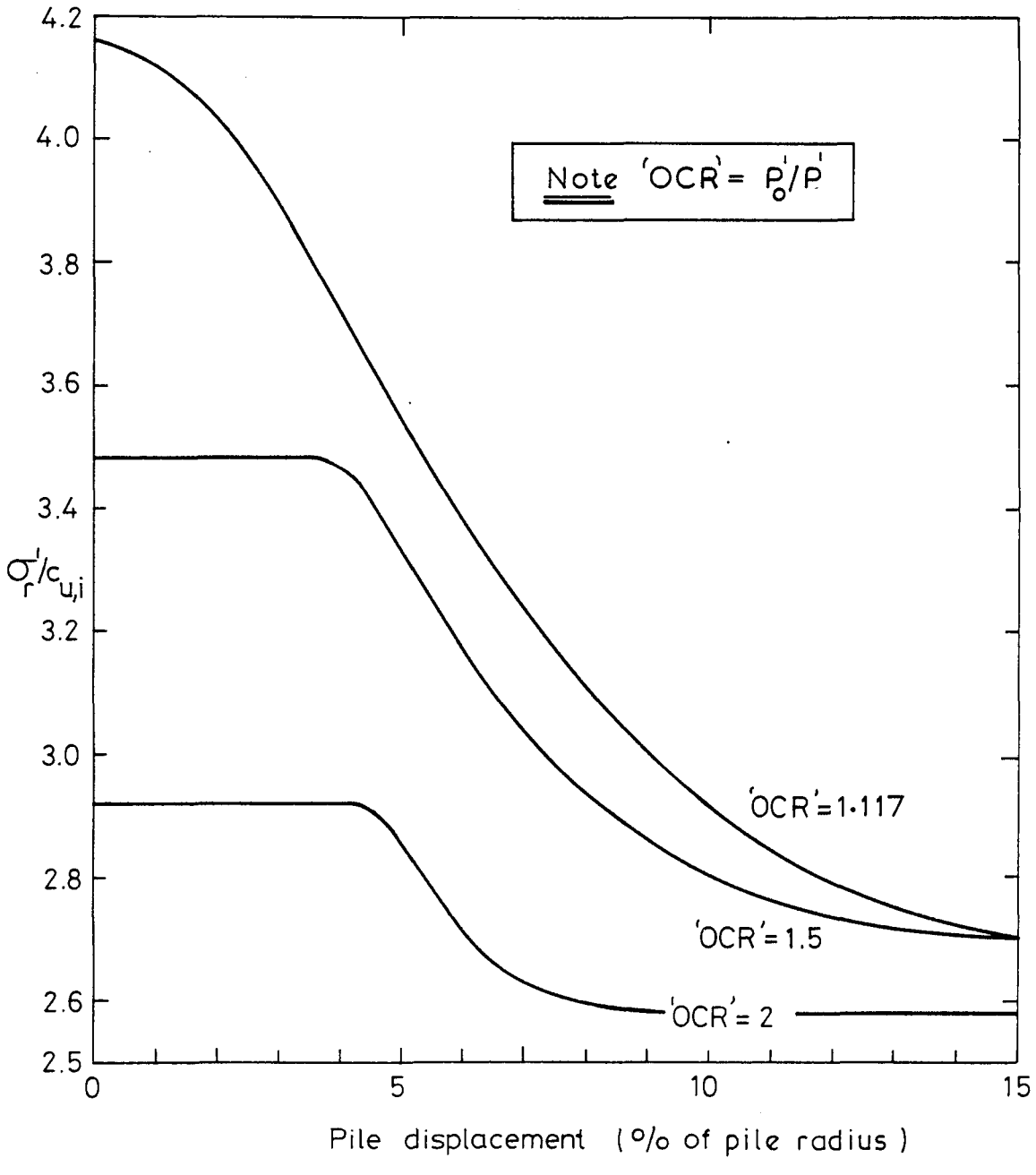
Relative initial stresses for the three analyses considering overconsolidated clay beside piles.

Fig. 9.12



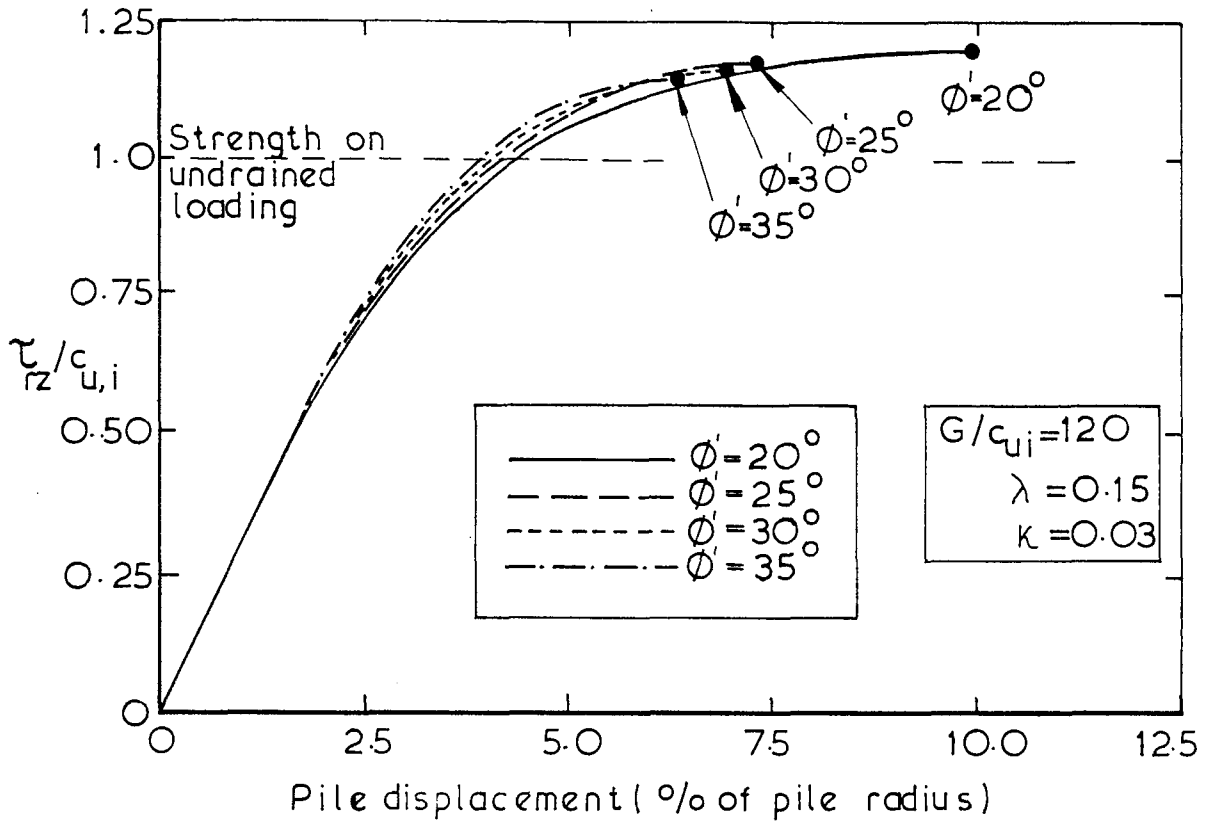
Stress paths as a function of the degree of overconsolidation in the clay adjacent to the pile shaft (drained loading).

Fig. 9.13



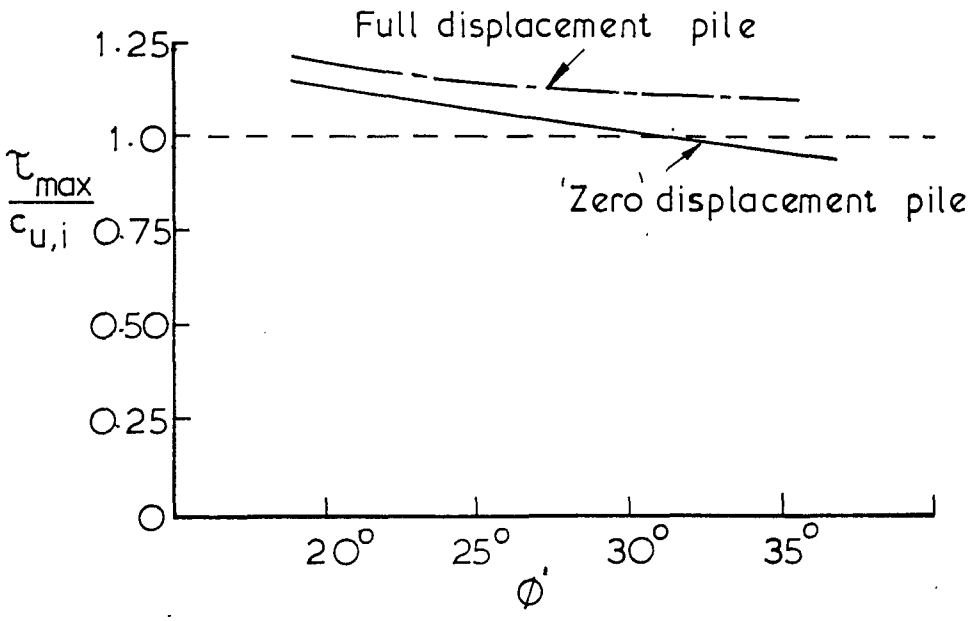
Variation of the radial stresses acting on a pile as a function of the degree of initial 'overconsolidation' beside the pile

Fig. 9.14



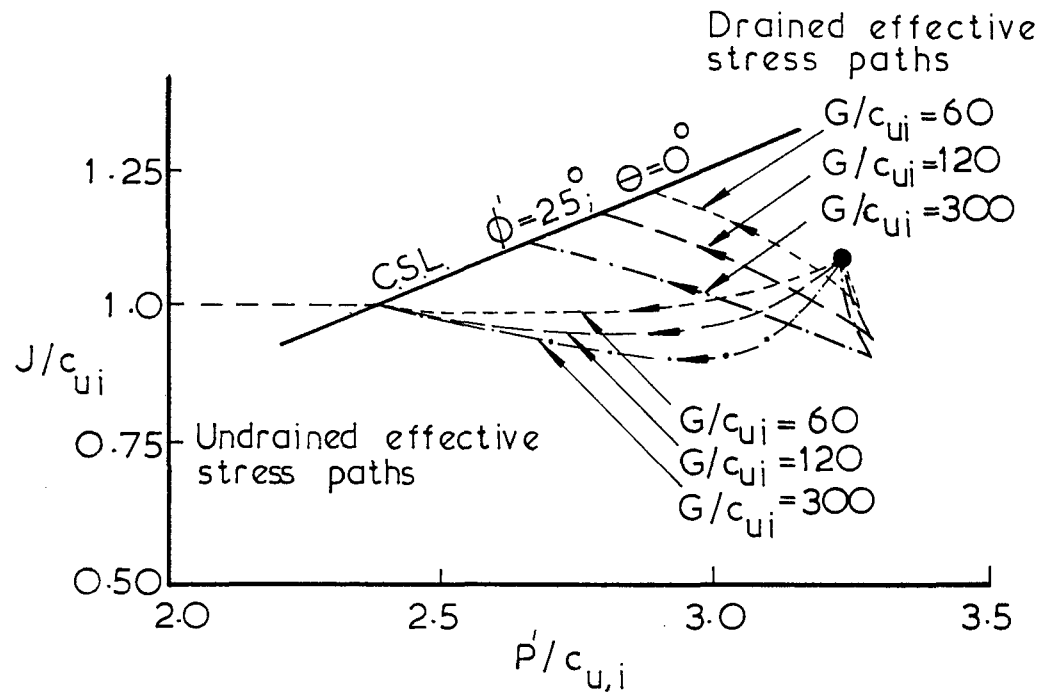
Drained 'load' / displacement behaviour for various values of ϕ'

Fig.9.15



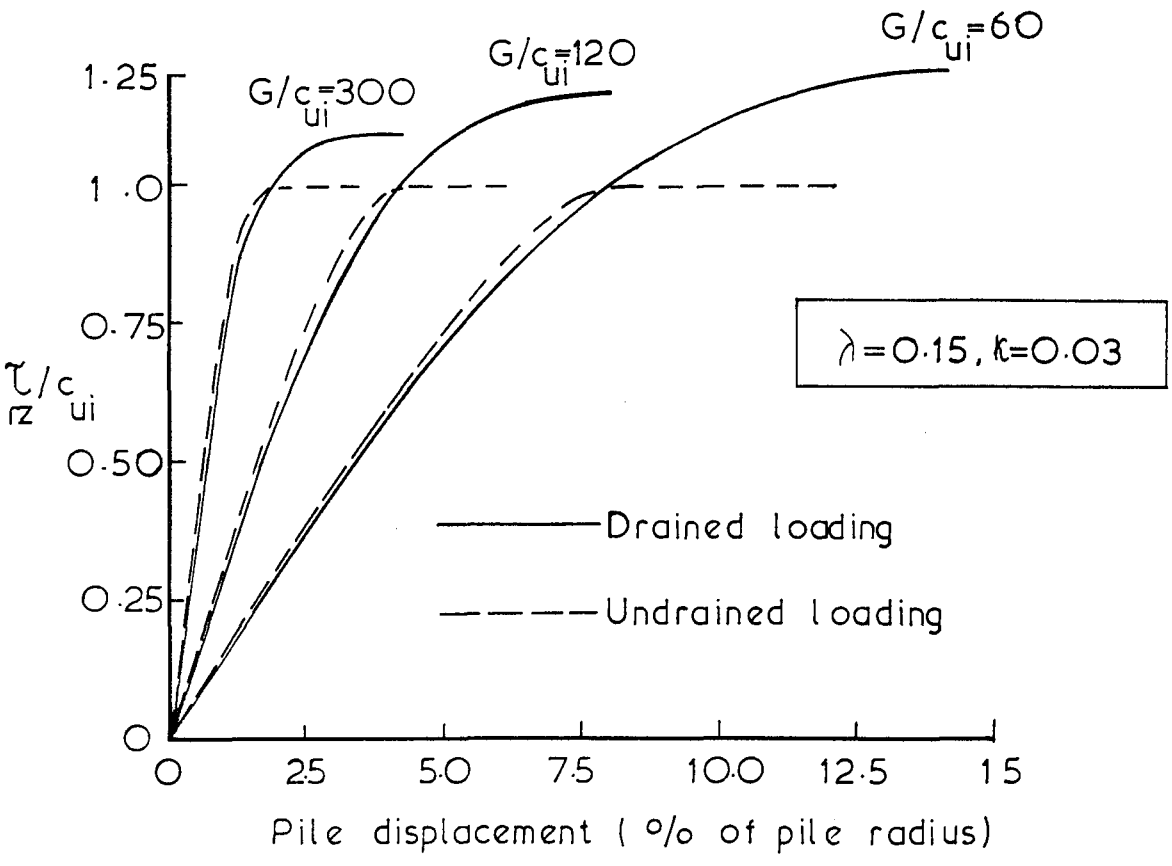
Peak shaft friction as a function of ϕ'

Fig.9.16



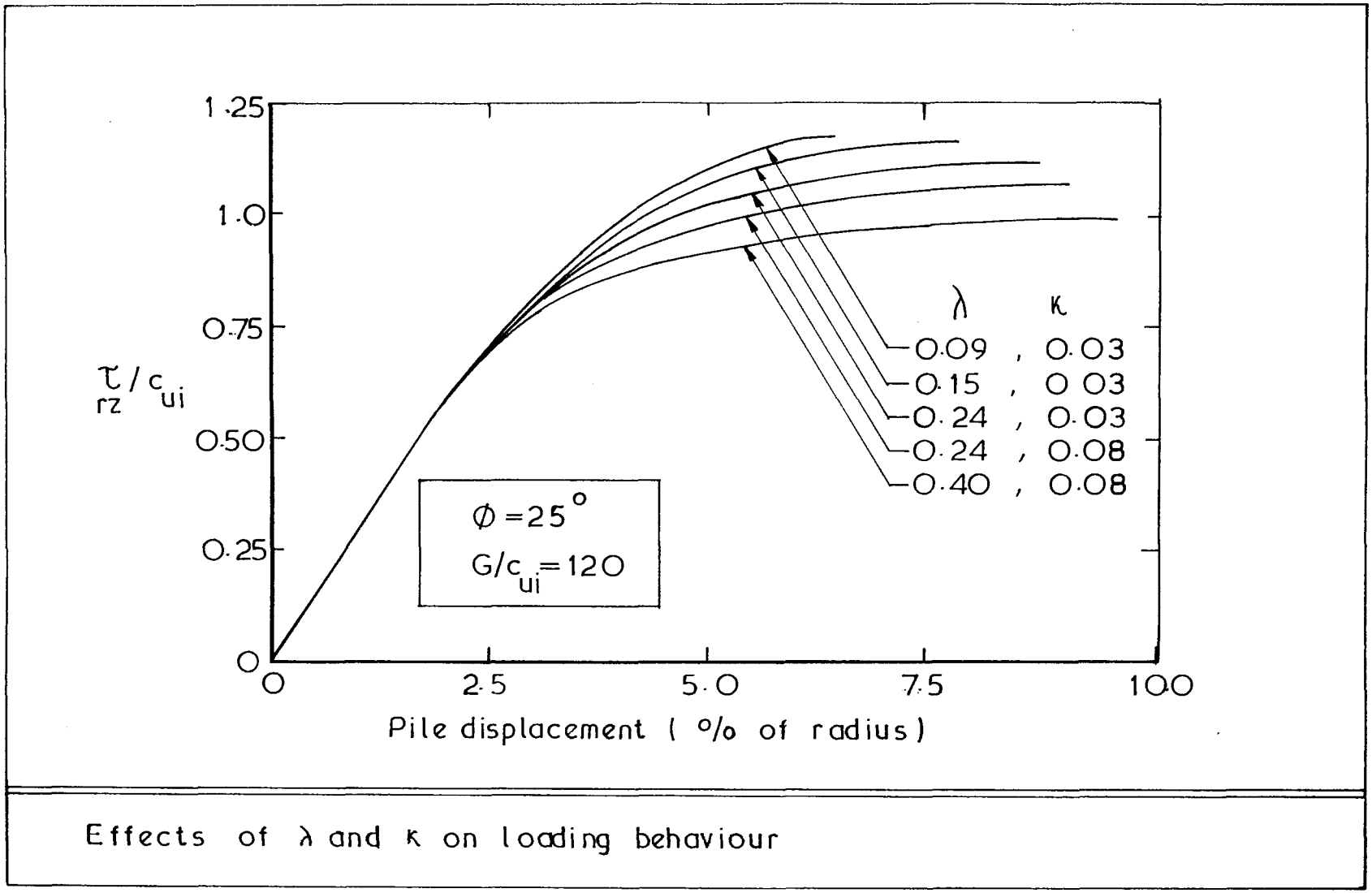
Effects of shear modulus on drained and undrained effective stress paths

Fig. 9.17



Effects of shear modulus on load / displacement behaviour

Fig. 9.18



Effects of λ and κ on loading behaviour

Fig. 9.19

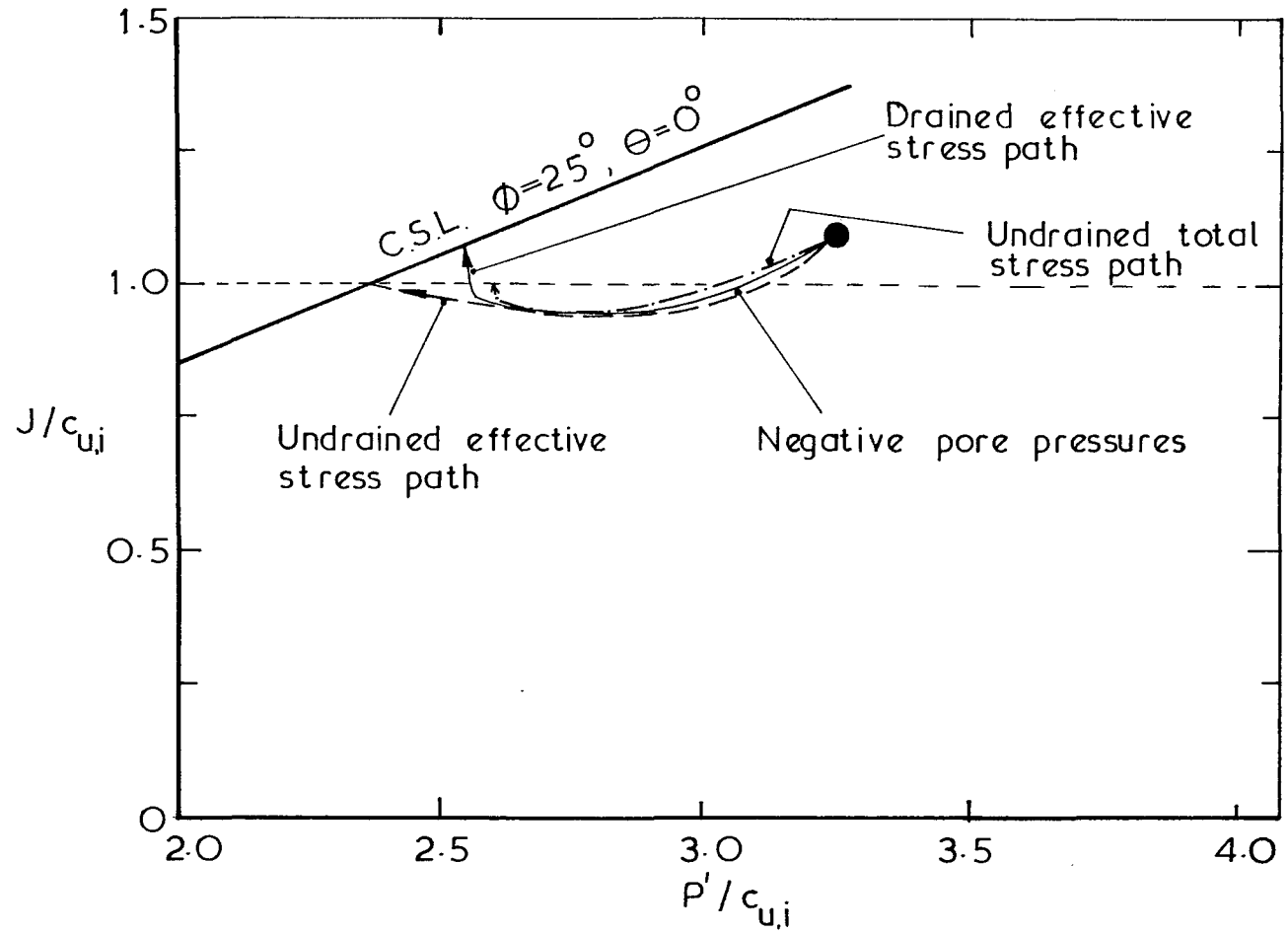
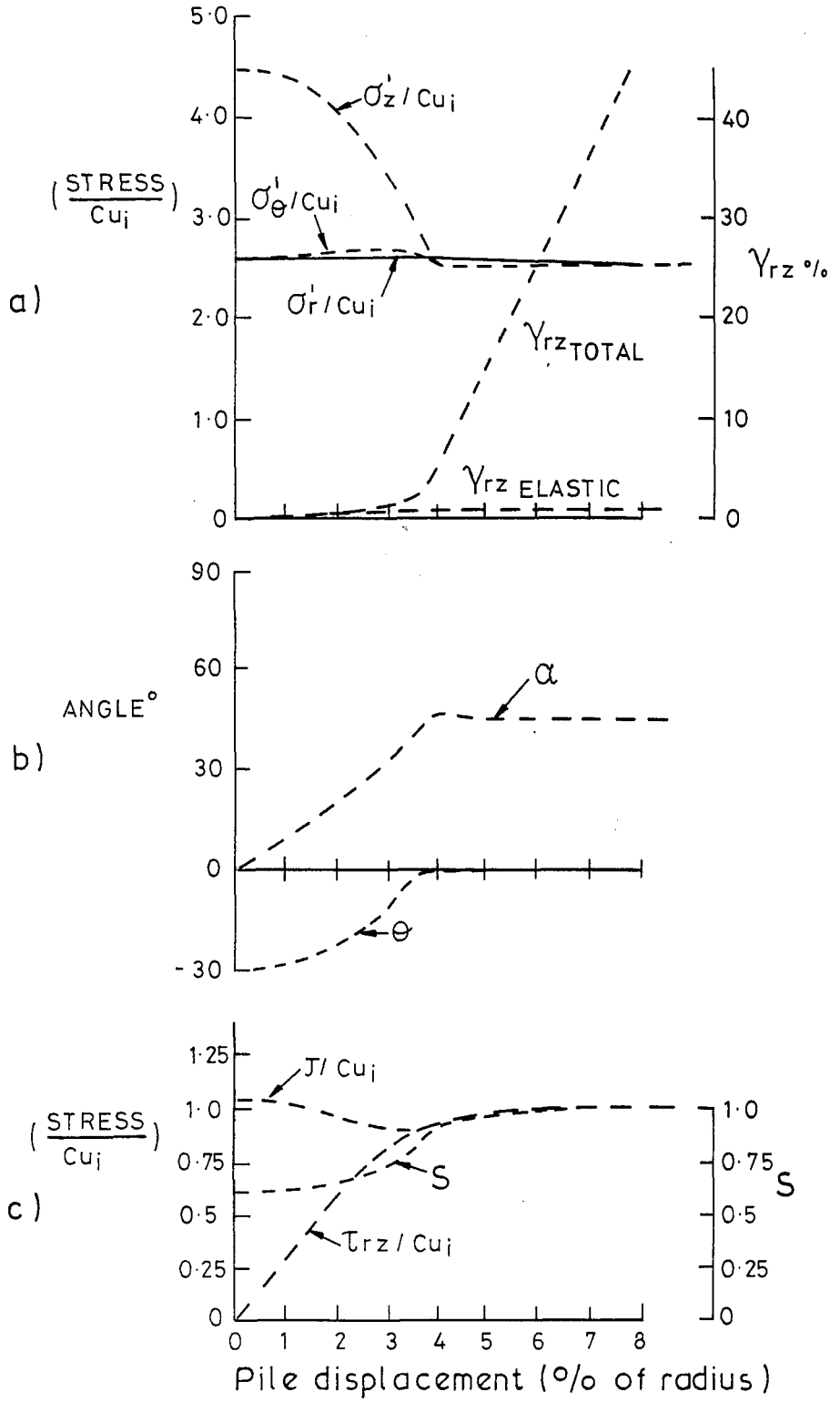


Fig. 9.20

Stress paths followed by an element of soil adjacent to a driven 'zero' displacement pile, on drained and undrained loading.



Variation with pile displacement of various components of stress and strain adjacent to a zero displacement pile loaded under drained conditions.

Fig. 9·21

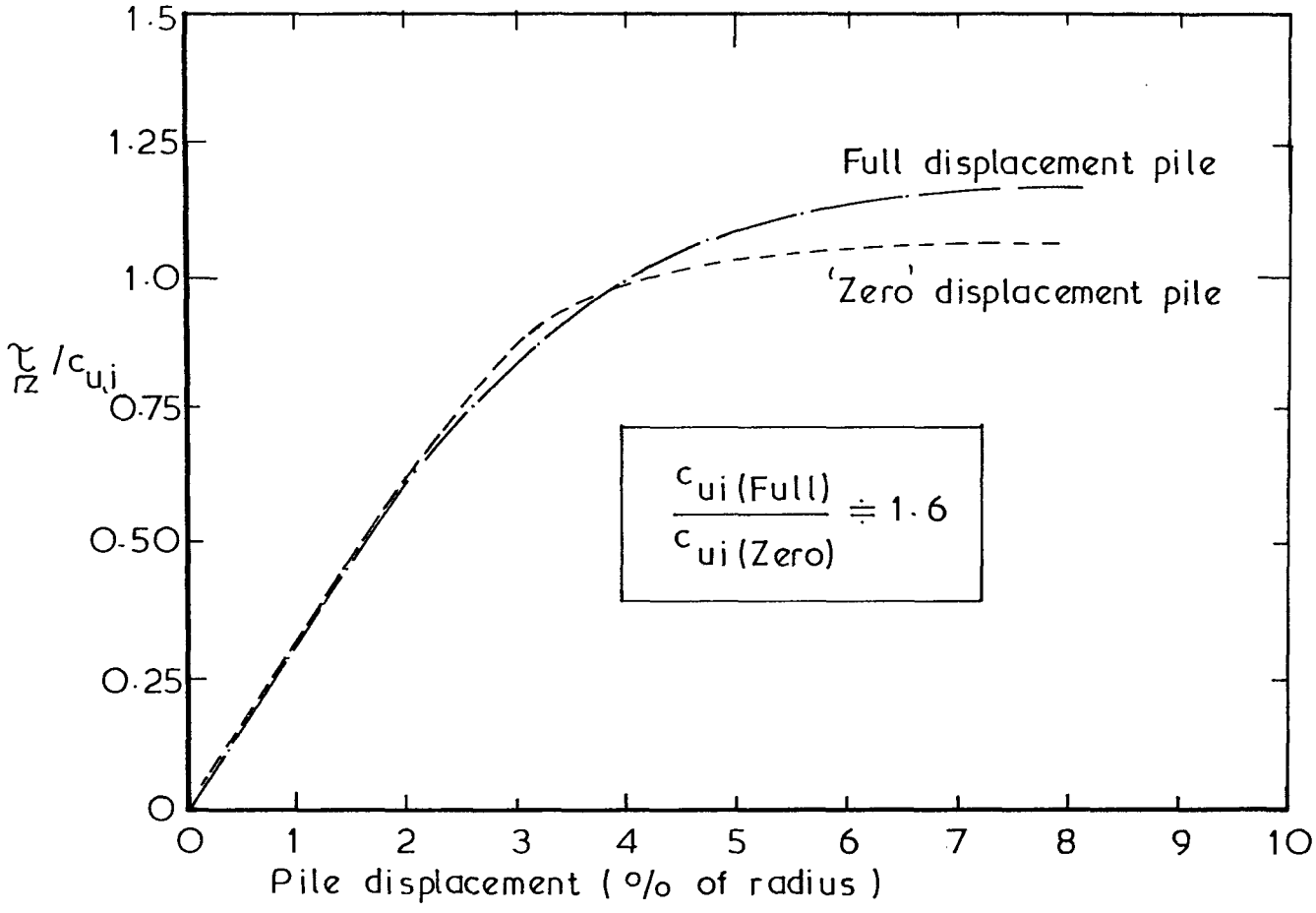
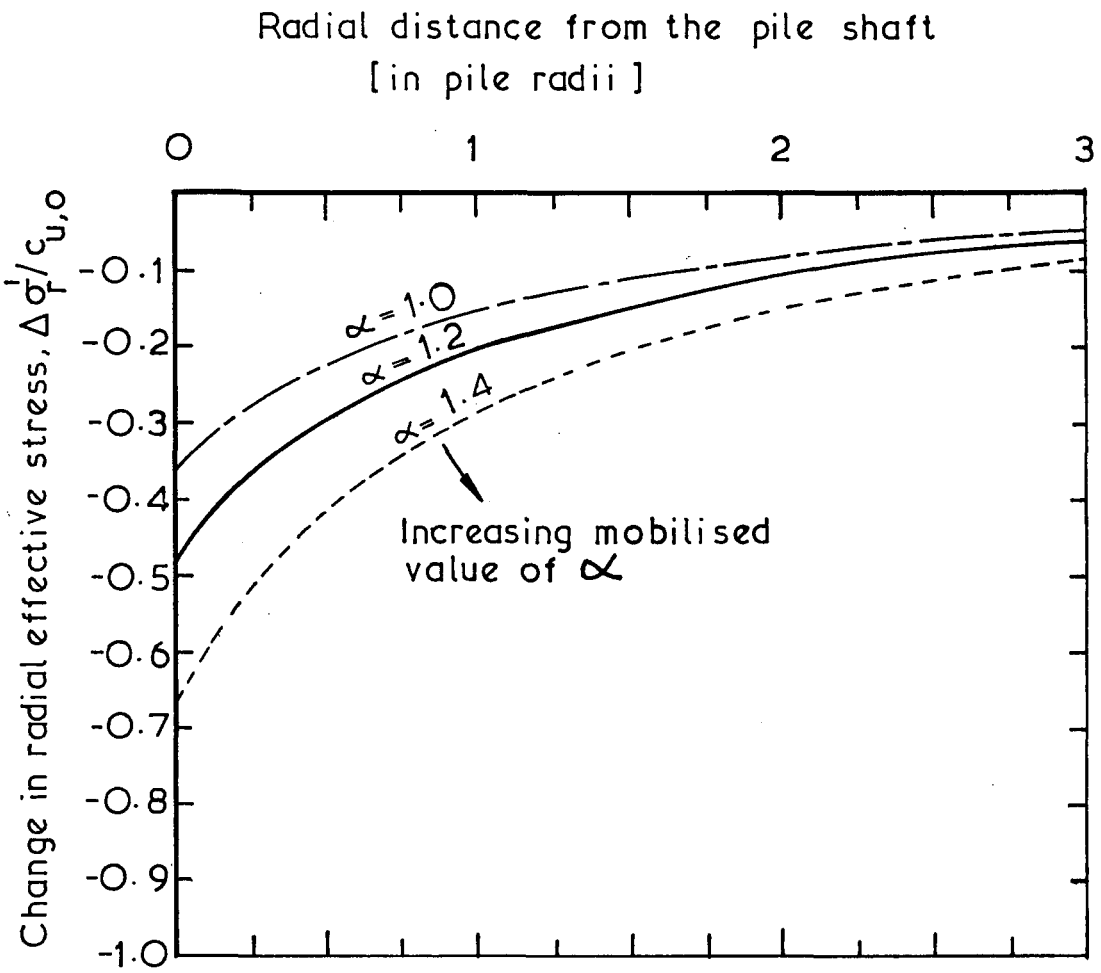


Fig. 9.22

Comparison between the shear stress displacement behaviours of Full and Zero displacement piles on drained loading.

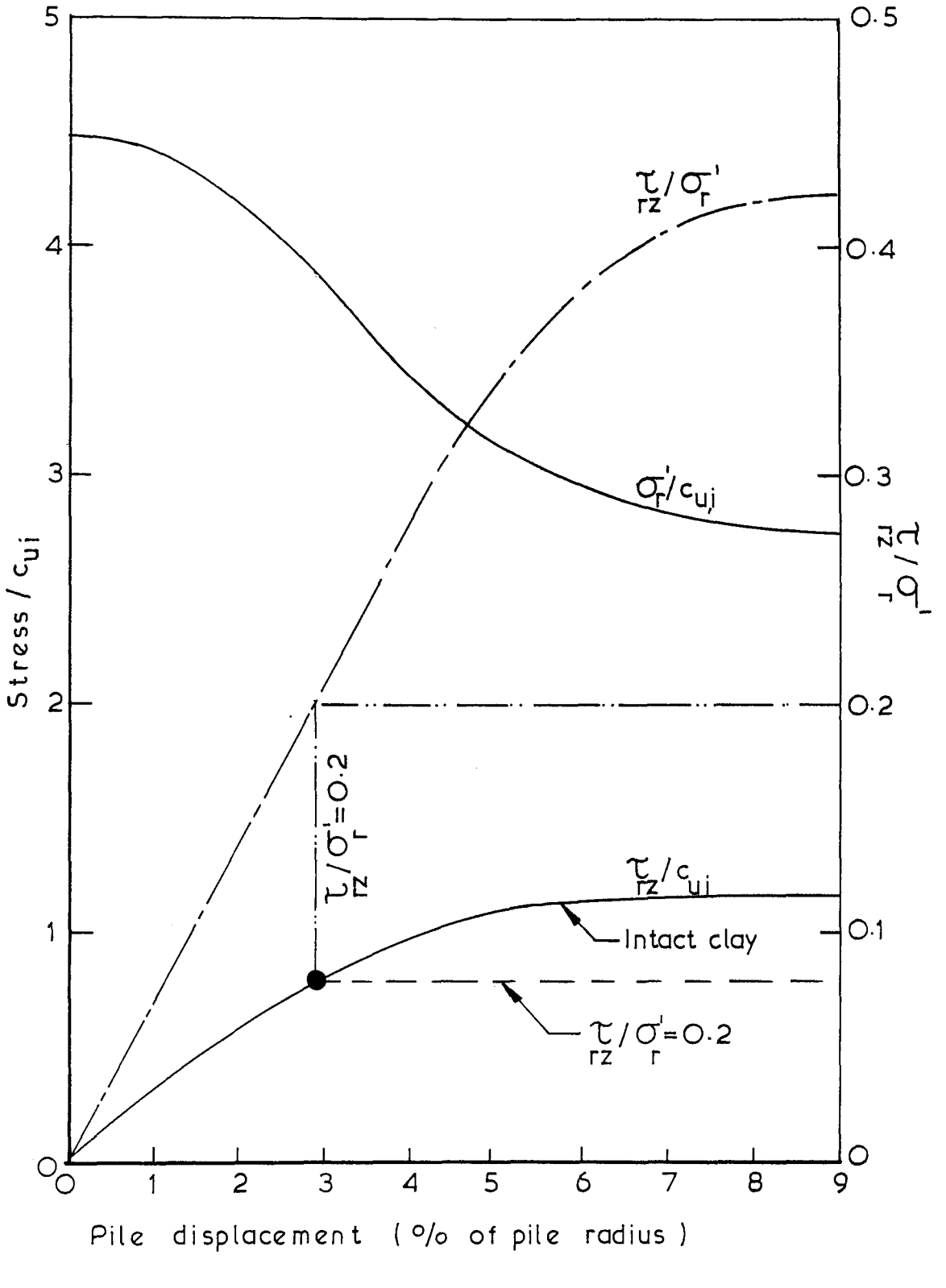


Notes [i] radial stress distribution prior to loading taken from Randolph et al (1979)

[ii] pile loading drained

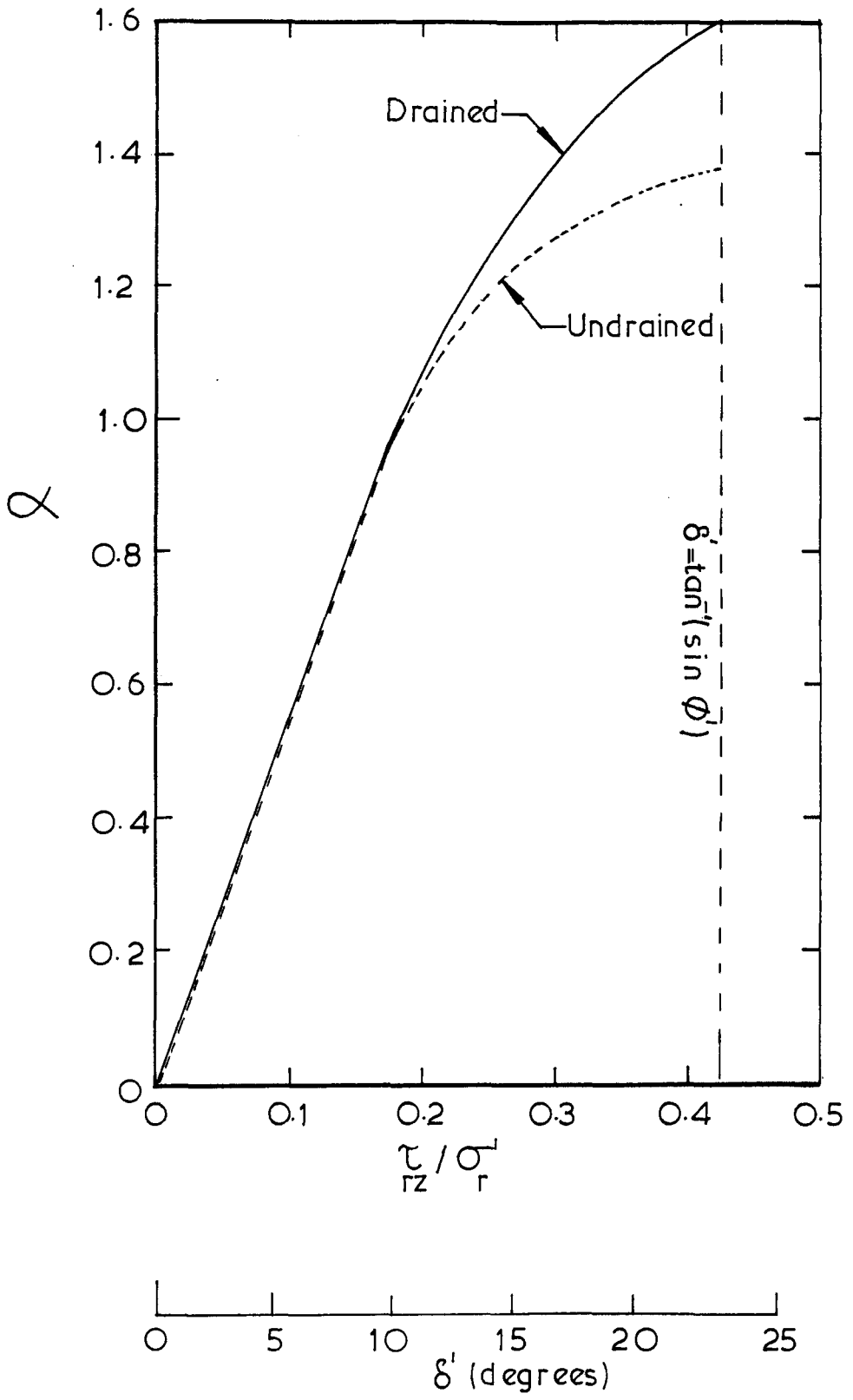
Change in radial effective stress, as a function of radial distance from the pile, at various stages during the loading of a pile installed in Boston Blue Clay

Fig. 9.23



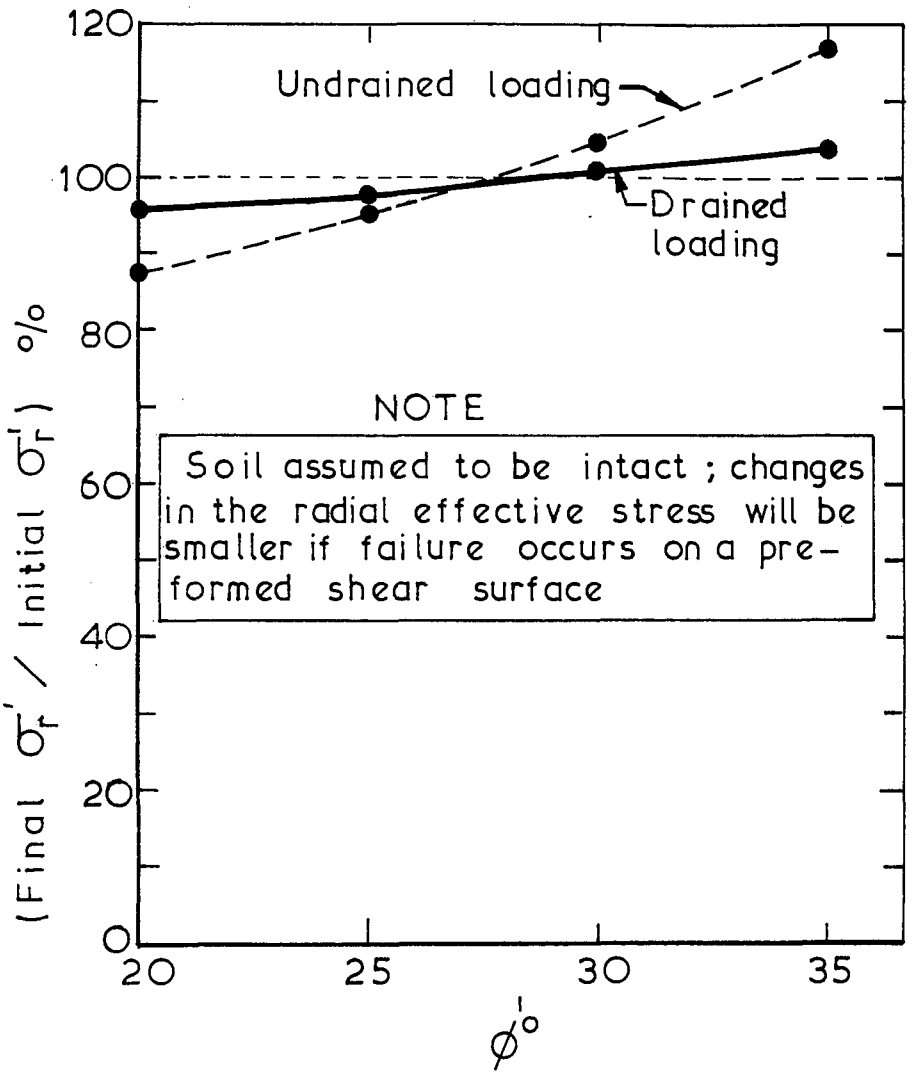
The possible influence of shear surfaces on the behaviour of a driven pile on drained loading

Fig.9.24



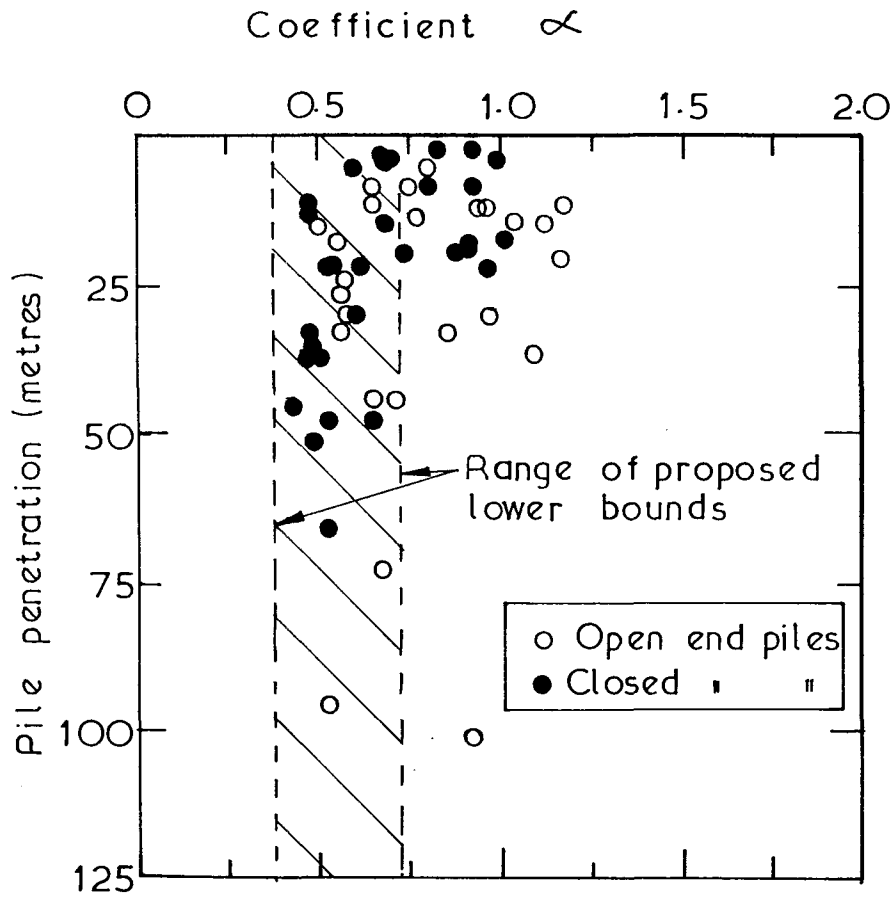
Variation of α with the angle of friction δ' mobilised on a vertical plane adjacent to a driven pile

Fig. 9·25



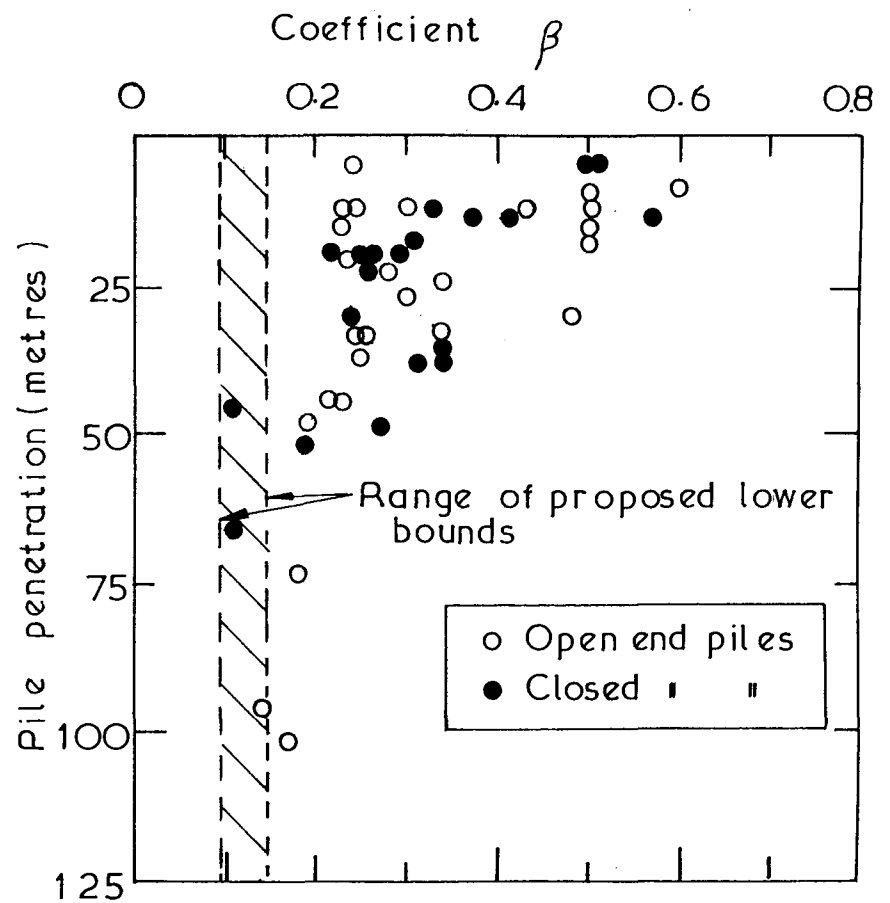
'Zero' displacement piles ; effect of ϕ' on the changes in the radial effective stress on loading to peak

Fig. 9.26



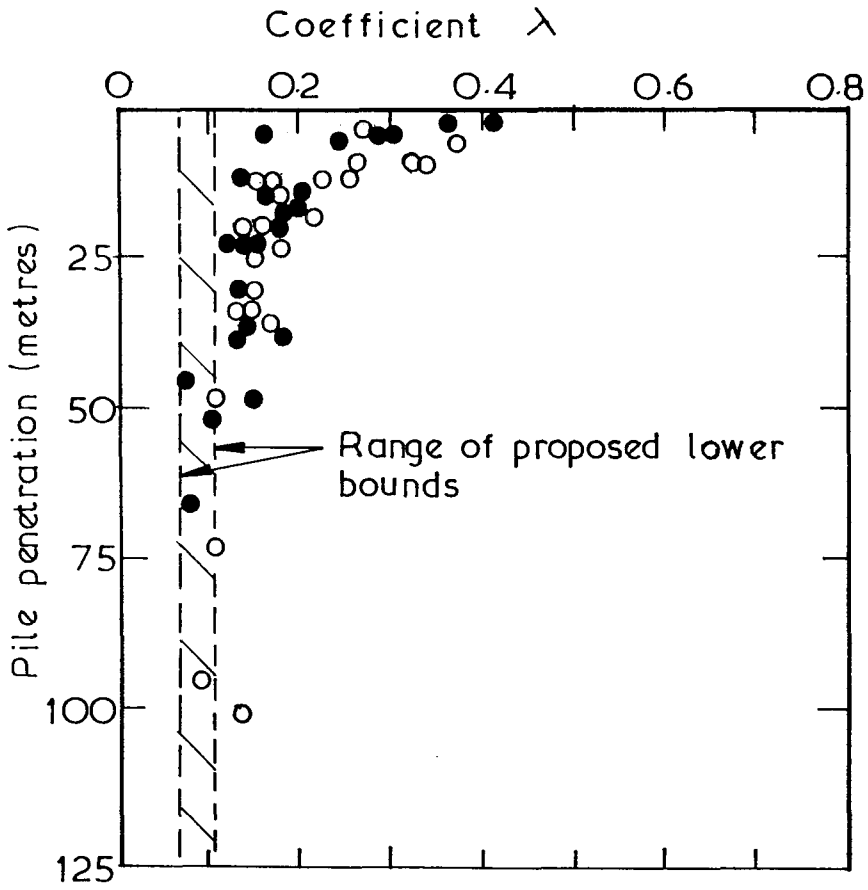
Profile of ∝ values (Kraft et al(1981))

Fig 9.27



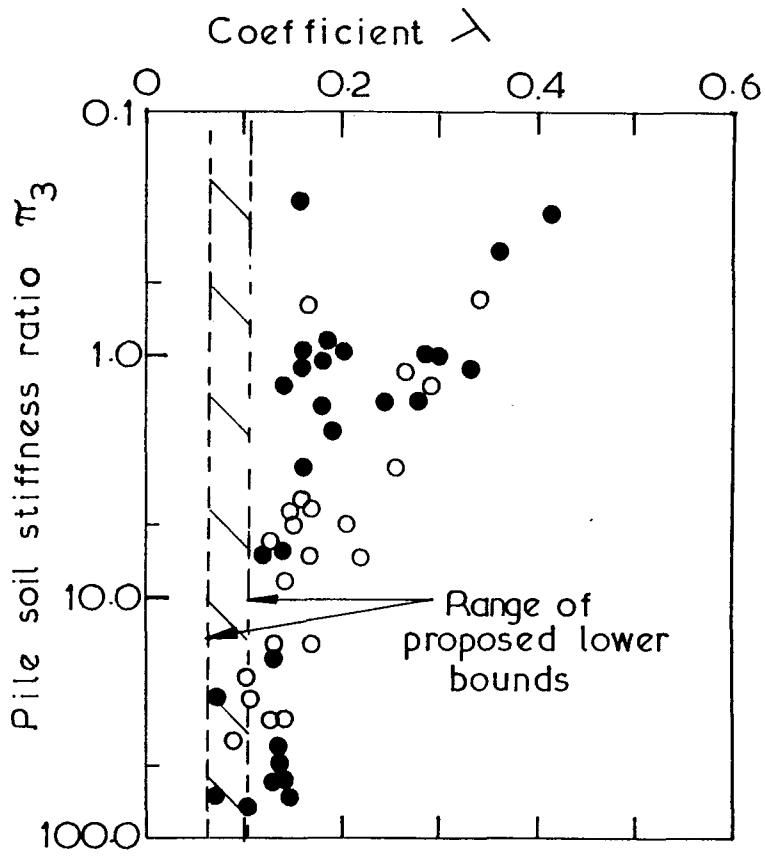
Profile of β values

Fig.9.28



Profile of λ values

Fig. 9. 29



Profile of λ values
(from Kraft et al (1981))

Fig. 9. 30

APPENDIX 9.1

CONSOLIDATION AROUND PILES

A.9.1 Introduction

Randolph and Wroth (1979) produced analytical solutions for the dissipation of excess pore pressures around driven piles, assuming the soil skeleton to deform in an elastic manner. They showed that the partial differential equation governing the plane strain radial consolidation reduced to the Terzaghi equation for one-dimensional consolidation, which was then solved by the method of separation of variables; also see Sills (1975).

Carter, Randolph and Wroth (1979) employed finite element methods to investigate the consolidation around piles, assuming the soil to behave in an elastoplastic manner during consolidation. Comparison between these predictions and those obtained analytically assuming the soil to behave elastically,showed that the dissipation of excess pore pressures with time is relatively unaffected by the choice of soil model, and therefore that a good estimate can be obtained by assuming a linear elastic soil. However, it was shown that the predicted stress changes are much more dependent on the type of soil model.

In the present study, it was desired to be able to determine the rates of dissipation of excess pore pressures around loaded piles. On the basis of the work described above it was considered appropriate to assume the soil to deform in a linear elastic manner, and a finite difference program was written to solve Terzaghi's equation for one-dimensional radial consolidation (Terzaghi, 1943);

$$\frac{\partial u}{\partial t} = C_v \{ \frac{1}{r} \frac{\partial}{\partial r} (r \times \frac{\partial u}{\partial r})\} \qquad \text{A.9.1(1)}$$

A.9.1.1 Finite Difference Method

When considering the dissipation of pore pressures around piles, it is necessary to establish the outer boundary at a distance of between thirty and eighty times the pile radius from the pile (see Randolph and Wroth, 1979). Because of the rapid spacial variation of the pore pressures close to the piles it is necessary to use closely spaced nodes near to the pile, if a finite difference solution procedure is adopted; on the other hand a much coarser spacing can be tolerated towards the outer boundary

where the spacial variation of pore pressures is much smaller. It was, therefore, decided to adopt a mesh in which the spacing of the nodes increased is a geometric progression with distance from the pile.

Because the spacing of the nodes was not uniform, additional ('correction') terms were introduced into the formultion of the finite difference equation, as shown below.

A.9.1.2 Finite Difference Formulation to Solve the One-dimensional Consolidation Equation

Considering a node i as illustrated in Fig. A.9.1.1, the forward and backward finite difference equations are obtained from the expansion of Taylor's series. Thus,

Forward differences;

$$u(r+\Delta^{+}r) = u(r)+ \Delta^{+}r\, u'(r) + \tfrac{1}{2}(\Delta r^{+})^{2}\, u''(r) + O(\Delta^{+}r)^{3} \qquad \text{A.9.1(2)}$$

Backward differences;

$$u(r-\Delta^{-}r) = u(r) - \Delta^{-}r\, u'(r) + \tfrac{1}{2}(\Delta^{-}r)^{2}\, u''(r) - O(\Delta^{-}r)^{3} \qquad \text{A.9.1(3)}$$

where $\Delta^{+}r = r_{i+1} - r_i$

and $\Delta^{-}r = r_i - r_{i-1}$

In general, let $\dfrac{r_{i+1}}{r_i} = \text{constant} = x$ A.9.1(4)

so $r_i = r_o x^i$, where r_o is the pile radius

Thus $\Delta^{+}r = r_o(x-1)x^i$

and $\Delta^{-}r = r_o(x-1)x^{i-1}$ 4.9.1(5)

The forward and backward difference equations were used to derive the following explicit finite difference equation

$$u_i(t+\Delta t) = u_i(t) + \frac{C_v \Delta t}{r_o^2} \; x^{-2i} \; \{P\, u_{i+1}(t) + Q\, u_i(t) + R\, u_{i-1}(r)\}$$

A.9.1(6)

where P,Q and R are constants which depend on the selected value of x.

$$\left.\begin{aligned} P &= (x-1)^2/(x^4-1) + (2x^2)/((1+x^2)(x-1)^2) \\ Q &= ((x-1)^2 - 4x^2/(x-1)^2)/(1+x^2) \end{aligned}\right\} \quad \text{A.9.1(7)}$$

and

$$R = x^2(2/(x-1)^2 - (x-1)/(x+1))/(1+x^2)$$

The condition for stability of the solution routine is that

$$\frac{C_v \Delta t}{(\Delta r_{min})^2} = \alpha < \tfrac{1}{2}$$

$$\Delta r_{min} = (x-1) r_o$$

so

$$\frac{C_v \Delta t}{r_o^2 (x-1)^2} = \alpha < \tfrac{1}{2}$$

Thus the final equation may be written as

$$u(t+\Delta t) = u(t) + \alpha (x-1)^2 \; x^{-2i} \; \{P\, u_{i+1}(r) + Q\, u_i(r) + R\, u_{i-1}(t)\}$$

A.9.1(8)

where the condition for stability is $\alpha < \tfrac{1}{2}$.

A.9.1.3 Boundary Conditions

The outer boundary (typically at a distance of about 90 pile radii from the shaft) was set to a constant excess pore pressure of zero. The pile itself was assumed impermeable and so a condition of no flow across the boundary was imposed by means of an additional imaginary node within the pile.

A.9.1.4 Solution

A program for an HP41 cv calculator (with printer) was written to solve the set of finite difference equations represented by eqn. A.9.1(8). Typically twenty nodes were employed, and the spacing of the nodes beside the pile was between 0.18 and 0.25 times the pile radius. For accuracy α was chosen to be 0.125 in the early stages of calculation, but was increased to 0.25 after the pore pressure at the pile face had decreased to about 25% of its initial value. Thus, at the start of the analysis the time increments (in terms of $T_v = \frac{C_v t}{r_o^2}$) were between 1/125 and 1/250.

A.9.1.5 Check Solution

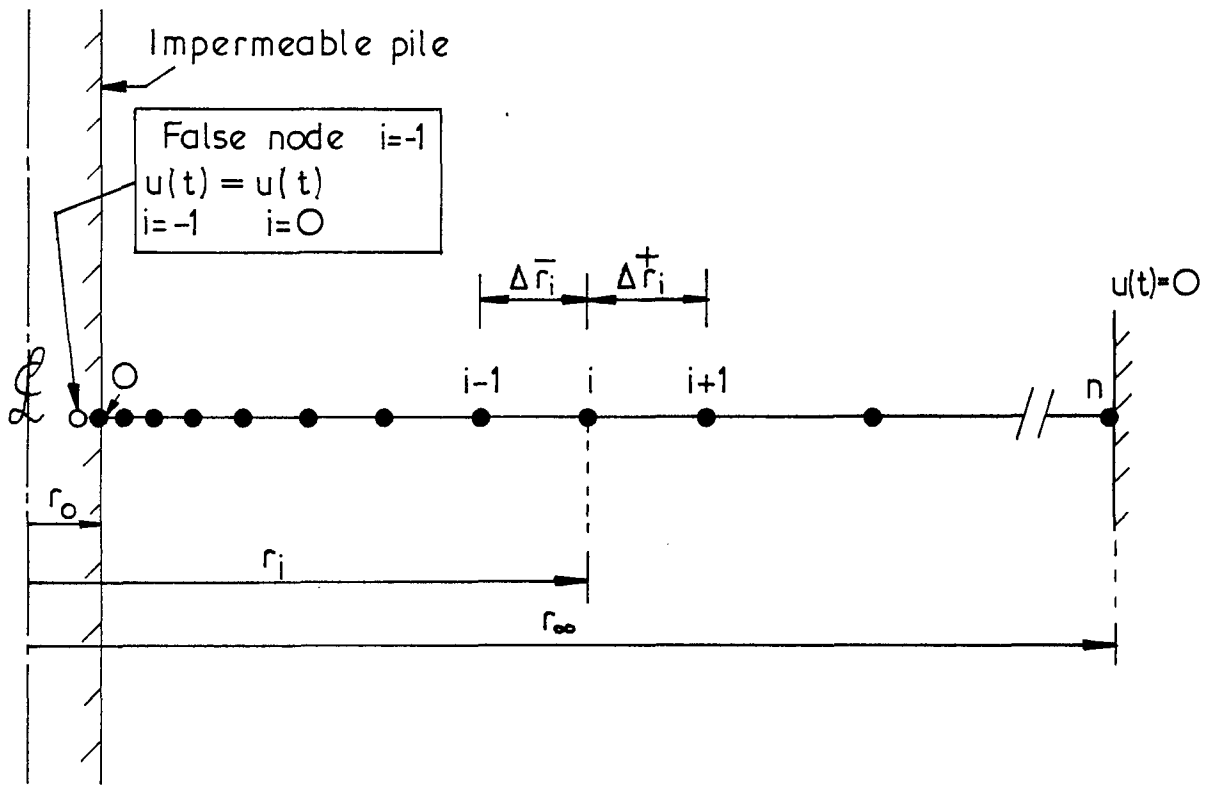
Randolph and Wroth (1979) presented the results of analytical solutions for the decay of excess pore pressures around a driven pile. The initial logarithmic variation of the excess pore pressures assumed by Randolph and Wroth (for the case of G/Cu = 50) were entered into the above program, and the results were compared with the analytical solution. In Fig. A.9.1.2 the predicted variations with time of the excess pore pressures at the pile face are compared, and the very close agreement may be seen. Having established the validity of the calculator program, it was then used to consider times for the dissipation of excess pore pressures around loaded piles.

$\frac{r_i}{r_{i-1}} = x$, so $r_i = r_o x^i$

Typically n=20

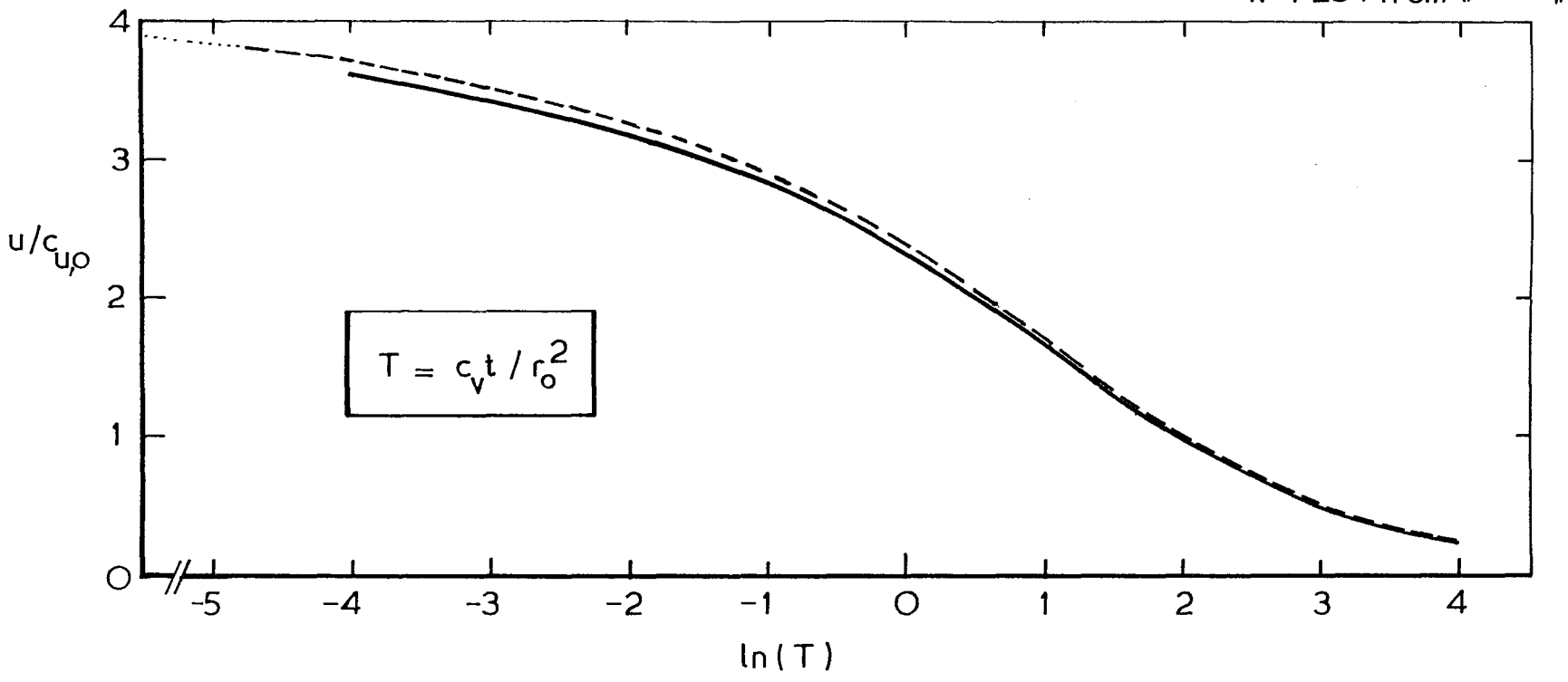
$1{\cdot}18 < x \leq 1{\cdot}254$

If $x=1{\cdot}254$, $(r_\infty / r_o) \doteq 93$



Schematic view of mesh employed in Finite difference program — to illustrate nomenclature

Fig. A.9.1. 1



Pore pressure dissipation at the face of a driven pile ; comparison between the Finite Difference predictions and the analytical solution from Randolph and Wroth (1979)

Fig. A.9.1. 2

APPENDIX 9.2

DERIVATION OF A VARIETY OF EQUATIONS EMPLOYED IN THE TEXT

A.9.2.1 Relationship between P', P'_o and P'_u

The quantities considered are illustrated in Fig. A.9.2.1.

Along the swelling line;

$$v_o + \kappa \ell n\, P'_o = v_u + \kappa \ell n\, P' \qquad \text{A.9.2(1)}$$

Along the consolidation line;

$$v_u + \lambda \ell n\, P'_u = v_o + \lambda \ell n\, P'_o \qquad \text{A.9.2(2)}$$

Thus

$$v_u - v_o = \kappa\, \ell n(P'_o/P') = \lambda\, \ell n(P'_o/P'_u) \qquad \text{A.9.2(3)}$$

$$\left(\frac{P'_o}{P'}\right)^{\kappa} = \left(\frac{P'_o}{P'_u}\right)^{\lambda} \qquad \text{A.9.2.(4)}$$

This leads, on manipulation to

$$\left(\frac{P'_o}{P'}\right) = \left(\frac{P'_u}{P'}\right)^{1/\mathcal{N}} \qquad \text{A.9.2(5)}$$

where $\mathcal{N} = (1-\kappa/\lambda)$

A.9.2.2 Relationship between the Stresses Acting in the Soil Beside a Full-displacement Pile at the Start and the End of Loading to Undrained Failure

Initial conditions

These are denoted by the subscript (i). From Randolph et al (1979) the initial stress state will be taken to obey the following relations,

(i) $\sigma'_{z,i} = \sigma'_{\theta,i} = K_o\, \sigma'_{r,i}$

(ii) the soil is normally consolidated.

Thus, $$J_i = \sigma'_{r,i}\, (1-K_o)/\sqrt{3} \qquad \text{A.9.2(6)}$$

and $$P'_i = \sigma'_{r,i}\, (1 + 2K_o)/3 \qquad \text{A.9.2(7)}$$

Because the minor and intermediate stresses ($\sigma'_{\theta,i}$ and $\sigma'_{z,i}$) are equal, the soil is initially in a state of triaxial compression (T.C.) and so the Lode

angle, θ_i, = -30°.

Thus $$g(\theta)_i = g(\theta)_{T.C.} \qquad A.9.2(8)$$

Failure conditions

Referring to Fig. A.9.2.1(b) it may be seen that as the case considered is undrained, the values of P'_u and P'_f (the value of P' at failure) are determined by the current water content. Thus P'_f is independent of the stress path to failure and of the shape of the yield function in the deviatoric plane.

In this analysis the yield function may take any shape in the deviatoric plane, as may the plastic potential. The boundary conditions of the problem together with the shape of the plastic potential dictate the Lode angle at failure (θ_f) (see Potts and Gens, 1982). This value may be used in conjunction with the yield function to define $g(\theta)_f$ for the pile loading. It may be seen from Fig. A.9.2.1(b) that the value of J at failure is given by

$$J_f = P'_f \, g(\theta)_f \qquad A.9.2(9)$$

$$C_u = J_f \cos \theta_f \qquad \text{from eqn. (A.7.14)}$$

and so

$$C_u = P'_f \, g(\theta)_f \cos \theta_f \qquad A.9.2(10)$$

It is illustrated in Fig. 8.9 that at failure the shear stress acting on the shaft is equal to C_u, so

$$\tau_{rz_{max}} = P'_f \, g(\theta)_f \cos \theta_f \qquad A.9.2(11)$$

All that is now required is to determine P'_f from the initial conditions.

The yield function is given by

$$\left(\frac{P'_o}{P'}\right) = 1 + S^2 = 1 + \left\{\frac{J}{P' g(\theta)}\right\}^2 \qquad A.9.2(12)$$

At failure

$$P' = P'_f, \text{ and } S = 1 \text{ so } \frac{P'_o}{P'_f} = 2$$

Using eqn. A.9.2(5) to eliminate P'_o which varies with the current stress state,

$$\left(\frac{P'_f}{P'_u}\right) = 0.5^{\Lambda} \qquad \text{A.9.2(13)}$$

The yield function may be rewritten as

$$\left(\frac{P'_o}{P'}\right) = \left(\frac{P'_u}{P'}\right)^{1/\Lambda} = 1 + \left\{\frac{J}{P'g(\theta)}\right\}^2$$

so

$$P_u = P' \left\{1 + \left\{\frac{J}{P'g(\theta)}\right\}^2\right\}^{\Lambda}$$

$$P_f = 0.5^{\Lambda} P' \left\{1 + \left\{\frac{J}{P'g(\theta)}\right\}^2\right\}^{\Lambda}$$

$$P_f = P' \left\{0.5\left(1 + \left(\frac{J}{P'g(\theta)}\right)^2\right)\right\}^{\Lambda} \qquad \text{A.9.2(14)}$$

Substituting the initial stress conditions into the above expression,

$$P_f = \sigma'_{r,i}\,(1 + 2K_o)/3 \left\{0.5\left(1 + \left(\frac{\sigma'_{r,i}(1-K_o)/\sqrt{3}}{\sigma'_{r,i}(1+2K_o)/3 \times g(\theta)_{TC}}\right)^2\right)\right\}^{\Lambda}$$

$$P_f = \sigma'_{r,i}\left(\frac{1+2K_o}{3}\right)\left\{0.5\left(1 + 3\left(\frac{1-K_o}{(1+2K_o)\,g(\theta)_{TC}}\right)^2\right)\right\}^{\Lambda} \qquad \text{A.9.2(15)}$$

Substituting into eqn. A.9.2(11),

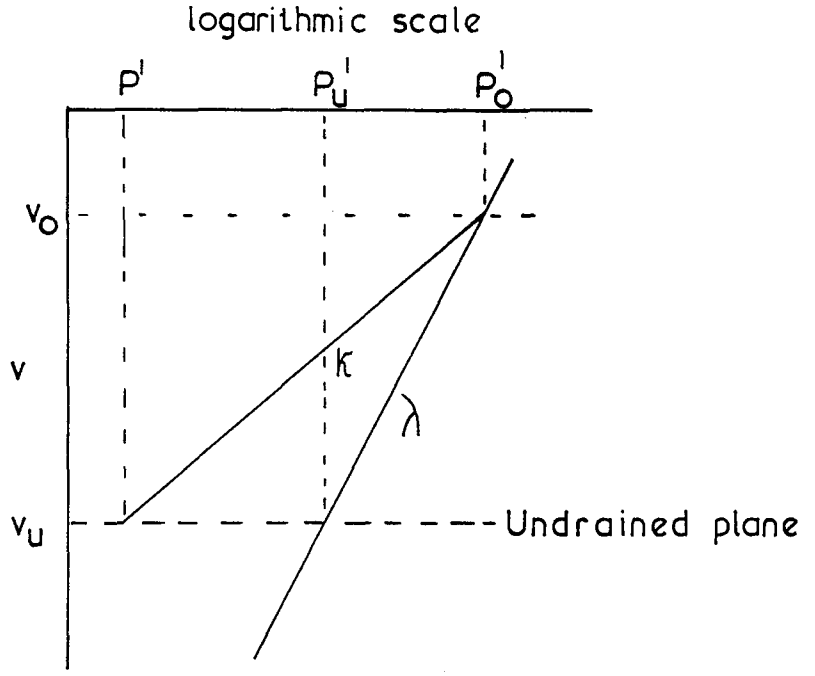
$$\tau_{rz\ max} = \sigma'_{r,i}\left(\frac{1+2K_o}{3}\right)\left\{0.5\left(1 + 3\left(\frac{1-K_o}{(1+2K_o)g(\theta)_{TC}}\right)^2\right)\right\}^{\Lambda} g(\theta)_f \cos\theta_f$$

A.9.2(16)

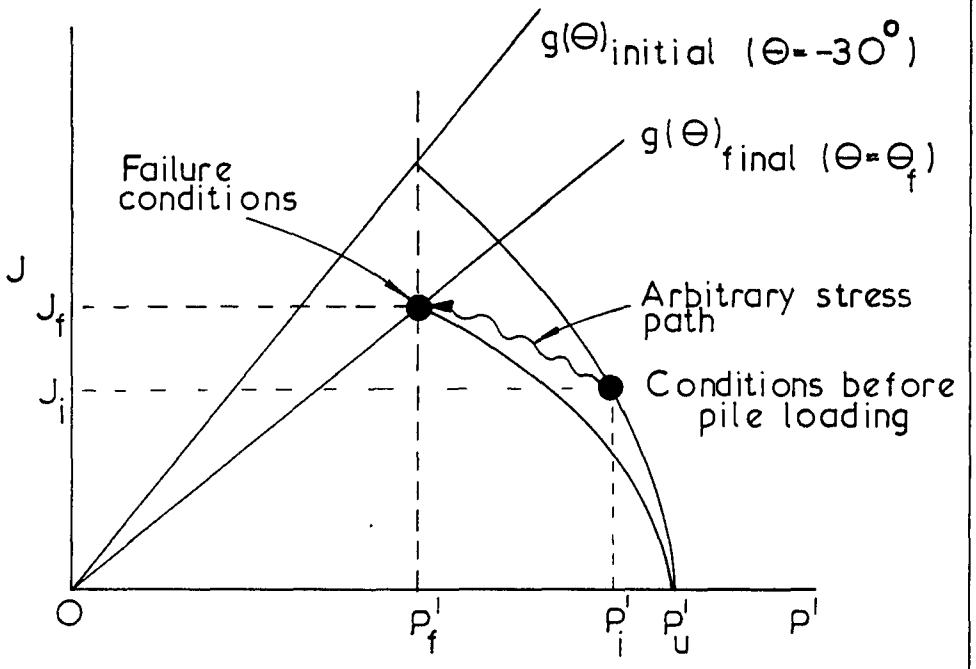
Finally, it will be recalled that if the soil is initiallly intact, failure is predicted to occur when the mobilised angle of friction is given by,

$$\delta' = \tan^{-1}(\sin\theta')_{\theta = \theta_f} \qquad \text{(see Fig. 8.9)}$$

Further relations between the stresses acting at failure may be derived as necessary from the equations presented above.



(a) Consolidation and swelling lines



(b) Stress conditions beside a driven pile loaded under undrained conditions

Fig.A.9.2.1

CHAPTER 10

CONCLUDING REMARKS

10.1 CONCLUSIONS

The work presented in this thesis is intended as a contribution towards a general effective stress theory of pile behaviour, and is concerned primarily with the response of normally-consolidated clay adjacent to loaded piles. The clay adjacent to a pile shaft is subject to an uncommonly high degree of kinematic restraint and so three independent, although complementary, approaches were adopted in this study;

(i) carefully controlled model pile tests;

(ii) micro-fabric studies of the clay adjacent to piles;

(iii) theoretical (numerical) modelling of the behaviour.

The first series of model tests was conducted on single piles installed into samples of anisotropically consolidated Speswhite Kaolin, by a technique which was demonstrated to cause minimal disturbance to either the stress field or the micro-fabric of the clay. The piles were loaded under fully drained conditions whilst the load-displacement behaviour was carefully monitored; in two of the tests the radial stresses acting on the piles were successfully measured. Following each test, the micro-fabric of the clay adjacent to the pile was studied.

The results demonstrate that the radial effective stress acting on a pile shaft typically varies during loading. In a test on a pile installed in over-consolidated Kaolin the radial stress increased by about 15%, whereas in tests on piles installed in normally-consolidated Kaolin the radial stresses decreased (the change in stress increased with increasing initial stress ratio).

The peak mobilised angle of shaft resistance appears to be independent of the initial stress ratio, and is slightly less than ϕ'. In tests conducted on piles installed in normally-consolidated Kaolin, the peak unit shaft resistance mobilised along the pile exceeds the initial undrained shear strength in triaxial compression by between 20% and 60%. It is suggested that this result is a consequence both of consolidation during the

pile loading, and the absence of pre-existing micro-fabric disturbance. The post-peak behaviour is brittle, the residual shaft resistance being roughly one-half of the peak value. The residual angle of shaft resistance is similar to the value measured by means of a Ring Shear apparatus at the same effective stress level and rate of displacement.

Micro-fabric studies performed in conjunction with these tests showed that 'Riedel' structures, which are associated with peak conditions, are formed at inclinations of between 10° and 15° to the direction of pile loading; the inclination appears to be independent of the initial stress ratio. Comparisons with predictions based on finite element analyses suggest that there are similarities between the Riedel structures and stress characteristics. In loading a pile up to peak conditions, permanent clay deformations were observed at distances of over one-half of one pile radius from the shaft. However, post-peak deformations were accommodated in a much narrower zone (less than one millimeter wide) and eventually a displacement discontinuity was formed parallel to the shaft. The clay particles adjacent to the discontinuity were strongly aligned sub-parallel to the direction of pile displacement, and the strength decreased to a residual value.

In order to examine the nature, and importance, of micro-fabric disturbance resulting from the installation of displacement piles, model piles were driven and jacked into samples of normally-consolidated Kaolin. After permitting complete consolidation, two of the three piles tested were loaded under drained conditions until residual strengths were achieved. The micro-fabric study demonstrated that the installation of displacement piles results in severe, permanent, fabric disturbance adjacent to the pile. Thus, before the pile is loaded, there exists, close to the pile, a shear zone which is at a residual strength appropriate to the peak pile velocities and the effective stress levels operating during installation. When the pile is loaded, peak conditions are achieved when the mobilised angle of shaft friction is equal to the residual angle of friction corresponding to the installation process. Thereafter the mobilised angle of friction decreases towards a residual value which depends on the rate of pile displacement during loading and the current effective stress level.

The load-displacement behaviour of the jacked and driven piles was in marked contrast to the behaviour of the piles installed with minimal disturbance into otherwise similar samples of Kaolin. The normalised peak shaft resistance of driven pile was slightly greater than that of the jacked

pile, but only 65% of that corresponding to a pile installed with minimal disturbance. On the other hand, the normalised residual shaft resistances of the three types of pile were very similar; the driven pile was about 10% stronger than the idealised pile.

It is considered that the post-peak brittleness observed during the loading of displacement piles (in the field as well as in the laboratory) is largely a result of a decrease in the angle of shaft friction from a residual value appropriate to installation conditions, to a lower value appropriate to slow loading. This post-peak brittleness is responsible for the progressive failure of long, compressible, piles. The experimental results have been combined with those from theoretical studies to provide a new, simple, method for calculating a lower bound to the ultimate shaft resistance of compressible piles. The predictions based on this method were shown to be in good agreement with the available field data, and with current empirical design procedures.

Finite element modelling of the behaviour of loaded piles, employing a form of the Modified Cam Clay constitutive law, has given very encouraging agreement with the results of model pile tests and the micro-fabric studies. The theoretical analyses were extended to consider the behaviour of loaded full-displacement piles; the stress states in the clay after pile installation and consolidation were taken from analyses based on cavity expansion theory (e.g. Randolph et al, 1979).

It has been shown that during the drained loading of a displacement pile, kinematic restraints force the effective stress path followed by an element of clay adjacent to the pile to be very similar to that which would be followed on undrained loading. For this reason, it is predicted that the peak drained and undrained shaft resistances are similar; this is supported by field measurements (e.g. Eide et al, 1961).

The excess pore pressures predicted to be generated on undrained Loading are smaller and much more localised than those generated during pile driving. It has also been shown that the excess pressures generated on loading will tend to dissipate roughly an order of magnitude faster than those generated on installation. It is suggested that in many instances (particularly on land) pile loading will tend to be a drained phenomenon.

Analyses of the drained loading of full-displacement piles have shown that the radial effective stress acting on the piles may decrease by as much as 40% during loading; it would, therefore, be highly unsafe to

assume that the radial stress acting on a pile following installation and consolidation, would continue to act whilst the pile is loaded to peak. Pile capacities, predicted on the basis of analyses which ignore the presence of pre-existing shear surfaces beside displacement piles, are well in excess of values measured in the field (despite the predicted reductions in the radial effective stress). Analyses which incorporate realistic strengths for the pre-existing shear surfaces lead to predictions which are in more reasonable agreement with field observations, but are still not conservative. There are a number of possible reasons for the over-esimation of pile capacities. One of these may be that the stresses assumed to exist around displacement piles following installation and consolidation were too high; the stresses were taken from Randolph et al (1979), and were derived from cavity expansion theory, employing the Modified Cam Clay constitutive law with a surface of revolution for both the yield function and the plastic potential. Reliable field measurements of radial effective stresses will be needed to resolve this matter.

10.2 IMPLICATIONS FOR THE DESIGN

10.2.1 Prediction of the Capacities of Compressible Piles

A method has been outlined (in Chapter 9) whereby a conservative estimate of the ultimate capacity of a long, compressible, pile may simply and cheaply be established. The only parameters required are the angles of shearing resistance of the intact soil, ϕ', the residual angles of interface friction, $\delta'_{r,i}$, and the bulk unit weights of the various strata. Estimates of ϕ' and $\delta'_{r,i}$ may be obtained without using undisturbed samples.

10.2.2 The Design of More Efficient Piles

An important conclusion from the work presented so far is that the peak shaft capacity of a displacement pile is limited by the presence of shear surfaces formed parallel to the pile during installation. Such surfaces are of particular importance around compressible piles because progressive failure may cause the peak pile capacity to tend rapidly towards the ultimate residual strength.

Another common method of installing piles, particularly in heavily over-consolidated clays, is to bore a hole (sometimes with the aid of bentonite mud) which is then filled with concrete. It is probable that the fabric disturbance caused by the drilling is less severe than that which

would have resulted had the pile been driven. However, the effects of stress relief and local swelling of the clay tend to reduce the final radial effective stress which acts on the pile, and so the peak capacity of the pile is again well below that which might have been obtained, had the pile been installed with no disturbance.

A method by which the capacity of a pile of given dimensions might be improved would be to install the pile by drilling and grouting under pressure. The result of this would be reduced fabric disturbance and an increased radial stress acting on the pile (the radial stress could presumably be made to exceed the initial in situ value). Thus the pile capacity might exceed that of an otherwise similar pile installed with no disturbance.

The results from the model pile tests suggest that the displacements required to mobilise the peak shaft resistance around drilled and grouted piles are considerably greater than those required for displacement piles. Thus, in the case of rigid piles, the settlement criteria may tend to reduce the advantages of pressure grouted piles. However, in the case of compressible piles, such as those used offshore, the advantages of the pressure-grouted piles are more obvious. The greater displacements required by drilled and grouted piles to reach peak conditions imply that for a given pile compressibility there will be a smaller propensity towards progressive failure than would be expected from a displacement pile. In addition, the model tests have shown that the post-peak rate of loss of shaft resistance with pile displacement is less for grouted piles than for displacement piles. Thus, for a given pile-head deflection, a pressure grouted pile should be able to mobilise a greater load than a displacement pile of similar dimensions.

Gouvenot and Gabaix (1975) report the results of tests conducted on pressure-grouted piles installed in sand and in clay. The authors conclude that the capacities of the pressure-grouted piles are between two and three times higher than those of similar piles grouted under gravity head.

Presumably Franki piles enjoy similar advantages of high lateral stresses and the fabric disturbance is probably not as severe as that encountered around driven piles.

This discussion is not pursued further, and is left as a suggestion for further consideration by others.

10.3 SUGGESTIONS FOR FUTURE RESEARCH

10.3.1 Field Measurements of Stresses

Theoretical procedures based on effective stress methods have been developed by many workers, in an attempt to model the history of the soil around a loaded pile. Predictions are made about the magnitudes of the radial total stresses, the excess pore pressures, and the shear stresses acting on the pile shaft at various stages in the pile's history. Unfortunately, in many instances, the validity of alternative approaches cannot be determined for lack of reliable field measurements. The most important quantity, the radial stress, has proved particularly difficult to measure, although not impossible (Butterfield and Johnston, 1973). There is now a great need for reliable field measurements of the stresses acting on piles installed in a variety of clays.

10.3.2 Interface Behaviour

The behaviour of clays when sheared against rigid interfaces has received surprisingly little attention, particularly in the last few years. On the basis of the work presented in this thesis it is suggested that direct shear interface tests should be performed routinely in the course of the site investigation for a piled foundation. There are also a large number of questions concerning interface behaviour which need to be addressed. For example;

(a) how do δ'_{peak} and $\delta'_{residual}$ depend on the interface material and the soil type (PI, grading etc.)?

(b) what is the influence of the rate of relative displacement for various interface roughnesses and particle gradings?

(c) what is the influence of the effective stress level?

(d) what is the effect of reversal, or of cyclic loading?

(e) under what circumstances does the failure plane occur within the soil, and when does it occur at the interface?

10.3.3 Industrially Important Problems

Much of the recent impetus, and money, for research into piling has come from oil companies who need to design foundations for large offshore structures. There is currently a trend towards the use of Tension Leg

Platforms (TLPs) in deep water. The piles involved will be required to act permanently in tension, and to sustain large cyclic loadings. Much work will be required before the behaviour of piles under such conditions can reliably be predicted; it would be helpful first to understand the response of piles subjected to monotonic compressive loadings!

REFERENCES

AIRHART, T.P., COYLE, H.M., HIRSCH, T.J. and BUCHANAN, S.J. (1969)

Pile-soil response in a cohesive soil. ASTM STP 444.

AMERASINGHE, S.F. and PARRY, R.H.G. (1975)

Anisotropy in heavily overconsolidated kaolin. ASCE, Journal of the Geotechnical Engineering Division, GT12, Dec. 1975.

APPENDINO, M., JAMIOLKOWSKI, M. and LANCELLOTTA, R. (1979)

Pore pressures of NC soft silty clay around driven displacement piles. Recent developments in the design and construction of piles, ICE, London, 1979.

D'APPOLONIA, D.J. and SAADA, A.S. (1972)

Discussion on: Bearing capacity of anisotropic cohesive soil. Journal of Geotechnical Engineering Division, ASCE: SMI, 126, 1972.

ARTHUR, J.R.F., CHUA, K.S., DUNSTAN, T. and RODRIGUEZ DEL C J.I. (1980)

Principal stress rotation: a missing parameter. ASCE, Journal of the Geotechnical Engineering Division, GT4, April 1980.

ARTHUR, J.R.F., DUNSTAN, T., AL-ANI, Q.A.J.L. and ASSADI, A. (1977)

Plastic deformation and failure in granular media. Geotechnique 27, no. 1, 53-74, 1977.

ATKINSON, J.H. (1973)

The deformation of undisturbed London Clay. Ph.D. Thesis, University of London.

ATKINSON, J.H. and POTTS, D.M. (1975)

Technical Note:
Geotechnique,vol.25,pp.379-384, 1975.

AURORA, R.P., PETERSON, E.H. and O'NEILL, M.W. (1980)

Model Study of load transfer in slender pile.
Technical Note: ASCE, Jounral of Geotechnical Engineering Division, August 1980.

AURORA, R.P. and O'NEILL, M.W. (1981)

Model studies of long piles in clay. Offshore Technology Conference, Paper DTC 4149.

BAGUELIN, F. and FRANK, R. (1980)

Theoretical studies of piles using the finite element method. ICE, Numerical methods in offshore piling. London, 1980, pp. 83-91.

BALIGH, M.M. and LEVADOUX, J-N. (1980)

Pore pressure dissipation after cone penetration. Massachusetts Institute of Technology, Report MITSG 80-13, Index No. 80-313-CIM.

BANNERJEE, P.K. and FATHALLAH, R.C. (1979)

An Eulerian formulation of the finite element method for predicting the stresses and pore water pressures around a driven pile. 3rd Int. Conf. Numerical Methods in Geomechanics, Aachen 1979, pp. 1053-1060.

BANNERJEE, P.K. and STIPHO, A.S. (1977).

Associated and non-associated constitutive relations for undrained behaviour of isotropic soft clays. Int. Jour. for Numerical and Analytical Methods in Geomechanics,

BEA, R.G. and DOYLE, E.H. (1975)

Parameters affecting axial capacity of piles in clays. Offshore Technology Conference, Paper OTC 2307, 1975.

BERGDAHL, U. and HULT, G. (1981)

Load tests on friction piles in clay. Int. Conf. SMFE, Stockholm, 1981.

BISHOP, A.W., GREEN, G.E., GARGA, U.K., ANDERSEN, A. and BROWN, J.D. (1971)

A new ring shear apparatus and its application to the measurement of residual strength. Geotechnique 21, no. 4, pp. 273-328.

BISHOP, A.W. and HENKEL, D.J. (1962)

The measurement of soil properties in the triaxial test. Edward Arnold, London.

BISHOP, A.W., KUMAPLEY, N.K. and EL RUWAYIH, A. (1975)

The influence of pore water tension on the strnegth of clay. Philosophical Transactions of The Royal Society of London. A. Mathematical and Physical Sciences, vol. 278, pp. 511-554, no. 1286, 1975.

BISHOP, A.W. and WESLEY, L.D. (1975)

A hydraulic triaxial apparatus for controlled stress path testing. Geotechnique 25, no. 4, pp. 657-670.

BJERRUM, L. (1975)

Problems of soil mechanics and construction on soft clays. Int. Conf. S.M. and F.E., 8, Moscow 1973, Proc. vol. 3, pp. 111-159.

BJERRUM, L. and JOHANNSEN, I. (1961)

Pore pressures resulting from driving piles in soft clay. Proc. Conf. on Pore Pressures and Suction in Soils, London.

BLANCHET, R., TAVERNAS, F. and GARNEAU, R. (1980).

Behaviour of friction piles in soft sensitive clays. Canadian Geotechnical J. vol. 17, 1980.

BOOKER, E.W. and IRELAND, H.O. (1965)

Earth pressures at rest related to stress history. Canadian Geotechnical J. vol. II, no. 1.

BORIN, D.L. (1973)

The behaviour of saturated kaolin in the simple shear apparatus. Ph.D. Thesis, University of Cambridge.

BOWDEN, F.P. and TABOR, D. (1950)

The friction and lubrication of solids, part 1. Oxford University Press,London (1950).

BOWDEN, F.P. and TABOR, D. (1964)

The friction and lubrication of solids, part II. Oxford University Press, London.

BOZOZUK, M., FELLENIUS, B.H. and SAMSON, L. (1978).

Soil disturbance from pile driving in sensitive clay. Canadian Geotechnical J., 15, 346-361 (1978).

BROMS, B.B. and MASSARSCH, R. (1979)

Discussion on: Recent developments in the design and construction of piles. ICE, London, 177-178.

BUCHER, F. (1975)

Die Restscherfestigkeit natürlicher Böden, ihre Einflussgrössen und Beziehungen als Ergeboris experimentaller Unter suchangen. Mitteilungen des Institutes für Grundbau und Bodenmecharik Eidgenössische Technische Hochschule Zürich, no. 103, 99 pages.

BURGHIGNOLI, A. and CARUANA, R. (1979)

Small scale experiment of pile driving in soft clay. RIN.Ita. Geotech., 13, no. 2, 87-93.

BURLAND, J.B. (1973)

Shaft friction of piles in clay - a simple fundamental approach. Ground Engng. 6, no. 3, 30-42.

BURLAND, J.B. (1978)

Skin friction on piles. Ground Engineering, Nov. 1978.

BURLAND, J.B., BUTLER, F.G. and DUNICAN, P.

The behaviour and design of large diameter bored piles in stiff clay. Proc. Symp. on Large Bored Piles, ICE, London, 51-71 (1966).

BUTTERFIELD, R. (1979)

A natural compression law for soils (an advance on e-log P'). Geotechnique, vol. 29, pp. 469-480.

BUTTERFIELD , R. and ANDRAWES, Z.K. (1972)

On the angles of friction between sand and plane surfaces. J. of Terramechanics, 8, 4, 15-23.

BUTTERFIELD, R. and BANNERJEE, P.K. (1970)

The effect of porewater pressures on the ultimate bearing capacity of driven piles. Proc. Second South East Asian Conf. on Soil Engineering, Bangkok, 385-394 (1970).

BUTTERFIELD, R. and JOHNSTON, I.W. (1973)

Stresses acting on a continuously penetrating pile. Proc. Eighth Int. Conf. Soil Mech. Jnl. Eng. Moscow, 2, 1, 39-46.

BUTTERFIELD, R. and JOHNSTON, I. (1980)

The influence of electro-osmosis on metallic piles in clay. Geotechnique, 30, no. 1, 17-38.

CARTER, J.P., RANDOLPH, M.F. adn WROTH, C.P. (1980)

Some aspects of the performance of open- and closed-ended piles. 'Numerical methods in offshore piling', ICE, London, pp. 165-170.

CARTER, J.P., RANDOLPH, M.F. and WROTH, C.P. (1979)

Stress and pore pressure changes in clay during and after the expansion of a cylindrical cavity. Int. Journ. for Numerical and Analytical Methods in Geomechanics, 1979.

CHANDLER, R.J. (1968)

The shaft friction of piles in cohesive soils in terms of effective stress. Civ. Eng. and Pub. Wks Rev., Jan. 1968, 48-51.

CHANDLER, R.J. and MARTINS, J.P. (1982)

An experimental study of skin friction around piles in clay. Geotechnique 32, no. 2, pp. 119-132.

CHODOROWSKI, A.R. (1982)

The generation and dissipation of excess pore water pressures during the driving of piles. M.Sc. dissertation, University of London.

CLARK, J.I. and MEYERHOF, G.G. (1972)

The behaviour of piles driven in clay. I. An investigation of soil stress and pore water pressure as related to soil properties. Canadian Geotechnical J., 9, 351 (1972).

CLARK, J.I. and MEYERHOF, G.G. (1973)

The behaviour of piles driven in clay. II. Investigation of the bearing capacity using total and effective strength parameters. Canadian Geotechnical J., 10, 86 (1973).

COOKE, R.W. and PRICE, G. (1973)

Strains and displacements around friction piles. Proc. 8th Int. Conf. Soil Mech. Fdn. Engrg., Moscow 2, no. 1, 53-60.

COOKE, R.W., PRICE, G. and TARR, K. (1979)

Jacked piles in London clay: a study of load transfer and settlement under working conditions. Geotechnique 29, no. 2, 113-147.

COYLE, H.M. and REESE, L.C. (1966)

Load transfer for axially loaded piles in clay. Journ. of the Soil Mechanics and Foundation Division, ASCE, vol. 92, no. SM2, 1966, pp. 1-26.

COX, W.R., KRAFT, L.M. and VERNER, E.A. (1979)

Axial load tests on 14-inch pipe piles in clay. Offshore Technology Conference, OTC 3491, 1979.

CUMMINGS, A.E., KERKHOFF, G.O. and PECK, R.B. (1950)

Effect of driving piles into soft clay. Trans. ASCE, 115, pp. 275-285.

DAVIS, E.H. (1968)

Theories of plasticity and the failure of soil masses. 'Soil Mechanics - Selected Topics', LEE, ed., Butterworths, 1968.

DE, P.K. (1973)

Electron microscopic investigation of kink band phenomena in shear induced consolidated kaolinite. Indian Geotechnical Journ., vol. 3, part 2, pp. 129-142.

DESAI, C.S. (1977)

The effects of driving and subsequent consolidation on behaviour of driven piles. International Journal for Numerical and Analytical Methods in Geomechanics.

DEWEY, J.F. (1965)

Nature and origin of kinkbands. Tectonophysics 1, 459-494.

DOLWIN, J., LEONARD, C.L. and POSKITT, T.J. (1979)

A study of two instrumented piles during driving. Paper No. E2006, Dept. of Civil Engineering, Queen Mary College, University of London.

DUNCAN, J.M. and DUNLOP, P. (1969)

Behaviour of soils in simple shear tests. Proc. 7th Int. Conf. Soil Mech., Mexico, 101-109.

EIDE, O., HUTCHINSON, J.N. and LANDVA, A. (1961)

Short and long term loading of a friction pile in clay. Proc. 5th Int. Conf. on Soil Mech. and Journ. Engng, Paris, 2, 1961.

EL RUWAYIH, A.A. (1975)

Stress strain characteristic of Rockfill, and of clays under high pore water tension. Ph.D. Thesis, University of London.

ESRIG, M.I., KIRBY, R.C., BEA, R.G. and MURPHY, B.S. (1977)

Initial development of a general effective stress method for the prediction of axial capacity for driven piles in clay. Offshore Technology Conf., Houston, Texas, Paper OTC 2943, 1977.

ESRIG, M.E. and KIRBY, R.C. (1979)

Advances in general effective stress method for the prediction of axial capacity for driven piles in clay. Offshore Technology Conf., Houston, Texas, Paper OTC 3406, 1979.

FELLENIUS, B.H. (1972)

Downdrag on piles in clay due to negative skin friction. Canadian Geotechnical J. 9(4), pp. 323-337.

FELLENIUS, B.H. (1975)

Test loading of piles and new proof testing procedures. Journ. Geot. Engng. Div. ASCE, GT9, 1975.

FELLENIUS, B.H. and SAMSON, L. (1976)

Testing of drivability of concrete piles and disturbance to sensitive clay. Canadian Geot. J., 13, 139 (1976).

FLAATE, K. (1972)

Effects of pile driving in clays. Canadian Geotech. J., 9, 81 (1972).

FOSTER, R.H. and DE, P.K. (1971)

Optical and electron microscopic investigation of shear induced structures in highly over-consolidated (soft) and heaving consolidated (hard) kaolinite. Proc. Clays and Clay Materials, vol. 19, pp. 30-48.

FOX, D.A. et al. (1970)

Pile driving into North Sea boulder clay. Proc. Offshore Tech. Conf. Houston, Paper OTC 1200, 535-548, 1970.

FREUND, R. (1974)

Kinematics of transform and transcurrent faults. Tectonophysics, 21, 1974, 93-134.

GALLAGHER, K.A. and ST. JOHN, H.D. (1980)

Field scale model studies of piles as anchorages for buoyant platforms. European Offshore Petroleum Conf. and Exhib., London, 1980.

GARNEAU, R. and SAMSON, L. (1974)

A device for the constant rate of penetration test for piles. Canadian Geotech. J, 11, 298 (1974).

GAY, N.C. and WEISS, L.E. (1974)

The relationship between principal stress directions and the geometry of kinks in foliated rock. Tectonphysics, 21 (1974), 287-300.

GENS, A. (1982)

Stress-strain and strength characteristics of a low plasticity clay. Ph.D. Thesis, University of London, Imperial College.

GIBSON, R.E. and ANDERSON, W.F. (1961)

Insitu measurement of soil properties with the pressuremeter. Civ. Engng Public Works Review, 56, pp. 615-618.

GOUVENOT, D. and GABAIX, J.C. (1975)

A new foundation technique using piles sealed by cement grout under high pressure. Proc. OTC, Houston, Paper OTC 2310, 1975.

GRIFFITHS, D.V. (1981)

Elasto plastic analyses of deep foundations in cohesive soil. Int. Journ. for Numerical and Analytical Methods in Geomechanics.

GROSCH, J.J. and REESE, L.C. (1980)

Field Tests of small scale pile segments in a soft clay deposit under repeated axial loading. Offshore Technology Conf., Houston, Texas, Paper OTC 3869, 1980.

HAGERTY, D.J. and GARLANGER, J.E. (1972)

Consolidation effects around driven piles. Proc. of Specialty Conf. on Earth Supported Structures, Purdue University, vol. II, 1207-1221.

HAGERTY, D.J. and PECK, R.B. (1971)

Heave and lateral movements due to pile driving. ASCE J. Soil Mech. Found. Div. 97, Proc. Paper 8497, pp. 1513-1532.

HEEREMA, E.P. (1979)

Pile driving and static load tests on piles in stiff clay. Offshore Technology Conf., Paper OTC 3490, 1979.

HELEY, W. and MacIVER, B.N. (1971)

Technical Report S-71-6, Report No. 1, Engineering properties of clay shales, U.S. Army Waterways Experimental Station.

HENKEL, D.J. (1960)

The shear strength of saturated remoulded clays. Research Conf. on Shear Strength of Cohesive Soils, Boulder, Colorado, p. 551.

HILL, R. (1950)

The mathematical theory of plasticity. Oxford University Press, London, 1950.

HOLLOWAY, D.M., CLOUGH, G.W. and VESIC, A.S. (1978)

The effects of residual driving stresses on the performance under axial loads. Offshore Technology Conference, Houston, Texas, Paper OTC 3306, 1978.

HOLMQUIST, D.V. and MATLOCK, H. (1976)

Resistance-displacement relationships for axially-loaded piles in soft clay. Offshore Techology Conf., Houston, Texas, Paper OTC 2474, 1976.

HOLTZ, W.G. and LOWITZ, C.A. (1965)

Effects of driving displacement piles in clear clay. ASCE J. SMF Div. 91 (SM5), Proc. Paper 4476, pp. 1-13.

HORN, H.M. and DEERE, D.V. (1962)

Frictional characteristics of minerals. Geotechnique, vol. 12, no. 4, pp. 319-335.

HOULSBY, G.T. and WROTH, C.P. (1980)

Strain and displacement discontinuities in soil. ASCE J. of the Engineering Mechanics Div., EM4, August 1980.

HOUSTON, W.N. and MITCHELL, J.K. (1969)

Property interrelationships in sensitive clays. J. Geot. Eng. Div. ASCE, SM4, 1037, 1969.

JAEGER, J.C. and COOK, N.G.W. (1977)

Fundamentals of rock mechanics. Chapman and Hall, London.

JOHANNESSEN, I.J. and BJERRUM, L. (1965)

Measurements of the compression of a steel pile to rock due to settlement of the surrounding clay. Proc. 6th Int. Conf. Soil Mech. and Found. Eng., II, pp. 261-264.

DE JOSSELIN and DE JONG (1971)

Discussion in Session II of the Roscoe Memorial Symposium. Stress-strain behaviour of soils, ed. R.H.G. Parry, Foulis, Cambridge, 258-261.

KIRBY, R.C. and ESRIG, M.I. (1980)

Further development of a general effective stress method for prediction of axial capacity for driven piles in clay. Recent developments in design and construction of piles, I.C.E., London, 1979.

KIRBY, R.G. and WROTH, C.P. (1977)

Application of critical state soil mechanics to the prediction of axial capacity of driven piles in clay. Offshore Technology Conference, Houston, Texas, Paper OTC 2942, 1977.

KLOHN, E.J. (1961)

Pile heave and redriving. Proc. ASCE,J. Soil Mech. Found. Div. 87 (SM4).

KOIZUMI, Y. and ITO, K. (1967)

Field tests with regard to pile driving and bearing capacity of pile foundations. Soils and Foundations, Japan 4, pp. 30-52.

KRAFT, L.M. Jr., COX, W.R. and VENER, E.A. (1981)

Pile load tests; cyclic loads and varying load rates. ASCE, Journ. of the Geotech. Eng. Div., January 1981.

KRAFT, L.M., RAY, R.P. and KAGANA, T. (1981)

Theoretical t-z curves. Proc. ASCE, J. Geot. Eng. Div., vol. 107, No. GT11, November 1981.

KRAFT, L.M., FOCHT, J.A. and AMERASINGHE, S.F. (1981)

Friction capacity of piles driven into clay. ASCE, Journ. of Geotech. Eng. Div., vol. 107, No. GT11, pp. 1521-1541.

KRYNINE, D.P. (1950)

Discussions of effect of driving piles into soft clay by Cummings et al. Trans. ASCE, vol. 115, pp. 315.

KULHANY, F.H. and PETERSON, M.S. (1979)

Behaviour of sand-concrete interfaces. Proc. of the Sixth Panamerican Conference on Soil Mechanics and Foundation Engineering, vol. 11, Lima 1979.

LADD, C.C. (1965)

Stress-strain behaviour of anisotropically consolidated clays during undraines shear. 6th Int. Conf. S.M. and F.E., Montreal, 1965.

LADD, C.C., BOVEE, R.B., EDGERS, L. and RIXNER, J.J. (1971)

Consolidated undrained plane strain shear tests on Boston Blue Clay. MIT Research Report R71-13.

LADD, C.C. and EDGERS, L. (1972)

Consolidated undrained direct-simple shear tests on saturated clays. MIT Research Report, T72-82.

LADE, P.V. and DUNCAN, J.M. (1973)

Cubical triaxial tests on cohesionless soil. J. Soil Mech. Found. Div., Proc. Am. Soc. Civ. Eng., 99, pp. 793-812.

LADE, P.V. and DUNCAN,J.M. (1975)

Elasto-plastic stress-strain theory for cohesionless soil. J. Geotech. Eng. Div., Proc. Am. Soc. Civ. Eng., 104, pp. 1037-1053.

LEVADOUX, J-N and BALIGH, M.M. (1980)

Pore pressure during cone penetration in clays. M.I.T., Report No. MIT S9 80-12.

LEWIN, P.I. (1970)

Stress-deformation characteristics of a saturated soil. Ph.D. Thesis, University of London, July 1970.

LITTLETON, I. (1976)

An experimental study of the adhesion between clay and steel. Journ. of Terrmechanics, vol. 13, no. 3, pp. 141-152.

LO,K.Y.and STERMAC, A.G. (1964).

Some pile loading tests in stiff clay. Canadian Geotech. J., 1, no. 2, 1964.

LO, K.Y. and STERMAC, A.G. (1965)

Induced pore pressures during pile driving operations. Proc. 6th Int. Conf. S.M. and F.E., vol. 2, 285.

LO, K.Y. and MORIN, J.P. (1972)

Strength anisotropy and time effects of two sensitive clays. Canadian Geotech. Journ. 9, 261 (1972).

LOPEZ, F. de Rezende (1979)

The undrained bearing capacity of piles and plates studied by the finite element method. Ph.D. Thesis, University of London, April 1979.

LOPEZ, F. de Rezende (1980)

Contribution to discussion; Conference on Recent Developments in Piling, ICE, London, 1979.

LUCKS, A.S., CHRISTIAN, J.T., BANDON, G.E. and HÖEG,K. (1972)

Stress conditions in NGI simple shear test. Journ. Geotech. Eng. Div. ASCE, SML 1972, 155-160.

LUPINI, J.F. (1981)

The residual strength of soils. Ph.D. Thesis, University of London.

LUPINI, J.F., SKINNER, A.E. and VAUGHAN, P.R. (1981)

The drained residual strength of cohesive soils. Geotechnique 31, no. 2, 181-213.

McCAMMON, N.R. and GOLDER, H.Q. (1970)

Some loading tests on long pipe piles. Geotechnique 20, no. 2, 171-184.

MARTIN, R.T. (1962)

Research on the physical properties of marine soils. Res. Rep. R62-42, Soil Eng. Div. Publ. No. 127.

MARTIN, R.T. (1966)

Quantitative fabric of wet kaolinite. Proc. 14th Nat. Conf. Clays and Clay Minerals, New York, Pergamon Press, pp. 271-287.

MARTIN, R.T. and LADD, C.C. (1970)

Fabric of consolidated kaolinite. MIT Research Report R70-15, Soils Publ. No. 254.

MARTINS, J.P. (1979)

A review of plastic field theory and its application to soil mechanics. M.Sc. dissertation, University of London.

MARTINS, J.P. and POTTS, D.M. (1982)

A numerical study of skin friction around driven piles. Behaviour of Offshore Structures, Boston, 1982.

MASSARSCH, K.R. (1976)

Soil movements caused by pile driving in clay. Dept. of Soil and Rock Mechanics, Royal Institute of Technology, Report No. 6, Sweden, pp. 269.

MASSARSCH, K.R. (1978)

New aspects of soil fracturing in clay. J. Geotech. Eng. Div. Am. Soc. Civ. Engrs, GT8, 1109-1123.

MASSARCH, K.R., BROMS, B.B. and SUNDQUIST, Q. (1975)

Pore pressure determinations with multiple piezometer. ASCE Conf. on In-Situ Measurements of Soil Properties.

MASSARSCH, K.R. and BROMS, B.B. (1977)

Fracturing of soil caused by pile driving in clay. Proc. 9th Int. Conf. Soil Mech. Found. Eng., Tokyo, vol. I, 197-200.

MATSUI, T., ITO, T., MITCHELL, J.K. and ABE, N. (1980)

Microscopic study of shear mechanism in soils. Journ. of Geotech. Div., ASCE, vol. 109, no. GT2, pp. 137-152.

MEYERHOF, G.G. and MURDOCK, L.J. (1953)

An investigation of the heaving capacity of some bored and driven piles in London Clay. Geotechnique 3, 267-282.

MEYERHOF, G.G. (1976)

Bearing capacity and settlement of pile foundations. J. Geotech. Eng. Div. ASCE, 102, GT3, 197-228.

MILLER, T.W., MURFF, J.D. and KRAFT, L.M. (1978)

Critical state soil mechanics model of soil consolidation stresses around a driven pile. 10th Offshore Technology Conference, Houston, Texas, OTC 3307.

MILLIGAN, V., SODERMAN, L.G. and RUTKA, A. (1962)

Experience with Canadian varied clay. J. Soil Mech. Found. Div. ASCE, 88, SM4, 31-67.

MITCHELL, J.K. (1956)

The fabric of natural clays and its relation to engineering properties. Highway Res. Bd., 35, pp. 693-713.

MITCHELL, J.K. and HOUSTON, W.N. (1969)

Causes of clay sensitivity. Journ. Geotech. Eng. Div. ASCE, vol. 93, SM3, May 1969, pp. 845-871.

MITCHELL, J.K. (1976)

Fundamentals of soil behaviour. John Wiley & Sons, Inc. New York (1976)

MITCHELL, R.J. (1970)

On the yielding and mechanical strength of Leda Clays. Canadian Geotech. Journ, 7, 297 (1970).

MORGENSTERN,N.R. and TCHALENKO, J.S. (1967a,b)

The optical determination of preferred orientation in clays and its application to the microstructure in consolidated kaolin, I,II. Proc. Roy. Soc., A 300, pp. 218-234 and pp. 235-250.

MORGENSTERN, N.R. and TCHALENKO , J.S. (1967c)

Microstructural observations on shear zones from slips in natural clays. Proc. Geotech. Conf. Oslo, pp. 147-152.

MORGENSTERN, N.R. and TCHALENKO, J.S. (1967d)

Microscopic structures in kaolin subjected to direct shear. Geotechnique, 17, 309-328.

NAYAK, G.C. and ZIENKIEWICZ, O.C. (1972)

Elasto-plastic stress analysis. A generalization for various constitutive relations including strain softening. Int. Journ. for Numerical Methods in Engineering, vol. 5, pp. 113-135.

NISHIDA, Y. (1964)

A basic calculation of the failure zone and the initial pore pressure around a driven pile in clay. Proc. 2nd Reg. Asian Conf. on Soil Mech. Found. Eng., 1, 217-219.

NISHIDA, Y. (1981)

Discussion on Randolph et al. (1979b). Geotechnique, 31, no. 2, 293-294.

O'NEIL, M.W. and REESE, L.C. (1972)

Behaviour of bored piles in Beaumont Clay. Journ. of Geotech. Eng. Div. ASCE, SM2, 1972, 195-213.

O'RIORDAN, N.N. (1982)

The mobilization of shaft adhesion down a bored, cast-in-situ pile in the Woolwich and Reading beds. Ground Engineering, 1982, vol. 15, nc. 3, pp. 17-26.

ORRJIE, O. and BROMS, B. (1967)

Effects of pile driving on soil properties. Proc. ASCE J. SMF Div. 93 (SM5), pp. 59-73.

PALMER, A.C. (1972)

Undrained plane-strain expansion of a cylindrical cavity in clay: a simple interpretation of the pressuremeter test. Teotechnique 22, no. 3, 451-457.

PARRY, R.H.G. (1971)

Undrained shear strengths in clays. Proc. 1st Australian-New Zealand Conf. Geomech.

PARRY, R.H.G. (1980)

A study of pile capacity for the Heather platform. Ground Engineering, March 1980.

PARRY, R.H.G. and NADARAJAH, V. (1973)

Observations on laboratory prepared, lightly overconsolidated specimens of kaolin. Geotechnique 24, no. 3, 345-358, 1973.

PARRY, R.H.G. and SWAIN, C.W. (1977a)

Effective stress methods of calculating skin friction on driven piles in soft clay. Ground Engineering, 1977, 10, 3, 24-26.

PARRY, R.H.G. and SWAIN, C.W. (1977b)

A study of skin friction on piles in stiff clay. Ground Engineering, 1977, 19, 8, 33-37.

PATERSON, M.S. and WEISS, L.E. (1966)

Experimental deformation and folding in phyllite. Geol. Sov. Am. Bull. 77, pp. 343-374.

POTTS, D.M. and GENS, A. (1983)

The effect of the plastic potential in boundary value problems. Int. Jl. for Numerical and Analytical Methods in Geomechanics (accepted for publication).

POTTS, D.M. and MARTINS, J.P. (1981)

The shaft resistance of driven piles in clay. 2nd Int. Conf. Numerical Methods in Offshore Piling, Houston, Texas.

POTTS, D.M. and MARTINS, J.P. (1982)

The shaft resistance of axially loaded piles in clay. Geotechnique, vol. 32, no. 4, December.

POTYONDY, J.G. (1961)

Skin friction between cohesive granular soils and construction materials. Geotechnique, 1961, 11, 4, 339-353.

POULOS, H.G. (1975)

Torsional response of piles. Journ. Geol. Eng. Div. ASCE, GT10, 1019, 1975.

POULOS, H.G. (1981)

Cyclic axial response of single pile. ASCE, Journ. of Geotech. Eng. Div., January 1981, ST1.

POULOS, H.G. and DAVIS, E.H. (1980)

Pile foundation analysis and design. John Wiley & Sons, 1980.

PREVOST, J.H. (1979)

Undrained shear tests on clay. Journ. Geotech. Eng. Div. ASCE, 105, GT1, 49-64.

PREVOST, J.H. and HØEG, K. (1976)

Reanalysis of simple shear soil testing. Canadian Geotech. Journ. 13, 418 (1976).

PREVOST. J-H. and HÖEG, K. (1975)

Effective stress-strain strength model for soils. Journ. Geotech. Eng. Div. ASCE, GT3, 1975.

PREVOST, J-H. and HÖEG, K. (1975)

Soil mechanics and plasticity analysis strain softening. Geotechnique, vol. 25, no. 1, March 1975.

PUECH, A. and JEZEQUEL, J-F (1980)

The effects of long time cyclic loadings on the behaviour of a tension pile. Offshore Technology Conference, Houston, Texas, 1980, OTC 3870.

QUIGLEY, R.M. and THOMPSON, C.D. (1966)

The fabric of anisotropically consolidated sensitive marine clay. Canadian Geotech. Journ. 3, no. 2, pp. 61-73.

RAMSAY, J.G. (1967)

Folding and fracturing of rocks, McGraw-Hill, New York, N.Y.

RANDOLPH, M.F. and CARTER, J.P. (1979)

The effect of pile permeability on the stress changes around a pile driven into clay. 3rd Int. Conf. Numerical Methods in Geomechanics, Aachen, pp. 1097-1105.

RANDOLPH, M.F., CARTER, J.P. and WROTH, C.P. (1979)

Driven piles in clay - the effects of installation and subsequent consolidation. Geotechnique 29, no. 4, 361-393, 1979.

RANDOLPH, M.F., STEENFELT, J.S. and WROTH, C.P. (1979)

The effect of pile type on design parameters for driven piles. Design parameters in Geotechnical Eng., B.G.S., London, 1978, vol. 2.

RANDOLPH, M.F. and WROTH, C.P. (1978)

Analysis of deformation of vertically loaded piles. ASCE, Journ. Geotech. Eng. Div., GT12, December 1978.

RANDOLPH, M.F. and WROTH, C.P.

An analytical solution for the consolidation around a driven pile. Int. Journ. for Numerical and Analytical Methods in Geomechanics, vol. 3, 217-229, 1979.

RANDOLPH, M.F. and WROTH, C.P. (1979)

An analysis of the vertical deformation of pile groups. Geotechnique vol. 29, no. 4, 1979.

RANDOLPH M.F. and WROTH, C.P. (1981)

Application of the failure state in undrained simple shear to the shaft capacity of driven piles. Geotechnique 31, no. 1, 143-157.

REESE, L.C., HUDSON, B.S. and VIJAYVERGIYA, B.S. (1969)

An investigation of the interaction between bored piles and soil. Proc. 7th Int. Conf. S.M. and F.E., vol. 2, pp. 211-215.

RIGDEN, W.J., PETTITT, J.J., ST. JOHN, H.D. and POSKITT, T.J. (1979)

Developments in piling for offshore structures. 2nd Int. Conf. on Beheaviour of Offshore Structures, London 1979, paper 67.

ROBINSKY, E.I. and MORRISON, C.E. (1964)

Sand displacement and compaction around model friction piles. Canadian Geotech. Journ., vol. 1, no. 2, 81.

ROSCOE, K.H., BASSETT, R.H. and COLE E.R.L. (1967)

Principal axes observed during simple shear of a sand. Proc. Geotech. Conf. Oslo, vol. 1, pp. 231-237.

ROSCOE, K.H. and BURLAND, J.B. (1968)

On the generalized stress-strain behaviour of 'wet' clays. Eng. Plast. eds.J. Heyman and F.A. Lekie, Cambridge University Press.

ROSCOE, K.H., SCHOFIELD, A.N. and WROTH, C.P. (1958)

On the yielding of soils. Geotechnique, 8, no. 1, pp. 22-53.

ROSCOE, K.H., THURAIRAJAH, A. (1964)

On the uniqueness of yield surfaces for wet clays. Proc. IUTAM Symp. on Rheology and Soil Mech., Grenoble, 1964, pp. 364-384, Berlin: Springer-Verlag, 1966.

ROY, M. (1980)

Discussion presented at Session VII: Recent developments in the design and construction of piles. pp. 378-380, ICE, London, 1980.

ROY, M., MICHAUD, D., TAVERNAS, F., LEROUEIL, S. and LA ROCHELLE, P. (1974)

The interpretation of static cone penetration tests in sensitive clays. Proc. Eur. Symp. on Penetration Testing, Stockholm, vol. 2.2, pp. 323-330.

ROY, M., BLANCHET, R., TAVERNAS, F. and LA ROCHELLE, P. (1981)

Behaviour of a sensitive clay during pile driving. Canadian Geotech. Journ. 18, 67-85 (1981).

ROY, M., TREMBLAY, M., TAVERNAS, F.A. and LA ROCHELLE, P. (1982)

Development of pore pressure in quasi-static penetration tests in sensitive clay. Canadian Geotech. Journ., 19, no. 1, pp. 124-138.

SCHOFIELD, A.N. and WROTH, C.P. (1968)

Critical state soil mechanics. McGraw-Hill Book Co., London, 1968.

SEARLE, I. (1980)

The design of bored piles in overconsolidated clays using effective stresses. Recent developments in the design and construction of piles, ICE, London, 1979.

SEED, H.B. and REESE, L.C. (1955)

The action of soft clay along friction piles. Proc. ASCE, Geotech. Eng. Div., December 1955.

SEMPLE, R.M. and GEMEINHARDT, J.P. (1981)

Stress history approach to analysis of soil resistance to pile driving. 13th Offshore Technology, Conference, Houston, Texas, Paper OTC 3969.

SILLS, G.C. (1975)

Some conditions under which Biot's equations of consolidation reduce to Terzaghi's equation. Geotechnique, vol. 25, no. 1, 1975, pp. 129-132.

SKEMPTON, A.W. (1954)

Pore pressure parameters A and B. Geotechnique 4, pp. 143.

SKEMPTON, A.W. (1959)

Cast-in-situ bored piles in London Clay. Geotechnique, 9, 158.

SKEMPTON, A.W. (1964)

Long term stability of clay slopes. Geotechnique, 14, pp. 72-101.

SKEMPTON, A.W. (1966)

Some observations on tectonic shear zones. Proc. 1st Int. Congr. Rock Mech. 1, pp. 329-335.

SKREDE, A. (1967)

An analysis of the changes in stresses and properties in the clay around a driven pile. Norwegian Thesis, Tech. Univ. of Norway, Trondheim.

SLOAN, S.W. and RANDOLPH, M.F. (1982)

Numerical prediction of collapse loads using finite element methods. Int. Journ. for Numerical and Analytical Methods in Geomechanics, vol. 6, pp. 47-76.

SMITH, R.E. (1964)

Discussion on Soderberg (1962). Geotechnique, 14, no. 1, 61.

ST. JOHN, H.D. (1980)

A review of current practice in the design and installation of piles for offshore structures. Dept. of Energy, Offshore Technology Report 5.

SÖDERBERG, L.O. (1962)

Consolidation theory applied to foundation pile time effects. Geotechnique, 12, 3, pp. 217-225.

STEENFELT, J.S., RANDOLPH, M.F. and WROTH, C.P. (1981)

Instrumented model piles jacked into clay. Int. Conf. Soil Mech. and Found. Eng., Stockholm, vol. 2.

STERMAC, A.G., SELBY, K.G. and DEVATA, M. (1969)

Behaviour of various types of piles in a stiff clay. Proc. 7th Int. Conf. S.M. and F.E., Mexico, 1969, p. 239.

SUTTON, V.J., RIGDEN, W.J., JAMES, , ST. JOHN, H.D. and POSKITT, R.J. (1979)

Full scale instrumented pile test in the North Sea. Offshore Technology Conf., Houston, Texas, 1979, OTC 3489.

SWANN, L. (1979)

Pore pressure generation around driven piles. M.Sc. Thesis, University of London.

TOMLINSON, M.J. (1970a)

Some effects of pile driving on skin friction. Proc. Conf. on Behaviour of Piles, I.C.E., London, 1970.

TOMLINSON, M.J. (1970b)

Adhesion of piles in stiff clays. CIRIA Report 26, November 1970.

TAVERNAS, F. and LEROUEIL, S. (1979)

Clay behaviour and the selection of design parameters. Design parameters in Geotechnical Eng: BGS, London 1971, vol. 1.

TCHALENKO, J.S. (1967)

The influence of shear and consolidation on the microscopic structure of some clays. Ph.D. Thesis, University of London (Imperial College), 1967.

TCHALENKO, J.S. (1968)

The evolution of kink bands and the development of compression textures in sheared clays. Tectonophysics 6(2), 1968, 159-174.

TERZAGHI, K. (1943)

Theoretical soil mechanics. John Wiley & Sons, New York.

THORBURN, S. and RIGDEN, W.J. (1980)

A practical study of pile behaviour. Offshore Technology Conf. Houston, Texas, 1980, OTC 3825.

THURAIRAJAH, A. (1961)

Some shear properties of kaolin and of sand. Ph.D. Thesis, University of Cambridge (1961).

TOH, C.T. and SLOAN, S.W. (1980)

Finite element analysis of isotropic and anisotropic cohesive soils with a view to correctly predicting impending collapse. Int. Journ. for Numerical and Analytical Methods in Geomechanics.

TORSTENSSON, B.A. (1973)

The behaviour of a cohesion pile group in clay. Proc. 8th Int. Conf S.M.and F.E. Moscow (USSR), vol. 2.1, pp. 237-242.

VAID YOGINDER, P. and CAMPANELLA, R.G. (1974)

Triaxial and plane strain behaviour of natural clay. Journ. of Geotech. Eng. Div., ASCE, GT3, 1974.

VAN EEKELEN, H.A.M., POTTS, D.M. (1978)

The behaviour of Drammen Clay under cyclic loading. Geotechnique 28, no. 2, 173-196.

VAN EEKELEN, H.A.M. (1980)

Isotropic yield surfaces in three dimensions for use in soil mechanics. Int. Journ. for Numerical and Analytical Methods in Geomechanics.

VIJAYVERIGA, V.N. (1980)

Soil response during pile driving. Conf. Numerical Methods in Offshore Piling, London, ICE, 53-58.

VIJAYVERGIYA, V.N. and FOCHT, J.A. (1972)

A new way to predict capacity of piles in clay. Proc. 4th. A Offshore Tech. Conf. Houston, Texas, paper .

VIJAYVERGIYA, V.N. (1977)

Friction capacity of driven piles in clay. Offshore Technology Conf. Houston, Texas, paper 2939.

WEISS, L.E. (1980)

Nucleation and growth of kink bands. Tectonophysics, 65 (1980) 1-38.

WERNICK, E. (1979)

A 'true' direct shear apparatus to measure soil parameters of shear bands. Design Parameters in Geotechnical Engineering, BGS, London, 1979, vol. 2.

WHITAKER, T. and COOKE, R.W. (1966)

An investigation of the shaft and base resistance of large bored piles in London Clay. Proc. Symp. on Large Bored Piles 7-49, I.C.E., London 1966.

WOOD, D.M. (1981)

Discussion on Randolph et al (1979). Geotechnique, 31, no. 2, 291-293.

WOOD, D.M, DRESCHER, A. and BUDHU, M. (1979)

On the determination of stress state in the simple shear apparatus. Geotechnical Testing Journ. vol. 2, no. , 1979.

WOOD, D.M. and WROTH, C.P. (1976)

The correlation of some basic engineering properties of soils. Boss '76, Behaviour of Offshore Structures.

WROTH, C.P. (1969)

Some recent developments of the simple shear apparatus at Cambridge. Discussion of Specialty Session 16, Proc. 7th ICSMFE, Mexico, vol. 3, pp. 526-527.

WROTH, C.P. (1979)

Correlations of the engineering properties of soils. Behaviour of Offshore Structures, London, 1979.

WROTH, C.P., CARTER, J.P. and RANDOLPH, M.F. (1980)

Stress changes around a pile driven into cohesive soil. Recent developments in the design and construction of piles. ICE, London, 1979.

YANG, N.C. (1956)

Redriving characteristics of piles. Proc. ASCE, SM3, vol. 82, p. 17.

YONG KWET, YEW (1979)

A laboratory study of the shaft resistance of bored piles. Ph.D. Thesis, University of Sheffield.

YONG, R.N. and SILVESTRI, V. (1979)

Anisotropic behaviour of a sensitive clay. Canadian Geotech. Jour. 16, 335-350 (1979).

ZEEVAERT, L. (1950)

Discussion of effect of driving piles into soft clay by Cummings et al. Trans. ASCE, vol. 115, 1950, pp. 287-292.

ZEEVAERT, L. (1960)

Reduction of point bearing capacity of piles because of negative skin friction. Panamerican Conf. on Soil Mechanics and Found. Eng. 1, Mexico, 1959, Proc. vol. 3, pp. 1145-1152.

ZIENKIEWICZ, O.C. (1977)

The finite element method (3rd ed.), McGraw-Hill Book Company (UK) Ltd.

ZIENKIEWICZ, O.C., VALLIAPPAN, S. and KING, I.P. (1969)

Elasto-plastic solutions of engineering problems: Initial stress; finite element approach. Int. Jour. for Numerical Methods in Eng., vol. 1, 75-100.

ZIENKIEWICZ, O. and NAYLOR, D.J. (1971)

The adaption of critical state soil mechanics theory for use in finite elements. Stress-Strain Behaviour of Soils, ed. R.H.G. Parry, Foulis, 1971, pp. 537-547.

ZYTYNSKI, M., RANDOLPH, M.F., NOVA, R. and WROTH, C.P. (1975)

On modelling the unloading-reloading behaviour of soils. Int. Jour. Numer. Anal. Methods in Geomechanics 1975, 2, 1, 87-93.